CATALYTIC C-C (C-N) BOND FORMATION AND C-O BOND CLEAVAGE BY PINCER-LIGATED IRIDIUM COMPLEXES

By

Bo Li

A dissertation submitted to the

School of Graduate Studies

Rutgers, The State University of New Jersey

In partial fulfillment of the requirements

For the degree of

Doctor of Philosophy

Graduate Program in Chemistry and Chemical Biology

Written under the direction of

Alan S. Goldman

And approved by

_____

_____

_____

_____

New Brunswick, New Jersey

May, 2019

ABSTRACT OF THE DISSERTATION

CATALYTIC C-C (C-N) BOND FORMATION AND C-O BOND CLEAVAGE BY PINCER-LIGATED IRIDIUM COMPLEXES

By

Bo Li

Dissertation Director:

Alan S. Goldman

Since the initial reports of catalytic alkane dehydrogenation by (^{tBu}PCP)Ir (^{tBu}PCP = κ^3-2,6-$C_6H_3(CH_2tBu_2)_2$) in 1996, pincer-iridium complexes have grown rapidly to include a family of derivatives. No longer limited to the original application of dehydrogenation, this new growing family shows versatile applications such as activation of X-H (X = C, N, O, Si) bonds, tandem dehydrogenation/olefin-metathesis, activation of other strong bonds, catalytic phenol-type C-O bond formation and cleavage. However, there are surprisingly few examples of dehydrogenative couplings of C−H bonds catalyzed by pincer-iridium complex, though it shows to be the ideal route for C-C bond formation. The substrates for catalytic C-O bond cleavage were also limited to alkyl phenol ethers. My PhD dissertation research aimed to discover and elucidate the mechanisms of a wider range of C-C (C-N) bond formation and C-O cleavage reactions catalyzed by pincer-ligated iridium complexes.

Chapter 2 presents the development of a tandem catalytic system for aryl-alkyl coupling. Iridium pincer complexes together with zeolites are used to convert pentylbenzene to methylnaphthalene, with hydrogen gas as the only byproduct. The utility of this method is demonstrated in the preparation of 2,6-dimethylnaphthalene, a feedstock for high performance polyesters.

Chapter 3, 4 and 5 describes the development and mechanistic investigation of dehydrogenative coupling reactions. Diaryl butadienes are obtained by homo-coupling. Cross-dehydrogenative coupling vinyl arenes with furan, thiophene, aromatics, and olefins is also demonstrated. A metalloindene complex is shown to be the key intermediate in these reactions. An intramolecular dehydrogenative coupling for the synthesis of indene and indole from vinyl arene and vinyl aniline, respectively, is further shown.

In Chapter 6, the catalytic hydrogenolysis of C-O bonds by pincer iridium complexes is shown. 1,3-diols and triols are partially deoxygenated under H_2 atmosphere. An important application for this reaction is illustrated by the high yielding conversion of glycerol, an abundant side product from biofuel production, to 1,2-propanediol, a useful solvent and chemical intermediate.

Lastly, I synthesized a new pincer-iridium complex (^{iPr}NCOP)Ir and utilized it for C-C bond formation and C-O bond cleavage.

Acknowledgement

The first person that comes to my mind to thank is Prof. Alan S. Goldman. I would not have a clear idea for my graduate school if I had not met you in 2012. Your guidance, encouragement, help, and patience kept me growing for last 7 years. You've done more than I could expect from an advisor: you are a friend and a supporter. I express my special thanks for you.

Another special person to mention here is Prof. Fuat E. Celik. As co-advisor and committee member, you are supportive, helpful, and suggestive. I learned a lot from you and really enjoyed my time as part of the Celik group.

I owe additional thanks to Prof. Charles Dismukes for his service as committee member since 2015; and to Prof. Martha Greenblatt for serving as a committee member for my Out-of-Field Research Proposal. Thanks to Prof. Mark Lipke and Prof. Demyan Prokopchuk, who stepped up for my defense. Thanks to Prof. Karsten Krogh-Jespersen and Prof. Faraj Hasanayn for the collaboration and contribution towards computational chemistry. Thanks to Prof. Enver Cagri Izgu for the help of job hunting. Thanks to Prof. William D. Jones for his collaboration on dehydrogenative coupling of vinyl arenes.

Thanks to Prof. Eric Garfunkel and Prof. Laurence S. Romsted for being close friends and supporters. Thanks to all the course instructors, including Prof. Kai Hultzsch, Prof. Spencer Knapp, Prof. Ralf Warmuth, Prof. Laurence S. Romsted, Prof. Leslie Jimenez, for preparing me good for my research.

I would like to thank all members from both Goldman group and Celik group. Thank you for joining my journey here at Rutgers and thanks for your suggestions and help

on problems I occurred. I really enjoy your company and have a good time here in NJ. I would particularly like to thank Dr. Michael C. Haibach and Dr. Akshai Kumar for helping me to initiate my research. Also special thanks to Dr. Tian Zhou, Dr. Changjian Guan and Santanu Malakar for your contribution to the computational chemistry studies. Special thanks to Arun Shada, Benjamin Gordon, Boris Sheludko, Santanu Malakar, and Tariq Bhatti for their editing for this thesis.

Thank you Dr. Thomas Emge for all the fancy crystal structure determination. Thank you Dr. William W. Brennessel for all the elemental analysis. Thank you Dr. Nagarajan Murali for all the NMR related issues. Thank you Dr. Alexei Ermakov for all the instrument related issues. Thank you Andrew M De Zaio for make facilities working and lab safe. Thank you Steven W Young for all the quick delivery. Thank you Mark F Dority for all the solution of computer related issues.

Thanks to our all other sweet staffs at CCB. It was all of you guy make me stay here just like home. Special thanks to Allison Larkin, Karen Fowler, Arielle L'Esperance, Lydia Haynes, and Ann Doeffinger. I have to say Ann Doeffinger is the sweetest administrative assistant I ever met.

The support and encouragement from my family and friends is a huge contributor to my success. I express my sincere thanks to all of you. As the most unselfish people in my life, I owe a huge thank you to my mom, dad, and my wife. You three make my life colorful and meaningful.

Dedication

To my family, and to science.

Table of Contents

Abstract **ii**

Acknowledgements **iv**

Dedication **vi**

Table of Contents **vii**

List of Figures **xiv**

List of Schemes **xxii**

List of Tables **xxv**

Chapter 1. Introduction **1**

1.1. Importance of dehydrogenation 1

1.2. History of transition-metal-mediated alkane dehydrogenation 1

1.3. Dehydrogenation and bond activation using pincer-iridium complexes 3

1.4. Research goals of this thesis 9

Chapter 2. Alkyl-aryl coupling catalyzed by tandem systems of pincer-ligated iridium complexes and zeolites **16**

Abstract 17

2.1. Introduction 18

2.2. Results and discussion 19

2.3. Conclusion 28

2.4. Experimental information 29

2.4.1 General information and experimental methods 29

2.4.2. Gas chromatography (GC) Methods 31

2.4.3. Identification of major products 32

2.4.4. Reactions with 0.58 g zeolites 34

2.4.5. Zeolite-catalyzed methylnaphthalene isomerization 36

2.4.6. Recyclability 37

2.4.7. Decrease of total solution mass (loss of volatile products) 37

2.9. Reference 39

Chapter 3. Catalytic dehydrogenative C-C coupling by a pincer-ligated iridium complex 42

Abstract 43

3.1. Introduction 44

3.2. Results and discussion 46

3.2.1. Catalytic intermolecular coupling by (iPrPCP)Ir 46

3.2.2. Catalytic intramolecular coupling by (^{iPr}PCP)Ir. 56

3.2.3. Stoichiometric reactions of (tBuPCP)Ir with styrenes 57

3.3. DFT calculations and mechanistic discussion 59

3.3.1. Double bond insertion mechanisms 59

3.3.2. A “direct” coupling mechanism 61

3.3.3. Metalloindene mechanism 64

3.3.4. Intramolecular coupling 68

3.3.5. Hetero-coupling with pentafluorophenylethylene 70

3.4. Summary and conclusions 74

3.5. Experimental information 77

3.5.1. General information 77

3.5.2. General procedure for coupling of vinyl arenes with (^{ipr}PCP)IrHCl as precatalyst 78

3.5.3. General procedure for coupling of vinyl arenes with (^{ipr}PCP)Ir(ethylene) as precatalyst 78

3.5.4. Computational information 79

3.5.5. Product identification 80

3.5.5.1. (*E*, *E*)-1,4-Diphenyl-1,3-butadiene 80

3.5.5.2. (*E*, *E*)-1,4-Di-(4-tolyl)-1,3-butadiene 80

3.5.5.3. (*E*, *E*)-1,4-Di-(2-tolyl)-1,3-butadiene 81

3.5.5.4. (*E*, *E*)-1,4-Di-[4-(trifluoromethyl)phenyl]butadiene 81

3.5.5.5. (*E*, *E*)-1,4- Di-(4-fluorophenyl)butadiene 81

3.5.5.6. (*E*, *E*)-1,4-Di-(4-tert-butylphenyl)-1,3-butadiene 81

3.5.5.7. (*E*, *E*)-1,4-Di-(4-methoxyphenyl)-1,3-butadiene 81

3.5.5.8. (*E*, *E*)-1,4-Di-(3,5-dimethylphenyl)-1,3-butadiene 82

3.5.5.9. (*E*, *E*)-1,4-Di-(3,5-trifluoromethylphenyl)-1,3-butadiene 82

3.5.5.10. (*E*, *E*)-1,4-(2-Naphthyl)-1,3-butadiene 82

3.5.5.11. 1,2,3,4,5-Pentafluoro-6-[(1*E*, 3*E*)-4-phenyl-1,3-butadien-1-yl]benzene 83

3.5.5.12. 4,6-Dimethylindene (A) and 5,7-dimethylindene (B) 83

3.5.5.13. 4,6-Dimethylindane (C) and 1-ethyl-2,4,6-trimethylbenzene (D) 84

3.5.5.14. 4,6-Dimethylindane 85

3.5.6. Iridium complexes 85

3.5.6.1. (^{iPr}PCP)Ir(η^2-H_2C=CHPh) (2) 85

3.5.6.2. Metalloindene complex 3 86

3.5.6.3. Metalloindene complex 4 87

3.5.6.4. Metalloindene complex 5 88

3.5.6.5. Metalloindene complex 7 88

3.5.6.6. Metalloindene complex 8 89

3.5.6.7. Metalloindene complex 9 90

3.5.7. Isomerization experiments 92

3.5.8. NMR spectra of coupling products and metal complexes 94

3.5.9. X-Ray structures 120

3.5.9.1. General information 120

3.5.9.2. Structural data for complex 2 122

3.5.9.3. Structural data for complex 3 135

3.5.9.4. Structural data for complex 4 149

3.5.9.5. Structural data for complex 5 166

3.5.9.6. Structural data for complex 7 180

3.5.9.7. Structural data for complex 8 205

3.5.9.8. Structural data for complex 9 219

3.5.9.9. Structural data for (*E*, *E*)-1,4-(2-naphthyl)-1,3-butadiene 233

3.5.10. Reaction mechanisms and free energies 243

Chapter 4. Cross-dehydrogenative coupling vinyl arenes with aromatics and olefins 262

Abstract 262

4.1. Introduction 263

4.2. Results and discussion 265

4.2.1. Cross-coupling styrene with stoichiometric amount benzene or TBE using (^{iPr}PCP)Ir as catalyst 266

4.2.2. Cross-coupling styrene with excess amount benzene by pincer-iridium complex 267

4.2.3. Cross-coupling vinyl arenes with aromatics by pincer-iridium complex 269

4.2.4. Cross-coupling vinyl arenes with heterocyclic compounds by pincer-iridium complex 271

4.2.5. Cross-coupling vinyl arenes with non-functionalized alkenes by pincer-iridium complex 272

4.3. Conclusion 275

4.4 Experimental information 276

4.4.1. General information 276

4.4.2. Product identification 277

4.4.3. NMR Spectra of cross-coupling products 278

Chapter 5. Direct synthesis of indene and indole through intramolecular dehydrogenative coupling 283

Abstract 283

5.1. Introduction 284

5.2. Results and discussion 286

5.2.1. Doubly ortho-methylated vinyl arenes undergo intramolecular dehydrogenative coupling 286

5.2.2. Intramolecular dehydrogenative coupling of vinyl aniline 289

5.3. Conclusion 295

5.4. Experiment information 296

5.4.1. General information 296

5.4.2. Product identification 297

5.4.2.1. 3-methylindole 297

5.4.2.2. 2-methylindole 297

5.4.2.3. Ir 1 297

5.4.3. NMR spectra 299

5.4.4. X-Ray structure data 306

5.4.3.1. ORTEP Diagram Ir 1 306

5.5. Reference 321

Chapter 6. Partial deoxygenation of diols and triols by a pincer-ligated iridium complex 325

Abstract 325

6.1. Introduction 326

6.2. Results and discussion 328

6.2.1. Dehydration by pincer iridium complex 328

6.2.2. Partial deoxygenation of diols 329

6.2.3. Partial deoxygenation of triols 335

6.2.4. Demethoxylation of 3-methoxy-1-propanol 343

6.2.5. Mechanism studies 344

6.3. Conclusion 347

6.4. Experimental information 348

6.4.1. General experimental information 348

6.5. Reference 350

Chapter 7. Synthesis and reactivity of a new pincer-ligated iridium complex for C-C bond formation and C-O bond cleavage 353

Abstract 353

7.1. Introduction 354

7.2. Results and discussion 356

7.2.1. Catalyst synthesis 356

7.2.2. Using (^{iPr}NCOP)Ir(ethylene) for C-C bond formation 359

7.2.3. Discovering C-O bond cleavage reaction by new catalyst (^{iPr}NCOP)Ir(ethylene) 361

7.2.4. C-O bond cleavage reaction scope and proposed mechanism 365

7. 3. Conclusion 367

7. 4. Experimental information 367

7.4.1. General information 368

7.4.2. Catalyst synthesis and product identification 368

7.4.2.1. (^{iPr}NCOP)Ir(HCl) synthesis and NMR data 368

7.4.2.2. (^{iPr}NCOP)Ir(ethylene) synthesis and NMR data 369

7.4.2.3. (^{iPr}NCOP)Ir(CO) synthesis and NMR data 369

7.4.3. NMR spectra 371

7.4.4. X-Ray structure data 374

7.5. Reference 384

List of Figures

Figure 1. 1. Pincer ligand and pincer-metal complexes 3

Figure 1. 2. Various pincer-ligated iridium complexes 5

Figure 1. 3. Bond activations by pincer-iridium complexes 7

Figure 1. 4. Ph.D. research summary 10

Figure 2. 1. Reaction vessel 30

Figure 2. 2. GC trace showing product separation 32

Figure 2. 3. GC trace of region of the major cyclized products with identification 33

Figure 3. 1. ORTEP representations of complex 2 and 3 53

Figure 3. 2. ORTEP representations of complex 4 and 5 55

Figure 3. 3. ORTEP representation of complex 7 58

Figure 3. 4. ORTEP representation of complex 8 and 9 59

Figure 3. 5. Dehydrogenative styrene coupling via consecutive vinylic C-H additions followed by loss of H_2, olefin hydrogenation and C-C elimination 62

Figure 3. 6. Calculated free energies (kcal/mol) for the tail-to-tail coupling of styrene via a cyclometalation (metalloindene) mechanism. 65

Figure 3. 7. Calculated free energies and enthalpies (below, italic) for the (^{iPr}PCP)Ir-catalyzed conversion of 2,4,6-trimethylstyrene to 4,6-dimethylindene at 150 °C. 69

Figure 3. 8. Products of (^{iPr}PCP)Ir-catalyzed dehydrogenative coupling of styrene and F_5-styrene (150 °C). 71

Figure 3. 9. Schematic diagrams of the TSs for the calculated rate-determining step for dehydrogenative coupling, via the “direct mechanism”, for homocoupling of styrene 73

Figure 3. 10. Schematic diagrams of the TSs for the calculated rate-determining step 74

Figure 3. 11. Crystal structure of (E, E)-1,4-(2-naphthyl)-1,3-butadiene 83

Figure 3. 12. GC-MS traces of isomerization experiment 93

Figure 3. 13. ^{1}H NMR of (*E*,*E*)-1,4-diphenyl-1,3-butadiene (500 MHz, $CDCl_3$) 94

Figure 3. 14. ^{13}C NMR of (*E*,*E*)-1,4-diphenyl-1,3-butadiene (500 MHz, $CDCl_3$) 94

Figure 3. 15. ^{1}H NMR of (*E*,*E*)-1,4-di-(4-tolyl)-1,3-butadiene (500 MHz, $CDCl_3$) 95

Figure 3. 16. ^{13}C NMR of (*E*,*E*)-1,4-di-(4-tolyl)-1,3-butadiene (500 MHz, $CDCl_3$) 95

Figure 3. 17. ^{1}H NMR of (*E*,*E*)-1,4-di-(2-tolyl)-1,3-butadiene (500 MHz, $CDCl_3$) 96

Figure 3. 18. ^{13}C NMR of (*E*,*E*)-1,4-di-(2-tolyl)-1,3-butadiene (500 MHz, $CDCl_3$) 96

Figure 3. 19. ^{1}H NMR of (*E*,*E*)-1,4-di-[4-(Trifluoromethyl)phenyl]-1,3-butadiene (500 MHz, $CDCl_3$) 97

Figure 3. 20. ^{13}C NMR of (*E*,*E*)-1,4-di-[4-(trifluoromethyl)phenyl]-1,3-butadiene (500 MHz, $CDCl_3$) 97

Figure 3. 21. ^{1}H NMR of (*E*,*E*)-1,4- di-(4-fluorophenyl)-1,3-butadiene (500 MHz, $CDCl_3$) 98

Figure 3. 22. ^{13}C NMR of (*E*,*E*)-1,4- di-(4-fluorophenyl)-1,3-butadiene (500 MHz, $CDCl_3$) 98

Figure 3. 23. ^{1}H NMR of (*E*,*E*)-1,4-di-(4-tert-butylphenyl)-1,3-butadiene (500 MHz, $CDCl_3$) 99

Figure 3. 24. ^{13}C NMR of (*E*,*E*)-1,4-di-(4-tert-butylphenyl)-1,3-butadiene (500 MHz, $CDCl_3$) 99

Figure 3. 25. ^{1}H NMR of (*E*,*E*)-1,4-di-(4-methoxyphenyl)-1,3-butadiene (500 MHz, $CDCl_3$) 100

Figure 3. 26. ^{13}C NMR of (*E*,*E*)-1,4-di-(4-methoxyphenyl)-1,3-butadiene (500 MHz, $CDCl_3$) 100

Figure 3. 27. ^{1}H NMR of (*E*,*E*)-1,4-di-(3,5-dimethylphenyl)-1,3-butadiene (500 MHz, $CDCl_3$) 101

Figure 3. 28. ^{13}C NMR of (*E*,*E*)-1,4-d-(3,5-dimethylphenyl)-1,3-butadiene (500 MHz, $CDCl_3$) 101

Figure 3. 29.^{1}H NMR of (*E*,*E*)-1,4-di-(3,5-ditrifluoromethylphenyl)-1,3-butadiene (500 MHz, $CDCl_3$) 102

Figure 3. 30. ^{1}H NMR of (*E*,*E*)-1,4-(2-naphthyl)-1,3-butadiene (400 MHz, CD_2Cl_2) 102

Figure 3. 31. ^{1}H NMR of 1,2,3,4,5-pentafluoro-6-[(1*E*,3*E*)-4-phenyl-1,3-butadien-1-yl]benzene 103

Figure 3. 32. ^{13}C NMR of 1,2,3,4,5-pentafluoro-6-[(1*E*,3*E*)-4-phenyl-1,3-butadien-1-yl]benzene 103

Figure 3. 33. ^{1}H NMR of 4,6-dimethylindene and 5,7-dimethylindene mixture 104

Figure 3. 34. ^{13}C NMR of 4,6-dimethylindene and 5,7-dimethylindene mixture 104

Figure 3. 35. ^{1}H NMR of 1-ethyl-2,4,6-trimethylbenzene and 4,6-dimethylindane mixture 105

Figure 3. 36. ^{13}C NMR of 1-ethyl-2,4,6-trimethylbenzene and 4,6-dimethylindane mixture 105

Figure 3. 37. ^{1}H NMR of 4,6-dimethylindane 106

Figure 3. 38. ^{13}C NMR of 4,6-dimethylindane 106

Figure 3. 39. ^{1}H NMR of (^{iPr}PCP)Ir(η^2-H_2C=CH-phenyl), 2 107

Figure 3. 40. ^{31}P NMR of (^{iPr}PCP)Ir(η^2-H_2C=CH-phenyl), 2 107

Figure 3. 41. ^{1}H NMR of metalloindene complex 3 108

Figure 3. 42. ^{13}C NMR metalloindene complex 3 108

Figure 3. 43. ^{31}P NMR of metalloindene complex 3 109

Figure 3. 44. ^{1}H NMR of metalloindene complex 4 109

Figure 3. 45. ^{13}C NMR of metalloindene complex 4 110

Figure 3. 46. ^{31}P NMR of metalloindene complex 4 110

Figure 3. 47. ^{1}H NMR of metalloindene complex 5 111

Figure 3. 48. ^{31}P NMR of metalloindene complex 5 111

Figure 3. 49. ^{1}H NMR of metalloindene complex 7 112

Figure 3. 50. ^{13}C NMR of metalloindene complex 7 112

Figure 3. 51. ^{31}P NMR of metalloindene complex 7 113

Figure 3. 52. ^{1}H NMR of metalloindene complex 8 113

Figure 3. 53. ^{13}C NMR of metalloindene complex 8 114

Figure 3. 54. ^{31}P NMR of metalloindene complex 8 114

Figure 3. 55. ^{1}H NMR of metalloindene complex 9 at 25°C 115

Figure 3. 56. ^{13}C NMR of metalloindene complex 9 at 25°C 115

Figure 3. 57. ^{31}P NMR of metalloindene complex 9 at 25°C 116

Figure 3. 58. ^{1}H NMR of metalloindene complex 9 at different Temperature 116

Figure 3. 59. ^{13}C NMR of metalloindene complex 9 at different Temperature 117

Figure 3. 60. ^{1}H NMR of metalloindene complex 9 at 115 °C 117

Figure 3. 61. ^{31}P NMR of metalloindene complex 9 at 115 °C 118

Figure 3. 62. ^{1}H NMR of metalloindene-CO complex 9-CO 118

Figure 3. 63. ^{13}C NMR of metalloindene-CO complex 9-CO 119

Figure 3. 64. ^{31}P NMR of metalloindene-CO complex 9-CO 119

Figure 3. 65. ORTEP diagram of complex 2 122

Figure 3. 66. ORTEP diagram of complex 3 135

Figure 3. 67. ORTEP diagram of complex 4 149

Figure 3. 68. ORTEP diagram of complex 5 166

Figure 3. 69. ORTEP diagram of complex 7 180

Figure 3. 70. ORTEP diagram of complex 8 205

Figure 3. 71. ORTEP diagram of complex 9 219

Figure 3. 72. ORTEP diagram of (*E*, *E*)-1,4-(2-naphthyl)-1,3-butadiene 233

Figure 3. 73. Ir(V) reaction mechanism and free energy values for styrene coupling catalyzed by (^{iPr}PCP)Ir. 243

Figure 3. 74. Vinylidene reaction mechanism and free energy values for styrene coupling catalyzed by (^{iPr}PCP)Ir. 245

Figure 3. 75. Ir-C bond insertion reaction mechanism and free energy values for styrene coupling catalyzed by (^{iPr}PCP)Ir. 247

Figure 3. 76. Ir-H bond insertion reaction mechanism and free energy values for styrene coupling catalyzed by (^{iPr}PCP)Ir. 249

Figure 3. 77. Metalloindene reaction mechanism and free energy values for styrene coupling catalyzed by (^{iPr}PCP)Ir. 251

Figure 3. 78. Metalloindene reaction mechanism and corrected free energy values for 2,4,6-triMe-styrene coupling vs cyclization catalyzed by (^{iPr}PCP)Ir. 253

Figure 4. 1. Proposed mechanism for styrene homo-coupling reaction 264

Figure 4. 2. Different pincer-iridium catalysts used for CDC reaction 266

Figure 4. 3. Cross-coupling vinyl arenes with aromatics 270

Figure 4. 4. Cross-coupling vinyl arenes with heterocyclic compound 272

Figure 4. 5. Cross-coupling vinyl arenes with non-functionalized alkenes 275

Figure 4. 6. ^{1}H NMR of [(1*E*,3*E*)-5,5-Dimethyl-1,3-hexadien-1-yl]benzene (500 MHz, $CDCl_3$) 278

Figure 4. 7. ^{13}C NMR of [(1*E*,3*E*)-5,5-Dimethyl-1,3-hexadien-1-yl]benzene (500 MHz, $CDCl_3$) 278

Figure 5. 1. Chemical structure of indole and indene 284

Figure 5. 2. Mechanism for Intramolecular dehydrogenative coupling of 2,4,6-trimethylstyrene 288

Figure 5. 3. ORTEP diagram of Ir 1 290

Figure 5. 4. ^{1}H NMR of intramolecular dehydrogenative coupling of 2-isopropenylaniline 292

Figure 5. 5. ^{31}P NMR of intramolecular dehydrogenative coupling of 2-isopropenylaniline 293

Figure 5. 6. Substrates for indoles synthesis by intramolecular dehydrogenative coupling 294

Figure 5. 7. Mechanism for intramolecular dehydrogenative coupling of 2-isopropenylaniline 295

Figure 5. 8. Insertion mechanism 295

Figure 5. 9. ^{1}H NMR of 3-methylindole 299

Figure 5. 10. ^{13}C NMR of 3-methylindole 299

Figure 5. 11. ^{1}H NMR of 2-methylindole 300

Figure 5. 12. ^{13}C NMR of 2-methylindole 300

Figure 5. 13. ^{1}H NMR of Ir 1 301

Figure 5. 14. ^{13}C NMR of Ir 1 301

Figure 5. 15. ^{31}P NMR of Ir 1 302

Figure 5. 16. COSY of Ir 1 302

Figure 5. 17. HSQC of Ir 1 303

Figure 5. 18. HMBC of Ir 1 303

Figure 5. 19. NOSEY of Ir 1 304

Figure 5. 20. ^{1}H NMR assignment of Ir 1 304

Figure 5. 21. ^{1}H NMR assignment of Ir 1 305

Figure 6. 1. Proposed new metallocycle 329

Figure 6. 2. Catalyst species in the reaction 331

Figure 6. 3. Diols with 1,3-hydroxyl group went through deoxygenation 334

Figure 6. 4. Diols with 1,3-hydroxygroup did not go through deoxygenation 335

Figure 6. 5. Diols could not undergo deoxygenation 335

Figure 6. 6. Partial deoxygenation of glycerol 336

Figure 6. 7. Different catalysts used for partial deoxygenation of glycerol 340

Figure 6. 8. Partial deoxygenation of glycerol with different catalysts 341

Figure 6. 9. Partial deoxygenation of glycerol under varied CO partial pressure 342

Figure 6. 10. Triols could effect partial deoxygenation 343

Figure 6. 11. Comparing glycerol and 1,3-propanediol as substrate 345

Figure 6. 12. Comparing 2-methyl-1,3-propanediol and 1,3-propanediol as substrate 346

Figure 6. 13. Proposed reaction mechanism for deoxygenation 347

Figure 7. 1. Various pincer-ligated iridium complexes 355

Figure 7. 2. Design of new catalyst with a possible hemi-labile amine arm 356

Figure 7. 3. Synthetic route for ^{iPr}NCOPH ligand 356

Figure 7. 4. ORTEP diagram of (^{iPr}NCOP)Ir(ethylene) 358

Figure 7. 5. ^{31}P NMR of ^{iPr}NCOPH ligand metalation 359

Figure 7. 6. Designed catalytic cycle for methyl acrylate dimerization 361

Figure 7. 7. Reaction involved vinyl acetate and (^{iPr}NCOP)Ir(ethylene) 362

Figure 7. 8. Other substrate and catalyst for C-O bond cleavage 365

Figure 7. 9. Substrates could undergo C-O bond cleavage 365

Figure 7. 10. Proposed mechanism 367

Figure 7. 11. ^{1}H NMR of (^{iPr}NCOP)Ir(HCl) 371

Figure 7. 12. ^{31}P NMR of (^{iPr}NCOP)Ir(HCl) 371

Figure 7. 13. ^{1}H NMR of (^{iPr}NCOP)Ir(ethylene) 372

Figure 7. 14. ^{31}P NMR of (^{iPr}NCOP)Ir(ethylene) 372

Figure 7. 15. ^{1}H NMR of (^{iPr}NCOP)Ir(CO) 373

Figure 7. 16. ^{31}P NMR of (^{iPr}NCOP)Ir(CO) 373

Figure 7. 17. ORTEP diagram of (^{iPr}NCOP)Ir(ethylene) 374

List of Schemes

Scheme 1. 1. Ir(III) Cationic species effected stoichiometric cycloalkane dehydrogenation 2

Scheme 1. 2. Iridium complexes catalyzed thermal and photochemical dehydrogenation of cyclooctane 2

Scheme 1. 3. Pincer-iridium complexes catalyzed transfer dehydrogenation of cyclooctane 4

Scheme 1. 4. Pincer-iridium complexes catalyzed dehydrogenation 5

Scheme 1. 5. Pincer-iridium complexes catalyzed linear alkane to alkylbenzene 6

Scheme 1. 6. Alkane metathesis by tandem alkane-dehydrogenation and olefin-metathesis catalysts 6

Scheme 1. 7. Iridium-catalyzed reduction of alkyl halides by triethylsilane 8

Scheme 1. 8. Iridium-catalyzed olefin hydroaryloxylation and cleavage of simple aryl alkyl ethers 8

Scheme 1. 9. Iridium-catalyzed dehydrogenative coupling of silane 8

Scheme 2. 1. Proposed intermolecular alkane-arene dehydrocoupling by tandem (pincer)Ir-catalyzed dehydrogenation and zeolite-catalyzed alkylation 19

Scheme 2. 2. Intramolecular dehydrocoupling by tandem (pincer)Ir-catalyzed dehydrogenation and zeolite-catalyzed alkylation 20

Scheme 2. 3. Acceptorless dehydrogenation of *n*-pentylbenzene in the absence of zeolite 23

Scheme 2. 4. Zeolite-catalyzed cyclization of 5-phenylpent-1-ene 24

Scheme 3. 1. Reported examples of dehydrogenative coupling of vinyl arenes 45

Scheme 3. 2. Simplified catalytic cycle for dehydrogenative coupling by (^{R}PCP)Ir proceeding via C-H addition to yield an Ir(III) hydrocarbyl hydride followed by a second C-H addition to the Ir(III) species 47

Scheme 3. 3. Reactions of (^{iPr}PCP)Ir with styrenes 53

Scheme 3. 4. Intramolecular C(sp^{3})-C(sp^{2}) dehydrogenative coupling catalyzed by (^{iPr}PCP)Ir 57

Scheme 3. 5. Dehydrogenative styrene coupling via C-H addition and insertion into the resulting Ir-C bond 60

Scheme 3. 6. Dehydrogenative styrene coupling via C-H addition and insertion into Ir-H bond 61

Scheme 4. 1. Different method for C-C bond formation by transitional metal 264

Scheme 4. 2. Proposed CDC reaction route 265

Scheme 4. 3. Proposed CDC reaction equation 265

Scheme 4. 4. Proposed CDC reaction route with excess amount of aromatics and alkene 267

Scheme 4. 5. Tandem dehydrogenation and coupling 274

Scheme 5. 1. Two categories of indoles synthesis methods 285

Scheme 5. 2. Synthesis indoles using dehydrogenative coupling 286

Scheme 5. 3. Intramolecular dehydrogenative coupling route for indenes and indoles synthesis 286

Scheme 5. 4. Intramolecular dehydrogenative coupling of 2,4,6-trimethylstyrene 287

Scheme 5. 5. Coupling reaction of 2,5-dimethyl styrene 289

Scheme 5. 6. N-H activation of 2-isopropenyl aniline by pincer-iridium complex 290

Scheme 5. 7. Intramolecular dehydrogenative coupling of 2-isopropenylaniline 291

Scheme 6. 1. Tandem acid and metal catalyst for partial deoxygenation of glycerol 327

Scheme 6. 2. Dehydration by pincer-iridium complex 328

Scheme 6. 3. Pincer-iridium complex for partial deoxygenation of glycerol 328

Scheme 6. 4. Tandem dehydration and transfer dehydrogenation 329

Scheme 6. 5. Partial deoxygenation of 1,3-propanediol 331

Scheme 6. 6. Decarbonylation route of 1,3-propanediol by pincer-iridium complex 332

Scheme 6. 7. Partial deoxygenation of 1,2-propanediol 334

Scheme 6. 8. Catalytic hydrogenation of ether 343

Scheme 6. 9. Electronic effects of substrates 345

Scheme 7. 1. Metalation of ^{iPr}NCOPH ligand 357

Scheme 7. 2. Homo-coupling of styrene by (^{iPr}NCOP)Ir(ethylene) 359

Scheme 7. 3. Methyl acrylate dimerization 361

Scheme 7. 4. C-O bond cleavage by (^{iPr}NCOP)Ir(ethylene) 363

Scheme 7. 5. C-O bond cleavage by (^{iPr}NCOP)Ir(CO) 363

List of Tables

Table 2. 1. Dehydrocyclization of *n*-pentylbenzene (5.8 M) co-catalyzed by H-SSZ-25 zeolite and various pincer-ligated iridium catalyst precursors 21

Table 2. 2. Reaction of 5-phenylpent-1-ene with zeolites 25

Table 2. 3. Dehydrocyclization of *n*-pentylbenzene co-catalyzed by H-beta zeolite and various pincer-ligated iridium catalyst precursors 26

Table 2. 4. Dehydrocyclization of *n*-pentylbenzene co-catalyzed by H-SSZ-25 zeolite 34

Table 2. 5. Dehydrocyclization of *n*-pentylbenzene co-catalyzed by H-beta zeolite 35

Table 2. 6. Methylnaphthalene isomerization catalyzed by H-SSZ-25 and H-beta zeolite 36

Table 2. 7. Recycle the catalysts 37

Table 3. 1. Catalytic dehydrogenative coupling of vinyl arenes to form diarylbutadienes at 150 °C 48

Table 3. 2. Catalytic dehydrogenative coupling of styrene to form 1,4-diphenylbutadiene in the presence of added hydrogen acceptors at 150 °C 51

Table 3. 3. Crystal data and structure refinement for complex 2 123

Table 3. 4. Atomic coordinates (x 10^4) and equivalent isotropic displacement parameters (Å^{2}x 10^3) for complex 2 124

Table 3. 5. Bond lengths [Å] and angles [°] for complex 2 126

Table 3. 6. Anisotropic displacement parameters (Å^{2}x 10^3) for complex 2 130

Table 3. 7. Hydrogen coordinates (x 10^4) and isotropic displacement parameters (Å^2 x 10^3) for complex 2 132

Table 3. 8. Torsion angles [°] for complex 2 134

Table 3. 9. Crystal data and structure refinement for complex 3 136

Table 3. 10. Atomic coordinates (x 10^4) and equivalent isotropic displacement parameters (Å^{2}x 10^3) 137

Table 3. 11. Bond lengths [Å] and angles [°] for complex 3 139

Table 3. 12. Anisotropic displacement parameters (Å^{2}x 10^3) for complex 3 143

Table 3. 13. Hydrogen coordinates (x 10^4) and isotropic displacement parameters (Å^{2}x 10^3) for complex 3 145

Table 3. 14. Torsion angles [°] for complex 3 147

Table 3. 15. Crystal data and structure refinement for complex 4 150

Table 3. 16. Atomic coordinates (x 10^4) and equivalent isotropic displacement parameters (Å^{2}x 10^3) for complex 4 151

Table 3. 17. Bond lengths [Å] and angles [°] for complex 4 153

Table 3. 18. Anisotropic displacement parameters (Å^{2}x 10^3) for complex 4 159

Table 3. 19. Hydrogen coordinates (x 10^4) and isotropic displacement parameters (Å^{2}x 10^3) for complex 4 161

Table 3. 20. Torsion angles [°] for complex 4 164

Table 3. 21. Crystal data and structure refinement for complex 5 167

Table 3. 22. Atomic coordinates (x 10^4) and equivalent isotropic displacement parameters (Å^{2}x 10^3) for complex 5 168

Table 3. 23. Bond lengths [Å] and angles [°] for complex 5 170

Table 3. 24. Anisotropic displacement parameters (Å^{2}x 10^3) for complex 5 174

Table 3. 25. Hydrogen coordinates (x 10^4) and isotropic displacement parameters (Å^2 x 10^3) for complex 5 176

Table 3. 26. Torsion angles [°] for complex 5 178

Table 3. 27. Crystal data and structure refinement for complex 7 181

Table 3. 28. Atomic coordinates (x 10^4) and equivalent isotropic displacement parameters (Å^{2}x 10^3) for complex 7 182

Table 3. 29. Bond lengths [Å] and angles [°] for complex 7 185

Table 3. 30. Anisotropic displacement parameters (Å^{2}x 10^3) for complex 7 195

Table 3. 31. Hydrogen coordinates (x 10^4) and isotropic displacement parameters (Å^{2}x 10^3) for complex 7 198

Table 3. 32. Torsion angles [°] for complex 7 202

Table 3. 33. Crystal data and structure refinement for complex 8 206

Table 3. 34. Atomic coordinates (x 10^4) and equivalent isotropic displacement parameters (Å^{2}x 10^3) for complex 8 207

Table 3. 35. Bond lengths [Å] and angles [°] for complex 8 209

Table 3. 36. Anisotropic displacement parameters (Å^{2}x 10^3) for complex 8 213

Table 3. 37. Hydrogen coordinates (x 10^4) and isotropic displacement parameters (Å^{2}x 10^3) for complex 8 215

Table 3. 38. Torsion angles [°] for complex 8 217

Table 3. 39. Crystal data and structure refinement for complex 9 220

Table 3. 40. Atomic coordinates (x 10^4) and equivalent isotropic displacement parameters (Å^{2}x 10^3) for complex 9 221

Table 3. 41. Bond lengths [Å] and angles [°] for complex 9 223

Table 3. 42. Anisotropic displacement parameters ($Å^2$x 10^3) for complex 9 227

Table 3. 43. Hydrogen coordinates (x 10^4) and isotropic displacement parameters ($Å^2$x 10^3) for complex 9 229

Table 3. 44. Torsion angles [°] for complex 9 231

Table 3. 45. Crystal data and structure refinement for (*E*, *E*)-1,4-(2-naphthyl)-1,3-butadiene 234

Table 3. 46. Atomic coordinates (x 10^4) and equivalent isotropic displacement parameters ($Å^2$x 10^3) for (*E*, *E*)-1,4-(2-naphthyl)-1,3-butadiene 235

Table 3. 47. Bond lengths [Å] and angles [°] for (*E*, *E*)-1,4-(2-naphthyl)-1,3-butadiene 237

Table 3. 48. Anisotropic displacement parameters ($Å^2$x 10^3) for (*E*, *E*)-1,4-(2-naphthyl)-1,3-butadiene 239

Table 3. 49. Hydrogen coordinates (x 10^4) and isotropic displacement parameters ($Å^2$ x 10^3) for (*E*, *E*)-1,4-(2-naphthyl)-1,3-butadiene 241

Table 3. 50. Torsion angles [°] for (*E*, *E*)-1,4-(2-naphthyl)-1,3-butadiene 242

Table 3. 51. Ir(V) reaction mechanism and free energy values for styrene coupling catalyzed by (^{iPr}PCP)Ir 244

Table 3. 52. Vinylidene reaction mechanism and free energy values for styrene coupling catalyzed by (^{iPr}PCP)Ir 246

Table 3. 53. Ir-C bond insertion reaction mechanism and free energy values for styrene coupling catalyzed by (^{iPr}PCP)Ir 248

Table 3. 54. Ir-H bond insertion reaction mechanism and free energy values for styrene coupling catalyzed by (^{iPr}PCP)Ir 250

Table 3. 55. Metalloindene reaction mechanism and free energy values for styrene coupling catalyzed by (^{iPr}PCP)Ir 252

Table 3. 56. Metalloindene reaction mechanism and free energy values for 2,4,6-triMe-styrene coupling vs cyclization catalyzed by (^{iPr}PCP)Ir 254

Table 3. 57. Energetic effects of solvation on the metalloindene reaction mechanism for styrene coupling by (^{iPr}PCP)Ir 255

Table 4. 1. Evaluation of reaction condition and catalysts 268

Table 4. 2. Evaluation of catalysts for cross-coupling styrene with TBE 273

Table 5. 1. Crystal data and structure refinement for Ir 1 307

Table 5. 2. Atomic coordinates (x 10^4) and equivalent isotropic displacement parameters (Å^{2}x 10^3) for Ir 1 308

Table 5. 3. Bond lengths [Å] and angles [°] for Ir 1 310

Table 5. 4. Anisotropic displacement parameters (Å^{2}x 10^3) for Ir 1 314

Table 5. 5. Hydrogen coordinates (x 10^4) and isotropic displacement parameters (Å^{2}x 10^3) for Ir 1 316

Table 5. 6. Torsion angles [°] for Ir 1 318

Table 5. 7. Hydrogen bonds for Ir 1 [Å and °] 320

Table 6. 1. Partial deoxygenation of 1,3-propanediol with different gases component 333

Table 6. 2. (^{iPr}POCOP)Ir catalyzed partial deoxygenation of glycerol with different hydrogen pressure 338

Table 6. 3. Partial deoxygenation of glycerol in mixed solvents 339

Table 6. 4. Partial deoxygenation of glycerol with different catalysts 340

Table 7. 1. Crystal data and structure refinement for (^{iPr}NCOP)Ir(ethylene) 375

Table 7. 2. Atomic coordinates (x 10^4) and equivalent isotropic displacement parameters (Å^{2}x 10^3) for (^{iPr}NCOP)Ir(ethylene) 376

Table 7. 3. Bond lengths [Å] and angles [°] for (^{iPr}NCOP)Ir(ethylene) 377

Table 7. 4. Anisotropic displacement parameters (Å^{2}x 10^3) for (^{iPr}NCOP)Ir(ethylene) 380

Table 7. 5. Hydrogen coordinates (x 10^4) and isotropic displacement parameters (Å^{2}x 10^3) for (^{iPr}NCOP)Ir(ethylene) 381

Table 7. 6. Torsion angles [°] for (^{iPr}NCOP)Ir(ethylene) 383

Chapter 1. Introduction

1.1. Importance of dehydrogenation

Alkenes are among the most important and widely used organic chemical feedstocks in the chemical industry. They are readily transformed into a wide range of value-added fine chemicals, polymers, commodity chemicals, and fuels. Alkanes are the most abundant organic natural resources in the world, but are generally difficult to react in controlled ways. Producing alkenes through dehydrogenating abundant and inexpensive alkanes is a simple and attractive route. The well-known catalysts for dehydrogenation are major heterogeneous, which required high operation temperature (> 500°C). The low selectivity of these catalyst and coking reaction resulted in the substrate limiting to simple molecules. The development of transition-metal-based catalysts (organometallic complexes) is a new strategy to address this problem by providing desirable terminal selectivity leading to α-olefins and high productivity under mild reaction condition (100-250°C).[1-2]

1.2. History of transition-metal-mediated alkane dehydrogenation

$[IrH_2(acetone)_2(PPh_3)_2][BF_4]$ effected alkane dehydrogenation was discovered by Crabtree in 1979.[3] It was the first example of transition-metal-mediated alkane dehydrogenation. Under refluxing condition with 3,3-dimethyl-1-butene (tert-butylethylene, TBE) as hydrogen acceptor, Ir(III) cationic species transformed to cyclopentadienyl or cyclooctadiene iridium complexes by reacting with cyclopentane or cyclooctane, respectively (scheme 1.1). Felkin group subsequently achieved stoichiometric cycloalkane dehydrogenation reaction by using the compound $(PPh_3)_2ReH_7$.[4-5]

Scheme 1. 1. Ir(III) Cationic species effected stoichiometric cycloalkane dehydrogenation

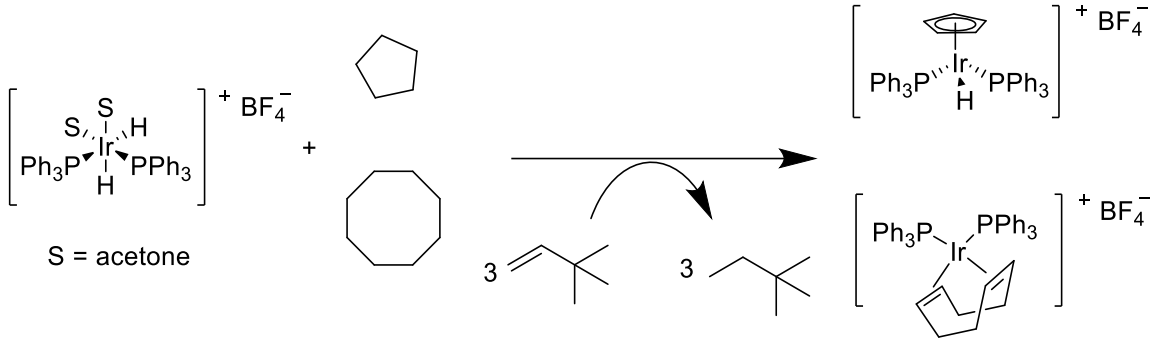

The two pioneering groups in transition-metal-mediated stoichiometric cycloalkane dehydrogenation, Felkin[6-8] and Crabtree groups[9-10], also independently discovered the first homogeneous catalysts for alkane transfer-dehydrogenation. In Crabtree's case, the Ir(III) species, $IrH_2(\eta^2\text{-}O_2CCF_3)(PR_3)_2$ [R = *p*-FC_6H_4 or cyclohexyl (Cy)], in the presence of TBE as hydrogen acceptor, could catalyze the dehydrogenation of cyclooctane under either thermal or photochemical conditions with up to 28 turnovers. Photolysis-driven dehydrogenation of alkanes could even occur without hydrogen acceptor at room temperature. However, the thermal and optical stability of the iridium complex became the major obstacle limiting the turnover number (TON).

Scheme 1. 2. Iridium complexes catalyzed thermal and photochemical dehydrogenation of cyclooctane

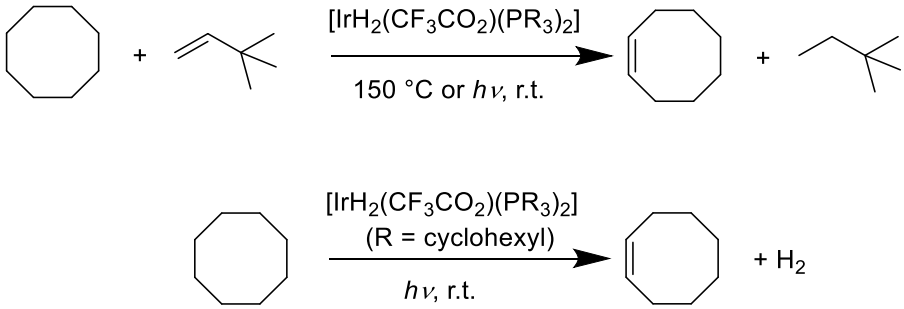

1.3. Dehydrogenation and bond activation using pincer-iridium complexes

The introduction of pincer ligands greatly increased the stability of the iridium catalysts, and subsequently increased their activity in alkane dehydrogenation. 1,3-bis[(di-t-butylphosphino)methyl]benzene (PCPH) was first designed and used as ligand to synthesize different organometallic complexes [(PCP)M] by Moulton and Shaw in 1976,[11] shown in figure 1.1. Meridionally-bound tridentate ligands such as (PCPH) were later referred to as "pincer ligands". However, it was not until the initial report of alkane dehydrogenation by (^{tBu}PCP)Ir (**1**) (^{tBu}PCP = κ^3-2,6-$C_6H_3(CH_2{}^tBu_2)_2$) in 1996 by Jensen and Kaska[12] that people realized pincer-iridium complexes' great potential in catalysis more broadly. In Jensen and Kaska's case, under typical transfer dehydrogenation condition, remarkable turnover frequencies (TOF) 82 turnovers per hour (TO/h) (150°C) and 720 TO/h (200°C) were achieved. To be noticed, no catalyst decomposition was observed over one week under all the study temperatures.

Figure 1. 1. Pincer ligand and pincer-metal complexes

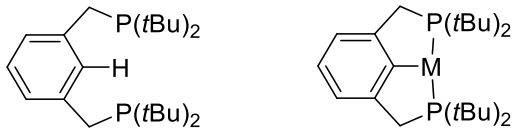

PCPH (PCP)M

Scheme 1. 3. Pincer-iridium complexes catalyzed transfer dehydrogenation of cyclooctane

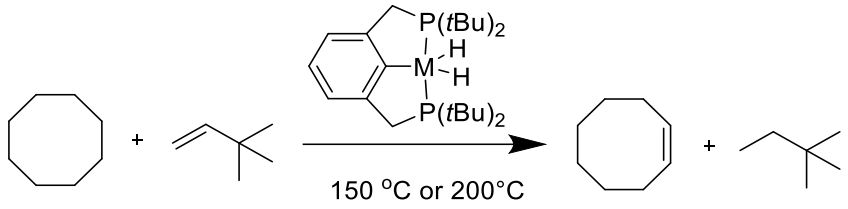

In the absence of hydrogen acceptor, the high endothermicity of alkane dehydrogenation requires high thermal stability of catalysts. Taking advantage of the extraordinary thermal stability of ($^{t\mathrm{Bu}}$PCP)Ir, Kaska, Jensen and Goldman jointly investigated the acceptorless dehydrogenation of alkanes. Using cyclodecane as substrate, together with catalyst **1**, 360 TONs were obtained after heating at 200 °C for 24h.[13] The sterically less-crowded analog of **1**, ($^{i\mathrm{Pr}}$PCP)IrH_2, **2**, can be even more effective compared to **1**, which gave up to 1000 TONs for acceptorless dehydrogenation of cyclodecane.[14]

Since these initial reports of alkane dehydrogenation by ($^{t\mathrm{Bu}}$PCP)Ir, pincer-ligated iridium complexes have grown rapidly to include a family of derivatives, as shown in Figure 1.2.[1-2] By introducing different substituents on the pincer ligand, the steric and electronic property of the iridium can be tuned to maximize their reactivity and selectivity towards different reactions. Pincer-iridium catalyzed dehydrogenation reaction now includes both transfer and acceptorless dehydrogenation of cycloalkanes and linear alkanes, as showed in scheme 1.4.

Figure 1. 2. Various pincer-ligated iridium complexes

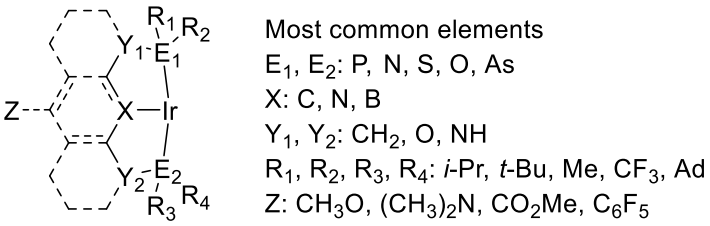

Scheme 1. 4. Pincer-iridium complexes catalyzed dehydrogenation

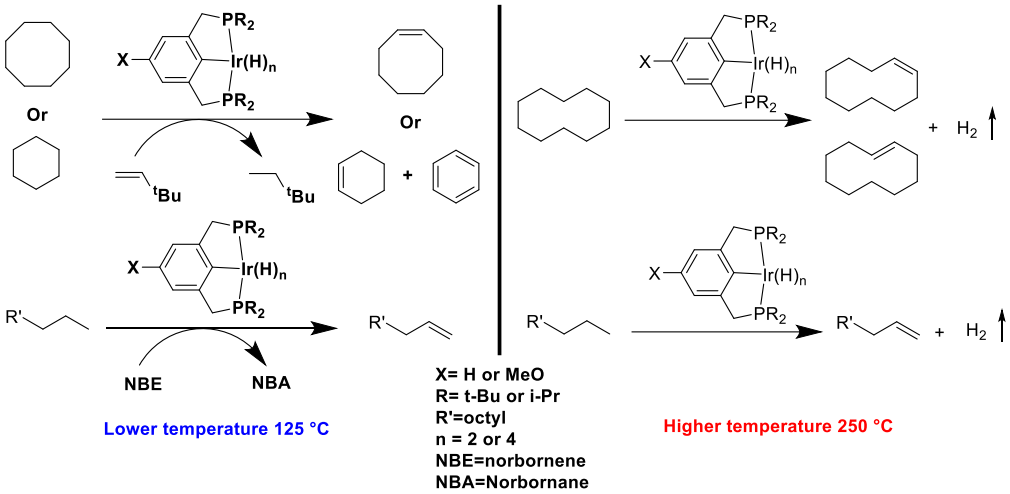

Reactions based on pincer-iridium catalyzed dehydrogenation has been studied extensively as a result of its great potential in the petroleum industry. Pincer-iridium complexes catalyzed selective conversion of linear alkanes to alkylbenzenes (dehydroaromatization) was first reported by Goldman's group in 2011,[15] shown in scheme 1.5. Starting with n-dodecane, they can make over 35% C12 aromatics and 17% benzene. In 2006, Goldman and Brookhart reported that dehydrogenation catalysts in tandem with olefin metathesis catalyst disproportionated alkane chains.[16] Different dehydrogenation catalysts in tandem with olefin metathesis catalysts were later reported to afford catalytic systems for the metathesis of alkanes or alkyl-groups, shown in scheme 1.6.[17]

Scheme 1. 5. Pincer-iridium complexes catalyzed linear alkane to alkylbenzene

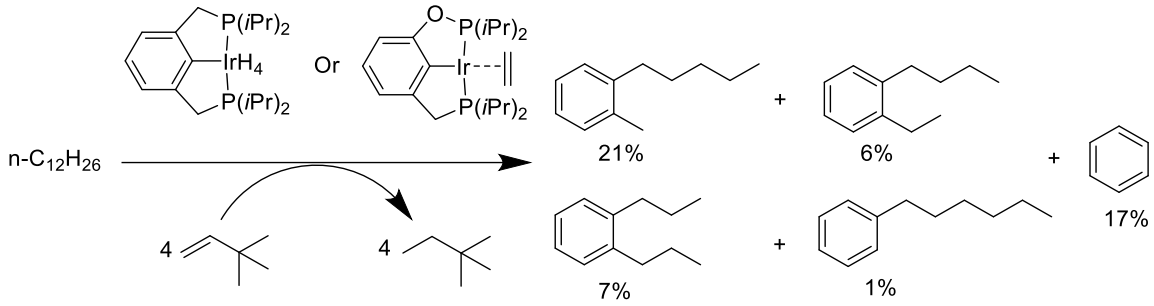

Scheme 1. 6. Alkane metathesis by tandem alkane-dehydrogenation and olefin-metathesis catalysts

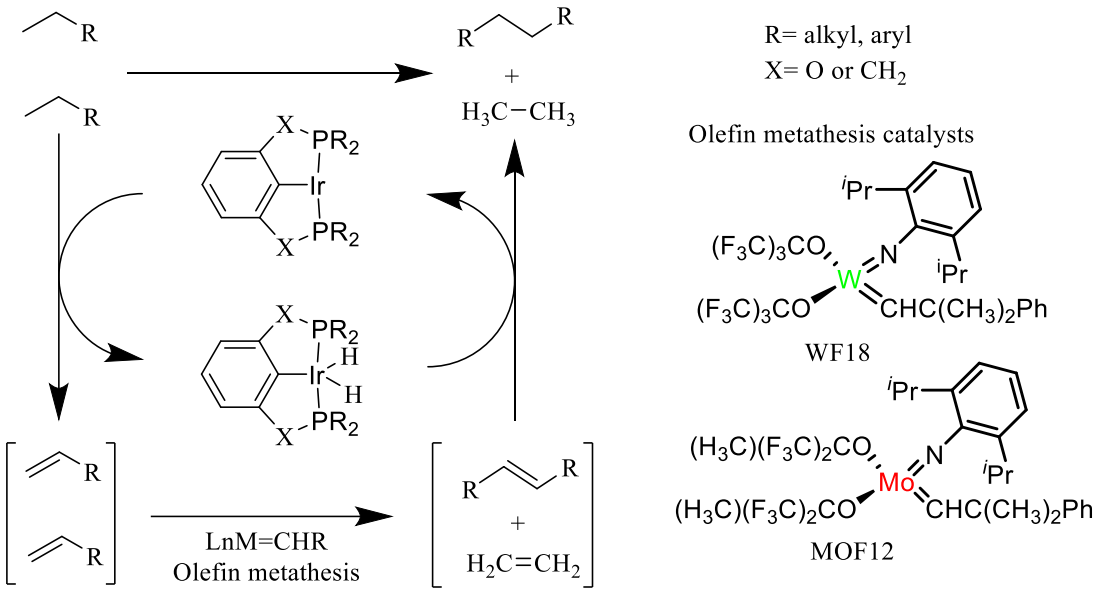

Beyond the original application of dehydrogenation, pincer iridium complexes could be used to activate different types of bonds, such as X-H (X = C, N, O) bonds[18-20] and C-Y (Y = C, N, O, F)[21-25], as showed in figure 1.3. Although these bond activation reactions are stoichiometric, the potential of using pincer-iridium into catalytic bond formation and cleavage reaction were significant and fulfilled by later work.

Figure 1. 3. Bond activations by pincer-iridium complexes

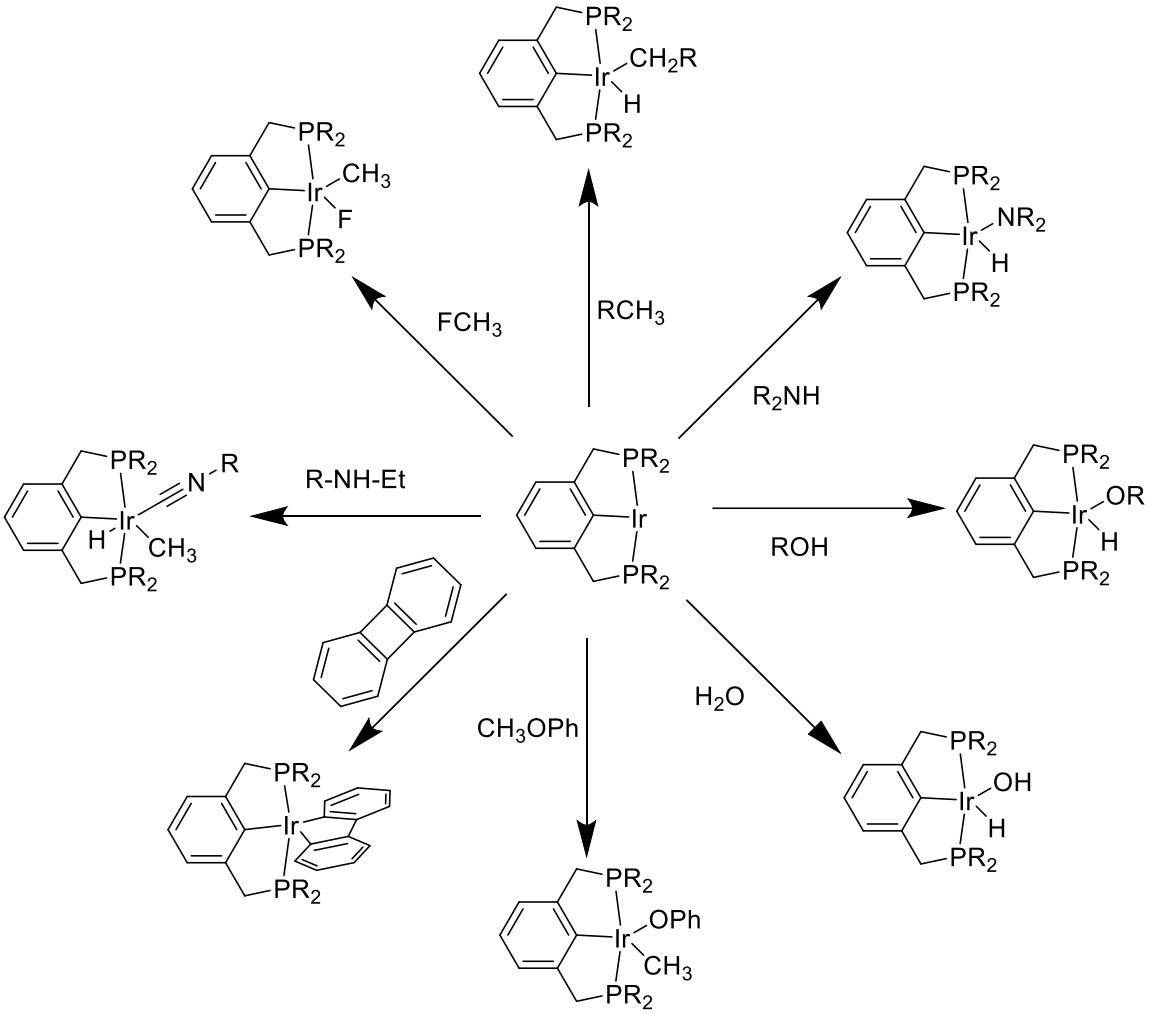

Iridium-catalyzed reduction of alkyl halides by triethylsilane (scheme 1.7), as reported by the Brookhart group in 2007, is one such example based on bond activation of pincer-iridium complexes.[26] Iridium-catalyzed olefin hydroaryloxylation[27] and cleavage of simple aryl alkyl ethers[28] (scheme 1.8) reported by Goldman illustrated the potential pincer-iridium as catalysts in bond formation and cleavage. In 2015, the Waterman group demonstrated the utility of pincer-iridium complexes in the dehydrogenative coupling of silanes (scheme 1.9).[29]

Scheme 1. 7. Iridium-catalyzed reduction of alkyl halides by triethylsilane

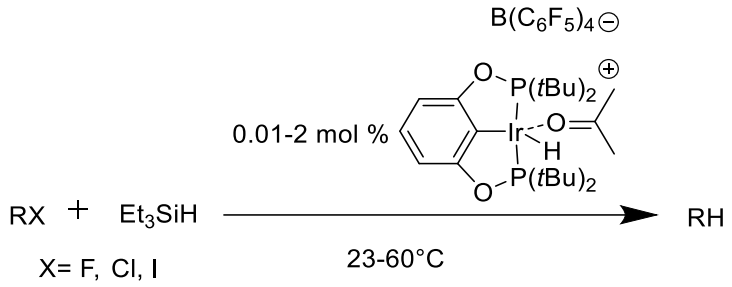

Scheme 1. 8. Iridium-catalyzed olefin hydroaryloxylation and cleavage of simple aryl alkyl ethers

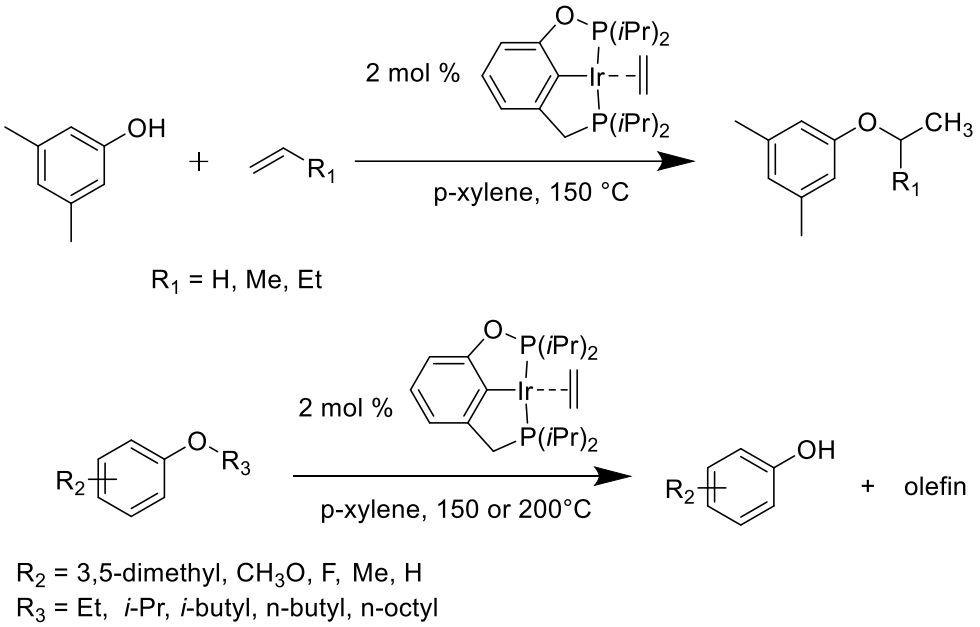

Scheme 1. 9. Iridium-catalyzed dehydrogenative coupling of silane

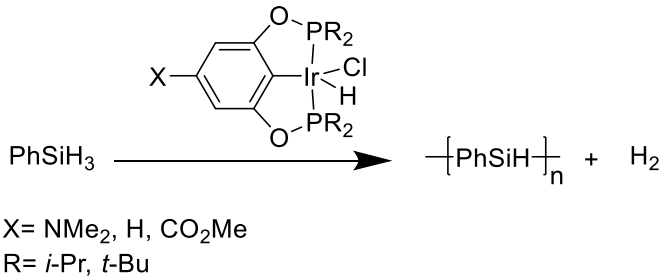

1.4. Research goals of this thesis

Although pincer-iridium complex family shows versatile applications including dehydrogenation, tandem dehydrogenation/olefin-metathesis, activation of bonds, catalytic reduction of alkyl halides, catalytic phenol-type C-O bond formation and cleavage, and dehydrogenative coupling of silane, in many cases catalyst productivity, substrate scope and reaction generality remains limited. My PhD thesis research aimed to investigate and discover a wider range of C-C and C-X (X = N, O) bond formation and cleavage reactions catalyzed by pincer-ligated iridium complexes, shown in figure 1.4.

Figure 1. 4. Ph.D. research summary

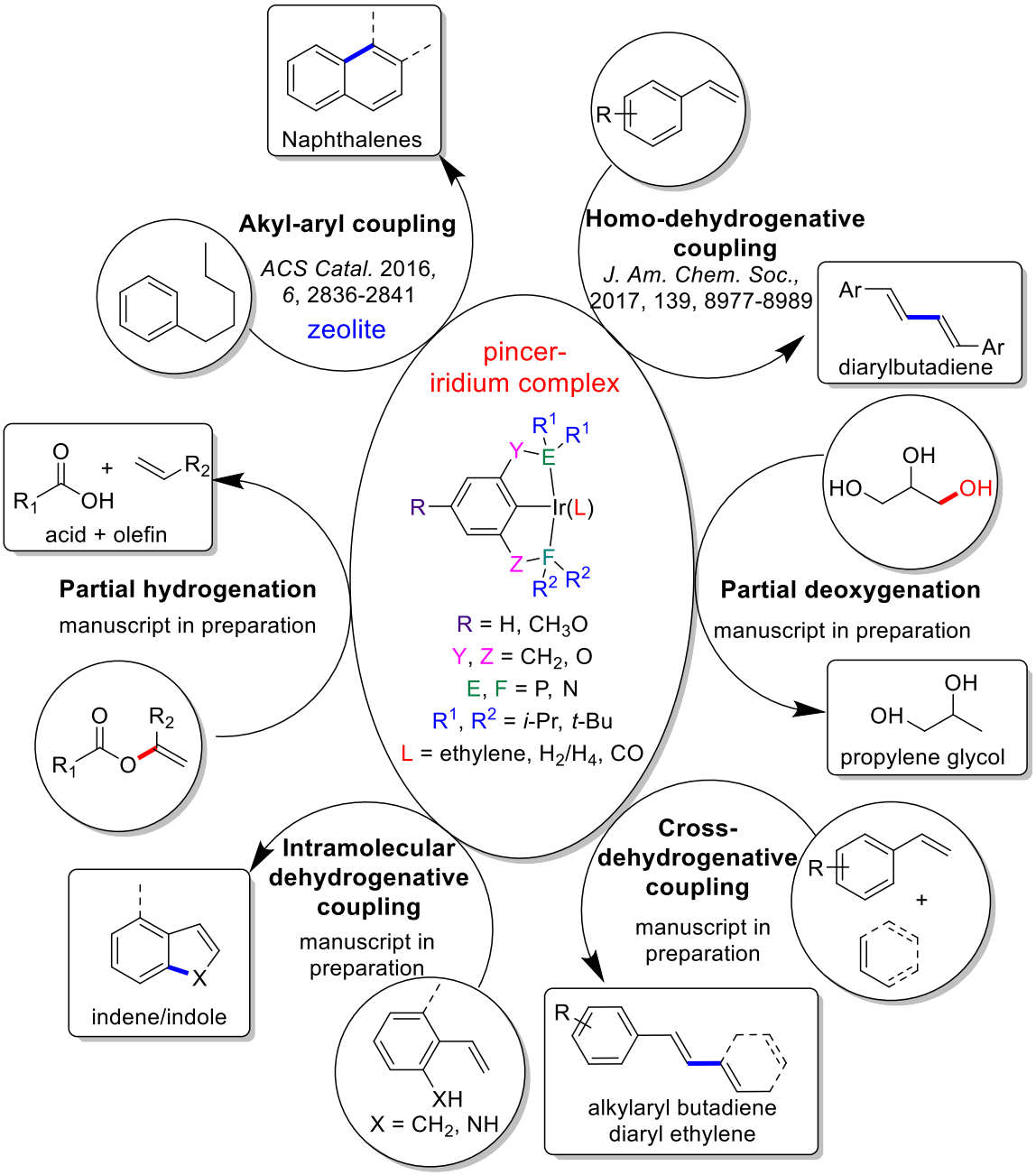

The concept of tandem reactions based on pincer-iridium catalyzed dehydrogenation allowed the development of a formal alkane metathesis system using pincer-iridium complex in combination with Schrock's olefin metathesis catalyst. To extend this general concept, we attempted to couple alkanes with arenes via

dehydrogenation in tandem with arene alkylation through the use of zeolites as alkylation catalysts. In chapter 2, an intramolecular alkyl-aryl dehydrogenative coupling employing zeolites as the co-catalyst of pincer-iridium complex will be discussed. It should be noted that this reaction could perform up to 6860 turnovers (in terms of mole of H_2 to per mole iridium catalyst) without the use of a sacrificial hydrogen acceptor. And this successful example can be applied to pentyltoluene, which could give dimethylnaphthalene as product. One of the major products, 2,6-dimethylnaphthalene is industrial precursor of polyethylene naphthalate (PEN).

There are surprisingly few examples of iridium-catalyzed dehydrogenative couplings of C−H bonds. It has been reported that pincer-ligated iridium complexes (^{tBu}PCP)Ir and (^{iPr}PCP)Ir can form metallocycles through double C-H activation or C-C cleavage[22, 30-31]. However, these studies never led to catalytic C-C bond formation. In chapter 3-5, dehydrogenative coupling reactions catalyzed by pincer- iridium complexes, which effected homo-dehydrogenative coupling to covert vinyl arenes to diaryl butadiene, cross-dehydrogenative coupling (CDC) to react vinyl arenes with furan, thiophene, aromatics and olefins, and intramolecular dehydrogenative coupling to directly synthesize indene and indole from vinyl arene and vinyl aniline. A metalloindene mechanism of these dehydrogenative coupling reactions was proposed based on both experimental and computational results.

Pincer-ligated iridium complexes are not typically studied for dehydration reactions, as they are thought to be moisture sensitive. However, we discovered that (^{iPr}POCOP)Ir could dehydrate tert-butanol to give isobutene. Moreover, tandem dehydration and transfer dehydrogenation can yield a secondary olefin. In the chapter 6, we will discuss diols and

triols partial deoxygenation by pincer-iridium complexes. One important substrate for this type reaction is glycerol, a biodiesel by-product, could be converted to 1,2-propanediol, an important polymer precursor (2.12 million tons consumed in 2013).

To obtain better reactivity toward C-C bond formation and C-O cleavage catalysis, we designed a more sterically open catalyst with a possibly hemi-labile amine arm, (^{iPr}NCOP)Ir, which will be presented in chapter 7. This complex catalyzed styrene homo-coupling at lower temperatures; however, the catalyst decomposed and thus could not give many turnovers. An non-dehydrogenative coupling of methyl acrylate to form dimethyl (E)-hex-2-enedioate was observed with this catalyst. Interestingly, (^{iPr}NCOP)Ir could catalyze hydrogenation of unsaturated ester, which selectively break the C-O bond of vinylic ester to give acid and olefin.

1.4. Reference

1. Choi, J.; MacArthur, A. H.; Brookhart, M.; Goldman, A. S., Dehydrogenation and related reactions catalyzed by iridium pincer complexes. *Chemical reviews* **2011,** *111* (3), 1761-79.
2. Kumar, A.; Bhatti, T. M.; Goldman, A. S., Dehydrogenation of Alkanes and Aliphatic Groups by Pincer-Ligated Metal Complexes. *Chemical reviews* **2017,** *117* (19), 12357-12384.
3. Crabtree, R. H.; Mihelcic, J. M.; Quirk, J. M., Iridium complexes in alkane dehydrogenation. *Journal of the American Chemical Society* **1979,** *101* (26), 7738-7740.
4. Baudry, D.; Ephritikhine, M.; Felkin, H., The activation of C–H bonds in cycloalkanes by rhenium complexes. *Journal of the Chemical Society, Chemical Communications* **1982,** (11), 606-607.
5. Baudry, D.; Ephritikhine, M.; Felkin, H., The activation of C–H bonds in cyclopentane by bis(phosphine)rhenium heptahydrides. *Journal of the Chemical Society, Chemical Communications* **1980,** (24), 1243-1244.
6. Baudry, D.; Ephritikhine, M.; Felkin, H.; Holmes-Smith, R., The selective catalytic conversion of cycloalkanes into cycloalkenes using a soluble rhenium polyhydride system. *Journal of the Chemical Society, Chemical Communications* **1983,** (14), 788-789.
7. Felkin, H.; Fillebeen-Khan, T.; Gault, Y.; Holmes-Smith, R.; Zakrzewski, J., Activation of Carbon-Hydrogen Bonds in Saturated Hydrocarbons. The Catalytic Functionalization of Cyclooctane by means of some Soluble Iridium and Ruthenium Polyhydride Systems. *Tetrahedron Lett.* **1984,** *25* (12), 1279-1282.
8. Felkin, H.; Fillebeen-Khan, T.; Holmes-Smith, R.; Lin, Y., Activation of Carbon-Hydrogen Bonds in Saturated Hydrocarbons. The Selective, Catalytic Functionalization of Methyl Groups by Means of a Soluble Iridium Polyhydride System. *Tetrahedron Lett.* **1985,** *26* (16), 1999-2000.
9. Burk, M. J.; Crabtree, R. H.; Parnell, C. P.; Uriarte, R. J., Selective Stoichiometric and Catalytic C-H Bond Cleavage Reactions in Hydrocarbons. *Organometallics* **1984,** *3*, 816-817.
10. Burk, M. J.; Crabtree, R. H.; McGrath, D. V., Thermal and Photochemical Catalytic Dehydrogenation of Alkanes with $[IrH_2(CF_3CO_2)(PR_3)_2]$ (R = C_6H_4F-p and cyclohexyl). *J. Chem. Soc., Chem. Commun.* **1985,** (24), 1829-1830.
11. Moulton, C. J.; Shaw, B. L., Transition metal–carbon bonds. Part XLII. Complexes of nickel, palladium, platinum, rhodium and iridium with the tridentate ligand 2,6-bis[(di-t-butylphosphino)methyl]phenyl. *Journal of the Chemical Society, Dalton Transactions* **1976,** (11), 1020-1024.
12. Gupta, M.; Hagen, C.; Flesher, R. J.; Kaska, W. C.; Jensen, C. M., A highly active alkane dehydrogenation catalyst: stabilization of dihydrido rhodium and iridium complexes by a P-C-P pincer ligand. *Chemical Communications* **1996,** (17), 2083-2084.
13. Xu, W. W.; Rosini, G. P.; Gupta, M.; Jensen, C. M.; Kaska, W. C.; KroghJespersen, K.; Goldman, A. S., Thermochemical alkane dehydrogenation catalyzed in solution without the use of a hydrogen acceptor. *Chemical Communications* **1997,** (23), 2273-2274.
14. Liu, F.; S. Goldman, A., Efficient thermochemical alkane dehydrogenation and isomerization catalyzed by an iridium pincer complex. *Chemical Communications* **1999,** (7), 655-656.

15. Ahuja, R.; Punji, B.; Findlater, M.; Supplee, C.; Schinski, W.; Brookhart, M.; Goldman, A. S., Catalytic dehydroaromatization of n-alkanes by pincer-ligated iridium complexes. *Nat Chem* **2011,** *3* (2), 167-171.
16. Goldman, A. S.; Roy, A. H.; Huang, Z.; Ahuja, R.; Schinski, W.; Brookhart, M., Catalytic alkane metathesis by tandem alkane dehydrogenation olefin metathesis. *Science* **2006,** *312* (5771), 257-261.
17. Haibach, M. C.; Kundu, S.; Brookhart, M.; Goldman, A. S., Alkane Metathesis by Tandem Alkane-Dehydrogenation-Olefin-Metathesis Catalysis and Related Chemistry. *Accounts of Chemical Research* **2012,** *45* (6), 947-958.
18. Kanzelberger, M.; Zhang, X. W.; Emge, T. J.; Goldman, A. S.; Zhao, J.; Incarvito, C.; Hartwig, J. F., Distinct thermodynamics for the formation and cleavage of N-H bonds in aniline and ammonia. Directly-observed reductive elimination of ammonia from an isolated amido hydride complex. *Journal of the American Chemical Society* **2003,** *125* (45), 13644-13645.
19. Lee, D. W.; Jensen, C. M.; Morales-Morales, D., Reactivity of Iridium PCP Pincer Complexes toward CO and CO2. Crystal Structures of IrH(κ2-O2COH){C6H3-2,6-(CH2PBut2)2} and IrH(C(O)OH){C6H3-2,6-(CH2PBut2)2}·H2O. *Organometallics* **2003,** *22* (23), 4744-4749.
20. Zhao, J.; Goldman, A. S.; Hartwig, J. F., Oxidative addition of ammonia to form a stable monomeric amido hydride complex. *Science* **2005,** *307* (5712), 1080-2.
21. Zhang, X.; Emge, T. J.; Ghosh, R.; Goldman, A. S., Selective Cleavage of the C−C Bonds of Aminoethyl Groups, via a Multistep Pathway, by a Pincer Iridium Complex. *Journal of the American Chemical Society* **2005,** *127* (23), 8250-8251.
22. Laviska, D. A.; Guan, C.; Emge, T. J.; Wilklow-Marnell, M.; Brennessel, W. W.; Jones, W. D.; Krogh-Jespersen, K.; Goldman, A. S., Addition of C–C and C–H bonds by pincer-iridium complexes: a combined experimental and computational study. *Dalton T* **2014,** *43* (43), 16354-16365.
23. Choi, J.; Choliy, Y.; Zhang, X.; Emge, T. J.; Krogh-Jespersen, K.; Goldman, A. S., Cleavage of sp3 C−O Bonds via Oxidative Addition of C−H Bonds. *Journal of the American Chemical Society* **2009,** *131* (43), 15627-15629.
24. Kundu, S.; Choi, J.; Wang, D. Y.; Choliy, Y.; Emge, T. J.; Krogh-Jespersen, K.; Goldman, A. S., Cleavage of Ether, Ester, and Tosylate C(sp3)–O Bonds by an Iridium Complex, Initiated by Oxidative Addition of C–H Bonds. Experimental and Computational Studies. *Journal of the American Chemical Society* **2013,** *135* (13), 5127-5143.
25. Choi, J.; Wang, D. Y.; Kundu, S.; Choliy, Y.; Emge, T. J.; Krogh-Jespersen, K.; Goldman, A. S., Net Oxidative Addition of C(sp³)-F Bonds to Iridium via Initial C-H Bond Activation. *Science* **2011,** *332* (6037), 1545-1548.
26. Yang, J.; Brookhart, M., Iridium-Catalyzed Reduction of Alkyl Halides by Triethylsilane. *Journal of the American Chemical Society* **2007,** *129* (42), 12656-12657.
27. Haibach, M. C.; Guan, C. J.; Wang, D. Y.; Li, B.; Lease, N.; Steffens, A. M.; Krogh-Jespersen, K.; Goldman, A. S., Olefin Hydroaryloxylation Catalyzed by Pincer-Iridium Complexes. *Journal of the American Chemical Society* **2013,** *135* (40), 15062-15070.
28. Haibach, M. C.; Lease, N.; Goldman, A. S., Catalytic Cleavage of Ether C□O Bonds by Pincer Iridium Complexes. *Angewandte Chemie International Edition* **2014,** *53* (38), 10160-10163.

29. Mucha, N. T.; Waterman, R., Iridium Pincer Catalysts for Silane Dehydrocoupling: Ligand Effects on Selectivity and Activity. *Organometallics* **2015,** *34* (15), 3865-3872.
30. Laviska, D. A.; Zhou, T.; Kumar, A.; Emge, T. J.; Krogh-Jespersen, K.; Goldman, A. S., Single and Double C–H Activation of Biphenyl or Phenanthrene. An Example of C–H Addition to Ir(III) More Facile than Addition to Ir(I). *Organometallics* **2016**.
31. Wilklow-Marnell, M.; Brennessel, W. W.; Jones, W. D., Formation of 5-membered metallacycles at iPrPCPIr by C–H, O–H, and C–CO bond cleavage. *Polyhedron* **2016,** *116*, 38-46.

Chapter 2. Alkyl-aryl coupling catalyzed by tandem systems of pincer-ligated iridium complexes and zeolites

This chapter is reproduced with permission from

Alkyl-Aryl Coupling Catalyzed by Tandem Systems of Pincer-Ligated Iridium Complexes and Zeolites

Long V. Dinh, Bo Li, Akshai Kumar, William Schinski, Kathleen D. Field, Alexander Kuperman, Fuat E. Celik, and Alan S. Goldman

ACS Catal. **2016**, *6*, 2836−2841

Copyright © 2016 American Chemical Society

Abstract: We report that pincer-ligated-iridium catalysts for alkane dehydrogenation can operate in tandem with zeolite catalysts for arene-alkene coupling, to effect the overall intramolecular dehydrocoupling of alkyl-H and aryl-H bonds, i.e. the dehydrocyclization of alkyl benzene. Thus zeolite and soluble iridium co-catalysts in refluxing pentylbenzene (205 °C) gave high yields of 1-methyl-1,2,3,4-tetrahydronaphthalene. Subsequent dehydrogenation and isomerization affords 1- and 2-methylnaphthalene and 2-methyl-1,2,3,4-tetrahydronaphthalene. Total yields of cyclized product as high as 5.4 M (94%) have been obtained, corresponding to 6800 turnovers per mol Ir. Turnover numbers for the tandem-catalyzed dehydrocyclization are much greater than those obtained for simple dehydrogenation by Ir catalysts (to give olefins) in the absence of zeolite.

2.1. Introduction

The selective functionalization of C-H bonds of alkanes or alkyl groups is a major goal of modern catalysis. Organometallic complexes have shown great promise with respect to alkyl C-H bond activation.[1] Perhaps the most well developed organometallic-catalyzed alkane conversion is dehydrogenation to give olefins, first reported as early as 1979,[2] and developed extensively over the years since then.[3] But while such dehydrogenation systems show great potential for the production of olefins, their utility is limited by several factors. Typically, an olefinic acceptor is sacrificed since dehydrogenation is highly endothermic; acceptorless dehydrogenation has been reported but yields and rates tend to be much lower, particularly with acyclic alkanes.[3] High regioselectivity for dehydrogenation at the terminal position of *n*-alkanes has been reported, but subsequent isomerization results in loss of the valuable α-olefins.[4-5] The build-up of olefin can result in catalyst inhibition.[6] Secondary reactions limit yields of mono-olefins (although the secondary products may themselves be of value[7]).

We have found that employing dehydrogenation catalysts in tandem[8-9] with catalysts for olefin metathesis affords catalytic systems for the metathesis of alkanes or alkyl groups.[10-11] In this article we report a new tandem dehydrogenation-based system, in which the net reaction is the formation of an alkyl-aryl bond from the coupling of alkyl-H and aryl-H units (eq 1) with liberation of H_2.[12] In view of the importance of alkyl-aryl bonds in organic chemistry, coupling reactions of this type have great potential applicability. No hydrogen acceptor is required so the system is highly atom-economical. Although we herein report only intramolecular couplings, in principle it should be possible to extend this to intermolecular couplings.

$$\text{alkyl-H} + \text{aryl-H} \longrightarrow \text{alkyl-aryl} + H_2 \qquad (1)$$

2.2. Results and discussion

Our approach to the development of a system for the catalysis of eq 1 was based on pincer-iridium-catalyzed acceptorless dehydrogenation[13-14] of an alkyl group, followed by arene alkylation with the resulting olefin.[15] While classical alkylation catalysts such as HF[16] would presumably react with and deactivate the iridium catalysts, we hoped that solid-phase alkylation catalysts, in particular zeolites, would be compatible with the iridium catalysts.[17] We set out to effect the reaction without any hydrogen acceptor, in part because that is obviously a more atom-economical approach, but also to avoid the problem of alkylation or other zeolite-catalyzed reactions (e.g. oligomerization) of any sacrificial acceptor.

Scheme 2. 1. Proposed intermolecular alkane-arene dehydrocoupling by tandem (pincer)Ir-catalyzed dehydrogenation and zeolite-catalyzed alkylation

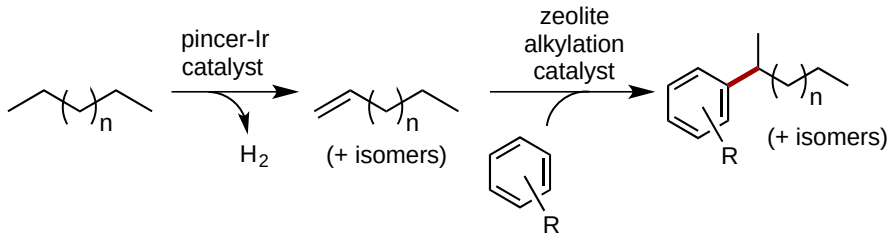

Initial attempts to effect the reaction of Scheme 2.1 with *n*-alkanes and arenes, for example, refluxing a solution of pincer-iridium catalyst, *n*-dodecane, and biphenyl, in the presence of zeolites under conditions previously reported for acceptorless alkane dehydrogenation, did not give appreciable yields of the desired coupling product. In contrast, remarkably high turnover numbers were obtained when we attempted the *intramolecular* version of this reaction, a dehydrocyclization, as shown in Scheme 2.2.

Scheme 2. 2. Intramolecular dehydrocoupling by tandem (pincer)Ir-catalyzed dehydrogenation and zeolite-catalyzed alkylation

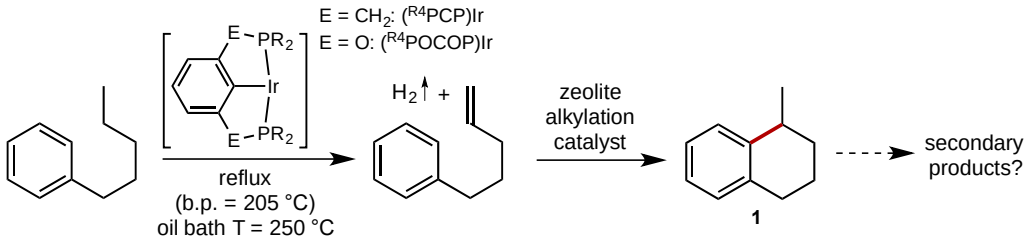

For example, an *n*-pentylbenzene (b.p. = 205 °C) solution of (^{tBu4}PCP)IrH_n (n = 2 or 4; 2.0 mM) with H-SSZ-25 zeolite[18] (0.30 g / 2.7 mL) was immersed in an oil bath held at 250 °C and allowed to reflux. As previously described for acceptorless dehydrogenation, an argon flow above the top of the condenser allowed the escape of H_2.[19-22] After 8 h the reaction gave 790 mM 1-methyl-1,2,3,4-tetrahydronaphthalene (**1**) as the major product (Scheme 2.2; Table 2.1, entry 1) as determined by gas chromatographic analysis. In addition, 53 mM 1-methyl-naphthalene, **3**, was observed; this is presumably attributable to the secondary dehydrogenation of **1**. Somewhat more surprisingly, the formation of 2-methyl-1,2,3,4-tetrahydronaphthalene (**2**), 2-methyl-naphthalene (**4**), 2-ethyl indane (**5**), and 5-methyl-1,2,3,4-tetrahydronaphthalene (**6**) were also observed, giving a total of 890 mM cyclized product. (See section 2.4 for full characterization of products.)

Table 2. 1. Dehydrocyclization of *n*-pentylbenzene (5.8 M) co-catalyzed by H-SSZ-25 zeolite and various pincer-ligated iridium catalyst precursors

entry	Ir catalyst (2.0 mM)	zeolite	time (h)	**1**	**2**	**3**	**4**	**5**	**6**	Total Cyclized Product	TON (H_2/Ir)	Yield Cyclized Product
1	(^{tBu4}PCP)Ir	H-SSZ-25	8	790 (13.6)	11 (0.2)	53 (0.9)	22 (0.4)	11 (0.2)	4 (0.1)	890	520	15%
			24	1510 (26.0)	94 (1.6)	340 (5.9)	260 (4.5)	44 (0.8)	8 (0.1)	2260	1730	39%
			72	340 (5.9)	360 (6.2)	1060 (18.3)	2410 (41.6)	150 (2.6)	200 (3.4)	4520	5730	78%
2	none	H-SSZ-25	8	27 (0.5)	7 (0.1)	0	0	4 (0.1)	0	38		1%
			24	97 (1.7)	12 (0.2)	0	0	7 (0.1)	2 (0.0)	120		2%
			72	250 (4.3)	76 (1.3)	7 (0.1)	17 (0.3)	0	5 (0.1)	360		6%
3	(^{iPr4}PCP)Ir	H-SSZ-25	8	380 (6.6)	13 (0.2)	8 (0.1)	10 (0.2)	14 (0.2)	2 (0.0)	430	230	7%
			24	690 (11.9)	73 (1.3)	36 (0.6)	53 (0.9)	33 (0.6)	5 (0.1)	890	530	15%
			72	1030 (17.8)	300 (5.2)	160 (2.8)	220 (3.8)	94 (1.6)	13 (0.2)	1820	1290	31%
4	(MeO-^{tBu4}PCP)Ir	H-SSZ-25	8	330 (5.7)	35 (0.6)	6 (0.1)	0	18 (0.3)	3 (0.1)	390	200	7%
			24	1110 (19.1)	52 (0.9)	280 (4.8)	170 (2.9)	32 (0.6)	8 (0.1)	1650	1280	28%
			72	240 (4.1)	160 (2.8)	1180 (20.3)	2550 (44.0)	100 (1.7)	140 (2.4)	4370	5920	75%
5	(MeO-^{iPr4}PCP)Ir	H-SSZ-25	8	860 (14.8)	23 (0.4)	32 (0.6)	20 (0.3)	14 (0.2)	4 (0.1)	950	530	16%
			24	1860 (32.1)	150 (2.6)	380 (6.6)	320 (5.5)	76 (1.3)	15 (0.3)	2800	2100	48%
6	(^{tBu4}POCOP)Ir	H-SSZ-25	8h	1210 (20.9)	25 (0.4)	180 (3.1)	110 (1.9)	19 (0.3)	29 (0.5)	1570	1080	27%
			24	720 (12.4)	290 (5.0)	1560 (26.9)	2580 (44.5)	130 (2.2)	150 (2.6)	5430	6860	94%
7	(Me_2N-^{tBu4}PCP)Ir	H-SSZ-25	8	180 (3.1)	25 (0.4)	5 (0.1)	2 (0.0)	10 (0.2)	4 (0.1)	230	120	4%
			24	810 (14.0)	54 (0.9)	72 (1.2)	84 (1.4)	36 (0.6)	6 (0.1)	1060	690	18%
			72	670 (11.6)	340 (5.9)	870 (15.0)	1530 (26.4)	150 (2.6)	130 (2.2)	3690	4250	64%

Dehydrocyclization of refluxing (205 °C) *n*-pentylbenzene (5.8 M) co-catalyzed by H-SSZ-25 zeolite (0.30 g/2.7 mL) and various pincer-ligated iridium catalyst (2.0 mM) precursors.[a] a) Product concentrations in mM; percent yields in parentheses. For catalysts (tBu4PCP)Ir, (p-OMe-tBu4PCP)Ir, (Me2N-tBu4PCP)Ir, the catalyst precursors were the corresponding hydrides (typically a mixture of dihydride and tetrahydride), while for (tBu4POCOP)Ir, (iPr4PCP)Ir and (p-OMe-iPr4PCP)Ir the precursors were the corresponding ethylene adducts. (See section 2.4 for full experimental details).

After 24 h under the same conditions, 1.51 M **1** and a total of 2.3 M cyclized product was observed (Table 2.1, entry 1). While this represents a substantial increase in the concentration of **1** compared with that after 8 h (ca. 2-fold), in relative terms the increase in concentrations of products **2-5** was much greater (ca. 4-12 fold), consistent with these species being secondary products. After 72 h, the concentration of **1** had *decreased* to 340 mM but the total concentration of cyclized products had increased to 4.52 M, for an overall yield of 78%. The total number of turnovers, calculated based on the inferred number of moles H_2 lost from the product mixture per mol Ir catalyst, was ca. 5700.

Control experiments performed under the same conditions revealed that the zeolite in the absence of pincer-Ir catalyst catalyzed the formation of cyclic product at rates only ca. 5% of those obtained in the tandem systems (Table 2.1, entry 2). Conversely, pincer-Ir complexes in the absence of zeolite gave no cyclized product. Furthermore, total turnover numbers of dehydrogenated products (alkenyl benzenes) were much lower in the absence of zeolite (Scheme 2.3). Thus the results obtained with the combination of zeolite and pincer-ligated iridium indicate not only that the catalysts are highly compatible and able to operate in tandem,[8] but that the combination moreover affords a strong synergistic effect. This synergistic effect may be attributable to one or more independent factors including the following: (1) The *n*-alkenyl arenes which build up in the absence of zeolite presumably can bind to the iridium center, inhibiting catalysis. Linear olefins bind much more strongly than arenes,[23] and, moreover, alkenyl arenes may bind in a bidentate fashion through both aryl C-H activation and either π-coordination or C-H activation of the vinyl unit. (2) As olefin concentration builds up, the hydrogen (free H_2 and/or iridium-bound) resulting from dehydrogenation is more likely to be added back to olefin as opposed to escaping from

solution. The cyclization of the initial dehydrogenated product, presumably catalyzed by zeolite, precludes these reactions, greatly increasing the overall efficiency of iridium-catalyzed dehydrogenation.

Scheme 2. 3. Acceptorless dehydrogenation of *n*-pentylbenzene in the absence of zeolite

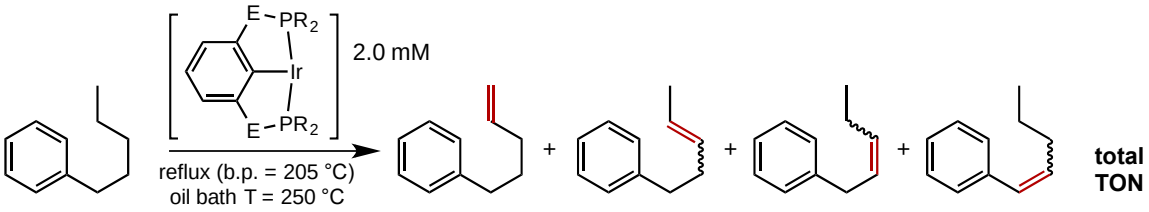

(^{tBu4}PCP)Ir	**8 h**	7 mM	39 mM	15 mM	38 mM	**51**
	72 h	1 mM	42 mM	17 mM	37 mM	**51**
(^{tBu4}POCOP)Ir	**8 h**	1 mM	55 mM	23 mM	63 mM	**75**
	72 h	5 mM	53 mM	24 mM	102 mM	**98**
(^{iPr4}PCP)Ir	**8 h**	1 mM	22 mM	6 mM	24 mM	**28**
	72 h	1 mM	25 mM	8 mM	37 mM	**37**

The ability of zeolites to catalyze alkylations of the type implied in Scheme 2.2 is well known.[17] Accordingly, under the conditions of our dehydrocyclization reactions, 5-phenylpent-1-ene (1.1 M in *n*-pentylbenzene) in the presence of H-SSZ-25 zeolite afforded nearly quantitative yield of cyclized product **1** within 5 min. This rate of cyclization is much greater than that of the overall tandem-catalyzed dehydrocyclizations (Table 2.1), indicating that the dehydrogenation step of Scheme 2.2 may be rate-determining.

Scheme 2. 4**. Zeolite-catalyzed cyclization of 5-phenylpent-1-ene**

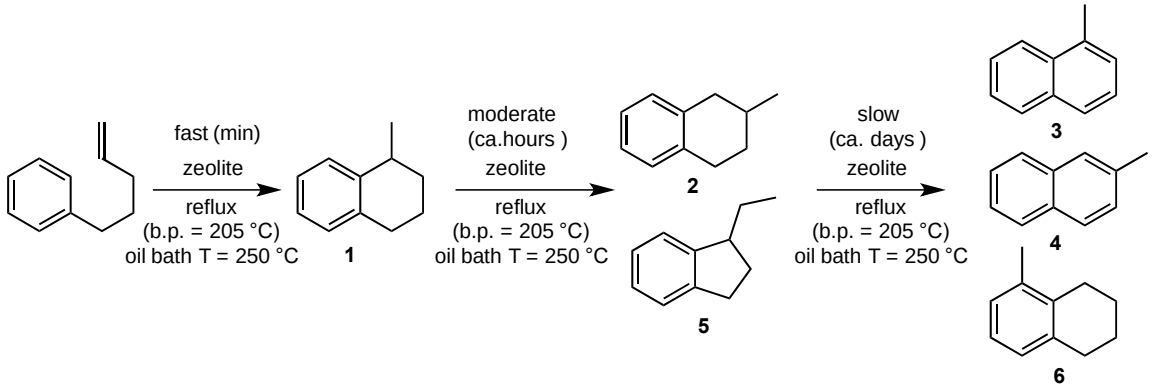

Further thermolysis of the 5-phenylpent-1-ene reaction mixture in the presence of H-SSZ-25 initially revealed (30 min to ca. 8 h) isomerization of **1** to give **2** and **5** (Scheme 2.4; Table 2.2). The concentration of the methyl-migration product **2** exceeded that of **1** within 32 h. Slow dehydrogenation catalyzed by the zeolite gave relatively small quantities of the corresponding naphthalene. Additionally, in independent experiments,[21] solutions of either 1-methylnaphthalene (**3**) or 2-methylnaphthalene (**4**) over either H-SSZ-25 or H-beta[24], under the same conditions (refluxing *n*-pentylbenzene), revealed isomerization between these species to give, within 16 h, a ratio of **4**:**3** = 2.1 ± 0.2.

The above results are all consistent with the tandem catalysis scheme indicated in Scheme 2.2, in which the pincer-Ir complex catalyzes dehydrogenation (of *n*-pentylbenzene and also the initially formed 1-methyltetralin) while the zeolite catalyzes alkylation/cyclization as well as isomerization.

Table 2. 2. Reaction of 5-phenylpent-1-ene with zeolites

entry	Ir catalyst	zeolite	time	**1**	**2**	**3**	**4**	**5**	**6**	Total Cyclized Product
1	none	H-SSZ-25	5 min	1110	0	0	0	4	0	1110
			30 min	1070	14	0	0	8	0	1090
			2 h	970	58	5	3	20	0	1060
			8 h	880	250	15	21	86	4	1260
			24 h	470	470	28	56	140	19	1180
			32 h	390	510	27	66	140	27	1160
2	none	H-beta	5 min	920	22	0	0	4	0	950
			30 min	830	89	0	0	19	0	940
			2 h	560	240	1	4	59	0	860
			8 h	260	460	4	9	100	6	840
			24 h	210	610	7	22	110	22	980
			32 h	210	620	12	29	120	32	1020

Reaction of 5-phenylpent-1-ene (1.1 M) with zeolites (in the absence of pincer-Ir catalyst).[a]
a) Refluxing (205 °C) *n*-pentylbenzene solvent. Product concentrations in mM. (See section 2.4 for full experimental details).

The rate of the dehydrocyclization reactions by (^{tBu4}PCP)Ir and zeolite is not dramatically different when H-beta zeolite is used in place of H-SSZ-25 (Table 2.3, entry 1, vs. Table 2.1, entry 1). This is consistent with the observation that the cyclization of 5-phenylpent-1-ene is fast with either of these zeolites (Scheme 2.4), and thus dehydrogenation by the pincer-Ir catalyst is expected to be rate-determining. Likewise rates and yields are increased only modestly (much less than a factor of two) when 0.58 g zeolite was used instead of 0.30 g (see section 2.5).

Table 2. 3. Dehydrocyclization of *n*-pentylbenzene co-catalyzed by H-beta zeolite and various pincer-ligated iridium catalyst precursors

entry	Ir catalyst	zeolite	time (h)	**1**	**2**	**3**	**4**	**5**	**6**	Total Cyclized Product	TON (H_2/Ir)	Yield Cyclized Product
1	(^{tBu4}PCP)Ir	H-beta	8	630 (10.9)	180 (3.1)	30 (0.5)	49 (0.8)	80 (1.4)	5 (0.1)	970	570	17%
			24	520 (9.0)	860 (14.8)	220 (3.8)	480 (8.3)	190 (3.3)	71 (1.2)	2340	1870	40%
			72	95 (1.6)	200 (3.4)	730 (12.6)	1740 (30.0)	200 (3.4)	160 (2.8)	3130	4030	54%
2	none	H-beta	8	5 (0.1)	0	0	0	0	0	5		0.1%
			24	6 (0.1)	3 (0.1)	0	0	0	0	9		0.2%
			72	21 (0.4)	12 (0.2)	3 (0.1)	1 (0.0)	11 (0.2)	4 (0.1)	52		1%
3	(^{iPr4}PCP)Ir	H-beta	8	410 (7.1)	78 (1.3)	8 (0.1)	15 (0.3)	56 (1.0)	3 (0.1)	570	310	10%
			24	420 (7.2)	400 (6.9)	33 (0.6)	67 (1.2)	110 (1.9)	12 (0.2)	1040	620	18%
			72	390 (6.7)	890 (15.3)	190 (3.3)	390 (6.7)	210 (3.6)	81 (1.4)	2150	1660	37%
4	(MeO-^{tBu4}PCP)Ir	H-beta	8	520 (9.0)	130 (2.2)	26 (0.4)	71 (1.2)	66 (1.1)	6 (0.1)	820	510	14%
			24	350 (6.0)	520 (9.0)	330 (5.7)	830 (14.3)	150 (2.6)	150 (2.6)	2330	2330	40%
			72	69 (1.2)	83 (1.4)	780 (13.4)	1860 (32.1)	47 (0.8)	94 (1.6)	2930	4110	51%
5	(MeO-^{iPr4}PCP)Ir	H-beta	8	960 (16.6)	1060 (18.3)	240 (4.1)	490 (8.4)	220 (3.8)	43 (0.7)	3010	2240	52%
			24	140 (2.4)	270 (4.7)	850 (14.7)	2060 (35.5)	110 (1.9)	250 (4.3)	3680	4750	63%
6	(^{tBu4}POCOP)Ir	H-beta	8	560 (9.7)	670 (11.6)	240 (4.1)	530 (9.1)	120 (2.1)	25 (0.4)	2150	1840	37%
			24	110 (1.9)	210 (3.6)	970 (16.7)	2310 (39.8)	87 (1.5)	120 (2.1)	3810	5180	66%
7	(Me_2N-^{tBu4}PCP)Ir	H-beta	8	450 (7.8)	43 (0.7)	9 (0.2)	16 (0.3)	46 (0.8)	2 (0.0)	570	310	10%
			24	510 (8.8)	840 (14.5)	270 (4.7)	600 (10.3)	210 (3.6)	120 (2.1)	2550	2150	44%
			72	36 (0.6)	70 (1.2)	810 (14.0)	1930 (33.3)	45 (0.8)	100 (1.7)	2990	4240	52%

Dehydrocyclization of n-pentylbenzene (5.8 M) co-catalyzed by H-beta zeolite (0.30 g/2.7 mL) and various pincer-ligated iridium catalyst (2.0 mM) precursors.a a) Product concentrations in mM; percent yields in parentheses. For catalysts (^{tBu4}PCP)Ir, (*p*-OMe-^{tBu4}PCP)Ir, (Me_2N-^{tBu4}PCP)Ir, the catalyst precursors were the corresponding hydrides (typically a mixture of dihydride and tetrahydride), while for (^{tBu4}POCOP)Ir, (^{iPr4}PCP)Ir

and (*p*-OMe-^{iPr4}PCP)Ir the precursors were the corresponding ethylene adducts. (See section 2.4 for full experimental details).

We investigated pincer-Ir catalysts other than (^{tBu4}PCP)Ir for the tandem iridium-zeolite chemistry. We have previously reported that (^{iPr4}PCP)Ir is more effective than (^{tBu4}PCP)Ir for other, related, catalysis including acceptorless dehydrogenation and dehydroaromatization of *n*-alkanes.[5, 7, 19, 25] We find, however (Scheme 2.3), that this is not the case for the acceptorless dehydrogenation of *n*-pentylbenzene (ca. 37 turnovers after 72 h); this may attributable to strong inhibition of this sterically unhindered catalyst by the alkenyl benzene product (this will be the subject of further investigation). Accordingly, turnover numbers obtained with (^{iPr4}PCP)Ir and either H-SSZ-25 or H-beta zeolite are lower than obtained with (^{tBu4}PCP)Ir, but still far greater (>500 after 24 h) than in the absence of zeolite, highlighting the ability of these species to operate in tandem effectively and synergistically.

(^{tBu4}POCOP)Ir is one of the less effective catalysts of this class for dehydrogenation reactions including dehydroaromatization and *n*-alkane transfer dehydrogenation.[5, 7, 10-11, 26] It was found however to be more effective than (^{tBu4}PCP)Ir, and much more effective than (^{iPr4}PCP)Ir, for acceptorless dehydrogenation of *n*-pentylbenzene (Scheme 2.3). We attribute this to a reduced tendency of (^{R4}POCOP)Ir, relative to (^{R4}PCP)Ir complexes, to form stable 18-electron complexes[23, 27] including bidentate-coordinated alkenyl benzene adducts of the type considered above. Indeed, (^{tBu4}POCOP)Ir is the most effective pincer-Ir catalyst yet investigated for the tandem-catalyzed cyclizations; in tandem with H-SSZ-25, (^{tBu4}POCOP)Ir(C_2H_4) gave 5.4 M cyclized product (6900 turnovers and 94% yield) in 24 h.

Finally, we investigated the recyclability of the pincer-Ir/zeolite system. In two case, volatiles were removed by vacuum (at ca. 60 °C) after the tandem-catalyzed cyclization reaction had proceeded (at reflux). Fresh *n*-pentylbenzene was then added to the remaining solids and GC analysis revealed that almost all cyclized product had been removed. The systems were then brought to reflux again.[21] In one experiment, with (^{iPr4}PCP)Ir and zeolite H-beta, after 8 h at reflux the concentration of cyclized species was 440 mM; upon removal of volatiles, addition of fresh *n*-pentylbenzene, and then another 8 h at reflux, the yield of cyclized species was 240 mM or 55% of that obtained in the initial run. In another experiment, with (MeO-^{iPr4}PCP)Ir and zeolite H-beta, the total cyclization yield after 8 h was 2.89 M. Following removal of volatiles and addition of *n*-pentylbenzene, 2.13 M cyclized species was observed after 8 h reflux, or 74% of the yield obtained before recycling. That same mixture was then allowed to undergo further reaction at reflux for another 16 h (i.e. a total of 24 h reflux) resulting in a total yield of 3.52 M. The volatiles were then removed for a second time and fresh *n*-pentylbenzene was again added to the remaining solids. The mixture was then allowed to undergo reaction at reflux for another 24 h, and GC analysis revealed 2.52 M or 72% of the corresponding yields observed in the previous 24 h run. Thus, apparently partial catalyst decomposition did occur, but further experiments will be required to determine the nature of the decomposition and to what extent it took place during the cyclization reaction vs. during the catalyst recycling process.

2.3. Conclusion

In summary, catalysis by pincer-iridium alkane dehydrogenation catalysts in tandem with zeolite arene-alkylation catalysts effects the intramolecular coupling of alkyl and aryl C-H bonds with the loss of free H_2. The systems give far greater turnover numbers

than are obtained from dehydrogenation alone using only the pincer-iridium catalysts. This reaction may provide a useful route to naphthalene derivatives. More broadly, efforts are currently underway to extend this approach to intermolecular alkyl-aryl coupling and to other reactions that exploit the compatibility of pincer-iridium and zeolite catalysts.

2.4. Experimental information

2.4.1 General information and experimental methods

All manipulations were conducted under an argon atmosphere either in a glovebox or using standard Schlenk techniques. All anhydrous solvents were purchased from Aldrich, flushed with argon, and stored in an argon atmosphere in a glovebox. *n*-Pentylbenzene (99%), 1-methylnaphthalene (**3**; 95%), 2-methylnaphthalene (**4**; 97%) and mesitylene (99%) were purchased from Aldrich. *n*-Pentylbenzene and 1-methylnaphthalene were degassed under vacuum and dried over activated neutral alumina, then stored over activated 3Å molecular sieves. 2-methylnaphthalene was put in the glovebox vacuum chamber overnight before being brought inside the glovebox for use. Pincer-ligated iridium catalysts, (^{tBu4}PCP)IrH$_n$,[28] (*p*-OMe-^{tBu4}PCP)IrH$_n$,[29] (Me$_2$N-^{tBu4}PCP)IrH$_n$,[30] (^{tBu4}POCOP)IrH$_n$,[31] (^{iPr4}PCP)Ir(C$_2$H$_4$),[32] (*p*-OMe-^{iPr4}PCP)Ir(C$_2$H$_4$)[25] were synthesized as previously reported and characterized by ^{1}H and ^{31}P NMR. 1-methyltetralin (**1**),[33] 2-methyltetralin (**2**),[34] 1-ethylindane(**5**),[35] and 5-phenylpent-1-ene,[36] were synthesized as previously reported and characterized by ^{1}H and ^{13}C NMR before use as standards for GC and GC/MS. Calcined zeolites were received from Chevron Energy Technology Company. All other reagents were obtained from commercial sources and used as received. All glassware was dried in a vacuum oven for at least 24 h prior to use.

As with previously reported studies of acceptorless dehydrogenation, the reactor used consisted of a glass flask of ca. 5 mL total volume, fused to a condenser, above which were fused two Kontes exposed O-ring tip valves (see Fig. 2.1). Inside the glovebox, 2.7 mL of a 2.0 mM *n*-pentylbenzene (b.p. = 205 °C) solution of pincer-iridium catalyst was combined with zeolite (0.30 g or 0.58 g) in the reactor. The bulb containing the solution was heated in an oil bath at 250 °C, resulting in vigorous reflux. The condenser was water-cooled and argon flowed above the condenser via the two opened Kontes valves, allowing the escape of evolved dihydrogen.

After allowing the solution to cool down, an argon-purged syringe with a long needle was used to obtain aliquots of 0.05 mL, for GC or GC-MS analysis, under a strong counter-flow of argon via the fully opened top Kontes valve. 0.030 mL of the sample was mixed with 0.005 mL mesitylene as a GC standard before injection into the GC.

Figure 2. 1. Reaction vessel

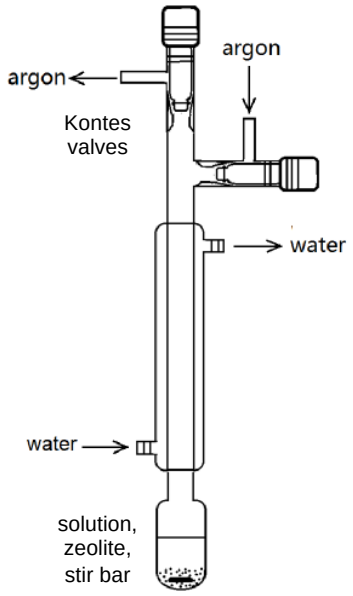

2.4.2. Gas chromatography (GC) Methods

Gas chromatography was performed on a Varian 430 gas chromatograph utilizing flame ionization detection with the following parameters:

GC Method 1 (for typical dehydrocyclization GC runs)

Column: 30 m × 0.25 mm × 0.5 μm (Supelco) fused silica capillary column, Petrocol, HD

Starting temperature: 38 °C

Time at starting temp: 1.4 min

Ramp: 20 °C/min to 250 °C, hold time 3 min

Ramp: 30 °C/min to 280 °C, hold time 35 min

Flow rate: 1 mL/min (He)

Split ratio: 90

Ending temp: 280 °C

Injector temp: 300 °C

Detector temp: 310 °C

GC Method 2 (for olefin separations)

Column: 30 m × 0.25 mm × 0.5 μm (Supelco) fused silica capillary column, Petrocol, HD

Starting temperature: 40 °C

Time at starting temp: 1.4 min

Ramp: 5 °C/min to 90 °C, hold time 3 min

Ramp: 2.5 °C/min to 155 °C, hold time 1 min

Ramp: 20 °C/min to 260 °C, hold time 20 min

Flow rate: 1 mL/min (He)

Split ratio: 500

Ending temp: 260 °C

Injector temp: 270 °C

Detector temp: 300 °C

2.4.3. Identification of major products

Authentic samples were used as standards to identify the reaction products by GC and GC-MS. Figures 2.2 and 2.3 show an example of the GC trace of a typical dehydrocyclization experiment. 1-methyltetralin (**1**), 2-methyltetralin (**2**), 1-methylnaphthalene (**3**), 2-methylnaphthalene (**4**) and 1-ethylindane (**5**), were identified by comparison of their GC and GC-MS with authentic samples. The assignment of 5-methyltetralin (**6**) was inferred based on the correlation of boiling point (234 °C) with GC retention time (Figure 2.3) relative to the known products, and the mass spectrometry data.

Figure 2. 2. GC trace showing product separation

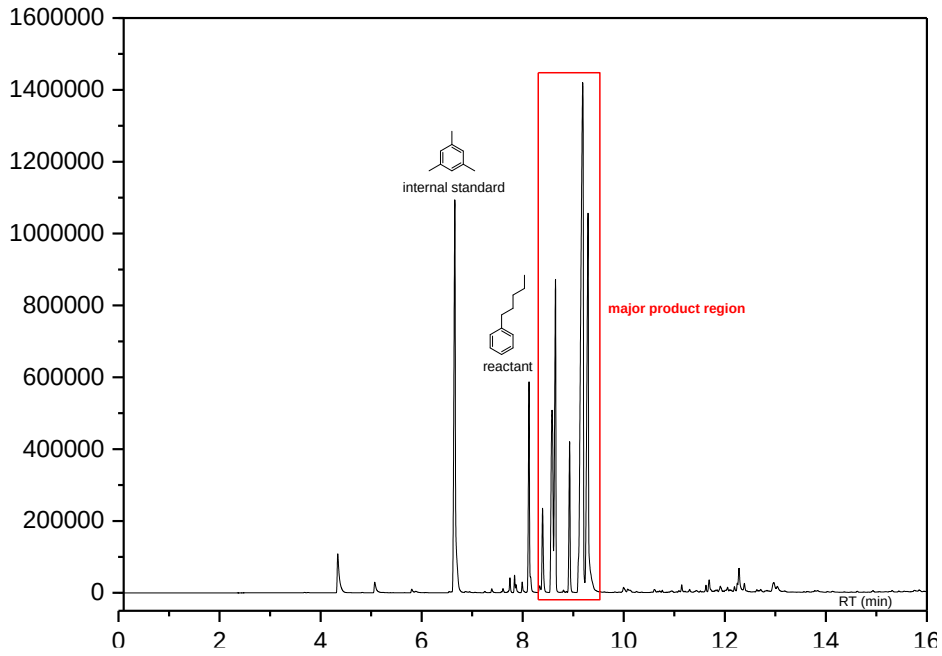

Reaction run with 2 mM (^{tBu4}POCOP)Ir(ethylene) and 0.58g H-SSZ-25 zeolite as catalyst.

Figure 2. 3. GC trace of region of the major cyclized products with identification

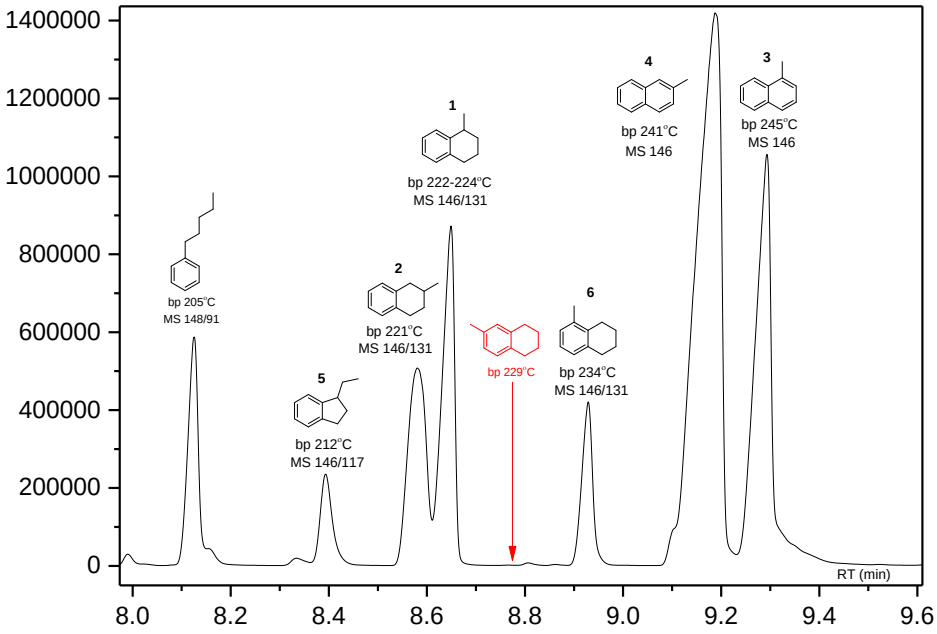

Reaction run with 2 mM (^{tBu4}POCOP)Ir(ethylene) and 0.58g H-SSZ-25 zeolite as catalyst.

2.4.4. Reactions with 0.58 g zeolites

Table 2. 4. Dehydrocyclization of *n*-pentylbenzene co-catalyzed by H-SSZ-25 zeolite

entry	Ir catalyst (2.0 mM)	zeolite	time (h)	**1**	**2**	**3**	**4**	**5**	**6**	Total Cyclized Product	TON (H_2/Ir)	Yield Cyclized Product
1	(^{tBu4}PCP)Ir	H-SSZ-25	8	440	20	13	16	18	3	510	280	9
			24	830	150	120	150	67	11	1330	930	23
			72	79	190	680	1610	75	150	2780	3680	48
2	none	H-SSZ-25	8	55	14	2	6	7	5	90	50	2
			24	140	47	2	8	10	37	240	130	4
			72	200	200	23	77	0	43	540	370	9
3	(^{iPr4}PCP)Ir	H-SSZ-25	8	580	26	14	14	24	6	660	360	11
			24	980	220	77	100	78	9	1460	910	25
			72	670	770	410	840	210	93	2990	2750	52
4	(MeO-^{tBu4}PCP)Ir	H-SSZ-25	8	430	25	23	34	23	4	540	330	9
			24	850	170	330	440	81	36	1910	1720	33
			72	15	9	910	2080	7	9	3030	4510	52
5	(MeO-^{iPr4}PCP)Ir	H-SSZ-25	8	1220	94	100	79	41	5	1540	950	27
			24	920	520	810	1380	150	100	3880	4130	67
6	(^{tBu4}POCOP)Ir	H-SSZ-25	8h	1580	62	220	170	40	8	2080	1430	36
			24	580	490	980	1910	160	240	4360	5070	75

Dehydrocyclization of n-pentylbenzene co-catalyzed by H-SSZ-25 zeolite (0.58 g/ 2.7 mL) and various pincer-ligated iridium catalyst (2.0 mM) precursors.[a] a) Product concentrations in mM. For catalysts (^{tBu4}PCP)Ir and (*p*-OMe-^{tBu4}PCP)Ir, the catalyst precursors were the corresponding hydrides (typically a mixture of dihydride and tetrahydride), while for (^{tBu4}POCOP)Ir, (^{iPr4}PCP)Ir and (*p*-OMe-^{iPr4}PCP)Ir the precursors were the corresponding ethylene adducts.

Table 2. 5. Dehydrocyclization of *n*-pentylbenzene co-catalyzed by H-beta zeolite

entry	Ir catalyst	zeolite	time (h)	**1**	**2**	**3**	**4**	**5**	**6**	Total Cyclized Product	TON (H_2/Ir)	Yield Cyclized Product
1	(^{tBu4}PCP)Ir	H-beta	8	310	130	6	17	64	8	540	290	9
			24	350	620	48	150	140	44	1350	870	23
			72	130	270	460	980	110	160	2110	2500	36
2	none	H-beta	8	28	7	0	0	7	8	50	30	1
			24	62	53	2	0	18	28	160	80	3
			72	140	340	15	8	75	70	650	350	11
3	(^{iPr4}PCP)Ir	H-beta	8	340	110	7	1	71	2	530	270	9
			24	330	610	27	55	140	18	1180	670	20
			72	180	460	330	720	140	170	2000	2050	34
4	(MeO-^{tBu4}PCP)Ir	H-beta	8	390	240	35	95	79	13	850	560	15
			24	260	440	310	720	120	180	2030	2050	35
			72	62	110	640	1480	55	99	2450	3340	42
5	(MeO-^{iPr4}PCP)Ir	H-beta	8	640	1200	290	630	250	86	3100	2470	53
			24	55	120	720	1710	72	170	2850	3850	49
6	(^{tBu4}POCOP)Ir	H-beta	8h	580	1100	400	930	250	130	3390	3030	58
			24	14	37	900	2110	37	47	3150	4580	54

Dehydrocyclization of n-pentylbenzene co-catalyzed by H-beta zeolite (0.58 g/ 2.7 mL) and various pincer-ligated iridium catalyst (2.0 mM) precursors.[a] a) Product concentrations in mM. For catalysts (^{tBu4}PCP)Ir and (*p*-OMe-^{tBu4}PCP)Ir, the catalyst precursors were the corresponding hydrides (typically a mixture of dihydride and tetrahydride), while for (^{tBu4}POCOP)Ir, (^{iPr4}PCP)Ir and (*p*-OMe-^{iPr4}PCP)Ir the precursors were the corresponding ethylene adducts.

2.4.5. Zeolite-catalyzed methylnaphthalene isomerization

Table 2. 6. Methylnaphthalene isomerization catalyzed by H-SSZ-25 and H-beta zeolite

entry	Ir catalyst	zeolite	time	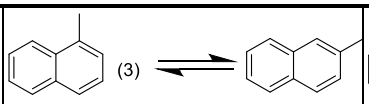			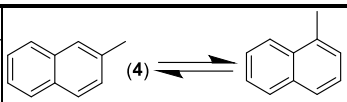		
				4/(4+3)	**4/(4+3)**	**4/3**	**4/(4+3)**	**4/(4+3)**	**4/3**
1	No Ir	H-SSZ-25	0	1	0	0	0	1	
			5min	0.97	0.03	0.03	0.07	0.93	12.51
			30min	0.86	0.14	0.16	0.13	0.87	6.69
			2h	0.61	0.39	0.64	0.18	0.82	4.62
			4h	0.44	0.56	1.28	0.23	0.78	3.44
			8h	0.36	0.64	1.79	0.29	0.71	2.47
			16h	0.30	0.70	2.29	0.32	0.68	2.11
			24h	0.32	0.68	2.13	0.33	0.67	2.07
			32h	0.33	0.67	2.04	0.33	0.67	2.02
2	No Ir	H-beta	0	1	0	0	0	1	
			8h	0.28	0.72	2.57	0.32	0.68	2.26
			24h	0.28	0.72	2.56	0.31	0.69	2.6
			72h	0.27	0.73	2.73	0.28	0.72	2.13

Methylnaphthalene (1.0 M in pentylbenzene) isomerization catalyzed by H-SSZ-25 and H-beta zeolite (0.58 g/2.7 mL). Same experimental condition as dehydrocyclization of n-pentylbenzene, but start with 1.0 M methyl naphthalene in pentylbenzene without pincer iridium complexes. 3, 4, and 3+4 are standing for concentration of 1-methylnaphthalene, 2-methylnaphthalene, and total of these two accordingly.

2.4.6. Recyclability

Table 2. 7. Recycle the catalysts

Ir catalyst	time (h)	**1**	**2**	**3**	**4**	**5**	**6**	Total Cyclized Product	TON (H_2/Ir)	Yield Cyclized Product
(^{iPr4}PCP)Ir	8	350	40	6	1	44	3	440	230	4.0 %
	Recycle									
	8	180	36	2	0	17	2	240	120	2.1%
	24	390	210	10	21	84	6	720	390	6.7%
	72	470	1010	170	340	220	60	2270	1640	28%
(MeO-^{iPr4}PCP)Ir	8	1050	1000	200	390	210	39	2890	2030	35%
	Recycle 1									
	8	1000	580	120	258	150	23	2130	1450	25%
	24	360	750	570	1390	210	250	3520	3720	64%
	Recycle 2									
	8	760	84	64	130	61	18	1110	750	13%
	24	720	570	320	670	180	67	2520	2250	39%
	72	120	190	900	2130	90	140	3570	4820	83%

a) Product concentrations in mM. For catalyst (*p*-OMe-^{tBu4}PCP)Ir, the catalyst precursor was the corresponding mixture of dihydride and tetrahydride, while for (^{iPr4}PCP)Ir the precursor was the corresponding ethylene adduct. Volatiles were removed by vacuum (at ca. 60 °C) after the tandem-catalyzed cyclization reaction had proceeded (at reflux). Fresh *n*-pentylbenzene was then added to the remaining solids; GC analysis revealed that almost all cyclized product had been removed. The systems were then brought to reflux again for the specified times.

2.4.7. Decrease of total solution mass (loss of volatile products)

In an experiment with (^{iPr4}PCP)Ir catalyst (2 mM) and H-SSZ-25 zeolite (0.30 g) in 2.7 mL *n*-pentylbenzene, after 8 h, 24 h, and 72 h of reflux, total turnover numbers for H_2 loss were 310, 840, and 2460 respectively. We observed a total loss of mass of 0.051 g,

0.059 g, and 0.231 g after each of these intervals (thus cumulative totals are 0.051 g, 0.110 g, and 0.341 g). The expected losses of H_2 based on the dehydrocyclized product yields are 0.0034 g, 0.0092 g, and 0.027 g respectively, or ca. 8% of the observed decrease of mass. The remainder of the decrease of mass is presumably attributable to loss of *n*-pentylbenzene, (e.g. 0.341 g - 0.027 g = 0.314 g after 72 h) corresponding to 2.12 mmol *n*-pentylbenzene. Thus up to approximately 16% (2.12 mmol/13.3 mmol) of the hydrogen is lost as *n*-pentylbenzene hydrogenation products. (This is an upper limit since it assumes that each mol of *n*-pentylbenzene is lost as benzene plus *n*-pentane; but it is also possible that the pentylbenzene lost is *not* fully hydrogenated, i.e. that it is lost as pentene plus benzene). Thus we conclude that >80% of hydrogen lost is indeed lost as H_2 gas.

2.9. Reference

1. CHrevsMarch2016, Recent CHRevs - KIG chapter not book. In *Revs2014*.
2. DeHtnEarlyStoichCat2, DeHtnEarlyStoichCat.
3. GeneralDehtn2011-16, General Dehydrogenation 2011-16 8 refs including Choi 2011 and Kumar 2016.
4. Liu, F.; Pak, E. B.; Singh, B.; Jensen, C. M.; Goldman, A. S., Dehydrogenation of n-Alkanes Catalyzed by Iridium "Pincer" Complexes. Regioselective Formation of Alpha-Olefins. *J. Am. Chem. Soc.* **1999,** *121* (16), 4086-4087.
5. Kumar, A.; Zhou, T.; Emge, T. J.; Mironov, O.; Saxton, R. J.; Krogh-Jespersen, K.; Goldman, A. S., Dehydrogenation of n-Alkanes by Solid-Phase Molecular Pincer-Iridium Catalysts. High Yields of α-Olefin Product. *J. Am. Chem. Soc.* **2015,** *137* (31), 9894-9911.
6. Renkema, K. B.; Kissin, Y. V.; Goldman, A. S., The Mechanism of Alkane Transfer-Dehydrogenation Catalyzed by a Pincer–Ligated Iridium Complex. *J. Am. Chem. Soc.* **2003,** *125* (26), 7770-7771.
7. Ahuja, R.; Punji, B.; Findlater, M.; Supplee, C.; Schinski, W.; Brookhart, M.; Goldman, A. S., Catalytic dehydroaromatization of n-alkanes by pincer-ligated iridium complexes. *Nature Chem.* **2011,** *3* (2), 167-171.
8. BakerMarksTandemCatRevs, For in-depth reviews of tandem catalysis see BakerMarksTandemCatRevs.
9. TandemDehtnCrabtreeChemRev2010, review of tandem catalysis based on dehydrogenation see Dobereiner, G. E.; Crabtree, R. H. Chem. Rev. 2010, 110, 681-703.
10. Haibach, M. C.; Kundu, S.; Brookhart, M.; Goldman, A. S., Alkane Metathesis by Tandem Alkane-Dehydrogenation-Olefin-Metathesis Catalysis and Related Chemistry. *Acc. Chem. Res.* **2012,** *45* (Copyright (C) 2012 American Chemical Society (ACS). All Rights Reserved.), 947-958.
11. Dobereiner, G. E.; Yuan, J.; Schrock, R. R.; Goldman, A. S.; Hackenberg, J. D., Catalytic Synthesis of n-Alkyl Arenes through Alkyl Group Cross-Metathesis. *J. Am. Chem. Soc.* **2013,** *135* (34), 12572-12575.
12. DehydrogenativeCouplingOfCH_Bonds, As a catalytic dehydrogenative C-C bond formation, this reaction is closely related, at least formally, to the rich chemistry of oxidations of C-H bonds resulting in C-C bond coupling. See for example: 9 refs.
13. Xu, W.; Rosini, G. P.; Gupta, M.; Jensen, C. M.; Kaska, W. C.; Krogh-Jespersen, K.; Goldman, A. S., Thermochemical Alkane Dehydrogenation Catalyzed in Solution Without the Use of a Hydrogen Acceptor. *Chem. Commun.* **1997**, 2273-2274.
14. Krogh-Jespersen, K.; Czerw, M.; Kanzelberger, M.; Goldman, A. S., DFT/ECP Study of C-H Activation by (PCP)Ir and (PCP)Ir$(H)_2$. Enthalpies and Free Energies of Associative and Dissociative Pathways. *J. Chem. Inf. Comput. Sci.* **2001,** *41* (1), 56-63.
15. Clerici, M. G., Zeolites for fine chemicals production. *Top. Catal.* **2000,** *13* (4), 373-386.
16. Kocal, J. A.; Vora, B. V.; Imai, T., Production of linear alkylbenzenes. *Appl. Catal., A* **2001,** *221* (1-2), 295-301.
17. ZeoliteAlkylationRevs, ZeoliteAlkylationRevs 6.
18. Zones, S. I.; Hwang, S.-J.; Davis, M. E., Studies of the Synthesis of SSZ-25 Zeolite in a "Mixed-Template" System. *Chemistry – A European Journal* **2001,** *7* (9), 1990-2001.

19. Liu, F.; Goldman, A. S., Efficient thermochemical alkane dehydrogenation and isomerization catalyzed by an iridium pincer complex. *Chem. Commun.* **1999**, 655-656.
20. Punji, B.; Emge, T. J.; Goldman, A. S., A Highly Stable Adamantyl-Substituted Pincer-Ligated Iridium Catalyst for Alkane Dehydrogenation. *Organometallics* **2010,** *29* (12), 2702-2709.
21. SeeSuppInfo, See Supporting Information. In *See Supporting Information for details. All reactions were conducted under argon atmosphere.*
22. DecSoltnVolume, A very small decrease in solution volume was observed after long reaction times; this was quantified in one experiment....
23. Field, K. D. Activation of Small Molecules by Pincer Iridium Catalysts. Ph. D. thesis, Rugers University, Piscataway, 2014.
24. Deem, M. W.; Newsam, J. M.; Creighton, J. A., Fluctuations in zeolite aperture dimensions simulated by crystal dynamics. *J. Am. Chem. Soc.* **1992,** *114* (18), 7198-7207.
25. Kundu, S.; Choliy, Y.; Zhuo, G.; Ahuja, R.; Emge, T. J.; Warmuth, R.; Brookhart, M.; Krogh-Jespersen, K.; Goldman, A. S., Rational Design and Synthesis of Highly Active Pincer-Iridium Catalysts for Alkane Dehydrogenation. *Organometallics* **2009,** *28* (18), 5432-5444.
26. Biswas, S.; Brookhart, M.; Choliy, Y.; Goldman, A.; Huang, Z.; Krogh-Jespersen, K., Catalytic dehydrogenation and metathesis of alkanes: Selectivity and mechanistic aspects. *Abstracts of Papers, 239th ACS National Meeting, San Francisco, CA, United States, March 21-25,* **2010**, INOR-670.
27. Zhu, K.; Achord, P. D.; Zhang, X.; Krogh-Jespersen, K.; Goldman, A. S., Highly Effective Pincer-Ligated Iridium Catalysts for Alkane Dehydrogenation. DFT Calculations of Relevant Thermodynamic, Kinetic, and Spectroscopic Properties. *Journal of the American Chemical Society* **2004,** *126* (40), 13044-13053.
28. Gupta, M.; Hagen, C.; Flesher, R. J.; Kaska, W. C.; Jensen, C. M., A highly active alkane dehydrogenation catalyst: stabilization of dihydrido rhodium and iridium complexes by a P-C-P pincer ligand. *Chemical Communications* **1996,** (17), 2083-2084.
29. Krogh-Jespersen, K.; Czerw, M.; Zhu, K. M.; Singh, B.; Kanzelberger, M.; Darji, N.; Achord, P. D.; Renkema, K. B.; Goldman, A. S., Combined computational and experimental study of substituent effects on the thermodynamics of H-2, CO, arene, and alkane addition to iridium. *Journal of the American Chemical Society* **2002,** *124* (36), 10797-10809.
30. Huang, Z.; Brookhart, M.; Goldman, A. S.; Kundu, S.; Ray, A.; Scott, S. L.; Vicente, B. C., Highly Active and Recyclable Heterogeneous Iridium Pincer Catalysts for Transfer Dehydrogenation of Alkanes. *Advanced Synthesis & Catalysis* **2009,** *351* (1-2), 188-206.
31. Göttker-Schnetmann, I.; White, P.; Brookhart, M., Iridium Bis(phosphinite) p-XPCP Pincer Complexes: Highly Active Catalysts for the Transfer Dehydrogenation of Alkanes. *Journal of the American Chemical Society* **2004,** *126* (6), 1804-1811.
32. Kumar, A.; Zhou, T.; Emge, T. J.; Mironov, O.; Saxton, R. J.; Krogh-Jespersen, K.; Goldman, A. S., Dehydrogenation of n-Alkanes by Solid-Phase Molecular Pincer-Iridium Catalysts. High Yields of α-Olefin Product. *Journal of the American Chemical Society* **2015,** *137* (31), 9894-9911.
33. Xie, K.; Wang, S.; Li, P.; Li, X.; Yang, Z.; An, X.; Guo, C.-C.; Tan, Z., Synthesis of tetralin and chromane derivatives via In-catalyzed intramolecular hydroarylation. *Tetrahedron Letters* **2010,** *51* (33), 4466-4469.

34. Fujita, M.; Kim, W. H.; Sakanishi, Y.; Fujiwara, K.; Hirayama, S.; Okuyama, T.; Ohki, Y.; Tatsumi, K.; Yoshioka, Y., Elimination−Addition Mechanism for Nucleophilic Substitution Reaction of Cyclohexenyl Iodonium Salts and Regioselectivity of Nucleophilic Addition to the Cyclohexyne Intermediate. *Journal of the American Chemical Society* **2004,** *126* (24), 7548-7558.
35. Adamczyk, M.; Watt, D. S.; Netzel, D. A., Synthesis of biological markers in fossil fuels. 2. Synthesis and carbon-13 NMR studies of substituted indans and tetralins. *The Journal of Organic Chemistry* **1984,** *49* (22), 4226-4237.
36. Anderson, J. C.; Munday, R. H., Vinyldimethylphenylsilanes as Safety Catch Silanols in Fluoride-Free Palladium-Catalyzed Cross-Coupling Reactions. *The Journal of Organic Chemistry* **2004,** *69* (25), 8971-8974.

Chapter 3. Catalytic dehydrogenative C-C coupling by a pincer-ligated iridium complex

This chapter is reproduced with permission from

Catalytic Dehydrogenative C-C Coupling by a Pincer-Ligated Iridium Complex

Miles Wilklow-Marnell, Bo Li, Tian Zhou, Karsten Krogh-Jespersen, William W. Brennessel, Thomas J. Emge, Alan S. Goldman, and William D. Jones

J. Am. Chem. Soc. **2017**, *139*, 8977−8989

Copyright © 2017 American Chemical Society

Abstract: The pincer-iridium fragment (^{iPr}PCP)Ir (^{R}PCP = $\boldsymbol{\kappa}^3$-2,6-$C_6H_3(CH_2PR_2)_2$) has been found to catalyze the dehydrogenative coupling of vinyl arenes to afford predominantly (*E*,*E*)-1,4-diaryl-1,3-butadienes. The eliminated hydrogen can undergo addition to another molecule of vinyl arene, resulting in an overall disproportionation reaction with one equivalent of ethyl arene formed for each equivalent of diarylbutadiene produced. Alternatively, sacrificial hydrogen acceptors (e.g. *t*-butylethylene) can be added to the solution for this purpose. Diarylbutadienes are isolated in moderate to good yields, up to ca. 90% based on the disproportionation reaction. The results of DFT calculations and experiments with substituted styrenes indicate that the coupling proceeds via double C-H addition of a styrene molecule, at *β*-vinyl and ortho-aryl positions, to give an iridium(III) metalloindene intermediate; this intermediate then adds a *β*-vinyl C-H bond of a second styrene molecule before reductively eliminating product. Several metalloindene complexes have been isolated and crystallographically characterized. In accord with the proposed mechanism, substitution at the ortho-aryl positions of the styrene precludes dehydrogenative homocoupling. In the case of 2,4,6-trimethylstyrene, dehydrogenative coupling of *β*-vinyl and ortho-methyl C-H bonds affords dimethylindene, demonstrating that the dehydrogenative coupling is not limited to C(sp^2)-H bonds.

3.1. Introduction

Carbon-carbon bond forming reactions are clearly among the most useful and important reactions in organic synthesis. Over the past several decades, transition metal complexes have revolutionized the ability to effect C-C bond formation. The majority of transition metal catalyzed systems for C-C bond formations require pre-activated substrates, including organometallic and/or organohalide species.[1-9] (Of course this applies even more so to non-transition-metal catalyzed C-C bond formations.) Significant progress has been made with respect to C-C bond formation between non-functionalized[10-14] alkanes, alkenes, and alkynes, with the dehydrogenative Heck (or Fujiwara-Moritani) reaction, an aryl-vinyl $C(sp^2)$-$C(sp^2)$ coupling, being perhaps the most well developed class of such reactions. However, these methodologies often require high to stoichiometric amounts of Pd species and/or oxidants, and the presence of directing groups, and often display poor selectivity and/or yields.[15-18] The few examples of C_{vinyl}-C_{vinyl} bond formation by double C_{vinyl}-H activation suffer from the same issues.[19]

Examples of the direct formation of C_{vinyl}-C_{vinyl} bonds by transition metal mediated dehydrogenative coupling of vinyl arenes to form specifically aryl substituted 1,3-butadienes are particularly quite limited. Scheme 3.1 depicts notable examples to date. In an early example, Yatsimirsky *et al.* studied the kinetics of stoichiometric dehydrogenative coupling of styrene by various palladium(II) acetate species in glacial acetic acid.[20] Much later, in 2006 the formation of 1,4-diphenyl-1,3-butadiene was identified by Kim *et al.* as a component (up to 53%) in the product mixture resulting from Fujiwara-Moritani coupling between benzene and styrene using $Pd(CF_3CO_2)_2$ as catalyst in the presence of thioether type ligands and 3.4 atm O_2.[21] Recently, 4-vinylbiphenyl was shown to undergo

dehydrogenative coupling when deposited as a monolayer on copper surfaces;[22] however, the coupled product was only observed *in situ*. Also in 2015, the dehydrogenative coupling of various vinyl arenes was reported in up to 66% yield using $Pd(OAc)_2$ as catalyst (20 mol %) and $Cu(OAc)_2$ as oxidant under 1 atm O_2.[23] In addition, the reaction required one equivalent of benzyl chloride.

Scheme 3. 1. Reported examples of dehydrogenative coupling of vinyl arenes

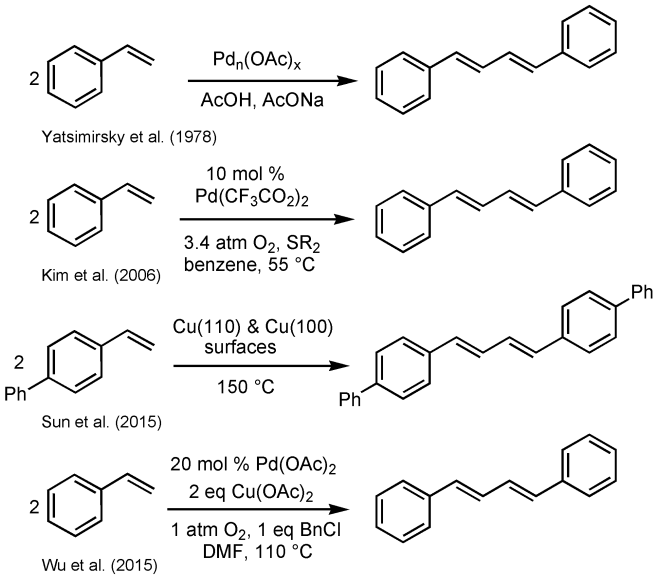

Although iridium has played a leading role in the development of stoichiometric C-H bond activation,[24] as well as catalytic C-H bond functionalization,[25-26] particularly alkane dehydrogenation,[27-28] there are surprisingly few examples of iridium-catalyzed dehydrogenative couplings of C-H bonds. Intramolecular ligand-based C(sp^3)-H couplings forming new C-C double bonds,[29-30] and several inter- and intramolecular couplings to form heterocycles[31-32] and fluorenols[33] have been reported. In the present work, we report the efficient dehydrogenative coupling of vinyl arenes to form (*E*,*E*)-1,4-diaryl-1,3-butadienes catalyzed by the reactive (^{iPr}PCP)Ir fragment. In addition we demonstrate efficient catalytic intramolecular C(sp^3)-C(sp^2) dehydrogenative coupling. These results

indicate that the established ability of pincer-ligated iridium complexes to effect both C-H addition and C-C bond coupling,[34] can be integrated into productive catalytic dehydrogenative coupling reactions that do not require the use of an oxidizing agent.

3.2. Results and discussion

3.2.1. Catalytic intermolecular coupling by (iPrPCP)Ir

Pincer-ligated iridium fragments (^{R}PCP)Ir have been reported to undergo facile and rapid addition of aryl and vinyl C-H bonds at room temperature,[35] (Scheme 3.2) as well as catalyzing alkane dehydrogenation. More recently, we have also reported the *double* C-H activation of biphenyl and phenanthrene to form iridacycles at (^{R}PCP)Ir with concomitant release of H_2.[36-37] In addition we have demonstrated that (^{R}PCP)IrRR' complexes can undergo relatively facile C-C bond reductive elimination[34] and, conversely, (^{R}PCP)Ir fragments can oxidatively add strained C-C bonds.[38] With this in mind, we have attempted to determine whether these stoichiometric reactions could be employed in catalytic dehydrogenative C-C bond coupling reactions as indicated in Scheme 3.2.

Scheme 3. 2. Simplified catalytic cycle for dehydrogenative coupling by (^{R}PCP)Ir proceeding via C-H addition to yield an Ir(III) hydrocarbyl hydride followed by a second C-H addition to the Ir(III) species

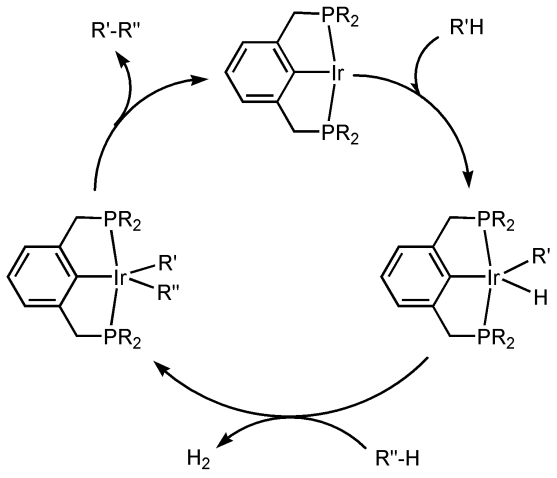

Simplified catalytic cycle for dehydrogenative coupling by (^{R}PCP)Ir proceeding via C-H addition to yield an Ir(III) hydrocarbyl hydride followed by a second C-H addition to the Ir(III) species

Table 3. 1. Catalytic dehydrogenative coupling of vinyl arenes to form diarylbutadienes at 150 °C

Entry	Substrate	Catalyst Precursor (% loading)	time	Conversion (%)[a]	Yield (%)[b]
1		(^{iPr}PCP)IrHCl (5%)[c]	24 h	92	70[e], 77[g]
		(^{iPr}PCP)Ir(C_2H_4) (1%)[d]	72 h	96	92[f], 83[e]
2		(^{iPr}PCP)IrHCl (5%)[c]	24 h	98	48[e]
		(^{iPr}PCP)Ir(C_2H_4) (1%)[d]	72 h	94	88[f], 81[e]
3	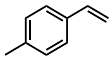	(^{iPr}PCP)Ir(C_2H_4) (1%)[d]	72 h	93	82[e]
4	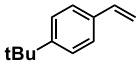	(^{iPr}PCP)Ir(C_2H_4) (1%)[d]	96 h	92	88[f], 80[e]
5	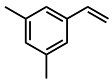	(^{iPr}PCP)Ir(C_2H_4) (2%)[d]	120 h	43	31[f], 26[e]
6		(^{iPr}PCP)IrHCl (5%)[c]	24 h	9	trace[h]
7	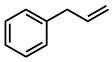	(^{iPr}PCP)IrHCl (5%)[c]	24 h	82	0[i]
8	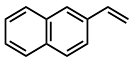	(^{iPr}PCP)IrHCl (5%)[c]	24 h	98	55[e]
9	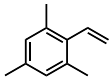	(^{iPr}PCP)Ir(C_2H_4) (1%)[d]	48 h	95	0 (93)[j]
10	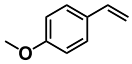	(^{iPr}PCP)IrHCl (5%)[c]	24 h	76	50[e]
		(^{iPr}PCP)Ir(C_2H_4) (1%)[d]	158 h	67	58[e]
11	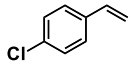	(^{iPr}PCP)IrHCl (5%)[c]	24 h	20	~ 16[k]
12	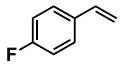	(^{iPr}PCP)Ir(C_2H_4) (1%)[d]	145 h	88	75[f], 67[e]
13	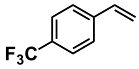	(^{iPr}PCP)Ir(C_2H_4) (1%)[d]	145 h	90	70[f], 60[e]
14	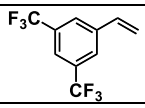	(^{iPr}PCP)Ir(C_2H_4) (1%)[d]	120 h	36	13[f], 7[e]

(a) Percent disappearance of substrate. (b) Yields based on assumption of one equiv ethylbenzene produced for each equiv diarylbutadiene formed; all diarylbutadiene mixtures are > 90% (*E, E)* isomer and ca.5–9% (*E,Z)* isomer. (c) (^{iPr}PCP)IrHCl, 2 equiv KO^{t}Bu, 654 mM substrate in toluene. (d) (^{iPr}PCP)Ir(C_2H_4), 500 mM substrate in *p*-xylene-d_{10}. (e) Isolated yield. Entries 1, 2, 8, and 10 are yields of purified (*E, E)* isomer only. (f) Yield determined by ^{1}H NMR spectroscopy. (g) Yield determined by GC-MS, dodecane standard. (h) Identified by GC-MS, dodecane standard. (i) Only isomerization to form 1-phenyl-1-propene was observed. (j) 93% yield of 4,6-dimethylindene. (k) Extensive hydrogen/halogen exchange, total yield mixed halogenated coupling products, yield estimated by GC-MS, dodecane standard.

A solution of styrene (0.654 M) in toluene containing 5 mol % (^{iPr}PCP)IrHCl and 2 equivalents KO^{t}Bu (based on Ir) was heated at 150 °C in a sealed ampule, with stirring, for 24 h. It is presumed that the KO^{t}Bu reacts with (^{iPr}PCP)IrHCl to generate the reactive fragment (^{iPr}PCP)Ir.[39] In accord with the hypothesis indicated above, (*E*,*E*)-1,4-diphenyl-1,3-butadiene (**1**) was observed as one of two major organic products as indicated by GC-MS and ^{1}H NMR spectroscopy, in comparison with an authentic sample (Entry 1, Table 3.1). (*E*,*Z*)-1,4-diphenyl-1,3-butadiene was also observed, at a concentration less than ca. 10% of the *E*,*E* isomer, in this reaction as well as in the reactions of the various styrene derivatives that yield dehydrogenative coupling product (discussed below). The other major product was ethylbenzene, resulting from the hydrogenation of styrene (eq 1). Thus the reaction is a disproportionation wherein one equivalent of styrene is hydrogenated to form ethylbenzene for each equivalent of **1** produced. In the absence of (^{iPr}PCP)IrHCl, under otherwise identical conditions (including the presence of KO^{t}Bu), the formation of **1** was not observed.

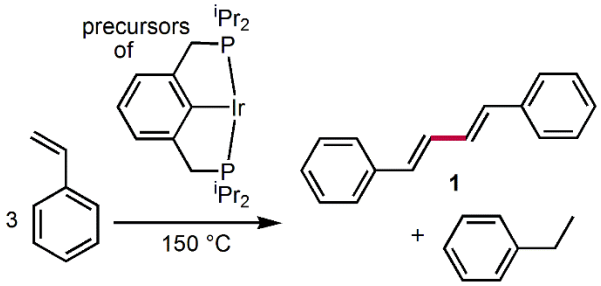

(1)

(^{iPr}PCP)Ir(C_2H_4)[40] was also found to be an effective precatalyst for dehydrogenative coupling, presumably yielding the active (^{iPr}PCP)Ir fragment by dissociation of ethylene without the need for base or other activating agents. Our typical protocol with this precatalyst used 1 mole % (^{iPr}PCP)Ir(C_2H_4) with respect to substrate, in *p*-xylene-d_{10} heated at 150 °C (entry 1, Table 3.1). The (^{iPr}PCP)Ir catalyst was found to tolerate various substituents at the para-position of the aryl ring, including methyl, *t*-butyl, trifluoromethyl, methoxy, and fluorine, (Table 3.1, entries 3, 4, 10, 12, and 13) although conversions were lowered in some cases, perhaps due to C-H activation at the position ortho to the substituent.[41] 2-vinylnaphthalene (entry 8) was also converted to the corresponding dimer. Functional groups at the para position that are known to react with (PCP)Ir derivatives, such as C-Cl bonds (entry 11) or ester groups[42-43], as well as a diphenylphosphino group, prevented catalytic coupling. Vinylferrocene and 2-vinylpyridine also proved incompatible, affording low conversions or complicated product mixtures.

Substitution with a methyl group at only one of the styrene ortho positions did not significantly inhibit the reaction (Table 3.1, entry 2). Substitution at the vinylic positions, however, severely limited coupling. α-Methylstyrene (entry 6) and 1-phenylpropene (β-methylstyrene) afforded no more than trace amounts of coupling product. Allylbenzene also did not produce observable coupling products (entry 7); instead, only isomerization to form 1-phenylpropene was observed.

The use of sacrificial hydrogen acceptors, *t*-butylethylene (TBE), norbornene (NBE), ethylene and propene was investigated as a means of achieving coupling without loss of an equivalent of styrene. The formation of ethylbenzene by-product (Table 3.2) was thereby indeed significantly decreased and the amount of 1,4-diphenylbutadiene produced

was increased (entries 2, 3, 5-8). However, unidentified products, some possibly attributable to cross-coupling between styrene and the acceptor alkene, were also detected, particularly in the case of norbornene.

Table 3. 2. Catalytic dehydrogenative coupling of styrene to form 1,4-diphenylbutadiene in the presence of added hydrogen acceptors at 150 °C.

Entry	Catalyst Precursor (% loading)	Acceptor	time	Conversion (%)[a]	[ethylbenzene]	[diphenyl-butadiene]
1	(^{iPr}PCP)IrHCl (5%)[b]	none	24 h	92	241 mM[d]	168 mM[d]
2	(^{iPr}PCP)IrHCl (5%)[b]	TBE	24 h	80	126 mM[d]	190 mM[d]
3	(^{iPr}PCP)IrHCl (5%)[b]	NBE	24 h	78	54 mM[d]	183 mM[d]
4	(^{iPr}PCP)Ir(C_2H_4) (1%)[c]	none	72 h	96	151 mM[e]	153 mM[e]
5	(^{iPr}PCP)Ir(C_2H_4) (1%)[c]	TBE (500 mM)	72 h	87	57 mM[e]	184 mM[e]
6	(^{iPr}PCP)Ir(C_2H_4) (1%)[c]	NBE (500 mM)	72 h	82	37 mM[e]	181 mM[e]
7	(^{iPr}PCP)Ir(C_2H_4) (1%)[c]	ethylene (1.5 atm)	72 h	79	12 mM[e]	187 mM[e]
8	(^{iPr}PCP)Ir(C_2H_4) (1%)[c]	propene (1.5 atm)	72 h	85	40 mM[e]	187 mM[e]

(a) Percent disappearance of substrate. (b) (^{iPr}PCP)IrHCl, 2 equiv KO^{t}Bu, 654 mM styrene in toluene. (c) (^{iPr}PCP)Ir(C_2H_4), 500 mM styrene in *p*-xylene-d_{10}. (d) Determined by GC-MS, dodecane standard. (e) Determined by ^{1}H NMR spectroscopy.

The formation of almost exclusively the (*E*,*E*)-stereoisomer of 1,4-diphenyl-1,3-butadiene is noteworthy. GC-MS revealed that an additional species with the same mass and very similar GC retention time as the major (*E*,*E*) product, presumably the (*E*,*Z*) isomer, was present in all reaction samples in low concentration (ca. 7% of the (*E*,*E*) isomer concentration).

We considered the possibility that that the (*E*,*Z*) isomer was actually a major kinetic product but underwent isomerization to the more thermodynamically stable (*E*,*E*) isomer. To assess this possibility, a mixture of (*E*,*E*) and (*E*,*Z*)-diphenylbutadiene (approximately 40:60) was independently generated[44] and was then used to prepare a toluene solution 0.2 M in total 1,4-diphenyl-1,3-butadienes. When samples of this solution were heated at 150 °C for 24 hours in the presence of KO^{t}Bu/(^{iPr}PCP)IrHCl, almost all (*E*,*Z*) isomer was converted to the (*E*,*E*) isomer, along with some formation of diphenylbutene and diphenylbutane (see SI). In the absence of (^{iPr}PCP)IrHCl, under otherwise identical conditions, no isomerization was observed. Thus the observation of predominantly (*E*,*E*) product in the coupling reaction does not indicate that this isomer is the major kinetic product.

Dehydrogenation of (^{iPr}PCP)IrH$_4$ with TBE in toluene solution at room temperature, followed by addition of styrene gives nearly quantitative conversion to a single product with a chemical shift of δ 45.7 ppm in the ^{31}P NMR spectrum (see SI); this is also the major signal observed at early times in the ^{31}P NMR spectrum during styrene coupling catalyzed by (^{iPr}PCP)Ir(C_2H_4). Removal of volatiles by vacuum and subsequent crystallization from pentane at -17 °C provided crystals suitable for X-ray diffraction, which allowed assignment as the styrene π-adduct (^{iPr}PCP)Ir(η^2-CH_2=CHC_6H_5) (**2**), shown in Figure 3.1a (Scheme 3.3).

Scheme 3. 3. Reactions of (^{iPr}PCP)Ir with styrenes

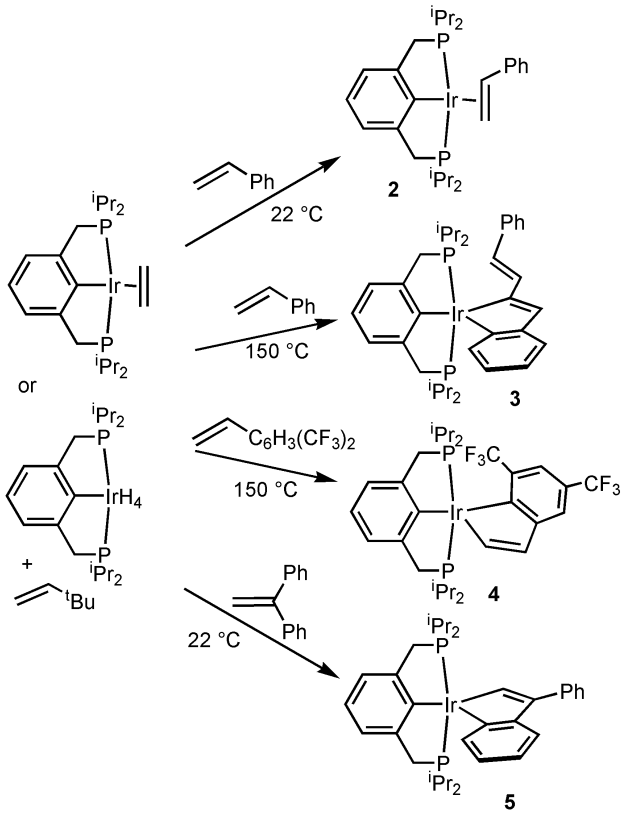

Figure 3. 1. ORTEP representations of complex 2 and 3

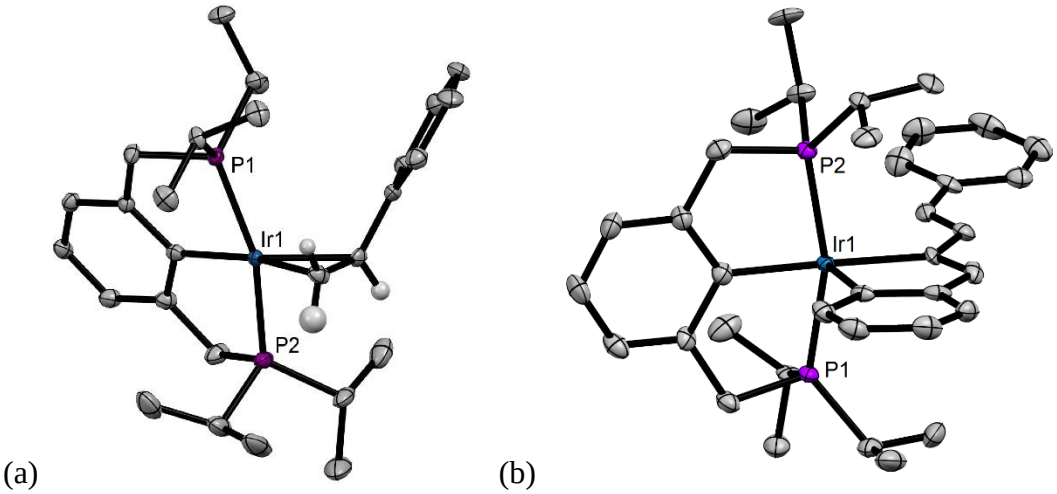

(a) (b)

ORTEP representations (50% probability ellipsoids) of (a) (^{iPr}PCP)Ir(η^2-styrene) (2) and (b) metalloindene complex 3. (Hydrogen atoms omitted for clarity except vinylic H atoms of styrene in 2.)

After 20 h at 150 °C, ^{1}H NMR and ^{31}P NMR spectroscopy of a toluene solution of (^{iPr}PCP)Ir(C_2H_4) and styrene revealed that the major iridium-containing species present was a complex with C_s symmetry (equivalent P nuclei and four sets of inequivalent *i*-Pr methyl groups). The ^{1}H NMR spectrum was consistent with that expected for the metalloindene complex **3** (Scheme 3.3, see SI) presumably formed by addition of *β*-vinyl and ortho aryl C-H bonds of **1** to an (^{iPr}PCP)Ir fragment. Crystals were obtained from a reaction solution, and X-ray diffraction confirmed this assignment (Figure 3.1b). Under the same conditions, a toluene solution of diphenylbutadiene **1**, (^{iPr}PCP)Ir(C_2H_4), and TBE gave the same product (**3**), as indicated by ^{1}H NMR and ^{31}P NMR. In addition to metalloindene **3**, two other (^{iPr}PCP)Ir metalloindenes, obtained from reactions of substituted styrenes with precursors of the (^{iPr}PCP)Ir fragment, have been characterized. The reaction of (^{iPr}PCP)Ir(C_2H_4) with 3,5-bis-trifluoromethylstyrene at 150 °C afforded the corresponding metalloindene, **4** (Scheme 3.3). Crystals were obtained by recrystallization in hexane at -40 °C, and the structure (of what appears to be the *n*-hexane solvate) was obtained by X-ray diffraction (Figure 3.2a). It has previously been reported that the presence of an ortho-trifluoromethyl group greatly stabilizes (PCP)Ir(aryl)H[41, 45]; the apparently greater stability of **4** as compared with its unsubstituted analogue presumably derives from the same or closely related factors. In addition, dehydrogenation of (^{iPr}PCP)IrH_4 with TBE followed by addition of 1,1'-diphenylethylene in toluene (see SI) also affords a stable metalloindene (**5**) as determined by ^{1}H and ^{31}P NMR as well as single crystal X-ray diffraction (Figure 3.2b, Scheme 3.3). In contrast to **4**, formation of **5** does not require heating, perhaps because the very crowded styrene derivative 1,1'-diphenylethylene does not allow formation of a relatively stable *π*-adduct.

Figure 3. 2. ORTEP representations of complex 4 and 5

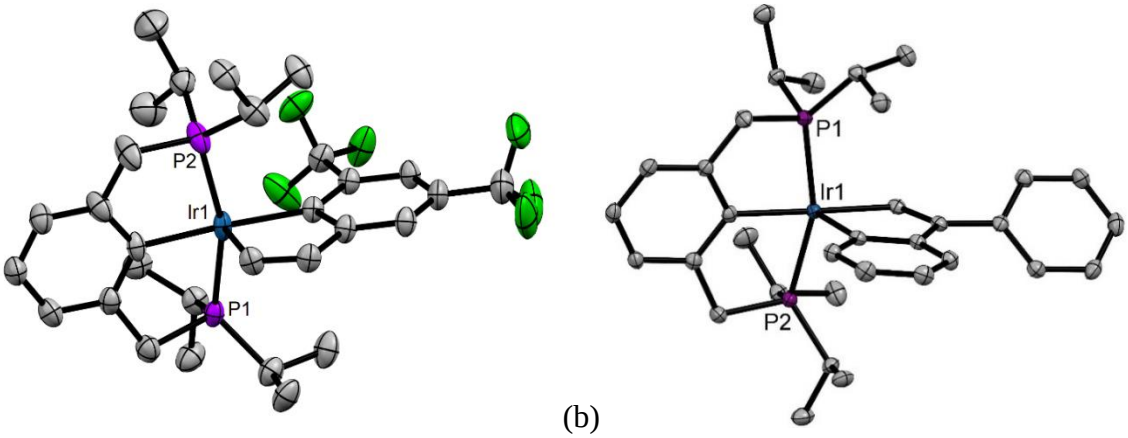

(a) (b)

ORTEP representations (50% probability ellipsoids) of metalloindene complex 4 (a) and 5 (b).

Complex **3** (along with complex **2**) is a major species present in solution even after only 1 h of thermolysis, at which time less than 50% of the styrene has undergone conversion to **1**. It may seem surprising that the parent (unsubstituted) (^{iPr}PCP)Ir metalloindene, **6**, is not observed under the same conditions. The results of DFT calculations (discussed in full in Section 3, below), however, explain the failure to observe **6** under the same conditions that allow observation of **3**. Formation of **3**, from **1** and (^{iPr}PCP)Ir, is calculated to be 2.9 kcal/mol more favorable than formation of **6** from styrene and (^{iPr}PCP)Ir. This corresponds to an equilibrium value of >30 for eq 2, suggesting that **6** would not be observable in the presence of a significant concentration of **1** (assuming that the formation of **3** from the reaction of **1** is kinetically facile, even if it is less rapid than formation of **6** from reaction of styrene). Moreover, since complexes **2** and **3** are present in comparable concentrations in the presence of **1**, this suggests, in accord with observation, that before significant concentrations of **1** (or **3**) are formed, the only major species present at very early reaction times would be the π-styrene complex **2**.

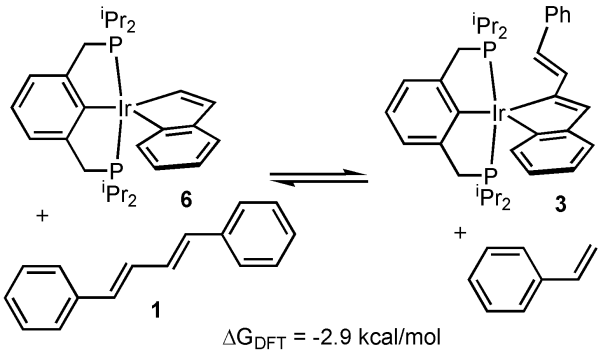

(2)

3.2.2. Catalytic intramolecular coupling by (^{iPr}PCP)Ir.

Surprisingly, in contrast with the fairly efficient coupling observed with *p*-substituted or mono-ortho substituted substrates, no diarylbutadiene coupling product was observed from the reaction of 2,4,6-trimethylstyrene. Instead, however, intramolecular C(sp^3)-C(sp^2) coupling was achieved, with >80% yield (87% total conversion) giving two major dehydrogenative coupling products, 4,6-dimethylindene and 5,7-dimethylindene, as well as 2-ethylmesitylene (Scheme 3.4). The identity of the dimethylindenes was determined by ^{1}H and ^{13}C NMR spectroscopy and GC-MS. Further support for their assignment was obtained by Pd-catalyzed hydrogenation of the mixture which gave a single major product, 4, 6-dimethylindane, also assigned on the basis of ^{1}H and ^{13}C NMR and GC-MS (see SI).

Scheme 3. 4. Intramolecular C(sp^3)-C(sp^2) dehydrogenative coupling catalyzed by (^{iPr}PCP)Ir

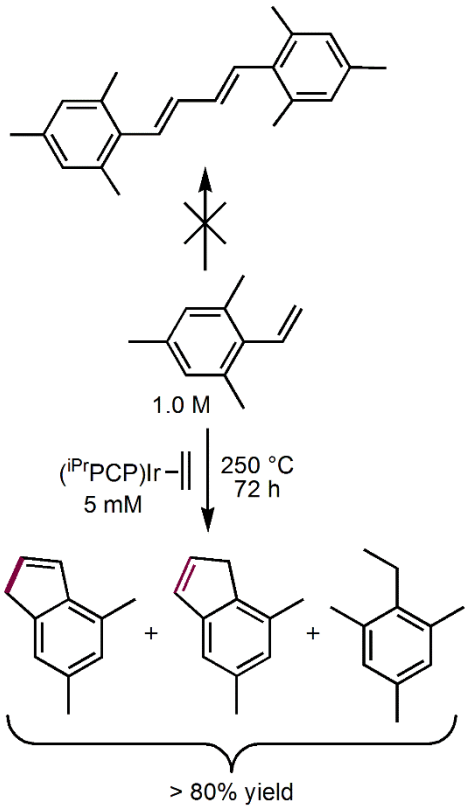

3.2.3. Stoichiometric reactions of (tBuPCP)Ir with styrenes

In contrast to the ^{iPr}PCP analogs, no catalysis was obtained with the more crowded pincer-iridium species (^{tBu}PCP)Ir. The reaction of (^{tBu}PCP)IrH$_4$ (20 mM) with styrene (120 mM) at 150 °C for 6 h instead resulted in the formation of a metalloindene species, **7**, in 80% yield (by ^{1}H NMR), which may be described as the product of dehydrogenative coupling of a phosphino-*t*-butyl methyl group and a molecule of styrene, plus C-H addition of the styrene *β*-vinyl and ortho-aryl C-H bonds (eq 3). Crystals were obtained by recrystallization in hexane at -40°C, and X-ray diffraction revealed the structure shown in Figure 3.3.

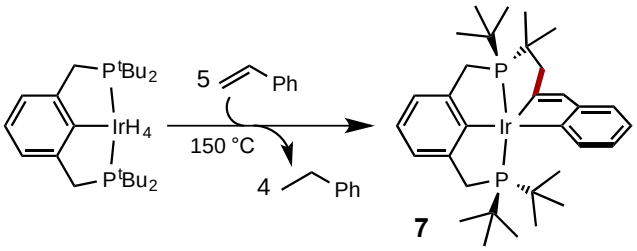

(3)

Figure 3. 3. ORTEP representation of complex 7

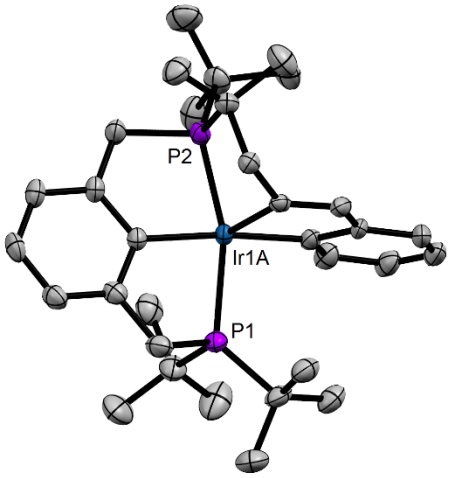

ORTEP representation of complex 7 with 50% probability ellipsoids

With either *α*-methylstyrene or β-methylstyrene, the reaction of (^{tBu}PCP)IrH$_4$ at 150 °C gave the simple metalloindene complexes (eq 4, complexes **8** and **9**, respectively) resulting from C-H addition of the *β*-vinyl and ortho-aryl C-H bonds of the respective uncoupled styrene (and presumably hydrogenation of another molecule of styrene). The iridium-containing products were identified by ^{1}H and ^{31}P NMR spectroscopy of the reaction solutions, as well as single-crystal X-ray diffraction (Figure 3.4).

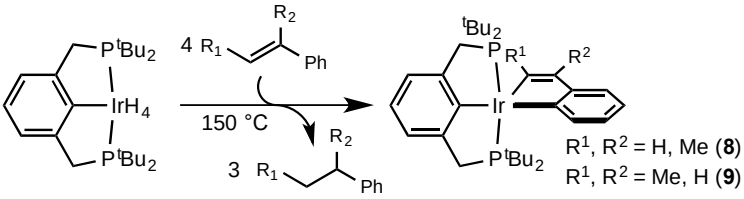

(4)

Figure 3. 4. ORTEP representation of complex 8 and 9

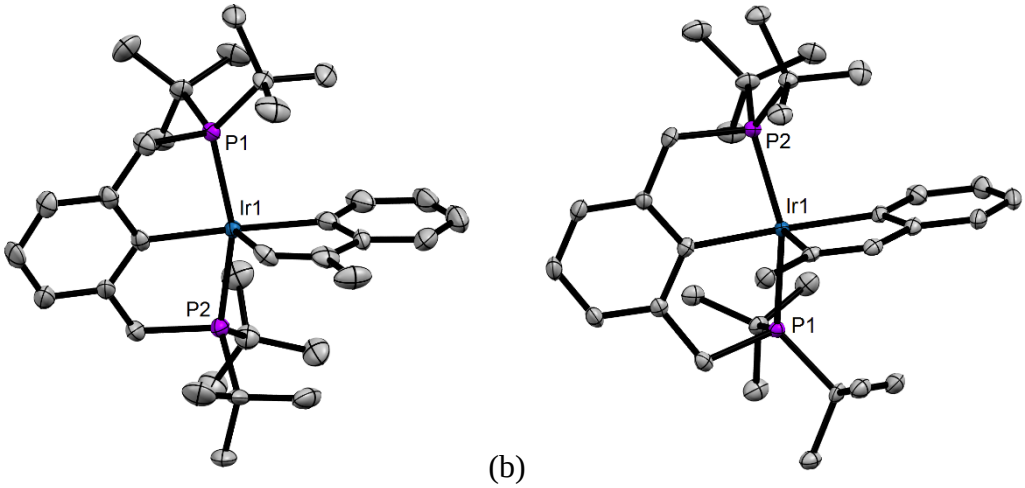

(a) (b)

ORTEP representation of products of reaction of (^{iPr}PCP)Ir(C_2H_4) with (a) *α*-methylstyrene, 8, and (b) *β*-methylstyrene, 9 (50% probability ellipsoids).

Thus, it is seen that both (^{iPr}PCP)Ir and (^{tBu}PCP)Ir fragments have a strong tendency to react with vinylarenes to form metalloindenes (complexes **3**, **4**, **5**, **7**, **8**, **9**). It appears likely that the greater steric bulk of the *t*-Bu groups mitigates the reactivity of the (^{tBu}PCP) complexes, facilitating their isolation.

3.3. DFT calculations and mechanistic discussion

3.3.1. Double bond insertion mechanisms

A priori, several possible mechanisms for the tail-to-tail coupling reactions (Scheme 3.5) can be envisaged. In general, olefin dimerization probably proceeds most commonly via insertion of an olefin into a metal-carbon bond. The 14e fragments (^{R}PCP)Ir have been well established to oxidatively add C-H bonds, including the addition of a *trans*-*β*-C-H bond of a terminal olefin[35] to give observable 16e products. Addition of the styrene *trans*-*β*-C-H bond, followed by 2,1-insertion of a second styrene molecule into the resulting Ir-C bond, and then *β*-H elimination (which is known to be facile for (^{iPr}PCP)Ir(alkyl)H)

would give the observed diphenylbutadiene (Scheme 3.5). Insertion of double bonds into Ir-C bonds, and metal-vinyl bonds more generally, however, is relatively rare.

Scheme 3. 5. Dehydrogenative styrene coupling via C-H addition and insertion into the resulting Ir-C bond

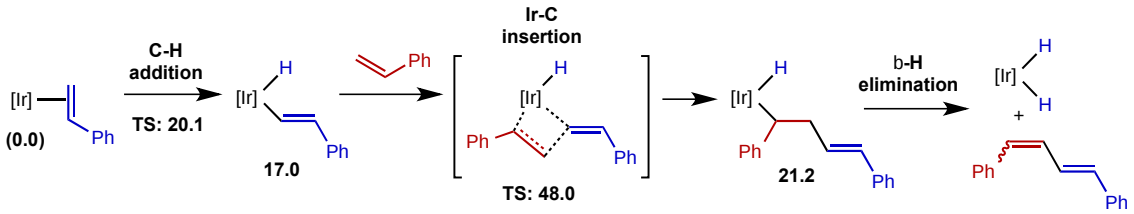

Dehydrogenative styrene coupling via C-H addition and insertion into the resulting Ir-C bond; calculated pathway with free energies (150 °C; kcal/mol)

DFT calculations (see Computational Section for details) indicate that the kinetics of styrene β-vinylic C-H addition to (^{iPr}PCP)Ir are facile (in accord with experimental results with C-H addition of TBE to (^{tBu}PCP)Ir[35]), giving an oxidative addition product calculated to be 17.0 kcal/mol higher in free energy than the isomeric styrene π-adduct. Following C-H addition, however, coordination of a second molecule of styrene is endoergic by 0.8 kcal mol and insertion of its double bond into the Ir-vinyl bond is calculated to have a very high barrier, $\Delta G^{\neq}$ = 30.2 kcal/mol. The computed TS for insertion is thus 48.0 kcal/mol above the resting state free energy, arguing against the likelihood of such a mechanism.

Insertion of olefins into Ir-H bonds is much more facile than insertion into Ir-C bonds. Styrene insertion into the Ir-H bond of the C-H addition product (^{iPr}PCP)Ir(H)(CH=CHPh) yields (^{iPr}PCP)Ir(CH_2CH_2Ph)(CH=CHPh) (Scheme 3.6); the styrene insertion TS and product are calculated to be 31.5 kcal/mol and 26.0 kcal/mol above the π-styrene complex, respectively, presenting a substantial but not prohibitively high barrier. However, C-C elimination from this complex has a calculated barrier of $\Delta G^{\ddagger}$

= 24.3 kcal/mol and thus a prohibitively high-energy TS, 50.3 kcal/mol above the resting state. (Moreover, the monoene resulting from such a reaction would need to undergo subsequent dehydrogenation to give the observed diphenylbutadiene.) Our electronic structure calculations therefore argue strongly against this pathway.

Scheme 3. 6. Dehydrogenative styrene coupling via C-H addition and insertion into Ir-H bond

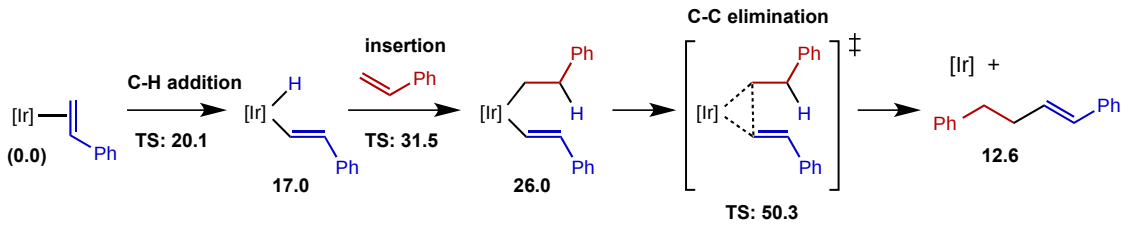

Dehydrogenative styrene coupling via C-H addition and insertion into Ir-H bond; calculated pathway with free energies (150 °C; kcal/mol)

3.3.2. A "direct" coupling mechanism

We have previously demonstrated that 16e Ir(III) complexes such as (^{R}PCP)IrH$_2$[46] and (^{R}PCP)Ir(CCPh)(H)[47] will undergo addition of C-H bonds. Further, we have shown that C-C bond reductive elimination from complexes (PCP)IrRR' can be relatively favorable for C(sp^2)-bound R groups.[34, 47] Thus, there is good precedent for a mechanism involving initial oxidative addition of a styrene *trans-β* vinylic C-H bond to (^{iPr}PCP)Ir, followed by addition of the same bond of a second styrene molecule to the resulting Ir(III) center; subsequent loss of H_2 and then C-C elimination would afford the coupled product (Figure 3.5). We will refer to this as the "direct" coupling pathway (to distinguish it from a more indirect pathway, proposed later, which also involves vinylic C-H additions to Ir(I) and Ir(III), and subsequent loss of H_2 followed by C-C elimination).

Following the same C-H addition to (^{iPr}PCP)Ir(I) that was considered in the pathways discussed above, C-H addition of a second molecule of styrene is calculated to

proceed via a TS that is clearly Ir(V) in character (Figure 3.5); the Ir-H distances (1.62 Å and 1.66 Å) are typical of stable Ir hydrides, the C-H bond is essentially fully cleaved (d_{C-H} = 1.59 Å), and the H-H distance (1.68 Å) is greater than that of even an elongated dihydrogen complex.[48] This second C-H addition step is calculated to have a free energy barrier of $\Delta G^{\ddagger}$ = 25.8 kcal/mol, arising from a very small activation enthalpy, $\Delta H^{\ddagger}$ = 5.1 kcal/mol, and a very unfavorable activation entropy, $\Delta S^{\ddagger}$ = -49 eu ($-T\Delta S^{\ddagger}$ = 20.7 kcal/mol). Although the crowded TS has largely Ir(V) character, it does not lead to an Ir(V) intermediate, but rather to an Ir(III) dihydrogen complex (**10•H₂**, d_{H-H} = 0.85 Å). Periana has termed processes that proceed through such TSs without a net change in oxidation state as Oxidative Hydrogen Migrations.[49-50]

Figure 3. 5. Dehydrogenative styrene coupling via consecutive vinylic C-H additions followed by loss of H_2, olefin hydrogenation and C-C elimination

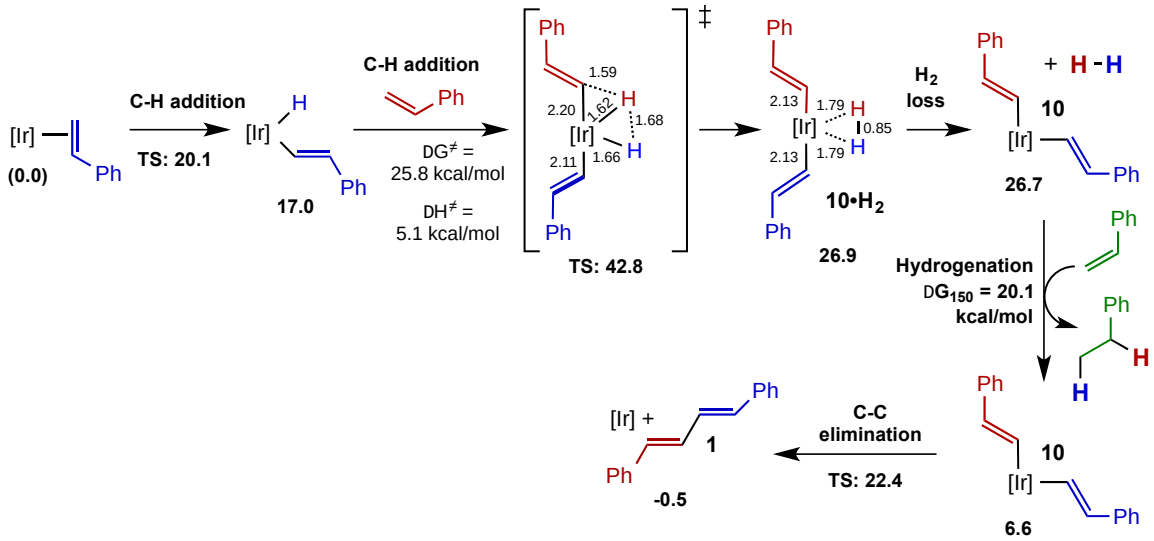

Calculated pathway with free energies (150 °C; kcal/mol) and selected internuclear distances (Å) indicated.

The next step in this pathway would be loss of H_2 from **10•H₂** to afford products (^{iPr}PCP)Ir(CH=CHPh)$_2$ (**10**) and H_2, which have a free energy 26.7 kcal/mol above the π-

styrene complex. Hydrogenation of another molecule of styrene (indicated in green in Figure 3.5) is likely to be very rapid on the overall time-scale of this reaction, and certainly more rapid than the back reaction with **10** which would be present in an extremely small concentration. The free energy of the resulting products, (^{iPr}PCP)Ir(CH=CHPh)$_2$ (**10**) plus PhEt, is 6.6 kcal/mol above that of complex **2** plus two molecules of free styrene. C-C reductive elimination from **10** would afford the observed coupling product, *E,E*-1,4-diphenylbutadiene.

Thus, the calculated overall barrier to the pathway of Figure 3.5 is 42.8 kcal/mol, assuming that C-H addition of the second styrene molecule is rate-determining. Although this is less than the barriers to the insertion mechanisms discussed above, it is significantly greater than the barrier that would be inferred from the very approximately determined rate of styrene coupling (ca. 3 x 10^{-4} s^{-1}), $\Delta G^{\ddagger}$ ~ 32 kcal/mol.

Perhaps arguing against the mechanism of Figure 3.5 even more strongly than the calculated barrier is a combination of experimental results and DFT calculations with 2,4,6-trimethylstyrene as the substrate. As discussed in the experimental section above, the presence of *o*-methyl groups completely inhibited the tail-to-tail dimerization reaction. Based only on cursory consideration of the structures shown in Figure 3.5, such a result would probably not be expected. Indeed, the DFT calculations predict that the overall barrier to tail-to-tail dimerization via the mechanism of Figure 3.5 is *lower* for 2,6-dimethylstyrene by 4.4 kcal/mol than for styrene (this is attributable to the lower binding energy of the π-olefin complex of the sterically hindered olefin in the π-olefin complex, not to any advantage conferred by the methyl groups to the TS.

3.3.3. Metalloindene mechanism

Figure 3.6 shows our proposed pathway for the tail-to-tail coupling of styrene. Like the coupling mechanisms considered above (Schemes 3.5 and 3.6, Figure 3.5), the proposed initial in-cycle step is addition of a styrene *β*-vinyl C-H bond but in this case it is addition of the *β*-C-H bond that is *cis* to the phenyl group. This is kinetically and thermodynamically less favorable than addition trans to phenyl ($\Delta\Delta G^{\ddagger}$ = 4.4 kcal/mol and $\Delta\Delta G$ = 0.5 kcal/mol, respectively) but the overall predicted barrier ($\Delta G^{\ddagger}$ = 24.5 kcal/mol) is certainly not prohibitive. Subsequent intramolecular addition of a styrenyl *o*-C-H bond is calculated to have a low barrier: $\Delta G^{\ddagger}$ = 8.9 kcal/mol and $\Delta H^{\ddagger}$ = 7.8 kcal/mol. As in the case of the vinylic C-H bond addition to (^{iPr}PCP)Ir(CH=CHPh)(H) (Figure 3.5), the C-H addition to this Ir(III) center proceeds via a TS that is essentially Ir(V) in character, to give an Ir(III) metalloindene dihydrogen complex, **6•H$_2$**.

Figure 3. 6. Calculated free energies (kcal/mol) for the tail-to-tail coupling of styrene via a cyclometalation (metalloindene) mechanism.

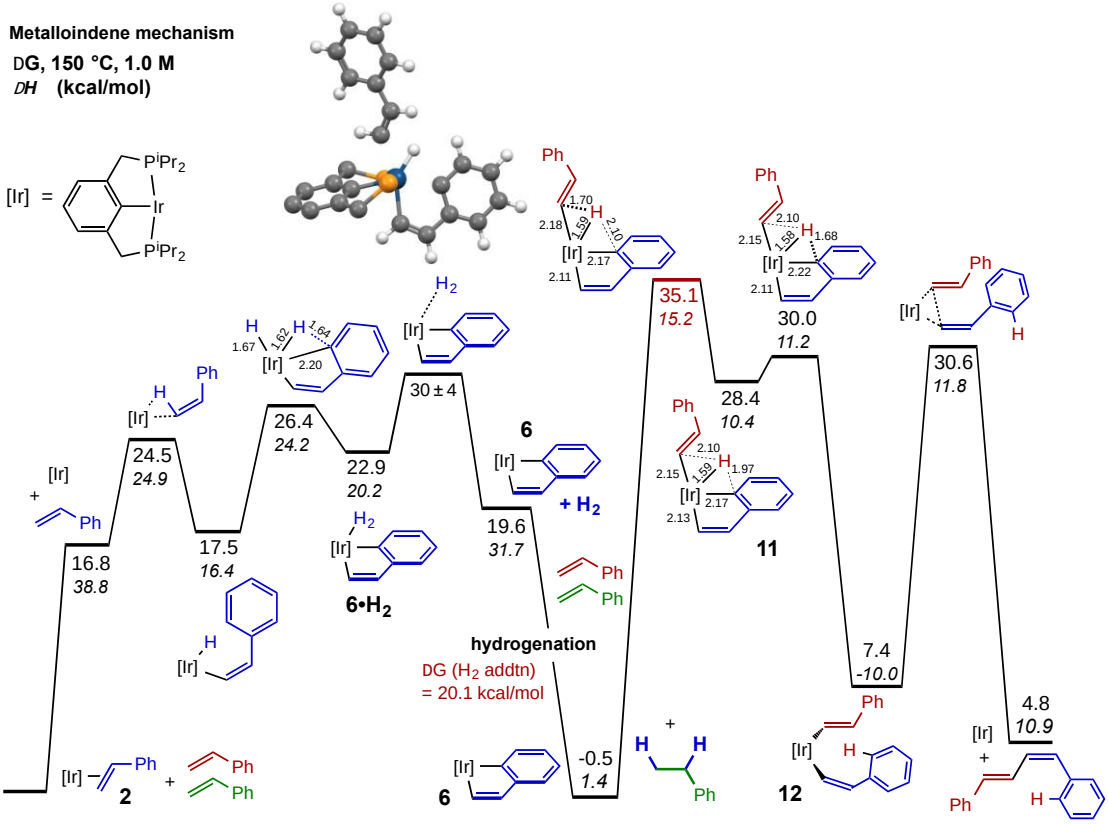

Ball-and-stick model of calculated highest-energy TS shown (^{i}Pr groups and pincer-backbone H atoms omitted for clarity). Energy values (kcal/mol) are referenced to T = 423 K (150 °C) and concentrations of 1 M for each species participating in the reaction. Selected internuclear distances (Å) are indicated.

The facile cyclometalation to give metalloindene dihydrogen complex **6•H$_2$** is followed by loss of H_2. This reaction appears to have no barrier on the potential energy surface in the reverse direction, and we were unable to locate a true TS (first-order saddle point on the potential energy surface). If we assume that the enthalpic barrier to H_2 loss is at least equal to the (thermodynamic) enthalpy of H_2 loss, which is 11.5 kcal/mol in the present case, while the entropy of activation is ≥ 0 but no more than ca. 20 eu, then the

highest point on the free energy surface for H_2 loss from the metalloindene dihydride is ca. 26 - 34 kcal/mol above the π-styrene complex.

The H_2 lost from **6•H₂** is presumably consumed relatively quickly in the hydrogenation of styrene (or other olefin if added). The resulting products, metalloindene **6** plus ethylbenzene, are calculated to have a free energy that is 0.5 kcal below that of the □-styrene complex (**2**) plus an additional styrene molecule (indicated in green in Figure 3.6). **6** then undergoes addition of the *trans-β* C-H bond of another molecule of styrene. This reaction is calculated to proceed via a TS with a free energy that is 35.1 kcal/mol above the π-styrene complex, and 35.6 kcal/mol above **6**, leading to the Ir(V) metalloindene complex, **11**. Aryl-H reductive elimination from this species has an extremely low kinetic barrier ($\Delta G^{\ddagger}$ = 1.6 kcal/mol and $\Delta H^{\ddagger}$ = 0.8 kcal/mol), leading to [Ir](*cis*-CH=CHPh)(*trans*-CH=CHPh), **12**.

The bis(vinyl) complex (^{iPr}PCP)Ir(*cis*-CH=CHPh)(*trans*-CH=CHPh) (**12**, Figure 3.6) is only slightly higher in free energy than the *trans,trans* isomer (**10**, Figure 3.5). More significantly, the calculated barrier to C-C elimination from **12** is $\Delta G^{\ddagger}$ = 23.2 kcal/mol, as compared with □$G^{\ddagger}$ = 15.8 kcal/mol for **10**. Nevertheless, this TS is calculated to be 4.5 kcal/mol lower in free energy than the TS for C-H addition to the metalloindene to give **11**, which necessarily gives rise to a cis-vinyl unit and ultimately the E,Z isomeric product. As noted above, control experiments show that cis-trans isomerization of this species to give the observed E,E isomer is rapid relative to the overall reaction.

The overall barrier calculated for the metalloindene mechanism of Figure 3.6 (35.6 kcal/mol) is thus significantly lower than that for the “direct” addition mechanism of Figure

3.5 (42.8 kcal/mol) and in good agreement with the approximate experimentally determined barrier, $\Delta G^{\ddagger} \sim 32$ kcal/mol.

Additional calculations in which the effects of bulk solvation were included (CPCM continuum dielectric model, toluene model solvent) anticipate very small changes relative to the idealized gas-phase energy profile presented in Figure 3.6 (cf. Table 3.57 in Supporting Information). Computed changes in TS free energies from solvation in toluene are all less than 2 kcal/mol and, in particular, the barrier for the rate determining step of the metalloindene mechanism, namely addition of the *trans-β* C-H bond of a styrene molecule to **6**, is predicted to increase modestly by just 0.9 kcal/mol.

The energy profile of the proposed mechanism of Figure 3.6 suggests that addition of the phenyl *ortho*-C-H bond leads reversibly to the metalloindene dihydrogen complex **6•H$_2$**. Assuming that the dihydrogen ligand can undergo rotation, this process would lead to H/D exchange. When the reaction is conducted with $C_6H_5C_2D_3$ we see extensive H/D scrambling at all sites on styrene, including the styrene *o*-C-H bond. Exchange at the meta and para positions is presumably the result of intermolecular H-D scrambling. However, we have previously found that any substituent on an arene ring, even a methyl group, strongly inhibits C-H addition;[35, 42, 51] the failure of the vinyl group to block H/D exchange at the *o*-C-H position is consistent with the reversible cyclometallation implied by Figure 3.6.

3.3.4. Intramolecular coupling

Consistent with the proposed mechanism of Figure 3.6, tail-to-tail coupling is not observed for 2,4,6-trimethylstyrene, which cannot form a metalloindene intermediate as it lacks an ortho-C-H bond. Instead, the conversion of 2,4,6-trimethylstyrene to dimethylindenes occurs, representing an unusual example of dehydrogenative C(sp^3)-C(sp^2) coupling with an unfunctionalized hydrocarbon. For this reaction, a "direct" C-C coupling pathway is calculated (Figure 3.7). As in the case of the metalloindene mechanism (Figure 3.6), the coupling pathway begins with C-H addition to give the cis-2-arylvinyl iridium hydride (Figure 3.7). The bulkiness of the trimethylphenyl group slightly raises the barrier to vinylic C-H addition to the 14e (^{iPr}PCP)Ir fragment, but it raises the relative energy of the π-olefin complex even more. Cis-β-vinyl C-H addition of 2,4,6-trimethylstyrene is thus kinetically, as well as thermodynamically, slightly more favorable, relative to the respective π-complex, than is the case for the parent styrene (cf. Figure 3.6; $\Delta\Delta G^{\ddagger}$ = -2.1 kcal/mol and $\Delta\Delta G$ = -1.5 kcal/mol).

Figure 3. 7. Calculated free energies and enthalpies (below, italic) for the (^{iPr}PCP)Ir-catalyzed conversion of 2,4,6-trimethylstyrene to 4,6-dimethylindene at 150 °C.

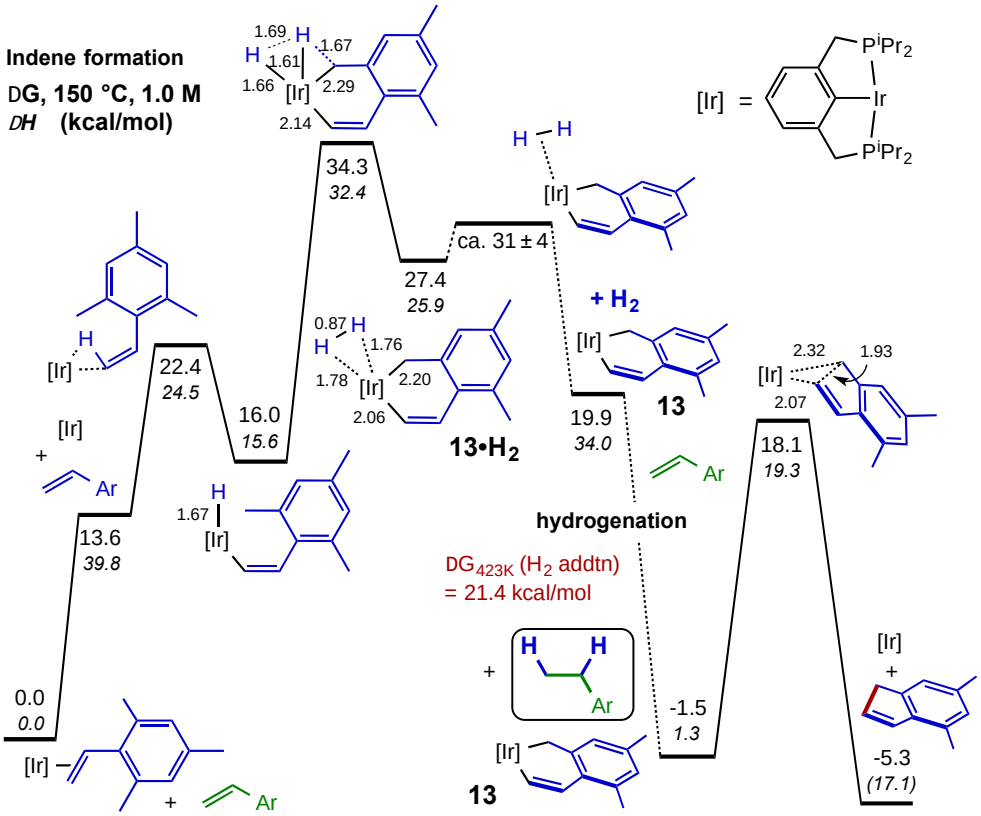

Energy values (kcal/mol) are referenced to T = 423 K (150 °C) and concentrations of 1 M for each species participating in the reaction. Selected internuclear distances (Å) are indicated.

Intramolecular addition of an ortho-methyl C-H bond then proceeds through a TS with significant Ir(V) character (Figure 3.7). The length of the newly formed Ir-H bond in the TS (1.61 Å) is actually slightly less than that of the Ir-H bond in the preceding intermediate or that same bond in the TS (1.67 Å and 1.66 Å respectively). The incipient Ir-C bond is nearly, but not quite fully, formed ($d_{C\text{-}Ir}$ = 2.29 Å) and the C-H bond is fully or nearly fully cleaved ($d_{C\text{-}H}$ = 1.67 Å). This addition of the methyl C-H bond (Figure 3.7) has a barrier $\Delta G^{\ddagger}$ = 18.3 kcal/mol resulting in a TS with free energy 34.3 kcal/mol above

the π-complex resting state. The product of this benzylic C-H activation is an Ir(III) dihydrogen complex (d_{H-H} = 0.87 Å), **13•H₂**.

The TS for loss of H_2 from **13•H₂** could not be located but, again, in the reverse direction, addition of H_2 to **13** appears to be barrierless on the potential energy surface. This implies a TS enthalpy equal to that of the product and, again assuming that $\Delta S^{\ddagger} = 0$ to 20 eu, a free energy of the TS approximately 27-35 kcal/mol above the resting state. Following hydrogenation of an additional molecule of styrene (ΔG = -21.4 kcal/mol), C-C reductive elimination from **13** is relatively facile ($\Delta G^{\ddagger}$ = 19.6 kcal/mol), releasing indene and regenerating the 14e (^{iPr}PCP)Ir intermediate.

Hence, the overall barrier to the intramolecular dehydrogenative C(sp^3)-C(sp^2) coupling is calculated to be 34.3 kcal/mol with C-H addition to give **13•H₂** as the rate-determining step (Figure 3.7). Loss of dihydrogen from **13•H₂** appears to have a lower calculated barrier, although we cannot rule out that step as rate-determining, particularly in view of the error limits of the calculations. In either case, the calculations seem to be in very good agreement with the experimental rate of the cyclization which implies a barrier of ca. 32 kcal/mol.

3.3.5. Hetero-coupling with pentafluorophenylethylene

Like 2,4,6-trimethylstyrene, pentafluorophenylethylene (F_5-styrene) cannot undergo dehydrogenative coupling via the proposed metalloindene mechanism; accordingly, F_5-styrene is found to undergo no detectable homocoupling. However, addition of the F_5-styrene β-vinyl C-H bond to the (unsubstituted) metalloindene complex **6** is calculated to be *more* favorable (by 1.4 kcal/mol) than addition of the corresponding styrene bond which is the rate-determining step proposed for the mechanism of Figure 3.6.

Accordingly, a *p*-xylene-d_{10} solution with (^{iPr}PCP)Ir(C_2H_4) catalyst (5 mM) and roughly equal concentrations of F_5-styrene (270 mM) and styrene (230 mM) reveals high selectivity for dehydrogenative heterocoupled product, $C_6F_5CH{=}CHCH{=}CHPh$, **1-F$_5$**. Over the course of the first five hours at 150 °C, with 46% of total styrenes consumed, the ratio of **1-F$_5$** : **1** remains constant at ca. 11:1 (Figure 3.8), implying that $\Delta G^{\ddagger}$ is 1.9 kcal/mol lower for C-H addition of F_5-styrene than for styrene, in excellent agreement with the calculated value of 1.4 kcal/mol. It should also be noted that F_5-styrene is preferentially hydrogenated vs. styrene (ca. 4.5:1). Hence, the ratio of F_5-styrene:styrene decreases during the course of the reaction and styrene is present in greater concentration after 4 hours, although the rate of formation of heterocoupled product continues to greatly exceed that of homocoupled product. After 40 hours, quantitative conversion to dimer and hydrogenated products is observed; the observed (^{1}H NMR) concentrations of heterodimer and styrene homodimer are 161 mM and 19 mM respectively, while concentrations of $C_6F_5CH_2CH_3$ and ethylbenzene are 124 mM and 28 mM respectively.

Figure 3. 8. Products of (^{iPr}PCP)Ir-catalyzed dehydrogenative coupling of styrene and F$_5$-styrene (150 °C).

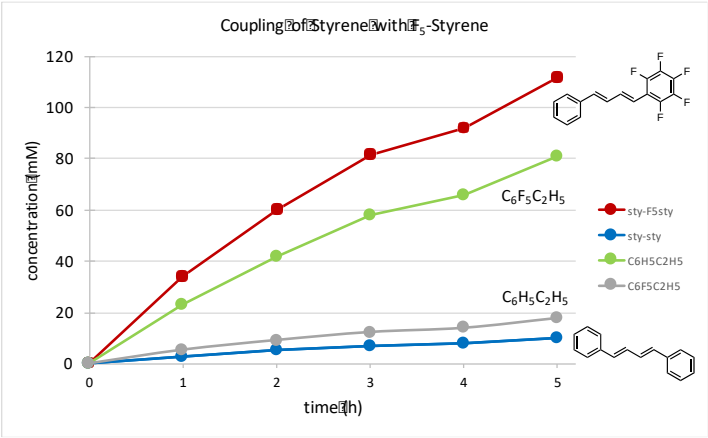

The failure of F_5-styrene to undergo homodimerization, even under conditions where styrene homodimerization and cross-coupling occurs, argues strongly against the "direct" addition mechanism (Figure 3.5). With a common resting state (as is necessarily the case in a single-solution competition experiment of the type described above) the rate-determining step for homocoupling of F_5-styrene via the “direct addition” mechanism is calculated to be 2.8 kcal/mol lower in free energy than that for styrene (Figure 3.9). (Thus it is 40.0 kcal/mol above the styrene π-complex plus two molecules of free F_5-styrene, but the nature of the actual resting state affects only this absolute value and not the relevant differences). This would imply that the rate of F_5-styrene homocoupling would be ca. 30-fold greater than that of styrene homocoupling, in direct contradiction with the failure to observe *any* F_5-styrene homocoupling product. The TS for F_5-styrene homocoupling in the "direct" mechanism is also calculated to be slightly lower in free energy than those for heterocoupling (40.6 kcal/mol above the styrene π-complex for styrene C-H addition to the C-H adduct of F_5-styrene, and 41.4 kcal/mol for the converse heterocoupling TS) again in contradiction with experimental results. Since the expected errors in computed free energies for such isodesmic comparisons are quite small, the implication that the “direct addition” mechanism would strongly favor formation of the F_5-styrene homocoupling product (which is experimentally not observed) argues strongly against this being the operative mechanism.

Figure 3. 9. Schematic diagrams of the TSs for the calculated rate-determining step for dehydrogenative coupling, via the "direct mechanism", for homocoupling of styrene

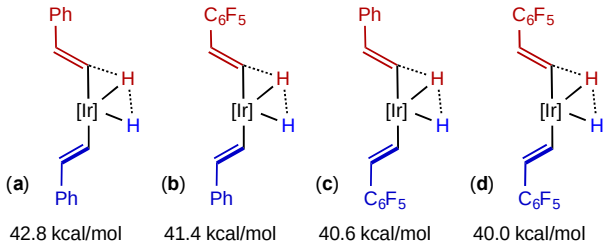

(**a**); heterocoupling of F_5-styrene with styrene (**b**) and (**c**); homocoupling of F_5-styrene (**d**). (Absolute energies are given relative to the non-fluorinated (^{iPr}PCP)Ir(π-styrene) complex plus the corresponding two molecules of styrene. Note that relative energies, which are relevant to the results of a competition experiment, are not affected by the choice of reference state.)

Additionally, the greater rate of hydrogenation of F_5-styrene relative to that of styrene, noted above, suggests that F_5-styrene inserts more favorably into an Ir-H bond. This observation offers an additional argument against the insertion-based mechanisms of Scheme 3.5 (proceeding through insertion into an Ir-C bond) and particularly Scheme 3.6 (insertion into an Ir-H bond). In agreement with this inference, DFT calculations indicate that the TS for the rate-determining step (C-C elimination) for the mechanism of Scheme 3.6 is 7.8 kcal/mol lower in free energy for the homocoupling of F_5-styrene than for styrene, and 2.8 kcal/mol lower than for heterocoupling of F_5-styrene and styrene (Figure 3.10, structures a - c). Likewise, for the mechanism of Scheme 3.5, the TS of the rate-determining step (insertion into the Ir-C bond) is 5.7 kcal/mol lower in free energy for homocoupling of F_5-styrene than for styrene, and 1.9 kcal/mol lower than for heterocoupling (Figure 3.10, structures d - f).

Figure 3. 10. Schematic diagrams of the TSs for the calculated rate-determining step

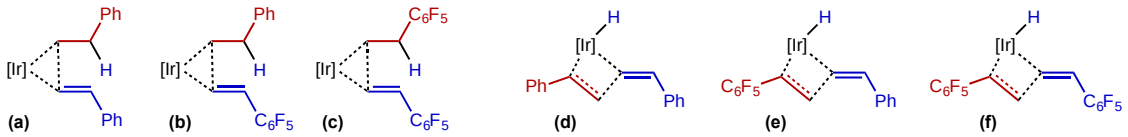

50.3 kcal/mol 45.3 kcal/mol 42.5 kcal/mol 48.0 kcal/mol 44.2 kcal/mol 42.3 kcal/mol

Schematic diagrams of the TSs for the calculated rate-determining step for homocoupling of styrene, heterocoupling of F_5-styrene with styrene, and homocoupling of F_5-styrene, via mechanism of Scheme 3.6 (insertion into Ir-H bond of arylvinyl hydride followed by rate-determining C-C eliminationa, b, and c) and mechanism of Scheme 3.5 (rate-determining insertion into Ir-C bond of arylvinyl hydride; d, e, and f). (Absolute energies are given relative to the non-fluorinated (^{iPr}PCP)Ir(π-styrene) complex plus the corresponding two molecules of styrene; relative energies, which are relevant to the results of a competition experiment, are not affected by the choice of reference state.)

3.4. Summary and conclusions

Dehydrogenative coupling of unactivated C-H bonds (intermolecular vinyl-vinyl, intramolecular vinyl-benzyl) is found to be catalyzed by precursors of the (^{iPr}PCP)Ir fragment. The reactions proceed via C-H activation to (^{iPr}PCP)Ir(I) followed by a second C-H activation by the resulting (^{iPr}PCP)Ir(III) product. The C-H additions to Ir(III) occur via TSs that are strongly Ir(V) in character although the reactions generally do not lead to an Ir(V) product, but rather to the formation of a new Ir(III) dihydrogen complex.

For intermolecular dehydrogenative vinyl-vinyl coupling, addition of a vinylic C-H bond to Ir(I), followed by addition of a second vinylic C-H bond to the resulting Ir(III) vinyl hydride, loss of H_2, and then C-C elimination would comprise what we refer to as a “direct” pathway (Figure 3.5). Instead, however, the Ir(III) vinyl hydride complex undergoes addition of an aryl ring ortho C-H bond to give an Ir(III) metalloindene, **6**, plus H_2 (Figure 3.6). The activation enthalpy of this reaction (7.8 kcal mol) is slightly greater than the intermolecular addition (5.1 kcal/mol), but the entropic penalty is much less. Subsequent, intermolecular, vinyl C-H addition to the Ir(III) metalloindene **6** has a much *greater*

calculated barrier ($\Delta G^{\ddagger}$ = 35.6 kcal/mol) than vinyl C-H addition to the Ir(III) vinyl hydride (25.8 kcal/mol) in the "direct" mechanism. However, the metalloindene pathway is driven by addition of the released dihydrogen to another mol of olefin, prior to the second vinylic C-H addition; this significantly lowers the free energy of the system (by ca. 20 kcal/mol), which would lead to a commensurately much greater concentration of Ir(III) metalloindene **6**, thus favoring occurrence of the subsequent intermolecular reaction. In contrast, in the case of the "direct" mechanism, loss of H_2 and hydrogenation of styrene does not occur until after the entropically unfavorable second addition of a vinyl C-H bond (which is calculated to be rate-determining), and thus cannot provide any driving force.

As we have shown previously, C-C elimination from (pincer)IrRR' complexes can be relatively facile when R and R' are sp^2-C-bound fragments.[34] Accordingly in all mechanisms investigated, C-C elimination is not calculated to be rate-determining.

Although in most of this work the H_2 by-product of the reaction is consumed by an additional molecule of styrene, it is found that other olefins can play the same role as hydrogen-acceptor; this allows, in principle, complete conversion of the styrene to dehydrogenatively coupled dimer. Either with or without added olefin, no conventional oxidizing agent (including acids) is required.

In accord with the proposed metalloindene mechanism, styrenes that lack a C-H bond ortho to the vinyl group are found not to undergo tail-to-tail homocoupling. In contrast, the DFT calculations predict that the ortho-substituents would not adversely affect coupling via the "direct" mechanism. In the case of 2,4,6-trimethylstyrene, the product of vinylic C-H addition to (^{iPr}PCP)Ir(I) undergoes cyclometallation by subsequent C-H addition of an ortho-methyl C-H bond. This reaction is enthalpically much less favorable

than any of the C(sp^2) C-H bond additions considered above but, due to the low entropic penalty, the calculated barrier, although high, is not prohibitive. Subsequent loss of H_2 and then C-C elimination to give indene are calculated to proceed relatively rapidly. The calculated overall barrier, corresponding to the cyclometallation TS, is 34.3 kcal/mol above the π-complex resting state, in good agreement with the observed rates.

The absence of an ortho-C-H bond precludes homocoupling of $C_6F_5CH{=}CH_2$ (F_5-styrene) via the metalloindene mechanism; this is fully confirmed experimentally. However, although F_5-styrene cannot undergo double C-H activation to form a metalloindene complex, the fluorination of the aryl ring is calculated to favor β-vinylic C-H bond addition to a metalloindene complex. Accordingly, although it undergoes no homocoupling, the dehydrogenative hetero-coupling of F_5-styrene with styrene is much more favorable than styrene homocoupling. This is well explained by the metalloindene mechanism and the calculations even capture fairly well the ratio of hetero- to homocoupling. Conversely, the calculations predict that if any of the other mechanisms investigated were operative, the homocoupling of F_5-styrene would be *more* favorable than either heterocoupling or styrene homocoupling.

We believe that the principles elucidated in this work will be applicable to the development of more general dehydrogenative coupling reactions. Most obviously, the metalloindene mechanism should be viable for the coupling of styrenes and their derivatives with other C-H bonds (including both alkenes and non-alkenes). While a “direct” mechanism was found to not be operative in the intermolecular case studied in this work, it was found to operate for intramolecular coupling involving sp^3 C-H bonds. Even for the intermolecular case, the barrier to the direct mechanism was not calculated to be extremely

high. Thus such a mechanism, or more generally sequential C-H activations and C-C coupling, may well be viable with closely related catalysts. In that context, efforts in our lab are underway to determine the factors that favor such pathways.

3.5. Experimental information

3.5.1. General information

All manipulations were carried out under an inert atmosphere of dry argon either in a glovebox or using a standard double manifold. All NMR spectra were acquired on a 500-MHz Varian VNMRS or a Bruker AMX 400-MHz spectrometer. ^{1}H and ^{13}C NMR spectra were referenced to residual deuterated solvent signal. The signal of the residual protio methyl group of *p*-xylene-d_{10} was set at δ 2.296 in the ^{1}H NMR and at δ 20.90 in the ^{13}C NMR spectrum and the signal of residual $CHCl_3$ was set at δ 7.258. Chemical shifts for ^{31}P-NMR spectra were referenced to external H_3PO_4, PMe_3 (set at δ 62.40), or $P(OEt)_3$ (set at δ 139). NMR yields were calculated based on comparing the vinyl or aryl signals in the ^{1}H NMR spectrum to the signal of the methylene group of the $P(OEt)_3$ standard. All vinyl arenes were obtained from commercial sources or synthesized based on reported methods. Further treatment was carried out by drying them over calcium hydride, then distilling under reduced pressure. All aromatic solvents were dried over sodium/benzophenone, distilled from the resultant purple solution prior to use, and stored over 3 Å molecular sieves. X-ray structure collection was conducted on a Bruker Smart APEX CCD diffractometer or a Bruker SMART APEX II CCD platform diffractometer. GCMS analysis was conducted using a Shimadzu GCMS-QP5000 with an Equity-1701 column, helium as carrier gas, and dodecane used as internal standard, or a Varian 3900 GC with a 30-m capillary column coupled with a Saturn 2100T MS, also using helium carrier gas. For

elemental analysis, samples were weighed with a PerkinElmer Model AD-6 Autobalance and their compositions were determined with a PerkinElmer 2400 Series II Analyzer. Air-sensitive samples were handled in VAC Atmospheres gloveboxes. Melting points (uncorrected) were determined on a Laboratory Devices Mel-Temp instrument. The ^{iPr}PCPH ligand precursor[52], (^{iPr}PCP)IrHCl[53], (^{iPr}PCP)IrH_4[53], and the (^{iPr}PCP)Ir(ethylene)[54] complex were synthesized by literature methods.

3.5.2. General procedure for coupling of vinyl arenes with (^{ipr}PCP)IrHCl as precatalyst

To a 4-mL glass ampoule with Teflon closure, 10 mg (0.0177 mmol) (^{iPr}PCP)IrHCl, 4 mg (0.0356 mmol) potassium *tert*-butoxide, a stir bar, and 0.5 mL toluene were added. This was followed by addition of 0.354 mmol vinyl arene. The sealed vessel was then heated, with stirring, at 150 °C for 24 h in an aluminum heating block. Soluble products were isolated as a crude mixture by removal of volatiles in vacuo, redissolution in petroleum ether, and passage of this concentrated solution through a short plug of silica to remove catalyst. Several washes with petroleum ether were conducted to collect organics and concentration of the combined solutions to dryness provided the crude product. The desired (*E*, *E*)-1,4-diaryl-1,3-butadienes could be further purified by vacuum sublimation or recrystallization from aliphatic alcohols.

3.5.3. General procedure for coupling of vinyl arenes with (^{ipr}PCP)Ir(ethylene) as precatalyst

To an NMR tube attached to a short extension of glass tubing, 1.4 mg (0.0025 mmol) (^{iPr}PCP)Ir(ethylene) complex and 0.25 mmol vinyl arene in 0.5 mL *p*-xylene-d_{10} were added (for cross-couplings a total of 0.25 mmol vinyl arene was used, in a 1:1 ratio). A

sealed capillary tube with triethyl phosphite in *p*-xylene-d_{10} inside the NMR tube provided an external standard. The NMR tube was connected to a closed Kontes valve by a piece of Tygon tubing. The contents of the tube were then frozen with liquid nitrogen, and the tube was flame-sealed under vacuum. The sealed NMR tube was then heated at 150 °C inside an oven and the reaction was then monitored by NMR spectroscopy. Products were isolated by column chromatography using hexane as the eluent, which gives a mixture of both (*E*, *E*) and (*E*, *Z*) isomers. Further purification was carried out by recrystallization in hexane to give pure (*E*, *E*) isomer.

3.5.4. Computational information

All electronic structure calculations employed the DFT method.[55] Data presented in the text result from calculations which employed the M06-L exchange-correlation functional.[56] We also examined two additional functionals, M06[57] and PBE [58], in selected calculations; the results obtained with these functionals fully support the mechanisms we propose based on calculations with the M06-L functional. For Ir, we applied the Hay-Wadt relativistic effective (small) core potential[59] and the LANL2TZ basis set[60] augmented by a set of diffuse d-type functions (exponent=0.07645)[61]; all other atoms (P, F, C, and H) were assigned 6-311G(d,p) basis sets.[62]

Geometries were calculated for stationary points along the reaction paths by standard optimization procedures.[63] Normal mode analysis was performed to further verify the nature of a particular stationary point (minimum or transition state). The resulting set of vibrational frequencies was employed (without scaling) to determine zero-point energy corrections. Enthalpies (ΔH, $\Delta H^{\ddagger}$) and Gibbs' free energies (ΔG, $\Delta G^{\ddagger}$; T = 298.15 K, P = 1 atm) were subsequently obtained from the potential energies using standard statistical

mechanical expressions.[64] For better comparisons with measured energetics, we further corrected the Gibbs' free energies so they corresponded to a standard state of 1 M for all species and T = 423 K (the temperature applied in the experiments reported here).[64] In order to enhance computational stability and accuracy[65] in geometry optimizations and normal mode calculations, we used increased atomic grid sizes (grid=ultrafine option).[66] All calculations made use of the Gaussian 09 electronic structure program.[67] Geometries of all calculated species and energetic quantities are available in Supporting Information.

3.5.5. Product identification

All homo-coupling and cross-coupling products were isolated and compared with both reported ^{1}H and ^{13}C NMR spectra[68-72]; further characterization was carried out by GC-MS.

3.5.5.1. (*E*, *E*)-1,4-Diphenyl-1,3-butadiene

^{1}H NMR (500 MHz, chloroform-*d*): δ 7.45 (dd, *J* = 8.2, 1.4 Hz, 4H_{Ar}), 7.33 (ddt, *J* = 8.3, 7.2 Hz, 1.3 Hz, 4H_{Ar}), 7.24 (tt, *J* = 7.3, 1.3 Hz, 2H_{Ar}), 6.96 (AA' of AA'BB', 2H, vinyl-H), 6.68 (BB' of AA'BB', 2H, vinyl-H). ^{13}C NMR (126 MHz, chloroform-*d*): δ 137.33, 132.79, 129.22, 128.63, 127.53, 126.35. M.P. = 152-154 °C.

3.5.5.2. (*E*, *E*)-1,4-Di-(4-tolyl)-1,3-butadiene

^{1}H NMR (500 MHz, chloroform-*d*): δ 7.33 (d, *J* = 8.1 Hz, 4H_{Ar}), 7.14 (d, *J* = 8.1 Hz, 4H_{Ar}), 6.90 (AA' of AA'BB', 2H, vinyl-H), 6.63 (BB' of AA'BB', 2H, vinyl-H), 2.35(s, 6H, CH_3). ^{13}C NMR (126 MHz, chloroform-*d*): δ 137.32, 134.68, 132.22, 129.33, 128.47, 126.21, 21.24.

3.5.5.3. (*E*, *E*)-1,4-Di-(2-tolyl)-1,3-butadiene

^{1}H NMR (500 MHz, chloroform-*d*): 7.57 (d, *J* = 7.8 Hz, 2H_{Ar}), 7.23-7.12 (m, 6H_{Ar}), 6.97-6.86 (m, 4H, vinyl-H), 2.40 (s, 6H, CH_3). ^{13}C NMR (126 MHz, chloroform-*d*): δ 136.16, 135.58, 130.66, 130.45, 130.25, 127.42, 126.11, 124.99, 19.87. M.P. = 130-134 °C.

3.5.5.4. (*E*, *E*)-1,4-Di-[4-(trifluoromethyl)phenyl]butadiene

^{1}H NMR (500 MHz, chloroform-*d*): δ 7.59 (d, *J* = 8.3 Hz, 4H_{Ar}), 7.53 (d, *J* = 8.2 Hz, 4H_{Ar}), 7.03 (AA' of AA'BB', 2 H, vinyl-H), 6.75 (BB' of AA'BB', 2 H, vinyl-H). ^{13}C NMR (126 MHz, chloroform-*d*): δ 140.37 (q, *J* = 1.3 Hz), 132.66, 130.93, 129.49 (q, *J* = 32.6 Hz), 126.56, 125.64 (q, *J* = 3.8 Hz), 124.11 (q, *J* = 272.4 Hz).

3.5.5.5. (*E*, *E*)-1,4- Di-(4-fluorophenyl)butadiene

^{1}H NMR (500 MHz, chloroform-*d*): δ 7.42-7.36 (m, 4H_{Ar}), 7.05-6.98 (m, 4H_{Ar}), 6.84 (AA' of AA'BB', 2 H, vinyl-H), 6.62 (BB' of AA'BB', 2H, vinyl-H). ^{13}C NMR (126 MHz, chloroform-*d*): δ 162.27 (d, *J* = 247.4 Hz), 133.47 (d, *J* = 3.4 Hz), 131.51, 128.77 (d, *J* = 3.0 Hz), 127.80 (d, *J* = 7.9 Hz), 115.61 (d, *J* = 21.8 Hz).

3.5.5.6. (*E*, *E*)-1,4-Di-(4-tert-butylphenyl)-1,3-butadiene

^{1}H NMR (500 MHz, chloroform-*d*): δ 7.41-7.31 (m, 8H_{Ar}), 6.92 (AA' of AA'BB', 2H, vinyl-H), 6.64 (BB' of AA'BB', 2H, vinyl-H), 1.33 (s, 18H, CH_3). ^{13}C NMR (126 MHz, chloroform-*d*): δ 150.59, 134.69, 132.12, 128.73, 126.04, 125.56, 34.60, 31.26.

3.5.5.7. (*E*, *E*)-1,4-Di-(4-methoxyphenyl)-1,3-butadiene

^{1}H NMR (500 MHz, chloroform-*d*): δ 7.40-7.33 (m, 4H_{Ar}), 6.90-6.83 (m, 4H_{Ar}), 6.81 (AA' of AA'BB', 2H, vinyl-H), 6.57 (BB' of AA'BB', 2H, vinyl-H), 3.82 (s, 6H, CH_3). ^{13}C NMR (126 MHz, chloroform-*d*): ^{13}C NMR δ 159.07, 131.27, 130.40, 127.52, 127.43, 114.09, 55.30.

3.5.5.8. (*E, E*)-1,4-Di-(3,5-dimethylphenyl)-1,3-butadiene

^{1}H NMR (500 MHz, chloroform-*d*): δ 7.06 (s, 4H_{Ar}), 6.92 (AA' of AA'BB', 2H, vinyl-H), 6.88 (s, 2H), 6.59 (BB' of AA'BB', 2H, vinyl-H), 2.32 (s, 12H, CH_3). ^{13}C NMR (126 MHz, chloroform-*d*): δ 138.03, 137.33, 132.66, 129.29, 129.09, 124.23, 21.27.

3.5.5.9. (*E, E*)-1,4-Di-(3,5-trifluoromethylphenyl)-1,3-butadiene

^{1}H NMR (500 MHz, benzene-d_6): δ 7.60-7.58 (m, 2H_{Ar}), 7.51 – 7.45 (m, 4H_{Ar}), 6.30 (AA' of AA'BB', 2H, vinyl-H), 5.95 (BB' of AA'BB', 2H, vinyl-H). We were unable to obtain an acceptable ^{13}C NMR spectrum due to the extremely low solubility of this compound in common organic solvents[70].

3.5.5.10. (*E, E*)-1,4-(2-Naphthyl)-1,3-butadiene

The very poor solubility of this product allowed for simple isolation by filtration of the reaction mixture cooled to 0 °C with a fine frit. The collected solid was washed sequentially with cold toluene, isopropanol, and water, then dried at 80 °C to give a yellowish solid. Several crystals of X-ray diffraction quality were obtained from these solids, and the structure obtained conclusively determined the formation of (*E*,*E*)-1,4-(2-naphthyl)-1,3-butadiene. The poor solubility of the product precluded collection of a ^{13}C NMR spectrum. However, in CD_2Cl_2 after 664 scans an acceptable ^{1}H NMR spectrum was obtained, which has not previously been reported. ^{1}H NMR 400 MHz (CD_2Cl_2): δ 7.83 (bs, 8H_{Ar}), 7.72 (d, J_{HH} = 8.8 Hz, 2H_{Ar}), 7.47 (p, J_{HH} = 6.8 Hz, 4H_{Ar}), 7.19 (AA' of AA'BB', 2H, vinyl-H), 6.92 (BB' of AA'BB', 2H, vinyl-H). M.P. = 266-270 °C

Figure 3. 11. Crystal structure of (E, E)-1,4-(2-naphthyl)-1,3-butadiene

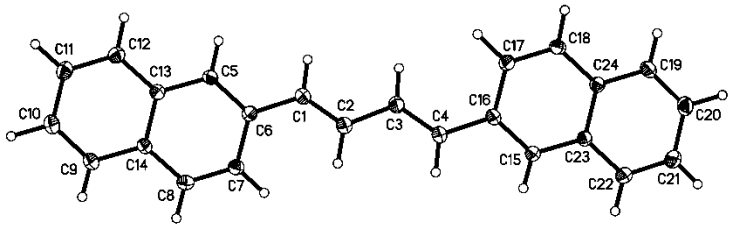

3.5.5.11. 1,2,3,4,5-Pentafluoro-6-[(1*E*, 3*E*)-4-phenyl-1,3-butadien-1-yl]benzene

This cross-coupling product was isolated by column chromatography using 98:2 hexane and ethyl acetate as the eluent, which gives 1,2,3,4,5-pentafluoro-6-[(1*E*,3*E*)-4-phenyl-1,3-butadien-1-yl]benzene and (*E*, *E*)-1,4-diphenyl-1,3-butadiene. ^{1}H and ^{13}C NMR of 1,2,3,4,5-pentafluoro-6-[(1*E*,3*E*)-4-phenyl-1,3-butadien-1-yl]benzene is reported below, which matches reported values.[71] ^{1}H NMR (500 MHz, chloroform-*d*): δ 7.49 – 7.44 (m, 2H), 7.38 – 7.33 (m, 2H), 7.30 – 7.26 (m, 1H), 7.24 (d, *J* = 10.5 Hz, 1H, vinyl-H), 6.93 (ddq, *J* = 15.7, 10.5, 1.1 Hz, 1H, vinyl-H), 6.78 (d, *J* = 15.5 Hz, 1H, vinyl-H), 6.56 (d, *J* = 16.0 Hz, 1H, vinyl-H). ^{13}C NMR (126 MHz, chloroform-*d*): 148.00-113.00 (low intensity, -C_6F_5, described by literature[71], but barely observed), δ 137.62 (m), 136.57, 136.23, 128.94, 128.74, 128.34, 126.75, 116.25 – 115.99 (m). MS (EI): m/z calcd. for $C_{16}H_9F_5$: 296.06, GC-MS: m/z 296.80.

3.5.5.12. 4,6-Dimethylindene (A) and 5,7-dimethylindene (B)

The intramolecular coupling of 2,4,6-trimethylstyrene gives two inseparable indene products, 4,6dimethylindene and 5,7-dimethylindene, as well as a small amount of 1-ethyl-2,4,6-trimethylbenzene after flash column chromatography using hexane as eluent. The ^{1}H NMR spectrum was assigned as follows: 4,6-Dimethylindene. ^{1}H NMR (500 MHz, chloroform-*d*): δ 7.15 (dd, *J* = 1.5, 0.8 Hz, $1H_{Ar}$), 6.95 (dtd, *J* = 5.6, 2.0, 0.8 Hz, $1H_{Ar}$), 6.92 (dt, *J* = 1.6, 0.9 Hz, 1H, vinyl-H), 6.49 (dt, *J* = 5.6, 2.0 Hz, 1H, vinyl-H), 3.38 (td, *J* =

1.9, 0.9 Hz, 2H, CH_2), 2.43 (s, 3H, CH_3), 2.37 (s, 3H, CH_3). GC-MS: m/z 144. 5,7-Dimethylindene. ^{1}H NMR (500 MHz, chloroform-*d*): δ 7.10 – 7.09 (m, 1H), 6.86 (dt, *J* = 5.7, 2.0 Hz, 2H, H_{Ar} + vinyl-H), 6.56 (dt, *J* = 5.5, 2.0 Hz, 1H, vinyl-H), 3.27 (t, *J* = 2.0 Hz, 2H, CH_2), 2.38 (s, 3H, CH_3), 2.35 (s, 3H, CH_3). 4,6-Dimethylindene and 5,7-Dimethylindene. ^{13}C NMR (126 MHz, chloroform-*d*): δ 144.73, 143.93, 141.11, 139.43, 136.17, 134.28, 133.98, 132.51, 132.48, 132.2, 129.97, 129.75, 128.07, 126.68, 122.03, 119.31, 39.13, 37.56, 21.32, 18.67. MS (EI): m/z calcd. for $C_{11}H_{12}$: 144.09 GC-MS: m/z 143.80. Anal. Calcd.: C, 91.61; H, 8.39. Found: C, 91.96; H, 8.79.

3.5.5.13. 4,6-Dimethylindane (C) and 1-ethyl-2,4,6-trimethylbenzene (D)

The (^{iPr}PCP)Ir(ethylene)-catalyzed reaction of 2,4,6-trimethylstyrene was taken to 90% conversion and the resulting mixture was then hydrogenated with 5% Pd/C under 1 atm H_2, giving NMR spectra attributable to a ~1.25:1 mixture of 1-Ethyl-2,4,6-trimethylbenzene and 4,6-dimethylindane. The mixture could not be separated by standard purification methods. 4,6-Dimethylindane. ^{1}H NMR (500 MHz, chloroform-*d*): δ 6.93 (s, 1H_{Ar}), 6.82 (s, 1H_{Ar}), 2.92 (t, *J* = 7.5 Hz, 2H, CH_2), 2.82 (t, *J* = 7.4 Hz, 2H, CH_2), 2.28 (s, 3H, CH_3), 2.26 (s, 3H, CH_3), 2.09 (p, *J* = 7.5 Hz, 2H, CH_2).1-Ethyl-2,4,6-trimethylbenzene ^{1}H NMR (500 MHz, chloroform-*d*): δ 6.86 (s, 2 H_{Ar}), 2.65 (q, *J* = 7.6 Hz, 9H, CH_3), 2.32 (s, 2H, CH_2), 1.13 (t, *J* = 7.6 Hz, 3H, CH_3). 4,6-dimethylindane and 1-Ethyl-2,4,6-trimethylbenzene ^{13}C NMR (126 MHz, chloroform-*d*): δ 144.11, 139.96, 137.82, 135.81, 135.66, 134.74, 133.47, 128.8, 127.72, 122.38, 32.99, 30.98, 24.93, 22.27, 21.11, 20.78, 19.50, 19.12, 13.46.

3.5.5.14. 4,6-Dimethylindane

Hydrogenation of mixtures of isolated products 4,6-dimethylindene and 5,7-dimethylindene using 5% Pd/C under H_2 atmosphere gave one product 4,6-dimethylindane with a trace amount of 1-ethyl-2,4,6-trimethylbenzene. ^{1}H NMR (500 MHz, chloroform-*d*): δ 6.91 (s, 1H_{Ar}), 6.80 (s, 1 H_{Ar}), 2.90 (t, *J* = 7.5 Hz, 2H, CH_2), 2.80 (t, *J* = 7.4 Hz, 2H, CH_2), 2.31 (s, 3H, CH_3), 2.24 (s, 3H, CH_3), 2.07 (p, *J* = 7.5 Hz, 2H, CH_2). ^{13}C NMR (126 MHz, chloroform-*d*): δ 144.10, 139.96, 135.80, 133.47, 127.71, 122.37, 32.98, 30.97, 24.92, 21.10, 19.12. MS (EI): m/z calcd. for $C_{11}H_{14}$: 146.10 [M+]; found: 146.20. All values match with reported values.[72] Anal. Calcd.: C, 90.35; H, 9.65. Found: C, 90.67; H, 9.99.

3.5.6. Iridium complexes

3.5.6.1. (^{iPr}PCP)Ir(η^2-H_2C=CHPh) (2)

To a J. Young NMR tube, 15 mg (0.0281 mmol) (^{iPr}PCP)IrH_4, 0.5 mL toluene, and 8.5 μL (0.066 mmol) TBE were added, yielding a red solution. 4 μL (0.035 mmol) styrene was then added, after which the solution quickly turned brown. A single major product was observed by ^{31}P NMR spectroscopy in ≥ 98% yield within 5-10 min. The volatiles were then removed by vacuum and the residue re-dissolved in pentane. Crystals suitable for X-ray diffraction were grown from this solution by slow evaporation at -17 °C in 40-50% yield. Attempts to wash these crystals of the oily residue in which they formed resulted in complete dissolution; elemental analysis was therefore not conducted.

^{31}P[73] NMR 400 MHz (C_6D_6): δ 45.72 (s). ^{1}H NMR 400 MHz (C_6D_6): δ 7.6 (d, J_{HH} = 7.6 Hz, 2H, meta-PCP), 7.32 (d, J_{HH} = 7.2 Hz, 2H, Ar-H styrene), 7.24-7.10 (m, 4H, Ar-H styrene, obscured by solvent), 7.06 (t, J_{HH} = 7.2 Hz, 1H, para-PCP), 5.07 (m, 1H, CH-

styrene), 3.55 (overlapping dt, 1H, CH_2-styrene), 3.10 (overlapping qvt, 4H, CH_2-PCP), 2.99 (d, J_{HH} = 7.2 Hz, 1H, CH_2-styrene), 2.15 (vp, 2H, CH-PCP), 1.61 (vp, 2H, CH-PCP), 1.24 (q, J_{HP} = 6.8 Hz, 6H, CH_3-PCP), 0.99 (q, J_{HP} = 6.4 Hz, 6H, CH_3-PCP), 0.81 (q, J_{HP} = 6.4 Hz, 6H, CH_3-PCP), 0.70 (q, J_{HP} = 7.2 Hz, 6H, CH_3-PCP).

3.5.6.2. Metalloindene complex 3

To a J. Young NMR tube, 5.6 mg (0.010 mmol) (^{iPr}PCP)Ir(ethylene), 0.5 mL *p*-xylene, and 4.6 μL (0.040 mmol) styrene were added. Upon mixing the solution quickly turned brown and was then heated at 150 °C for 20 h, whereupon the solution turned black. The reaction was monitored by ^{31}P NMR spectroscopy, which gave >99% conversion to a major product (singlet, >90% yield). Volatiles were then removed under vacuum and the residue re-dissolved in a very small amount of hexane. Crystals suitable for X-ray diffraction were grown from this solution at -40 °C in 50-60% yield. Purified product was obtained from washing the solid with a solvent mixture of hexane and isopropanol (v:v, 1:5; 2x2 mL). The same compound was obtained by combining 5.6 mg (0.010 mmol) (^{iPr}PCP)Ir(ethylene), 2.1 mg (0.010 mmol) (*E*, *E*)-1,4-diphenyl-1,3-butadiene and 2.6 μL (0.020 mmol) TBE in 0.5 ml *p*-xylene and heating at 150 °C for 2 h.

^{1}H NMR (500 MHz, *p*-xylene-d_{10}): δ 8.87 (d, *J* = 15.5 Hz, $1H_{Ar}$), 7.88 (s, 1H, vinyl-H), 7.66 – 7.58 (m, $2H_{Ar}$), 7.54 (d, *J* = 7.4 Hz, $2H_{Ar}$), 7.37 – 7.31 (m, $3H_{Ar}$), 7.20 – 7.14 (m, $2H_{Ar}$), 6.89 (td, *J* = 7.3, 1.0 Hz, $1H_{Ar}$), 6.57 (d, *J* = 15.5 Hz, $1H_{Ar}$), 6.51 (d, *J* = 7.9 Hz, 1H, vinyl-H), 6.29 (td, *J* = 7.6, 1.8 Hz, 1H, vinyl-H), 3.48 (t, *J* = 4.4 Hz, 4H, CH_2), 2.57 (pt, *J* = 7.1, 2.6 Hz, 2H, CH), 1.97 – 1.86 (m, 2H, CH), 0.99 (q, *J* = 7.3 Hz, 6H, CH_3), 0.94 (q, *J* = 7.3 Hz, 12H, CH_3), 0.69 (q, *J* = 7.4 Hz, 6H, CH_3). ^{13}C NMR (126 MHz, *p*-xylene-d_{10}): δ 186.37 (t, *J* = 2.0 Hz), 176.77 (t, *J* = 6.8 Hz), 156.30, 153.46 (t, *J* = 8.2 Hz), 146.64 –

146.57 (m), 146.53 – 146.47 (m), 143.50, 141.00, 132.39, 131.22, 129.76, 127.17, 127.10, 126.07, 123.94, 123.19, 122.67, 121.64 (t, *J* = 8.1 Hz), 40.08 (t, *J* = 15.8 Hz), 27.45 (t, *J* = 13.1 Hz), 25.58 (t, *J* = 14.2 Hz), 21.78, 20.19, 18.78, 18.77. ^{31}P NMR (202 MHz, *p*-xylene-d_{10}): δ 40.31. Anal. Calcd.: C, 58.91; H, 6.46. Found: C 58.83; H 6.60.

3.5.6.3. Metalloindene complex 4

To a J. Young NMR tube, 5.6 mg (0.010 mmol) (^{iPr}PCP)Ir(ethylene), 0.5 mL *p*-xylene, and 7.2 μL (0.040 mmol) 3,5-bis(trifluoromethyl)styrene were added. Upon mixing the solution quickly turned dark. It was then heated at 150 °C for 2 h, whereupon the solution turned to deep red. The reaction was monitored by ^{31}P NMR spectroscopy, which gave >99% conversion to a single product (singlet, >95% yield). Volatiles were then removed under vacuum and the residue re-dissolved in a very small amount of hexane. Crystals suitable for X-ray diffraction were grown from this solution at -40 °C in 40-50% yield. ^{1}H NMR (500 MHz, *p*-xylene-d_{10}): δ 8.16 (s, 1H_{Ar}), 7.75 (s, 1H_{Ar}), 7.44 (d, *J* = 7.5 Hz, 2H_{Ar}), 7.26 – 7.21 (m, 1H_{Ar}), 5.72 (ddt, *J* = 4.3, 2.1, 1.0 Hz, 1H, vinyl-H), 5.54 (dt, *J* = 4.6, 2.7 Hz, 1H, vinyl-H), 3.50 (td, J =4.2Hz, 1H, CH_2), 3.47 (d, J = 4.2 Hz, 1H, CH_2), 3.17 (t, J = 4.4 Hz, 1H, CH_2), 3.14 (t, J = 4.4 Hz, 1H, CH_2), δ 2.50 (pt, *J* = 7.1, 2.2 Hz, 2H, CH), 1.98 (ddtd, *J* = 13.5, 10.5, 7.1, 3.4 Hz, 2H, CH)., 0.92 (q, *J* = 6.6 Hz, 6H, CH_3), 0.82 (q, *J* = 7.4 Hz, 6H, CH_3), 0.72 (q, *J* = 7.4 Hz, 6H, CH_3), 0.67(q, *J* = 7.4 Hz, 6H, CH_3). ^{13}C NMR (126 MHz, *p*-xylene-d_{10}): δ 182.39 (q, *J* = 6.8 Hz), 177.99 (t, *J* = 2.1 Hz), 155.57, 152.78 (t, *J* = 8.2 Hz), 139.27 (q, *J* = 26.3 Hz), 136.32 (t, *J* = 3.1 Hz), 130.02 (q, J = 274.4Hz), 127.14 (q, *J* = 271.3Hz), 126.05, 125.67 (q, *J* = 31.8 Hz), 122.67 (t, *J* = 7.3 Hz), 121.80 (t, *J* = 8.3 Hz), 120.26 – 119.93 (m), 119.59 (td, *J* = 8.2, 4.0 Hz), 38.68 (t, *J* = 16.0 Hz), 25.50 (t, *J* = 13.2 Hz), 24.06 (t, *J* = 14.4 Hz), 21.58 – 21.45 (m), 19.56, 18.67, 18.24.

^{31}P NMR (202 MHz, *p*-xylene-d_{10}): δ 43.25. Anal. Calcd.: C, 46.93; H, 5.12. Found: C, 46.86; H, 4.97.

3.5.6.4. Metalloindene complex 5

To a J. Young NMR tube, 10 mg (0.0187 mmol) (^{iPr}PCP)IrH_4, 0.5 mL toluene, and 4.9 μL (0.038 mmol) TBE were added followed by 3.3 μL (0.0187 mmol) 1,1'-diphenylethylene (DPE). Upon mixing the solution quickly turned brown, and within one hour ≥ 97% conversion to a single product was observed by ^{31}P NMR spectroscopy. Complete conversion was achieved by stirring at room temperature overnight. Volatiles were then removed by vacuum and the residue re-dissolved in pentane. Crystals suitable for X-ray diffraction were grown from this solution at -17 °C in 60-70% yield. ^{31}P NMR 400 MHz (C_6D_6): δ 45.13 (s). ^{1}H NMR 400 MHz (C_6D_6): δ 8.63 (s, 1H, CH-DPE), 7.74 (d, J_{HH} = 7.2 Hz, 2H, meta-PCP), 7.50 (d, J_{HH} = 7.6 Hz, 1H, Ar-H DPE), 7.47-7.34 (m, 5H, Ar-H DPE), 7.29 (t, J_{HH} = 7.2 Hz, 1H, Ar-H DPE), 7.21 (d partially obscured by solvent, J_{HH} = 7.6 Hz, 1H, Ar-H DPE), 7.03 (t, J_{HH} = 7.2 Hz, 1H, para-PCP), 6.83 (t, J_{HH} = 7.2 Hz, 1H, Ar-H DPE), 3.33 (dvt left side AB pattern, J_{HH} = 16.8, J_{HP} = 3 Hz, 2H, CH_2-PCP), 3.18 (dvt right side AB pattern, J_{HH} = 17.2, J_{HP} = 3.6 Hz, 2H, CH_2-PCP), 2.00 (m, 4H, CH-PCP), 0.71 (m, 24H, CH_3-PCP). Anal Calcd: C = 57.69%, H = 6.41%. Found: C = 57.72%, H = 6.18%.

3.5.6.5. Metalloindene complex 7

To a J. Young NMR tube, 5.9 mg (0.010 mmol) (^{tBu}PCP)Ir$(H)_4$, 0.5 mL *p*-xylene, and 6.9 μL (0.060 mmol) styrene were added. Upon mixing the solution quickly turned dark. The solution was then heated at 150 °C for 5 h, whereupon the solution turned red. The reaction gave >99% conversion to two major products as determined by ^{31}P NMR

spectroscopy [major: δ 74.63 (d, *J* = 304.8 Hz), 50.13 (d, *J* = 304.6 Hz), minor: δ 86.84 (d, *J* = 313.6 Hz), 61.75 (d, *J* = 311.3 Hz)]. Volatiles were then removed under vacuum and the residue re-dissolved in a very small amount of hexane. Crystals of major species suitable for X-ray diffraction were grown from this solution at -40 °C in 30-40% yield. ^{1}H NMR (500 MHz, *p*-xylene-d_{10}): δ 8.29 – 8.22 (m, 1H, H_{Ar}), 7.50 (dd, *J* = 6.4, 2.3 Hz, 1H_{Ar}), 7.45 (dd, *J* = 7.5, 3.5 Hz, 2H_{Ar}), 7.33 (t, *J* = 7.5 Hz, 1H_{Ar}), 7.26 – 7.18 (m, 2H_{Ar}), 6.02 (d, *J* = 1.5 Hz, 1H, vinyl-H), 3.88 (ddd, *J* = 16.1, 12.0, 4.1 Hz, 1H, CH_2), 3.67 – 3.48 (m, 3H, CH_2), 2.48 (d, *J* = 11.1 Hz, 1H, CH_2), 1.31 (d, *J* = 11.2 Hz,6H, CH_3), 1.21 (d, *J* = 11.2 Hz, 1H, CH_2), 1.11 (d, *J* = 13.5 Hz, 9H, CH_3), 1.03 (d, *J* = 13.0 Hz, 9H, CH_3), 0.89 (d, *J* = 12.2 Hz, 9H, CH_3). ^{13}C NMR (126 MHz, *p*-xylene-d_{10}): δ 180.39 (dd, *J* = 4.0, 2.1 Hz), 170.42 (dd, *J* = 9.1, 3.7 Hz), 158.55, 151.24 (dd, *J* = 11.6, 4.1 Hz), 150.99 (dd, *J* = 10.8, 3.3 Hz), 144.10 (dd, *J* = 5.2, 3.5 Hz), 140.46 – 140.33 (m), 140.32 – 140.24 (m), 135.37, 126.13, 124.04, 122.52, 122.27, 121.91 (dd, *J* = 15.0, 12.6 Hz), 62.93 (d, *J* = 15.1 Hz), 45.74 (dd, *J* = 27.8, 1.4 Hz), 45.18 (dd, *J* = 15.1, 2.6 Hz), 42.14 (d, *J* = 28.9 Hz), 41.22 (d, *J* = 27.5 Hz), 35.90 (dd, *J* = 14.1, 4.5 Hz), 34.22 (dd, *J* = 15.0, 5.3 Hz), 31.57 (d, *J* = 3.5 Hz), 29.72 – 29.41 (m), 29.00, 28.75 (d, *J* = 4.2 Hz), 28.16 (t, *J* = 1.8 Hz). ^{31}P NMR (202 MHz, *p*-xylene-d_{10}): δ 74.63 (d, *J* = 304.5 Hz), 50.13 (d, *J* = 304.7 Hz). Anal. Calcd.: C, 56.04; H, 6.91. Found: C, 56.42; H, 6.92.

3.5.6.6. Metalloindene complex 8

To a J. Young NMR tube, 5.9 mg (0.010 mmol) (^{tBu}PCP)Ir(H)$_4$, 0.5 mL *p*-xylene, and 6.9 μL (0.060 mmol) *α*-methyl-styrene were added. Upon mixing the solution quickly turned dark. The solution was then heated at 150°C for 2 h, whereupon the solution turned deep red. >99% conversion to a single product (a singlet) can be observed by ^{31}P NMR

spectroscopy. The volatiles were then removed under vacuum and the residue re-dissolved in a very small amount of hexane. Crystals suitable for X-ray diffraction were grown from this solution by slowly evaporating the solvent. ^{1}H NMR (500 MHz, *p*-xylene-d_{10}): δ 7.71 (d, J = 7.4 Hz, 1H$_{Ar}$), 7.50 (d, J = 7.4 Hz, 2H$_{Ar}$), 7.32 – 7.28 (m, 1H$_{Ar}$), 7.20 (s, broad, 1H$_{Ar}$), 7.18 (dd, J = 7.4, 1.7 Hz, 1H$_{Ar}$), 7.14 (td, J = 7.3, 1.2 Hz, 1H$_{Ar}$), 6.97 (td, J = 7.2, 1.7 Hz, 1H, vinyl-H), 3.63 – 3.49 (m, 4H, CH$_2$), 2.39 (q, J = 1.6 Hz, 3H, CH$_3$), 1.02 (td, J = 6.3, 4.5 Hz, 36H, CH$_3$). ^{13}C NMR (126 MHz, *p*-xylene-d_{10}): δ 184.16 (t, J = 1.7 Hz), 157.31, 152.47 (t, J = 7.6 Hz), 142.49 (t, J = 2.5 Hz), 138.94, 134.69 – 134.22 (m), 125.39, 124.49, 122.47, 121.55 (t, J = 7.7 Hz), 121.33, 40.69 (t, J = 13.8 Hz), 38.57 (t, J = 10.4 Hz), 37.75 (t, J = 10.1 Hz), 30.93 (t, J = 2.0 Hz), 30.58 (t, J = 1.9 Hz), 19.37 (t, J = 1.1 Hz). ^{31}P NMR (202 MHz, *p*-xylene-d_{10}): δ 48.20. Anal. Calcd.: C, 56.47; H, 7.32. Found: C, 55.74; H, 7.44.

3.5.6.7. Metalloindene complex 9

To a J. Young NMR tube, 5.9 mg (0.010 mmol) (^{tBu}PCP)Ir(H)$_4$, 0.5 mL *p*-xylene, and 6.9 μL (0.060 mmol) *β*-methyl-styrene were added. Upon mixing the solution quickly turned dark. The solution was heated to 150°C for 2 h, whereupon the solution turned black. All of the phosphorus signal converted to a single broad peak by ^{31}P NMR spectroscopy. The volatiles were then removed under vacuum and the residue re-dissolved in a very small amount of hexane. Crystals suitable for X-ray diffraction were grown from this solution by slowly evaporating the solvent.

^{1}H NMR (500 MHz, *p*-xylene-d_{10}): All signals from the metalloindene parts are broad and poorly defined at ambient temperature due to fluxional behavior of the complex in solution; only the signals from the ^{tBu4}PCP ligand could be identified, as has been

previously reported for related biphenylene complexes and attributed to fluxional behavior[37-38]. ^{1}H NMR (500 MHz, *p*-xylene-d_{10}): δ 7.47 (d, J = 7.4 Hz, 2H_{Ar}), 7.27 (t, J = 7.4 Hz, 1H_{Ar}), 3.65 (t, J = 4.2 Hz, 1H, CH_2), 3.62 (t, J = 4.2 Hz, 1H, CH_2), 3.52 (t, J = 4.0 Hz, 1H, CH_2), 3.48 (t, J = 4.0 Hz, 1H, CH_2), 1.06 (dt, J = 11.6, 6.4 Hz, 36H, CH_3). ^{13}C NMR (126 MHz, *p*-xylene-d_{10}): A similar situation happened as in the ^{1}H NMR spectrum. δ 183.62, 152.44, 136.98, 125.08, 122.87, 121.85, 121.52 (t, J = 7.7 Hz), 40.39 (t, J = 13.4 Hz), 38.52, 31.81, 30.42. ^{31}P NMR (202 MHz, *p*-xylene-d_{10}): δ 43.08(broad). Anal. Calcd.: C, 56.47; H, 7.32. Found: C, 56.75; H, 7.34.

To overcome the difficulty assigning the spectrum resulting from the fluxional behavior, we increased the temperature. From 25 °C to 115 °C, we can clearly see the broad ^{31}P signal become sharper, and new peaks gradually appear in the ^{1}H NMR spectrum. At 115 °C, ^{1}H NMR (500 MHz, *p*-xylene-d_{10}): δ 7.49 (d, J = 7.0 Hz, 1H_{Ar}), 7.43 (d, J = 7.4 Hz, 2H_{Ar}), 7.22 – 7.13 (m, 2H_{Ar}), 6.97 (t, J = 7.2 Hz, 1H_{Ar}), 6.84 (t, J = 7.3 Hz, 1H_{Ar}), 6.19 (s, broad peaks, 1H, vinyl-H), 3.75 (t, J = 4.2 Hz, 1H, CH_2), 3.72 (t, J = 4.1 Hz, 1H, CH_2), 3.62 (t, J = 4.0 Hz, 1H, CH_2), 3.59 (t, J = 3.9 Hz, 1H, CH_2), 2.19 (s, 3H, CH_3), 1.15 (t, J = 6.4 Hz, 18H, CH_3), 1.12 (t, J = 6.2 Hz, 18H, CH_3). ^{31}P NMR (202 MHz, *p*-xylene-d_{10}): δ 45.97.

In a further effort to characterize this complex, the J. Young NMR tube with a *p*-xylene-d_{10} solution of the complex was charged with 1 atm CO, which changed the solution from dark to light yellow. A single signal in the ^{31}P NMR spectrum was observed, which was assigned to the metalloindene-CO complex **9-CO** in analogy with previously reported, related, biphenylene complexes.[74-75] ^{1}H NMR (500 MHz, *p*-xylene-d_{10}): δ 7.42 (q, J = 1.4 Hz, 1H_{Ar}), 7.32 – 7.19 (m, 5H_{Ar}), 7.16 (td, J = 7.3, 1.1 Hz, 1H_{Ar}), 6.78 (td, J = 7.3, 1.5 Hz,

1H, vinyl-H), 3.92 (t, J = 4.0 Hz, 1H, CH_2), 3.89 (t, J = 4.0 Hz, 1H, CH_2), 3.29 (d, J = 1.4 Hz, 1H, CH_2), 3.25 (t, J = 3.3 Hz, 1H, CH_2), 3.22 (t, J = 3.4 Hz, 1H, CH_2), 1.32 (t, J = 6.3 Hz, 18H, CH_3), 0.81 (t, J = 6.2 Hz, 18H, CH_3). ^{13}C NMR (126 MHz, *p*-xylene-d_{10}): δ 185.27 (t, J = 8.1 Hz), 167.82, 158.15 (t, J = 1.2 Hz), 155.52 (t, J = 5.8 Hz), 149.02 (t, J = 5.1 Hz), 145.54 (t, J = t3.3 Hz), 145.39 (t, J = 10.4 Hz), 140.35, 135.04, 125.85, 125.43, 122.34, 122.26 (t, J = 6.7 Hz), 121.60, 41.22 (t, J = 14.3 Hz), 39.86 (t, J = 9.8 Hz), 39.51 (t, J = 9.8 Hz), 35.81, 32.17 (t, J = 1.5 Hz), 31.48 (t, J = 1.4 Hz). ^{31}P NMR (202 MHz, *p*-xylene-d_{10}): δ 36.36.

3.5.7. Isomerization experiments

To a 50-mL volumetric flask, 50 mg (*E*,*E*)-1,4-diphenyl-1,3-butadiene was added and the vessel made up to volume with hexane. From this solution, 0.1 mL was removed as a sample and analyzed by GC-MS (Figure 3.12). The flask was then subject to irradiation from a 200-W Hg-Xe lamp with UV-filter (ORIEL Corp. model 6137 lamp) at a distance of approximately 8 cm for 2.5 h. At this point 1 μL was withdrawn as a sample. The solution was then transferred to a Teflon sealed ampoule and all residues were rinsed with additional hexane. The hexane was then removed by vacuum leaving an oily partially solid yellow residue. This residue was then dissolved in 1.15 mL toluene providing a 0.2 M solution. From this solution two 0.5 mL aliquots were withdrawn and each delivered to 4 mL ampoules. To one ampoule 4 mg KO^{t}Bu was added, and to the other 4 mg KO^{t}Bu with 10 mg (^{iPr}PCP)IrHCl was added (equal to an approximately 7.5 mole % catalyst loading under normal reaction conditions). The sealed vessels were then heated with stirring in an aluminum heating block at 150 °C for 24 h. After this time, each vessel was cooled to room temperature and the reaction mixture filtered through a short plug of silica. The silica was

rinsed several times with additional toluene. The filtrate was then evaporated to dryness and redissolved in hexane to the original concentration before irradiation (21.9 mL hexane per reaction). These solutions were used for GC-MS analysis (Figures 3.12).

Figure 3. 12. GC-MS traces of isomerization experiment

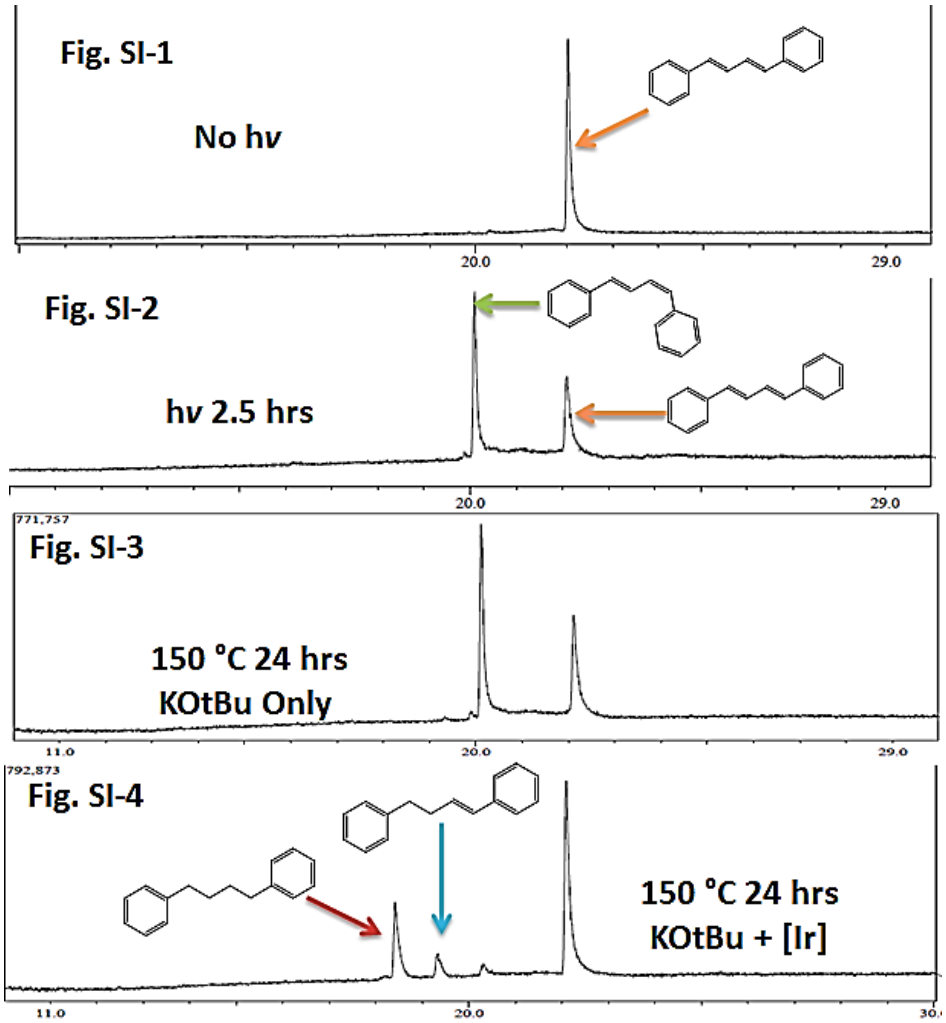

3.5.8. NMR spectra of coupling products and metal complexes

Figure 3. 13. ^{1}H NMR of (*E*,*E*)-1,4-diphenyl-1,3-butadiene (500 MHz, $CDCl_3$)

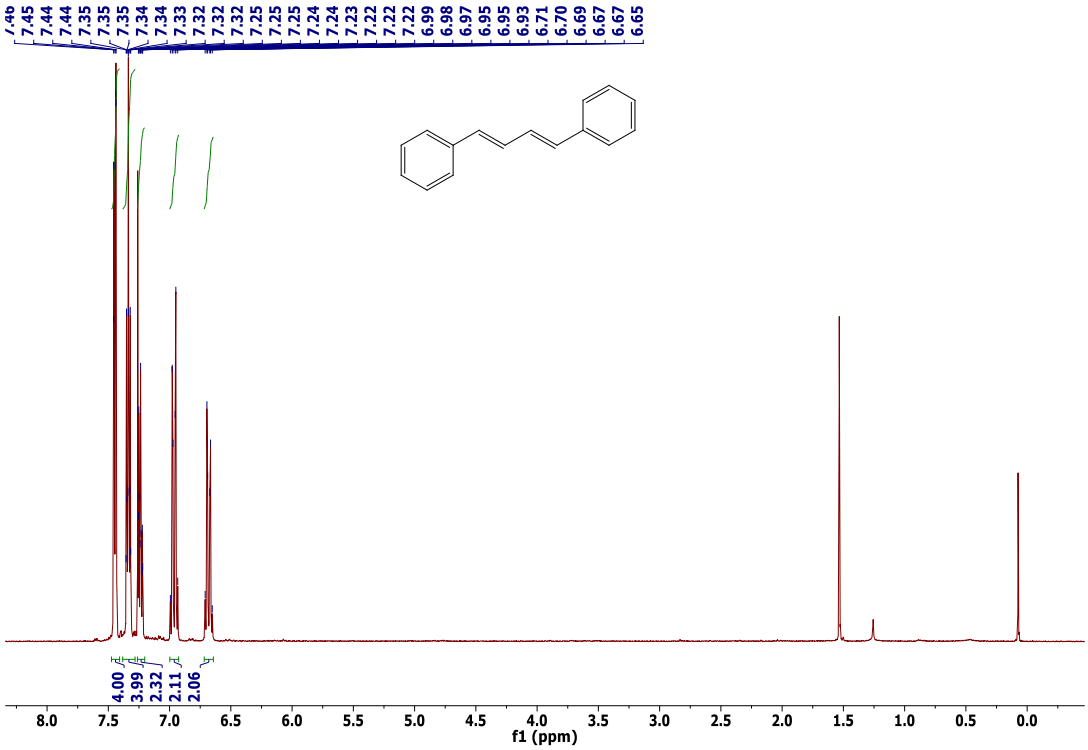

Figure 3. 14. ^{13}C NMR of (*E*,*E*)-1,4-diphenyl-1,3-butadiene (500 MHz, $CDCl_3$)

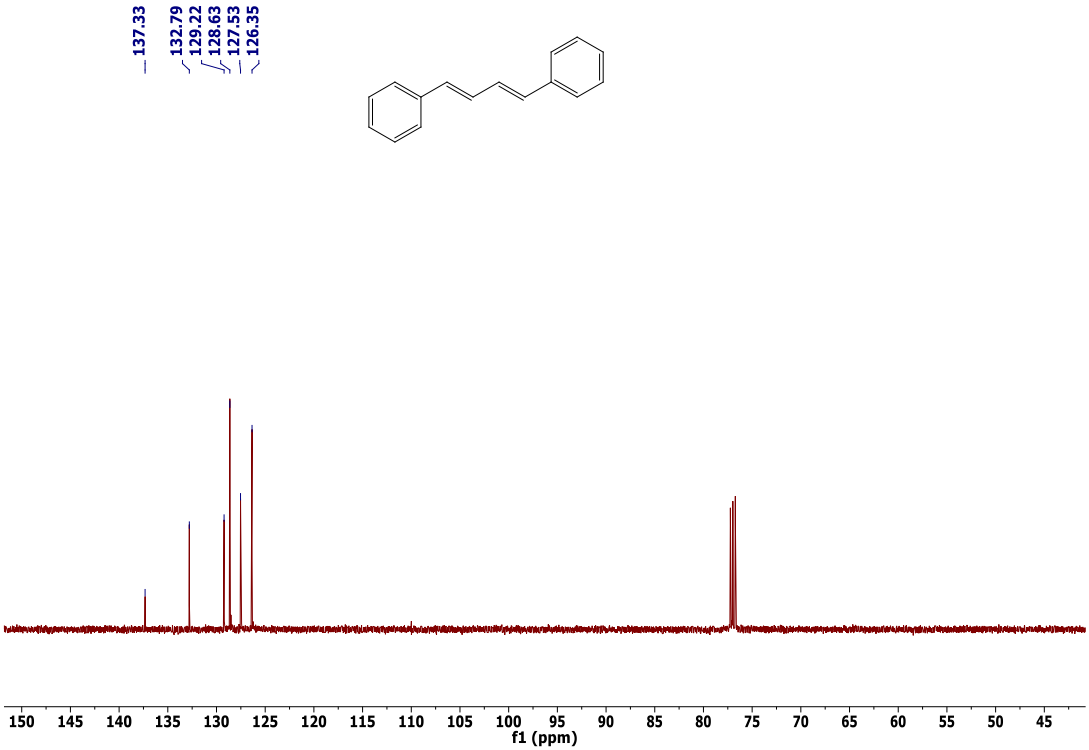

Figure 3. 15. ^{1}H NMR of (*E*,*E*)-1,4-di-(4-tolyl)-1,3-butadiene (500 MHz, $CDCl_3$)

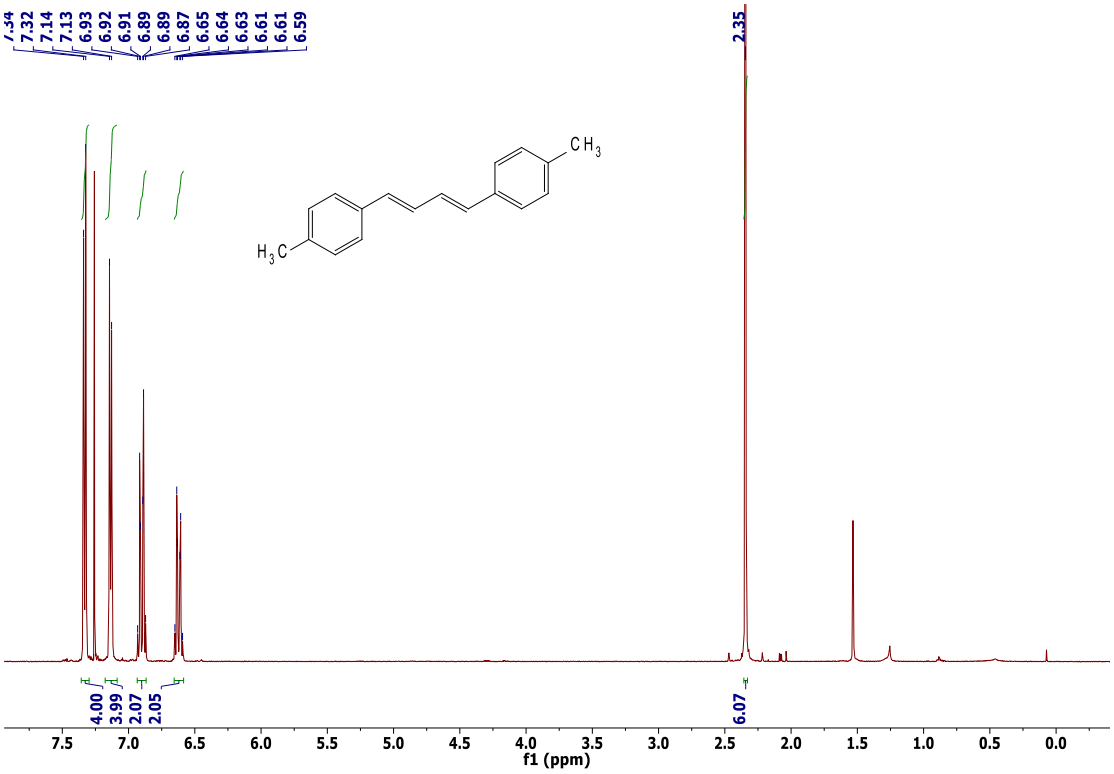

Figure 3. 16. ^{13}C NMR of (*E*,*E*)-1,4-di-(4-tolyl)-1,3-butadiene (500 MHz, $CDCl_3$)

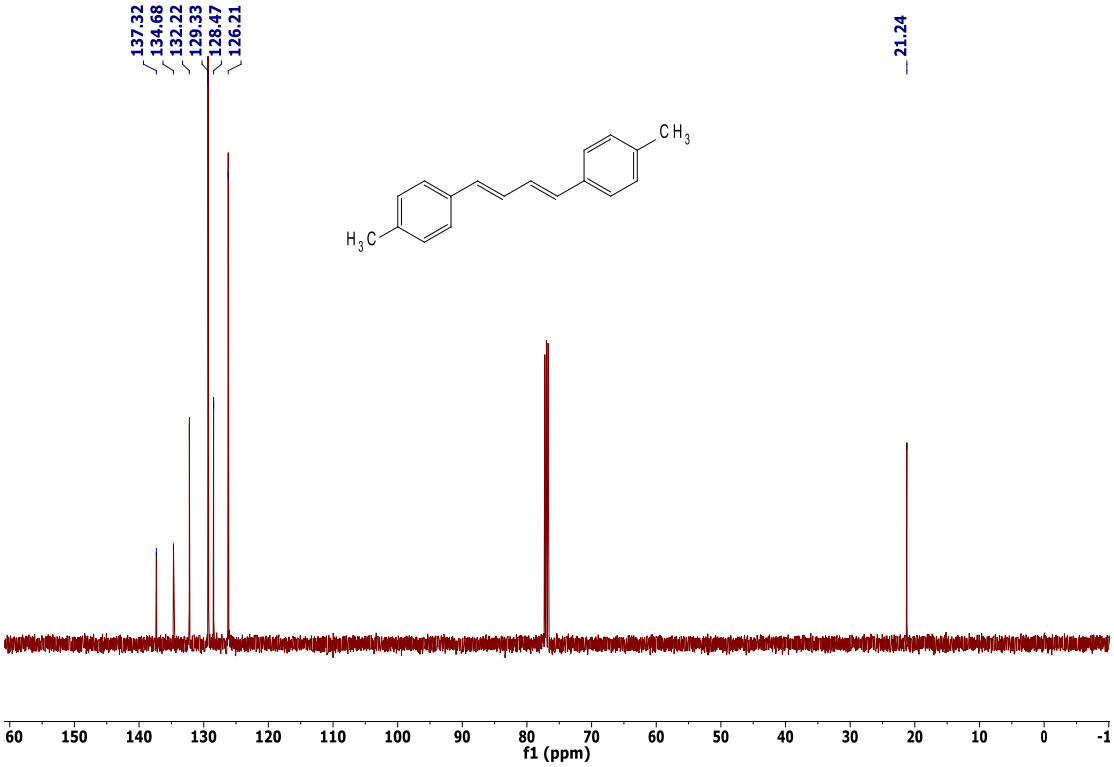

Figure 3. 17. ^{1}H NMR of (*E*,*E*)-1,4-di-(2-tolyl)-1,3-butadiene (500 MHz, $CDCl_3$)

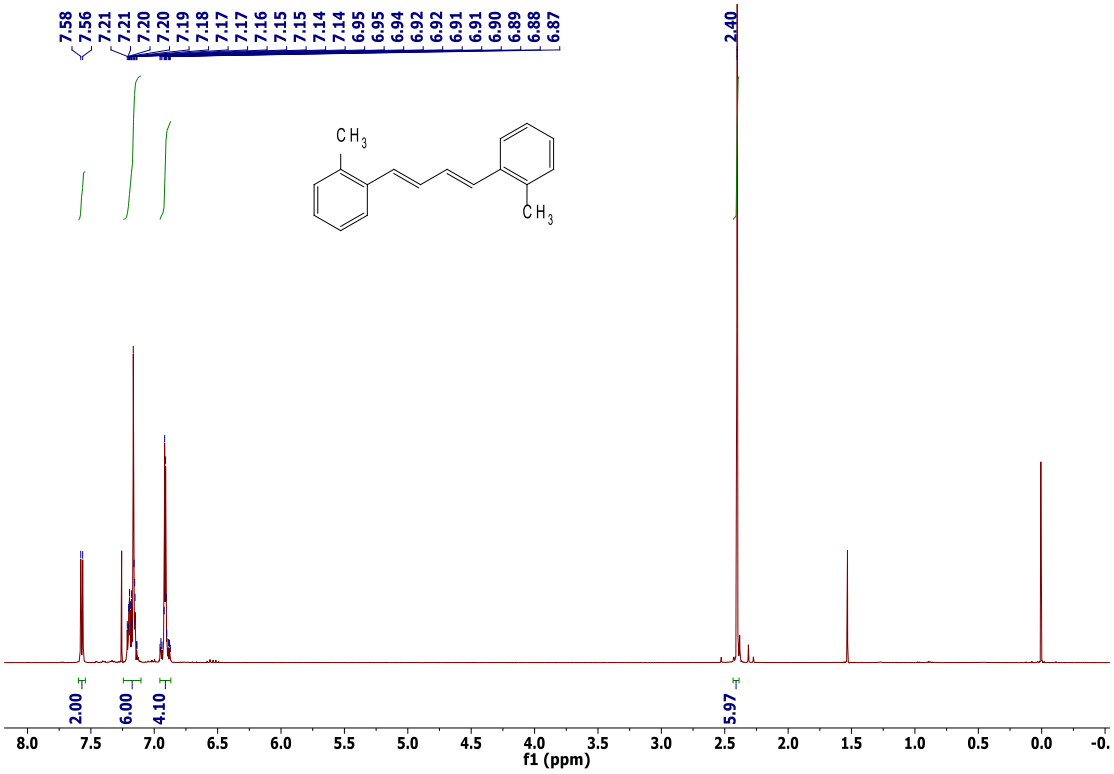

Figure 3. 18. ^{13}C NMR of (*E*,*E*)-1,4-di-(2-tolyl)-1,3-butadiene (500 MHz, $CDCl_3$)

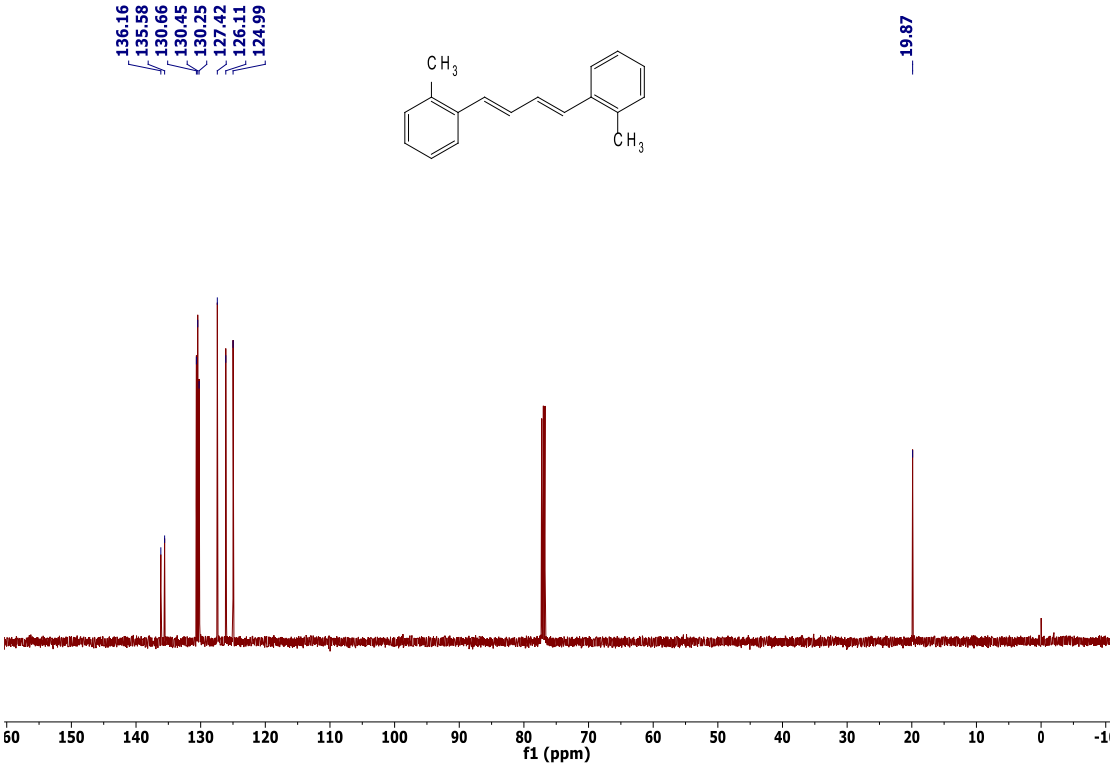

Figure 3. 19. ^{1}H NMR of (*E*,*E*)-1,4-di-[4-(Trifluoromethyl)phenyl]-1,3-butadiene (500 MHz, $CDCl_3$)

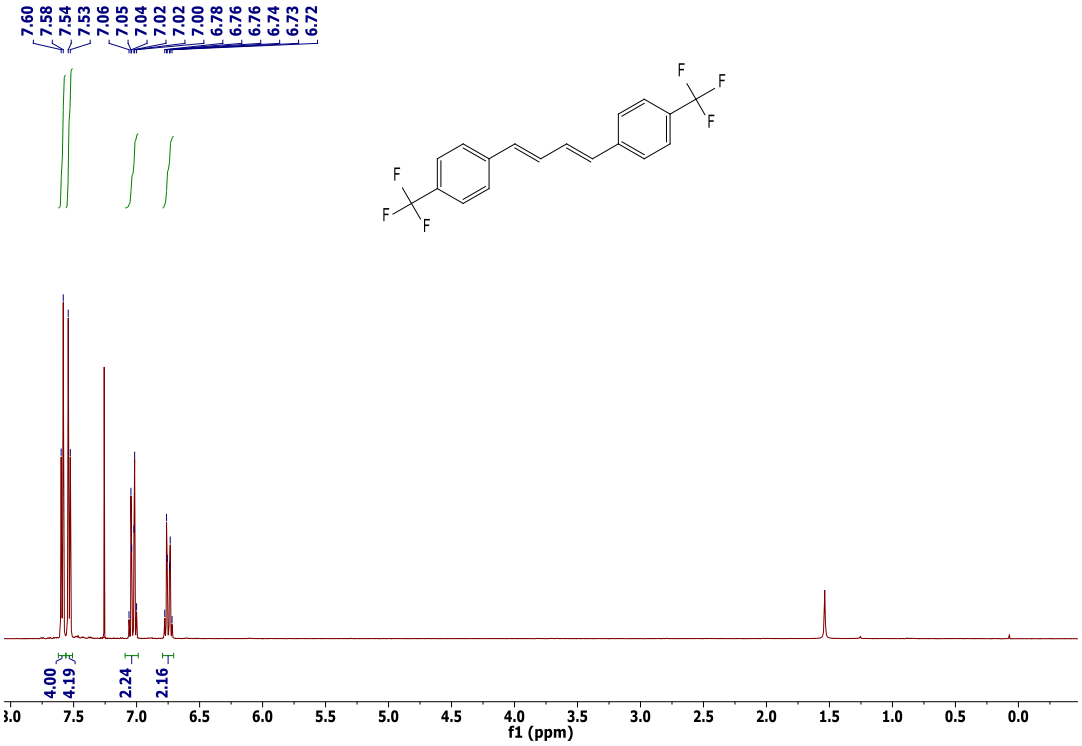

Figure 3. 20. ^{13}C NMR of (*E*,*E*)-1,4-di-[4-(trifluoromethyl)phenyl]-1,3-butadiene (500 MHz, $CDCl_3$)

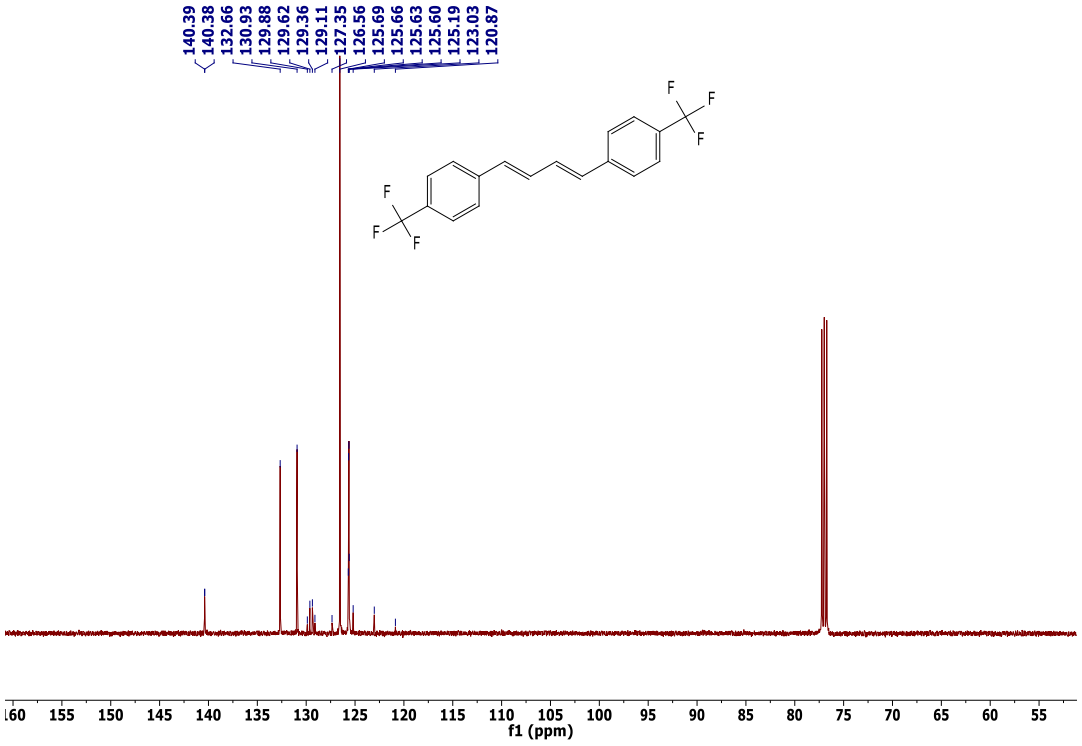

Figure 3. 21. ^{1}H NMR of (*E*,*E*)-1,4- di-(4-fluorophenyl)-1,3-butadiene (500 MHz, $CDCl_3$)

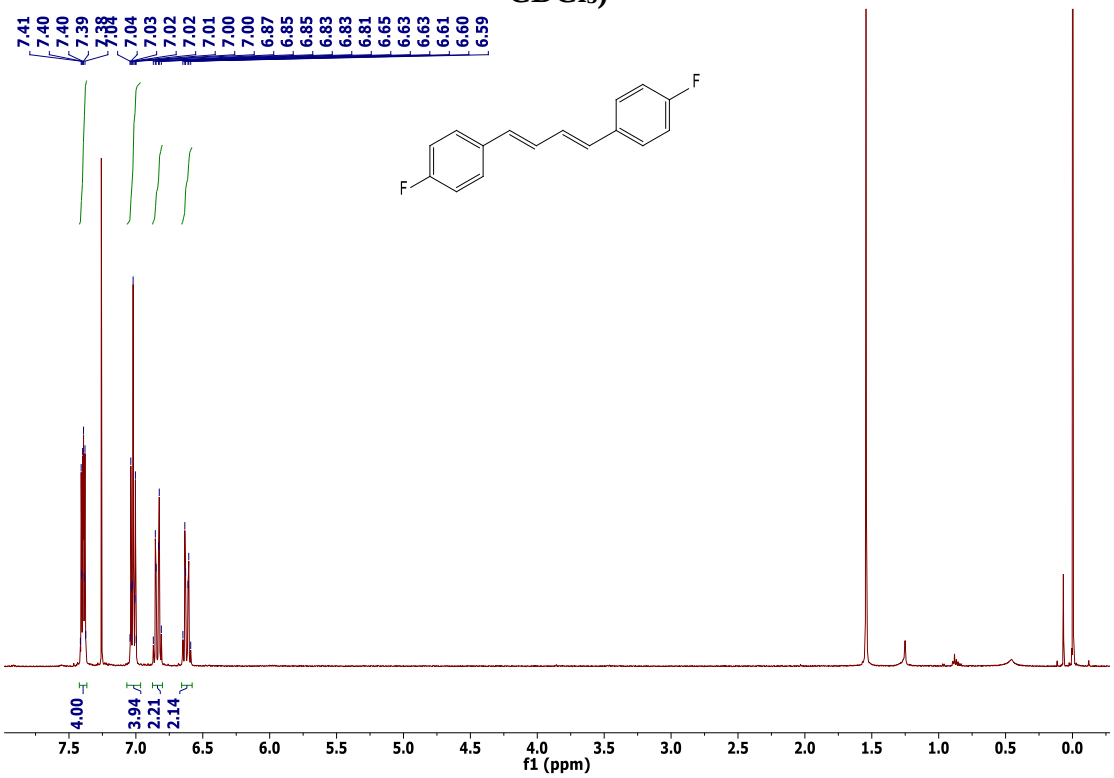

Figure 3. 22. ^{13}C NMR of (*E*,*E*)-1,4- di-(4-fluorophenyl)-1,3-butadiene (500 MHz, $CDCl_3$)

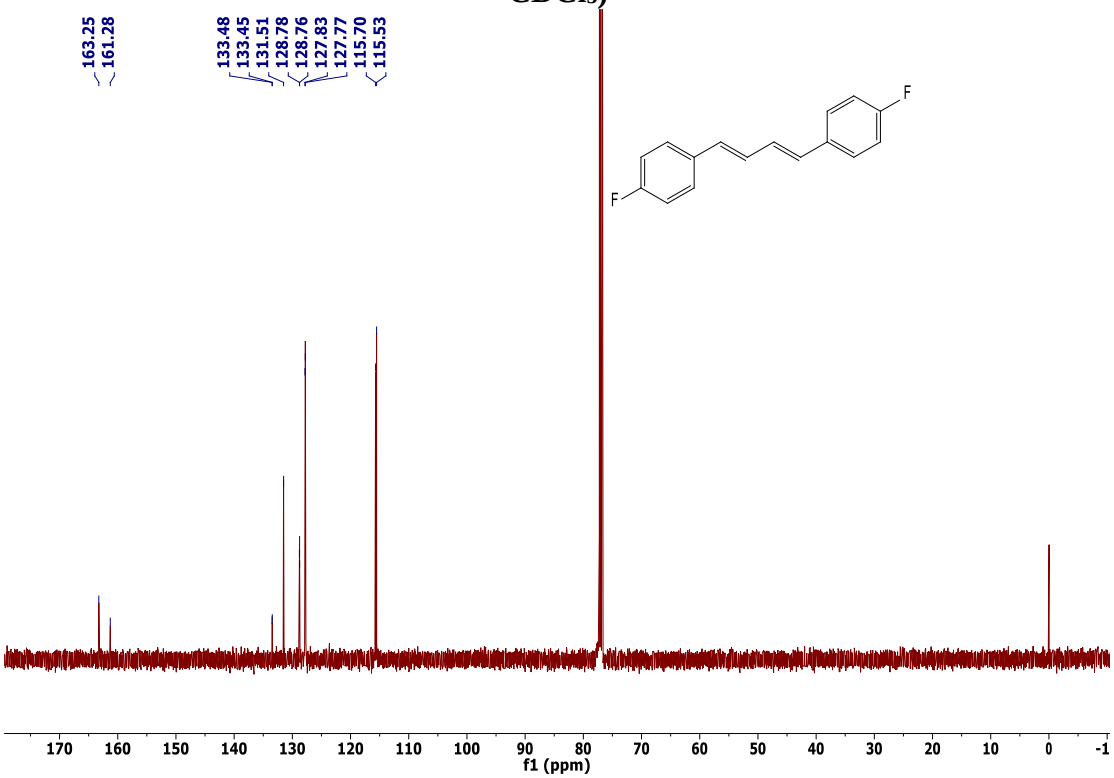

Figure 3. 23. ^{1}H NMR of (*E*,*E*)-1,4-di-(4-tert-butylphenyl)-1,3-butadiene (500 MHz, $CDCl_3$)

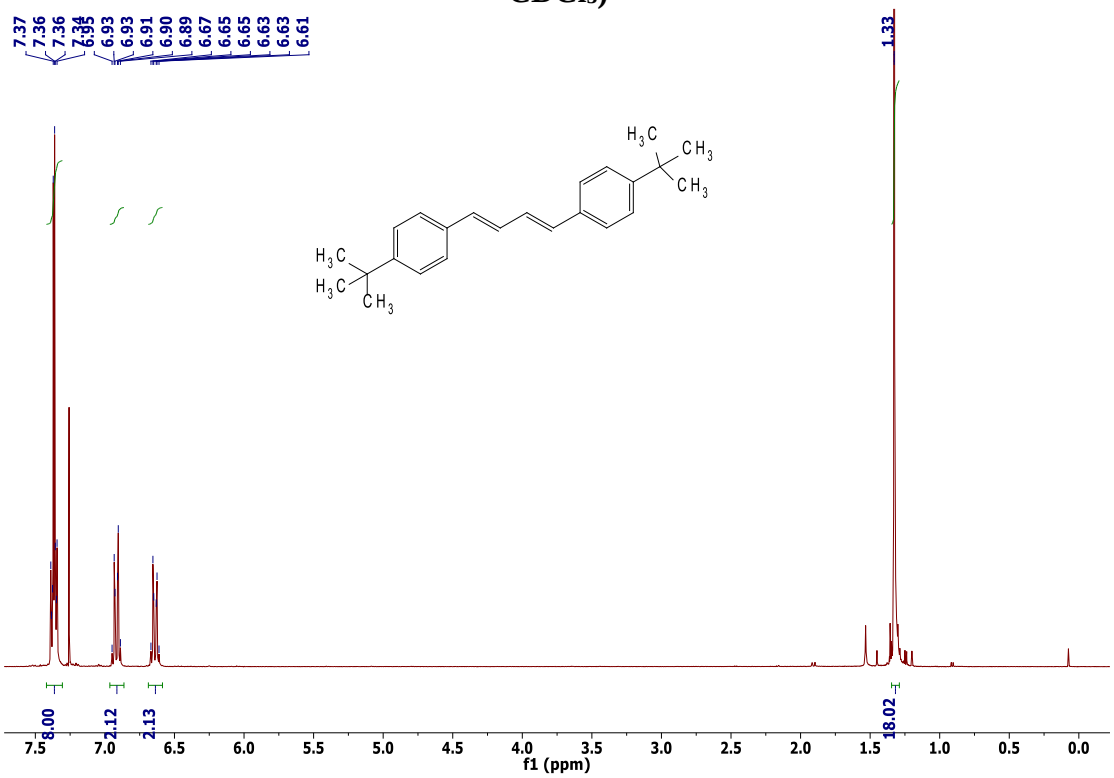

Figure 3. 24. ^{13}C NMR of (*E*,*E*)-1,4-di-(4-tert-butylphenyl)-1,3-butadiene (500 MHz, $CDCl_3$)

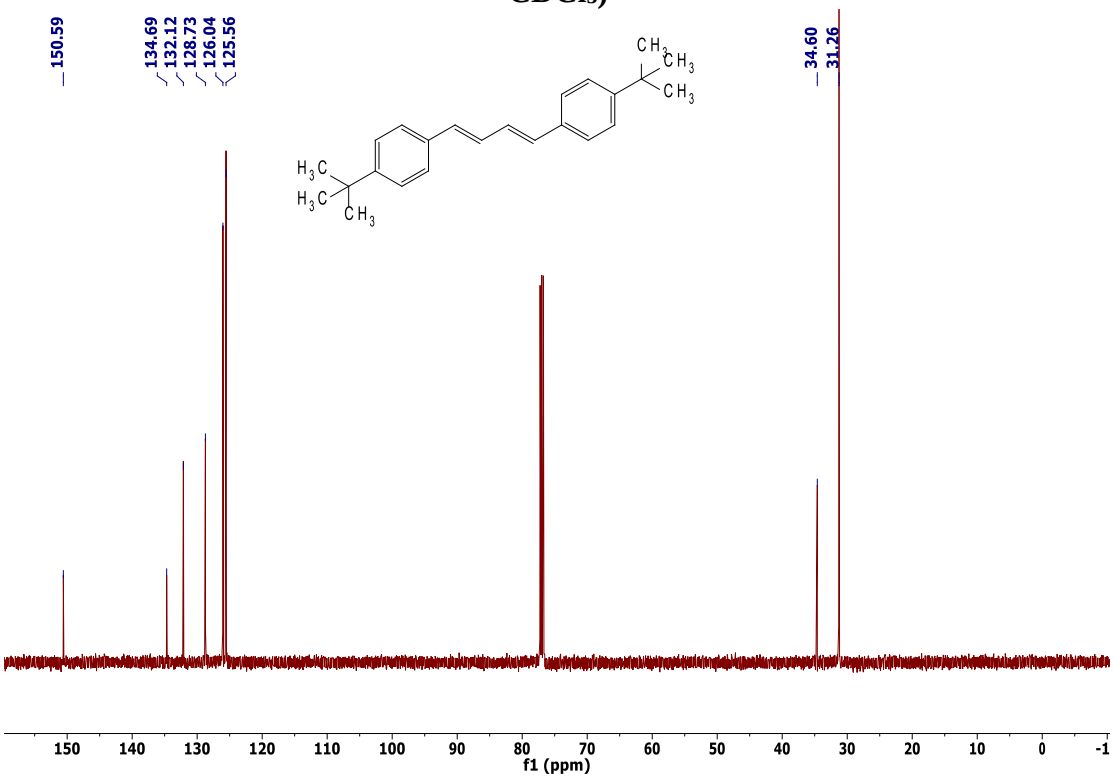

Figure 3. 25. ^{1}H NMR of (*E*,*E*)-1,4-di-(4-methoxyphenyl)-1,3-butadiene (500 MHz, $CDCl_3$)

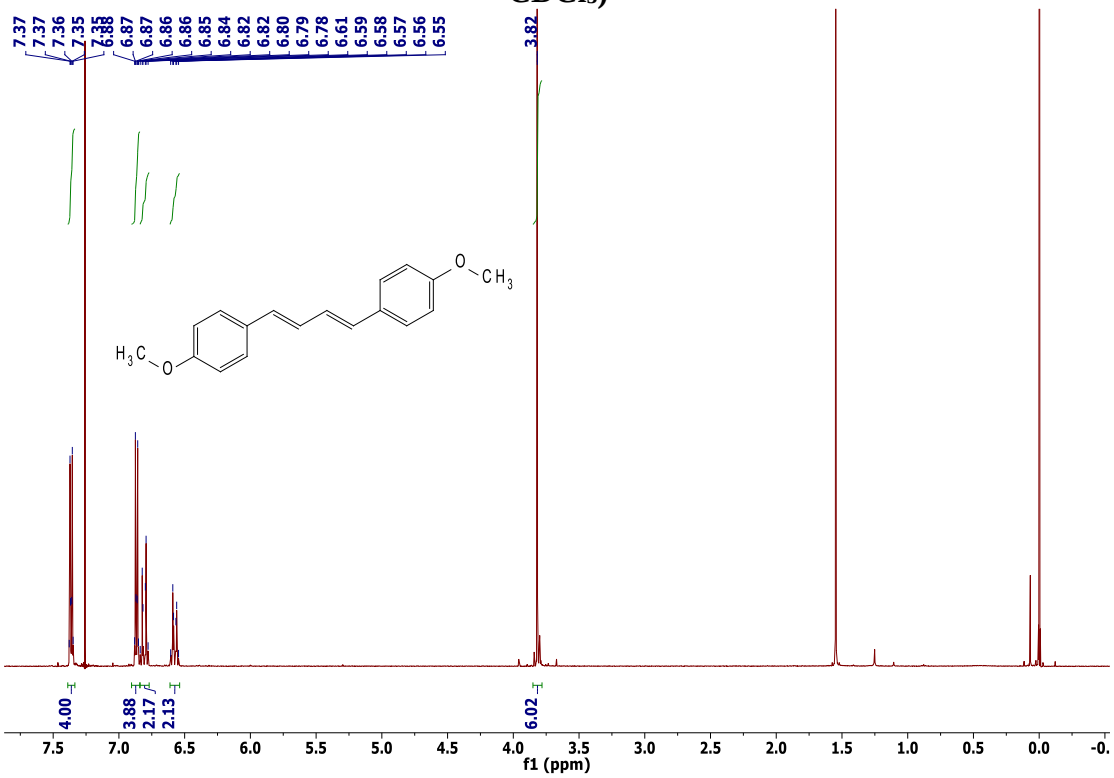

Figure 3. 26. ^{13}C NMR of (*E*,*E*)-1,4-di-(4-methoxyphenyl)-1,3-butadiene (500 MHz, $CDCl_3$)

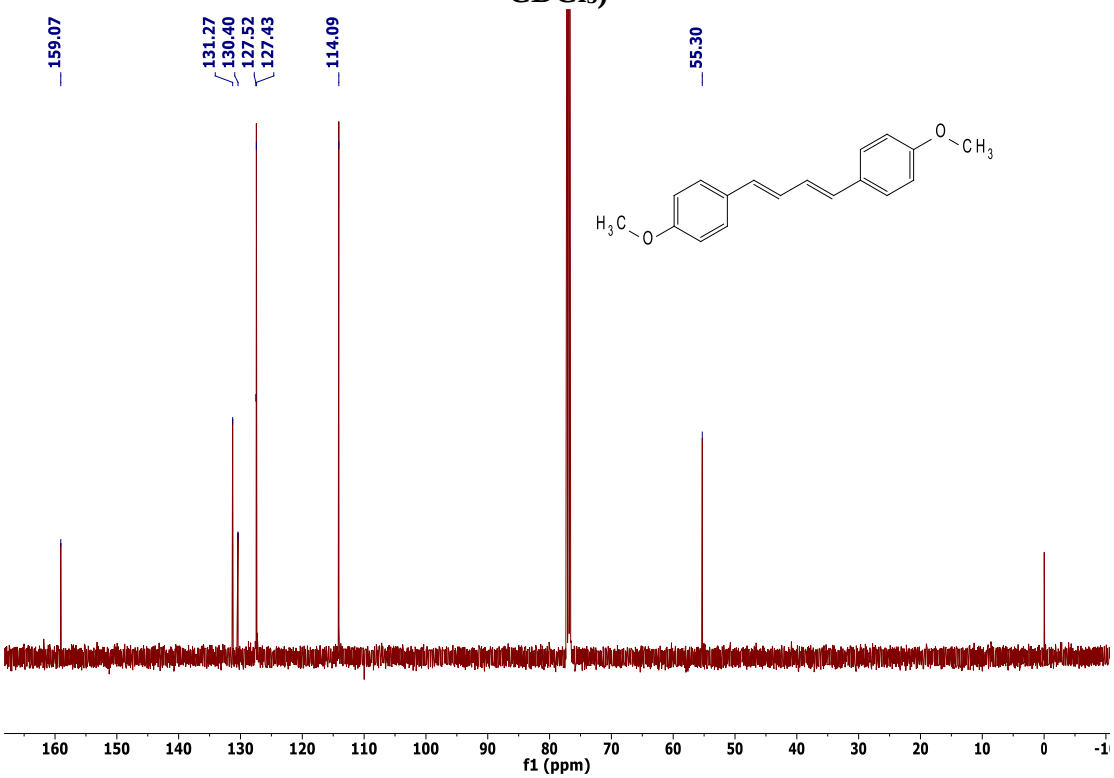

Figure 3. 27. ^{1}H NMR of (*E*,*E*)-1,4-di-(3,5-dimethylphenyl)-1,3-butadiene (500 MHz, $CDCl_3$)

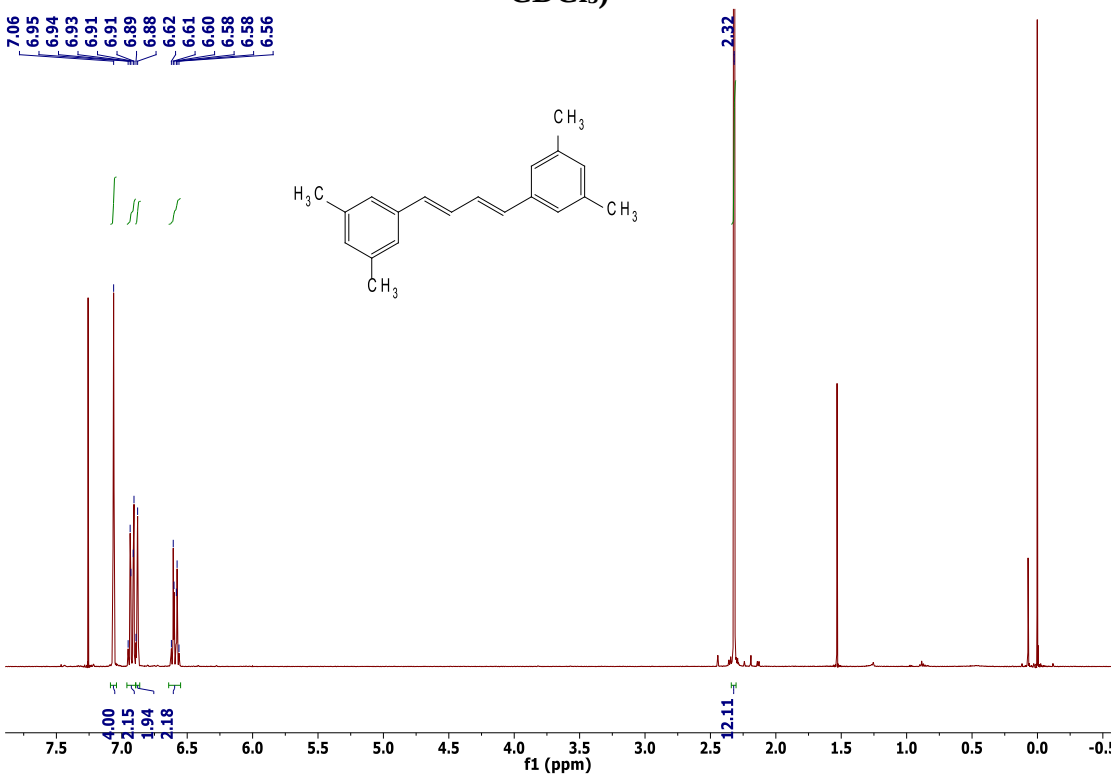

Figure 3. 28. ^{13}C NMR of (*E*,*E*)-1,4-d-(3,5-dimethylphenyl)-1,3-butadiene (500 MHz, $CDCl_3$)

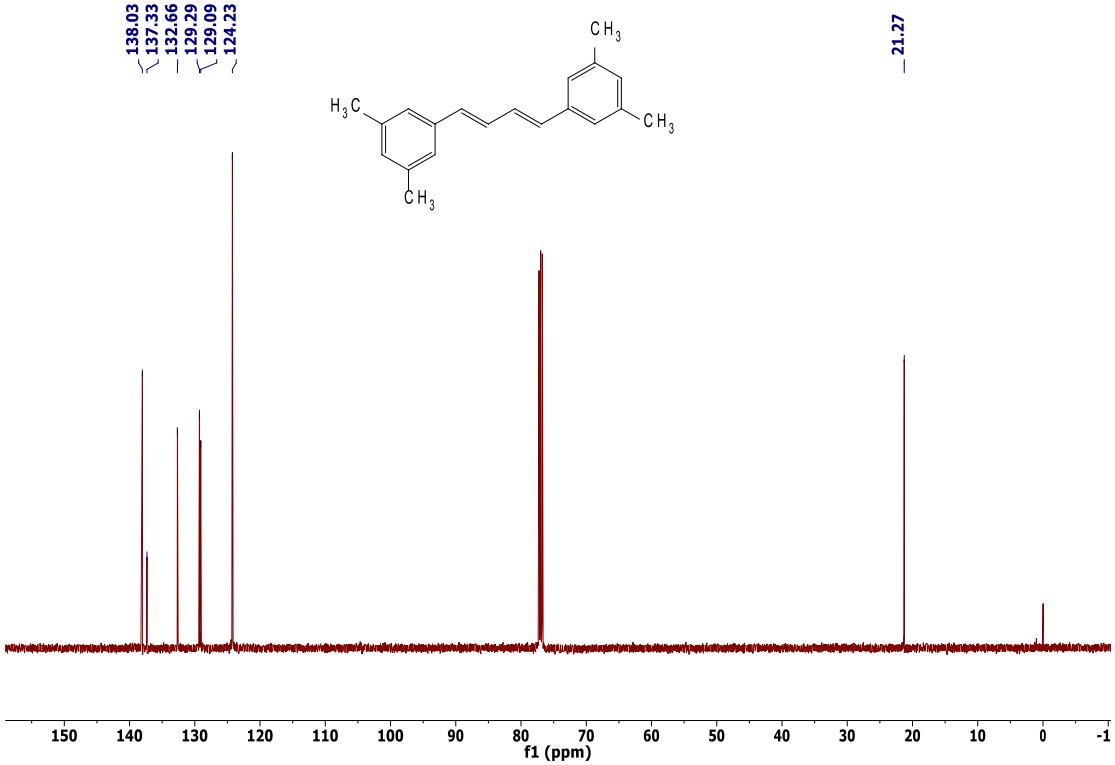

Figure 3. 29.^{1}H NMR of (*E*,*E*)-1,4-di-(3,5-ditrifluoromethylphenyl)-1,3-butadiene (500 MHz, $CDCl_3$)

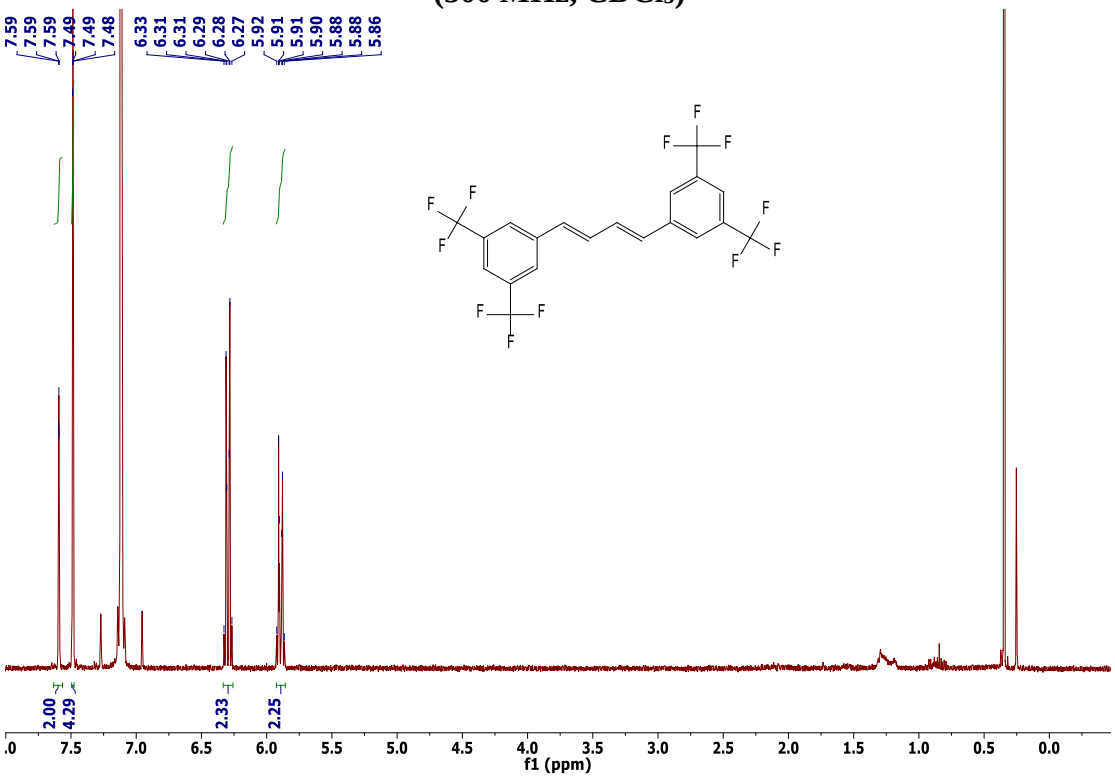

Figure 3. 30. ^{1}H NMR of (*E*,*E*)-1,4-(2-naphthyl)-1,3-butadiene (400 MHz, CD_2Cl_2)

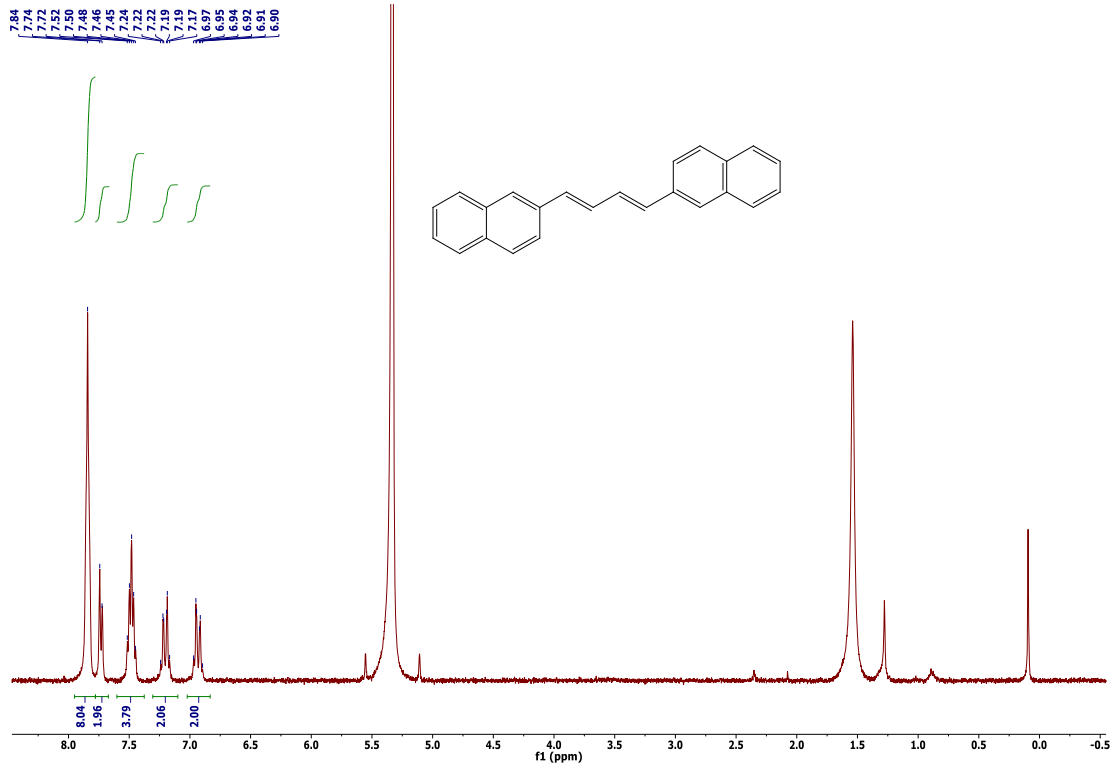

Figure 3. 31. ^{1}H NMR of 1,2,3,4,5-pentafluoro-6-[(1*E*,3*E*)-4-phenyl-1,3-butadien-1-yl]benzene

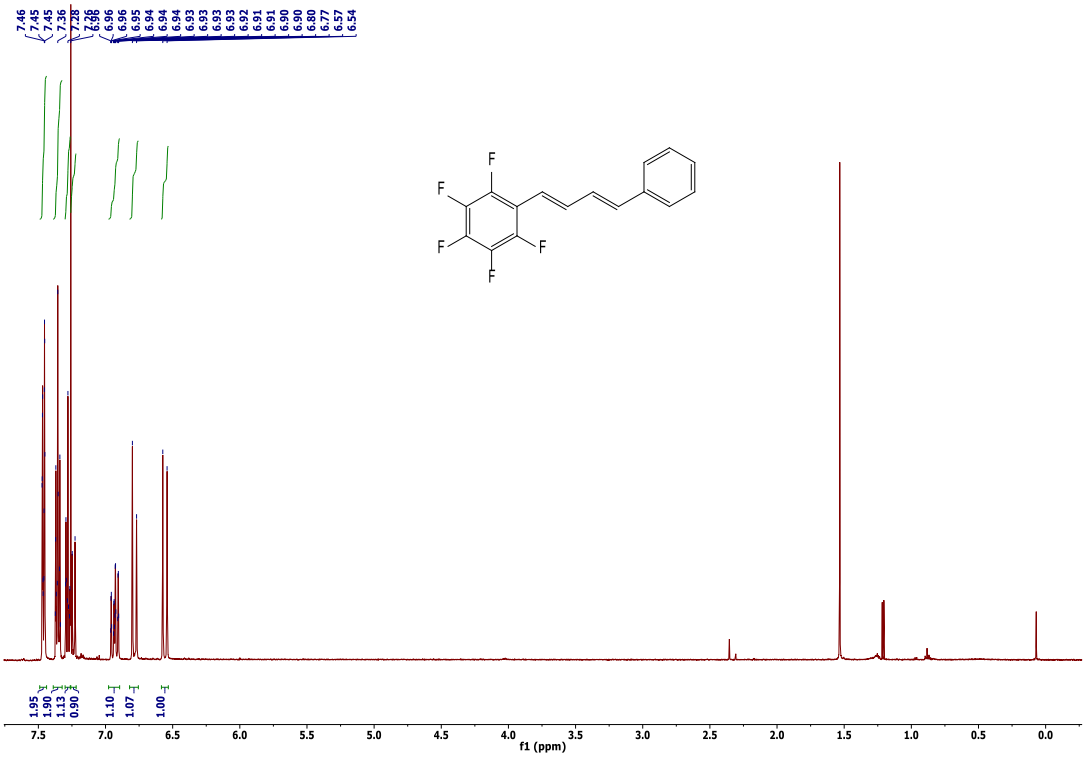

Figure 3. 32. ^{13}C NMR of 1,2,3,4,5-pentafluoro-6-[(1*E*,3*E*)-4-phenyl-1,3-butadien-1-yl]benzene

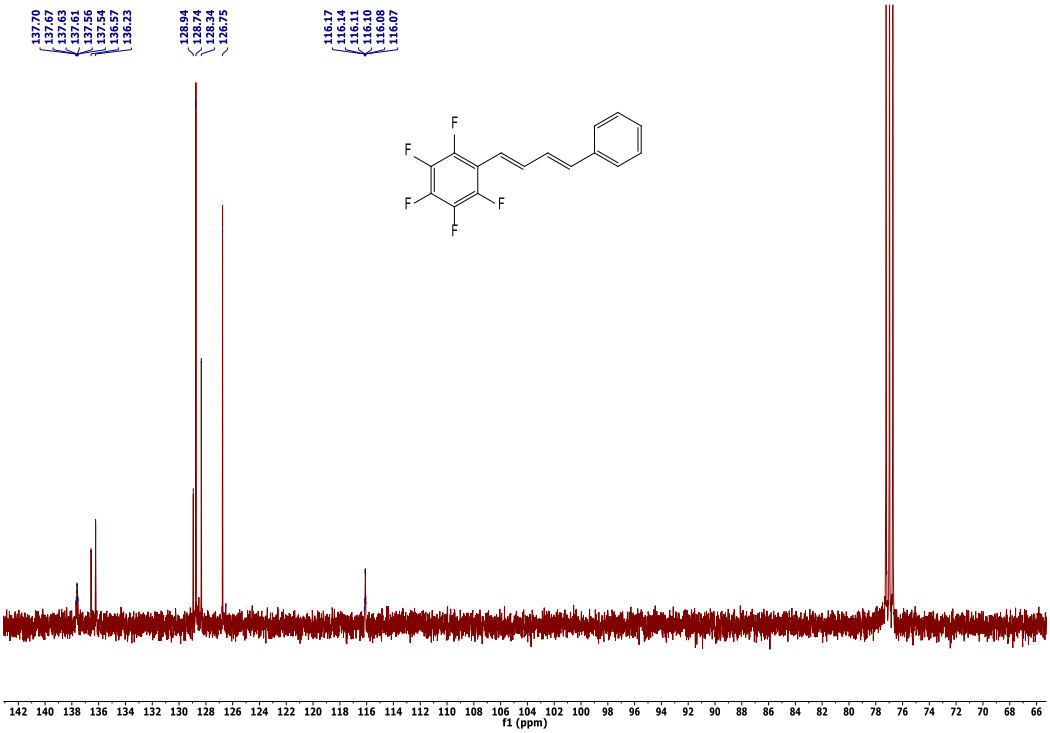

Figure 3. 33. ^{1}H NMR of 4,6-dimethylindene and 5,7-dimethylindene mixture

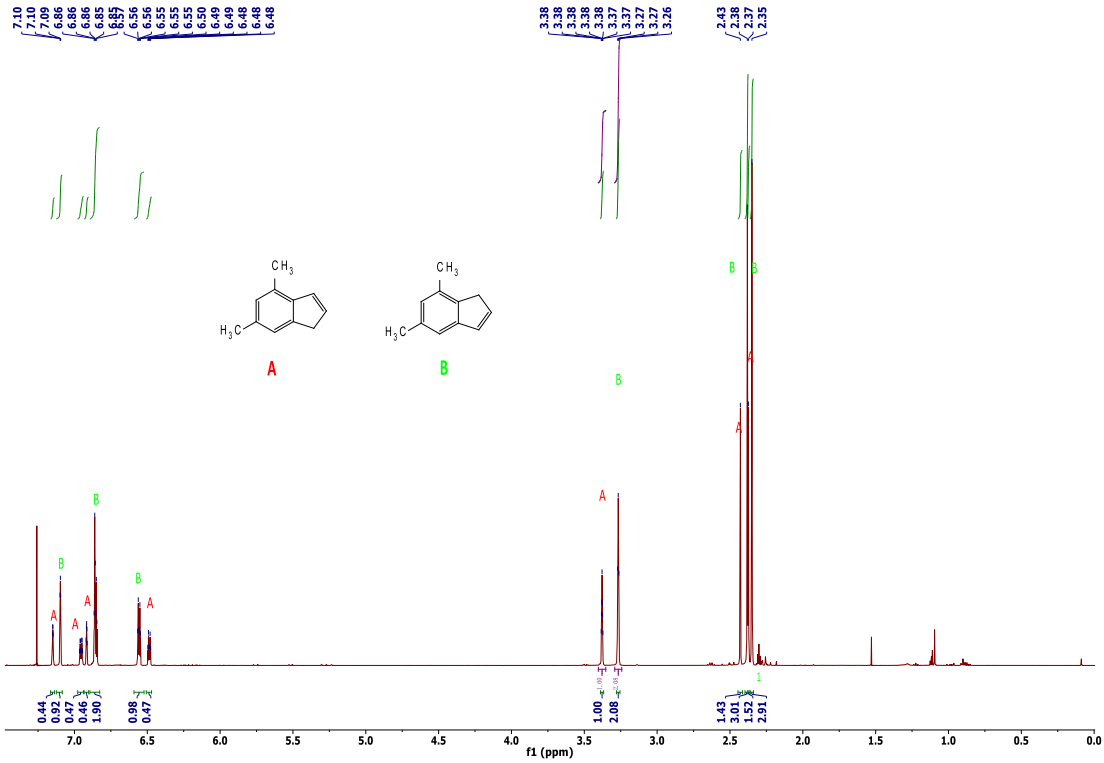

Figure 3. 34. ^{13}C NMR of 4,6-dimethylindene and 5,7-dimethylindene mixture

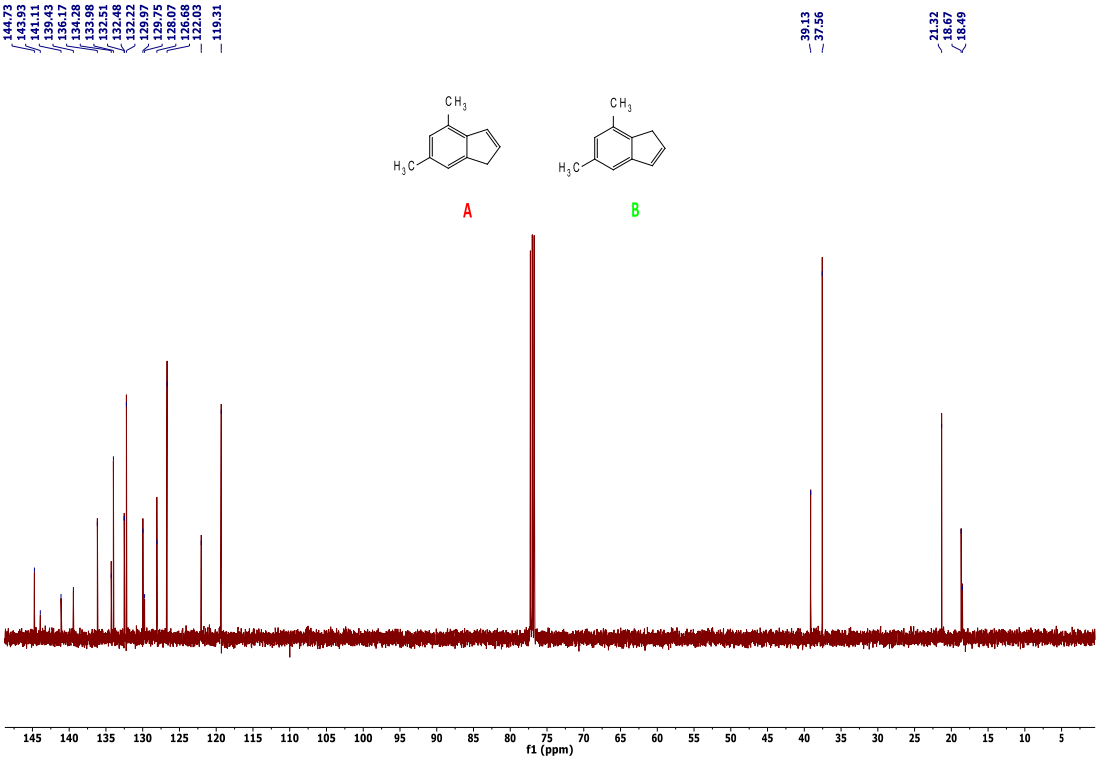

Figure 3. 35. ^{1}H NMR of 1-ethyl-2,4,6-trimethylbenzene and 4,6-dimethylindane mixture

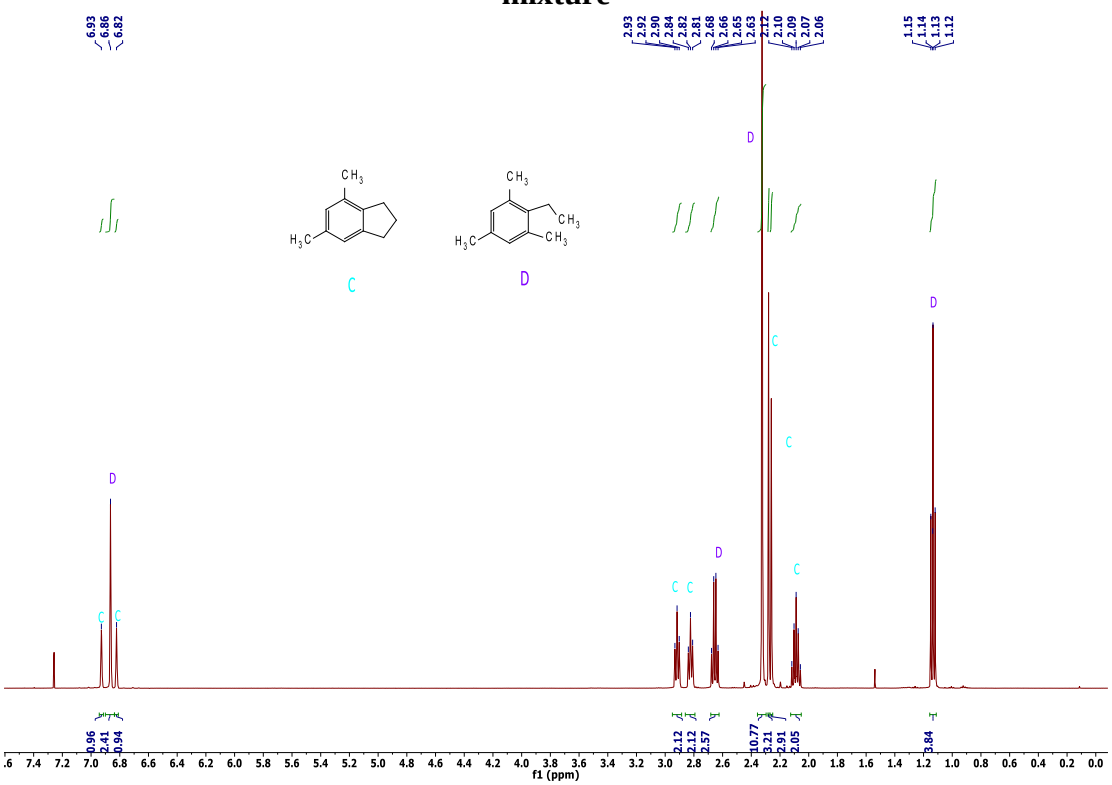

Figure 3. 36. ^{13}C NMR of 1-ethyl-2,4,6-trimethylbenzene and 4,6-dimethylindane mixture

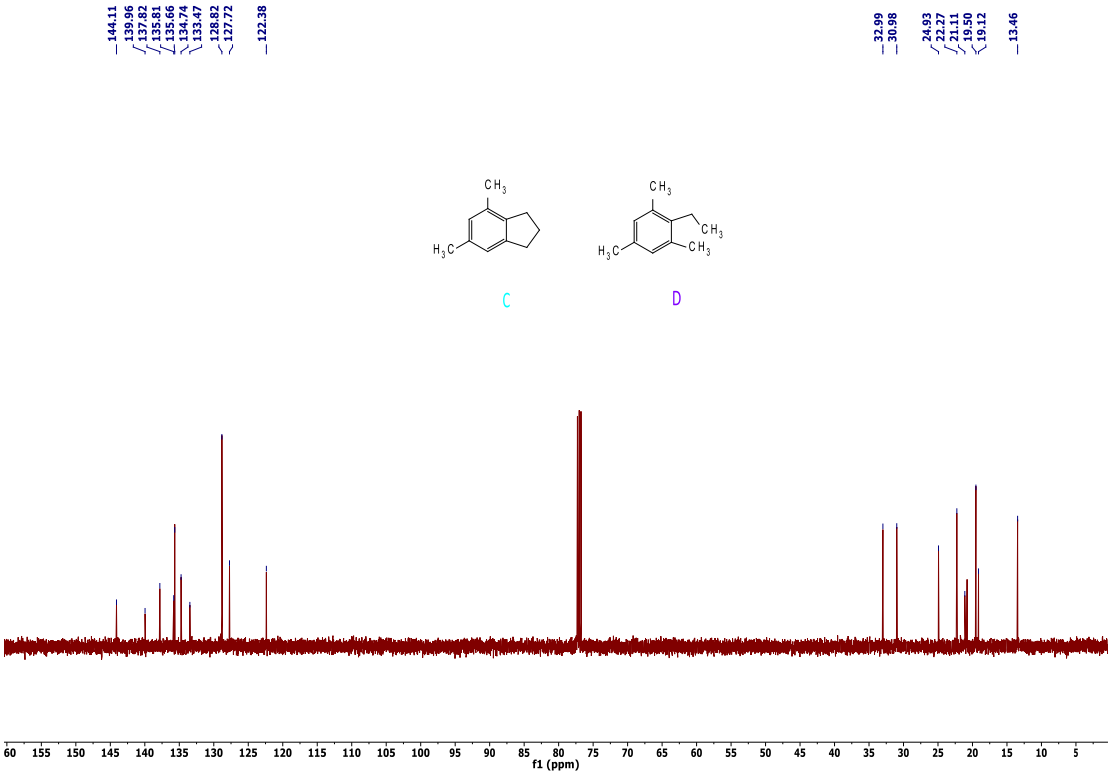

Figure 3. 37. ^{1}H NMR of 4,6-dimethylindane

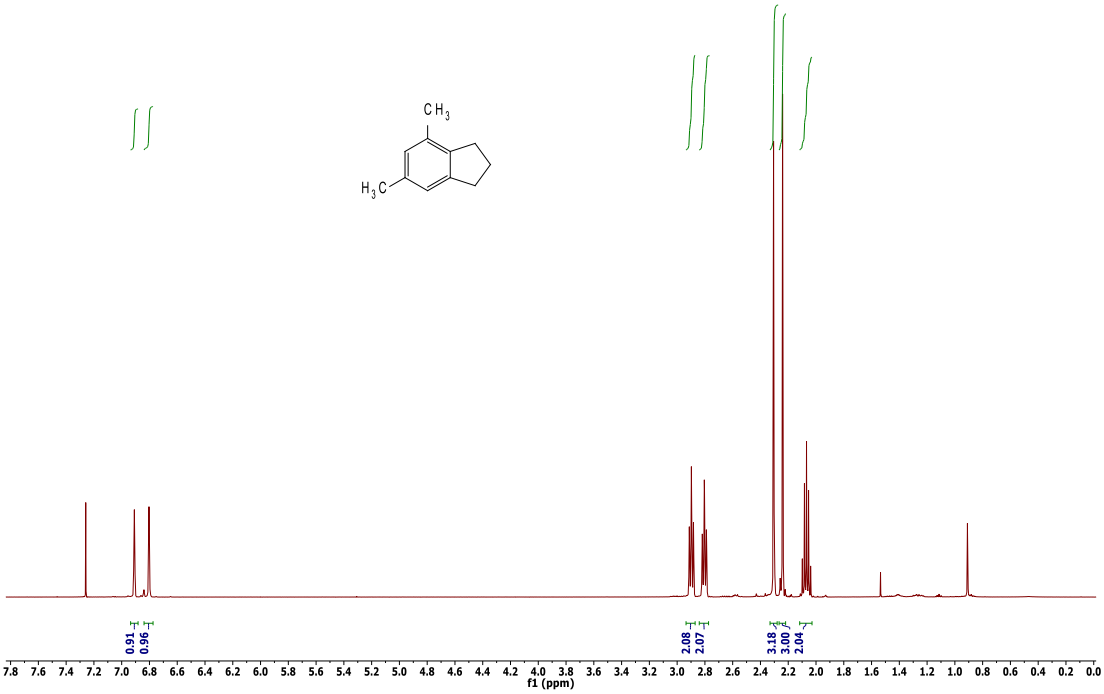

Figure 3. 38. ^{13}C NMR of 4,6-dimethylindane

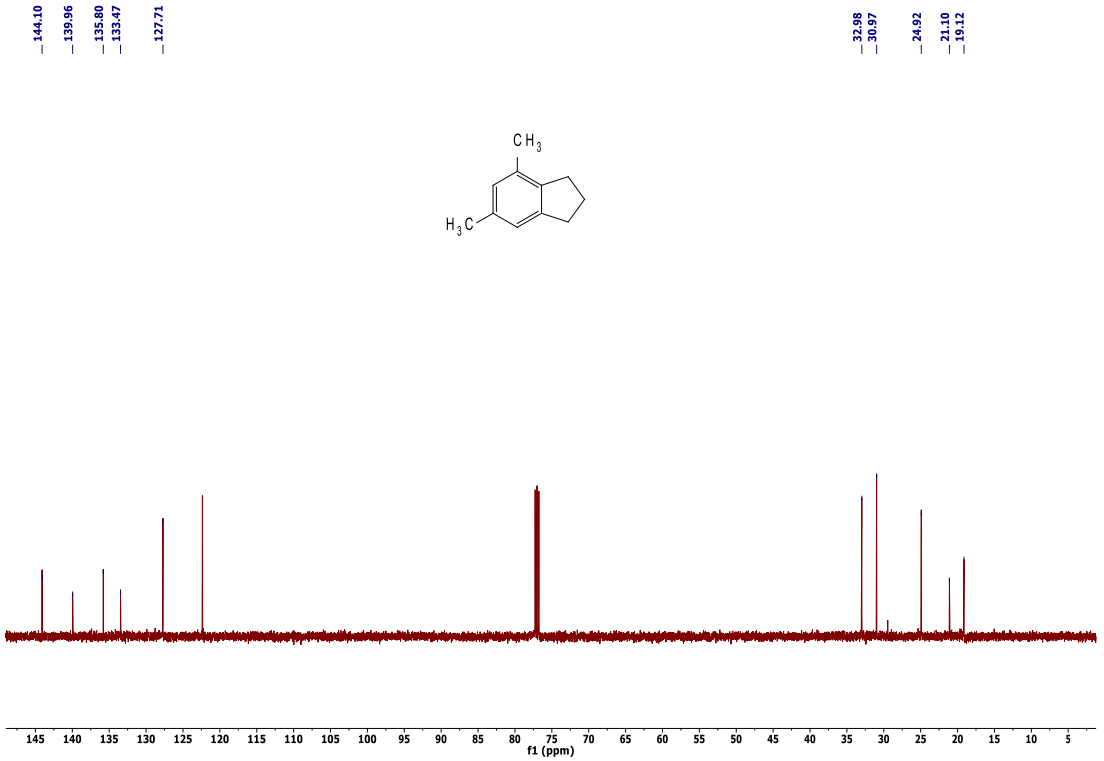

Figure 3. 39. ^{1}H NMR of (^{iPr}PCP)Ir(η^2-H$_2$C=CH-phenyl), 2

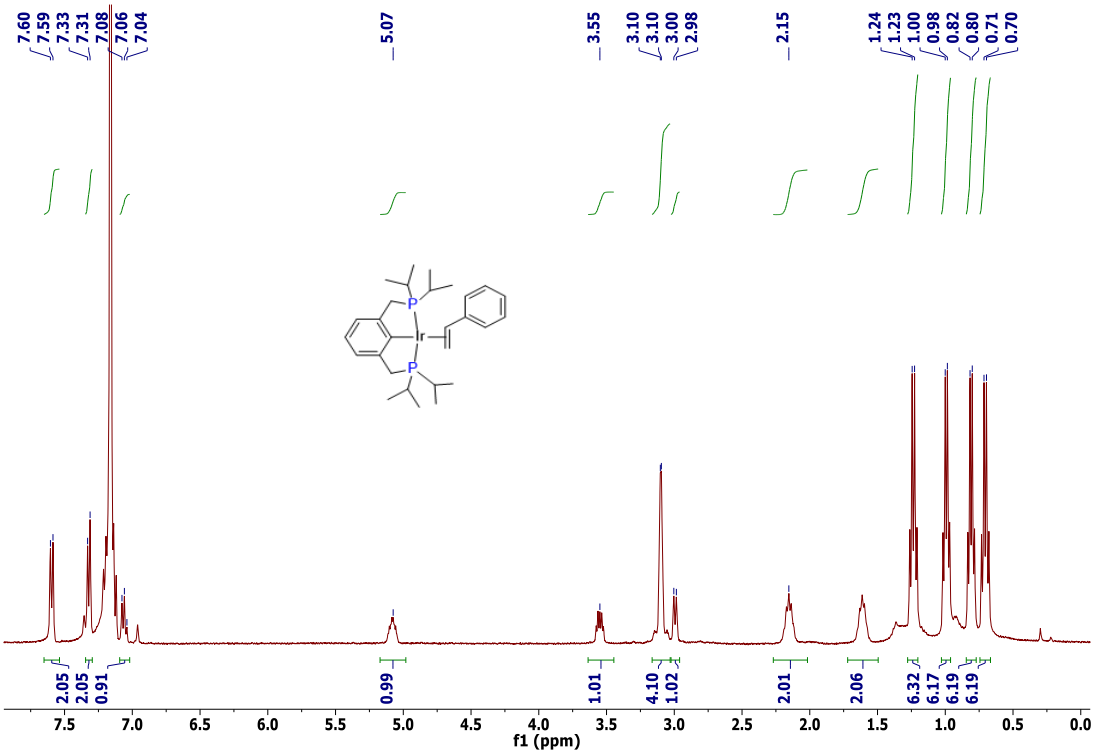

Figure 3. 40. ^{31}P NMR of (^{iPr}PCP)Ir(η^2-H$_2$C=CH-phenyl), 2

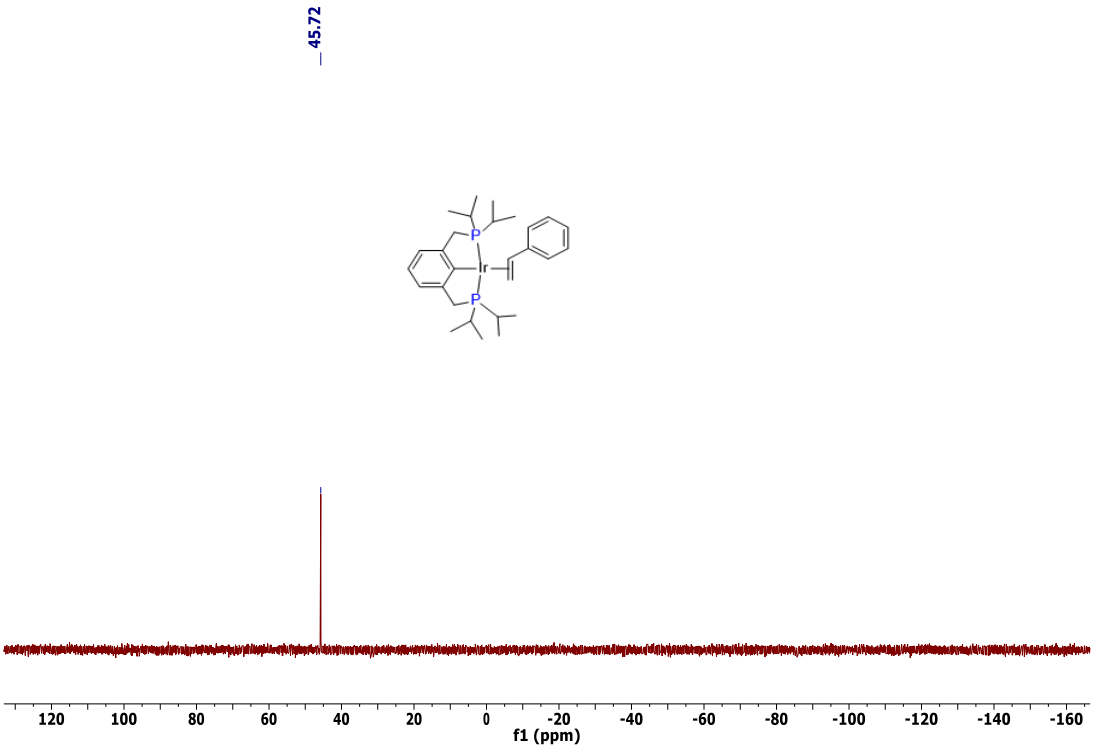

Figure 3. 41. ^{1}H NMR of metalloindene complex 3

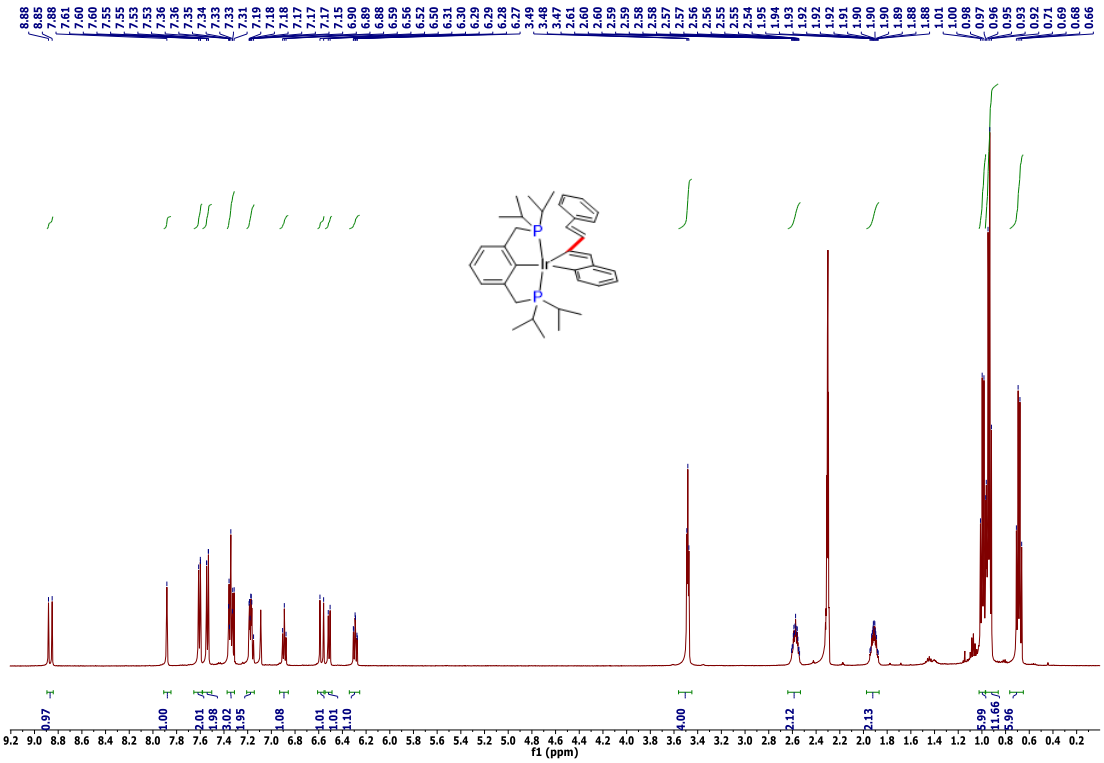

Figure 3. 42. ^{13}C NMR metalloindene complex 3

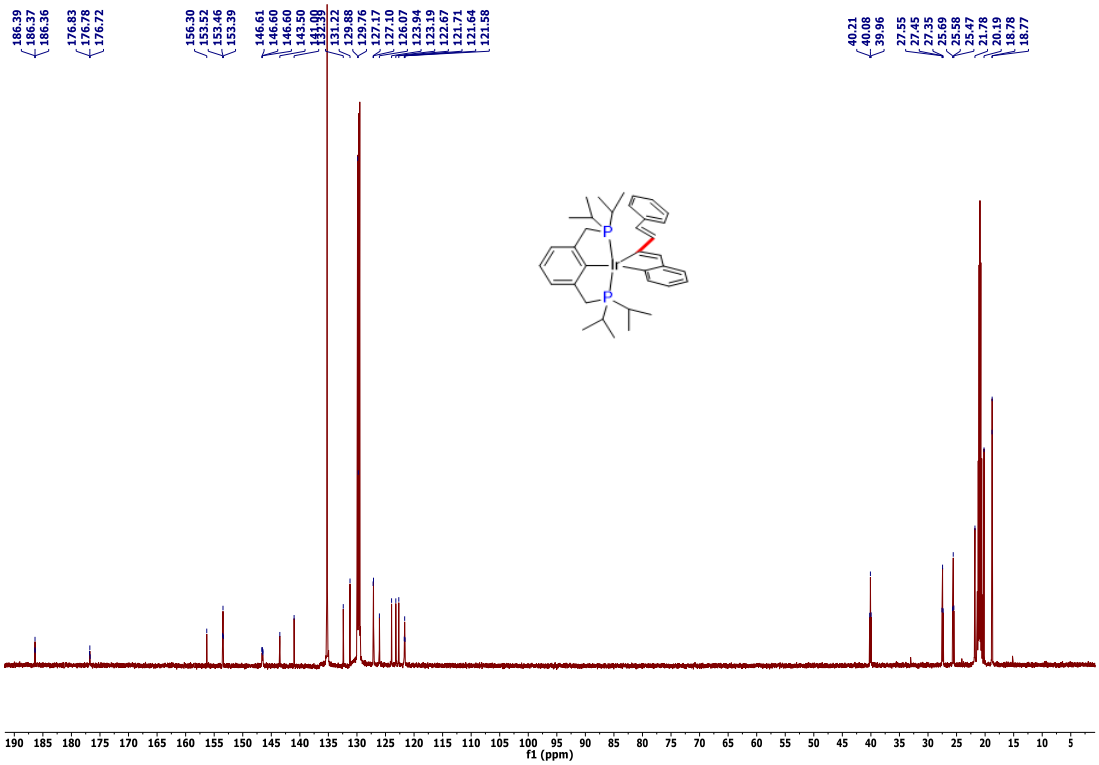

Figure 3. 43. ^{31}P NMR of metalloindene complex 3

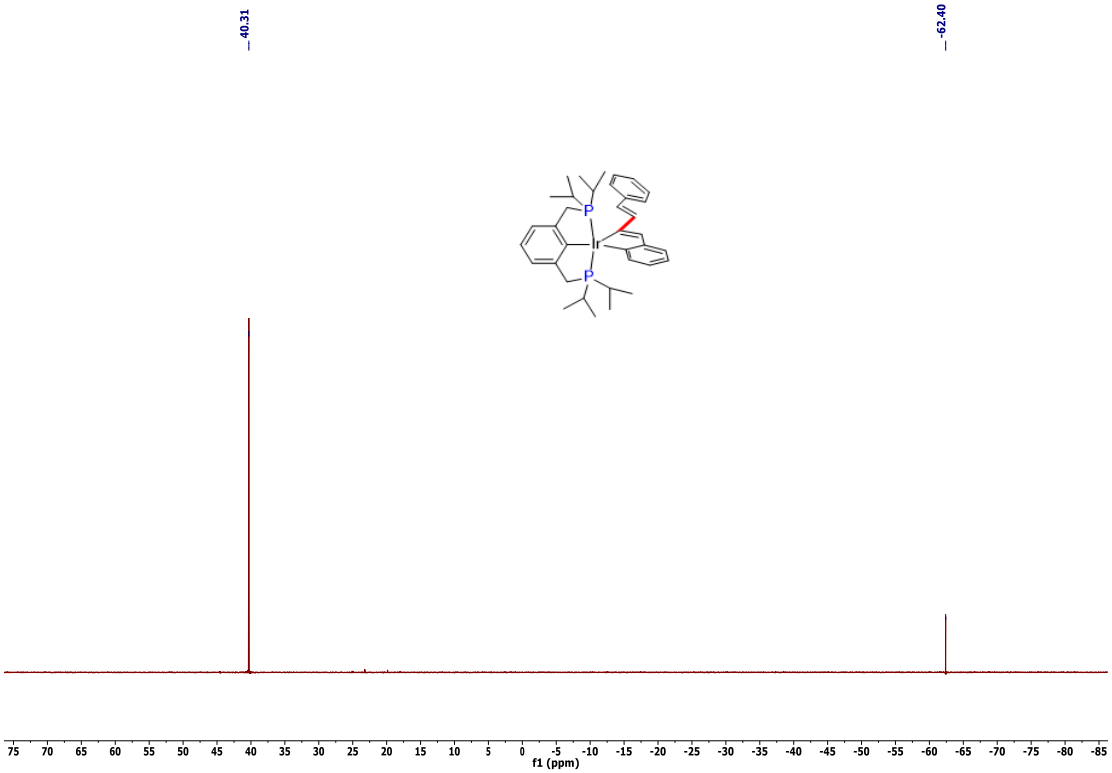

Figure 3. 44. ^{1}H NMR of metalloindene complex 4

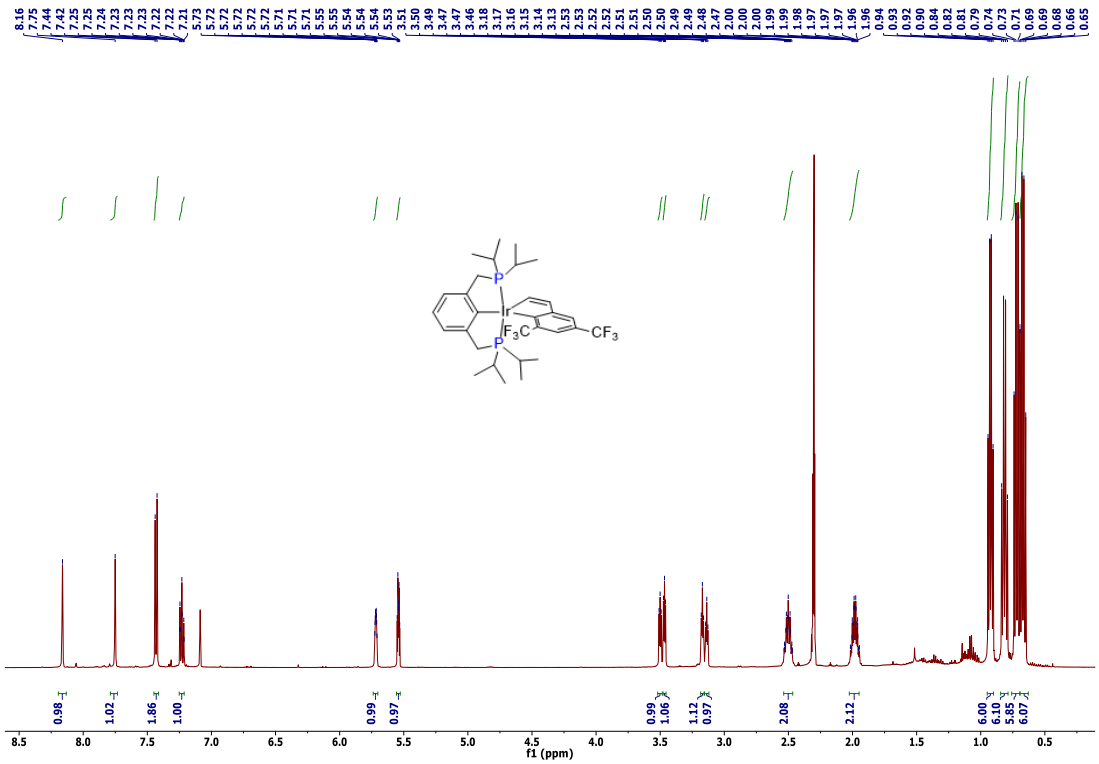

Figure 3. 45. ^{13}C NMR of metalloindene complex 4

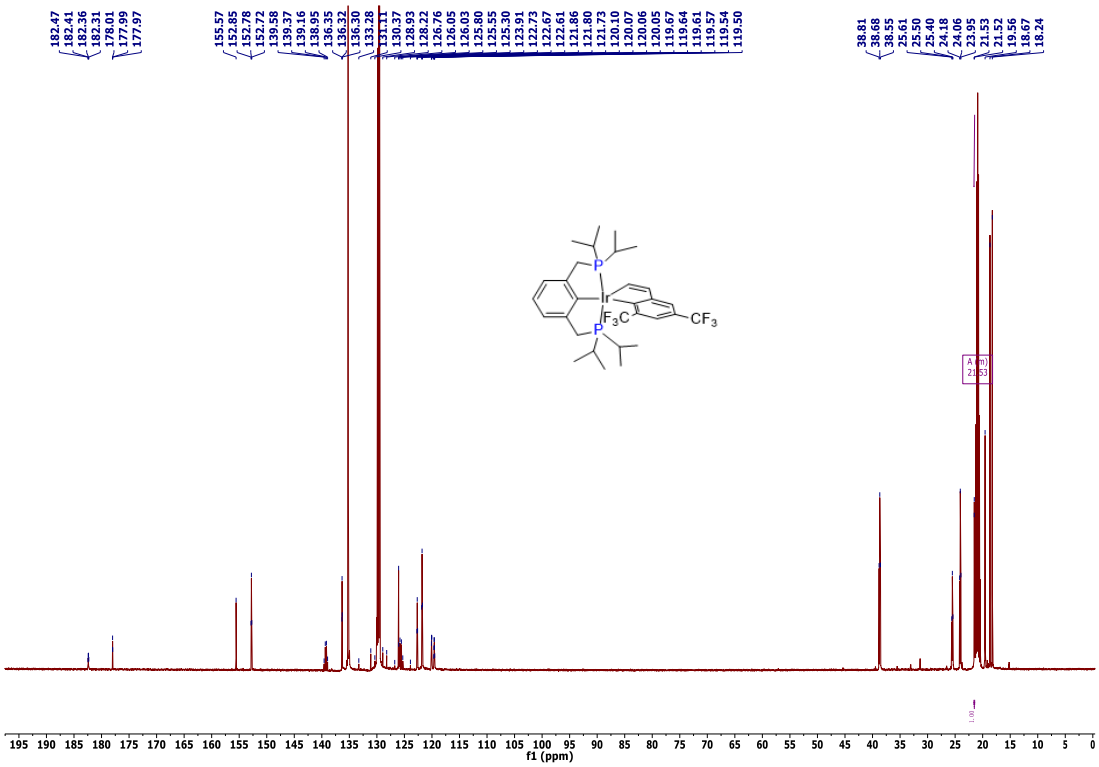

Figure 3. 46. ^{31}P NMR of metalloindene complex 4

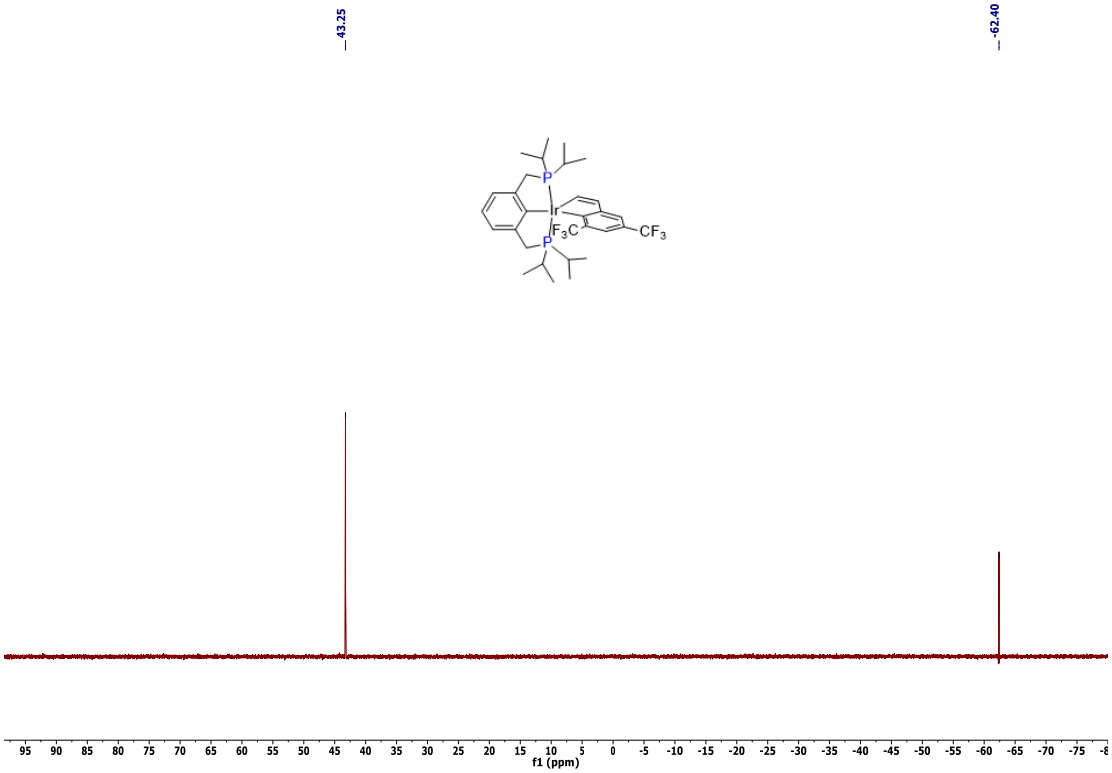

Figure 3. 47. ^{1}H NMR of metalloindene complex 5

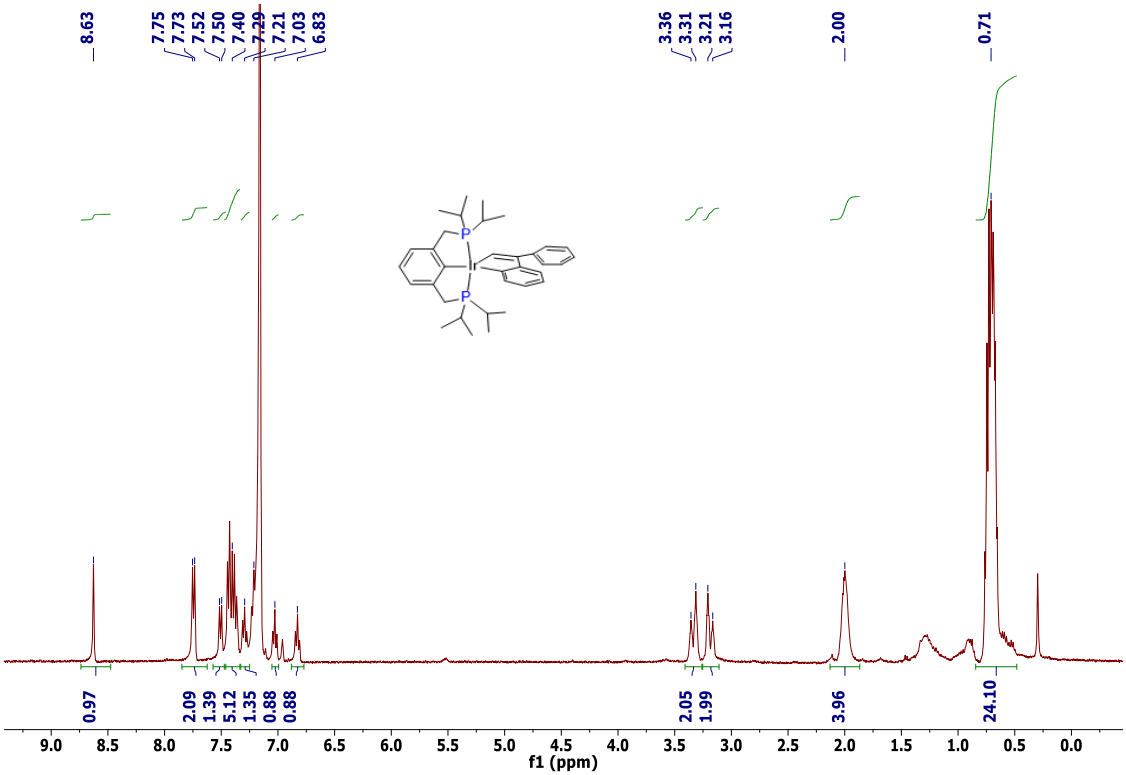

Figure 3. 48. ^{31}P NMR of metalloindene complex 5

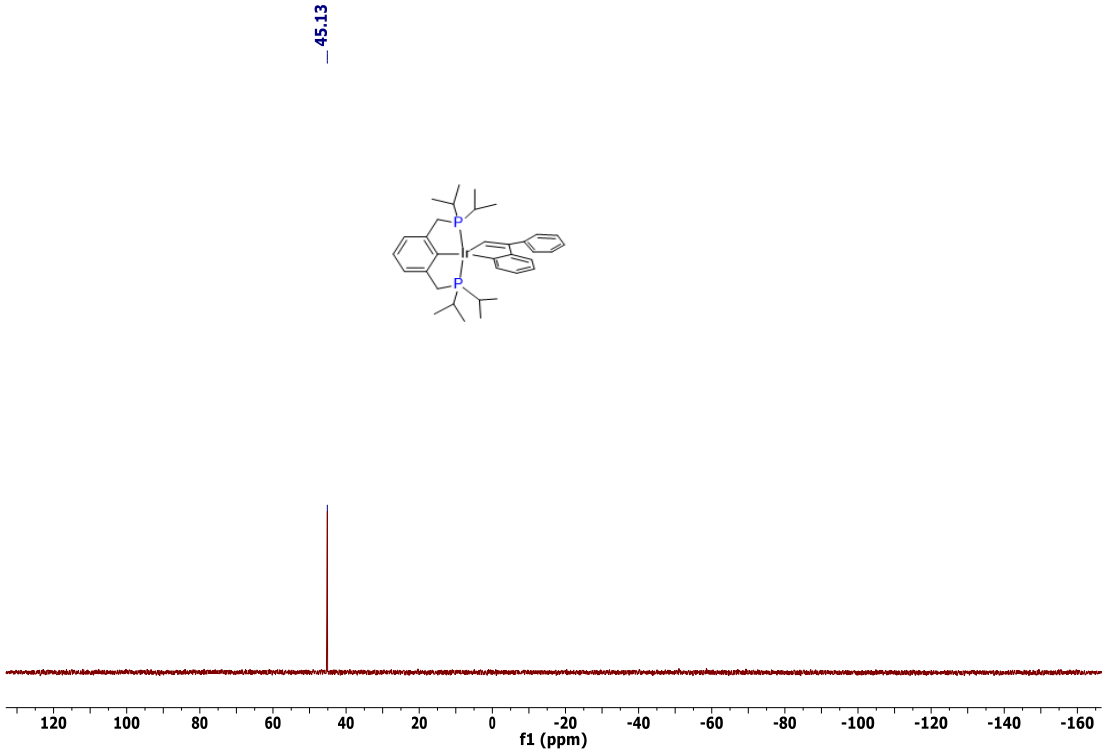

Figure 3. 49. ^{1}H NMR of metalloindene complex 7

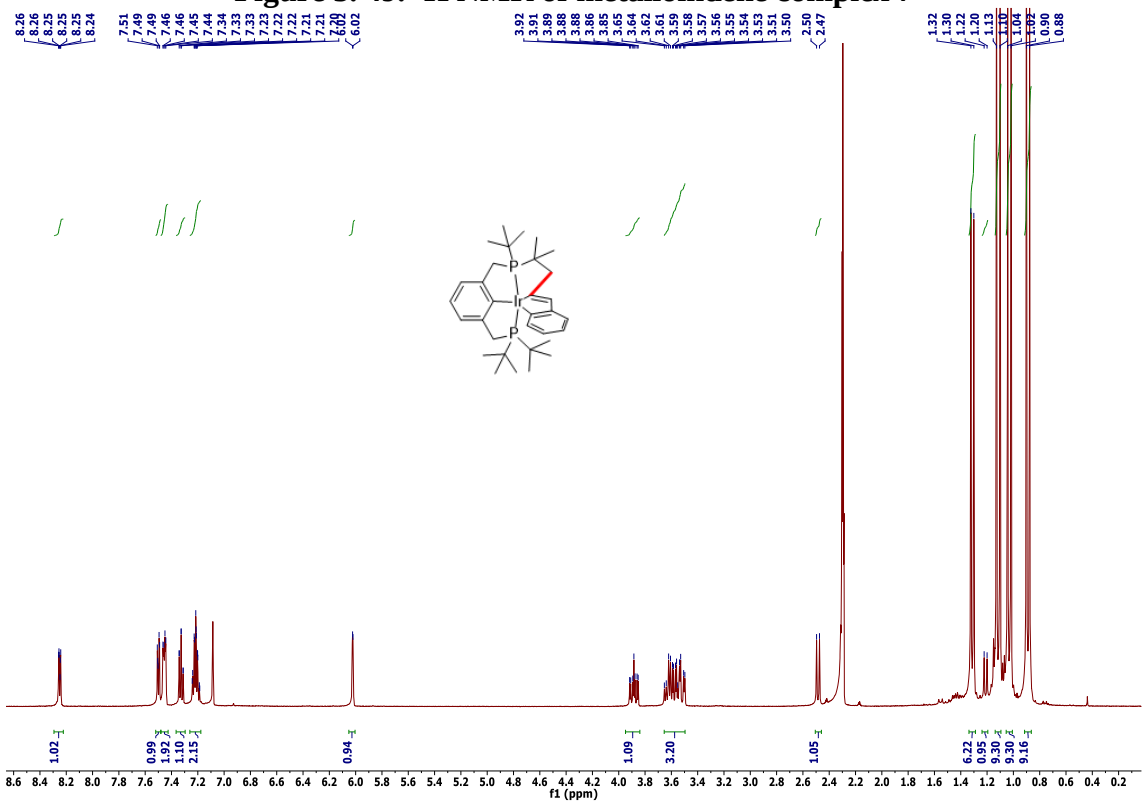

Figure 3. 50. ^{13}C NMR of metalloindene complex 7

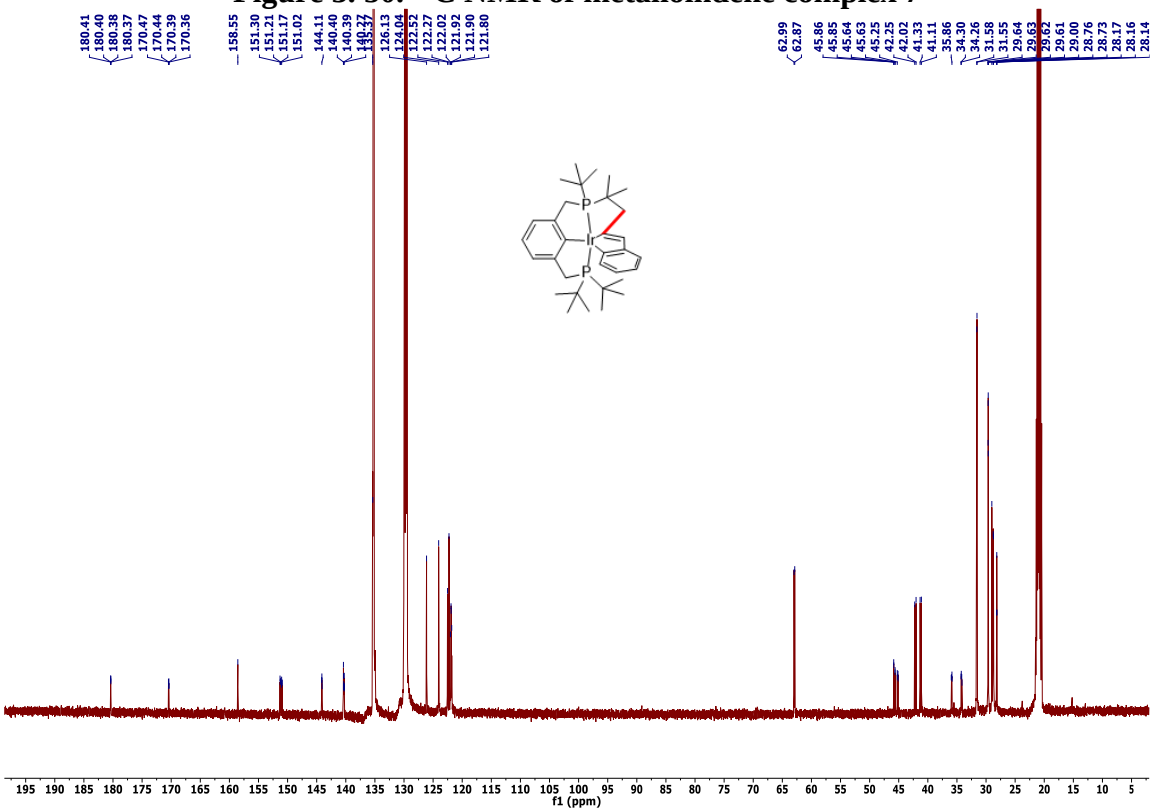

Figure 3. 51. ^{31}P NMR of metalloindene complex 7

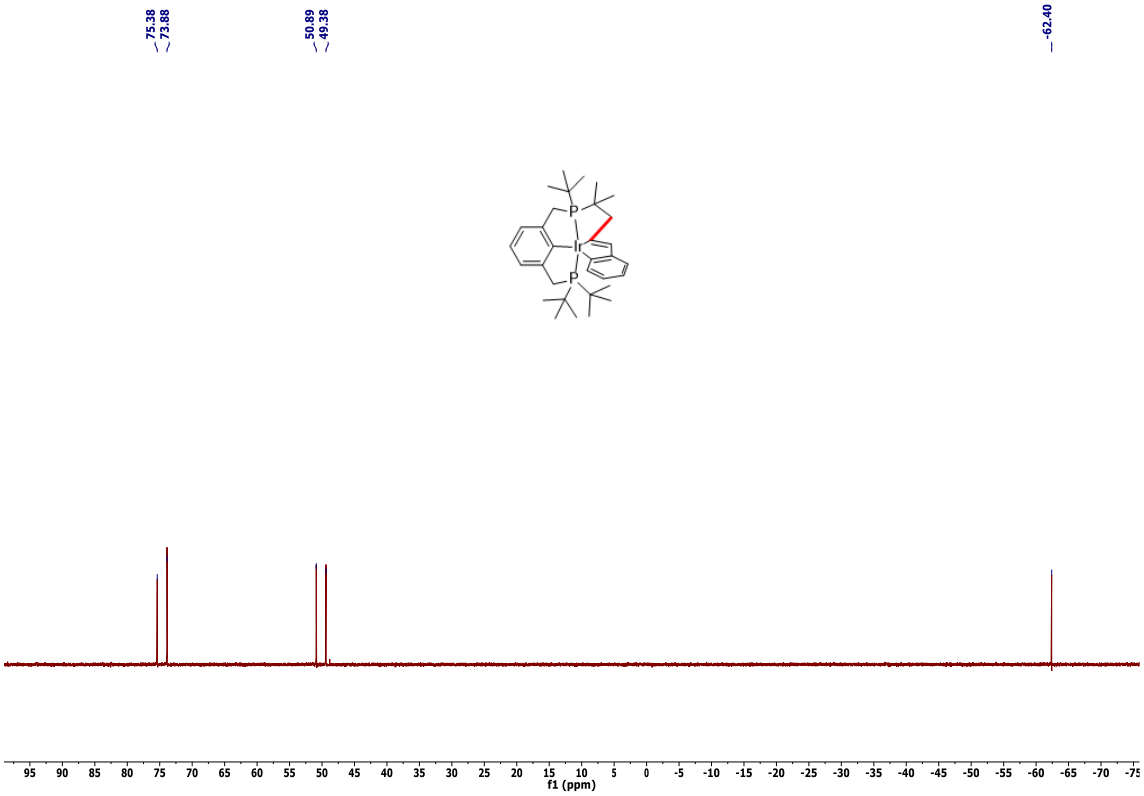

Figure 3. 52. ^{1}H NMR of metalloindene complex 8

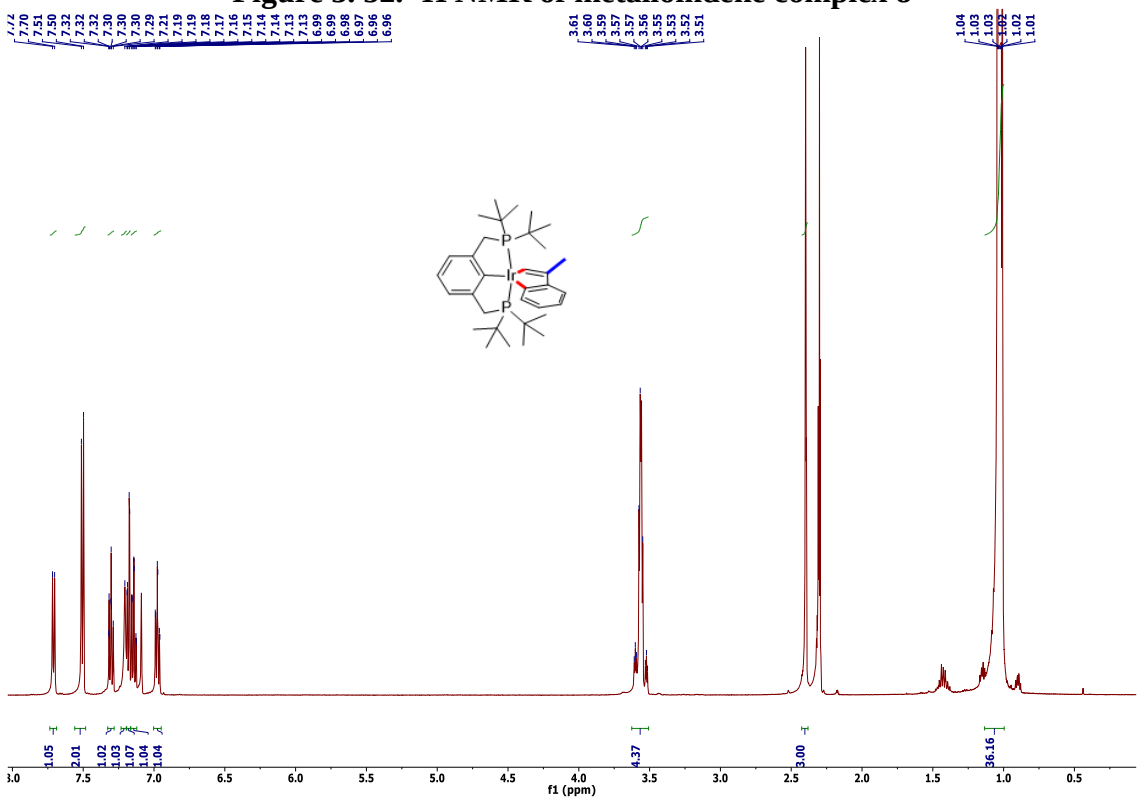

Figure 3. 53. ^{13}C NMR of metalloindene complex 8

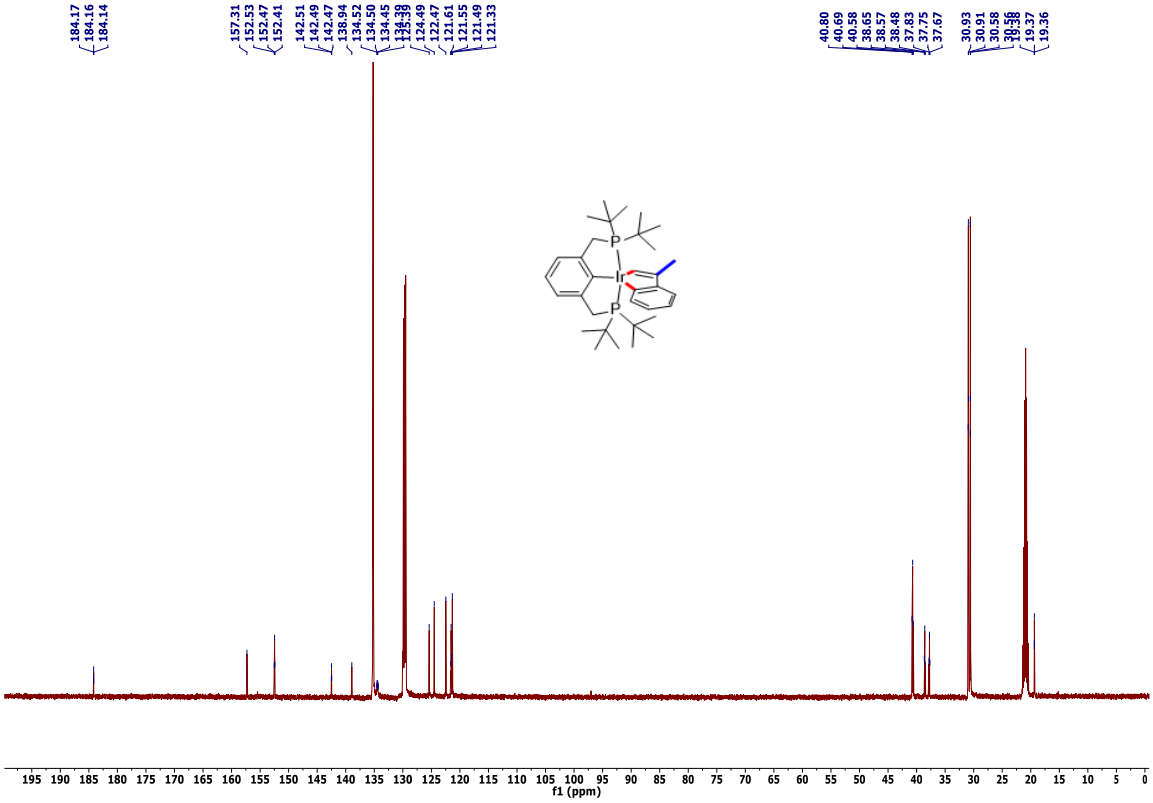

Figure 3. 54. ^{31}P NMR of metalloindene complex 8

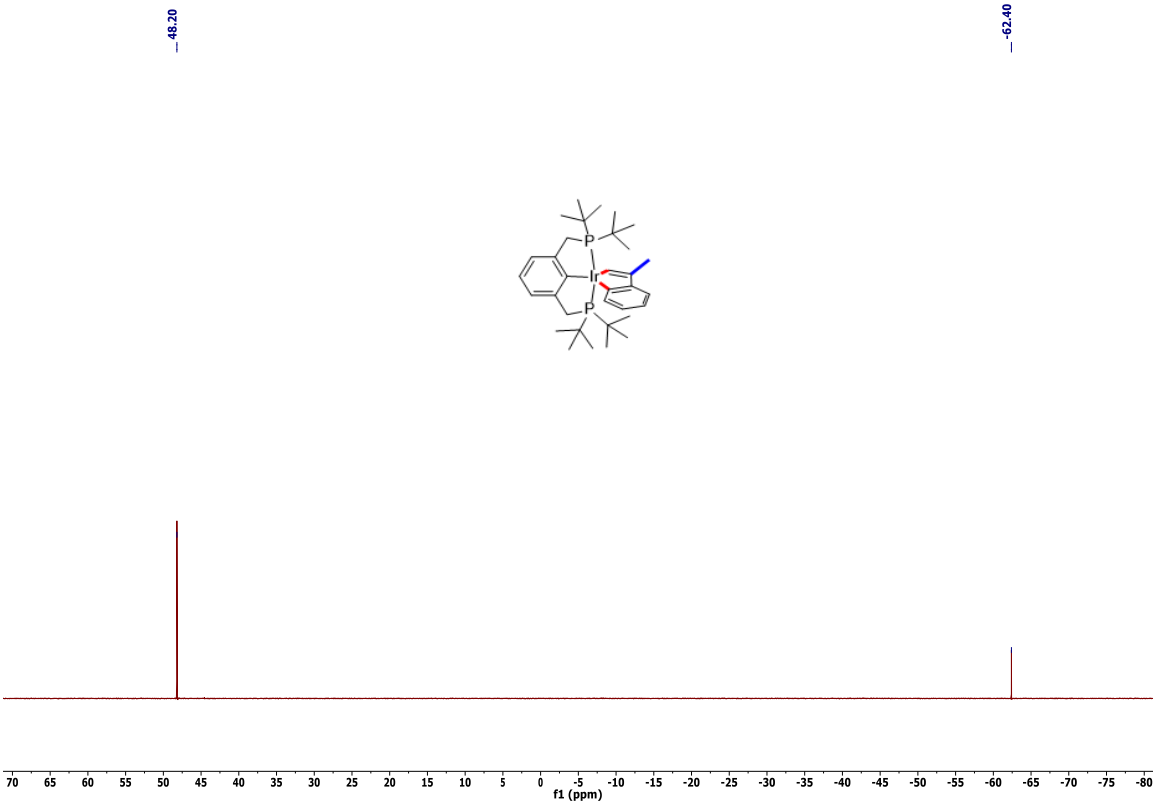

Figure 3. 55. ^{1}H NMR of metalloindene complex 9 at 25°C

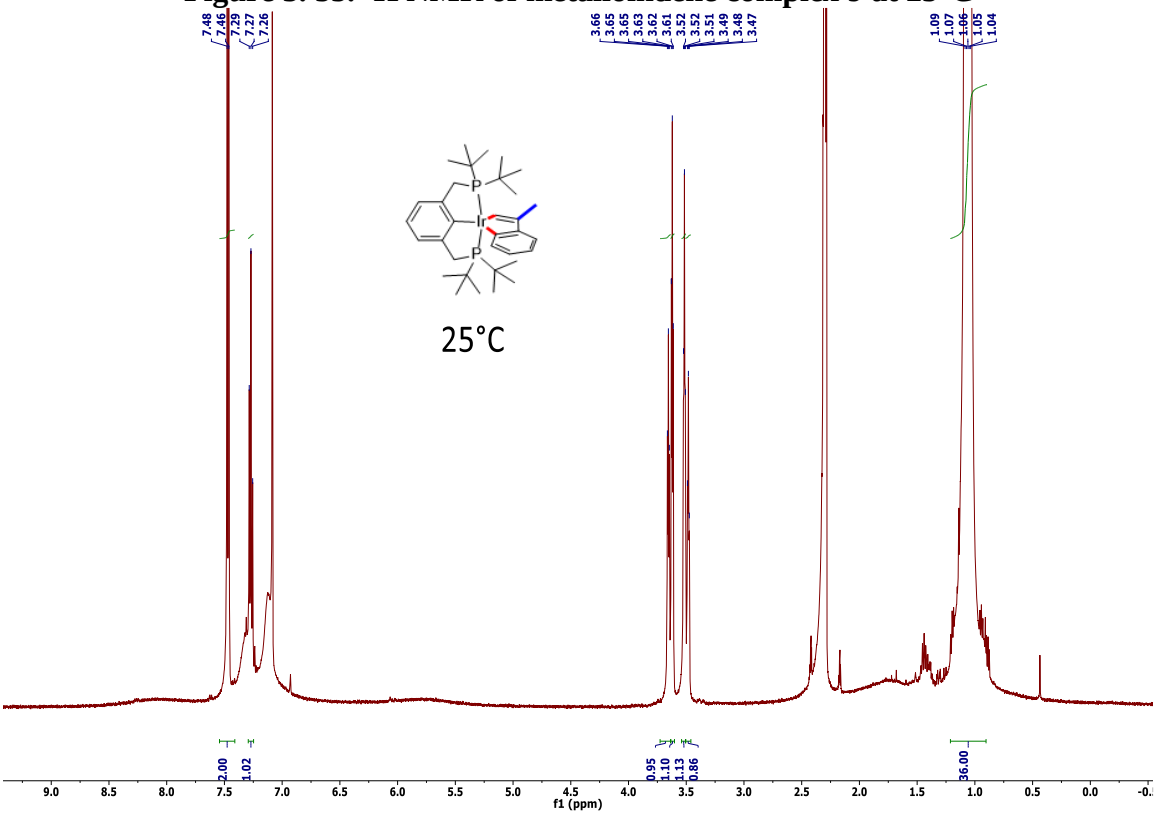

Figure 3. 56. ^{13}C NMR of metalloindene complex 9 at 25°C

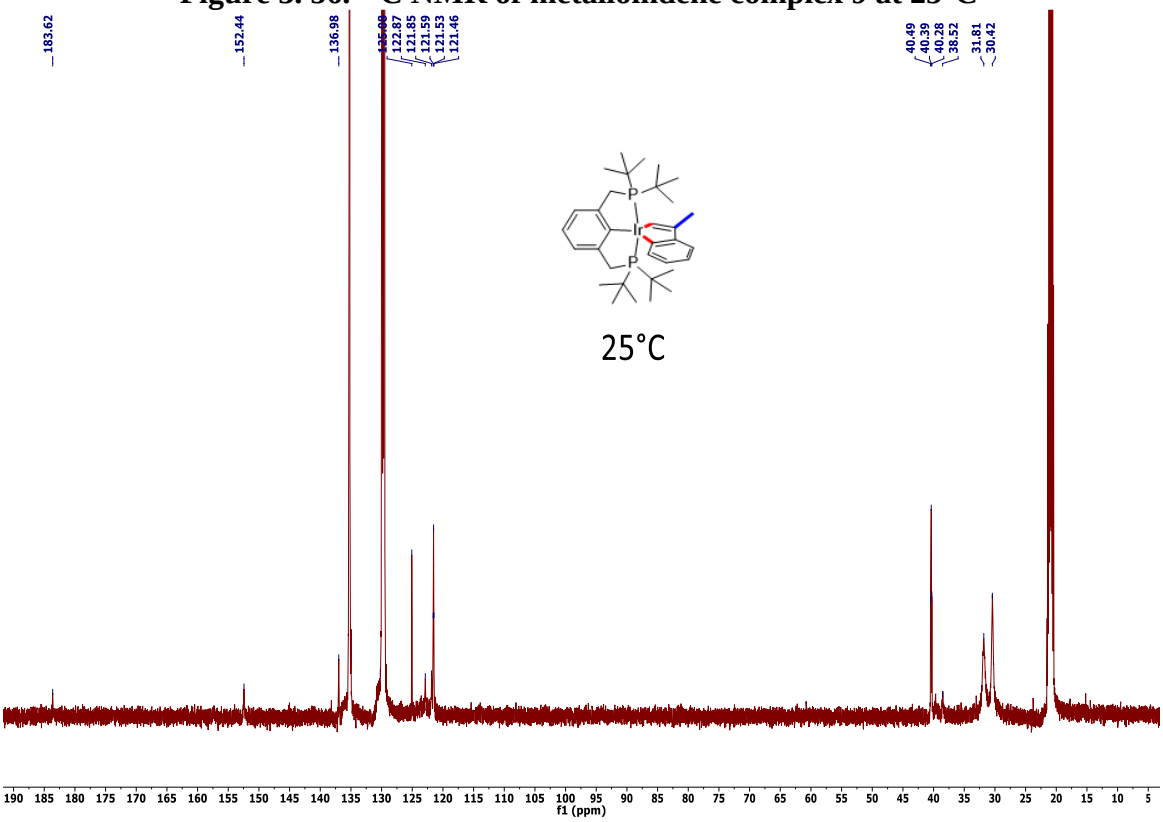

Figure 3. 57. ^{31}P NMR of metalloindene complex 9 at 25°C

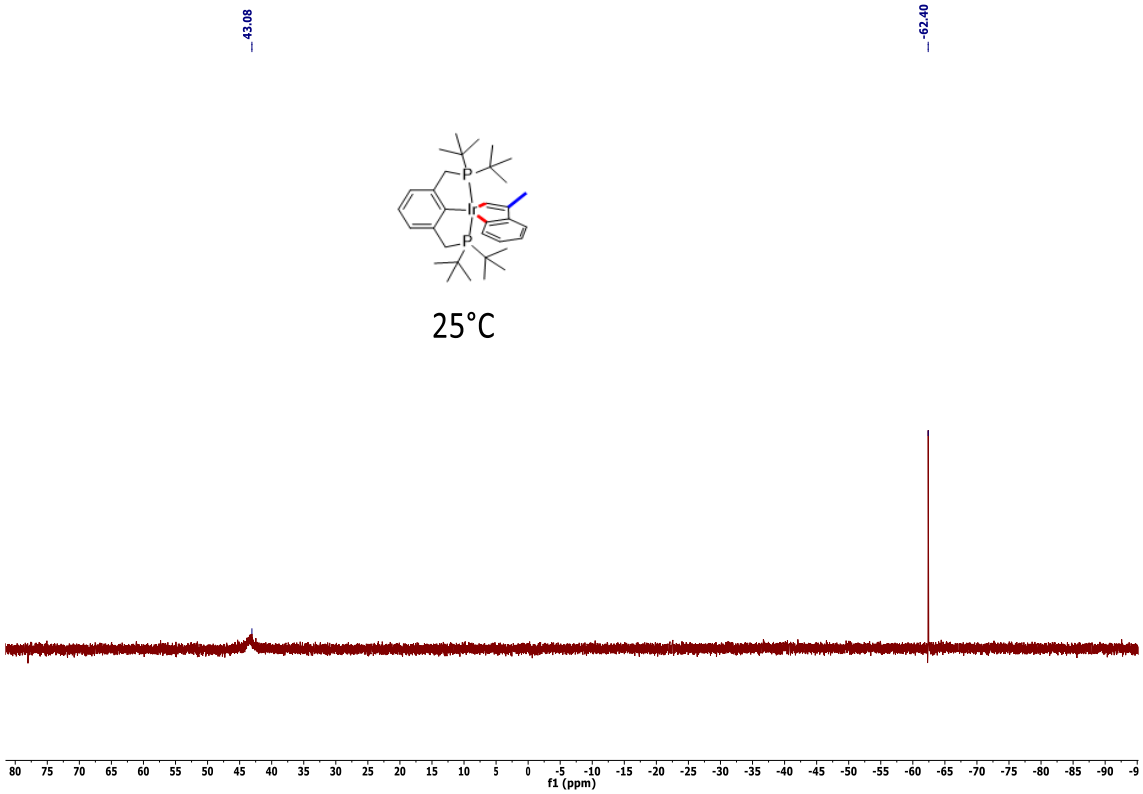

Figure 3. 58. ^{1}H NMR of metalloindene complex 9 at different Temperature

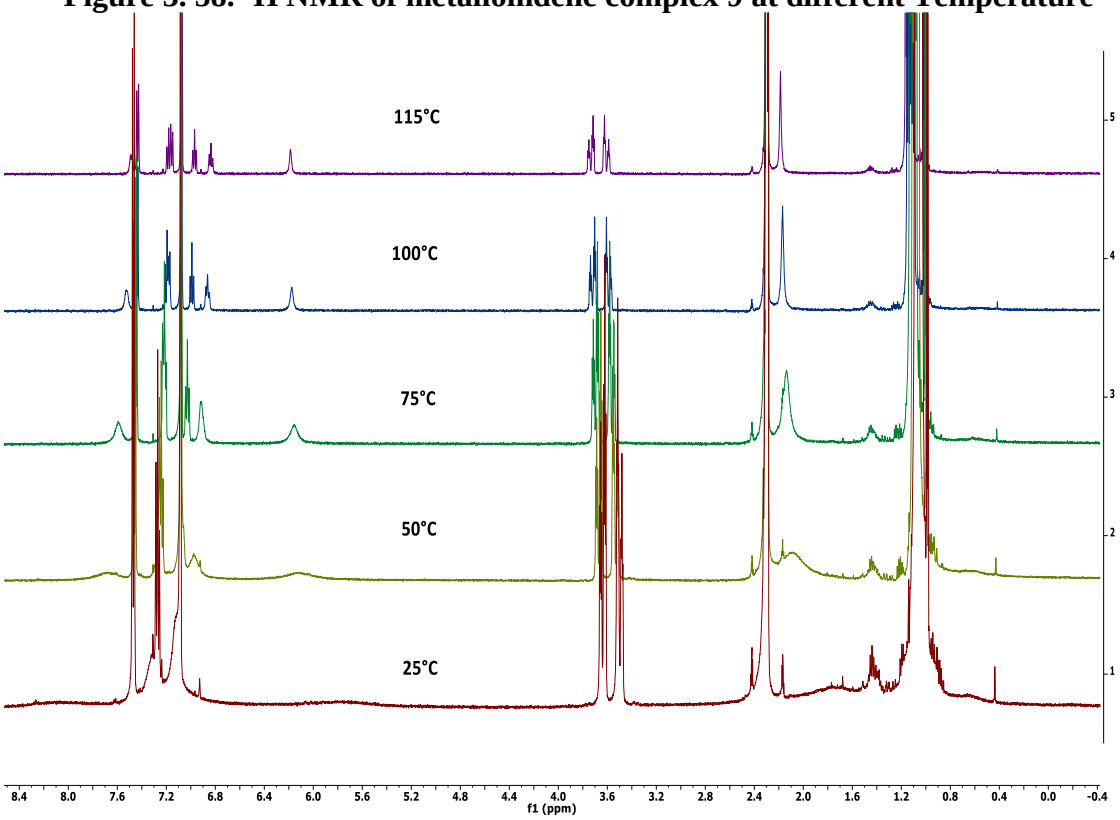

Figure 3. 59. ^{13}C NMR of metalloindene complex 9 at different Temperature

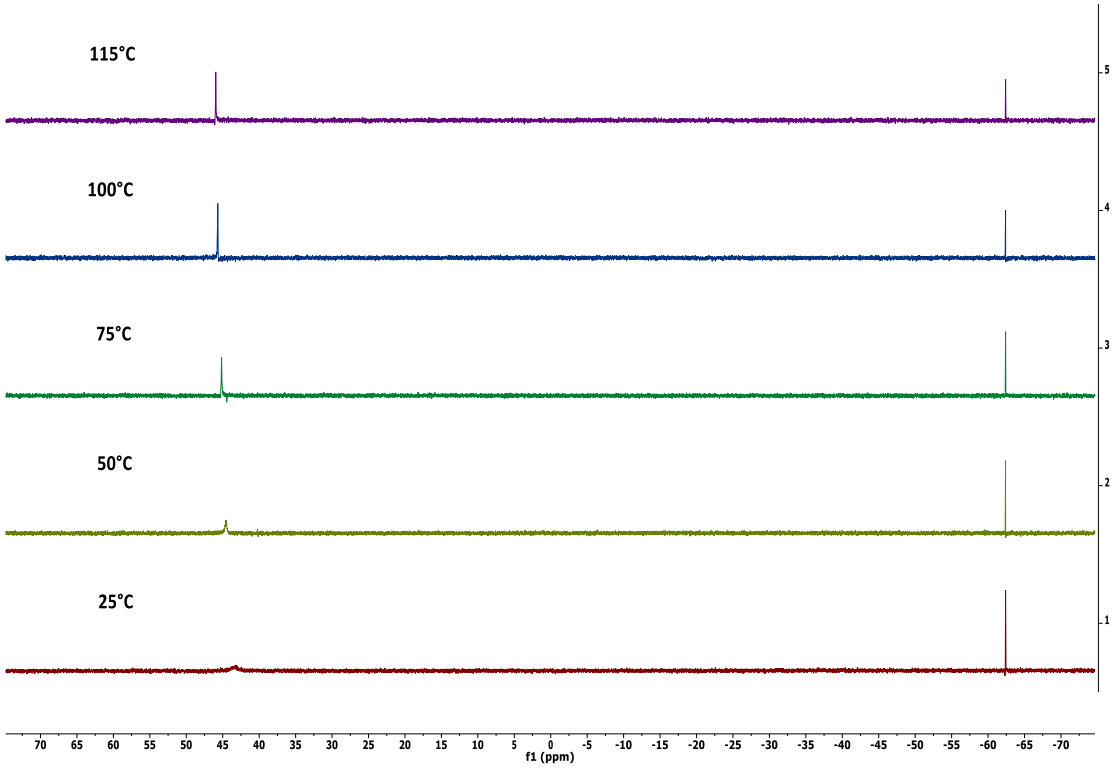

Figure 3. 60. ^{1}H NMR of metalloindene complex 9 at 115 °C

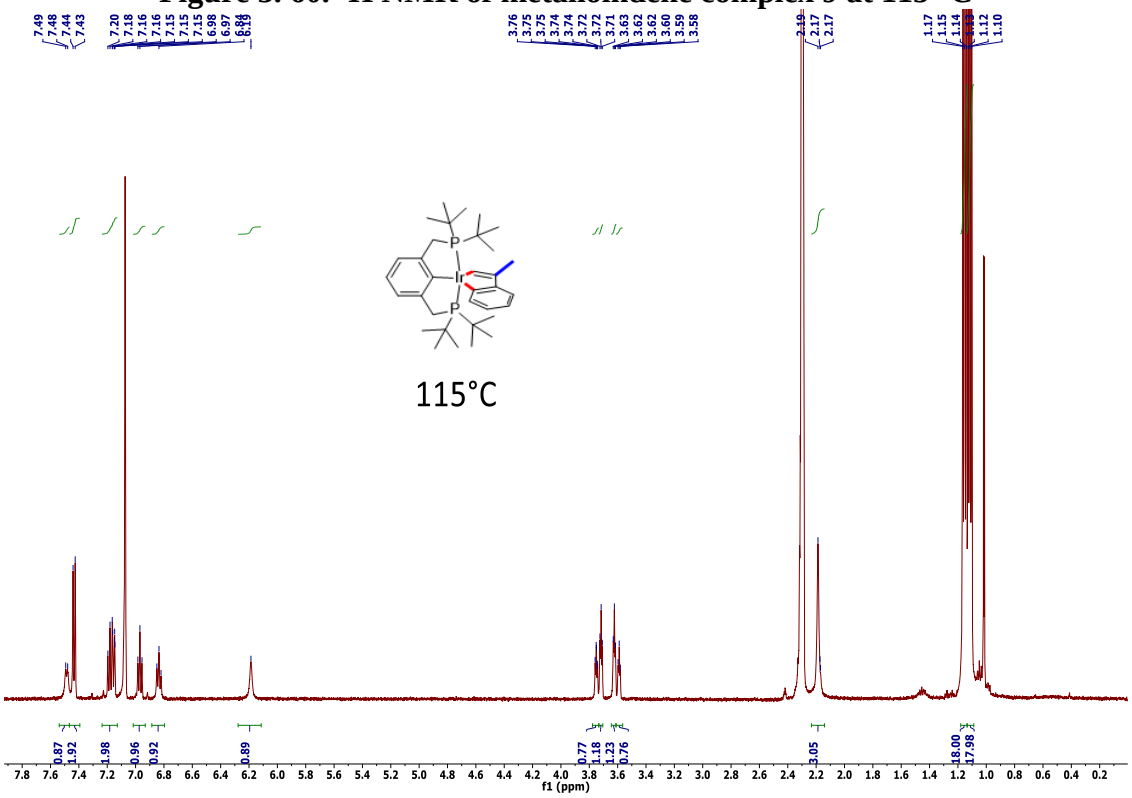

Figure 3. 61. ^{31}P NMR of metalloindene complex 9 at 115 °C

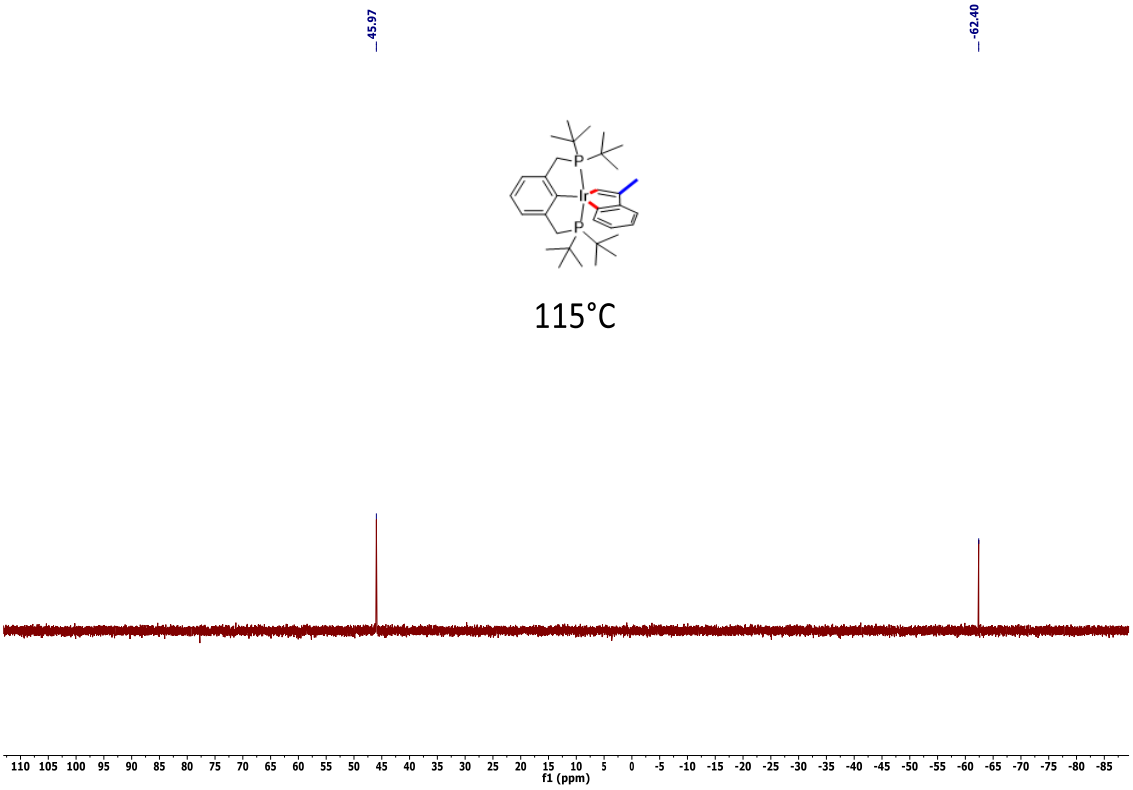

Figure 3. 62. ^{1}H NMR of metalloindene-CO complex 9-CO

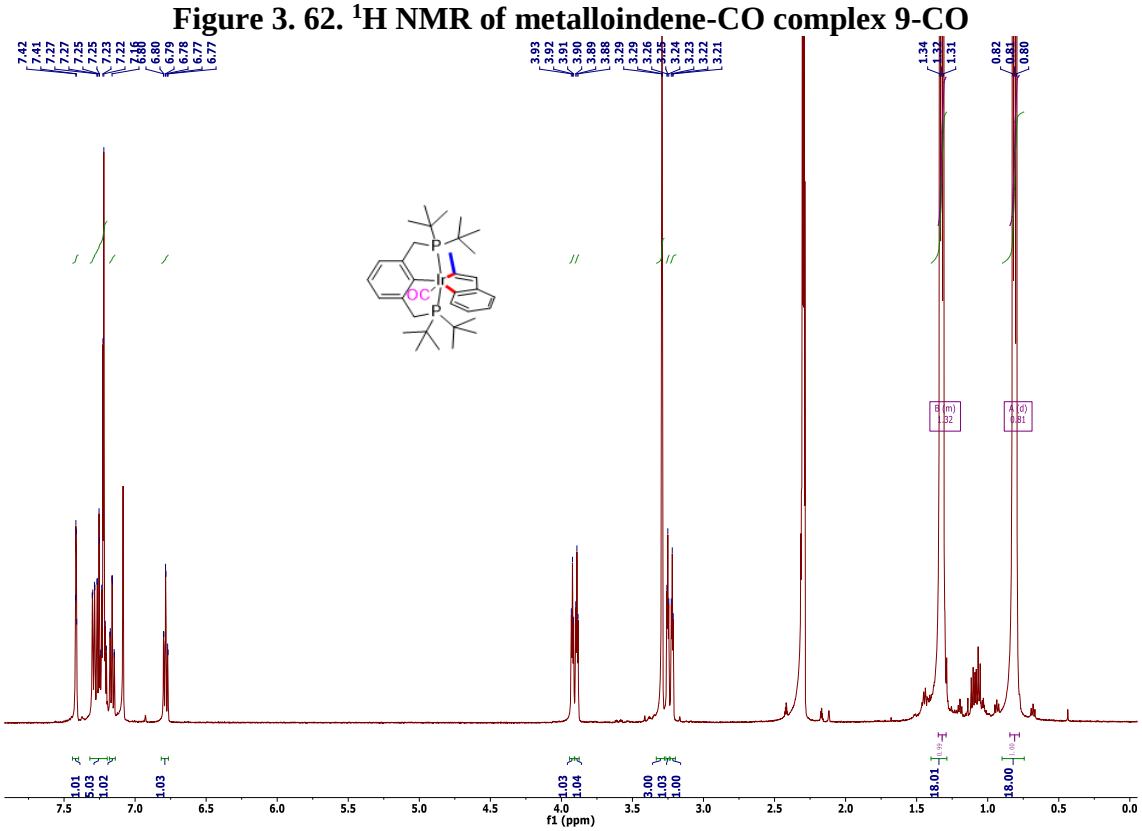

Figure 3. 63. ^{13}C NMR of metalloindene-CO complex 9-CO

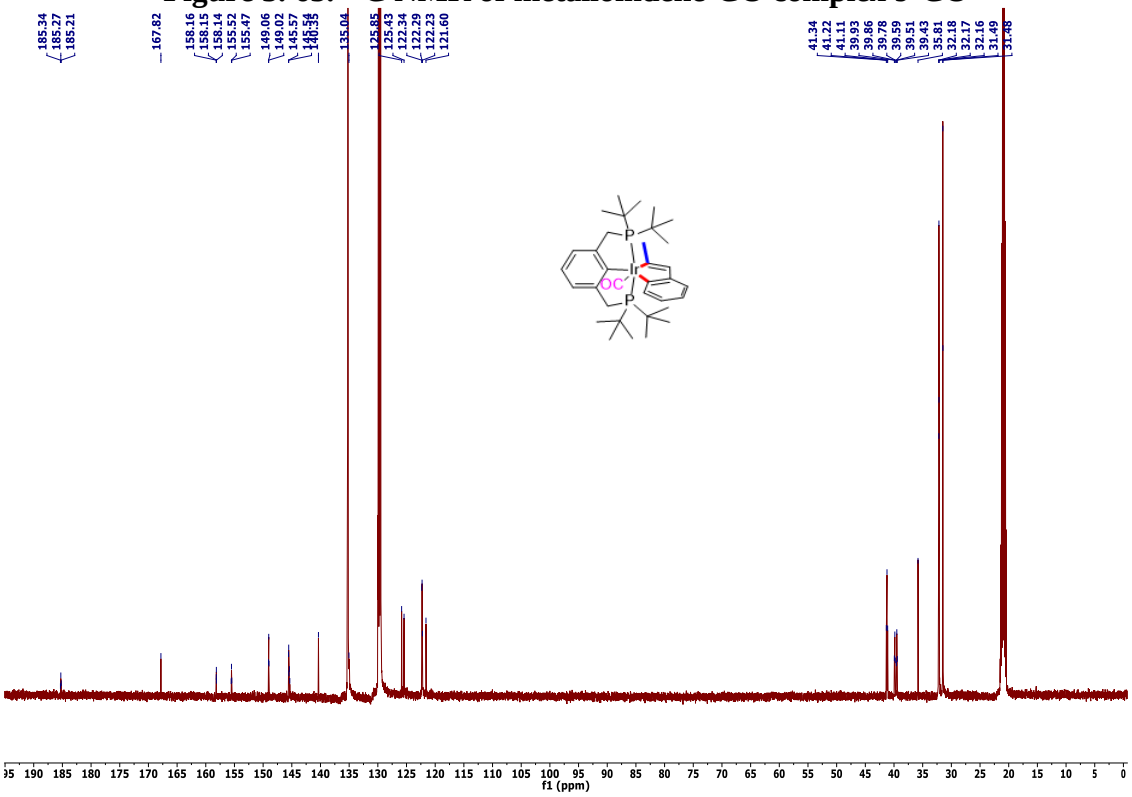

Figure 3. 64. ^{31}P NMR of metalloindene-CO complex 9-CO

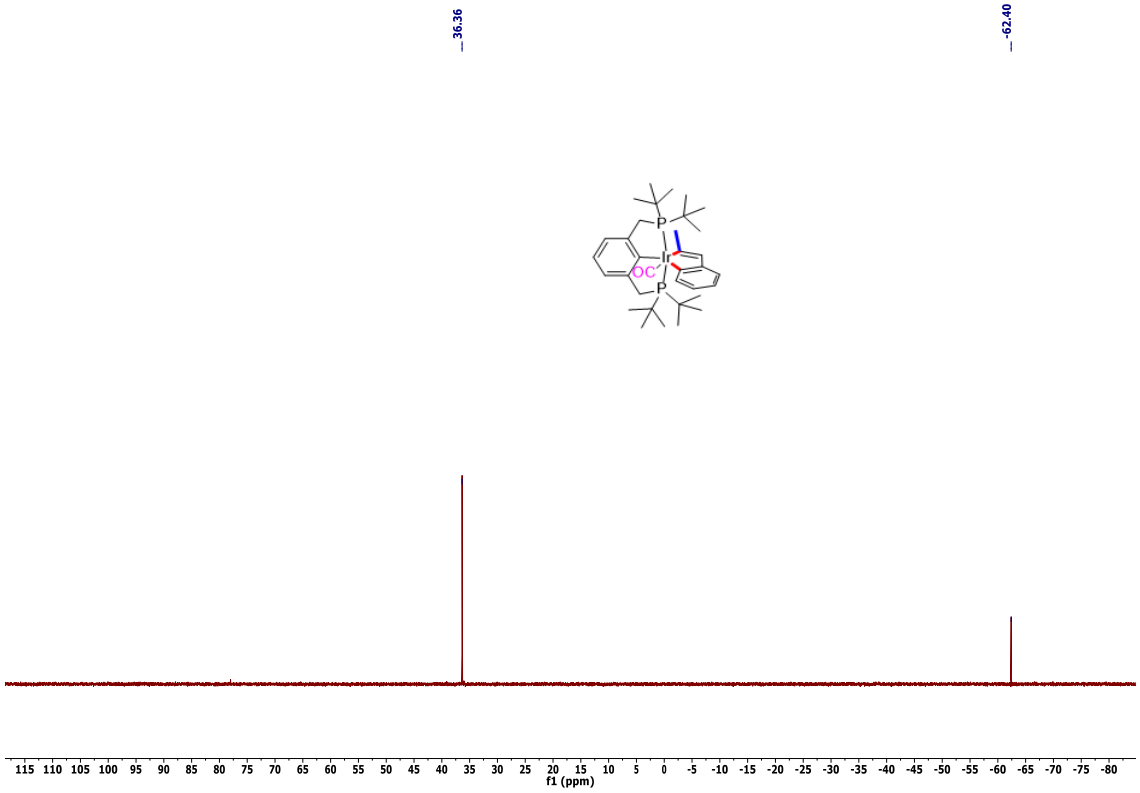

3.5.9. X-Ray structures

3.5.9.1. General information

For complex 2, 5, and 10, A crystal was placed onto the tip of a thin glass optical fiber and mounted on a Bruker SMART APEX II CCD platform diffractometer for a data collection at 100.0(5) K.[76] A preliminary set of cell constants and an orientation matrix were calculated from reflections harvested from three orthogonal wedges of reciprocal space. The full data collection was carried out using MoKα radiation (graphite monochromator) with a frame time of 25 seconds and a detector distance of 3.99 cm. A randomly oriented region of reciprocal space was surveyed: six major sections of frames were collected with 0.50° steps in ω at six different ϕ *settings* and a detector position of -38° in 2θ. The intensity data were corrected for absorption.[77] Final cell constants were calculated from the xyz centroids of 3913 strong reflections from the actual data collection after integration.[78] The structure was solved using SHELXT-2014/5[79] and refined using SHELXL-2014/7.[80] The space group *C*2/*c* was determined based on systematic absences and intensity statistics. A direct-methods solution was calculated which provided most non-hydrogen atoms from the E-map. Full-matrix least squares / difference Fourier cycles were performed which located the remaining non-hydrogen atoms. All non-hydrogen atoms were refined with anisotropic displacement parameters. All hydrogen atoms were placed in ideal positions and refined as riding atoms with relative isotropic displacement parameters. The final full matrix least squares refinement converged to $R1 = 0.0391$ (F^2, $I > 2\sigma(I)$) and $wR2 = 0.0782$ (F^2, all data).

For complex 3, 4, 7, 8, and 9, X-ray diffraction data were collected on a Bruker Smart APEX CCD diffractometer with graphite monochromatized MoKα radiation (λ =

0.71073Å) at 100 or 120 K. Crystals were immersed in Paratone oil and placed on a glass needle or nylon loop. The data were corrected for Lorenz effects, polarization, and absorption, the latter by a multiscan (SADABS) method.[81] The structures were solved by direct methods (SHELXS86).[82] All non-hydrogen atoms were refined (SHELXL97)3 based upon Fobs.[83] All hydrogen atom coordinates were calculated with idealized geometries (SHELXL97). Scattering factors (fo, f', f'') are as described in SHELXL97.

3.5.9.2. Structural data for complex 2

CCDC # 1540145

Figure 3. 65. ORTEP diagram of complex 2

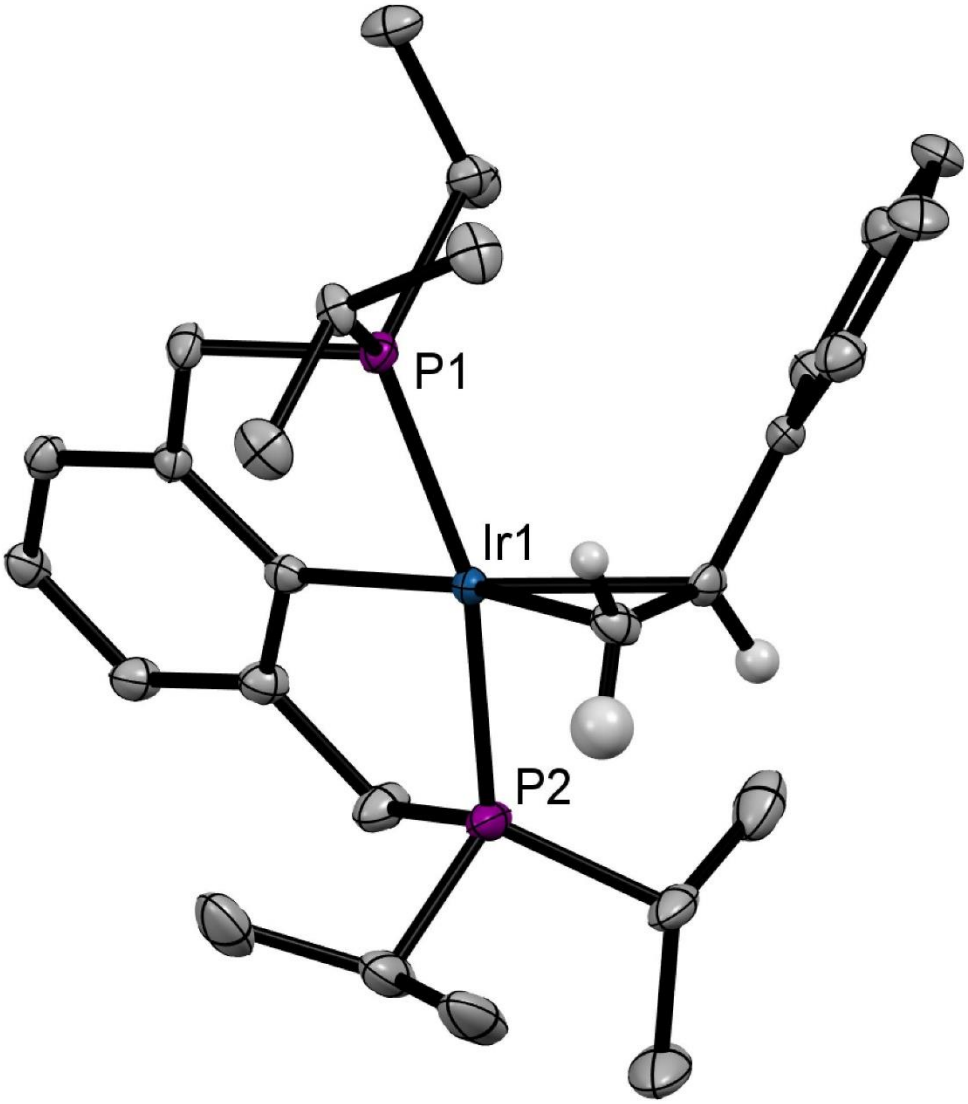

Table 3. 3. Crystal data and structure refinement for complex 2.

Identification code	jonmm35	
Empirical formula	C28 H43 Ir P2	
Formula weight	633.76	
Temperature	100.0(5) K	
Wavelength	0.71073 Å	
Crystal system	monoclinic	
Space group	$P2_1/c$	
Unit cell dimensions	a = 11.6684(13) Å	α = 90°
	b = 14.5529(16) Å	β = 103.837(2)°
	c = 16.9045(19) Å	γ = 90°
Volume	2787.2(5) $Å^3$	
Z	4	
Density (calculated)	1.510 Mg/m^3	
Absorption coefficient	4.918 mm^{-1}	
F(000)	1272	
Crystal color, morphology	dark red, plate	
Crystal size	0.16 x 0.12 x 0.06 mm^3	
Theta range for data collection	1.797 to 38.856°	
Index ranges	$-20 \leq h \leq 20$, $-25 \leq k \leq 25$, $-29 \leq l \leq 29$	
Reflections collected	100793	
Independent reflections	15523 [R(int) = 0.1148]	
Observed reflections	8031	
Completeness to theta = 37.785°	99.5%	
Absorption correction	Multi-scan	
Max. and min. transmission	0.4406 and 0.3562	
Refinement method	Full-matrix least-squares on F^2	
Data / restraints / parameters	15523 / 0 / 300	
Goodness-of-fit on F^2	0.997	
Final R indices [I>2sigma(I)]	$R1$ = 0.0425, $wR2$ = 0.0737	
R indices (all data)	$R1$ = 0.1081, $wR2$ = 0.0920	
Largest diff. peak and hole	1.981 and -2.435 e.$Å^{-3}$	

Table 3. 4. Atomic coordinates (x 10^4) and equivalent isotropic displacement parameters (Å^{2}x 10^3) for complex 2.

U_{eq} is defined as one third of the trace of the orthogonalized U_{ij} tensor.

	x	y	z	U_{eq}
Ir1	6394(1)	7521(1)	5614(1)	12(1)
P1	4828(1)	7392(1)	6215(1)	13(1)
P2	8236(1)	7488(1)	5393(1)	20(1)
C1	5714(4)	8740(3)	4874(2)	19(1)
C2	5575(3)	7957(2)	4372(2)	16(1)
C3	4407(3)	7534(3)	4009(2)	16(1)
C4	4331(3)	6587(3)	3861(2)	19(1)
C5	3251(4)	6167(3)	3514(2)	23(1)
C6	2241(4)	6696(3)	3303(2)	24(1)
C7	2295(3)	7641(3)	3418(3)	27(1)
C8	3373(4)	8062(3)	3779(2)	22(1)
C21	7194(3)	6664(2)	6562(2)	15(1)
C22	6672(3)	6474(2)	7219(2)	14(1)
C23	7243(3)	5913(2)	7870(2)	16(1)
C24	8341(3)	5537(2)	7895(2)	17(1)
C25	8884(3)	5724(2)	7269(2)	19(1)
C26	8317(3)	6267(2)	6609(2)	18(1)
C27	5505(3)	6911(3)	7226(2)	16(1)
C28	8925(4)	6453(3)	5927(3)	24(1)
C29	3623(3)	6576(2)	5787(2)	16(1)
C30	4162(4)	5622(2)	5713(2)	22(1)
C31	2656(4)	6495(3)	6269(3)	23(1)
C32	4069(3)	8411(2)	6509(2)	16(1)
C33	4971(4)	9159(3)	6858(3)	24(1)
C34	3081(4)	8793(3)	5819(2)	23(1)
C35	8517(3)	7397(3)	4360(2)	27(1)
C36	7927(4)	6556(3)	3915(3)	36(1)
C37	9828(4)	7433(5)	4350(3)	48(1)
C38	9223(4)	8421(3)	5899(3)	30(1)
C39	8888(4)	9348(3)	5465(3)	40(1)

C40	9192(5)	8499(3)	6795(3)	36(1)

Table 3. 5. Bond lengths [Å] and angles [°] for complex 2.

Ir(1)-C(21)	2.068(4)	C(24)-C(25)	1.384(5)
Ir(1)-C(2)	2.183(4)	C(24)-H(24)	0.9500
Ir(1)-C(1)	2.206(4)	C(25)-C(26)	1.397(5)
Ir(1)-P(2)	2.2686(9)	C(25)-H(25)	0.9500
Ir(1)-P(1)	2.3007(9)	C(26)-C(28)	1.516(5)
P(1)-C(27)	1.842(4)	C(27)-H(27A)	0.9900
P(1)-C(29)	1.850(4)	C(27)-H(27B)	0.9900
P(1)-C(32)	1.855(3)	C(28)-H(28A)	0.9900
P(2)-C(28)	1.839(4)	C(28)-H(28B)	0.9900
P(2)-C(38)	1.852(5)	C(29)-C(30)	1.541(5)
P(2)-C(35)	1.858(4)	C(29)-C(31)	1.547(5)
C(1)-C(2)	1.406(5)	C(29)-H(29)	1.0000
C(1)-H(1A)	0.95(4)	C(30)-H(30A)	0.9800
C(1)-H(1B)	0.92(5)	C(30)-H(30B)	0.9800
C(2)-C(3)	1.488(5)	C(30)-H(30C)	0.9800
C(2)-H(2)	0.91(4)	C(31)-H(31A)	0.9800
C(3)-C(4)	1.400(6)	C(31)-H(31B)	0.9800
C(3)-C(8)	1.404(5)	C(31)-H(31C)	0.9800
C(4)-C(5)	1.398(5)	C(32)-C(33)	1.532(5)
C(4)-H(4)	0.9500	C(32)-C(34)	1.535(5)
C(5)-C(6)	1.381(6)	C(32)-H(32)	1.0000
C(5)-H(5)	0.9500	C(33)-H(33A)	0.9800
C(6)-C(7)	1.389(6)	C(33)-H(33B)	0.9800
C(6)-H(6)	0.9500	C(33)-H(33C)	0.9800
C(7)-C(8)	1.401(6)	C(34)-H(34A)	0.9800
C(7)-H(7)	0.9500	C(34)-H(34B)	0.9800
C(8)-H(8)	0.9500	C(34)-H(34C)	0.9800
C(21)-C(26)	1.417(5)	C(35)-C(36)	1.514(6)
C(21)-C(22)	1.417(5)	C(35)-C(37)	1.535(5)
C(22)-C(23)	1.403(5)	C(35)-H(35)	1.0000
C(22)-C(27)	1.505(5)	C(36)-H(36A)	0.9800
C(23)-C(24)	1.385(5)	C(36)-H(36B)	0.9800
C(23)-H(23)	0.9500	C(36)-H(36C)	0.9800

C(37)-H(37A)	0.9800	C(2)-C(1)-H(1A)	126(2)
C(37)-H(37B)	0.9800	Ir(1)-C(1)-H(1A)	113(2)
C(37)-H(37C)	0.9800	C(2)-C(1)-H(1B)	118(3)
C(38)-C(40)	1.529(6)	Ir(1)-C(1)-H(1B)	103(3)
C(38)-C(39)	1.541(6)	H(1A)-C(1)-H(1B)	113(4)
C(38)-H(38)	1.0000	C(1)-C(2)-C(3)	123.2(4)
C(39)-H(39A)	0.9800	C(1)-C(2)-Ir(1)	72.2(2)
C(39)-H(39B)	0.9800	C(3)-C(2)-Ir(1)	115.0(2)
C(39)-H(39C)	0.9800	C(1)-C(2)-H(2)	117(3)
C(40)-H(40A)	0.9800	C(3)-C(2)-H(2)	113(3)
C(40)-H(40B)	0.9800	Ir(1)-C(2)-H(2)	109(3)
C(40)-H(40C)	0.9800	C(4)-C(3)-C(8)	118.4(3)
C(21)-Ir(1)-C(2)	158.95(14)	C(4)-C(3)-C(2)	119.6(3)
C(21)-Ir(1)-C(1)	163.43(14)	C(8)-C(3)-C(2)	121.9(4)
C(2)-Ir(1)-C(1)	37.36(14)	C(5)-C(4)-C(3)	121.2(4)
C(21)-Ir(1)-P(2)	81.07(10)	C(5)-C(4)-H(4)	119.4
C(2)-Ir(1)-P(2)	93.57(10)	C(3)-C(4)-H(4)	119.4
C(1)-Ir(1)-P(2)	98.62(11)	C(6)-C(5)-C(4)	119.5(4)
C(21)-Ir(1)-P(1)	82.41(10)	C(6)-C(5)-H(5)	120.2
C(2)-Ir(1)-P(1)	103.71(10)	C(4)-C(5)-H(5)	120.2
C(1)-Ir(1)-P(1)	95.74(11)	C(5)-C(6)-C(7)	120.6(4)
P(2)-Ir(1)-P(1)	162.69(3)	C(5)-C(6)-H(6)	119.7
C(27)-P(1)-C(29)	103.64(17)	C(7)-C(6)-H(6)	119.7
C(27)-P(1)-C(32)	100.46(16)	C(6)-C(7)-C(8)	119.9(4)
C(29)-P(1)-C(32)	104.54(17)	C(6)-C(7)-H(7)	120.0
C(27)-P(1)-Ir(1)	103.38(12)	C(8)-C(7)-H(7)	120.0
C(29)-P(1)-Ir(1)	119.25(12)	C(7)-C(8)-C(3)	120.3(4)
C(32)-P(1)-Ir(1)	122.29(13)	C(7)-C(8)-H(8)	119.9
C(28)-P(2)-C(38)	102.9(2)	C(3)-C(8)-H(8)	119.9
C(28)-P(2)-C(35)	104.4(2)	C(26)-C(21)-C(22)	116.2(3)
C(38)-P(2)-C(35)	104.8(2)	C(26)-C(21)-Ir(1)	122.0(3)
C(28)-P(2)-Ir(1)	104.87(13)	C(22)-C(21)-Ir(1)	121.8(3)
C(38)-P(2)-Ir(1)	114.69(17)	C(23)-C(22)-C(21)	121.1(3)
C(35)-P(2)-Ir(1)	122.90(13)	C(23)-C(22)-C(27)	120.0(3)
C(2)-C(1)-Ir(1)	70.4(2)	C(21)-C(22)-C(27)	118.9(3)

C(24)-C(23)-C(22)	121.1(3)	H(30B)-C(30)-H(30C)	109.5
C(24)-C(23)-H(23)	119.5	C(29)-C(31)-H(31A)	109.5
C(22)-C(23)-H(23)	119.5	C(29)-C(31)-H(31B)	109.5
C(25)-C(24)-C(23)	119.2(3)	H(31A)-C(31)-H(31B)	109.5
C(25)-C(24)-H(24)	120.4	C(29)-C(31)-H(31C)	109.5
C(23)-C(24)-H(24)	120.4	H(31A)-C(31)-H(31C)	109.5
C(24)-C(25)-C(26)	120.4(4)	H(31B)-C(31)-H(31C)	109.5
C(24)-C(25)-H(25)	119.8	C(33)-C(32)-C(34)	111.0(3)
C(26)-C(25)-H(25)	119.8	C(33)-C(32)-P(1)	110.1(3)
C(25)-C(26)-C(21)	122.1(3)	C(34)-C(32)-P(1)	113.9(2)
C(25)-C(26)-C(28)	119.3(3)	C(33)-C(32)-H(32)	107.2
C(21)-C(26)-C(28)	118.6(3)	C(34)-C(32)-H(32)	107.2
C(22)-C(27)-P(1)	110.0(2)	P(1)-C(32)-H(32)	107.2
C(22)-C(27)-H(27A)	109.7	C(32)-C(33)-H(33A)	109.5
P(1)-C(27)-H(27A)	109.7	C(32)-C(33)-H(33B)	109.5
C(22)-C(27)-H(27B)	109.7	H(33A)-C(33)-H(33B)	109.5
P(1)-C(27)-H(27B)	109.7	C(32)-C(33)-H(33C)	109.5
H(27A)-C(27)-H(27B)	108.2	H(33A)-C(33)-H(33C)	109.5
C(26)-C(28)-P(2)	106.9(3)	H(33B)-C(33)-H(33C)	109.5
C(26)-C(28)-H(28A)	110.3	C(32)-C(34)-H(34A)	109.5
P(2)-C(28)-H(28A)	110.3	C(32)-C(34)-H(34B)	109.5
C(26)-C(28)-H(28B)	110.3	H(34A)-C(34)-H(34B)	109.5
P(2)-C(28)-H(28B)	110.3	C(32)-C(34)-H(34C)	109.5
H(28A)-C(28)-H(28B)	108.6	H(34A)-C(34)-H(34C)	109.5
C(30)-C(29)-C(31)	109.7(3)	H(34B)-C(34)-H(34C)	109.5
C(30)-C(29)-P(1)	108.9(3)	C(36)-C(35)-C(37)	111.0(4)
C(31)-C(29)-P(1)	115.1(3)	C(36)-C(35)-P(2)	111.3(3)
C(30)-C(29)-H(29)	107.6	C(37)-C(35)-P(2)	114.1(3)
C(31)-C(29)-H(29)	107.6	C(36)-C(35)-H(35)	106.7
P(1)-C(29)-H(29)	107.6	C(37)-C(35)-H(35)	106.7
C(29)-C(30)-H(30A)	109.5	P(2)-C(35)-H(35)	106.7
C(29)-C(30)-H(30B)	109.5	C(35)-C(36)-H(36A)	109.5
H(30A)-C(30)-H(30B)	109.5	C(35)-C(36)-H(36B)	109.5
C(29)-C(30)-H(30C)	109.5	H(36A)-C(36)-H(36B)	109.5
H(30A)-C(30)-H(30C)	109.5	C(35)-C(36)-H(36C)	109.5

H(36A)-C(36)-H(36C)	109.5	P(2)-C(38)-H(38)	108.2
H(36B)-C(36)-H(36C)	109.5	C(38)-C(39)-H(39A)	109.5
C(35)-C(37)-H(37A)	109.5	C(38)-C(39)-H(39B)	109.5
C(35)-C(37)-H(37B)	109.5	H(39A)-C(39)-H(39B)	109.5
H(37A)-C(37)-H(37B)	109.5	C(38)-C(39)-H(39C)	109.5
C(35)-C(37)-H(37C)	109.5	H(39A)-C(39)-H(39C)	109.5
H(37A)-C(37)-H(37C)	109.5	H(39B)-C(39)-H(39C)	109.5
H(37B)-C(37)-H(37C)	109.5	C(38)-C(40)-H(40A)	109.5
C(40)-C(38)-C(39)	110.1(4)	C(38)-C(40)-H(40B)	109.5
C(40)-C(38)-P(2)	110.6(3)	H(40A)-C(40)-H(40B)	109.5
C(39)-C(38)-P(2)	111.3(3)	C(38)-C(40)-H(40C)	109.5
C(40)-C(38)-H(38)	108.2	H(40A)-C(40)-H(40C)	109.5
C(39)-C(38)-H(38)	108.2	H(40B)-C(40)-H(40C)	109.5

Table 3. 6. Anisotropic displacement parameters (Å^{2}x 10^3) for complex 2.

The anisotropic displacement factor exponent takes the form: $-2\pi^2[h^2 a^{*2}U_{11} + ... + 2 h k a^* b^* U_{12}]$

	U_{11}	U_{22}	U_{33}	U_{23}	U_{13}	U_{12}
Ir1	11(1)	14(1)	11(1)	2(1)	2(1)	0(1)
P1	13(1)	16(1)	12(1)	0(1)	4(1)	2(1)
P2	12(1)	29(1)	18(1)	10(1)	4(1)	0(1)
C1	14(2)	19(2)	22(2)	6(1)	0(1)	0(1)
C2	16(2)	20(2)	13(2)	8(1)	3(1)	0(1)
C3	14(1)	23(2)	12(1)	1(2)	3(1)	-5(2)
C4	16(2)	24(2)	16(2)	-4(1)	5(1)	0(1)
C5	24(2)	26(2)	20(2)	-6(2)	6(2)	-6(2)
C6	15(2)	34(2)	22(2)	-4(2)	2(2)	-9(2)
C7	13(2)	37(3)	30(2)	0(2)	6(2)	1(2)
C8	20(2)	26(2)	21(2)	3(1)	6(2)	2(2)
C21	13(2)	14(1)	16(2)	-2(1)	3(1)	-2(1)
C22	15(2)	15(1)	12(1)	0(1)	3(1)	-1(1)
C23	18(2)	14(2)	14(2)	2(1)	4(1)	-1(1)
C24	15(2)	15(2)	19(2)	6(1)	0(1)	-1(1)
C25	15(2)	19(2)	24(2)	3(1)	4(2)	-1(1)
C26	14(2)	18(2)	21(2)	3(1)	4(1)	0(1)
C27	17(2)	22(2)	11(1)	1(1)	5(1)	3(1)
C28	18(2)	30(2)	26(2)	10(2)	9(2)	5(2)
C29	16(2)	17(2)	17(2)	0(1)	5(1)	-1(1)
C30	24(2)	18(2)	24(2)	-3(1)	8(2)	-3(1)
C31	20(2)	24(2)	29(2)	-1(2)	14(2)	-3(2)
C32	17(2)	15(2)	14(2)	-3(1)	1(1)	4(1)
C33	26(2)	17(2)	28(2)	-6(1)	3(2)	2(2)
C34	22(2)	21(2)	25(2)	-1(1)	3(2)	9(2)
C35	17(2)	47(3)	21(2)	11(2)	9(1)	3(2)
C36	35(3)	52(3)	23(2)	6(2)	14(2)	13(2)
C37	19(2)	96(4)	31(2)	9(3)	11(2)	-1(3)
C38	18(2)	38(2)	30(2)	12(2)	-4(2)	-8(2)
C39	30(3)	39(3)	43(3)	16(2)	-7(2)	-19(2)
C40	35(3)	33(2)	32(2)	-1(2)	-8(2)	-13(2)

Table 3. 7. Hydrogen coordinates (x 10^4) and isotropic displacement parameters (Å^2 x 10^3) for complex 2.

	x	y	z	U(eq)
H1A	5110(40)	9050(30)	5060(20)	12(10)
H1B	6390(40)	9090(30)	4910(30)	33(14)
H2	6100(40)	7880(30)	4060(30)	16(11)
H4	5027	6223	3999	22
H5	3211	5522	3424	28
H6	1503	6410	3078	29
H7	1601	8003	3252	32
H8	3405	8707	3869	27
H23	6870	5790	8300	19
H24	8718	5156	8337	21
H25	9646	5482	7288	23
H27A	5625	7405	7640	20
H27B	4971	6445	7372	20
H28A	8822	5924	5548	29
H28B	9780	6554	6151	29
H29	3235	6789	5224	20
H30A	3577	5235	5349	32
H30B	4390	5336	6253	32
H30C	4859	5689	5491	32
H31A	2038	6074	5984	34
H31B	2312	7102	6311	34
H31C	3005	6258	6816	34
H32	3696	8214	6956	19
H33A	4584	9648	7098	36
H33B	5294	9416	6421	36
H33C	5611	8893	7279	36
H34A	2623	9249	6040	35
H34B	2561	8290	5568	35
H34C	3427	9084	5407	35

H35	8134	7944	4045	33
H36A	7871	6623	3330	53
H36B	7134	6491	4007	53
H36C	8395	6009	4119	53
H37A	9909	7348	3791	72
H37B	10254	6943	4697	72
H37C	10157	8030	4555	72
H38	10048	8266	5872	36
H39A	9449	9821	5728	61
H39B	8090	9521	5499	61
H39C	8914	9292	4891	61
H40A	9686	9017	7045	54
H40B	9494	7930	7080	54
H40C	8378	8601	6836	54

Table 3. 8. Torsion angles [°] for complex 2.

Ir1-C1-C2-C3	108.7(3)	Ir1-P1-C27-C22	-19.2(3)
C1-C2-C3-C4	-149.7(3)	C25-C26-C28-P2	-159.3(3)
Ir1-C2-C3-C4	-65.3(4)	C21-C26-C28-P2	19.7(5)
C1-C2-C3-C8	32.7(5)	C38-P2-C28-C26	94.1(3)
Ir1-C2-C3-C8	117.2(3)	C35-P2-C28-C26	-156.6(3)
C8-C3-C4-C5	-1.8(5)	Ir1-P2-C28-C26	-26.1(3)
C2-C3-C4-C5	-179.4(3)	C27-P1-C29-C30	-61.6(3)
C3-C4-C5-C6	0.9(6)	C32-P1-C29-C30	-166.5(3)
C4-C5-C6-C7	1.3(6)	Ir1-P1-C29-C30	52.5(3)
C5-C6-C7-C8	-2.4(6)	C27-P1-C29-C31	62.0(3)
C6-C7-C8-C3	1.5(6)	C32-P1-C29-C31	-42.9(3)
C4-C3-C8-C7	0.6(5)	Ir1-P1-C29-C31	176.1(2)
C2-C3-C8-C7	178.2(3)	C27-P1-C32-C33	74.2(3)
C26-C21-C22-C23	-0.7(5)	C29-P1-C32-C33	-178.7(3)
Ir1-C21-C22-C23	-178.1(3)	Ir1-P1-C32-C33	-39.1(3)
C26-C21-C22-C27	177.2(3)	C27-P1-C32-C34	-160.5(3)
Ir1-C21-C22-C27	-0.1(4)	C29-P1-C32-C34	-53.3(3)
C21-C22-C23-C24	0.8(5)	Ir1-P1-C32-C34	86.3(3)
C27-C22-C23-C24	-177.1(3)	C28-P2-C35-C36	62.6(3)
C22-C23-C24-C25	0.4(5)	C38-P2-C35-C36	170.4(3)
C23-C24-C25-C26	-1.6(6)	Ir1-P2-C35-C36	-56.3(4)
C24-C25-C26-C21	1.7(6)	C28-P2-C35-C37	-63.9(4)
C24-C25-C26-C28	-179.4(4)	C38-P2-C35-C37	43.9(4)
C22-C21-C26-C25	-0.5(5)	Ir1-P2-C35-C37	177.2(3)
Ir1-C21-C26-C25	176.8(3)	C28-P2-C38-C40	-64.5(4)
C22-C21-C26-C28	-179.5(3)	C35-P2-C38-C40	-173.4(3)
Ir1-C21-C26-C28	-2.1(5)	Ir1-P2-C38-C40	48.8(4)
C23-C22-C27-P1	-168.0(3)	C28-P2-C38-C39	172.8(4)
C21-C22-C27-P1	14.1(4)	C35-P2-C38-C39	63.8(4)
C29-P1-C27-C22	105.8(3)	Ir1-P2-C38-C39	-73.9(4)
C32-P1-C27-C22	-146.2(3)		

3.5.9.3. Structural data for complex 3

CCDC # 1539911

Figure 3. 66. ORTEP diagram of complex 3

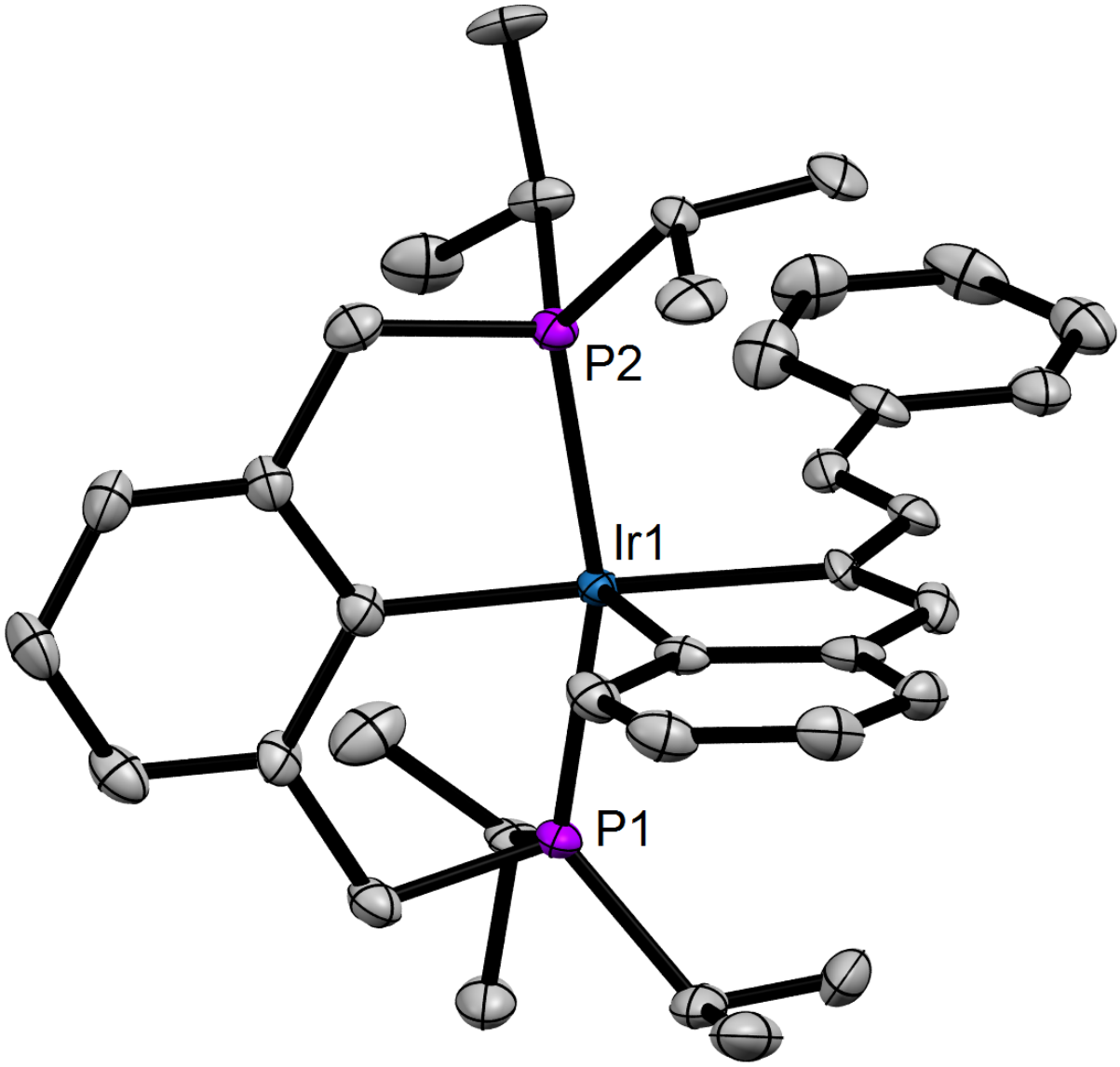

Table 3. 9. Crystal data and structure refinement for complex 3.

Identification code	twin4_P-1	
Empirical formula	C36 H47 Ir P2	
Formula weight	733.87	
Temperature	100(2) K	
Wavelength	0.71073 Å	
Crystal system	Triclinic	
Space group	P-1	
Unit cell dimensions	a = 9.9152(12) Å	α = 92.263(3)°.
	b = 11.9825(14) Å	β = 107.127(3)°.
	c = 14.1511(17) Å	γ = 91.127(3)°.
Volume	1604.6(3) $Å^3$	
Z	100	
Density (calculated)	1.519 Mg/m^3	
Absorption coefficient	4.283 mm^{-1}	
F(000)	740	
Crystal size	0.24 x 0.16 x 0.03 mm^3	
Theta range for data collection	1.507 to 30.003°.	
Index ranges	$-13 \leq h \leq 13$, $-16 \leq k \leq 16$, $-19 \leq l \leq 19$	
Reflections collected	18351	
Independent reflections	18351 [R(int) = 0.077 for component 1; 0.095 for all components]	
Completeness to theta = 25.242°	99.9 %	
Absorption correction	Semi-empirical from equivalents	
Max. and min. transmission	0.4322 and 0.2821	
Refinement method	Full-matrix least-squares on F^2	
Data / restraints / parameters	18351 / 0 / 362	
Goodness-of-fit on F^2	1.039	
Final R indices [I>2sigma(I)]	R1 = 0.0612, wR2 = 0.1449	
R indices (all data)	R1 = 0.0740, wR2 = 0.1516	
Extinction coefficient	n/a	
Largest diff. peak and hole	4.622 and -3.263 $e.Å^{-3}$	

Table 3. 10. Atomic coordinates (x 10^4) and equivalent isotropic displacement parameters ($Å^2$x 10^3) for complex 3. U(eq) is defined as one third of the trace of the orthogonalized U^{ij} tensor.

	x	y	z	U(eq)
Ir(1)	8384(1)	7573(1)	7273(1)	13(1)
P(1)	9941(2)	9050(2)	7378(2)	17(1)
P(2)	7465(2)	5794(2)	7267(2)	15(1)
C(1)	10145(9)	6911(8)	8243(7)	18(2)
C(2)	10179(9)	5791(8)	8553(7)	19(2)
C(3)	11383(10)	5360(8)	9197(7)	24(2)
C(4)	12608(10)	6022(9)	9567(8)	27(2)
C(5)	12614(10)	7123(9)	9306(7)	25(2)
C(6)	11414(9)	7569(8)	8674(7)	19(2)
C(7)	8803(10)	5087(8)	8204(7)	22(2)
C(8)	11398(9)	8801(8)	8483(7)	21(2)
C(9)	7396(11)	5017(8)	6092(7)	22(2)
C(10)	6838(12)	3799(8)	6032(8)	31(2)
C(11)	8819(12)	5071(9)	5899(8)	33(2)
C(12)	5774(9)	5435(7)	7481(7)	21(2)
C(13)	4529(10)	5746(9)	6618(8)	30(2)
C(14)	5654(11)	5934(8)	8476(8)	28(2)
C(15)	10745(9)	8987(7)	6344(7)	19(2)
C(16)	11793(10)	9947(8)	6369(8)	28(2)
C(17)	11483(12)	7869(8)	6319(9)	33(3)
C(18)	9533(10)	10546(8)	7480(8)	28(2)
C(19)	8533(11)	10891(9)	6502(9)	37(3)
C(20)	8939(11)	10817(9)	8338(9)	34(3)
C(21)	7578(9)	8191(7)	8311(6)	16(2)
C(22)	8145(10)	8100(8)	9331(7)	22(2)
C(23)	7486(11)	8511(8)	9989(8)	26(2)
C(24)	6181(10)	9037(8)	9639(8)	27(2)
C(25)	5610(10)	9158(8)	8634(7)	23(2)
C(26)	6260(10)	8735(8)	7949(7)	21(2)
C(27)	5744(9)	8784(8)	6884(7)	20(2)

C(28)	6553(9)	8290(7)	6384(8)	21(2)
C(29)	6108(9)	8245(7)	5294(7)	20(2)
C(30)	6854(9)	7733(7)	4755(7)	18(2)
C(31)	6500(9)	7570(8)	3673(7)	22(2)
C(32)	5326(10)	8025(8)	3007(7)	25(2)
C(33)	5030(11)	7819(9)	1994(8)	29(2)
C(34)	5915(12)	7158(10)	1627(7)	33(3)
C(35)	7063(13)	6703(10)	2266(8)	33(2)
C(36)	7379(12)	6921(10)	3279(8)	30(2)

Table 3. 11. Bond lengths [Å] and angles [°] for complex 3.

Ir(1)-C(21)	1.993(9)	C(11)-H(11B)	0.9800
Ir(1)-C(1)	2.071(9)	C(11)-H(11C)	0.9800
Ir(1)-C(28)	2.102(9)	C(12)-C(13)	1.524(13)
Ir(1)-P(1)	2.296(2)	C(12)-C(14)	1.545(13)
Ir(1)-P(2)	2.301(2)	C(12)-H(12)	1.0000
P(1)-C(8)	1.828(9)	C(13)-H(13A)	0.9800
P(1)-C(18)	1.854(10)	C(13)-H(13B)	0.9800
P(1)-C(15)	1.862(10)	C(13)-H(13C)	0.9800
P(2)-C(7)	1.825(10)	C(14)-H(14A)	0.9800
P(2)-C(12)	1.836(9)	C(14)-H(14B)	0.9800
P(2)-C(9)	1.856(9)	C(14)-H(14C)	0.9800
C(1)-C(2)	1.426(13)	C(15)-C(16)	1.527(12)
C(1)-C(6)	1.431(12)	C(15)-C(17)	1.543(13)
C(2)-C(3)	1.395(13)	C(15)-H(15)	1.0000
C(2)-C(7)	1.530(12)	C(16)-H(16A)	0.9800
C(3)-C(4)	1.390(13)	C(16)-H(16B)	0.9800
C(3)-H(3)	0.9500	C(16)-H(16C)	0.9800
C(4)-C(5)	1.385(14)	C(17)-H(17A)	0.9800
C(4)-H(4)	0.9500	C(17)-H(17B)	0.9800
C(5)-C(6)	1.391(13)	C(17)-H(17C)	0.9800
C(5)-H(5)	0.9500	C(18)-C(19)	1.524(15)
C(6)-C(8)	1.512(13)	C(18)-C(20)	1.525(15)
C(7)-H(7A)	0.9900	C(18)-H(18)	1.0000
C(7)-H(7B)	0.9900	C(19)-H(19A)	0.9800
C(8)-H(8A)	0.9900	C(19)-H(19B)	0.9800
C(8)-H(8B)	0.9900	C(19)-H(19C)	0.9800
C(9)-C(11)	1.515(14)	C(20)-H(20A)	0.9800
C(9)-C(10)	1.541(12)	C(20)-H(20B)	0.9800
C(9)-H(9)	1.0000	C(20)-H(20C)	0.9800
C(10)-H(10A)	0.9800	C(21)-C(22)	1.396(12)
C(10)-H(10B)	0.9800	C(21)-C(26)	1.435(13)
C(10)-H(10C)	0.9800	C(22)-C(23)	1.369(13)
C(11)-H(11A)	0.9800	C(22)-H(22)	0.9500

C(23)-C(24)	1.413(14)	C(30)-H(30)	0.9500
C(23)-H(23)	0.9500	C(31)-C(36)	1.398(14)
C(24)-C(25)	1.382(14)	C(31)-C(32)	1.399(13)
C(24)-H(24)	0.9500	C(32)-C(33)	1.387(14)
C(25)-C(26)	1.398(13)	C(32)-H(32)	0.9500
C(25)-H(25)	0.9500	C(33)-C(34)	1.390(16)
C(26)-C(27)	1.446(13)	C(33)-H(33)	0.9500
C(27)-C(28)	1.347(13)	C(34)-C(35)	1.367(16)
C(27)-H(27)	0.9500	C(34)-H(34)	0.9500
C(28)-C(29)	1.472(13)	C(35)-C(36)	1.386(14)
C(29)-C(30)	1.349(13)	C(35)-H(35)	0.9500
C(29)-H(29)	0.9500	C(36)-H(36)	0.9500
C(30)-C(31)	1.471(13)		

C(21)-Ir(1)-C(1)	96.0(3)	C(2)-C(1)-C(6)	115.0(8)
C(21)-Ir(1)-C(28)	79.6(4)	C(2)-C(1)-Ir(1)	123.2(7)
C(1)-Ir(1)-C(28)	175.6(4)	C(6)-C(1)-Ir(1)	121.7(7)
C(21)-Ir(1)-P(1)	95.5(2)	C(3)-C(2)-C(1)	122.2(8)
C(1)-Ir(1)-P(1)	81.9(3)	C(3)-C(2)-C(7)	120.3(8)
C(28)-Ir(1)-P(1)	98.3(2)	C(1)-C(2)-C(7)	117.4(8)
C(21)-Ir(1)-P(2)	94.6(2)	C(4)-C(3)-C(2)	120.5(9)
C(1)-Ir(1)-P(2)	82.3(3)	C(4)-C(3)-H(3)	119.8
C(28)-Ir(1)-P(2)	98.0(2)	C(2)-C(3)-H(3)	119.8
P(1)-Ir(1)-P(2)	162.08(8)	C(5)-C(4)-C(3)	119.4(9)
C(8)-P(1)-C(18)	106.0(5)	C(5)-C(4)-H(4)	120.3
C(8)-P(1)-C(15)	104.7(4)	C(3)-C(4)-H(4)	120.3
C(18)-P(1)-C(15)	103.4(4)	C(4)-C(5)-C(6)	120.8(9)
C(8)-P(1)-Ir(1)	103.9(3)	C(4)-C(5)-H(5)	119.6
C(18)-P(1)-Ir(1)	125.3(3)	C(6)-C(5)-H(5)	119.6
C(15)-P(1)-Ir(1)	111.8(3)	C(5)-C(6)-C(1)	122.0(9)
C(7)-P(2)-C(12)	105.7(4)	C(5)-C(6)-C(8)	119.8(8)
C(7)-P(2)-C(9)	103.9(5)	C(1)-C(6)-C(8)	118.1(8)
C(12)-P(2)-C(9)	104.5(4)	C(2)-C(7)-P(2)	110.9(6)
C(7)-P(2)-Ir(1)	105.1(3)	C(2)-C(7)-H(7A)	109.5
C(12)-P(2)-Ir(1)	125.7(3)	P(2)-C(7)-H(7A)	109.5
C(9)-P(2)-Ir(1)	109.9(3)	C(2)-C(7)-H(7B)	109.5

P(2)-C(7)-H(7B)	109.5	H(13A)-C(13)-H(13C)	109.5
H(7A)-C(7)-H(7B)	108.0	H(13B)-C(13)-H(13C)	109.5
C(6)-C(8)-P(1)	109.0(6)	C(12)-C(14)-H(14A)	109.5
C(6)-C(8)-H(8A)	109.9	C(12)-C(14)-H(14B)	109.5
P(1)-C(8)-H(8A)	109.9	H(14A)-C(14)-H(14B)	109.5
C(6)-C(8)-H(8B)	109.9	C(12)-C(14)-H(14C)	109.5
P(1)-C(8)-H(8B)	109.9	H(14A)-C(14)-H(14C)	109.5
H(8A)-C(8)-H(8B)	108.3	H(14B)-C(14)-H(14C)	109.5
C(11)-C(9)-C(10)	110.9(9)	C(16)-C(15)-C(17)	109.0(8)
C(11)-C(9)-P(2)	110.9(7)	C(16)-C(15)-P(1)	114.5(7)
C(10)-C(9)-P(2)	113.8(7)	C(17)-C(15)-P(1)	110.4(6)
C(11)-C(9)-H(9)	106.9	C(16)-C(15)-H(15)	107.6
C(10)-C(9)-H(9)	106.9	C(17)-C(15)-H(15)	107.6
P(2)-C(9)-H(9)	106.9	P(1)-C(15)-H(15)	107.6
C(9)-C(10)-H(10A)	109.5	C(15)-C(16)-H(16A)	109.5
C(9)-C(10)-H(10B)	109.5	C(15)-C(16)-H(16B)	109.5
H(10A)-C(10)-H(10B)	109.5	H(16A)-C(16)-H(16B)	109.5
C(9)-C(10)-H(10C)	109.5	C(15)-C(16)-H(16C)	109.5
H(10A)-C(10)-H(10C)	109.5	H(16A)-C(16)-H(16C)	109.5
H(10B)-C(10)-H(10C)	109.5	H(16B)-C(16)-H(16C)	109.5
C(9)-C(11)-H(11A)	109.5	C(15)-C(17)-H(17A)	109.5
C(9)-C(11)-H(11B)	109.5	C(15)-C(17)-H(17B)	109.5
H(11A)-C(11)-H(11B)	109.5	H(17A)-C(17)-H(17B)	109.5
C(9)-C(11)-H(11C)	109.5	C(15)-C(17)-H(17C)	109.5
H(11A)-C(11)-H(11C)	109.5	H(17A)-C(17)-H(17C)	109.5
H(11B)-C(11)-H(11C)	109.5	H(17B)-C(17)-H(17C)	109.5
C(13)-C(12)-C(14)	111.4(8)	C(19)-C(18)-C(20)	111.2(9)
C(13)-C(12)-P(2)	111.4(7)	C(19)-C(18)-P(1)	109.7(7)
C(14)-C(12)-P(2)	113.0(6)	C(20)-C(18)-P(1)	112.9(7)
C(13)-C(12)-H(12)	106.9	C(19)-C(18)-H(18)	107.6
C(14)-C(12)-H(12)	106.9	C(20)-C(18)-H(18)	107.6
P(2)-C(12)-H(12)	106.9	P(1)-C(18)-H(18)	107.6
C(12)-C(13)-H(13A)	109.5	C(18)-C(19)-H(19A)	109.5
C(12)-C(13)-H(13B)	109.5	C(18)-C(19)-H(19B)	109.5
H(13A)-C(13)-H(13B)	109.5	H(19A)-C(19)-H(19B)	109.5
C(12)-C(13)-H(13C)	109.5	C(18)-C(19)-H(19C)	109.5

H(19A)-C(19)-H(19C)	109.5	C(26)-C(27)-H(27)	122.4
H(19B)-C(19)-H(19C)	109.5	C(27)-C(28)-C(29)	120.3(8)
C(18)-C(20)-H(20A)	109.5	C(27)-C(28)-Ir(1)	114.9(7)
C(18)-C(20)-H(20B)	109.5	C(29)-C(28)-Ir(1)	124.7(7)
H(20A)-C(20)-H(20B)	109.5	C(30)-C(29)-C(28)	122.9(9)
C(18)-C(20)-H(20C)	109.5	C(30)-C(29)-H(29)	118.6
H(20A)-C(20)-H(20C)	109.5	C(28)-C(29)-H(29)	118.6
H(20B)-C(20)-H(20C)	109.5	C(29)-C(30)-C(31)	128.7(9)
C(22)-C(21)-C(26)	118.5(8)	C(29)-C(30)-H(30)	115.7
C(22)-C(21)-Ir(1)	126.1(7)	C(31)-C(30)-H(30)	115.7
C(26)-C(21)-Ir(1)	115.4(6)	C(36)-C(31)-C(32)	117.6(9)
C(23)-C(22)-C(21)	122.1(9)	C(36)-C(31)-C(30)	118.5(9)
C(23)-C(22)-H(22)	118.9	C(32)-C(31)-C(30)	123.8(9)
C(21)-C(22)-H(22)	118.9	C(33)-C(32)-C(31)	121.2(10)
C(22)-C(23)-C(24)	119.8(10)	C(33)-C(32)-H(32)	119.4
C(22)-C(23)-H(23)	120.1	C(31)-C(32)-H(32)	119.4
C(24)-C(23)-H(23)	120.1	C(32)-C(33)-C(34)	119.8(10)
C(25)-C(24)-C(23)	119.2(9)	C(32)-C(33)-H(33)	120.1
C(25)-C(24)-H(24)	120.4	C(34)-C(33)-H(33)	120.1
C(23)-C(24)-H(24)	120.4	C(35)-C(34)-C(33)	119.9(9)
C(24)-C(25)-C(26)	121.8(9)	C(35)-C(34)-H(34)	120.1
C(24)-C(25)-H(25)	119.1	C(33)-C(34)-H(34)	120.1
C(26)-C(25)-H(25)	119.1	C(34)-C(35)-C(36)	120.6(11)
C(25)-C(26)-C(21)	118.5(9)	C(34)-C(35)-H(35)	119.7
C(25)-C(26)-C(27)	126.7(9)	C(36)-C(35)-H(35)	119.7
C(21)-C(26)-C(27)	114.8(9)	C(35)-C(36)-C(31)	120.9(11)
C(28)-C(27)-C(26)	115.3(9)	C(35)-C(36)-H(36)	119.5
C(28)-C(27)-H(27)	122.4	C(31)-C(36)-H(36)	119.5

Table 3. 12. Anisotropic displacement parameters ($Å^2$x 10^3) for complex 3.

The anisotropic displacement factor exponent takes the form: $-2\pi^2[h^2 a^{*2}U^{11} + ... + 2 h k a^* b^* U^{12}]$

	U^{11}	U^{22}	U^{33}	U^{23}	U^{13}	U^{12}
Ir(1)	11(1)	12(1)	18(1)	0(1)	6(1)	-1(1)
P(1)	13(1)	13(1)	26(1)	1(1)	5(1)	-3(1)
P(2)	14(1)	15(1)	18(1)	2(1)	7(1)	-2(1)
C(1)	16(4)	20(5)	22(5)	3(4)	9(4)	1(3)
C(2)	17(4)	23(5)	18(5)	5(4)	6(4)	1(4)
C(3)	24(5)	22(5)	30(5)	8(4)	12(4)	8(4)
C(4)	17(5)	40(6)	21(5)	8(5)	1(4)	0(4)
C(5)	18(5)	34(5)	23(5)	4(4)	7(4)	-6(4)
C(6)	13(4)	21(4)	26(5)	5(4)	12(4)	2(3)
C(7)	27(5)	17(4)	24(5)	4(4)	10(4)	-1(4)
C(8)	16(4)	23(5)	25(5)	2(4)	5(4)	-5(4)
C(9)	31(5)	16(4)	18(5)	-1(4)	8(4)	-5(4)
C(10)	47(7)	12(4)	33(6)	-8(4)	14(5)	-8(4)
C(11)	42(6)	32(6)	30(6)	-8(5)	19(5)	-6(5)
C(12)	13(4)	16(4)	32(6)	3(4)	5(4)	-3(3)
C(13)	15(5)	26(5)	45(7)	4(5)	5(4)	-9(4)
C(14)	28(5)	20(5)	43(6)	3(4)	22(5)	-7(4)
C(15)	17(4)	16(4)	24(5)	4(4)	7(4)	-8(3)
C(16)	23(5)	22(5)	38(6)	7(4)	10(4)	-3(4)
C(17)	42(6)	24(5)	45(7)	6(5)	30(5)	1(5)
C(18)	21(5)	15(4)	47(7)	1(4)	10(5)	-4(4)
C(19)	26(5)	18(5)	64(8)	6(5)	9(5)	6(4)
C(20)	28(5)	24(5)	52(7)	-12(5)	16(5)	-7(4)
C(21)	19(4)	15(4)	13(4)	1(3)	6(3)	-6(3)
C(22)	16(4)	24(5)	27(5)	1(4)	8(4)	-4(4)
C(23)	27(5)	29(5)	26(5)	-4(4)	12(4)	-9(4)
C(24)	25(5)	27(5)	34(6)	-9(4)	20(5)	-5(4)
C(25)	18(4)	18(4)	33(6)	-4(4)	11(4)	0(4)
C(26)	23(5)	16(4)	25(5)	-3(4)	9(4)	-10(4)
C(27)	11(4)	21(4)	29(5)	7(4)	7(4)	0(3)

C(28)	6(4)	15(4)	37(6)	3(4)	1(4)	-1(3)
C(29)	14(4)	18(4)	24(5)	-2(4)	4(4)	-6(3)
C(30)	16(4)	14(4)	25(5)	7(4)	4(4)	-1(3)
C(31)	15(4)	24(5)	24(5)	-2(4)	5(4)	-10(4)
C(32)	23(5)	21(5)	30(6)	2(4)	8(4)	-6(4)
C(33)	26(5)	32(5)	26(5)	8(5)	4(4)	-8(5)
C(34)	37(6)	45(7)	15(5)	-3(5)	8(5)	-18(5)
C(35)	40(6)	32(6)	31(6)	-6(5)	20(5)	-1(5)
C(36)	32(6)	32(5)	31(6)	10(5)	16(5)	3(5)

Table 3. 13. Hydrogen coordinates (x 10^4) and isotropic displacement parameters (Å^{2}x 10^3) for complex 3.

	x	y	z	U(eq)
H(3)	11367	4608	9385	29
H(4)	13433	5722	9995	32
H(5)	13447	7579	9560	30
H(7A)	8450	4949	8775	26
H(7B)	8987	4355	7924	26
H(8A)	12304	9044	8383	26
H(8B)	11276	9237	9059	26
H(9)	6722	5409	5546	26
H(10A)	6977	3404	5450	46
H(10B)	5829	3790	5977	46
H(10C)	7353	3427	6631	46
H(11A)	9512	4690	6418	50
H(11B)	9126	5853	5902	50
H(11C)	8741	4703	5254	50
H(12)	5724	4603	7515	25
H(13A)	3645	5510	6739	44
H(13B)	4595	5371	6006	44
H(13C)	4546	6557	6553	44
H(14A)	5572	6746	8441	42
H(14B)	6498	5763	9010	42
H(14C)	4816	5609	8607	42
H(15)	9962	9015	5711	23
H(16A)	12526	9987	7010	41
H(16B)	11296	10652	6275	41
H(16C)	12230	9819	5839	41
H(17A)	11796	7808	5725	50
H(17B)	10820	7248	6309	50
H(17C)	12302	7842	6909	50
H(18)	10436	10992	7602	33

H(19A)	7688	10397	6317	55
H(19B)	9008	10833	5985	55
H(19C)	8261	11664	6574	55
H(20A)	8773	11619	8371	51
H(20B)	9616	10610	8959	51
H(20C)	8046	10395	8236	51
H(22)	9017	7741	9576	26
H(23)	7905	8443	10680	32
H(24)	5702	9305	10090	32
H(25)	4752	9539	8402	27
H(27)	4895	9139	6560	24
H(29)	5258	8591	4956	23
H(30)	7724	7438	5123	22
H(32)	4721	8482	3254	30
H(33)	4225	8130	1552	34
H(34)	5723	7022	933	39
H(35)	7650	6232	2015	39
H(36)	8205	6626	3711	36

Table 3. 14. Torsion angles [°] for complex 3.

C(6)-C(1)-C(2)-C(3)	-2.6(13)	C(7)-P(2)-C(12)-C(14)	66.6(7)
Ir(1)-C(1)-C(2)-C(3)	179.2(7)	C(9)-P(2)-C(12)-C(14)	175.9(7)
C(6)-C(1)-C(2)-C(7)	173.6(8)	Ir(1)-P(2)-C(12)-C(14)	-55.9(8)
Ir(1)-C(1)-C(2)-C(7)	-4.6(12)	C(8)-P(1)-C(15)-C(16)	-68.1(8)
C(1)-C(2)-C(3)-C(4)	0.3(15)	C(18)-P(1)-C(15)-C(16)	42.7(8)
C(7)-C(2)-C(3)-C(4)	-175.8(9)	Ir(1)-P(1)-C(15)-C(16)	180.0(6)
C(2)-C(3)-C(4)-C(5)	1.3(15)	C(8)-P(1)-C(15)-C(17)	55.3(8)
C(3)-C(4)-C(5)-C(6)	-0.4(16)	C(18)-P(1)-C(15)-C(17)	166.1(7)
C(4)-C(5)-C(6)-C(1)	-2.0(15)	Ir(1)-P(1)-C(15)-C(17)	-56.6(7)
C(4)-C(5)-C(6)-C(8)	173.8(9)	C(8)-P(1)-C(18)-C(19)	168.9(7)
C(2)-C(1)-C(6)-C(5)	3.4(13)	C(15)-P(1)-C(18)-C(19)	59.1(8)
Ir(1)-C(1)-C(6)-C(5)	-178.3(7)	Ir(1)-P(1)-C(18)-C(19)	-70.5(8)
C(2)-C(1)-C(6)-C(8)	-172.4(8)	C(8)-P(1)-C(18)-C(20)	-66.5(8)
Ir(1)-C(1)-C(6)-C(8)	5.8(12)	C(15)-P(1)-C(18)-C(20)	-176.3(7)
C(3)-C(2)-C(7)-P(2)	-173.8(7)	Ir(1)-P(1)-C(18)-C(20)	54.1(8)
C(1)-C(2)-C(7)-P(2)	10.0(11)	C(26)-C(21)-C(22)-C(23)	0.0(13)
C(12)-P(2)-C(7)-C(2)	-145.0(7)	Ir(1)-C(21)-C(22)-C(23)	-177.1(7)
C(9)-P(2)-C(7)-C(2)	105.3(7)	C(21)-C(22)-C(23)-C(24)	0.7(14)
Ir(1)-P(2)-C(7)-C(2)	-10.2(7)	C(22)-C(23)-C(24)-C(25)	-1.9(14)
C(5)-C(6)-C(8)-P(1)	163.4(8)	C(23)-C(24)-C(25)-C(26)	2.5(14)
C(1)-C(6)-C(8)-P(1)	-20.6(11)	C(24)-C(25)-C(26)-C(21)	-1.9(13)
C(18)-P(1)-C(8)-C(6)	157.6(6)	C(24)-C(25)-C(26)-C(27)	178.2(9)
C(15)-P(1)-C(8)-C(6)	-93.5(7)	C(22)-C(21)-C(26)-C(25)	0.6(12)
Ir(1)-P(1)-C(8)-C(6)	23.9(7)	Ir(1)-C(21)-C(26)-C(25)	178.0(6)
C(7)-P(2)-C(9)-C(11)	-59.8(8)	C(22)-C(21)-C(26)-C(27)	-179.5(8)
C(12)-P(2)-C(9)-C(11)	-170.4(7)	Ir(1)-C(21)-C(26)-C(27)	-2.1(10)
Ir(1)-P(2)-C(9)-C(11)	52.2(8)	C(25)-C(26)-C(27)-C(28)	-178.6(9)
C(7)-P(2)-C(9)-C(10)	66.0(8)	C(21)-C(26)-C(27)-C(28)	1.6(12)
C(12)-P(2)-C(9)-C(10)	-44.6(9)	C(26)-C(27)-C(28)-C(29)	177.5(8)
Ir(1)-P(2)-C(9)-C(10)	178.1(7)	C(26)-C(27)-C(28)-Ir(1)	-0.4(10)
C(7)-P(2)-C(12)-C(13)	-167.1(7)	C(27)-C(28)-C(29)-C(30)	-178.0(8)
C(9)-P(2)-C(12)-C(13)	-57.8(8)	Ir(1)-C(28)-C(29)-C(30)	-0.3(12)
Ir(1)-P(2)-C(12)-C(13)	70.4(8)	C(28)-C(29)-C(30)-C(31)	176.3(8)

C(29)-C(30)-C(31)-C(36)	-174.3(9)	C(33)-C(34)-C(35)-C(36)	-1.9(18)
C(29)-C(30)-C(31)-C(32)	5.5(15)	C(34)-C(35)-C(36)-C(31)	2.9(18)
C(36)-C(31)-C(32)-C(33)	1.3(15)	C(32)-C(31)-C(36)-C(35)	-2.5(16)
C(30)-C(31)-C(32)-C(33)	-178.5(9)	C(30)-C(31)-C(36)-C(35)	177.3(10)
C(31)-C(32)-C(33)-C(34)	-0.5(15)		
C(32)-C(33)-C(34)-C(35)	0.7(16)		

3.5.9.4. Structural data for complex 4

CCDC # 1539910

Figure 3. 67. ORTEP diagram of complex 4

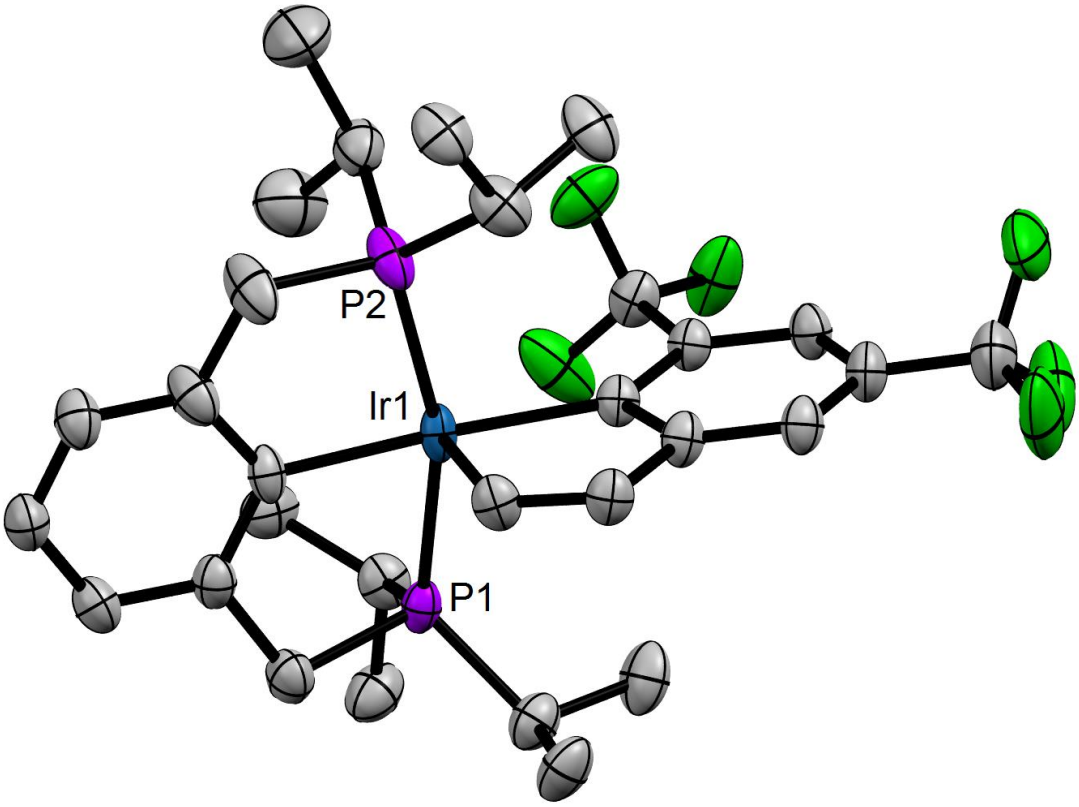

Table 3. 15. Crystal data and structure refinement for complex 4.

Identification code	irstyr9b_P-1final	
Empirical formula	C36 H53 F6 Ir P2	
Formula weight	853.92	
Temperature	120(2) K	
Wavelength	0.71073 Å	
Crystal system	Triclinic	
Space group	P-1	
Unit cell dimensions	a = 8.3236(7) Å	α = 103.023(2)°.
	b = 14.4951(13) Å	β = 94.075(2)°.
	c = 15.2260(13) Å	γ = 96.298(2)°.
Volume	1770.3(3) $Å^3$	
Z	2	
Density (calculated)	1.602 Mg/m^3	
Absorption coefficient	3.918 mm^{-1}	
F(000)	860	
Crystal size	0.170 x 0.110 x 0.002 mm^3	
Theta range for data collection	1.379 to 26.732°.	
Index ranges	$-10 \leq h \leq 10$, $-18 \leq k \leq 18$, $-19 \leq l \leq 19$	
Reflections collected	16876	
Independent reflections	7497 [R(int) = 0.0474]	
Completeness to theta = 25.242°	99.9 %	
Absorption correction	NUMERICAL	
Max. and min. transmission	0.9872 and 0.5232	
Refinement method	Full-matrix least-squares on F^2	
Data / restraints / parameters	7497 / 1062 / 512	
Goodness-of-fit on F^2	1.039	
Final R indices [I>2sigma(I)]	R1 = 0.0590, wR2 = 0.1472	
R indices (all data)	R1 = 0.0753, wR2 = 0.1574	
Extinction coefficient	n/a	
Largest diff. peak and hole	4.429 and -3.746 $e.Å^{-3}$	

Table 3. 16. Atomic coordinates (x 10^4) and equivalent isotropic displacement parameters ($Å^2$x 10^3) for complex 4.

U(eq) is defined as one third of the trace of the orthogonalized U^{ij} tensor.

	x	y	z	U(eq)
Ir(1)	2445(1)	6884(1)	2984(1)	27(1)
P(1)	2201(2)	7168(1)	4522(2)	28(1)
P(2)	2273(3)	7054(2)	1522(2)	38(1)
C(1)	2641(9)	8355(5)	3279(6)	29(2)
C(2)	2757(10)	8921(6)	4170(6)	32(2)
C(3)	2794(11)	9909(6)	4353(6)	36(2)
C(4)	2749(11)	10376(6)	3650(6)	38(2)
C(5)	2724(11)	9847(6)	2777(6)	38(2)
C(6)	2693(12)	8878(6)	2589(6)	41(2)
C(7)	2930(11)	8439(6)	4950(6)	38(2)
C(8)	2894(14)	8329(6)	1636(7)	50(2)
C(9)	3196(11)	6549(7)	5296(6)	39(2)
C(10)	5053(11)	6679(8)	5294(7)	48(2)
C(11)	2531(13)	5491(7)	5080(8)	50(2)
C(12)	66(10)	7069(6)	4777(6)	33(2)
C(13)	-861(11)	7764(7)	4368(6)	40(2)
C(14)	-157(13)	7229(8)	5776(6)	46(2)
C(15A)	3690(20)	6355(11)	767(11)	44(3)
C(16A)	4180(20)	6836(12)	39(12)	44(3)
C(17A)	2746(13)	5376(7)	318(7)	49(2)
C(15B)	3160(19)	6467(9)	515(15)	44(3)
C(16B)	4940(20)	6761(13)	590(13)	44(3)
C(17B)	2746(13)	5376(7)	318(7)	49(2)
C(18)	129(13)	6818(7)	1041(6)	43(2)
C(19)	-210(19)	7138(10)	156(8)	71(3)
C(20)	-936(15)	7245(10)	1745(8)	65(3)
C(21)	2622(9)	5423(5)	2680(5)	26(1)
C(22)	1470(10)	4577(6)	2459(5)	28(1)

C(23)	1896(10)	3658(6)	2261(6)	33(2)
C(24)	3519(11)	3530(6)	2252(6)	36(2)
C(25)	4706(10)	4319(6)	2442(6)	33(2)
C(26)	4265(10)	5228(6)	2652(6)	31(2)
C(27)	-285(10)	4667(6)	2448(6)	34(2)
F(1A)	-688(10)	5300(7)	3110(7)	66(3)
F(2A)	-1202(9)	3832(5)	2462(7)	54(2)
F(3A)	-884(9)	4857(7)	1701(5)	53(2)
F(1B)	-850(20)	4718(16)	3283(11)	46(4)
F(2B)	-1280(20)	4017(14)	1901(14)	56(4)
F(3B)	-670(20)	5510(13)	2309(15)	48(4)
C(28)	3971(14)	2560(7)	2021(8)	52(2)
F(4A)	3190(14)	1989(6)	2485(7)	79(3)
F(5A)	5507(11)	2500(6)	2180(9)	84(3)
F(6A)	3499(13)	2093(6)	1181(5)	69(2)
F(4B)	4620(40)	2260(20)	2681(16)	69(5)
F(5B)	5060(40)	2430(20)	1380(20)	70(5)
F(6B)	2740(30)	1888(19)	1650(20)	70(5)
C(29)	5432(10)	6087(6)	2884(6)	31(2)
C(30)	4844(9)	6910(6)	3053(6)	32(2)
C(31A)	7330(50)	-470(30)	2740(20)	99(4)
C(32A)	7070(30)	240(30)	2200(20)	110(3)
C(33A)	8730(30)	640(20)	2070(20)	109(4)
C(34A)	8540(40)	1230(20)	1411(18)	112(4)
C(35A)	7070(40)	790(20)	796(18)	115(4)
C(36A)	7580(50)	10(30)	110(20)	117(4)
C(31B)	7260(50)	-510(30)	3070(20)	99(4)
C(32B)	7350(40)	280(20)	2592(16)	110(3)
C(33B)	8330(30)	-40(20)	1829(15)	111(4)
C(34B)	7120(40)	-330(20)	1013(16)	115(4)
C(35B)	7570(50)	390(20)	483(18)	117(4)
C(36B)	8700(50)	1140(20)	1140(20)	115(4)

Table 3. 17. Bond lengths [Å] and angles [°] for complex 4.

Ir(1)-C(30)	1.988(8)	C(11)-H(11A)	0.9800
Ir(1)-C(1)	2.064(8)	C(11)-H(11B)	0.9800
Ir(1)-C(21)	2.087(8)	C(11)-H(11C)	0.9800
Ir(1)-P(2)	2.290(2)	C(12)-C(14)	1.514(13)
Ir(1)-P(1)	2.312(2)	C(12)-C(13)	1.543(12)
P(1)-C(7)	1.828(9)	C(12)-H(12)	1.0000
P(1)-C(9)	1.839(9)	C(13)-H(13A)	0.9800
P(1)-C(12)	1.843(8)	C(13)-H(13B)	0.9800
P(2)-C(15B)	1.826(19)	C(13)-H(13C)	0.9800
P(2)-C(8)	1.829(9)	C(14)-H(14A)	0.9800
P(2)-C(18)	1.845(11)	C(14)-H(14B)	0.9800
P(2)-C(15A)	1.92(2)	C(14)-H(14C)	0.9800
C(1)-C(2)	1.409(12)	C(15A)-C(16A)	1.493(17)
C(1)-C(6)	1.428(12)	C(15A)-C(17A)	1.530(15)
C(2)-C(3)	1.392(12)	C(15A)-H(15A)	1.0000
C(2)-C(7)	1.514(12)	C(16A)-H(16A)	0.9800
C(3)-C(4)	1.392(13)	C(16A)-H(16B)	0.9800
C(3)-H(3)	0.9500	C(16A)-H(16C)	0.9800
C(4)-C(5)	1.373(13)	C(17A)-H(17A)	0.9800
C(4)-H(4)	0.9500	C(17A)-H(17B)	0.9800
C(5)-C(6)	1.366(13)	C(17A)-H(17C)	0.9800
C(5)-H(5)	0.9500	C(15B)-C(16B)	1.482(17)
C(6)-C(8)	1.519(13)	C(15B)-C(17B)	1.536(15)
C(7)-H(7A)	0.9900	C(15B)-H(15B)	1.0000
C(7)-H(7B)	0.9900	C(16B)-H(16D)	0.9800
C(8)-H(8A)	0.9900	C(16B)-H(16E)	0.9800
C(8)-H(8B)	0.9900	C(16B)-H(16F)	0.9800
C(9)-C(11)	1.525(13)	C(17B)-H(17D)	0.9800
C(9)-C(10)	1.536(13)	C(17B)-H(17E)	0.9800
C(9)-H(9)	1.0000	C(17B)-H(17F)	0.9800
C(10)-H(10A)	0.9800	C(18)-C(20)	1.508(15)
C(10)-H(10B)	0.9800	C(18)-C(19)	1.540(14)
C(10)-H(10C)	0.9800	C(18)-H(18)	1.0000

C(19)-H(19A)	0.9800	C(31A)-H(31C)	0.9800
C(19)-H(19B)	0.9800	C(32A)-C(33A)	1.477(14)
C(19)-H(19C)	0.9800	C(32A)-H(32A)	0.9900
C(20)-H(20A)	0.9800	C(32A)-H(32B)	0.9900
C(20)-H(20B)	0.9800	C(33A)-C(34A)	1.465(14)
C(20)-H(20C)	0.9800	C(33A)-H(33A)	0.9900
C(21)-C(26)	1.429(11)	C(33A)-H(33B)	0.9900
C(21)-C(22)	1.431(11)	C(34A)-C(35A)	1.475(14)
C(22)-C(23)	1.389(11)	C(34A)-H(34A)	0.9900
C(22)-C(27)	1.480(11)	C(34A)-H(34B)	0.9900
C(23)-C(24)	1.385(12)	C(35A)-C(36A)	1.482(14)
C(23)-H(23)	0.9500	C(35A)-H(35A)	0.9900
C(24)-C(25)	1.390(12)	C(35A)-H(35B)	0.9900
C(24)-C(28)	1.467(13)	C(36A)-H(36A)	0.9800
C(25)-C(26)	1.380(11)	C(36A)-H(36B)	0.9800
C(25)-H(25)	0.9500	C(36A)-H(36C)	0.9800
C(26)-C(29)	1.451(11)	C(31B)-C(32B)	1.484(14)
C(27)-F(2B)	1.283(18)	C(31B)-H(31D)	0.9800
C(27)-F(1A)	1.292(11)	C(31B)-H(31E)	0.9800
C(27)-F(3A)	1.307(11)	C(31B)-H(31F)	0.9800
C(27)-F(3B)	1.353(18)	C(32B)-C(33B)	1.484(14)
C(27)-F(2A)	1.364(11)	C(32B)-H(32C)	0.9900
C(27)-F(1B)	1.376(18)	C(32B)-H(32D)	0.9900
C(28)-F(4B)	1.29(3)	C(33B)-C(34B)	1.491(14)
C(28)-F(5A)	1.300(14)	C(33B)-H(33C)	0.9900
C(28)-F(6A)	1.315(13)	C(33B)-H(33D)	0.9900
C(28)-F(6B)	1.33(3)	C(34B)-C(35B)	1.494(14)
C(28)-F(4A)	1.348(14)	C(34B)-H(34C)	0.9900
C(28)-F(5B)	1.37(3)	C(34B)-H(34D)	0.9900
C(29)-C(30)	1.319(12)	C(35B)-C(36B)	1.492(14)
C(29)-H(29)	0.9500	C(35B)-H(35C)	0.9900
C(30)-H(30)	0.9500	C(35B)-H(35D)	0.9900
C(31A)-C(32A)	1.489(14)	C(36B)-H(36D)	0.9800
C(31A)-H(31A)	0.9800	C(36B)-H(36E)	0.9800
C(31A)-H(31B)	0.9800	C(36B)-H(36F)	0.9800

C(30)-Ir(1)-C(1)	91.9(3)	C(3)-C(4)-H(4)	120.7
C(30)-Ir(1)-C(21)	79.6(3)	C(6)-C(5)-C(4)	121.5(9)
C(1)-Ir(1)-C(21)	171.5(3)	C(6)-C(5)-H(5)	119.2
C(30)-Ir(1)-P(2)	93.0(3)	C(4)-C(5)-H(5)	119.2
C(1)-Ir(1)-P(2)	82.6(2)	C(5)-C(6)-C(1)	122.2(8)
C(21)-Ir(1)-P(2)	96.8(2)	C(5)-C(6)-C(8)	120.2(9)
C(30)-Ir(1)-P(1)	97.4(2)	C(1)-C(6)-C(8)	117.3(8)
C(1)-Ir(1)-P(1)	81.0(2)	C(2)-C(7)-P(1)	108.0(6)
C(21)-Ir(1)-P(1)	100.8(2)	C(2)-C(7)-H(7A)	110.1
P(2)-Ir(1)-P(1)	160.82(8)	P(1)-C(7)-H(7A)	110.1
C(7)-P(1)-C(9)	106.1(4)	C(2)-C(7)-H(7B)	110.1
C(7)-P(1)-C(12)	103.7(4)	P(1)-C(7)-H(7B)	110.1
C(9)-P(1)-C(12)	103.7(4)	H(7A)-C(7)-H(7B)	108.4
C(7)-P(1)-Ir(1)	104.4(3)	C(6)-C(8)-P(2)	109.7(6)
C(9)-P(1)-Ir(1)	124.5(3)	C(6)-C(8)-H(8A)	109.7
C(12)-P(1)-Ir(1)	112.5(3)	P(2)-C(8)-H(8A)	109.7
C(15B)-P(2)-C(8)	104.6(5)	C(6)-C(8)-H(8B)	109.7
C(15B)-P(2)-C(18)	97.8(7)	P(2)-C(8)-H(8B)	109.7
C(8)-P(2)-C(18)	106.0(5)	H(8A)-C(8)-H(8B)	108.2
C(8)-P(2)-C(15A)	108.3(5)	C(11)-C(9)-C(10)	110.6(8)
C(18)-P(2)-C(15A)	113.5(6)	C(11)-C(9)-P(1)	111.3(7)
C(15B)-P(2)-Ir(1)	132.5(7)	C(10)-C(9)-P(1)	112.1(6)
C(8)-P(2)-Ir(1)	104.0(3)	C(11)-C(9)-H(9)	107.5
C(18)-P(2)-Ir(1)	109.7(3)	C(10)-C(9)-H(9)	107.5
C(15A)-P(2)-Ir(1)	114.6(6)	P(1)-C(9)-H(9)	107.5
C(2)-C(1)-C(6)	114.9(7)	C(9)-C(10)-H(10A)	109.5
C(2)-C(1)-Ir(1)	123.0(6)	C(9)-C(10)-H(10B)	109.5
C(6)-C(1)-Ir(1)	122.1(6)	H(10A)-C(10)-H(10B)	109.5
C(3)-C(2)-C(1)	122.2(8)	C(9)-C(10)-H(10C)	109.5
C(3)-C(2)-C(7)	119.3(8)	H(10A)-C(10)-H(10C)	109.5
C(1)-C(2)-C(7)	118.5(7)	H(10B)-C(10)-H(10C)	109.5
C(2)-C(3)-C(4)	120.4(8)	C(9)-C(11)-H(11A)	109.5
C(2)-C(3)-H(3)	119.8	C(9)-C(11)-H(11B)	109.5
C(4)-C(3)-H(3)	119.8	H(11A)-C(11)-H(11B)	109.5
C(5)-C(4)-C(3)	118.6(8)	C(9)-C(11)-H(11C)	109.5
C(5)-C(4)-H(4)	120.7	H(11A)-C(11)-H(11C)	109.5

H(11B)-C(11)-H(11C)	109.5	H(17B)-C(17A)-H(17C)	109.5
C(14)-C(12)-C(13)	109.2(7)	C(16B)-C(15B)-C(17B)	111.7(12)
C(14)-C(12)-P(1)	114.5(6)	C(16B)-C(15B)-P(2)	111.2(13)
C(13)-C(12)-P(1)	110.6(6)	C(17B)-C(15B)-P(2)	111.4(11)
C(14)-C(12)-H(12)	107.4	C(16B)-C(15B)-H(15B)	107.4
C(13)-C(12)-H(12)	107.4	C(17B)-C(15B)-H(15B)	107.4
P(1)-C(12)-H(12)	107.4	P(2)-C(15B)-H(15B)	107.4
C(12)-C(13)-H(13A)	109.5	C(15B)-C(16B)-H(16D)	109.5
C(12)-C(13)-H(13B)	109.5	C(15B)-C(16B)-H(16E)	109.5
H(13A)-C(13)-H(13B)	109.5	H(16D)-C(16B)-H(16E)	109.5
C(12)-C(13)-H(13C)	109.5	C(15B)-C(16B)-H(16F)	109.5
H(13A)-C(13)-H(13C)	109.5	H(16D)-C(16B)-H(16F)	109.5
H(13B)-C(13)-H(13C)	109.5	H(16E)-C(16B)-H(16F)	109.5
C(12)-C(14)-H(14A)	109.5	C(15B)-C(17B)-H(17D)	109.5
C(12)-C(14)-H(14B)	109.5	C(15B)-C(17B)-H(17E)	109.5
H(14A)-C(14)-H(14B)	109.5	H(17D)-C(17B)-H(17E)	109.5
C(12)-C(14)-H(14C)	109.5	C(15B)-C(17B)-H(17F)	109.5
H(14A)-C(14)-H(14C)	109.5	H(17D)-C(17B)-H(17F)	109.5
H(14B)-C(14)-H(14C)	109.5	H(17E)-C(17B)-H(17F)	109.5
C(16A)-C(15A)-C(17A)	108.3(11)	C(20)-C(18)-C(19)	110.9(10)
C(16A)-C(15A)-P(2)	111.7(14)	C(20)-C(18)-P(2)	110.0(7)
C(17A)-C(15A)-P(2)	107.1(11)	C(19)-C(18)-P(2)	115.0(8)
C(16A)-C(15A)-H(15A)	109.9	C(20)-C(18)-H(18)	106.8
C(17A)-C(15A)-H(15A)	109.9	C(19)-C(18)-H(18)	106.8
P(2)-C(15A)-H(15A)	109.9	P(2)-C(18)-H(18)	106.8
C(15A)-C(16A)-H(16A)	109.5	C(18)-C(19)-H(19A)	109.5
C(15A)-C(16A)-H(16B)	109.5	C(18)-C(19)-H(19B)	109.5
H(16A)-C(16A)-H(16B)	109.5	H(19A)-C(19)-H(19B)	109.5
C(15A)-C(16A)-H(16C)	109.5	C(18)-C(19)-H(19C)	109.5
H(16A)-C(16A)-H(16C)	109.5	H(19A)-C(19)-H(19C)	109.5
H(16B)-C(16A)-H(16C)	109.5	H(19B)-C(19)-H(19C)	109.5
C(15A)-C(17A)-H(17A)	109.5	C(18)-C(20)-H(20A)	109.5
C(15A)-C(17A)-H(17B)	109.5	C(18)-C(20)-H(20B)	109.5
H(17A)-C(17A)-H(17B)	109.5	H(20A)-C(20)-H(20B)	109.5
C(15A)-C(17A)-H(17C)	109.5	C(18)-C(20)-H(20C)	109.5
H(17A)-C(17A)-H(17C)	109.5	H(20A)-C(20)-H(20C)	109.5

H(20B)-C(20)-H(20C)	109.5	F(6B)-C(28)-F(5B)	102.8(17)
C(26)-C(21)-C(22)	113.0(7)	F(4B)-C(28)-C(24)	116.0(15)
C(26)-C(21)-Ir(1)	112.4(5)	F(5A)-C(28)-C(24)	115.3(9)
C(22)-C(21)-Ir(1)	134.5(6)	F(6A)-C(28)-C(24)	114.1(9)
C(23)-C(22)-C(21)	123.9(7)	F(6B)-C(28)-C(24)	114.1(15)
C(23)-C(22)-C(27)	117.0(7)	F(4A)-C(28)-C(24)	111.5(9)
C(21)-C(22)-C(27)	119.1(7)	F(5B)-C(28)-C(24)	114.1(14)
C(24)-C(23)-C(22)	119.5(8)	C(30)-C(29)-C(26)	117.0(7)
C(24)-C(23)-H(23)	120.2	C(30)-C(29)-H(29)	121.5
C(22)-C(23)-H(23)	120.2	C(26)-C(29)-H(29)	121.5
C(23)-C(24)-C(25)	119.8(8)	C(29)-C(30)-Ir(1)	117.9(6)
C(23)-C(24)-C(28)	119.6(8)	C(29)-C(30)-H(30)	121.0
C(25)-C(24)-C(28)	120.5(9)	Ir(1)-C(30)-H(30)	121.0
C(26)-C(25)-C(24)	120.0(8)	C(32A)-C(31A)-H(31A)	109.5
C(26)-C(25)-H(25)	120.0	C(32A)-C(31A)-H(31B)	109.5
C(24)-C(25)-H(25)	120.0	H(31A)-C(31A)-H(31B)	109.5
C(25)-C(26)-C(21)	123.8(8)	C(32A)-C(31A)-H(31C)	109.5
C(25)-C(26)-C(29)	123.3(8)	H(31A)-C(31A)-H(31C)	109.5
C(21)-C(26)-C(29)	112.9(7)	H(31B)-C(31A)-H(31C)	109.5
F(1A)-C(27)-F(3A)	106.7(9)	C(33A)-C(32A)-C(31A)	104.8(11)
F(2B)-C(27)-F(3B)	106.0(14)	C(33A)-C(32A)-H(32A)	110.8
F(1A)-C(27)-F(2A)	105.7(8)	C(31A)-C(32A)-H(32A)	110.8
F(3A)-C(27)-F(2A)	102.7(8)	C(33A)-C(32A)-H(32B)	110.8
F(2B)-C(27)-F(1B)	104.7(13)	C(31A)-C(32A)-H(32B)	110.8
F(3B)-C(27)-F(1B)	98.9(12)	H(32A)-C(32A)-H(32B)	108.9
F(2B)-C(27)-C(22)	118.3(12)	C(34A)-C(33A)-C(32A)	106.8(11)
F(1A)-C(27)-C(22)	115.5(8)	C(34A)-C(33A)-H(33A)	110.4
F(3A)-C(27)-C(22)	112.8(7)	C(32A)-C(33A)-H(33A)	110.4
F(3B)-C(27)-C(22)	114.1(10)	C(34A)-C(33A)-H(33B)	110.4
F(2A)-C(27)-C(22)	112.4(7)	C(32A)-C(33A)-H(33B)	110.4
F(1B)-C(27)-C(22)	112.7(10)	H(33A)-C(33A)-H(33B)	108.6
F(5A)-C(28)-F(6A)	108.0(10)	C(33A)-C(34A)-C(35A)	107.0(11)
F(4B)-C(28)-F(6B)	104.1(18)	C(33A)-C(34A)-H(34A)	110.3
F(5A)-C(28)-F(4A)	105.6(10)	C(35A)-C(34A)-H(34A)	110.3
F(6A)-C(28)-F(4A)	101.1(9)	C(33A)-C(34A)-H(34B)	110.3
F(4B)-C(28)-F(5B)	104.2(18)	C(35A)-C(34A)-H(34B)	110.3

H(34A)-C(34A)-H(34B)	108.6	C(32B)-C(33B)-C(34B)	104.6(11)
C(34A)-C(35A)-C(36A)	106.0(11)	C(32B)-C(33B)-H(33C)	110.8
C(34A)-C(35A)-H(35A)	110.5	C(34B)-C(33B)-H(33C)	110.8
C(36A)-C(35A)-H(35A)	110.5	C(32B)-C(33B)-H(33D)	110.8
C(34A)-C(35A)-H(35B)	110.5	C(34B)-C(33B)-H(33D)	110.8
C(36A)-C(35A)-H(35B)	110.5	H(33C)-C(33B)-H(33D)	108.9
H(35A)-C(35A)-H(35B)	108.7	C(33B)-C(34B)-C(35B)	103.4(10)
C(35A)-C(36A)-H(36A)	109.5	C(33B)-C(34B)-H(34C)	111.1
C(35A)-C(36A)-H(36B)	109.5	C(35B)-C(34B)-H(34C)	111.1
H(36A)-C(36A)-H(36B)	109.5	C(33B)-C(34B)-H(34D)	111.1
C(35A)-C(36A)-H(36C)	109.5	C(35B)-C(34B)-H(34D)	111.1
H(36A)-C(36A)-H(36C)	109.5	H(34C)-C(34B)-H(34D)	109.0
H(36B)-C(36A)-H(36C)	109.5	C(36B)-C(35B)-C(34B)	103.4(10)
C(32B)-C(31B)-H(31D)	109.5	C(36B)-C(35B)-H(35C)	111.1
C(32B)-C(31B)-H(31E)	109.5	C(34B)-C(35B)-H(35C)	111.1
H(31D)-C(31B)-H(31E)	109.5	C(36B)-C(35B)-H(35D)	111.1
C(32B)-C(31B)-H(31F)	109.5	C(34B)-C(35B)-H(35D)	111.1
H(31D)-C(31B)-H(31F)	109.5	H(35C)-C(35B)-H(35D)	109.0
H(31E)-C(31B)-H(31F)	109.5	C(35B)-C(36B)-H(36D)	109.5
C(33B)-C(32B)-C(31B)	104.5(11)	C(35B)-C(36B)-H(36E)	109.5
C(33B)-C(32B)-H(32C)	110.8	H(36D)-C(36B)-H(36E)	109.5
C(31B)-C(32B)-H(32C)	110.8	C(35B)-C(36B)-H(36F)	109.5
C(33B)-C(32B)-H(32D)	110.8	H(36D)-C(36B)-H(36F)	109.5
C(31B)-C(32B)-H(32D)	110.8	H(36E)-C(36B)-H(36F)	109.5
H(32C)-C(32B)-H(32D)	108.9		

Table 3. 18. Anisotropic displacement parameters ($Å^2$x 10^3) for complex 4.

The anisotropic displacement factor exponent takes the form: $-2\pi^2[h^2 a^{*2}U^{11} + ... + 2 h k a^* b^* U^{12}]$

	U^{11}	U^{22}	U^{33}	U^{23}	U^{13}	U^{12}
Ir(1)	19(1)	20(1)	44(1)	9(1)	13(1)	4(1)
P(1)	22(1)	24(1)	40(1)	11(1)	4(1)	4(1)
P(2)	47(1)	25(1)	43(1)	4(1)	26(1)	2(1)
C(1)	25(3)	22(3)	43(3)	6(3)	13(3)	7(3)
C(2)	27(3)	27(3)	42(3)	9(3)	4(3)	3(3)
C(3)	36(4)	29(3)	41(4)	3(3)	8(3)	1(3)
C(4)	41(4)	27(3)	45(4)	6(3)	5(3)	5(3)
C(5)	44(4)	30(3)	44(4)	11(3)	14(3)	6(3)
C(6)	47(4)	29(3)	44(3)	3(3)	15(3)	-4(3)
C(7)	39(4)	29(4)	43(4)	8(3)	2(3)	1(3)
C(8)	74(5)	27(4)	49(4)	8(3)	28(4)	-8(4)
C(9)	34(4)	43(4)	45(4)	18(4)	8(3)	10(3)
C(10)	32(4)	54(6)	64(6)	28(5)	0(4)	11(4)
C(11)	49(5)	40(5)	70(6)	30(5)	18(5)	7(4)
C(12)	22(3)	37(4)	41(4)	7(3)	10(3)	3(3)
C(13)	27(4)	57(5)	39(4)	11(4)	9(3)	15(4)
C(14)	46(5)	57(6)	44(5)	22(4)	13(4)	18(4)
C(15A)	37(4)	47(4)	45(4)	3(4)	15(4)	1(4)
C(16A)	40(5)	48(5)	43(6)	5(5)	21(4)	5(4)
C(17A)	51(5)	41(4)	51(5)	-1(4)	24(4)	5(4)
C(15B)	37(4)	47(4)	45(4)	3(4)	15(4)	1(4)
C(16B)	40(5)	48(5)	43(6)	5(5)	21(4)	5(4)
C(17B)	51(5)	41(4)	51(5)	-1(4)	24(4)	5(4)
C(18)	56(5)	36(4)	40(4)	12(4)	9(4)	9(4)
C(19)	101(9)	66(7)	51(5)	23(5)	2(6)	12(6)
C(20)	54(6)	82(7)	59(6)	8(6)	12(5)	19(6)
C(21)	22(3)	26(3)	32(3)	10(3)	11(3)	4(2)
C(22)	26(3)	27(3)	35(3)	11(3)	8(3)	3(2)
C(23)	33(3)	23(3)	42(4)	8(3)	6(3)	1(3)

C(24)	38(3)	26(3)	47(4)	11(3)	9(3)	10(3)
C(25)	29(3)	30(3)	44(4)	11(3)	12(3)	10(3)
C(26)	26(3)	30(3)	40(3)	12(3)	10(3)	7(3)
C(27)	25(3)	35(3)	45(3)	15(3)	6(3)	1(3)
F(1A)	29(4)	72(5)	77(5)	-25(5)	16(4)	4(4)
F(2A)	23(3)	46(4)	102(6)	39(4)	3(4)	-2(3)
F(3A)	33(4)	78(6)	61(4)	38(4)	6(3)	13(4)
F(1B)	31(7)	61(9)	55(6)	23(6)	18(6)	15(7)
F(2B)	28(6)	63(7)	65(8)	-6(7)	1(7)	4(7)
F(3B)	24(7)	51(6)	79(9)	33(6)	13(7)	8(6)
C(28)	61(4)	35(3)	64(4)	12(3)	10(4)	18(3)
F(4A)	124(7)	37(4)	93(6)	29(4)	54(5)	30(4)
F(5A)	62(5)	41(4)	141(8)	3(5)	-9(5)	29(4)
F(6A)	104(6)	46(4)	59(4)	2(3)	14(4)	39(4)
F(4B)	93(10)	40(8)	82(8)	17(7)	5(8)	43(8)
F(5B)	86(9)	46(9)	83(9)	6(8)	27(8)	31(7)
F(6B)	85(8)	33(7)	90(10)	4(8)	10(8)	16(7)
C(29)	22(3)	32(3)	43(4)	12(3)	8(3)	3(3)
C(30)	21(3)	30(3)	43(4)	6(3)	8(3)	0(3)
C(31A)	99(7)	94(6)	104(7)	19(6)	11(7)	21(6)
C(32A)	109(5)	112(5)	110(5)	26(4)	12(4)	15(4)
C(33A)	106(6)	113(6)	108(6)	24(5)	17(5)	13(5)
C(34A)	109(6)	110(6)	115(6)	25(5)	17(5)	12(5)
C(35A)	114(6)	113(6)	118(6)	24(5)	13(5)	15(5)
C(36A)	117(6)	115(6)	116(6)	24(4)	17(5)	12(5)
C(31B)	99(7)	94(6)	104(7)	19(6)	11(7)	21(6)
C(32B)	109(5)	112(5)	110(5)	26(4)	12(4)	15(4)
C(33B)	108(6)	114(6)	111(5)	25(5)	13(5)	15(5)
C(34B)	116(6)	114(6)	115(5)	26(5)	10(5)	13(5)
C(35B)	117(6)	115(6)	116(6)	24(4)	17(5)	12(5)
C(36B)	114(6)	113(6)	118(6)	24(5)	13(5)	15(5)

Table 3. 19. Hydrogen coordinates (x 10^4) and isotropic displacement parameters ($Å^2$x 10^3) for complex 4.

	x	y	z	U(eq)
H(3)	2851	10266	4963	43
H(4)	2735	11048	3770	46
H(5)	2728	10163	2294	46
H(7A)	2284	8723	5439	45
H(7B)	4083	8525	5200	45
H(8A)	4043	8436	1513	60
H(8B)	2220	8562	1190	60
H(9)	2942	6840	5923	47
H(10A)	5342	6389	4690	71
H(10B)	5538	6370	5738	71
H(10C)	5462	7362	5452	71
H(11A)	2970	5157	4535	74
H(11B)	1343	5418	4978	74
H(11C)	2851	5220	5590	74
H(12)	-450	6406	4477	40
H(13A)	-776	7636	3714	60
H(13B)	-388	8423	4652	60
H(13C)	-2006	7674	4479	60
H(14A)	-1283	7333	5869	69
H(14B)	578	7791	6115	69
H(14C)	88	6667	5991	69
H(15A)	4678	6277	1143	53
H(16A)	3208	6886	-343	66
H(16B)	4903	6461	-332	66
H(16C)	4745	7477	315	66
H(17A)	1682	5459	49	73
H(17B)	2597	5001	774	73
H(17C)	3354	5041	-156	73
H(15B)	2664	6680	-11	53

H(16D)	5327	6593	-11	66
H(16E)	5487	6432	996	66
H(16F)	5170	7453	834	66
H(17D)	1732	5177	-82	73
H(17E)	2615	5182	888	73
H(17F)	3626	5073	22	73
H(18)	-182	6110	899	52
H(19A)	432	6813	-306	107
H(19B)	90	7831	265	107
H(19C)	-1368	6976	-56	107
H(20A)	-698	7943	1887	98
H(20B)	-723	7017	2295	98
H(20C)	-2080	7054	1509	98
H(23)	1079	3121	2132	39
H(25)	5820	4234	2427	40
H(29)	6568	6057	2913	38
H(30)	5545	7498	3203	38
H(31A)	7389	-1093	2336	149
H(31B)	6418	-531	3112	149
H(31C)	8342	-268	3143	149
H(32A)	6442	-61	1615	132
H(32B)	6489	753	2535	132
H(33A)	9290	1034	2650	131
H(33B)	9370	118	1838	131
H(34A)	9502	1242	1065	134
H(34B)	8421	1890	1724	134
H(35A)	6625	1267	507	139
H(35B)	6223	530	1133	139
H(36A)	7747	-530	372	175
H(36B)	8602	244	-106	175
H(36C)	6742	-191	-408	175
H(31D)	7025	-1121	2633	149
H(31E)	6395	-435	3480	149
H(31F)	8301	-478	3430	149
H(32C)	6252	375	2365	132
H(32D)	7886	884	2996	132

H(33C)	8883	-591	1918	133
H(33D)	9153	480	1773	133
H(34C)	5999	-309	1184	138
H(34D)	7217	-985	663	138
H(35C)	8114	111	-53	140
H(35D)	6597	655	280	140
H(36D)	9824	1055	1028	173
H(36E)	8531	1089	1760	173
H(36F)	8488	1774	1071	173

Table 3. 20. Torsion angles [°] for complex 4.

C(6)-C(1)-C(2)-C(3)	4.7(12)	Ir(1)-P(1)-C(12)-C(14)	178.8(6)
Ir(1)-C(1)-C(2)-C(3)	-176.2(6)	C(7)-P(1)-C(12)-C(13)	54.8(7)
C(6)-C(1)-C(2)-C(7)	-172.2(8)	C(9)-P(1)-C(12)-C(13)	165.6(6)
Ir(1)-C(1)-C(2)-C(7)	6.8(11)	Ir(1)-P(1)-C(12)-C(13)	-57.3(7)
C(1)-C(2)-C(3)-C(4)	-1.3(13)	C(8)-P(2)-C(15B)-C(16B)	54.8(15)
C(7)-C(2)-C(3)-C(4)	175.6(8)	C(18)-P(2)-C(15B)-C(16B)	163.7(13)
C(2)-C(3)-C(4)-C(5)	-2.2(14)	Ir(1)-P(2)-C(15B)-C(16B)	-70.4(14)
C(3)-C(4)-C(5)-C(6)	2.0(14)	C(8)-P(2)-C(15B)-C(17B)	-179.9(11)
C(4)-C(5)-C(6)-C(1)	1.8(15)	C(18)-P(2)-C(15B)-C(17B)	-71.0(12)
C(4)-C(5)-C(6)-C(8)	-171.8(9)	Ir(1)-P(2)-C(15B)-C(17B)	54.9(14)
C(2)-C(1)-C(6)-C(5)	-5.0(13)	C(15B)-P(2)-C(18)-C(20)	-179.5(9)
Ir(1)-C(1)-C(6)-C(5)	176.0(7)	C(8)-P(2)-C(18)-C(20)	-71.8(8)
C(2)-C(1)-C(6)-C(8)	168.8(8)	C(15A)-P(2)-C(18)-C(20)	169.5(8)
Ir(1)-C(1)-C(6)-C(8)	-10.3(12)	Ir(1)-P(2)-C(18)-C(20)	39.9(8)
C(3)-C(2)-C(7)-P(1)	162.3(7)	C(15B)-P(2)-C(18)-C(19)	-53.4(9)
C(1)-C(2)-C(7)-P(1)	-20.7(10)	C(8)-P(2)-C(18)-C(19)	54.2(9)
C(9)-P(1)-C(7)-C(2)	156.3(6)	C(15A)-P(2)-C(18)-C(19)	-64.5(10)
C(12)-P(1)-C(7)-C(2)	-94.7(7)	Ir(1)-P(2)-C(18)-C(19)	165.9(7)
Ir(1)-P(1)-C(7)-C(2)	23.2(6)	C(26)-C(21)-C(22)-C(23)	1.6(12)
C(5)-C(6)-C(8)-P(2)	-165.1(8)	Ir(1)-C(21)-C(22)-C(23)	178.6(6)
C(1)-C(6)-C(8)-P(2)	21.0(12)	C(26)-C(21)-C(22)-C(27)	-179.2(7)
C(15B)-P(2)-C(8)-C(6)	-162.6(10)	Ir(1)-C(21)-C(22)-C(27)	-2.2(12)
C(18)-P(2)-C(8)-C(6)	94.7(8)	C(21)-C(22)-C(23)-C(24)	-1.4(13)
C(15A)-P(2)-C(8)-C(6)	-143.2(9)	C(27)-C(22)-C(23)-C(24)	179.3(8)
Ir(1)-P(2)-C(8)-C(6)	-21.0(9)	C(22)-C(23)-C(24)-C(25)	0.0(13)
C(7)-P(1)-C(9)-C(11)	173.0(7)	C(22)-C(23)-C(24)-C(28)	-178.5(9)
C(12)-P(1)-C(9)-C(11)	64.1(7)	C(23)-C(24)-C(25)-C(26)	1.0(14)
Ir(1)-P(1)-C(9)-C(11)	-66.1(7)	C(28)-C(24)-C(25)-C(26)	179.6(9)
C(7)-P(1)-C(9)-C(10)	-62.5(8)	C(24)-C(25)-C(26)-C(21)	-0.8(13)
C(12)-P(1)-C(9)-C(10)	-171.4(7)	C(24)-C(25)-C(26)-C(29)	178.1(8)
Ir(1)-P(1)-C(9)-C(10)	58.4(8)	C(22)-C(21)-C(26)-C(25)	-0.5(12)
C(7)-P(1)-C(12)-C(14)	-69.0(8)	Ir(1)-C(21)-C(26)-C(25)	-178.2(7)
C(9)-P(1)-C(12)-C(14)	41.7(8)	C(22)-C(21)-C(26)-C(29)	-179.5(7)

Ir(1)-C(21)-C(26)-C(29)	2.8(9)	C(23)-C(24)-C(28)-F(6A)	65.6(13)
C(23)-C(22)-C(27)-F(2B)	-31.0(17)	C(25)-C(24)-C(28)-F(6A)	-113.0(12)
C(21)-C(22)-C(27)-F(2B)	149.7(15)	C(23)-C(24)-C(28)-F(6B)	13(2)
C(23)-C(22)-C(27)-F(1A)	136.6(10)	C(25)-C(24)-C(28)-F(6B)	-165.2(19)
C(21)-C(22)-C(27)-F(1A)	-42.7(12)	C(23)-C(24)-C(28)-F(4A)	-48.2(14)
C(23)-C(22)-C(27)-F(3A)	-100.3(10)	C(25)-C(24)-C(28)-F(4A)	133.3(11)
C(21)-C(22)-C(27)-F(3A)	80.4(10)	C(23)-C(24)-C(28)-F(5B)	131.1(19)
C(23)-C(22)-C(27)-F(3B)	-156.7(13)	C(25)-C(24)-C(28)-F(5B)	-47(2)
C(21)-C(22)-C(27)-F(3B)	24.0(15)	C(25)-C(26)-C(29)-C(30)	178.7(8)
C(23)-C(22)-C(27)-F(2A)	15.3(12)	C(21)-C(26)-C(29)-C(30)	-2.3(11)
C(21)-C(22)-C(27)-F(2A)	-164.1(8)	C(26)-C(29)-C(30)-Ir(1)	0.6(11)
C(23)-C(22)-C(27)-F(1B)	91.5(14)	C(31A)-C(32A)-C(33A)-C(34A)	170(3)
C(21)-C(22)-C(27)-F(1B)	-87.8(14)	C(32A)-C(33A)-C(34A)-C(35A)	-31(4)
C(23)-C(24)-C(28)-F(4B)	-108(2)	C(33A)-C(34A)-C(35A)-C(36A)	-83(4)
C(25)-C(24)-C(28)-F(4B)	74(2)	C(31B)-C(32B)-C(33B)-C(34B)	106(3)
C(23)-C(24)-C(28)-F(5A)	-168.6(11)	C(32B)-C(33B)-C(34B)-C(35B)	113(3)
C(25)-C(24)-C(28)-F(5A)	12.9(16)	C(33B)-C(34B)-C(35B)-C(36B)	-13(4)

3.5.9.5. Structural data for complex 5

CCDC # 1540146

Figure 3. 68. ORTEP diagram of complex 5

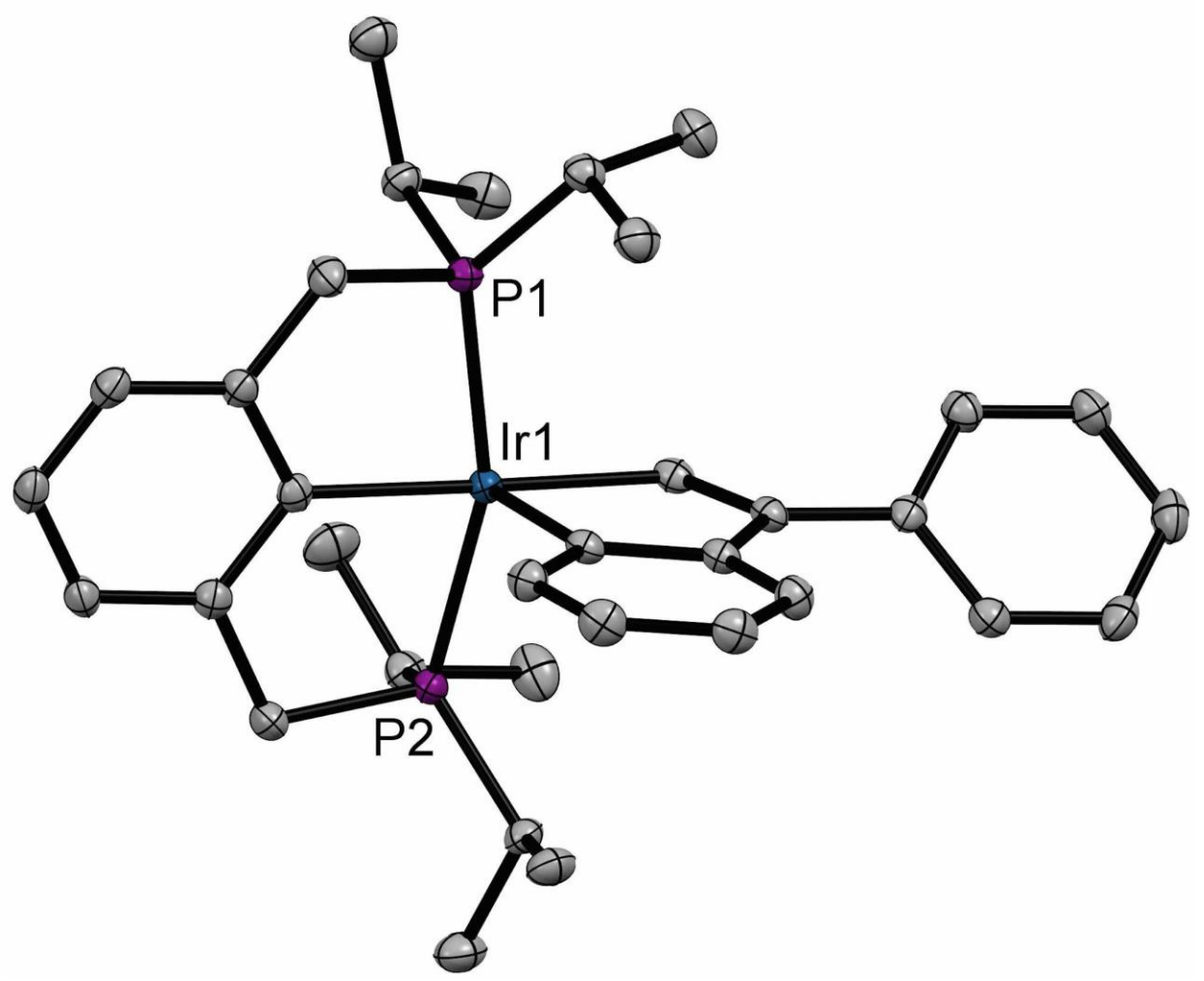

Table 3. 21. Crystal data and structure refinement for complex 5.

Identification code	jonmm34	
Empirical formula	C34 H45 Ir P2	
Formula weight	707.84	
Temperature	100.0(5) K	
Wavelength	0.71073 Å	
Crystal system	monoclinic	
Space group	*C*2/*c*	
Unit cell dimensions	*a* = 36.747(4) Å	α = 90°
	b = 9.5480(11) Å	β = 115.959(2) °
	c = 18.726(2) Å	γ = 90°
Volume	5907.2(12) $Å^3$	
Z	8	
Density (calculated)	1.592 Mg/m^3	
Absorption coefficient	4.650 mm^{-1}	
F(000)	2848	
Crystal color, morphology	pink-black, block	
Crystal size	0.20 x 0.14 x 0.12 mm^3	
Theta range for data collection	2.182 to 38.899°	
Index ranges	$-64 \leq h \leq 63$, $-16 \leq k \leq 16$, $-32 \leq l \leq 32$	
Reflections collected	111049	
Independent reflections	16637 [*R*(int) = 0.0957]	
Observed reflections	11406	
Completeness to theta = 37.785°	100.0%	
Absorption correction	Multi-scan	
Max. and min. transmission	0.2261 and 0.1432	
Refinement method	Full-matrix least-squares on F^2	
Data / restraints / parameters	16637 / 0 / 342	
Goodness-of-fit on F^2	1.023	
Final *R* indices [*I*>2sigma(*I*)]	*R*1 = 0.0391, *wR*2 = 0.0682	
R indices (all data)	*R*1 = 0.0727, *wR*2 = 0.0782	
Largest diff. peak and hole	2.919 and -1.686 e.$Å^{-3}$	

Table 3. 22. Atomic coordinates (x 10^4) and equivalent isotropic displacement parameters ($Å^2$x 10^3) for complex 5.

U_{eq} is defined as one third of the trace of the orthogonalized U_{ij} tensor.

	x	y	z	U_{eq}
Ir1	3769(1)	5598(1)	6948(1)	14(1)
P1	3600(1)	4519(1)	5748(1)	16(1)
P2	3962(1)	7330(1)	7896(1)	16(1)
C1	3398(1)	4425(3)	7306(2)	16(1)
C2	3570(1)	3333(3)	7803(2)	16(1)
C3	4002(1)	3144(3)	7999(2)	16(1)
C4	4153(1)	4127(3)	7627(2)	15(1)
C5	4555(1)	4039(3)	7749(2)	19(1)
C6	4809(1)	2990(3)	8232(2)	21(1)
C7	4663(1)	2029(3)	8592(2)	21(1)
C8	4261(1)	2096(3)	8475(2)	19(1)
C9	3347(1)	2406(3)	8114(2)	17(1)
C10	2954(1)	1960(3)	7626(2)	20(1)
C11	2735(1)	1144(3)	7917(2)	22(1)
C12	2903(1)	753(3)	8714(2)	25(1)
C13	3294(1)	1178(3)	9207(2)	23(1)
C14	3512(1)	1999(3)	8913(2)	20(1)
C21	4139(1)	6764(3)	6568(2)	16(1)
C22	4192(1)	6364(3)	5889(2)	17(1)
C23	4409(1)	7198(3)	5596(2)	19(1)
C24	4574(1)	8458(3)	5958(2)	20(1)
C25	4540(1)	8865(3)	6641(2)	19(1)
C26	4334(1)	8015(3)	6950(2)	17(1)
C27	4011(1)	4989(3)	5494(2)	20(1)
C28	4335(1)	8405(3)	7737(2)	20(1)
C29	3164(1)	5465(3)	4984(2)	19(1)
C30	2804(1)	5588(3)	5186(2)	27(1)
C31	3028(1)	4944(3)	4134(2)	26(1)

C32	3522(1)	2632(3)	5518(2)	19(1)
C33	3127(1)	2099(3)	5506(2)	25(1)
C34	3879(1)	1768(3)	6097(2)	24(1)
C35	3527(1)	8511(3)	7645(2)	21(1)
C36	3329(1)	8752(4)	6745(2)	31(1)
C37	3225(1)	7888(3)	7918(2)	27(1)
C38	4169(1)	7069(3)	8976(2)	18(1)
C39	4546(1)	6131(3)	9302(2)	23(1)
C40	4257(1)	8455(3)	9435(2)	26(1)

Table 3. 23. Bond lengths [Å] and angles [°] for complex 5.

Ir(1)-C(4)	2.002(3)	C(13)-C(14)	1.395(4)
Ir(1)-C(1)	2.086(3)	C(13)-H(13)	0.9500
Ir(1)-C(21)	2.109(2)	C(14)-H(14)	0.9500
Ir(1)-P(1)	2.2960(7)	C(21)-C(26)	1.415(4)
Ir(1)-P(2)	2.2999(7)	C(21)-C(22)	1.419(4)
P(1)-C(27)	1.828(3)	C(22)-C(23)	1.398(4)
P(1)-C(32)	1.845(3)	C(22)-C(27)	1.511(4)
P(1)-C(29)	1.848(3)	C(23)-C(24)	1.384(4)
P(2)-C(28)	1.837(3)	C(23)-H(23)	0.9500
P(2)-C(38)	1.841(3)	C(24)-C(25)	1.393(4)
P(2)-C(35)	1.842(3)	C(24)-H(24)	0.9500
C(1)-C(2)	1.356(4)	C(25)-C(26)	1.398(4)
C(1)-H(1)	0.9500	C(25)-H(25)	0.9500
C(2)-C(3)	1.475(3)	C(26)-C(28)	1.517(4)
C(2)-C(9)	1.487(4)	C(27)-H(27A)	0.9900
C(3)-C(8)	1.399(4)	C(27)-H(27B)	0.9900
C(3)-C(4)	1.419(4)	C(28)-H(28A)	0.9900
C(4)-C(5)	1.396(4)	C(28)-H(28B)	0.9900
C(5)-C(6)	1.397(4)	C(29)-C(31)	1.528(4)
C(5)-H(5)	0.9500	C(29)-C(30)	1.532(4)
C(6)-C(7)	1.379(4)	C(29)-H(29)	1.0000
C(6)-H(6)	0.9500	C(30)-H(30A)	0.9800
C(7)-C(8)	1.398(4)	C(30)-H(30B)	0.9800
C(7)-H(7)	0.9500	C(30)-H(30C)	0.9800
C(8)-H(8)	0.9500	C(31)-H(31A)	0.9800
C(9)-C(10)	1.397(4)	C(31)-H(31B)	0.9800
C(9)-C(14)	1.401(4)	C(31)-H(31C)	0.9800
C(10)-C(11)	1.390(4)	C(32)-C(34)	1.528(4)
C(10)-H(10)	0.9500	C(32)-C(33)	1.529(4)
C(11)-C(12)	1.393(4)	C(32)-H(32)	1.0000
C(11)-H(11)	0.9500	C(33)-H(33A)	0.9800
C(12)-C(13)	1.384(4)	C(33)-H(33B)	0.9800
C(12)-H(12)	0.9500	C(33)-H(33C)	0.9800

C(34)-H(34A)	0.9800	C(29)-P(1)-Ir(1)	108.01(9)
C(34)-H(34B)	0.9800	C(28)-P(2)-C(38)	106.02(12)
C(34)-H(34C)	0.9800	C(28)-P(2)-C(35)	104.05(13)
C(35)-C(37)	1.530(4)	C(38)-P(2)-C(35)	104.89(12)
C(35)-C(36)	1.532(4)	C(28)-P(2)-Ir(1)	106.10(9)
C(35)-H(35)	1.0000	C(38)-P(2)-Ir(1)	126.22(9)
C(36)-H(36A)	0.9800	C(35)-P(2)-Ir(1)	107.62(9)
C(36)-H(36B)	0.9800	C(2)-C(1)-Ir(1)	117.43(18)
C(36)-H(36C)	0.9800	C(2)-C(1)-H(1)	121.3
C(37)-H(37A)	0.9800	Ir(1)-C(1)-H(1)	121.3
C(37)-H(37B)	0.9800	C(1)-C(2)-C(3)	113.1(2)
C(37)-H(37C)	0.9800	C(1)-C(2)-C(9)	123.8(2)
C(38)-C(40)	1.533(4)	C(3)-C(2)-C(9)	123.1(2)
C(38)-C(39)	1.534(4)	C(8)-C(3)-C(4)	118.9(2)
C(38)-H(38)	1.0000	C(8)-C(3)-C(2)	127.1(2)
C(39)-H(39A)	0.9800	C(4)-C(3)-C(2)	113.9(2)
C(39)-H(39B)	0.9800	C(5)-C(4)-C(3)	119.5(2)
C(39)-H(39C)	0.9800	C(5)-C(4)-Ir(1)	123.2(2)
C(40)-H(40A)	0.9800	C(3)-C(4)-Ir(1)	117.24(18)
C(40)-H(40B)	0.9800	C(4)-C(5)-C(6)	120.5(3)
C(40)-H(40C)	0.9800	C(4)-C(5)-H(5)	119.7
C(4)-Ir(1)-C(1)	78.30(10)	C(6)-C(5)-H(5)	119.7
C(4)-Ir(1)-C(21)	101.85(10)	C(7)-C(6)-C(5)	120.1(3)
C(1)-Ir(1)-C(21)	179.05(10)	C(7)-C(6)-H(6)	119.9
C(4)-Ir(1)-P(1)	96.93(7)	C(5)-C(6)-H(6)	119.9
C(1)-Ir(1)-P(1)	97.98(7)	C(6)-C(7)-C(8)	120.3(3)
C(21)-Ir(1)-P(1)	81.08(7)	C(6)-C(7)-H(7)	119.9
C(4)-Ir(1)-P(2)	96.90(7)	C(8)-C(7)-H(7)	119.9
C(1)-Ir(1)-P(2)	99.35(7)	C(7)-C(8)-C(3)	120.6(3)
C(21)-Ir(1)-P(2)	81.57(7)	C(7)-C(8)-H(8)	119.7
P(1)-Ir(1)-P(2)	159.69(2)	C(3)-C(8)-H(8)	119.7
C(27)-P(1)-C(32)	103.92(13)	C(10)-C(9)-C(14)	117.0(2)
C(27)-P(1)-C(29)	102.29(13)	C(10)-C(9)-C(2)	121.0(2)
C(32)-P(1)-C(29)	107.65(12)	C(14)-C(9)-C(2)	122.0(2)
C(27)-P(1)-Ir(1)	104.15(9)	C(11)-C(10)-C(9)	121.7(3)
C(32)-P(1)-Ir(1)	127.89(9)	C(11)-C(10)-H(10)	119.2

C(9)-C(10)-H(10)	119.2	H(27A)-C(27)-H(27B)	108.3
C(10)-C(11)-C(12)	120.6(3)	C(26)-C(28)-P(2)	109.48(18)
C(10)-C(11)-H(11)	119.7	C(26)-C(28)-H(28A)	109.8
C(12)-C(11)-H(11)	119.7	P(2)-C(28)-H(28A)	109.8
C(13)-C(12)-C(11)	118.7(3)	C(26)-C(28)-H(28B)	109.8
C(13)-C(12)-H(12)	120.6	P(2)-C(28)-H(28B)	109.8
C(11)-C(12)-H(12)	120.6	H(28A)-C(28)-H(28B)	108.2
C(12)-C(13)-C(14)	120.5(3)	C(31)-C(29)-C(30)	110.9(2)
C(12)-C(13)-H(13)	119.7	C(31)-C(29)-P(1)	115.2(2)
C(14)-C(13)-H(13)	119.7	C(30)-C(29)-P(1)	113.31(19)
C(13)-C(14)-C(9)	121.5(3)	C(31)-C(29)-H(29)	105.5
C(13)-C(14)-H(14)	119.2	C(30)-C(29)-H(29)	105.5
C(9)-C(14)-H(14)	119.2	P(1)-C(29)-H(29)	105.5
C(26)-C(21)-C(22)	116.4(2)	C(29)-C(30)-H(30A)	109.5
C(26)-C(21)-Ir(1)	122.15(18)	C(29)-C(30)-H(30B)	109.5
C(22)-C(21)-Ir(1)	121.42(18)	H(30A)-C(30)-H(30B)	109.5
C(23)-C(22)-C(21)	121.5(2)	C(29)-C(30)-H(30C)	109.5
C(23)-C(22)-C(27)	120.5(2)	H(30A)-C(30)-H(30C)	109.5
C(21)-C(22)-C(27)	118.0(2)	H(30B)-C(30)-H(30C)	109.5
C(24)-C(23)-C(22)	120.4(2)	C(29)-C(31)-H(31A)	109.5
C(24)-C(23)-H(23)	119.8	C(29)-C(31)-H(31B)	109.5
C(22)-C(23)-H(23)	119.8	H(31A)-C(31)-H(31B)	109.5
C(23)-C(24)-C(25)	119.8(2)	C(29)-C(31)-H(31C)	109.5
C(23)-C(24)-H(24)	120.1	H(31A)-C(31)-H(31C)	109.5
C(25)-C(24)-H(24)	120.1	H(31B)-C(31)-H(31C)	109.5
C(24)-C(25)-C(26)	120.1(3)	C(34)-C(32)-C(33)	110.3(2)
C(24)-C(25)-H(25)	119.9	C(34)-C(32)-P(1)	111.35(19)
C(26)-C(25)-H(25)	119.9	C(33)-C(32)-P(1)	112.17(19)
C(25)-C(26)-C(21)	121.7(2)	C(34)-C(32)-H(32)	107.6
C(25)-C(26)-C(28)	119.2(2)	C(33)-C(32)-H(32)	107.6
C(21)-C(26)-C(28)	119.1(2)	P(1)-C(32)-H(32)	107.6
C(22)-C(27)-P(1)	108.82(18)	C(32)-C(33)-H(33A)	109.5
C(22)-C(27)-H(27A)	109.9	C(32)-C(33)-H(33B)	109.5
P(1)-C(27)-H(27A)	109.9	H(33A)-C(33)-H(33B)	109.5
C(22)-C(27)-H(27B)	109.9	C(32)-C(33)-H(33C)	109.5
P(1)-C(27)-H(27B)	109.9	H(33A)-C(33)-H(33C)	109.5

H(33B)-C(33)-H(33C)	109.5	C(35)-C(37)-H(37C)	109.5
C(32)-C(34)-H(34A)	109.5	H(37A)-C(37)-H(37C)	109.5
C(32)-C(34)-H(34B)	109.5	H(37B)-C(37)-H(37C)	109.5
H(34A)-C(34)-H(34B)	109.5	C(40)-C(38)-C(39)	110.3(2)
C(32)-C(34)-H(34C)	109.5	C(40)-C(38)-P(2)	112.53(19)
H(34A)-C(34)-H(34C)	109.5	C(39)-C(38)-P(2)	112.42(18)
H(34B)-C(34)-H(34C)	109.5	C(40)-C(38)-H(38)	107.1
C(37)-C(35)-C(36)	111.2(3)	C(39)-C(38)-H(38)	107.1
C(37)-C(35)-P(2)	110.62(19)	P(2)-C(38)-H(38)	107.1
C(36)-C(35)-P(2)	108.3(2)	C(38)-C(39)-H(39A)	109.5
C(37)-C(35)-H(35)	108.9	C(38)-C(39)-H(39B)	109.5
C(36)-C(35)-H(35)	108.9	H(39A)-C(39)-H(39B)	109.5
P(2)-C(35)-H(35)	108.9	C(38)-C(39)-H(39C)	109.5
C(35)-C(36)-H(36A)	109.5	H(39A)-C(39)-H(39C)	109.5
C(35)-C(36)-H(36B)	109.5	H(39B)-C(39)-H(39C)	109.5
H(36A)-C(36)-H(36B)	109.5	C(38)-C(40)-H(40A)	109.5
C(35)-C(36)-H(36C)	109.5	C(38)-C(40)-H(40B)	109.5
H(36A)-C(36)-H(36C)	109.5	H(40A)-C(40)-H(40B)	109.5
H(36B)-C(36)-H(36C)	109.5	C(38)-C(40)-H(40C)	109.5
C(35)-C(37)-H(37A)	109.5	H(40A)-C(40)-H(40C)	109.5
C(35)-C(37)-H(37B)	109.5	H(40B)-C(40)-H(40C)	109.5
H(37A)-C(37)-H(37B)	109.5		

Table 3. 24. Anisotropic displacement parameters ($Å^2$x 10^3) for complex 5.

The anisotropic displacement factor exponent takes the form: $-2\pi^2[h^2 a^{*2}U_{11} + ... + 2 h k a^* b^* U_{12}]$

	U_{11}	U_{22}	U_{33}	U_{23}	U_{13}	U_{12}
Ir1	14(1)	13(1)	14(1)	0(1)	6(1)	-1(1)
P1	16(1)	16(1)	15(1)	-1(1)	7(1)	-1(1)
P2	18(1)	14(1)	14(1)	0(1)	7(1)	-1(1)
C1	16(1)	15(1)	18(1)	-3(1)	7(1)	0(1)
C2	16(1)	15(1)	16(1)	-3(1)	7(1)	-2(1)
C3	16(1)	15(1)	16(1)	-3(1)	6(1)	-1(1)
C4	15(1)	14(1)	15(1)	-3(1)	6(1)	-1(1)
C5	18(1)	20(1)	20(1)	0(1)	9(1)	0(1)
C6	16(1)	22(1)	25(1)	1(1)	8(1)	4(1)
C7	20(1)	18(1)	23(1)	1(1)	6(1)	5(1)
C8	20(1)	16(1)	22(1)	2(1)	9(1)	2(1)
C9	21(1)	13(1)	17(1)	-1(1)	10(1)	1(1)
C10	18(1)	21(1)	21(1)	-1(1)	10(1)	-2(1)
C11	19(1)	22(1)	26(1)	-1(1)	10(1)	-4(1)
C12	29(1)	22(1)	32(2)	2(1)	21(1)	-3(1)
C13	30(2)	23(1)	20(1)	3(1)	15(1)	2(1)
C14	21(1)	18(1)	20(1)	-1(1)	9(1)	-1(1)
C21	15(1)	14(1)	16(1)	2(1)	6(1)	1(1)
C22	14(1)	19(1)	16(1)	2(1)	6(1)	0(1)
C23	18(1)	24(1)	17(1)	4(1)	9(1)	1(1)
C24	18(1)	23(1)	21(1)	6(1)	9(1)	-2(1)
C25	18(1)	16(1)	21(1)	2(1)	7(1)	-2(1)
C26	16(1)	18(1)	18(1)	2(1)	7(1)	1(1)
C27	22(1)	20(1)	22(1)	-3(1)	13(1)	-3(1)
C28	22(1)	20(1)	19(1)	-3(1)	9(1)	-6(1)
C29	21(1)	19(1)	16(1)	1(1)	6(1)	0(1)
C30	20(1)	28(2)	29(2)	-2(1)	8(1)	3(1)
C31	26(1)	28(2)	20(1)	3(1)	7(1)	2(1)
C32	20(1)	16(1)	19(1)	-2(1)	7(1)	0(1)

C33	25(1)	20(1)	29(2)	-2(1)	12(1)	-4(1)
C34	27(1)	19(1)	24(1)	0(1)	9(1)	1(1)
C35	24(1)	16(1)	22(1)	-1(1)	10(1)	1(1)
C36	29(2)	34(2)	23(2)	6(1)	6(1)	7(1)
C37	25(1)	24(1)	40(2)	-2(1)	21(1)	2(1)
C38	22(1)	20(1)	13(1)	0(1)	8(1)	0(1)
C39	25(1)	25(1)	15(1)	0(1)	5(1)	3(1)
C40	33(2)	24(1)	18(1)	-3(1)	8(1)	2(1)

Table 3. 25. Hydrogen coordinates (x 10^4) and isotropic displacement parameters (Å^2 x 10^3) for complex 5.

	x	y	z	U(eq)
H1	3120	4648	7127	19
H5	4657	4698	7502	23
H6	5082	2938	8312	26
H7	4836	1318	8921	26
H8	4162	1424	8721	23
H10	2832	2220	7082	24
H11	2469	851	7570	27
H12	2753	205	8915	30
H13	3414	909	9750	27
H14	3778	2288	9263	24
H23	4442	6900	5144	23
H24	4710	9043	5743	24
H25	4657	9721	6897	23
H27A	4221	4249	5677	24
H27B	3906	5079	4910	24
H28A	4268	9409	7734	24
H28B	4608	8247	8175	24
H29	3261	6446	4989	23
H30A	2614	6291	4841	40
H30B	2901	5872	5742	40
H30C	2667	4680	5104	40
H31A	2824	5586	3765	39
H31B	2910	4006	4081	39
H31C	3261	4907	4012	39
H32	3505	2492	4975	22
H33A	3109	1082	5428	37
H33B	2897	2549	5070	37
H33C	3121	2326	6011	37
H34A	3849	794	5915	36

H34B	3887	1803	6626	36
H34C	4132	2153	6122	36
H35	3626	9428	7919	25
H36A	3105	9417	6604	47
H36B	3225	7861	6471	47
H36C	3529	9132	6584	47
H37A	2976	8444	7701	41
H37B	3344	7902	8500	41
H37C	3164	6920	7730	41
H38	3956	6575	9078	22
H39A	4648	6040	9879	34
H39B	4755	6551	9180	34
H39C	4475	5203	9056	34
H40A	4350	8264	10002	40
H40B	4011	9024	9239	40
H40C	4469	8964	9357	40

Table 3. 26. Torsion angles [°] for complex 5.

Ir1-C1-C2-C3	-1.0(3)	C21-C22-C23-C24	-0.8(4)
Ir1-C1-C2-C9	179.60(18)	C27-C22-C23-C24	179.9(2)
C1-C2-C3-C8	-178.0(3)	C22-C23-C24-C25	2.9(4)
C9-C2-C3-C8	1.4(4)	C23-C24-C25-C26	-1.1(4)
C1-C2-C3-C4	-0.6(3)	C24-C25-C26-C21	-2.9(4)
C9-C2-C3-C4	178.8(2)	C24-C25-C26-C28	174.1(2)
C8-C3-C4-C5	-0.7(4)	C22-C21-C26-C25	4.8(4)
C2-C3-C4-C5	-178.4(2)	Ir1-C21-C26-C25	-172.5(2)
C8-C3-C4-Ir1	179.64(19)	C22-C21-C26-C28	-172.1(2)
C2-C3-C4-Ir1	2.0(3)	Ir1-C21-C26-C28	10.5(3)
C3-C4-C5-C6	0.2(4)	C23-C22-C27-P1	-158.1(2)
Ir1-C4-C5-C6	179.8(2)	C21-C22-C27-P1	22.6(3)
C4-C5-C6-C7	0.1(4)	C32-P1-C27-C22	-162.23(19)
C5-C6-C7-C8	0.1(4)	C29-P1-C27-C22	85.8(2)
C6-C7-C8-C3	-0.6(4)	Ir1-P1-C27-C22	-26.6(2)
C4-C3-C8-C7	0.9(4)	C25-C26-C28-P2	168.7(2)
C2-C3-C8-C7	178.3(3)	C21-C26-C28-P2	-14.3(3)
C1-C2-C9-C10	40.9(4)	C38-P2-C28-C26	147.83(19)
C3-C2-C9-C10	-138.4(3)	C35-P2-C28-C26	-101.8(2)
C1-C2-C9-C14	-135.9(3)	Ir1-P2-C28-C26	11.6(2)
C3-C2-C9-C14	44.8(4)	C27-P1-C29-C31	66.7(2)
C14-C9-C10-C11	-0.2(4)	C32-P1-C29-C31	-42.4(2)
C2-C9-C10-C11	-177.1(3)	Ir1-P1-C29-C31	176.20(19)
C9-C10-C11-C12	0.4(4)	C27-P1-C29-C30	-164.2(2)
C10-C11-C12-C13	-0.7(4)	C32-P1-C29-C30	86.7(2)
C11-C12-C13-C14	0.9(4)	Ir1-P1-C29-C30	-54.6(2)
C12-C13-C14-C9	-0.7(4)	C27-P1-C32-C34	69.2(2)
C10-C9-C14-C13	0.3(4)	C29-P1-C32-C34	177.15(19)
C2-C9-C14-C13	177.2(2)	Ir1-P1-C32-C34	-51.6(2)
C26-C21-C22-C23	-3.0(4)	C27-P1-C32-C33	-166.7(2)
Ir1-C21-C22-C23	174.39(19)	C29-P1-C32-C33	-58.7(2)
C26-C21-C22-C27	176.3(2)	Ir1-P1-C32-C33	72.5(2)
Ir1-C21-C22-C27	-6.3(3)	C28-P2-C35-C37	-167.5(2)

C38-P2-C35-C37	-56.3(2)	C35-P2-C38-C40	-53.1(2)
Ir1-P2-C35-C37	80.2(2)	Ir1-P2-C38-C40	-178.77(16)
C28-P2-C35-C36	70.4(2)	C28-P2-C38-C39	-68.7(2)
C38-P2-C35-C36	-178.4(2)	C35-P2-C38-C39	-178.4(2)
Ir1-P2-C35-C36	-41.9(2)	Ir1-P2-C38-C39	55.9(2)
C28-P2-C38-C40	56.6(2)		

3.5.9.6. Structural data for complex 7

CCDC # 1539912

Figure 3. 69. ORTEP diagram of complex 7

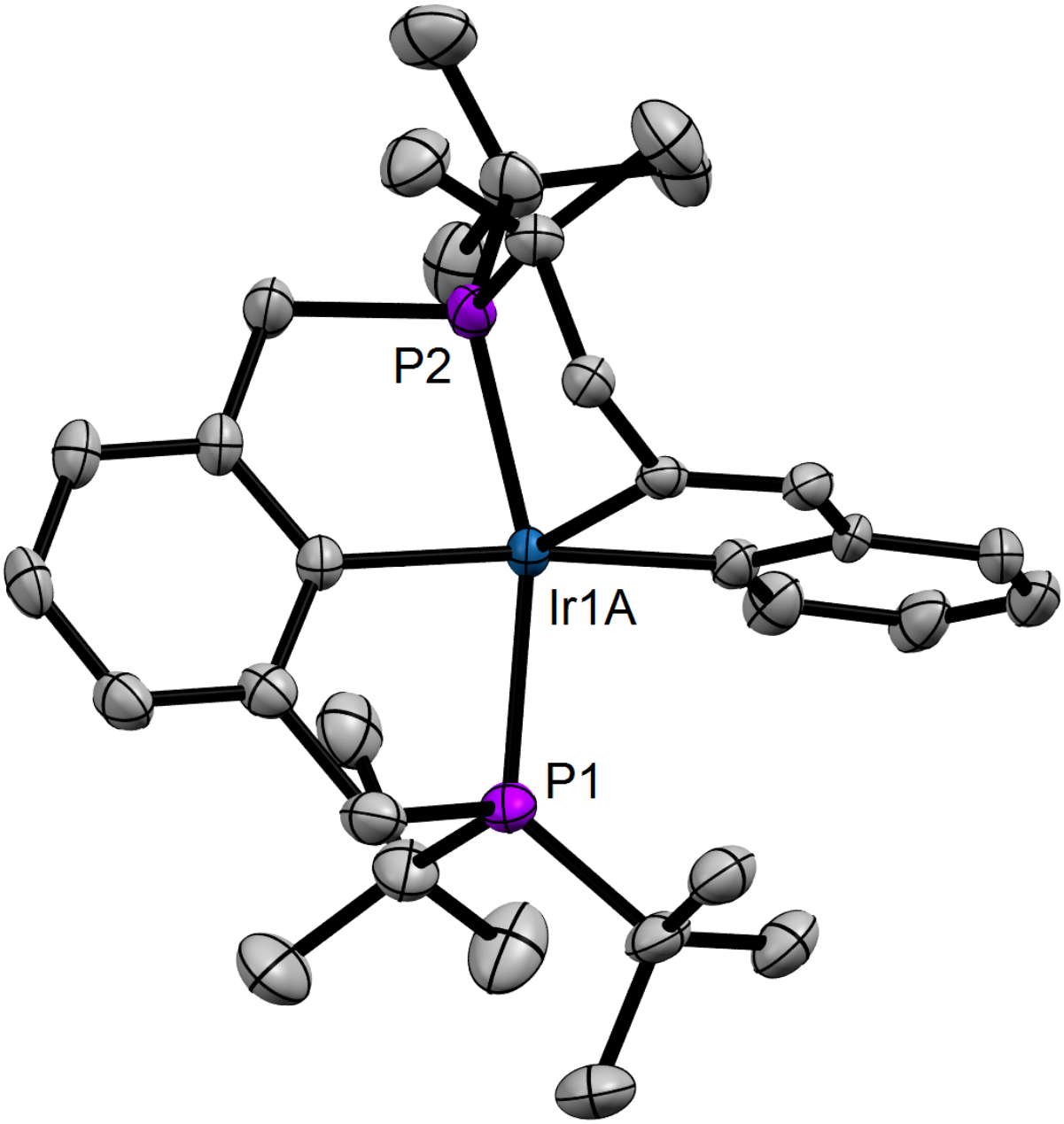

Table 3. 27. Crystal data and structure refinement for complex 7.

Identification code	ir_styrene_P-1	
Empirical formula	C32 H47 Ir P2	
Formula weight	685.83	
Temperature	150(2) K	
Wavelength	0.71073 Å	
Crystal system	Triclinic	
Space group	P-1	
Unit cell dimensions	a = 11.4853(4) Å	α= 109.9953(7)°.
	b = 16.6751(6) Å	β= 93.7505(7)°.
	c = 16.8477(6) Å	γ = 95.0066(7)°.
Volume	3004.90(19) $Å^3$	
Z	4	
Density (calculated)	1.516 Mg/m^3	
Absorption coefficient	4.568 mm^{-1}	
F(000)	1384	
Crystal size	0.220 x 0.200 x 0.060 mm^3	
Theta range for data collection	1.483 to 30.033°.	
Index ranges	$-16 \leq h \leq 16$, $-23 \leq k \leq 23$, $-23 \leq l \leq 23$	
Reflections collected	37056	
Independent reflections	17462 [R(int) = 0.0284]	
Completeness to theta = 25.242°	99.9 %	
Absorption correction	Numerical	
Max. and min. transmission	0.9165 and 0.6402	
Refinement method	Full-matrix least-squares on F^2	
Data / restraints / parameters	17462 / 358 / 743	
Goodness-of-fit on F^2	1.012	
Final R indices [I>2sigma(I)]	R1 = 0.0362, wR2 = 0.0739	
R indices (all data)	R1 = 0.0490, wR2 = 0.0781	
Extinction coefficient	n/a	
Largest diff. peak and hole	2.715 and -2.013 $e.Å^{-3}$	

Table 3. 28. Atomic coordinates (x 10^4) and equivalent isotropic displacement parameters ($Å^2$x 10^3) for complex 7.

U(eq) is defined as one third of the trace of the orthogonalized U^{ij} tensor.

	x	y	z	U(eq)
Ir(1A)	3329(1)	7088(1)	1226(1)	21(1)
C(25A)	4982(4)	6789(3)	1573(3)	25(1)
C(26A)	5487(4)	6022(4)	1296(4)	34(1)
C(27A)	6558(5)	5922(4)	1681(4)	38(1)
C(28A)	7156(5)	6595(5)	2350(4)	40(2)
C(29A)	6700(5)	7376(4)	2632(5)	36(1)
C(30A)	5617(5)	7478(4)	2248(4)	26(1)
C(31A)	5112(4)	8276(3)	2467(3)	26(1)
C(32A)	4079(4)	8246(3)	2037(2)	21(1)
C(24A)	3584(4)	8999(6)	1909(3)	26(1)
C(12A)	2054(6)	5355(4)	427(3)	44(1)
Ir(1B)	3281(3)	7146(2)	1387(2)	21(1)
C(25B)	4959(9)	6952(6)	1777(12)	25(1)
C(26B)	5797(13)	7522(10)	2399(16)	26(1)
C(27B)	6886(15)	7297(13)	2602(19)	36(1)
C(28B)	7200(12)	6509(12)	2149(18)	40(2)
C(29B)	6389(12)	5910(10)	1538(18)	38(1)
C(30B)	5277(9)	6132(7)	1366(13)	34(1)
C(31B)	4301(10)	5537(5)	811(12)	47(5)
C(32B)	3283(7)	5884(4)	761(7)	46(5)
C(12B)	2109(9)	5379(6)	446(6)	44(1)
C(24B)	3280(30)	8990(30)	1827(15)	26(1)
P(1)	2302(1)	6460(1)	2072(1)	27(1)
P(2)	3661(1)	7810(1)	339(1)	26(1)
C(1)	1592(3)	7325(2)	948(2)	24(1)
C(2)	657(3)	7199(2)	1413(2)	28(1)
C(3)	-500(3)	7256(3)	1154(3)	33(1)
C(4)	-757(3)	7460(3)	438(3)	34(1)

C(5)	134(3)	7610(2)	-22(3)	30(1)
C(6)	1289(3)	7534(2)	220(2)	26(1)
C(7)	954(4)	6994(3)	2204(3)	34(1)
C(8)	2256(3)	7633(3)	-315(2)	32(1)
C(9)	1828(4)	5326(3)	1297(3)	38(1)
C(10)	525(5)	5035(3)	1282(4)	56(1)
C(11)	2572(5)	4672(3)	1471(3)	59(2)
C(13)	2781(4)	6499(3)	3174(3)	34(1)
C(14)	1804(4)	6077(3)	3529(3)	50(1)
C(15)	3918(4)	6089(3)	3212(3)	41(1)
C(16)	3052(4)	7456(3)	3726(3)	39(1)
C(17)	4731(4)	7505(3)	-478(3)	35(1)
C(18)	4601(5)	7971(4)	-1112(3)	52(1)
C(19)	6001(4)	7652(3)	-63(3)	50(1)
C(20)	4447(4)	6532(3)	-934(3)	44(1)
C(21)	3851(3)	9001(2)	1016(2)	28(1)
C(22)	3045(4)	9531(3)	706(3)	43(1)
C(23)	5108(4)	9429(3)	1117(3)	48(1)
Ir(2A)	908(1)	1971(1)	3674(1)	21(1)
C(57A)	-247(4)	2741(3)	3367(3)	24(1)
C(58A)	-1289(4)	2991(3)	3712(3)	28(1)
C(59A)	-2034(5)	3445(4)	3391(4)	36(1)
C(60A)	-1749(5)	3679(4)	2718(4)	42(1)
C(61A)	-718(5)	3452(4)	2354(4)	38(1)
C(62A)	25(4)	2996(3)	2685(3)	27(1)
C(63A)	1155(4)	2749(3)	2384(3)	33(1)
C(64A)	1727(4)	2301(3)	2796(3)	28(1)
C(44A)	3006(6)	2219(4)	2802(3)	35(1)
C(56A)	-597(5)	1117(4)	4632(3)	44(1)
Ir(2B)	987(4)	1936(3)	3587(3)	21(1)
C(57B)	21(9)	2724(9)	3122(7)	24(1)
C(58B)	196(14)	3028(11)	2458(9)	27(1)
C(59B)	-545(16)	3571(15)	2256(13)	38(1)
C(60B)	-1492(16)	3812(14)	2708(13)	42(1)
C(61B)	-1706(12)	3515(11)	3366(11)	36(1)
C(62B)	-967(9)	2961(8)	3568(8)	28(1)

C(63B)	-1217(8)	2528(8)	4154(8)	35(4)
C(64B)	-447(7)	1996(5)	4231(5)	28(4)
C(56B)	-687(10)	1272(6)	4555(6)	44(1)
C(44B)	3180(30)	2023(11)	2927(14)	35(1)
P(3)	2483(1)	2911(1)	4438(1)	28(1)
P(4)	-237(1)	676(1)	2953(1)	24(1)
C(33)	1985(3)	1120(2)	3970(2)	27(1)
C(34)	2899(3)	1422(2)	4640(2)	28(1)
C(35)	3590(3)	863(3)	4850(3)	31(1)
C(36)	3371(4)	-15(3)	4409(3)	34(1)
C(37)	2458(3)	-330(2)	3765(2)	30(1)
C(38)	1784(3)	229(2)	3540(2)	26(1)
C(39)	3106(4)	2378(3)	5129(2)	34(1)
C(40)	842(4)	-108(2)	2800(3)	33(1)
C(41)	3608(4)	2891(3)	3652(3)	39(1)
C(42)	4798(4)	2661(4)	3917(4)	64(2)
C(43)	3838(5)	3735(4)	3484(4)	66(2)
C(45)	2275(4)	4005(2)	5175(3)	36(1)
C(46)	3390(4)	4438(3)	5774(3)	47(1)
C(47)	1872(5)	4575(3)	4691(3)	50(1)
C(48)	1280(4)	3857(3)	5689(3)	42(1)
C(49)	-1064(4)	375(3)	1876(2)	33(1)
C(50)	-1634(5)	-552(3)	1567(3)	55(1)
C(51)	-1996(4)	983(3)	1869(3)	37(1)
C(52)	-173(4)	486(3)	1274(3)	48(1)
C(53)	-1188(3)	495(3)	3767(3)	33(1)
C(54)	-1194(5)	-414(3)	3793(4)	55(1)
C(55)	-2438(4)	701(4)	3655(3)	54(1)

Table 3. 29. Bond lengths [Å] and angles [°] for complex 7.

Ir(1A)-C(32A)	2.022(4)	C(26B)-C(27B)	1.390(7)
Ir(1A)-C(25A)	2.102(4)	C(26B)-H(26B)	0.9500
Ir(1A)-C(1)	2.121(4)	C(27B)-C(28B)	1.369(9)
Ir(1A)-P(2)	2.2485(13)	C(27B)-H(27B)	0.9500
Ir(1A)-P(1)	2.3547(13)	C(28B)-C(29B)	1.391(8)
C(25A)-C(26A)	1.396(6)	C(28B)-H(28B)	0.9500
C(25A)-C(30A)	1.413(6)	C(29B)-C(30B)	1.400(7)
C(26A)-C(27A)	1.402(7)	C(29B)-H(29B)	0.9500
C(26A)-H(26A)	0.9500	C(30B)-C(31B)	1.466(7)
C(27A)-C(28A)	1.379(8)	C(31B)-C(32B)	1.361(7)
C(27A)-H(27A)	0.9500	C(31B)-H(31B)	0.9500
C(28A)-C(29A)	1.386(8)	C(32B)-C(12B)	1.487(8)
C(28A)-H(28A)	0.9500	C(12B)-C(9)	1.520(10)
C(29A)-C(30A)	1.415(6)	C(12B)-H(12D)	0.9900
C(29A)-H(29A)	0.9500	C(12B)-H(12E)	0.9900
C(30A)-C(31A)	1.438(7)	C(24B)-C(21)	1.559(10)
C(31A)-C(32A)	1.337(6)	C(24B)-H(24C)	0.9800
C(31A)-H(31A)	0.9500	C(24B)-H(24D)	0.9800
C(32A)-C(24A)	1.497(9)	C(24B)-H(24E)	0.9800
C(24A)-C(21)	1.557(5)	P(1)-C(7)	1.841(4)
C(24A)-H(24A)	0.9900	P(1)-C(13)	1.880(4)
C(24A)-H(24B)	0.9900	P(1)-C(9)	1.900(4)
C(12A)-C(9)	1.521(7)	P(2)-C(8)	1.836(4)
C(12A)-H(12A)	0.9800	P(2)-C(17)	1.875(4)
C(12A)-H(12B)	0.9800	P(2)-C(21)	1.907(4)
C(12A)-H(12C)	0.9800	C(1)-C(2)	1.412(5)
Ir(1B)-C(32B)	2.006(4)	C(1)-C(6)	1.415(5)
Ir(1B)-C(25B)	2.083(5)	C(2)-C(3)	1.393(5)
Ir(1B)-C(1)	2.113(5)	C(2)-C(7)	1.512(5)
Ir(1B)-P(1)	2.181(3)	C(3)-C(4)	1.382(6)
Ir(1B)-P(2)	2.426(3)	C(3)-H(3)	0.9500
C(25B)-C(30B)	1.398(6)	C(4)-C(5)	1.379(6)
C(25B)-C(26B)	1.398(6)	C(4)-H(4)	0.9500

C(5)-C(6)	1.391(5)	C(20)-H(20A)	0.9800
C(5)-H(5)	0.9500	C(20)-H(20B)	0.9800
C(6)-C(8)	1.508(5)	C(20)-H(20C)	0.9800
C(7)-H(7A)	0.9900	C(21)-C(22)	1.518(6)
C(7)-H(7B)	0.9900	C(21)-C(23)	1.525(6)
C(8)-H(8A)	0.9900	C(22)-H(22A)	0.9800
C(8)-H(8B)	0.9900	C(22)-H(22B)	0.9800
C(9)-C(10)	1.527(6)	C(22)-H(22C)	0.9800
C(9)-C(11)	1.534(6)	C(23)-H(23A)	0.9800
C(10)-H(10A)	0.9800	C(23)-H(23B)	0.9800
C(10)-H(10B)	0.9800	C(23)-H(23C)	0.9800
C(10)-H(10C)	0.9800	Ir(2A)-C(64A)	2.006(4)
C(11)-H(11A)	0.9800	Ir(2A)-C(57A)	2.083(4)
C(11)-H(11B)	0.9800	Ir(2A)-C(33)	2.121(4)
C(11)-H(11C)	0.9800	Ir(2A)-P(3)	2.2815(13)
C(13)-C(14)	1.533(6)	Ir(2A)-P(4)	2.3173(12)
C(13)-C(15)	1.534(6)	C(57A)-C(62A)	1.398(6)
C(13)-C(16)	1.538(6)	C(57A)-C(58A)	1.398(6)
C(14)-H(14A)	0.9800	C(58A)-C(59A)	1.390(7)
C(14)-H(14B)	0.9800	C(58A)-H(58A)	0.9500
C(14)-H(14C)	0.9800	C(59A)-C(60A)	1.368(8)
C(15)-H(15A)	0.9800	C(59A)-H(59A)	0.9500
C(15)-H(15B)	0.9800	C(60A)-C(61A)	1.391(8)
C(15)-H(15C)	0.9800	C(60A)-H(60A)	0.9500
C(16)-H(16A)	0.9800	C(61A)-C(62A)	1.399(7)
C(16)-H(16B)	0.9800	C(61A)-H(61A)	0.9500
C(16)-H(16C)	0.9800	C(62A)-C(63A)	1.466(7)
C(17)-C(18)	1.528(6)	C(63A)-C(64A)	1.361(7)
C(17)-C(20)	1.534(6)	C(63A)-H(63A)	0.9500
C(17)-C(19)	1.537(6)	C(64A)-C(44A)	1.487(8)
C(18)-H(18A)	0.9800	C(44A)-C(41)	1.557(6)
C(18)-H(18B)	0.9800	C(44A)-H(44A)	0.9900
C(18)-H(18C)	0.9800	C(44A)-H(44B)	0.9900
C(19)-H(19A)	0.9800	C(56A)-C(53)	1.541(6)
C(19)-H(19B)	0.9800	C(56A)-H(56A)	0.9800
C(19)-H(19C)	0.9800	C(56A)-H(56B)	0.9800

C(56A)-H(56C)	0.9800	C(34)-C(39)	1.512(5)
Ir(2B)-C(64B)	2.022(4)	C(35)-C(36)	1.388(6)
Ir(2B)-C(33)	2.088(6)	C(35)-H(35)	0.9500
Ir(2B)-C(57B)	2.101(4)	C(36)-C(37)	1.385(6)
Ir(2B)-P(3)	2.290(3)	C(36)-H(36)	0.9500
Ir(2B)-P(4)	2.299(3)	C(37)-C(38)	1.393(5)
C(57B)-C(58B)	1.395(7)	C(37)-H(37)	0.9500
C(57B)-C(62B)	1.413(6)	C(38)-C(40)	1.510(5)
C(58B)-C(59B)	1.402(7)	C(39)-H(39A)	0.9900
C(58B)-H(58B)	0.9500	C(39)-H(39B)	0.9900
C(59B)-C(60B)	1.379(8)	C(40)-H(40A)	0.9900
C(59B)-H(59B)	0.9500	C(40)-H(40B)	0.9900
C(60B)-C(61B)	1.386(8)	C(41)-C(42)	1.530(7)
C(60B)-H(60B)	0.9500	C(41)-C(43)	1.532(7)
C(61B)-C(62B)	1.415(6)	C(42)-H(42A)	0.9800
C(61B)-H(61B)	0.9500	C(42)-H(42B)	0.9800
C(62B)-C(63B)	1.438(7)	C(42)-H(42C)	0.9800
C(63B)-C(64B)	1.337(6)	C(43)-H(43A)	0.9800
C(63B)-H(63B)	0.9500	C(43)-H(43B)	0.9800
C(64B)-C(56B)	1.496(9)	C(43)-H(43C)	0.9800
C(56B)-C(53)	1.538(10)	C(45)-C(47)	1.529(6)
C(56B)-H(56D)	0.9900	C(45)-C(48)	1.532(6)
C(56B)-H(56E)	0.9900	C(45)-C(46)	1.533(6)
C(44B)-C(41)	1.554(11)	C(46)-H(46A)	0.9800
C(44B)-H(44C)	0.9800	C(46)-H(46B)	0.9800
C(44B)-H(44D)	0.9800	C(46)-H(46C)	0.9800
C(44B)-H(44E)	0.9800	C(47)-H(47A)	0.9800
P(3)-C(39)	1.836(4)	C(47)-H(47B)	0.9800
P(3)-C(45)	1.870(4)	C(47)-H(47C)	0.9800
P(3)-C(41)	1.903(4)	C(48)-H(48A)	0.9800
P(4)-C(40)	1.846(4)	C(48)-H(48B)	0.9800
P(4)-C(49)	1.874(4)	C(48)-H(48C)	0.9800
P(4)-C(53)	1.894(4)	C(49)-C(50)	1.523(6)
C(33)-C(38)	1.404(5)	C(49)-C(52)	1.531(6)
C(33)-C(34)	1.412(5)	C(49)-C(51)	1.539(6)
C(34)-C(35)	1.393(5)	C(50)-H(50A)	0.9800

C(50)-H(50B)	0.9800	C(53)-C(55)	1.520(6)
C(50)-H(50C)	0.9800	C(53)-C(54)	1.531(6)
C(51)-H(51A)	0.9800	C(54)-H(54A)	0.9800
C(51)-H(51B)	0.9800	C(54)-H(54B)	0.9800
C(51)-H(51C)	0.9800	C(54)-H(54C)	0.9800
C(52)-H(52A)	0.9800	C(55)-H(55A)	0.9800
C(52)-H(52B)	0.9800	C(55)-H(55B)	0.9800
C(52)-H(52C)	0.9800	C(55)-H(55C)	0.9800

C(32A)-Ir(1A)-C(25A)	78.65(18)	C(29A)-C(30A)-C(31A)	124.1(5)
C(32A)-Ir(1A)-C(1)	102.91(16)	C(32A)-C(31A)-C(30A)	115.4(4)
C(25A)-Ir(1A)-C(1)	174.53(18)	C(32A)-C(31A)-H(31A)	122.3
C(32A)-Ir(1A)-P(2)	78.16(11)	C(30A)-C(31A)-H(31A)	122.3
C(25A)-Ir(1A)-P(2)	105.43(16)	C(31A)-C(32A)-C(24A)	125.4(4)
C(1)-Ir(1A)-P(2)	80.04(10)	C(31A)-C(32A)-Ir(1A)	117.7(3)
C(32A)-Ir(1A)-P(1)	105.10(12)	C(24A)-C(32A)-Ir(1A)	114.6(3)
C(25A)-Ir(1A)-P(1)	95.12(15)	C(32A)-C(24A)-C(21)	107.9(5)
C(1)-Ir(1A)-P(1)	79.42(10)	C(32A)-C(24A)-H(24A)	110.1
P(2)-Ir(1A)-P(1)	159.40(5)	C(21)-C(24A)-H(24A)	110.1
C(26A)-C(25A)-C(30A)	117.0(4)	C(32A)-C(24A)-H(24B)	110.1
C(26A)-C(25A)-Ir(1A)	130.7(4)	C(21)-C(24A)-H(24B)	110.1
C(30A)-C(25A)-Ir(1A)	112.0(3)	H(24A)-C(24A)-H(24B)	108.4
C(25A)-C(26A)-C(27A)	122.0(5)	C(9)-C(12A)-H(12A)	109.5
C(25A)-C(26A)-H(26A)	119.0	C(9)-C(12A)-H(12B)	109.5
C(27A)-C(26A)-H(26A)	119.0	H(12A)-C(12A)-H(12B)	109.5
C(28A)-C(27A)-C(26A)	120.3(5)	C(9)-C(12A)-H(12C)	109.5
C(28A)-C(27A)-H(27A)	119.9	H(12A)-C(12A)-H(12C)	109.5
C(26A)-C(27A)-H(27A)	119.9	H(12B)-C(12A)-H(12C)	109.5
C(27A)-C(28A)-C(29A)	119.5(5)	C(32B)-Ir(1B)-C(25B)	78.5(2)
C(27A)-C(28A)-H(28A)	120.2	C(32B)-Ir(1B)-C(1)	100.4(3)
C(29A)-C(28A)-H(28A)	120.2	C(25B)-Ir(1B)-C(1)	178.0(6)
C(28A)-C(29A)-C(30A)	120.4(5)	C(32B)-Ir(1B)-P(1)	72.4(4)
C(28A)-C(29A)-H(29A)	119.8	C(25B)-Ir(1B)-P(1)	97.5(7)
C(30A)-C(29A)-H(29A)	119.8	C(1)-Ir(1B)-P(1)	83.71(14)
C(25A)-C(30A)-C(29A)	120.7(5)	C(32B)-Ir(1B)-P(2)	104.6(4)
C(25A)-C(30A)-C(31A)	115.1(4)	C(25B)-Ir(1B)-P(2)	102.5(7)

C(1)-Ir(1B)-P(2)	76.19(13)	H(24C)-C(24B)-H(24E)	109.5
P(1)-Ir(1B)-P(2)	158.86(15)	H(24D)-C(24B)-H(24E)	109.5
C(30B)-C(25B)-C(26B)	115.9(4)	C(7)-P(1)-C(13)	103.41(19)
C(30B)-C(25B)-Ir(1B)	115.1(4)	C(7)-P(1)-C(9)	105.4(2)
C(26B)-C(25B)-Ir(1B)	129.0(4)	C(13)-P(1)-C(9)	113.29(18)
C(27B)-C(26B)-C(25B)	122.7(5)	C(7)-P(1)-Ir(1B)	101.21(15)
C(27B)-C(26B)-H(26B)	118.7	C(13)-P(1)-Ir(1B)	124.22(16)
C(25B)-C(26B)-H(26B)	118.7	C(9)-P(1)-Ir(1B)	106.99(16)
C(28B)-C(27B)-C(26B)	119.9(5)	C(7)-P(1)-Ir(1A)	102.92(13)
C(28B)-C(27B)-H(27B)	120.1	C(13)-P(1)-Ir(1A)	127.74(14)
C(26B)-C(27B)-H(27B)	120.1	C(9)-P(1)-Ir(1A)	101.88(14)
C(27B)-C(28B)-C(29B)	119.6(5)	C(8)-P(2)-C(17)	102.46(18)
C(27B)-C(28B)-H(28B)	120.2	C(8)-P(2)-C(21)	105.09(18)
C(29B)-C(28B)-H(28B)	120.2	C(17)-P(2)-C(21)	114.01(18)
C(28B)-C(29B)-C(30B)	119.7(5)	C(8)-P(2)-Ir(1A)	104.39(13)
C(28B)-C(29B)-H(29B)	120.1	C(17)-P(2)-Ir(1A)	122.46(15)
C(30B)-C(29B)-H(29B)	120.1	C(21)-P(2)-Ir(1A)	106.56(12)
C(25B)-C(30B)-C(29B)	121.9(5)	C(8)-P(2)-Ir(1B)	105.15(15)
C(25B)-C(30B)-C(31B)	112.8(4)	C(17)-P(2)-Ir(1B)	126.41(16)
C(29B)-C(30B)-C(31B)	125.1(5)	C(21)-P(2)-Ir(1B)	101.78(14)
C(32B)-C(31B)-C(30B)	115.2(4)	C(2)-C(1)-C(6)	116.3(3)
C(32B)-C(31B)-H(31B)	122.4	C(2)-C(1)-Ir(1B)	116.8(3)
C(30B)-C(31B)-H(31B)	122.4	C(6)-C(1)-Ir(1B)	126.9(3)
C(31B)-C(32B)-C(12B)	124.6(5)	C(2)-C(1)-Ir(1A)	122.8(3)
C(31B)-C(32B)-Ir(1B)	118.0(4)	C(6)-C(1)-Ir(1A)	120.6(3)
C(12B)-C(32B)-Ir(1B)	115.9(4)	C(3)-C(2)-C(1)	121.6(4)
C(32B)-C(12B)-C(9)	95.8(8)	C(3)-C(2)-C(7)	120.8(3)
C(32B)-C(12B)-H(12D)	112.6	C(1)-C(2)-C(7)	117.6(3)
C(9)-C(12B)-H(12D)	112.6	C(4)-C(3)-C(2)	120.2(4)
C(32B)-C(12B)-H(12E)	112.6	C(4)-C(3)-H(3)	119.9
C(9)-C(12B)-H(12E)	112.6	C(2)-C(3)-H(3)	119.9
H(12D)-C(12B)-H(12E)	110.1	C(5)-C(4)-C(3)	120.0(4)
C(21)-C(24B)-H(24C)	109.5	C(5)-C(4)-H(4)	120.0
C(21)-C(24B)-H(24D)	109.5	C(3)-C(4)-H(4)	120.0
H(24C)-C(24B)-H(24D)	109.5	C(4)-C(5)-C(6)	120.2(4)
C(21)-C(24B)-H(24E)	109.5	C(4)-C(5)-H(5)	119.9

C(6)-C(5)-H(5)	119.9	H(11B)-C(11)-H(11C)	109.5
C(5)-C(6)-C(1)	121.7(4)	C(14)-C(13)-C(15)	110.4(3)
C(5)-C(6)-C(8)	120.5(3)	C(14)-C(13)-C(16)	109.5(4)
C(1)-C(6)-C(8)	117.7(3)	C(15)-C(13)-C(16)	106.9(4)
C(2)-C(7)-P(1)	107.9(3)	C(14)-C(13)-P(1)	111.0(3)
C(2)-C(7)-H(7A)	110.1	C(15)-C(13)-P(1)	112.2(3)
P(1)-C(7)-H(7A)	110.1	C(16)-C(13)-P(1)	106.5(3)
C(2)-C(7)-H(7B)	110.1	C(13)-C(14)-H(14A)	109.5
P(1)-C(7)-H(7B)	110.1	C(13)-C(14)-H(14B)	109.5
H(7A)-C(7)-H(7B)	108.4	H(14A)-C(14)-H(14B)	109.5
C(6)-C(8)-P(2)	107.7(3)	C(13)-C(14)-H(14C)	109.5
C(6)-C(8)-H(8A)	110.2	H(14A)-C(14)-H(14C)	109.5
P(2)-C(8)-H(8A)	110.2	H(14B)-C(14)-H(14C)	109.5
C(6)-C(8)-H(8B)	110.2	C(13)-C(15)-H(15A)	109.5
P(2)-C(8)-H(8B)	110.2	C(13)-C(15)-H(15B)	109.5
H(8A)-C(8)-H(8B)	108.5	H(15A)-C(15)-H(15B)	109.5
C(12B)-C(9)-C(10)	111.2(5)	C(13)-C(15)-H(15C)	109.5
C(12A)-C(9)-C(10)	108.6(4)	H(15A)-C(15)-H(15C)	109.5
C(12B)-C(9)-C(11)	107.0(6)	H(15B)-C(15)-H(15C)	109.5
C(12A)-C(9)-C(11)	107.7(4)	C(13)-C(16)-H(16A)	109.5
C(10)-C(9)-C(11)	109.8(4)	C(13)-C(16)-H(16B)	109.5
C(12B)-C(9)-P(1)	103.5(4)	H(16A)-C(16)-H(16B)	109.5
C(12A)-C(9)-P(1)	105.4(3)	C(13)-C(16)-H(16C)	109.5
C(10)-C(9)-P(1)	113.0(3)	H(16A)-C(16)-H(16C)	109.5
C(11)-C(9)-P(1)	111.9(3)	H(16B)-C(16)-H(16C)	109.5
C(9)-C(10)-H(10A)	109.5	C(18)-C(17)-C(20)	110.3(4)
C(9)-C(10)-H(10B)	109.5	C(18)-C(17)-C(19)	111.4(4)
H(10A)-C(10)-H(10B)	109.5	C(20)-C(17)-C(19)	106.2(4)
C(9)-C(10)-H(10C)	109.5	C(18)-C(17)-P(2)	111.6(3)
H(10A)-C(10)-H(10C)	109.5	C(20)-C(17)-P(2)	105.6(3)
H(10B)-C(10)-H(10C)	109.5	C(19)-C(17)-P(2)	111.5(3)
C(9)-C(11)-H(11A)	109.5	C(17)-C(18)-H(18A)	109.5
C(9)-C(11)-H(11B)	109.5	C(17)-C(18)-H(18B)	109.5
H(11A)-C(11)-H(11B)	109.5	H(18A)-C(18)-H(18B)	109.5
C(9)-C(11)-H(11C)	109.5	C(17)-C(18)-H(18C)	109.5
H(11A)-C(11)-H(11C)	109.5	H(18A)-C(18)-H(18C)	109.5

H(18B)-C(18)-H(18C)	109.5	C(57A)-Ir(2A)-C(33)	176.08(16)
C(17)-C(19)-H(19A)	109.5	C(64A)-Ir(2A)-P(3)	76.19(13)
C(17)-C(19)-H(19B)	109.5	C(57A)-Ir(2A)-P(3)	104.48(13)
H(19A)-C(19)-H(19B)	109.5	C(33)-Ir(2A)-P(3)	79.22(11)
C(17)-C(19)-H(19C)	109.5	C(64A)-Ir(2A)-P(4)	106.28(14)
H(19A)-C(19)-H(19C)	109.5	C(57A)-Ir(2A)-P(4)	95.94(13)
H(19B)-C(19)-H(19C)	109.5	C(33)-Ir(2A)-P(4)	80.43(11)
C(17)-C(20)-H(20A)	109.5	P(3)-Ir(2A)-P(4)	159.47(7)
C(17)-C(20)-H(20B)	109.5	C(62A)-C(57A)-C(58A)	115.9(4)
H(20A)-C(20)-H(20B)	109.5	C(62A)-C(57A)-Ir(2A)	115.0(3)
C(17)-C(20)-H(20C)	109.5	C(58A)-C(57A)-Ir(2A)	129.0(4)
H(20A)-C(20)-H(20C)	109.5	C(59A)-C(58A)-C(57A)	122.7(5)
H(20B)-C(20)-H(20C)	109.5	C(59A)-C(58A)-H(58A)	118.6
C(22)-C(21)-C(23)	107.9(4)	C(57A)-C(58A)-H(58A)	118.6
C(22)-C(21)-C(24A)	111.3(4)	C(60A)-C(59A)-C(58A)	120.0(5)
C(23)-C(21)-C(24A)	106.5(4)	C(60A)-C(59A)-H(59A)	120.0
C(22)-C(21)-C(24B)	100.7(15)	C(58A)-C(59A)-H(59A)	120.0
C(23)-C(21)-C(24B)	118.5(14)	C(59A)-C(60A)-C(61A)	119.7(5)
C(22)-C(21)-P(2)	114.2(3)	C(59A)-C(60A)-H(60A)	120.2
C(23)-C(21)-P(2)	113.5(3)	C(61A)-C(60A)-H(60A)	120.2
C(24A)-C(21)-P(2)	103.1(4)	C(60A)-C(61A)-C(62A)	119.7(5)
C(24B)-C(21)-P(2)	101.5(18)	C(60A)-C(61A)-H(61A)	120.1
C(21)-C(22)-H(22A)	109.5	C(62A)-C(61A)-H(61A)	120.1
C(21)-C(22)-H(22B)	109.5	C(57A)-C(62A)-C(61A)	122.0(5)
H(22A)-C(22)-H(22B)	109.5	C(57A)-C(62A)-C(63A)	112.8(4)
C(21)-C(22)-H(22C)	109.5	C(61A)-C(62A)-C(63A)	125.2(5)
H(22A)-C(22)-H(22C)	109.5	C(64A)-C(63A)-C(62A)	115.2(4)
H(22B)-C(22)-H(22C)	109.5	C(64A)-C(63A)-H(63A)	122.4
C(21)-C(23)-H(23A)	109.5	C(62A)-C(63A)-H(63A)	122.4
C(21)-C(23)-H(23B)	109.5	C(63A)-C(64A)-C(44A)	124.5(4)
H(23A)-C(23)-H(23B)	109.5	C(63A)-C(64A)-Ir(2A)	117.9(4)
C(21)-C(23)-H(23C)	109.5	C(44A)-C(64A)-Ir(2A)	115.9(3)
H(23A)-C(23)-H(23C)	109.5	C(64A)-C(44A)-C(41)	106.7(4)
H(23B)-C(23)-H(23C)	109.5	C(64A)-C(44A)-H(44A)	110.4
C(64A)-Ir(2A)-C(57A)	78.48(19)	C(41)-C(44A)-H(44A)	110.4
C(64A)-Ir(2A)-C(33)	103.89(18)	C(64A)-C(44A)-H(44B)	110.4

C(41)-C(44A)-H(44B)	110.4	C(64B)-C(63B)-C(62B)	115.4(4)
H(44A)-C(44A)-H(44B)	108.6	C(64B)-C(63B)-H(63B)	122.3
C(53)-C(56A)-H(56A)	109.5	C(62B)-C(63B)-H(63B)	122.3
C(53)-C(56A)-H(56B)	109.5	C(63B)-C(64B)-C(56B)	125.4(5)
H(56A)-C(56A)-H(56B)	109.5	C(63B)-C(64B)-Ir(2B)	117.8(3)
C(53)-C(56A)-H(56C)	109.5	C(56B)-C(64B)-Ir(2B)	114.7(4)
H(56A)-C(56A)-H(56C)	109.5	C(64B)-C(56B)-C(53)	105.0(7)
H(56B)-C(56A)-H(56C)	109.5	C(64B)-C(56B)-H(56D)	110.7
C(64B)-Ir(2B)-C(33)	104.5(3)	C(53)-C(56B)-H(56D)	110.7
C(64B)-Ir(2B)-C(57B)	78.64(19)	C(64B)-C(56B)-H(56E)	110.7
C(33)-Ir(2B)-C(57B)	176.2(3)	C(53)-C(56B)-H(56E)	110.7
C(64B)-Ir(2B)-P(3)	109.1(3)	H(56D)-C(56B)-H(56E)	108.8
C(33)-Ir(2B)-P(3)	79.70(18)	C(41)-C(44B)-H(44C)	109.5
C(57B)-Ir(2B)-P(3)	101.4(5)	C(41)-C(44B)-H(44D)	109.5
C(64B)-Ir(2B)-P(4)	71.7(3)	H(44C)-C(44B)-H(44D)	109.5
C(33)-Ir(2B)-P(4)	81.55(19)	C(41)-C(44B)-H(44E)	109.5
C(57B)-Ir(2B)-P(4)	97.6(4)	H(44C)-C(44B)-H(44E)	109.5
P(3)-Ir(2B)-P(4)	160.8(3)	H(44D)-C(44B)-H(44E)	109.5
C(58B)-C(57B)-C(62B)	117.1(4)	C(39)-P(3)-C(45)	104.64(19)
C(58B)-C(57B)-Ir(2B)	130.7(4)	C(39)-P(3)-C(41)	105.1(2)
C(62B)-C(57B)-Ir(2B)	112.2(3)	C(45)-P(3)-C(41)	115.0(2)
C(57B)-C(58B)-C(59B)	122.0(5)	C(39)-P(3)-Ir(2A)	103.97(14)
C(57B)-C(58B)-H(58B)	119.0	C(45)-P(3)-Ir(2A)	120.67(14)
C(59B)-C(58B)-H(58B)	119.0	C(41)-P(3)-Ir(2A)	105.82(14)
C(60B)-C(59B)-C(58B)	120.2(5)	C(39)-P(3)-Ir(2B)	104.85(19)
C(60B)-C(59B)-H(59B)	119.9	C(45)-P(3)-Ir(2B)	123.99(18)
C(58B)-C(59B)-H(59B)	119.9	C(41)-P(3)-Ir(2B)	101.54(18)
C(59B)-C(60B)-C(61B)	119.6(5)	C(40)-P(4)-C(49)	103.92(18)
C(59B)-C(60B)-H(60B)	120.2	C(40)-P(4)-C(53)	105.72(19)
C(61B)-C(60B)-H(60B)	120.2	C(49)-P(4)-C(53)	112.69(19)
C(60B)-C(61B)-C(62B)	120.4(5)	C(40)-P(4)-Ir(2B)	100.14(18)
C(60B)-C(61B)-H(61B)	119.8	C(49)-P(4)-Ir(2B)	123.42(19)
C(62B)-C(61B)-H(61B)	119.8	C(53)-P(4)-Ir(2B)	108.60(18)
C(57B)-C(62B)-C(61B)	120.6(5)	C(40)-P(4)-Ir(2A)	102.57(13)
C(57B)-C(62B)-C(63B)	115.1(4)	C(49)-P(4)-Ir(2A)	125.51(14)
C(61B)-C(62B)-C(63B)	124.0(5)	C(53)-P(4)-Ir(2A)	104.47(14)

C(38)-C(33)-C(34)	116.9(3)	C(43)-C(41)-C(44A)	105.8(4)
C(38)-C(33)-Ir(2B)	120.0(3)	C(42)-C(41)-P(3)	113.2(3)
C(34)-C(33)-Ir(2B)	123.1(3)	C(43)-C(41)-P(3)	114.1(4)
C(38)-C(33)-Ir(2A)	121.6(3)	C(44B)-C(41)-P(3)	101.5(14)
C(34)-C(33)-Ir(2A)	121.4(3)	C(44A)-C(41)-P(3)	103.7(3)
C(35)-C(34)-C(33)	121.6(4)	C(41)-C(42)-H(42A)	109.5
C(35)-C(34)-C(39)	120.7(4)	C(41)-C(42)-H(42B)	109.5
C(33)-C(34)-C(39)	117.7(3)	H(42A)-C(42)-H(42B)	109.5
C(36)-C(35)-C(34)	120.0(4)	C(41)-C(42)-H(42C)	109.5
C(36)-C(35)-H(35)	120.0	H(42A)-C(42)-H(42C)	109.5
C(34)-C(35)-H(35)	120.0	H(42B)-C(42)-H(42C)	109.5
C(37)-C(36)-C(35)	119.6(4)	C(41)-C(43)-H(43A)	109.5
C(37)-C(36)-H(36)	120.2	C(41)-C(43)-H(43B)	109.5
C(35)-C(36)-H(36)	120.2	H(43A)-C(43)-H(43B)	109.5
C(36)-C(37)-C(38)	120.5(4)	C(41)-C(43)-H(43C)	109.5
C(36)-C(37)-H(37)	119.7	H(43A)-C(43)-H(43C)	109.5
C(38)-C(37)-H(37)	119.7	H(43B)-C(43)-H(43C)	109.5
C(37)-C(38)-C(33)	121.4(4)	C(47)-C(45)-C(48)	107.7(4)
C(37)-C(38)-C(40)	120.6(3)	C(47)-C(45)-C(46)	110.9(4)
C(33)-C(38)-C(40)	117.9(3)	C(48)-C(45)-C(46)	109.8(4)
C(34)-C(39)-P(3)	106.9(3)	C(47)-C(45)-P(3)	111.6(3)
C(34)-C(39)-H(39A)	110.3	C(48)-C(45)-P(3)	105.1(3)
P(3)-C(39)-H(39A)	110.3	C(46)-C(45)-P(3)	111.5(3)
C(34)-C(39)-H(39B)	110.3	C(45)-C(46)-H(46A)	109.5
P(3)-C(39)-H(39B)	110.3	C(45)-C(46)-H(46B)	109.5
H(39A)-C(39)-H(39B)	108.6	H(46A)-C(46)-H(46B)	109.5
C(38)-C(40)-P(4)	108.2(3)	C(45)-C(46)-H(46C)	109.5
C(38)-C(40)-H(40A)	110.1	H(46A)-C(46)-H(46C)	109.5
P(4)-C(40)-H(40A)	110.1	H(46B)-C(46)-H(46C)	109.5
C(38)-C(40)-H(40B)	110.1	C(45)-C(47)-H(47A)	109.5
P(4)-C(40)-H(40B)	110.1	C(45)-C(47)-H(47B)	109.5
H(40A)-C(40)-H(40B)	108.4	H(47A)-C(47)-H(47B)	109.5
C(42)-C(41)-C(43)	107.3(4)	C(45)-C(47)-H(47C)	109.5
C(42)-C(41)-C(44B)	97.7(13)	H(47A)-C(47)-H(47C)	109.5
C(43)-C(41)-C(44B)	122.1(12)	H(47B)-C(47)-H(47C)	109.5
C(42)-C(41)-C(44A)	112.5(4)	C(45)-C(48)-H(48A)	109.5

C(45)-C(48)-H(48B)	109.5	H(52A)-C(52)-H(52B)	109.5
H(48A)-C(48)-H(48B)	109.5	C(49)-C(52)-H(52C)	109.5
C(45)-C(48)-H(48C)	109.5	H(52A)-C(52)-H(52C)	109.5
H(48A)-C(48)-H(48C)	109.5	H(52B)-C(52)-H(52C)	109.5
H(48B)-C(48)-H(48C)	109.5	C(55)-C(53)-C(54)	110.3(4)
C(50)-C(49)-C(52)	109.8(4)	C(55)-C(53)-C(56B)	100.6(6)
C(50)-C(49)-C(51)	110.2(4)	C(54)-C(53)-C(56B)	119.7(5)
C(52)-C(49)-C(51)	107.0(4)	C(55)-C(53)-C(56A)	108.5(4)
C(50)-C(49)-P(4)	111.1(3)	C(54)-C(53)-C(56A)	106.8(4)
C(52)-C(49)-P(4)	106.9(3)	C(55)-C(53)-P(4)	113.2(3)
C(51)-C(49)-P(4)	111.7(3)	C(54)-C(53)-P(4)	112.3(3)
C(49)-C(50)-H(50A)	109.5	C(56B)-C(53)-P(4)	100.2(4)
C(49)-C(50)-H(50B)	109.5	C(56A)-C(53)-P(4)	105.3(3)
H(50A)-C(50)-H(50B)	109.5	C(53)-C(54)-H(54A)	109.5
C(49)-C(50)-H(50C)	109.5	C(53)-C(54)-H(54B)	109.5
H(50A)-C(50)-H(50C)	109.5	H(54A)-C(54)-H(54B)	109.5
H(50B)-C(50)-H(50C)	109.5	C(53)-C(54)-H(54C)	109.5
C(49)-C(51)-H(51A)	109.5	H(54A)-C(54)-H(54C)	109.5
C(49)-C(51)-H(51B)	109.5	H(54B)-C(54)-H(54C)	109.5
H(51A)-C(51)-H(51B)	109.5	C(53)-C(55)-H(55A)	109.5
C(49)-C(51)-H(51C)	109.5	C(53)-C(55)-H(55B)	109.5
H(51A)-C(51)-H(51C)	109.5	H(55A)-C(55)-H(55B)	109.5
H(51B)-C(51)-H(51C)	109.5	C(53)-C(55)-H(55C)	109.5
C(49)-C(52)-H(52A)	109.5	H(55A)-C(55)-H(55C)	109.5
C(49)-C(52)-H(52B)	109.5	H(55B)-C(55)-H(55C)	109.5

Table 3. 30. Anisotropic displacement parameters ($Å^2$x 10^3) for complex 7.

The anisotropic displacement factor exponent takes the form: $-2\pi^2[h^2 a^{*2}U^{11} + ... + 2 h k a^* b^* U^{12}]$

	U^{11}	U^{22}	U^{33}	U^{23}	U^{13}	U^{12}
Ir(1A)	18(1)	23(1)	19(1)	6(1)	-1(1)	2(1)
C(25A)	22(2)	35(2)	22(3)	14(2)	3(2)	4(2)
C(26A)	29(2)	44(3)	32(2)	16(2)	9(2)	14(2)
C(27A)	31(2)	55(3)	39(3)	28(2)	8(2)	18(2)
C(28A)	24(2)	67(3)	42(4)	37(3)	2(2)	7(2)
C(29A)	22(2)	53(3)	39(2)	29(2)	-8(2)	-7(2)
C(30A)	19(2)	39(2)	25(3)	20(2)	-6(2)	-3(2)
C(31A)	29(2)	29(2)	22(2)	13(2)	-2(2)	-4(2)
C(32A)	25(2)	22(2)	16(2)	8(2)	4(2)	-1(2)
C(24A)	24(3)	29(2)	25(2)	11(2)	2(2)	3(3)
C(12A)	45(3)	33(2)	42(3)	4(2)	-6(2)	-4(2)
Ir(1B)	18(1)	23(1)	19(1)	6(1)	-1(1)	2(1)
C(25B)	22(2)	35(2)	22(3)	14(2)	3(2)	4(2)
C(26B)	19(2)	39(2)	25(3)	20(2)	-6(2)	-3(2)
C(27B)	22(2)	53(3)	39(2)	29(2)	-8(2)	-7(2)
C(28B)	24(2)	67(3)	42(4)	37(3)	2(2)	7(2)
C(29B)	31(2)	55(3)	39(3)	28(2)	8(2)	18(2)
C(30B)	29(2)	44(3)	32(2)	16(2)	9(2)	14(2)
C(31B)	53(8)	38(8)	45(9)	9(7)	5(8)	7(7)
C(32B)	51(8)	28(8)	47(10)	-3(7)	3(8)	8(7)
C(12B)	45(3)	33(2)	42(3)	4(2)	-6(2)	-4(2)
C(24B)	24(3)	29(2)	25(2)	11(2)	2(2)	3(3)
P(1)	29(1)	24(1)	31(1)	14(1)	-1(1)	0(1)
P(2)	19(1)	34(1)	24(1)	10(1)	3(1)	3(1)
C(1)	20(2)	27(2)	26(2)	10(1)	-2(1)	1(1)
C(2)	26(2)	26(2)	34(2)	11(2)	5(2)	3(2)
C(3)	23(2)	36(2)	45(2)	18(2)	7(2)	4(2)
C(4)	17(2)	36(2)	44(2)	11(2)	-3(2)	3(2)
C(5)	26(2)	32(2)	31(2)	9(2)	-4(2)	8(2)

C(6)	22(2)	30(2)	26(2)	8(2)	-3(1)	3(1)
C(7)	32(2)	36(2)	39(2)	20(2)	9(2)	3(2)
C(8)	24(2)	45(2)	26(2)	14(2)	-1(2)	2(2)
C(9)	41(2)	27(2)	46(3)	16(2)	-3(2)	-2(2)
C(10)	54(3)	45(3)	64(3)	20(3)	-6(3)	-19(2)
C(11)	80(4)	27(2)	61(3)	9(2)	-18(3)	9(2)
C(13)	44(2)	34(2)	32(2)	21(2)	2(2)	5(2)
C(14)	57(3)	54(3)	51(3)	36(2)	5(2)	-2(2)
C(15)	53(3)	39(2)	36(2)	20(2)	-3(2)	10(2)
C(16)	52(3)	37(2)	30(2)	16(2)	-1(2)	2(2)
C(17)	27(2)	45(2)	33(2)	11(2)	10(2)	7(2)
C(18)	49(3)	70(3)	52(3)	33(3)	25(2)	17(3)
C(19)	22(2)	67(3)	58(3)	16(3)	12(2)	9(2)
C(20)	38(2)	52(3)	36(2)	8(2)	2(2)	15(2)
C(21)	27(2)	33(2)	27(2)	14(2)	4(2)	1(2)
C(22)	53(3)	37(2)	41(3)	18(2)	-2(2)	5(2)
C(23)	37(2)	45(3)	54(3)	10(2)	3(2)	-7(2)
Ir(2A)	22(1)	24(1)	22(1)	12(1)	7(1)	5(1)
C(57A)	23(2)	21(2)	25(3)	8(2)	-4(2)	-3(2)
C(58A)	24(3)	24(2)	34(2)	6(2)	2(2)	6(2)
C(59A)	27(3)	26(2)	45(3)	-1(2)	-6(2)	6(2)
C(60A)	43(3)	29(3)	47(3)	9(2)	-20(2)	5(3)
C(61A)	50(3)	27(3)	36(3)	17(2)	-15(2)	-6(2)
C(62A)	31(2)	24(2)	28(3)	13(2)	-4(2)	-6(2)
C(63A)	36(3)	41(3)	23(2)	16(2)	-4(2)	-10(2)
C(64A)	29(2)	35(2)	21(2)	10(2)	6(2)	-5(2)
C(44A)	30(3)	46(3)	33(3)	18(2)	9(2)	0(2)
C(56A)	50(3)	56(3)	31(2)	22(2)	13(2)	3(2)
Ir(2B)	22(1)	24(1)	22(1)	12(1)	7(1)	5(1)
C(57B)	23(2)	21(2)	25(3)	8(2)	-4(2)	-3(2)
C(58B)	31(2)	24(2)	28(3)	13(2)	-4(2)	-6(2)
C(59B)	50(3)	27(3)	36(3)	17(2)	-15(2)	-6(2)
C(60B)	43(3)	29(3)	47(3)	9(2)	-20(2)	5(3)
C(61B)	27(3)	26(2)	45(3)	-1(2)	-6(2)	6(2)
C(62B)	24(3)	24(2)	34(2)	6(2)	2(2)	6(2)
C(63B)	36(8)	33(8)	29(8)	1(6)	4(7)	7(7)

C(64B)	37(8)	28(7)	18(7)	5(6)	20(6)	6(6)
C(56B)	50(3)	56(3)	31(2)	22(2)	13(2)	3(2)
C(44B)	30(3)	46(3)	33(3)	18(2)	9(2)	0(2)
P(3)	33(1)	25(1)	26(1)	10(1)	0(1)	1(1)
P(4)	24(1)	24(1)	23(1)	9(1)	0(1)	2(1)
C(33)	30(2)	27(2)	26(2)	12(2)	1(2)	6(2)
C(34)	33(2)	30(2)	25(2)	12(2)	5(2)	5(2)
C(35)	27(2)	38(2)	32(2)	18(2)	1(2)	6(2)
C(36)	36(2)	38(2)	37(2)	20(2)	9(2)	18(2)
C(37)	32(2)	28(2)	32(2)	11(2)	7(2)	10(2)
C(38)	28(2)	27(2)	27(2)	10(2)	7(2)	8(2)
C(39)	38(2)	33(2)	26(2)	9(2)	-7(2)	1(2)
C(40)	34(2)	28(2)	33(2)	6(2)	0(2)	7(2)
C(41)	33(2)	44(2)	43(2)	20(2)	6(2)	-2(2)
C(42)	26(2)	107(5)	68(4)	44(4)	6(2)	-2(3)
C(43)	71(4)	70(4)	70(4)	42(3)	21(3)	-7(3)
C(45)	40(2)	24(2)	38(2)	7(2)	-4(2)	-2(2)
C(46)	47(3)	31(2)	50(3)	1(2)	-12(2)	0(2)
C(47)	64(3)	26(2)	54(3)	10(2)	-9(2)	5(2)
C(48)	44(3)	36(2)	37(2)	2(2)	4(2)	9(2)
C(49)	35(2)	31(2)	26(2)	5(2)	-9(2)	0(2)
C(50)	55(3)	31(2)	62(3)	3(2)	-29(3)	-6(2)
C(51)	38(2)	39(2)	32(2)	13(2)	-9(2)	4(2)
C(52)	52(3)	65(3)	24(2)	10(2)	2(2)	15(2)
C(53)	28(2)	38(2)	38(2)	21(2)	7(2)	0(2)
C(54)	57(3)	44(3)	80(4)	40(3)	17(3)	-1(2)
C(55)	41(3)	77(4)	64(3)	44(3)	21(2)	15(3)

Table 3. 31. Hydrogen coordinates (x 10^4) and isotropic displacement parameters (Å^{2}x 10^3) for complex 7.

	x	y	z	U(eq)
H(26A)	5093	5552	832	40
H(27A)	6872	5388	1481	45
H(28A)	7876	6525	2615	48
H(29A)	7117	7844	3085	43
H(31A)	5488	8789	2888	31
H(24A)	3949	9539	2354	31
H(24B)	2726	8952	1945	31
H(12A)	2888	5542	429	52
H(12B)	1844	4782	-2	52
H(12C)	1577	5761	295	52
H(26B)	5615	8085	2695	31
H(27B)	7410	7691	3054	43
H(28B)	7968	6372	2251	48
H(29B)	6588	5353	1238	45
H(31B)	4375	4950	508	56
H(12D)	2154	4807	14	52
H(12E)	1552	5692	225	52
H(24C)	3728	8658	2098	31
H(24D)	3298	9577	2224	31
H(24E)	2469	8718	1670	31
H(3)	-1115	7155	1471	40
H(4)	-1548	7497	262	40
H(5)	-41	7766	-505	36
H(7A)	301	6611	2287	40
H(7B)	1080	7529	2708	40
H(8A)	2164	8127	-504	38
H(8B)	2226	7108	-824	38
H(10A)	52	5433	1131	84
H(10B)	363	5030	1844	84

H(10C)	325	4456	861	84
H(11A)	2449	4135	981	88
H(11B)	2338	4562	1976	88
H(11C)	3404	4902	1565	88
H(14A)	2061	6130	4113	75
H(14B)	1632	5467	3177	75
H(14C)	1095	6362	3523	75
H(15A)	4516	6336	2947	61
H(15B)	3764	5467	2908	61
H(15C)	4199	6200	3806	61
H(16A)	2324	7727	3776	58
H(16B)	3609	7741	3462	58
H(16C)	3396	7509	4292	58
H(18A)	5196	7818	-1513	79
H(18B)	4709	8593	-806	79
H(18C)	3816	7801	-1423	79
H(19A)	6513	7367	-490	75
H(19B)	6034	7414	394	75
H(19C)	6265	8270	172	75
H(20A)	3635	6401	-1198	65
H(20B)	4543	6240	-522	65
H(20C)	4982	6332	-1372	65
H(22A)	3134	10120	1116	64
H(22B)	2229	9276	649	64
H(22C)	3252	9540	154	64
H(23A)	5343	9395	559	72
H(23B)	5636	9134	1374	72
H(23C)	5152	10033	1484	72
H(58A)	-1495	2845	4187	34
H(59A)	-2741	3592	3638	43
H(60A)	-2252	3994	2500	50
H(61A)	-519	3606	1882	45
H(63A)	1465	2891	1934	40
H(44A)	3319	2335	2314	42
H(44B)	3151	1631	2766	42
H(56A)	211	992	4714	52

H(56B)	-588	1710	4647	52
H(56C)	-1037	1045	5087	52
H(58B)	836	2862	2133	33
H(59B)	-393	3774	1806	45
H(60B)	-1995	4178	2570	50
H(61B)	-2353	3684	3683	43
H(63B)	-1884	2614	4466	42
H(56D)	-1262	1409	4981	52
H(56E)	45	1157	4819	52
H(44C)	2403	2050	2671	42
H(44D)	3737	1914	2493	42
H(44E)	3142	1557	3158	42
H(35)	4212	1083	5295	37
H(36)	3843	-397	4549	41
H(37)	2290	-932	3474	36
H(39A)	3958	2568	5279	40
H(39B)	2717	2519	5659	40
H(40A)	451	-671	2771	39
H(40B)	1195	-184	2262	39
H(42A)	5310	2599	3462	96
H(42B)	4683	2118	4023	96
H(42C)	5162	3118	4435	96
H(43A)	4099	4204	4021	99
H(43B)	3113	3854	3228	99
H(43C)	4449	3685	3096	99
H(46A)	4031	4514	5441	71
H(46B)	3608	4076	6099	71
H(46C)	3243	5000	6165	71
H(47A)	1556	5071	5081	74
H(47B)	1260	4244	4235	74
H(47C)	2541	4774	4446	74
H(48A)	1133	4408	6100	62
H(48B)	1504	3476	5992	62
H(48C)	565	3591	5305	62
H(50A)	-2027	-702	993	83
H(50B)	-2212	-617	1950	83

H(50C)	-1030	-934	1559	83
H(51A)	-2344	851	1285	56
H(51B)	-1626	1579	2095	56
H(51C)	-2612	906	2221	56
H(52A)	354	37	1180	72
H(52B)	288	1052	1525	72
H(52C)	-589	438	730	72
H(54A)	-1678	-473	4232	83
H(54B)	-389	-516	3924	83
H(54C)	-1519	-833	3240	83
H(55A)	-2855	269	3139	82
H(55B)	-2421	1271	3605	82
H(55C)	-2844	696	4147	82

Table 3. 32. Torsion angles [°] for complex 7.

C(30A)-C(25A)-C(26A)-C(27A)	1.9(8)	Ir(1B)-C(32B)-C(12B)-C(9)	-78.5(9)
Ir(1A)-C(25A)-C(26A)-C(27A)	-172.2(5)	C(6)-C(1)-C(2)-C(3)	1.5(5)
C(25A)-C(26A)-C(27A)-C(28A)	-0.8(10)	Ir(1B)-C(1)-C(2)-C(3)	-176.6(3)
C(26A)-C(27A)-C(28A)-C(29A)	-0.9(10)	Ir(1A)-C(1)-C(2)-C(3)	-171.9(3)
C(27A)-C(28A)-C(29A)-C(30A)	1.2(11)	C(6)-C(1)-C(2)-C(7)	-178.7(3)
C(26A)-C(25A)-C(30A)-C(29A)	-1.6(9)	Ir(1B)-C(1)-C(2)-C(7)	3.1(5)
Ir(1A)-C(25A)-C(30A)-C(29A)	173.6(6)	Ir(1A)-C(1)-C(2)-C(7)	7.8(5)
C(26A)-C(25A)-C(30A)-C(31A)	175.1(5)	C(1)-C(2)-C(3)-C(4)	-1.5(6)
Ir(1A)-C(25A)-C(30A)-C(31A)	-9.7(7)	C(7)-C(2)-C(3)-C(4)	178.8(4)
C(28A)-C(29A)-C(30A)-C(25A)	0.1(11)	C(2)-C(3)-C(4)-C(5)	-0.2(6)
C(28A)-C(29A)-C(30A)-C(31A)	-176.3(7)	C(3)-C(4)-C(5)-C(6)	1.8(6)
C(25A)-C(30A)-C(31A)-C(32A)	3.7(7)	C(4)-C(5)-C(6)-C(1)	-1.7(6)
C(29A)-C(30A)-C(31A)-C(32A)	-179.7(6)	C(4)-C(5)-C(6)-C(8)	175.5(4)
C(30A)-C(31A)-C(32A)-C(24A)	-157.1(5)	C(2)-C(1)-C(6)-C(5)	0.0(5)
C(30A)-C(31A)-C(32A)-Ir(1A)	4.7(6)	Ir(1B)-C(1)-C(6)-C(5)	178.0(3)
C(31A)-C(32A)-C(24A)-C(21)	98.2(6)	Ir(1A)-C(1)-C(6)-C(5)	173.6(3)
Ir(1A)-C(32A)-C(24A)-C(21)	-64.1(5)	C(2)-C(1)-C(6)-C(8)	-177.2(3)
C(30B)-C(25B)-C(26B)-C(27B)	0(4)	Ir(1B)-C(1)-C(6)-C(8)	0.8(5)
Ir(1B)-C(25B)-C(26B)-C(27B)	179(3)	Ir(1A)-C(1)-C(6)-C(8)	-3.6(5)
C(25B)-C(26B)-C(27B)-C(28B)	4(5)	C(3)-C(2)-C(7)-P(1)	152.4(3)
C(26B)-C(27B)-C(28B)-C(29B)	-6(4)	C(1)-C(2)-C(7)-P(1)	-27.3(4)
C(27B)-C(28B)-C(29B)-C(30B)	3(4)	C(13)-P(1)-C(7)-C(2)	166.0(3)
C(26B)-C(25B)-C(30B)-C(29B)	-3(3)	C(9)-P(1)-C(7)-C(2)	-74.9(3)
Ir(1B)-C(25B)-C(30B)-C(29B)	177.9(19)	Ir(1B)-P(1)-C(7)-C(2)	36.5(3)
C(26B)-C(25B)-C(30B)-C(31B)	172(3)	Ir(1A)-P(1)-C(7)-C(2)	31.5(3)
Ir(1B)-C(25B)-C(30B)-C(31B)	-7.0(19)	C(5)-C(6)-C(8)-P(2)	163.6(3)
C(28B)-C(29B)-C(30B)-C(25B)	2(4)	C(1)-C(6)-C(8)-P(2)	-19.2(4)
C(28B)-C(29B)-C(30B)-C(31B)	-173(3)	C(17)-P(2)-C(8)-C(6)	159.4(3)
C(25B)-C(30B)-C(31B)-C(32B)	3(2)	C(21)-P(2)-C(8)-C(6)	-81.2(3)
C(29B)-C(30B)-C(31B)-C(32B)	178(2)	Ir(1A)-P(2)-C(8)-C(6)	30.7(3)
C(30B)-C(31B)-C(32B)-C(12B)	-162.2(17)	Ir(1B)-P(2)-C(8)-C(6)	25.8(3)
C(30B)-C(31B)-C(32B)-Ir(1B)	3.2(17)	C(32B)-C(12B)-C(9)-C(10)	165.5(4)
C(31B)-C(32B)-C(12B)-C(9)	87.1(11)	C(32B)-C(12B)-C(9)-C(11)	-74.5(5)

C(32B)-C(12B)-C(9)-P(1)	43.9(5)	Ir(2A)-C(57A)-C(62A)-C(63A)	-6.6(5)
C(7)-P(1)-C(13)-C(14)	56.4(3)	C(60A)-C(61A)-C(62A)-C(57A)	1.4(9)
C(9)-P(1)-C(13)-C(14)	-57.1(4)	C(60A)-C(61A)-C(62A)-C(63A)	-177.5(5)
Ir(1B)-P(1)-C(13)-C(14)	170.2(3)	C(57A)-C(62A)-C(63A)-C(64A)	1.6(6)
Ir(1A)-P(1)-C(13)-C(14)	174.8(3)	C(61A)-C(62A)-C(63A)-C(64A)	-179.5(5)
C(7)-P(1)-C(13)-C(15)	-179.5(3)	C(62A)-C(63A)-C(64A)-C(44A)	-159.9(5)
C(9)-P(1)-C(13)-C(15)	67.0(3)	C(62A)-C(63A)-C(64A)-Ir(2A)	4.6(6)
Ir(1B)-P(1)-C(13)-C(15)	-65.6(3)	C(63A)-C(64A)-C(44A)-C(41)	98.7(6)
Ir(1A)-P(1)-C(13)-C(15)	-61.1(3)	Ir(2A)-C(64A)-C(44A)-C(41)	-66.0(5)
C(7)-P(1)-C(13)-C(16)	-62.8(3)	C(62B)-C(57B)-C(58B)-C(59B)	2(3)
C(9)-P(1)-C(13)-C(16)	-176.3(3)	Ir(2B)-C(57B)-C(58B)-C(59B)	-178.5(17)
Ir(1B)-P(1)-C(13)-C(16)	51.1(4)	C(57B)-C(58B)-C(59B)-C(60B)	-1(4)
Ir(1A)-P(1)-C(13)-C(16)	55.6(3)	C(58B)-C(59B)-C(60B)-C(61B)	0(4)
C(8)-P(2)-C(17)-C(18)	51.7(4)	C(59B)-C(60B)-C(61B)-C(62B)	-1(3)
C(21)-P(2)-C(17)-C(18)	-61.3(4)	C(58B)-C(57B)-C(62B)-C(61B)	-3(2)
Ir(1A)-P(2)-C(17)-C(18)	168.0(3)	Ir(2B)-C(57B)-C(62B)-C(61B)	177.9(12)
Ir(1B)-P(2)-C(17)-C(18)	171.4(3)	C(58B)-C(57B)-C(62B)-C(63B)	170.7(16)
C(8)-P(2)-C(17)-C(20)	-68.1(3)	Ir(2B)-C(57B)-C(62B)-C(63B)	-8.6(14)
C(21)-P(2)-C(17)-C(20)	178.9(3)	C(60B)-C(61B)-C(62B)-C(57B)	2(2)
Ir(1A)-P(2)-C(17)-C(20)	48.1(3)	C(60B)-C(61B)-C(62B)-C(63B)	-171(2)
Ir(1B)-P(2)-C(17)-C(20)	51.6(3)	C(57B)-C(62B)-C(63B)-C(64B)	3.4(16)
C(8)-P(2)-C(17)-C(19)	177.0(3)	C(61B)-C(62B)-C(63B)-C(64B)	176.7(13)
C(21)-P(2)-C(17)-C(19)	64.0(4)	C(62B)-C(63B)-C(64B)-C(56B)	-158.7(11)
Ir(1A)-P(2)-C(17)-C(19)	-66.8(4)	C(62B)-C(63B)-C(64B)-Ir(2B)	4.0(12)
Ir(1B)-P(2)-C(17)-C(19)	-63.3(4)	C(63B)-C(64B)-C(56B)-C(53)	88.3(10)
C(32A)-C(24A)-C(21)-C(22)	160.3(4)	Ir(2B)-C(64B)-C(56B)-C(53)	-74.8(8)
C(32A)-C(24A)-C(21)-C(23)	-82.3(5)	C(38)-C(33)-C(34)-C(35)	1.7(6)
C(32A)-C(24A)-C(21)-P(2)	37.4(4)	Ir(2B)-C(33)-C(34)-C(35)	-176.5(3)
C(62A)-C(57A)-C(58A)-C(59A)	1.7(7)	Ir(2A)-C(33)-C(34)-C(35)	178.4(3)
Ir(2A)-C(57A)-C(58A)-C(59A)	-173.8(4)	C(38)-C(33)-C(34)-C(39)	-178.1(3)
C(57A)-C(58A)-C(59A)-C(60A)	-1.2(8)	Ir(2B)-C(33)-C(34)-C(39)	3.7(5)
C(58A)-C(59A)-C(60A)-C(61A)	0.7(9)	Ir(2A)-C(33)-C(34)-C(39)	-1.4(5)
C(59A)-C(60A)-C(61A)-C(62A)	-0.8(9)	C(33)-C(34)-C(35)-C(36)	-1.4(6)
C(58A)-C(57A)-C(62A)-C(61A)	-1.8(7)	C(39)-C(34)-C(35)-C(36)	178.4(4)
Ir(2A)-C(57A)-C(62A)-C(61A)	174.4(4)	C(34)-C(35)-C(36)-C(37)	-0.4(6)
C(58A)-C(57A)-C(62A)-C(63A)	177.2(4)	C(35)-C(36)-C(37)-C(38)	1.9(6)

C(36)-C(37)-C(38)-C(33)	-1.7(6)	C(41)-P(3)-C(45)-C(46)	-65.1(4)
C(36)-C(37)-C(38)-C(40)	175.8(4)	Ir(2A)-P(3)-C(45)-C(46)	166.1(3)
C(34)-C(33)-C(38)-C(37)	-0.1(6)	Ir(2B)-P(3)-C(45)-C(46)	169.3(3)
Ir(2B)-C(33)-C(38)-C(37)	178.1(3)	C(40)-P(4)-C(49)-C(50)	58.2(4)
Ir(2A)-C(33)-C(38)-C(37)	-176.8(3)	C(53)-P(4)-C(49)-C(50)	-55.8(4)
C(34)-C(33)-C(38)-C(40)	-177.7(3)	Ir(2B)-P(4)-C(49)-C(50)	170.5(3)
Ir(2B)-C(33)-C(38)-C(40)	0.5(5)	Ir(2A)-P(4)-C(49)-C(50)	175.0(3)
Ir(2A)-C(33)-C(38)-C(40)	5.6(5)	C(40)-P(4)-C(49)-C(52)	-61.6(3)
C(35)-C(34)-C(39)-P(3)	157.9(3)	C(53)-P(4)-C(49)-C(52)	-175.6(3)
C(33)-C(34)-C(39)-P(3)	-22.3(4)	Ir(2B)-P(4)-C(49)-C(52)	50.8(4)
C(45)-P(3)-C(39)-C(34)	160.4(3)	Ir(2A)-P(4)-C(49)-C(52)	55.3(3)
C(41)-P(3)-C(39)-C(34)	-78.0(3)	C(40)-P(4)-C(49)-C(51)	-178.3(3)
Ir(2A)-P(3)-C(39)-C(34)	33.0(3)	C(53)-P(4)-C(49)-C(51)	67.7(3)
Ir(2B)-P(3)-C(39)-C(34)	28.6(3)	Ir(2B)-P(4)-C(49)-C(51)	-65.9(4)
C(37)-C(38)-C(40)-P(4)	156.7(3)	Ir(2A)-P(4)-C(49)-C(51)	-61.4(3)
C(33)-C(38)-C(40)-P(4)	-25.7(4)	C(64B)-C(56B)-C(53)-C(55)	-77.5(6)
C(49)-P(4)-C(40)-C(38)	163.2(3)	C(64B)-C(56B)-C(53)-C(54)	161.7(4)
C(53)-P(4)-C(40)-C(38)	-78.0(3)	C(64B)-C(56B)-C(53)-P(4)	38.6(6)
Ir(2B)-P(4)-C(40)-C(38)	34.8(3)	C(40)-P(4)-C(53)-C(55)	-149.8(3)
Ir(2A)-P(4)-C(40)-C(38)	31.2(3)	C(49)-P(4)-C(53)-C(55)	-36.9(4)
C(64A)-C(44A)-C(41)-C(42)	157.3(4)	Ir(2B)-P(4)-C(53)-C(55)	103.5(4)
C(64A)-C(44A)-C(41)-C(43)	-85.7(5)	Ir(2A)-P(4)-C(53)-C(55)	102.4(3)
C(64A)-C(44A)-C(41)-P(3)	34.6(5)	C(40)-P(4)-C(53)-C(54)	-24.1(4)
C(39)-P(3)-C(45)-C(47)	174.3(3)	C(49)-P(4)-C(53)-C(54)	88.8(4)
C(41)-P(3)-C(45)-C(47)	59.5(4)	Ir(2B)-P(4)-C(53)-C(54)	-130.8(3)
Ir(2A)-P(3)-C(45)-C(47)	-69.3(4)	Ir(2A)-P(4)-C(53)-C(54)	-131.9(3)
Ir(2B)-P(3)-C(45)-C(47)	-66.0(4)	C(40)-P(4)-C(53)-C(56B)	104.0(5)
C(39)-P(3)-C(45)-C(48)	-69.2(3)	C(49)-P(4)-C(53)-C(56B)	-143.1(5)
C(41)-P(3)-C(45)-C(48)	176.0(3)	Ir(2B)-P(4)-C(53)-C(56B)	-2.7(5)
Ir(2A)-P(3)-C(45)-C(48)	47.2(3)	C(40)-P(4)-C(53)-C(56A)	91.8(3)
Ir(2B)-P(3)-C(45)-C(48)	50.5(4)	C(49)-P(4)-C(53)-C(56A)	-155.3(3)
C(39)-P(3)-C(45)-C(46)	49.6(4)	Ir(2A)-P(4)-C(53)-C(56A)	-16.0(3)

3.5.9.7. Structural data for complex 8

CCDC # 1539913

Figure 3. 70. ORTEP diagram of complex 8

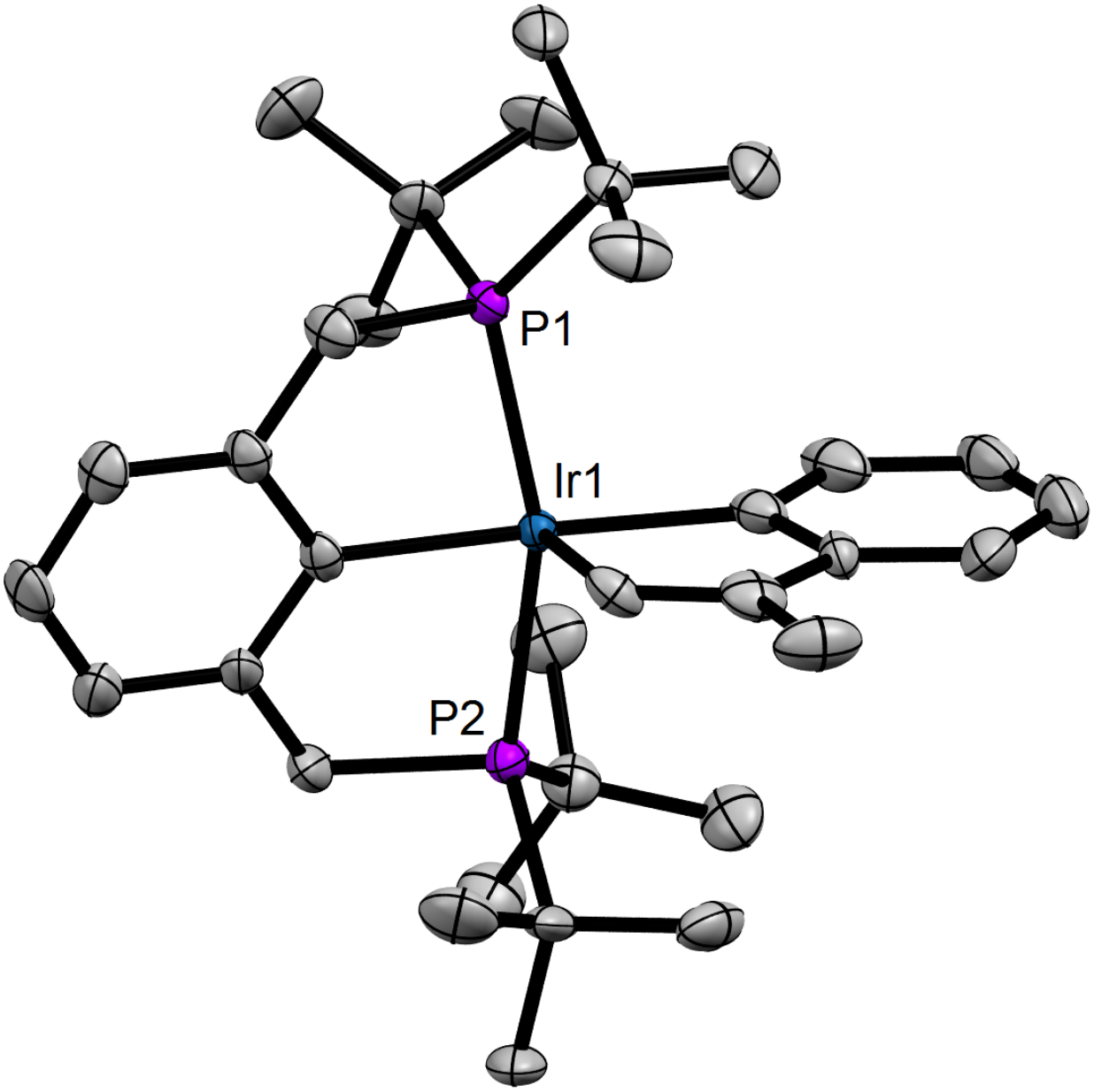

Table 3. 33. Crystal data and structure refinement for complex 8.

Identification code	irstyr-7-Me_Pbca	
Empirical formula	C33 H51 Ir P2	
Formula weight	701.87	
Temperature	100(2) K	
Wavelength	0.71073 Å	
Crystal system	Orthorhombic	
Space group	Pbca	
Unit cell dimensions	a = 13.7531(11) Å	α = 90°.
	b = 15.0329(12) Å	β = 90°.
	c = 29.851(2) Å	γ = 90°.
Volume	6171.7(8) $Å^3$	
Z	8	
Density (calculated)	1.511 Mg/m^3	
Absorption coefficient	4.450 mm^{-1}	
F(000)	2848	
Crystal size	0.480 x 0.060 x 0.010 mm^3	
Theta range for data collection	2.014 to 27.484°.	
Index ranges	$-17 \leq h \leq 17$, $-19 \leq k \leq 19$, $-38 \leq l \leq 38$	
Reflections collected	54694	
Independent reflections	7075 [R(int) = 0.1037]	
Completeness to theta = 25.242°	100.0 %	
Absorption correction	None	
Refinement method	Full-matrix least-squares on F^2	
Data / restraints / parameters	7075 / 0 / 338	
Goodness-of-fit on F^2	1.015	
Final R indices [I>2sigma(I)]	R1 = 0.0426, wR2 = 0.0816	
R indices (all data)	R1 = 0.0815, wR2 = 0.0943	
Extinction coefficient	n/a	
Largest diff. peak and hole	2.407 and -1.447 $e.Å^{-3}$	

Table 3. 34. Atomic coordinates (x 10^4) and equivalent isotropic displacement parameters ($Å^2$x 10^3) for complex 8.

U(eq) is defined as one third of the trace of the orthogonalized U^{ij} tensor.

	x	y	z	U(eq)
Ir(1)	1218(1)	896(1)	6232(1)	16(1)
P(1)	2850(1)	934(1)	6070(1)	17(1)
P(2)	-476(1)	904(1)	6140(1)	21(1)
C(1)	1162(5)	1573(4)	5622(2)	19(1)
C(2)	2004(5)	1958(4)	5430(2)	23(1)
C(3)	1973(6)	2401(4)	5022(2)	27(2)
C(4)	1099(5)	2491(4)	4796(2)	32(2)
C(5)	261(5)	2104(4)	4970(2)	30(2)
C(6)	297(5)	1640(4)	5372(2)	24(1)
C(7)	2938(5)	1884(4)	5689(2)	25(2)
C(8)	-578(4)	1128(5)	5531(2)	28(2)
C(9)	3076(5)	-73(4)	5708(2)	24(1)
C(10)	3423(5)	-862(5)	6000(3)	40(2)
C(11)	3755(6)	76(5)	5313(2)	42(2)
C(12)	2086(5)	-346(5)	5513(2)	32(2)
C(13)	3882(4)	1098(4)	6479(2)	24(1)
C(14)	3802(5)	463(5)	6867(2)	36(2)
C(15)	4886(4)	1016(5)	6245(2)	34(2)
C(16)	3809(6)	2044(5)	6675(3)	44(2)
C(17)	-1073(5)	-207(5)	6202(2)	31(2)
C(18)	-1295(6)	-401(5)	6697(2)	39(2)
C(19)	-2012(5)	-349(6)	5925(3)	42(2)
C(20)	-334(5)	-890(5)	6037(3)	40(2)
C(21)	-1242(5)	1798(5)	6400(2)	32(2)
C(22)	-1155(5)	1783(5)	6913(2)	38(2)
C(23)	-2329(4)	1724(5)	6282(2)	34(2)
C(24)	-869(5)	2687(5)	6218(3)	44(2)
C(25)	1268(5)	330(4)	6873(2)	27(1)

C(26)	1293(4)	987(4)	7219(2)	20(1)
C(27)	1309(5)	761(5)	7672(2)	40(2)
C(28)	1311(6)	-158(5)	7788(3)	43(2)
C(29)	1309(6)	-776(5)	7469(2)	40(2)
C(30)	1288(5)	-533(5)	7009(3)	40(2)
C(31)	1329(5)	1902(5)	7061(2)	31(2)
C(32)	1300(5)	1998(4)	6624(2)	24(1)
C(33)	1373(5)	2699(5)	7373(3)	42(2)

Table 3. 35. Bond lengths [Å] and angles [°] for complex 8.

Ir(1)-C(32)	2.030(6)	C(11)-H(11B)	0.9800
Ir(1)-C(1)	2.088(6)	C(11)-H(11C)	0.9800
Ir(1)-C(25)	2.095(6)	C(12)-H(12A)	0.9800
Ir(1)-P(1)	2.2970(15)	C(12)-H(12B)	0.9800
Ir(1)-P(2)	2.3455(15)	C(12)-H(12C)	0.9800
P(1)-C(7)	1.830(6)	C(13)-C(14)	1.506(9)
P(1)-C(9)	1.885(6)	C(13)-C(16)	1.542(9)
P(1)-C(13)	1.890(6)	C(13)-C(15)	1.553(9)
P(2)-C(8)	1.855(6)	C(14)-H(14A)	0.9800
P(2)-C(17)	1.870(7)	C(14)-H(14B)	0.9800
P(2)-C(21)	1.876(7)	C(14)-H(14C)	0.9800
C(1)-C(6)	1.408(8)	C(15)-H(15A)	0.9800
C(1)-C(2)	1.416(9)	C(15)-H(15B)	0.9800
C(2)-C(3)	1.387(9)	C(15)-H(15C)	0.9800
C(2)-C(7)	1.503(9)	C(16)-H(16A)	0.9800
C(3)-C(4)	1.385(10)	C(16)-H(16B)	0.9800
C(3)-H(3)	0.9500	C(16)-H(16C)	0.9800
C(4)-C(5)	1.390(10)	C(17)-C(20)	1.527(10)
C(4)-H(4)	0.9500	C(17)-C(18)	1.536(9)
C(5)-C(6)	1.389(9)	C(17)-C(19)	1.548(9)
C(5)-H(5)	0.9500	C(18)-H(18A)	0.9800
C(6)-C(8)	1.505(9)	C(18)-H(18B)	0.9800
C(7)-H(7A)	0.9900	C(18)-H(18C)	0.9800
C(7)-H(7B)	0.9900	C(19)-H(19A)	0.9800
C(8)-H(8A)	0.9900	C(19)-H(19B)	0.9800
C(8)-H(8B)	0.9900	C(19)-H(19C)	0.9800
C(9)-C(11)	1.520(9)	C(20)-H(20A)	0.9800
C(9)-C(12)	1.537(9)	C(20)-H(20B)	0.9800
C(9)-C(10)	1.547(9)	C(20)-H(20C)	0.9800
C(10)-H(10A)	0.9800	C(21)-C(24)	1.531(11)
C(10)-H(10B)	0.9800	C(21)-C(22)	1.534(9)
C(10)-H(10C)	0.9800	C(21)-C(23)	1.539(9)
C(11)-H(11A)	0.9800	C(22)-H(22A)	0.9800

C(22)-H(22B)	0.9800	C(27)-H(27)	0.9500
C(22)-H(22C)	0.9800	C(28)-C(29)	1.331(11)
C(23)-H(23A)	0.9800	C(28)-H(28)	0.9500
C(23)-H(23B)	0.9800	C(29)-C(30)	1.422(10)
C(23)-H(23C)	0.9800	C(29)-H(29)	0.9500
C(24)-H(24A)	0.9800	C(30)-H(30)	0.9500
C(24)-H(24B)	0.9800	C(31)-C(32)	1.313(9)
C(24)-H(24C)	0.9800	C(31)-C(33)	1.520(10)
C(25)-C(30)	1.360(9)	C(32)-H(32)	0.9500
C(25)-C(26)	1.431(9)	C(33)-H(33A)	0.9800
C(26)-C(27)	1.393(9)	C(33)-H(33B)	0.9800
C(26)-C(31)	1.456(9)	C(33)-H(33C)	0.9800
C(27)-C(28)	1.425(11)		

C(32)-Ir(1)-C(1)	96.1(2)	C(6)-C(1)-C(2)	116.6(5)
C(32)-Ir(1)-C(25)	78.7(2)	C(6)-C(1)-Ir(1)	121.8(5)
C(1)-Ir(1)-C(25)	174.8(2)	C(2)-C(1)-Ir(1)	121.5(4)
C(32)-Ir(1)-P(1)	92.68(19)	C(3)-C(2)-C(1)	121.7(6)
C(1)-Ir(1)-P(1)	80.77(18)	C(3)-C(2)-C(7)	120.9(6)
C(25)-Ir(1)-P(1)	99.80(18)	C(1)-C(2)-C(7)	117.4(5)
C(32)-Ir(1)-P(2)	96.81(19)	C(4)-C(3)-C(2)	120.0(7)
C(1)-Ir(1)-P(2)	81.92(18)	C(4)-C(3)-H(3)	120.0
C(25)-Ir(1)-P(2)	98.14(18)	C(2)-C(3)-H(3)	120.0
P(1)-Ir(1)-P(2)	161.05(5)	C(3)-C(4)-C(5)	119.8(6)
C(7)-P(1)-C(9)	105.1(3)	C(3)-C(4)-H(4)	120.1
C(7)-P(1)-C(13)	104.5(3)	C(5)-C(4)-H(4)	120.1
C(9)-P(1)-C(13)	110.6(3)	C(6)-C(5)-C(4)	120.2(6)
C(7)-P(1)-Ir(1)	102.4(2)	C(6)-C(5)-H(5)	119.9
C(9)-P(1)-Ir(1)	105.2(2)	C(4)-C(5)-H(5)	119.9
C(13)-P(1)-Ir(1)	126.9(2)	C(5)-C(6)-C(1)	121.5(6)
C(8)-P(2)-C(17)	103.0(3)	C(5)-C(6)-C(8)	120.1(6)
C(8)-P(2)-C(21)	103.5(3)	C(1)-C(6)-C(8)	118.2(5)
C(17)-P(2)-C(21)	110.6(3)	C(2)-C(7)-P(1)	108.7(4)
C(8)-P(2)-Ir(1)	101.0(2)	C(2)-C(7)-H(7A)	109.9
C(17)-P(2)-Ir(1)	114.8(2)	P(1)-C(7)-H(7A)	109.9
C(21)-P(2)-Ir(1)	120.9(2)	C(2)-C(7)-H(7B)	109.9

P(1)-C(7)-H(7B)	109.9	C(16)-C(13)-P(1)	108.5(4)
H(7A)-C(7)-H(7B)	108.3	C(15)-C(13)-P(1)	111.5(4)
C(6)-C(8)-P(2)	109.9(4)	C(13)-C(14)-H(14A)	109.5
C(6)-C(8)-H(8A)	109.7	C(13)-C(14)-H(14B)	109.5
P(2)-C(8)-H(8A)	109.7	H(14A)-C(14)-H(14B)	109.5
C(6)-C(8)-H(8B)	109.7	C(13)-C(14)-H(14C)	109.5
P(2)-C(8)-H(8B)	109.7	H(14A)-C(14)-H(14C)	109.5
H(8A)-C(8)-H(8B)	108.2	H(14B)-C(14)-H(14C)	109.5
C(11)-C(9)-C(12)	106.8(6)	C(13)-C(15)-H(15A)	109.5
C(11)-C(9)-C(10)	111.1(6)	C(13)-C(15)-H(15B)	109.5
C(12)-C(9)-C(10)	106.4(6)	H(15A)-C(15)-H(15B)	109.5
C(11)-C(9)-P(1)	115.3(5)	C(13)-C(15)-H(15C)	109.5
C(12)-C(9)-P(1)	106.6(4)	H(15A)-C(15)-H(15C)	109.5
C(10)-C(9)-P(1)	110.1(5)	H(15B)-C(15)-H(15C)	109.5
C(9)-C(10)-H(10A)	109.5	C(13)-C(16)-H(16A)	109.5
C(9)-C(10)-H(10B)	109.5	C(13)-C(16)-H(16B)	109.5
H(10A)-C(10)-H(10B)	109.5	H(16A)-C(16)-H(16B)	109.5
C(9)-C(10)-H(10C)	109.5	C(13)-C(16)-H(16C)	109.5
H(10A)-C(10)-H(10C)	109.5	H(16A)-C(16)-H(16C)	109.5
H(10B)-C(10)-H(10C)	109.5	H(16B)-C(16)-H(16C)	109.5
C(9)-C(11)-H(11A)	109.5	C(20)-C(17)-C(18)	108.3(6)
C(9)-C(11)-H(11B)	109.5	C(20)-C(17)-C(19)	106.9(6)
H(11A)-C(11)-H(11B)	109.5	C(18)-C(17)-C(19)	108.8(6)
C(9)-C(11)-H(11C)	109.5	C(20)-C(17)-P(2)	106.1(4)
H(11A)-C(11)-H(11C)	109.5	C(18)-C(17)-P(2)	110.6(5)
H(11B)-C(11)-H(11C)	109.5	C(19)-C(17)-P(2)	115.9(5)
C(9)-C(12)-H(12A)	109.5	C(17)-C(18)-H(18A)	109.5
C(9)-C(12)-H(12B)	109.5	C(17)-C(18)-H(18B)	109.5
H(12A)-C(12)-H(12B)	109.5	H(18A)-C(18)-H(18B)	109.5
C(9)-C(12)-H(12C)	109.5	C(17)-C(18)-H(18C)	109.5
H(12A)-C(12)-H(12C)	109.5	H(18A)-C(18)-H(18C)	109.5
H(12B)-C(12)-H(12C)	109.5	H(18B)-C(18)-H(18C)	109.5
C(14)-C(13)-C(16)	106.7(6)	C(17)-C(19)-H(19A)	109.5
C(14)-C(13)-C(15)	111.2(5)	C(17)-C(19)-H(19B)	109.5
C(16)-C(13)-C(15)	107.6(6)	H(19A)-C(19)-H(19B)	109.5
C(14)-C(13)-P(1)	111.1(4)	C(17)-C(19)-H(19C)	109.5

H(19A)-C(19)-H(19C)	109.5	H(24B)-C(24)-H(24C)	109.5
H(19B)-C(19)-H(19C)	109.5	C(30)-C(25)-C(26)	116.3(6)
C(17)-C(20)-H(20A)	109.5	C(30)-C(25)-Ir(1)	131.3(6)
C(17)-C(20)-H(20B)	109.5	C(26)-C(25)-Ir(1)	112.4(4)
H(20A)-C(20)-H(20B)	109.5	C(27)-C(26)-C(25)	122.2(6)
C(17)-C(20)-H(20C)	109.5	C(27)-C(26)-C(31)	123.1(6)
H(20A)-C(20)-H(20C)	109.5	C(25)-C(26)-C(31)	114.7(5)
H(20B)-C(20)-H(20C)	109.5	C(26)-C(27)-C(28)	118.2(7)
C(24)-C(21)-C(22)	109.9(6)	C(26)-C(27)-H(27)	120.9
C(24)-C(21)-C(23)	107.9(6)	C(28)-C(27)-H(27)	120.9
C(22)-C(21)-C(23)	107.6(6)	C(29)-C(28)-C(27)	120.1(7)
C(24)-C(21)-P(2)	106.9(5)	C(29)-C(28)-H(28)	119.9
C(22)-C(21)-P(2)	111.0(5)	C(27)-C(28)-H(28)	119.9
C(23)-C(21)-P(2)	113.5(5)	C(28)-C(29)-C(30)	120.9(7)
C(21)-C(22)-H(22A)	109.5	C(28)-C(29)-H(29)	119.5
C(21)-C(22)-H(22B)	109.5	C(30)-C(29)-H(29)	119.5
H(22A)-C(22)-H(22B)	109.5	C(25)-C(30)-C(29)	122.2(8)
C(21)-C(22)-H(22C)	109.5	C(25)-C(30)-H(30)	118.9
H(22A)-C(22)-H(22C)	109.5	C(29)-C(30)-H(30)	118.9
H(22B)-C(22)-H(22C)	109.5	C(32)-C(31)-C(26)	115.2(6)
C(21)-C(23)-H(23A)	109.5	C(32)-C(31)-C(33)	121.7(7)
C(21)-C(23)-H(23B)	109.5	C(26)-C(31)-C(33)	123.1(6)
H(23A)-C(23)-H(23B)	109.5	C(31)-C(32)-Ir(1)	119.0(5)
C(21)-C(23)-H(23C)	109.5	C(31)-C(32)-H(32)	120.5
H(23A)-C(23)-H(23C)	109.5	Ir(1)-C(32)-H(32)	120.5
H(23B)-C(23)-H(23C)	109.5	C(31)-C(33)-H(33A)	109.5
C(21)-C(24)-H(24A)	109.5	C(31)-C(33)-H(33B)	109.5
C(21)-C(24)-H(24B)	109.5	H(33A)-C(33)-H(33B)	109.5
H(24A)-C(24)-H(24B)	109.5	C(31)-C(33)-H(33C)	109.5
C(21)-C(24)-H(24C)	109.5	H(33A)-C(33)-H(33C)	109.5
H(24A)-C(24)-H(24C)	109.5	H(33B)-C(33)-H(33C)	109.5

Table 3. 36. Anisotropic displacement parameters ($Å^2$x 10^3) for complex 8.

The anisotropic displacement factor exponent takes the form: $-2\pi^2[h^2 a^{*2}U^{11} + ... + 2 h k a^* b^* U^{12}]$

	U^{11}	U^{22}	U^{33}	U^{23}	U^{13}	U^{12}
Ir(1)	16(1)	17(1)	14(1)	0(1)	-1(1)	-1(1)
P(1)	16(1)	16(1)	19(1)	2(1)	-1(1)	-1(1)
P(2)	18(1)	28(1)	16(1)	-2(1)	-1(1)	-1(1)
C(1)	25(3)	15(3)	18(3)	0(2)	-2(3)	3(3)
C(2)	27(3)	18(3)	25(3)	5(3)	-1(3)	2(3)
C(3)	35(4)	19(4)	28(4)	6(3)	3(3)	-3(3)
C(4)	43(5)	26(4)	28(4)	12(3)	-3(3)	9(3)
C(5)	34(4)	33(4)	22(3)	2(3)	3(3)	9(3)
C(6)	27(3)	29(4)	17(3)	2(3)	2(3)	12(3)
C(7)	24(3)	19(3)	32(4)	8(3)	-2(3)	-2(3)
C(8)	21(3)	43(4)	19(3)	0(3)	-3(2)	5(3)
C(9)	29(3)	18(3)	26(3)	-1(3)	3(3)	7(3)
C(10)	38(4)	21(4)	60(5)	5(4)	-6(4)	13(3)
C(11)	45(4)	48(5)	34(4)	-11(3)	14(4)	6(4)
C(12)	31(4)	24(4)	40(4)	-8(3)	-6(3)	5(3)
C(13)	16(3)	36(4)	21(3)	-1(3)	-4(2)	-4(3)
C(14)	24(3)	59(5)	24(3)	1(3)	-7(3)	-4(4)
C(15)	21(3)	51(5)	30(3)	9(4)	-2(3)	-4(3)
C(16)	31(4)	46(5)	55(5)	-16(4)	-15(4)	-2(4)
C(17)	28(4)	33(4)	31(4)	0(3)	-1(3)	-4(3)
C(18)	32(4)	42(4)	43(4)	10(3)	2(4)	-13(4)
C(19)	31(4)	54(5)	41(4)	-5(4)	-6(3)	-12(4)
C(20)	39(4)	29(4)	52(4)	-3(4)	5(4)	-10(4)
C(21)	16(3)	53(4)	26(3)	-6(3)	-2(3)	14(3)
C(22)	25(4)	57(5)	33(4)	-18(3)	2(3)	7(4)
C(23)	15(3)	55(5)	33(4)	3(4)	1(3)	6(3)
C(24)	40(4)	32(4)	59(5)	-1(4)	-2(4)	14(3)
C(25)	17(3)	30(4)	34(3)	6(3)	-1(3)	3(3)
C(26)	20(3)	24(3)	17(3)	4(2)	-3(2)	-2(3)
C(27)	27(4)	63(5)	28(3)	4(4)	6(3)	4(4)

C(28)	34(4)	58(5)	38(4)	25(4)	-3(4)	1(4)
C(29)	31(4)	41(4)	49(4)	24(4)	0(3)	6(5)
C(30)	25(4)	40(4)	54(5)	15(4)	0(4)	3(4)
C(31)	19(3)	37(4)	38(4)	-6(3)	-8(3)	-3(3)
C(32)	24(3)	20(3)	30(3)	-1(3)	-11(3)	1(3)
C(33)	29(4)	37(4)	61(5)	-23(4)	0(4)	1(4)

Table 3. 37. Hydrogen coordinates (x 10^4) and isotropic displacement parameters ($Å^2$x 10^3) for complex 8.

	x	y	z	U(eq)
H(3)	2552	2642	4898	33
H(4)	1071	2816	4524	39
H(5)	-337	2157	4813	36
H(7A)	3051	2436	5862	30
H(7B)	3490	1800	5480	30
H(8A)	-625	558	5365	33
H(8B)	-1176	1475	5470	33
H(10A)	3526	-1385	5810	59
H(10B)	2928	-997	6226	59
H(10C)	4033	-703	6149	59
H(11A)	3843	-485	5151	64
H(11B)	4386	287	5423	64
H(11C)	3473	521	5112	64
H(12A)	1846	125	5315	48
H(12B)	1621	-439	5757	48
H(12C)	2158	-899	5342	48
H(14A)	4336	571	7078	54
H(14B)	3837	-150	6757	54
H(14C)	3179	555	7020	54
H(15A)	5399	1204	6452	51
H(15B)	4898	1397	5978	51
H(15C)	4996	397	6156	51
H(16A)	3158	2135	6801	66
H(16B)	3925	2482	6438	66
H(16C)	4297	2118	6912	66
H(18A)	-1493	-1024	6730	58
H(18B)	-1822	-12	6799	58
H(18C)	-712	-291	6877	58
H(19A)	-1871	-254	5607	63

H(19B)	-2510	74	6023	63
H(19C)	-2248	-957	5970	63
H(20A)	279	-815	6201	60
H(20B)	-219	-804	5716	60
H(20C)	-586	-1491	6089	60
H(22A)	-478	1894	6999	58
H(22B)	-1359	1200	7025	58
H(22C)	-1573	2246	7041	58
H(23A)	-2606	1199	6429	52
H(23B)	-2403	1669	5957	52
H(23C)	-2670	2258	6386	52
H(24A)	-1225	3176	6361	66
H(24B)	-969	2709	5894	66
H(24C)	-174	2745	6285	66
H(27)	1319	1208	7897	48
H(28)	1313	-330	8095	52
H(29)	1321	-1387	7550	48
H(30)	1289	-990	6788	47
H(32)	1318	2573	6493	29
H(33A)	1451	3244	7197	63
H(33B)	1926	2633	7578	63
H(33C)	769	2733	7547	63

Table 3. 38. Torsion angles [°] for complex 8.

C(6)-C(1)-C(2)-C(3)	1.8(9)	C(7)-P(1)-C(13)-C(14)	169.5(5)
Ir(1)-C(1)-C(2)-C(3)	179.3(5)	C(9)-P(1)-C(13)-C(14)	-77.9(5)
C(6)-C(1)-C(2)-C(7)	-179.3(5)	Ir(1)-P(1)-C(13)-C(14)	51.3(6)
Ir(1)-C(1)-C(2)-C(7)	-1.8(8)	C(7)-P(1)-C(13)-C(16)	52.5(5)
C(1)-C(2)-C(3)-C(4)	1.3(10)	C(9)-P(1)-C(13)-C(16)	165.1(5)
C(7)-C(2)-C(3)-C(4)	-177.6(6)	Ir(1)-P(1)-C(13)-C(16)	-65.7(5)
C(2)-C(3)-C(4)-C(5)	-2.8(10)	C(7)-P(1)-C(13)-C(15)	-65.9(5)
C(3)-C(4)-C(5)-C(6)	1.0(10)	C(9)-P(1)-C(13)-C(15)	46.7(5)
C(4)-C(5)-C(6)-C(1)	2.2(10)	Ir(1)-P(1)-C(13)-C(15)	176.0(4)
C(4)-C(5)-C(6)-C(8)	-172.5(6)	C(8)-P(2)-C(17)-C(20)	77.3(5)
C(2)-C(1)-C(6)-C(5)	-3.6(9)	C(21)-P(2)-C(17)-C(20)	-172.7(5)
Ir(1)-C(1)-C(6)-C(5)	178.9(5)	Ir(1)-P(2)-C(17)-C(20)	-31.5(5)
C(2)-C(1)-C(6)-C(8)	171.3(6)	C(8)-P(2)-C(17)-C(18)	-165.5(5)
Ir(1)-C(1)-C(6)-C(8)	-6.2(8)	C(21)-P(2)-C(17)-C(18)	-55.4(5)
C(3)-C(2)-C(7)-P(1)	-157.8(5)	Ir(1)-P(2)-C(17)-C(18)	85.7(5)
C(1)-C(2)-C(7)-P(1)	23.3(7)	C(8)-P(2)-C(17)-C(19)	-41.1(6)
C(9)-P(1)-C(7)-C(2)	78.8(5)	C(21)-P(2)-C(17)-C(19)	69.0(6)
C(13)-P(1)-C(7)-C(2)	-164.8(4)	Ir(1)-P(2)-C(17)-C(19)	-149.9(4)
Ir(1)-P(1)-C(7)-C(2)	-30.9(5)	C(8)-P(2)-C(21)-C(24)	-53.9(5)
C(5)-C(6)-C(8)-P(2)	-161.2(5)	C(17)-P(2)-C(21)-C(24)	-163.7(5)
C(1)-C(6)-C(8)-P(2)	23.9(7)	Ir(1)-P(2)-C(21)-C(24)	57.9(5)
C(17)-P(2)-C(8)-C(6)	-146.3(5)	C(8)-P(2)-C(21)-C(22)	-173.7(5)
C(21)-P(2)-C(8)-C(6)	98.4(5)	C(17)-P(2)-C(21)-C(22)	76.5(6)
Ir(1)-P(2)-C(8)-C(6)	-27.3(5)	Ir(1)-P(2)-C(21)-C(22)	-61.9(6)
C(7)-P(1)-C(9)-C(11)	31.0(6)	C(8)-P(2)-C(21)-C(23)	65.0(6)
C(13)-P(1)-C(9)-C(11)	-81.2(6)	C(17)-P(2)-C(21)-C(23)	-44.8(6)
Ir(1)-P(1)-C(9)-C(11)	138.7(5)	Ir(1)-P(2)-C(21)-C(23)	176.8(4)
C(7)-P(1)-C(9)-C(12)	-87.3(5)	C(30)-C(25)-C(26)-C(27)	-1.7(10)
C(13)-P(1)-C(9)-C(12)	160.5(4)	Ir(1)-C(25)-C(26)-C(27)	178.7(5)
Ir(1)-P(1)-C(9)-C(12)	20.4(5)	C(30)-C(25)-C(26)-C(31)	176.5(6)
C(7)-P(1)-C(9)-C(10)	157.6(5)	Ir(1)-C(25)-C(26)-C(31)	-3.1(7)
C(13)-P(1)-C(9)-C(10)	45.4(5)	C(25)-C(26)-C(27)-C(28)	0.6(10)
Ir(1)-P(1)-C(9)-C(10)	-94.7(5)	C(31)-C(26)-C(27)-C(28)	-177.4(6)

C(26)-C(27)-C(28)-C(29)	0.8(11)	C(25)-C(26)-C(31)-C(32)	2.3(9)
C(27)-C(28)-C(29)-C(30)	-1.1(12)	C(27)-C(26)-C(31)-C(33)	-1.0(10)
C(26)-C(25)-C(30)-C(29)	1.5(11)	C(25)-C(26)-C(31)-C(33)	-179.2(6)
Ir(1)-C(25)-C(30)-C(29)	-179.1(5)	C(26)-C(31)-C(32)-Ir(1)	-0.3(8)
C(28)-C(29)-C(30)-C(25)	-0.1(12)	C(33)-C(31)-C(32)-Ir(1)	-178.9(5)
C(27)-C(26)-C(31)-C(32)	-179.5(6)		

3.5.9.8. Structural data for complex 9

CCDC # 1539909

Figure 3. 71. ORTEP diagram of complex 9

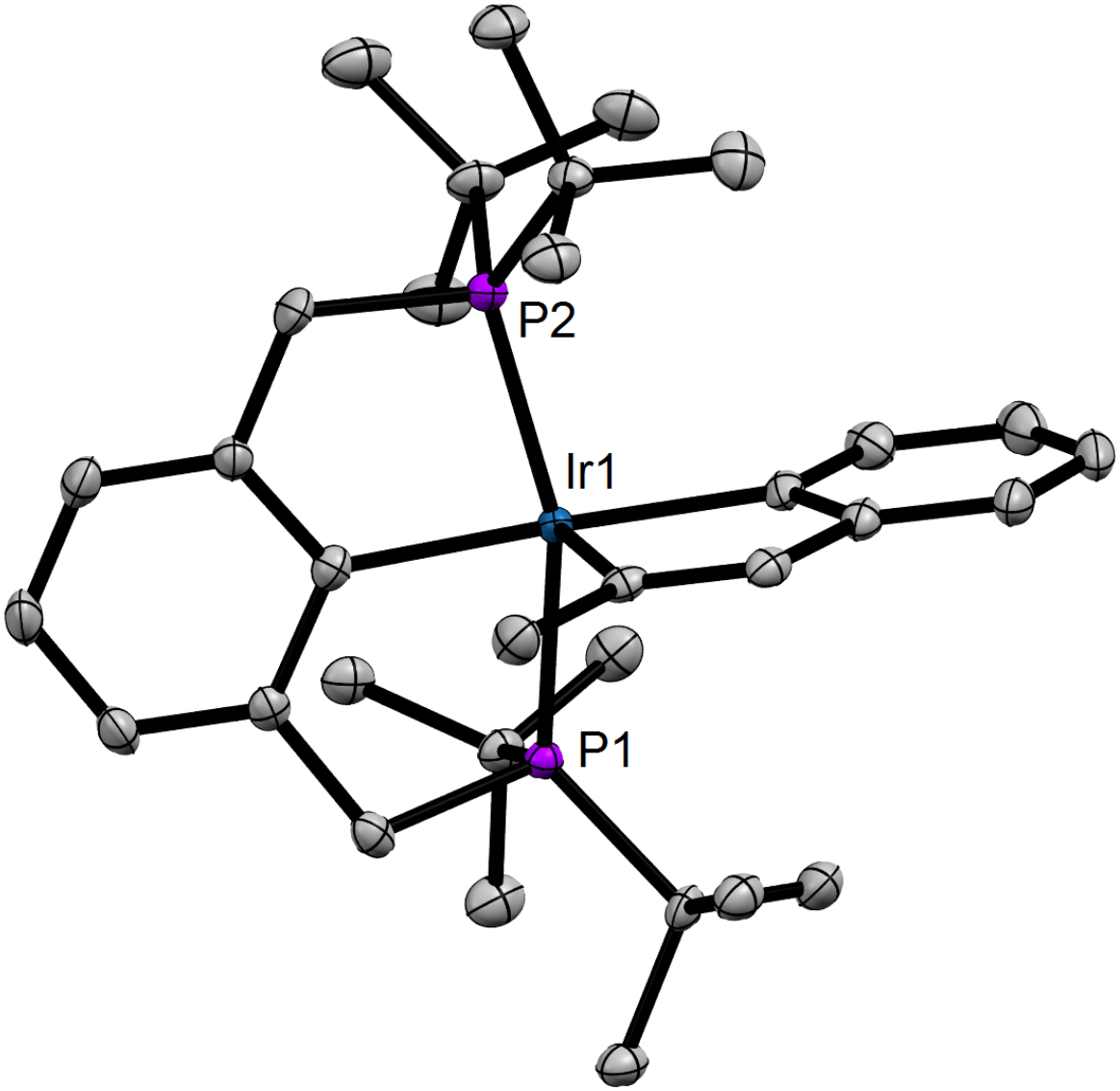

Table 3. 39. Crystal data and structure refinement for complex 9.

Identification code	irh_8_Me_styrene_P21n_a	
Empirical formula	C33 H51 Ir P2	
Formula weight	701.87	
Temperature	120(2) K	
Wavelength	0.71073 Å	
Crystal system	Monoclinic	
Space group	$P2_1/n$	
Unit cell dimensions	a = 8.8197(13) Å	α = 90°.
	b = 17.897(3) Å	β = 99.715(3)°.
	c = 19.538(3) Å	γ = 90°.
Volume	3039.8(8) $Å^3$	
Z	4	
Density (calculated)	1.534 Mg/m^3	
Absorption coefficient	4.518 mm^{-1}	
F(000)	1424	
Crystal size	0.200 x 0.100 x 0.050 mm^3	
Theta range for data collection	1.553 to 27.905°.	
Index ranges	$-11 \leq h \leq 11$, $-22 \leq k \leq 23$, $-23 \leq l \leq 25$	
Reflections collected	14659	
Independent reflections	6986 [R(int) = 0.0321]	
Completeness to theta = 25.242°	97.6 %	
Absorption correction	Semi-empirical from equivalents	
Max. and min. transmission	0.7457 and 0.5848	
Refinement method	Full-matrix least-squares on F^2	
Data / restraints / parameters	6986 / 0 / 338	
Goodness-of-fit on F^2	1.031	
Final R indices [I>2sigma(I)]	R1 = 0.0283, wR2 = 0.0647	
R indices (all data)	R1 = 0.0351, wR2 = 0.0674	
Extinction coefficient	n/a	
Largest diff. peak and hole	1.938 and -0.680 $e.Å^{-3}$	

Table 3. 40. Atomic coordinates (x 10^4) and equivalent isotropic displacement parameters (Å^{2}x 10^3) for complex 9.

U(eq) is defined as one third of the trace of the orthogonalized U^{ij} tensor.

	x	y	z	U(eq)
Ir(1)	4763(1)	6169(1)	7050(1)	11(1)
P(1)	3828(1)	6726(1)	5973(1)	13(1)
P(2)	4969(1)	5359(1)	7985(1)	14(1)
C(1)	3876(4)	5212(2)	6505(2)	16(1)
C(2)	3333(3)	5227(2)	5777(2)	15(1)
C(3)	2552(4)	4626(2)	5436(2)	21(1)
C(4)	2355(4)	3974(2)	5792(2)	23(1)
C(5)	2963(4)	3920(2)	6491(2)	21(1)
C(6)	3712(4)	4529(2)	6839(2)	16(1)
C(7)	3636(4)	5924(2)	5379(2)	17(1)
C(8)	4465(4)	4436(2)	7596(2)	21(1)
C(9)	1769(3)	7059(2)	5916(2)	16(1)
C(10)	1640(4)	7595(2)	6516(2)	23(1)
C(11)	1100(4)	7447(2)	5228(2)	25(1)
C(12)	743(4)	6376(2)	5977(2)	19(1)
C(13)	4928(4)	7442(2)	5547(2)	16(1)
C(14)	4754(4)	8222(2)	5848(2)	23(1)
C(15)	4486(4)	7452(2)	4751(2)	20(1)
C(16)	6639(4)	7242(2)	5709(2)	22(1)
C(17)	3290(4)	5610(2)	8426(2)	21(1)
C(18)	3718(5)	6241(2)	8960(2)	28(1)
C(19)	2540(4)	4965(3)	8763(2)	32(1)
C(20)	2099(4)	5912(2)	7827(2)	29(1)
C(21)	6737(4)	5160(2)	8650(2)	17(1)
C(22)	7421(4)	5883(2)	8989(2)	26(1)
C(23)	6387(4)	4620(2)	9206(2)	24(1)
C(24)	7976(4)	4812(2)	8282(2)	24(1)
C(25)	5777(4)	7127(2)	7569(2)	16(1)

C(26)	5157(4)	7725(2)	7888(2)	22(1)
C(27)	6058(5)	8306(2)	8212(2)	27(1)
C(28)	7635(4)	8304(2)	8228(2)	26(1)
C(29)	8306(4)	7726(2)	7910(2)	21(1)
C(30)	7395(4)	7148(2)	7586(2)	16(1)
C(31)	7970(4)	6523(2)	7240(2)	16(1)
C(32)	6961(4)	6017(2)	6930(2)	15(1)
C(33)	7392(4)	5367(2)	6526(2)	21(1)

Table 3. 41. Bond lengths [Å] and angles [°] for complex 9.

Ir(1)-C(32)	2.010(3)	C(11)-H(11B)	0.9800
Ir(1)-C(1)	2.098(3)	C(11)-H(11C)	0.9800
Ir(1)-C(25)	2.112(3)	C(12)-H(12A)	0.9800
Ir(1)-P(2)	2.3152(9)	C(12)-H(12B)	0.9800
Ir(1)-P(1)	2.3483(9)	C(12)-H(12C)	0.9800
P(1)-C(7)	1.837(4)	C(13)-C(16)	1.532(4)
P(1)-C(13)	1.883(3)	C(13)-C(14)	1.532(5)
P(1)-C(9)	1.897(3)	C(13)-C(15)	1.539(5)
P(2)-C(8)	1.840(4)	C(14)-H(14A)	0.9800
P(2)-C(21)	1.888(3)	C(14)-H(14B)	0.9800
P(2)-C(17)	1.889(3)	C(14)-H(14C)	0.9800
C(1)-C(6)	1.404(5)	C(15)-H(15A)	0.9800
C(1)-C(2)	1.422(5)	C(15)-H(15B)	0.9800
C(2)-C(3)	1.385(5)	C(15)-H(15C)	0.9800
C(2)-C(7)	1.517(5)	C(16)-H(16A)	0.9800
C(3)-C(4)	1.385(5)	C(16)-H(16B)	0.9800
C(3)-H(3)	0.9500	C(16)-H(16C)	0.9800
C(4)-C(5)	1.384(5)	C(17)-C(20)	1.533(5)
C(4)-H(4)	0.9500	C(17)-C(19)	1.534(5)
C(5)-C(6)	1.390(5)	C(17)-C(18)	1.539(5)
C(5)-H(5)	0.9500	C(18)-H(18A)	0.9800
C(6)-C(8)	1.526(5)	C(18)-H(18B)	0.9800
C(7)-H(7A)	0.9900	C(18)-H(18C)	0.9800
C(7)-H(7B)	0.9900	C(19)-H(19A)	0.9800
C(8)-H(8A)	0.9900	C(19)-H(19B)	0.9800
C(8)-H(8B)	0.9900	C(19)-H(19C)	0.9800
C(9)-C(10)	1.533(5)	C(20)-H(20A)	0.9800
C(9)-C(12)	1.538(5)	C(20)-H(20B)	0.9800
C(9)-C(11)	1.540(5)	C(20)-H(20C)	0.9800
C(10)-H(10A)	0.9800	C(21)-C(23)	1.523(5)
C(10)-H(10B)	0.9800	C(21)-C(22)	1.530(5)
C(10)-H(10C)	0.9800	C(21)-C(24)	1.538(5)
C(11)-H(11A)	0.9800	C(22)-H(22A)	0.9800

C(22)-H(22B)	0.9800	C(27)-H(27)	0.9500
C(22)-H(22C)	0.9800	C(28)-C(29)	1.389(5)
C(23)-H(23A)	0.9800	C(28)-H(28)	0.9500
C(23)-H(23B)	0.9800	C(29)-C(30)	1.394(5)
C(23)-H(23C)	0.9800	C(29)-H(29)	0.9500
C(24)-H(24A)	0.9800	C(30)-C(31)	1.442(5)
C(24)-H(24B)	0.9800	C(31)-C(32)	1.341(5)
C(24)-H(24C)	0.9800	C(31)-H(31)	0.9500
C(25)-C(26)	1.397(5)	C(32)-C(33)	1.492(5)
C(25)-C(30)	1.422(5)	C(33)-H(33A)	0.9800
C(26)-C(27)	1.394(5)	C(33)-H(33B)	0.9800
C(26)-H(26)	0.9500	C(33)-H(33C)	0.9800
C(27)-C(28)	1.386(6)		

C(32)-Ir(1)-C(1)	96.57(13)	C(6)-C(1)-C(2)	116.0(3)
C(32)-Ir(1)-C(25)	80.04(14)	C(6)-C(1)-Ir(1)	122.3(2)
C(1)-Ir(1)-C(25)	176.44(12)	C(2)-C(1)-Ir(1)	121.7(3)
C(32)-Ir(1)-P(2)	93.35(10)	C(3)-C(2)-C(1)	121.4(3)
C(1)-Ir(1)-P(2)	82.07(10)	C(3)-C(2)-C(7)	120.6(3)
C(25)-Ir(1)-P(2)	99.13(9)	C(1)-C(2)-C(7)	118.0(3)
C(32)-Ir(1)-P(1)	98.76(10)	C(4)-C(3)-C(2)	120.5(3)
C(1)-Ir(1)-P(1)	81.25(10)	C(4)-C(3)-H(3)	119.7
C(25)-Ir(1)-P(1)	98.14(9)	C(2)-C(3)-H(3)	119.7
P(2)-Ir(1)-P(1)	160.37(3)	C(5)-C(4)-C(3)	119.5(3)
C(7)-P(1)-C(13)	104.58(16)	C(5)-C(4)-H(4)	120.2
C(7)-P(1)-C(9)	102.91(15)	C(3)-C(4)-H(4)	120.2
C(13)-P(1)-C(9)	108.66(15)	C(4)-C(5)-C(6)	120.1(3)
C(7)-P(1)-Ir(1)	102.42(12)	C(4)-C(5)-H(5)	119.9
C(13)-P(1)-Ir(1)	123.79(11)	C(6)-C(5)-H(5)	119.9
C(9)-P(1)-Ir(1)	111.93(11)	C(5)-C(6)-C(1)	122.2(3)
C(8)-P(2)-C(21)	103.22(16)	C(5)-C(6)-C(8)	118.8(3)
C(8)-P(2)-C(17)	104.40(17)	C(1)-C(6)-C(8)	118.9(3)
C(21)-P(2)-C(17)	110.50(16)	C(2)-C(7)-P(1)	108.9(2)
C(8)-P(2)-Ir(1)	104.76(12)	C(2)-C(7)-H(7A)	109.9
C(21)-P(2)-Ir(1)	127.42(11)	P(1)-C(7)-H(7A)	109.9
C(17)-P(2)-Ir(1)	104.35(12)	C(2)-C(7)-H(7B)	109.9

P(1)-C(7)-H(7B)	109.9	C(14)-C(13)-P(1)	111.0(2)
H(7A)-C(7)-H(7B)	108.3	C(15)-C(13)-P(1)	113.2(2)
C(6)-C(8)-P(2)	109.8(2)	C(13)-C(14)-H(14A)	109.5
C(6)-C(8)-H(8A)	109.7	C(13)-C(14)-H(14B)	109.5
P(2)-C(8)-H(8A)	109.7	H(14A)-C(14)-H(14B)	109.5
C(6)-C(8)-H(8B)	109.7	C(13)-C(14)-H(14C)	109.5
P(2)-C(8)-H(8B)	109.7	H(14A)-C(14)-H(14C)	109.5
H(8A)-C(8)-H(8B)	108.2	H(14B)-C(14)-H(14C)	109.5
C(10)-C(9)-C(12)	108.5(3)	C(13)-C(15)-H(15A)	109.5
C(10)-C(9)-C(11)	108.6(3)	C(13)-C(15)-H(15B)	109.5
C(12)-C(9)-C(11)	106.4(3)	H(15A)-C(15)-H(15B)	109.5
C(10)-C(9)-P(1)	110.2(2)	C(13)-C(15)-H(15C)	109.5
C(12)-C(9)-P(1)	108.4(2)	H(15A)-C(15)-H(15C)	109.5
C(11)-C(9)-P(1)	114.5(2)	H(15B)-C(15)-H(15C)	109.5
C(9)-C(10)-H(10A)	109.5	C(13)-C(16)-H(16A)	109.5
C(9)-C(10)-H(10B)	109.5	C(13)-C(16)-H(16B)	109.5
H(10A)-C(10)-H(10B)	109.5	H(16A)-C(16)-H(16B)	109.5
C(9)-C(10)-H(10C)	109.5	C(13)-C(16)-H(16C)	109.5
H(10A)-C(10)-H(10C)	109.5	H(16A)-C(16)-H(16C)	109.5
H(10B)-C(10)-H(10C)	109.5	H(16B)-C(16)-H(16C)	109.5
C(9)-C(11)-H(11A)	109.5	C(20)-C(17)-C(19)	107.6(3)
C(9)-C(11)-H(11B)	109.5	C(20)-C(17)-C(18)	108.5(3)
H(11A)-C(11)-H(11B)	109.5	C(19)-C(17)-C(18)	109.6(3)
C(9)-C(11)-H(11C)	109.5	C(20)-C(17)-P(2)	103.0(2)
H(11A)-C(11)-H(11C)	109.5	C(19)-C(17)-P(2)	116.4(3)
H(11B)-C(11)-H(11C)	109.5	C(18)-C(17)-P(2)	111.2(2)
C(9)-C(12)-H(12A)	109.5	C(17)-C(18)-H(18A)	109.5
C(9)-C(12)-H(12B)	109.5	C(17)-C(18)-H(18B)	109.5
H(12A)-C(12)-H(12B)	109.5	H(18A)-C(18)-H(18B)	109.5
C(9)-C(12)-H(12C)	109.5	C(17)-C(18)-H(18C)	109.5
H(12A)-C(12)-H(12C)	109.5	H(18A)-C(18)-H(18C)	109.5
H(12B)-C(12)-H(12C)	109.5	H(18B)-C(18)-H(18C)	109.5
C(16)-C(13)-C(14)	107.0(3)	C(17)-C(19)-H(19A)	109.5
C(16)-C(13)-C(15)	106.5(3)	C(17)-C(19)-H(19B)	109.5
C(14)-C(13)-C(15)	110.7(3)	H(19A)-C(19)-H(19B)	109.5
C(16)-C(13)-P(1)	108.2(2)	C(17)-C(19)-H(19C)	109.5

H(19A)-C(19)-H(19C)	109.5	H(24B)-C(24)-H(24C)	109.5
H(19B)-C(19)-H(19C)	109.5	C(26)-C(25)-C(30)	115.8(3)
C(17)-C(20)-H(20A)	109.5	C(26)-C(25)-Ir(1)	132.2(2)
C(17)-C(20)-H(20B)	109.5	C(30)-C(25)-Ir(1)	112.0(2)
H(20A)-C(20)-H(20B)	109.5	C(27)-C(26)-C(25)	122.6(3)
C(17)-C(20)-H(20C)	109.5	C(27)-C(26)-H(26)	118.7
H(20A)-C(20)-H(20C)	109.5	C(25)-C(26)-H(26)	118.7
H(20B)-C(20)-H(20C)	109.5	C(28)-C(27)-C(26)	120.1(4)
C(23)-C(21)-C(22)	109.9(3)	C(28)-C(27)-H(27)	120.0
C(23)-C(21)-C(24)	108.8(3)	C(26)-C(27)-H(27)	120.0
C(22)-C(21)-C(24)	106.6(3)	C(27)-C(28)-C(29)	119.6(3)
C(23)-C(21)-P(2)	111.6(2)	C(27)-C(28)-H(28)	120.2
C(22)-C(21)-P(2)	110.9(2)	C(29)-C(28)-H(28)	120.2
C(24)-C(21)-P(2)	108.9(2)	C(28)-C(29)-C(30)	120.0(3)
C(21)-C(22)-H(22A)	109.5	C(28)-C(29)-H(29)	120.0
C(21)-C(22)-H(22B)	109.5	C(30)-C(29)-H(29)	120.0
H(22A)-C(22)-H(22B)	109.5	C(29)-C(30)-C(25)	122.0(3)
C(21)-C(22)-H(22C)	109.5	C(29)-C(30)-C(31)	124.5(3)
H(22A)-C(22)-H(22C)	109.5	C(25)-C(30)-C(31)	113.5(3)
H(22B)-C(22)-H(22C)	109.5	C(32)-C(31)-C(30)	118.5(3)
C(21)-C(23)-H(23A)	109.5	C(32)-C(31)-H(31)	120.8
C(21)-C(23)-H(23B)	109.5	C(30)-C(31)-H(31)	120.8
H(23A)-C(23)-H(23B)	109.5	C(31)-C(32)-C(33)	123.9(3)
C(21)-C(23)-H(23C)	109.5	C(31)-C(32)-Ir(1)	115.8(2)
H(23A)-C(23)-H(23C)	109.5	C(33)-C(32)-Ir(1)	120.3(2)
H(23B)-C(23)-H(23C)	109.5	C(32)-C(33)-H(33A)	109.5
C(21)-C(24)-H(24A)	109.5	C(32)-C(33)-H(33B)	109.5
C(21)-C(24)-H(24B)	109.5	H(33A)-C(33)-H(33B)	109.5
H(24A)-C(24)-H(24B)	109.5	C(32)-C(33)-H(33C)	109.5
C(21)-C(24)-H(24C)	109.5	H(33A)-C(33)-H(33C)	109.5
H(24A)-C(24)-H(24C)	109.5	H(33B)-C(33)-H(33C)	109.5

Table 3. 42. Anisotropic displacement parameters ($Å^2$x 10^3) for complex 9.

The anisotropic displacement factor exponent takes the form: $-2\pi^2[h^2 a^{*2}U^{11} + ... + 2 h k a^* b^* U^{12}]$

	U^{11}	U^{22}	U^{33}	U^{23}	U^{13}	U^{12}
Ir(1)	12(1)	11(1)	11(1)	0(1)	2(1)	-1(1)
P(1)	12(1)	14(1)	12(1)	1(1)	2(1)	-1(1)
P(2)	16(1)	15(1)	12(1)	1(1)	2(1)	0(1)
C(1)	15(2)	14(2)	18(2)	1(1)	3(1)	0(1)
C(2)	12(1)	17(2)	17(2)	-2(1)	4(1)	0(1)
C(3)	22(2)	23(2)	17(2)	-7(2)	2(1)	-3(2)
C(4)	24(2)	22(2)	24(2)	-7(2)	4(2)	-10(2)
C(5)	22(2)	15(2)	26(2)	0(2)	7(1)	-5(1)
C(6)	17(2)	15(2)	17(2)	-2(1)	4(1)	-2(1)
C(7)	12(2)	22(2)	16(2)	-2(2)	2(1)	-1(1)
C(8)	29(2)	12(2)	21(2)	2(2)	4(2)	-4(2)
C(9)	11(1)	19(2)	18(2)	3(2)	3(1)	0(1)
C(10)	21(2)	21(2)	29(2)	2(2)	9(2)	5(2)
C(11)	15(2)	31(2)	27(2)	9(2)	1(1)	2(2)
C(12)	12(2)	26(2)	20(2)	2(2)	4(1)	1(1)
C(13)	13(2)	14(2)	21(2)	2(2)	2(1)	-4(1)
C(14)	27(2)	19(2)	24(2)	3(2)	7(2)	-3(2)
C(15)	18(2)	25(2)	18(2)	6(2)	1(1)	-2(2)
C(16)	18(2)	24(2)	22(2)	5(2)	2(1)	-3(2)
C(17)	17(2)	27(2)	19(2)	3(2)	7(1)	2(2)
C(18)	27(2)	34(2)	23(2)	-2(2)	10(2)	6(2)
C(19)	24(2)	45(3)	27(2)	9(2)	7(2)	-1(2)
C(20)	24(2)	37(2)	25(2)	6(2)	4(2)	8(2)
C(21)	18(2)	17(2)	16(2)	3(2)	1(1)	0(1)
C(22)	19(2)	27(2)	28(2)	1(2)	-3(2)	2(2)
C(23)	24(2)	28(2)	20(2)	8(2)	2(1)	2(2)
C(24)	20(2)	28(2)	23(2)	5(2)	0(1)	4(2)
C(25)	19(2)	12(2)	15(2)	3(1)	-1(1)	-1(1)
C(26)	26(2)	19(2)	21(2)	1(2)	3(2)	3(2)

C(27)	40(2)	17(2)	22(2)	-2(2)	2(2)	2(2)
C(28)	37(2)	17(2)	20(2)	0(2)	-4(2)	-8(2)
C(29)	22(2)	20(2)	20(2)	2(2)	-1(1)	-8(2)
C(30)	16(2)	15(2)	16(2)	4(2)	-1(1)	-2(1)
C(31)	12(1)	19(2)	16(2)	5(2)	0(1)	0(1)
C(32)	14(2)	15(2)	16(2)	5(1)	3(1)	2(1)
C(33)	23(2)	18(2)	23(2)	-2(2)	8(1)	1(2)

Table 3. 43. Hydrogen coordinates (x 10^4) and isotropic displacement parameters ($Å^2$x 10^3) for complex 9.

	x	y	z	U(eq)
H(3)	2149	4662	4955	25
H(4)	1806	3565	5558	28
H(5)	2869	3467	6734	25
H(7A)	2776	6009	4991	20
H(7B)	4593	5861	5183	20
H(8A)	5405	4127	7624	25
H(8B)	3748	4178	7856	25
H(10A)	573	7766	6479	35
H(10B)	2315	8026	6493	35
H(10C)	1948	7335	6959	35
H(11A)	19	7574	5228	37
H(11B)	1172	7109	4840	37
H(11C)	1684	7904	5177	37
H(12A)	1199	6073	6377	29
H(12B)	659	6075	5553	29
H(12C)	-283	6544	6039	29
H(14A)	5021	8203	6355	34
H(14B)	3688	8391	5716	34
H(14C)	5442	8572	5665	34
H(15A)	3380	7547	4622	31
H(15B)	4734	6967	4563	31
H(15C)	5062	7847	4560	31
H(16A)	7219	7575	5449	33
H(16B)	6783	6723	5573	33
H(16C)	7011	7300	6208	33
H(18A)	4305	6626	8762	41
H(18B)	4343	6037	9381	41
H(18C)	2777	6462	9076	41
H(19A)	3304	4732	9123	48

H(19B)	2153	4592	8409	48
H(19C)	1685	5157	8973	48
H(20A)	1206	6102	8011	43
H(20B)	1772	5509	7495	43
H(20C)	2557	6316	7593	43
H(22A)	6706	6101	9267	38
H(22B)	7593	6237	8627	38
H(22C)	8402	5773	9290	38
H(23A)	7342	4494	9518	36
H(23B)	5925	4163	8984	36
H(23C)	5667	4854	9472	36
H(24A)	8191	5150	7915	36
H(24B)	7607	4332	8076	36
H(24C)	8919	4733	8619	36
H(26)	4078	7738	7883	26
H(27)	5591	8704	8423	32
H(28)	8254	8695	8455	31
H(29)	9384	7725	7912	25
H(31)	9039	6471	7233	19
H(33A)	8499	5380	6517	31
H(33B)	6825	5390	6050	31
H(33C)	7136	4902	6745	31

Table 3. 44. Torsion angles [°] for complex 9.

C(6)-C(1)-C(2)-C(3)	6.2(5)	C(7)-P(1)-C(13)-C(16)	-80.7(3)
Ir(1)-C(1)-C(2)-C(3)	-170.7(3)	C(9)-P(1)-C(13)-C(16)	169.9(2)
C(6)-C(1)-C(2)-C(7)	-173.6(3)	Ir(1)-P(1)-C(13)-C(16)	35.5(3)
Ir(1)-C(1)-C(2)-C(7)	9.5(4)	C(7)-P(1)-C(13)-C(14)	162.2(2)
C(1)-C(2)-C(3)-C(4)	-3.7(5)	C(9)-P(1)-C(13)-C(14)	52.8(3)
C(7)-C(2)-C(3)-C(4)	176.2(3)	Ir(1)-P(1)-C(13)-C(14)	-81.6(2)
C(2)-C(3)-C(4)-C(5)	-0.9(5)	C(7)-P(1)-C(13)-C(15)	37.1(3)
C(3)-C(4)-C(5)-C(6)	2.6(6)	C(9)-P(1)-C(13)-C(15)	-72.3(3)
C(4)-C(5)-C(6)-C(1)	0.3(5)	Ir(1)-P(1)-C(13)-C(15)	153.3(2)
C(4)-C(5)-C(6)-C(8)	-175.9(3)	C(8)-P(2)-C(17)-C(20)	-81.4(3)
C(2)-C(1)-C(6)-C(5)	-4.5(5)	C(21)-P(2)-C(17)-C(20)	168.3(3)
Ir(1)-C(1)-C(6)-C(5)	172.4(3)	Ir(1)-P(2)-C(17)-C(20)	28.3(3)
C(2)-C(1)-C(6)-C(8)	171.6(3)	C(8)-P(2)-C(17)-C(19)	36.1(3)
Ir(1)-C(1)-C(6)-C(8)	-11.5(4)	C(21)-P(2)-C(17)-C(19)	-74.3(3)
C(3)-C(2)-C(7)-P(1)	153.8(3)	Ir(1)-P(2)-C(17)-C(19)	145.8(3)
C(1)-C(2)-C(7)-P(1)	-26.3(4)	C(8)-P(2)-C(17)-C(18)	162.7(3)
C(13)-P(1)-C(7)-C(2)	158.6(2)	C(21)-P(2)-C(17)-C(18)	52.3(3)
C(9)-P(1)-C(7)-C(2)	-87.9(2)	Ir(1)-P(2)-C(17)-C(18)	-87.6(3)
Ir(1)-P(1)-C(7)-C(2)	28.4(2)	C(8)-P(2)-C(21)-C(23)	-62.1(3)
C(5)-C(6)-C(8)-P(2)	-167.0(3)	C(17)-P(2)-C(21)-C(23)	49.0(3)
C(1)-C(6)-C(8)-P(2)	16.7(4)	Ir(1)-P(2)-C(21)-C(23)	177.2(2)
C(21)-P(2)-C(8)-C(6)	-149.0(2)	C(8)-P(2)-C(21)-C(22)	174.9(2)
C(17)-P(2)-C(8)-C(6)	95.4(3)	C(17)-P(2)-C(21)-C(22)	-74.0(3)
Ir(1)-P(2)-C(8)-C(6)	-14.0(3)	Ir(1)-P(2)-C(21)-C(22)	54.3(3)
C(7)-P(1)-C(9)-C(10)	165.2(2)	C(8)-P(2)-C(21)-C(24)	57.9(3)
C(13)-P(1)-C(9)-C(10)	-84.3(3)	C(17)-P(2)-C(21)-C(24)	169.1(2)
Ir(1)-P(1)-C(9)-C(10)	55.9(3)	Ir(1)-P(2)-C(21)-C(24)	-62.7(3)
C(7)-P(1)-C(9)-C(12)	46.5(3)	C(30)-C(25)-C(26)-C(27)	-0.8(5)
C(13)-P(1)-C(9)-C(12)	157.0(2)	Ir(1)-C(25)-C(26)-C(27)	179.3(3)
Ir(1)-P(1)-C(9)-C(12)	-62.8(2)	C(25)-C(26)-C(27)-C(28)	-0.1(6)
C(7)-P(1)-C(9)-C(11)	-72.0(3)	C(26)-C(27)-C(28)-C(29)	1.0(6)
C(13)-P(1)-C(9)-C(11)	38.5(3)	C(27)-C(28)-C(29)-C(30)	-0.9(5)
Ir(1)-P(1)-C(9)-C(11)	178.7(2)	C(28)-C(29)-C(30)-C(25)	0.0(5)

C(28)-C(29)-C(30)-C(31)	180.0(3)	C(29)-C(30)-C(31)-C(32)	-177.9(3)
C(26)-C(25)-C(30)-C(29)	0.9(5)	C(25)-C(30)-C(31)-C(32)	2.1(5)
Ir(1)-C(25)-C(30)-C(29)	-179.2(3)	C(30)-C(31)-C(32)-C(33)	176.9(3)
C(26)-C(25)-C(30)-C(31)	-179.1(3)	C(30)-C(31)-C(32)-Ir(1)	-4.2(4)
Ir(1)-C(25)-C(30)-C(31)	0.8(4)		

3.5.9.9. Structural data for (*E*, *E*)-1,4-(2-naphthyl)-1,3-butadiene

CCDC # 1540144

Figure 3. 72. ORTEP diagram of (*E*, *E*)-1,4-(2-naphthyl)-1,3-butadiene

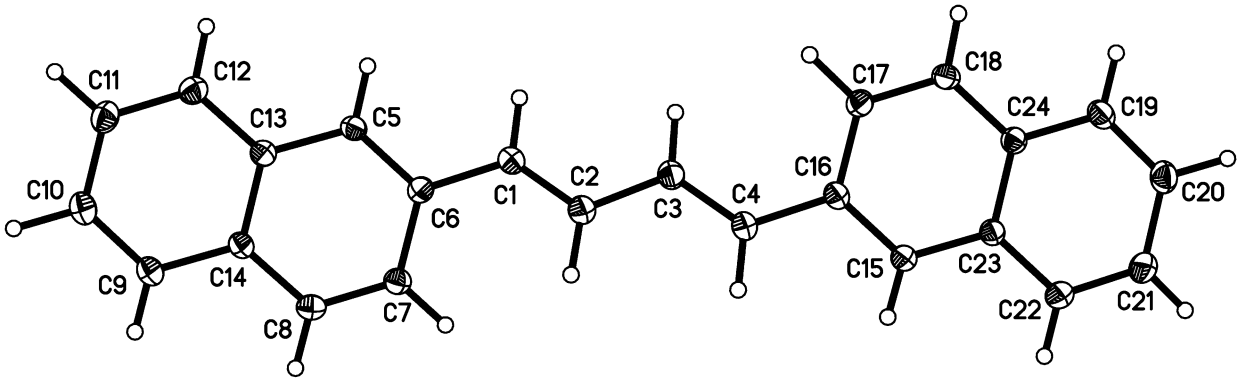

Table 3. 45. Crystal data and structure refinement for (*E*, *E*)-1,4-(2-naphthyl)-1,3-butadiene.

Identification code	jonmm24	
Empirical formula	C24 H18	
Formula weight	306.38	
Temperature	100.0(5) K	
Wavelength	0.71073 Å	
Crystal system	monoclinic	
Space group	$P2_1$	
Unit cell dimensions	a = 6.4734(9) Å	α = 90°
	b = 7.2485(10) Å	β = 96.619(3)°
	c = 16.941(2) Å	γ = 90°
Volume	789.62(19) $Å^3$	
Z	2	
Density (calculated)	1.289 Mg/m^3	
Absorption coefficient	0.073 mm^{-1}	
F(000)	324	
Crystal color, morphology	light yellow, block	
Crystal size	0.26 x 0.20 x 0.14 mm^3	
Theta range for data collection	2.421 to 38.663°	
Index ranges	$-10 \leq h \leq 11$, $-12 \leq k \leq 12$, $-29 \leq l \leq 29$	
Reflections collected	21417	
Independent reflections	8224 [R(int) = 0.0436]	
Observed reflections	5530	
Completeness to theta = 36.319°	98.4%	
Absorption correction	Multi-scan	
Max. and min. transmission	0.7476 and 0.6682	
Refinement method	Full-matrix least-squares on F^2	
Data / restraints / parameters	8224 / 1 / 289	
Goodness-of-fit on F^2	0.983	
Final R indices [I>2sigma(I)]	$R1$ = 0.0665, $wR2$ = 0.1552	
R indices (all data)	$R1$ = 0.0996, $wR2$ = 0.1789	
Largest diff. peak and hole	0.720 and -0.251 e.$Å^{-3}$	

Table 3. 46. Atomic coordinates (x 10^4) and equivalent isotropic displacement parameters ($Å^2$x 10^3) for (*E*, *E*)-1,4-(2-naphthyl)-1,3-butadiene.

U_{eq} is defined as one third of the trace of the orthogonalized U_{ij} tensor.

	x	y	z	U_{eq}
C1	8446(3)	4530(3)	5689(1)	18(1)
C2	7966(3)	5361(3)	4976(1)	19(1)
C3	6029(3)	5053(3)	4482(1)	19(1)
C4	5599(3)	5779(3)	3745(1)	17(1)
C5	10405(3)	4232(3)	7013(1)	16(1)
C6	10346(3)	4774(3)	6226(1)	16(1)
C7	12167(3)	5608(3)	5973(1)	17(1)
C8	13898(3)	5912(3)	6499(1)	17(1)
C9	15695(3)	5835(3)	7873(1)	18(1)
C10	15670(3)	5394(3)	8664(1)	22(1)
C11	13912(3)	4522(3)	8923(1)	22(1)
C12	12203(3)	4115(3)	8390(1)	19(1)
C13	12165(3)	4573(3)	7574(1)	16(1)
C14	13954(3)	5440(3)	7312(1)	16(1)
C15	3735(3)	5817(3)	2395(1)	16(1)
C16	3739(3)	5402(3)	3195(1)	16(1)
C17	1928(3)	4573(3)	3448(1)	18(1)
C18	221(3)	4173(3)	2913(1)	17(1)
C19	-1494(3)	4100(3)	1528(1)	19(1)
C20	-1427(3)	4457(3)	735(1)	22(1)
C21	347(3)	5290(3)	471(1)	22(1)
C22	2033(3)	5740(3)	1004(1)	20(1)
C23	2021(3)	5386(3)	1829(1)	16(1)
C24	227(3)	4549(3)	2090(1)	16(1)

Table 3. 47. Bond lengths [Å] and angles [°] for (*E*, *E*)-1,4-(2-naphthyl)-1,3-butadiene.

C(1)-C(2)	1.353(3)	C(18)-C(24)	1.422(3)
C(1)-C(6)	1.454(2)	C(18)-H(18)	0.97(3)
C(1)-H(1)	1.00(3)	C(19)-C(20)	1.374(3)
C(2)-C(3)	1.443(2)	C(19)-C(24)	1.417(3)
C(2)-H(2)	1.01(3)	C(19)-H(19)	0.96(3)
C(3)-C(4)	1.355(3)	C(20)-C(21)	1.415(3)
C(3)-H(3)	0.98(3)	C(20)-H(20)	1.05(3)
C(4)-C(16)	1.460(2)	C(21)-C(22)	1.374(3)
C(4)-H(4)	0.96(3)	C(21)-H(21)	0.97(3)
C(5)-C(6)	1.387(2)	C(22)-C(23)	1.421(3)
C(5)-C(13)	1.418(2)	C(22)-H(22)	0.95(3)
C(5)-H(5)	0.97(3)	C(23)-C(24)	1.425(3)
C(6)-C(7)	1.434(3)	C(2)-C(1)-C(6)	126.47(18)
C(7)-C(8)	1.366(3)	C(2)-C(1)-H(1)	120.1(15)
C(7)-H(7)	0.98(3)	C(6)-C(1)-H(1)	113.4(15)
C(8)-C(14)	1.416(3)	C(1)-C(2)-C(3)	122.92(17)
C(8)-H(8)	0.96(3)	C(1)-C(2)-H(2)	117.4(14)
C(9)-C(10)	1.380(3)	C(3)-C(2)-H(2)	119.7(13)
C(9)-C(14)	1.417(2)	C(4)-C(3)-C(2)	123.17(18)
C(9)-H(9)	0.94(3)	C(4)-C(3)-H(3)	122.0(13)
C(10)-C(11)	1.415(3)	C(2)-C(3)-H(3)	114.7(13)
C(10)-H(10)	1.07(3)	C(3)-C(4)-C(16)	125.55(18)
C(11)-C(12)	1.376(3)	C(3)-C(4)-H(4)	119.6(15)
C(11)-H(11)	1.01(3)	C(16)-C(4)-H(4)	114.4(15)
C(12)-C(13)	1.420(3)	C(6)-C(5)-C(13)	121.70(17)
C(12)-H(12)	0.99(2)	C(6)-C(5)-H(5)	120.4(14)
C(13)-C(14)	1.432(3)	C(13)-C(5)-H(5)	117.9(14)
C(15)-C(16)	1.389(3)	C(5)-C(6)-C(7)	118.36(16)
C(15)-C(23)	1.415(2)	C(5)-C(6)-C(1)	119.62(17)
C(15)-H(15)	0.92(3)	C(7)-C(6)-C(1)	122.00(16)
C(16)-C(17)	1.427(3)	C(8)-C(7)-C(6)	120.90(17)
C(17)-C(18)	1.376(3)	C(8)-C(7)-H(7)	120.9(16)
C(17)-H(17)	1.05(2)	C(6)-C(7)-H(7)	118.2(16)

C(7)-C(8)-C(14)	121.51(18)	C(17)-C(16)-C(4)	122.27(17)
C(7)-C(8)-H(8)	121.3(16)	C(18)-C(17)-C(16)	121.13(17)
C(14)-C(8)-H(8)	117.2(16)	C(18)-C(17)-H(17)	119.9(14)
C(10)-C(9)-C(14)	120.48(19)	C(16)-C(17)-H(17)	119.0(14)
C(10)-C(9)-H(9)	119.4(16)	C(17)-C(18)-C(24)	120.82(18)
C(14)-C(9)-H(9)	120.1(15)	C(17)-C(18)-H(18)	118.4(14)
C(9)-C(10)-C(11)	120.26(18)	C(24)-C(18)-H(18)	120.8(14)
C(9)-C(10)-H(10)	120.1(15)	C(20)-C(19)-C(24)	120.19(18)
C(11)-C(10)-H(10)	119.7(15)	C(20)-C(19)-H(19)	119.3(15)
C(12)-C(11)-C(10)	120.49(18)	C(24)-C(19)-H(19)	120.5(15)
C(12)-C(11)-H(11)	120.5(15)	C(19)-C(20)-C(21)	120.52(18)
C(10)-C(11)-H(11)	119.0(14)	C(19)-C(20)-H(20)	120.5(15)
C(11)-C(12)-C(13)	120.70(19)	C(21)-C(20)-H(20)	119.0(15)
C(11)-C(12)-H(12)	118.2(13)	C(22)-C(21)-C(20)	120.38(18)
C(13)-C(12)-H(12)	121.1(13)	C(22)-C(21)-H(21)	119.4(16)
C(5)-C(13)-C(12)	122.27(18)	C(20)-C(21)-H(21)	120.0(16)
C(5)-C(13)-C(14)	119.00(16)	C(21)-C(22)-C(23)	120.63(19)
C(12)-C(13)-C(14)	118.71(16)	C(21)-C(22)-H(22)	120.9(15)
C(8)-C(14)-C(9)	122.21(18)	C(23)-C(22)-H(22)	118.4(15)
C(8)-C(14)-C(13)	118.44(16)	C(15)-C(23)-C(22)	122.23(18)
C(9)-C(14)-C(13)	119.33(16)	C(15)-C(23)-C(24)	119.12(16)
C(16)-C(15)-C(23)	121.81(18)	C(22)-C(23)-C(24)	118.65(16)
C(16)-C(15)-H(15)	117.2(15)	C(19)-C(24)-C(18)	121.63(18)
C(23)-C(15)-H(15)	120.9(15)	C(19)-C(24)-C(23)	119.63(16)
C(15)-C(16)-C(17)	118.34(16)	C(18)-C(24)-C(23)	118.73(16)
C(15)-C(16)-C(4)	119.38(17)		

Table 3. 48. Anisotropic displacement parameters ($Å^2$x 10^3) for (*E*, *E*)-1,4-(2-naphthyl)-1,3-butadiene.

The anisotropic displacement factor exponent takes the form: $-2\pi^2[h^2 a^{*2}U_{11} + ... + 2 h k a^* b^* U_{12}]$

	U_{11}	U_{22}	U_{33}	U_{23}	U_{13}	U_{12}
C1	17(1)	18(1)	18(1)	0(1)	1(1)	-2(1)
C2	18(1)	21(1)	18(1)	-1(1)	1(1)	-1(1)
C3	18(1)	19(1)	18(1)	0(1)	0(1)	-1(1)
C4	16(1)	17(1)	17(1)	-1(1)	0(1)	0(1)
C5	15(1)	16(1)	17(1)	1(1)	2(1)	-2(1)
C6	17(1)	16(1)	15(1)	0(1)	2(1)	0(1)
C7	16(1)	17(1)	18(1)	1(1)	3(1)	0(1)
C8	17(1)	16(1)	20(1)	1(1)	5(1)	1(1)
C9	16(1)	18(1)	21(1)	-1(1)	0(1)	0(1)
C10	19(1)	23(1)	22(1)	-1(1)	-2(1)	0(1)
C11	22(1)	24(1)	17(1)	2(1)	0(1)	3(1)
C12	20(1)	19(1)	18(1)	2(1)	3(1)	0(1)
C13	15(1)	15(1)	16(1)	0(1)	2(1)	1(1)
C14	14(1)	15(1)	17(1)	0(1)	0(1)	0(1)
C15	15(1)	18(1)	16(1)	0(1)	2(1)	-1(1)
C16	14(1)	15(1)	18(1)	0(1)	0(1)	-1(1)
C17	18(1)	19(1)	16(1)	1(1)	2(1)	1(1)
C18	15(1)	18(1)	19(1)	1(1)	4(1)	-1(1)
C19	15(1)	19(1)	23(1)	1(1)	0(1)	-2(1)
C20	22(1)	25(1)	20(1)	-1(1)	-2(1)	-2(1)
C21	24(1)	26(1)	16(1)	0(1)	1(1)	-2(1)
C22	20(1)	23(1)	17(1)	1(1)	4(1)	-1(1)
C23	15(1)	16(1)	16(1)	0(1)	1(1)	0(1)
C24	16(1)	15(1)	17(1)	1(1)	1(1)	1(1)

Table 3. 49. Hydrogen coordinates (x 10^4) and isotropic displacement parameters (Å^2 x 10^3) for (*E*, *E*)-1,4-(2-naphthyl)-1,3-butadiene.

	x	y	z	U(eq)
H1	7430(40)	3680(40)	5899(15)	28(7)
H2	9030(40)	6220(40)	4790(14)	24(7)
H3	5070(40)	4220(40)	4708(13)	20(6)
H4	6640(40)	6500(40)	3522(15)	25(7)
H5	9230(40)	3580(40)	7195(14)	18(6)
H7	12140(40)	5960(40)	5410(15)	30(7)
H8	15140(40)	6420(40)	6330(15)	28(7)
H9	16900(40)	6370(40)	7705(15)	26(7)
H10	16980(40)	5720(40)	9085(15)	27(7)
H11	13930(40)	4200(40)	9506(15)	22(6)
H12	11030(30)	3450(30)	8589(13)	13(6)
H15	4920(40)	6330(40)	2241(15)	21(6)
H17	1890(40)	4300(40)	4056(14)	18(6)
H18	-970(40)	3580(40)	3109(14)	17(6)
H19	-2700(40)	3500(40)	1695(15)	23(7)
H20	-2700(40)	4140(40)	319(15)	32(7)
H21	430(40)	5440(40)	-91(16)	31(7)
H22	3250(40)	6270(40)	830(15)	26(7)

Table 3. 50. Torsion angles [°] for (*E*, *E*)-1,4-(2-naphthyl)-1,3-butadiene.

C6-C1-C2-C3	-179.4(2)	C12-C13-C14-C9	-0.7(3)
C1-C2-C3-C4	-175.3(2)	C23-C15-C16-C17	-2.0(3)
C2-C3-C4-C16	175.01(19)	C23-C15-C16-C4	176.39(17)
C13-C5-C6-C7	3.5(3)	C3-C4-C16-C15	-162.59(19)
C13-C5-C6-C1	-174.99(17)	C3-C4-C16-C17	15.7(3)
C2-C1-C6-C5	163.0(2)	C15-C16-C17-C18	0.6(3)
C2-C1-C6-C7	-15.3(3)	C4-C16-C17-C18	-177.7(2)
C5-C6-C7-C8	-1.9(3)	C16-C17-C18-C24	1.1(3)
C1-C6-C7-C8	176.50(18)	C24-C19-C20-C21	-0.6(3)
C6-C7-C8-C14	-0.8(3)	C19-C20-C21-C22	0.5(3)
C14-C9-C10-C11	0.8(3)	C20-C21-C22-C23	-0.3(3)
C9-C10-C11-C12	-0.5(3)	C16-C15-C23-C22	-177.53(18)
C10-C11-C12-C13	-0.5(3)	C16-C15-C23-C24	1.7(3)
C6-C5-C13-C12	176.51(19)	C21-C22-C23-C15	179.47(19)
C6-C5-C13-C14	-2.3(3)	C21-C22-C23-C24	0.2(3)
C11-C12-C13-C5	-177.80(18)	C20-C19-C24-C18	-179.06(19)
C11-C12-C13-C14	1.0(3)	C20-C19-C24-C23	0.5(3)
C7-C8-C14-C9	-176.59(18)	C17-C18-C24-C19	178.22(18)
C7-C8-C14-C13	2.0(3)	C17-C18-C24-C23	-1.3(3)
C10-C9-C14-C8	178.39(18)	C15-C23-C24-C19	-179.58(19)
C10-C9-C14-C13	-0.2(3)	C22-C23-C24-C19	-0.3(3)
C5-C13-C14-C8	-0.5(3)	C15-C23-C24-C18	0.0(3)
C12-C13-C14-C8	-179.32(19)	C22-C23-C24-C18	179.26(19)
C5-C13-C14-C9	178.16(19)		

3.5.10. Reaction mechanisms and free energies

Figure 3. 73. Ir(V) reaction mechanism and free energy values for styrene coupling catalyzed by (^{iPr}PCP)Ir.

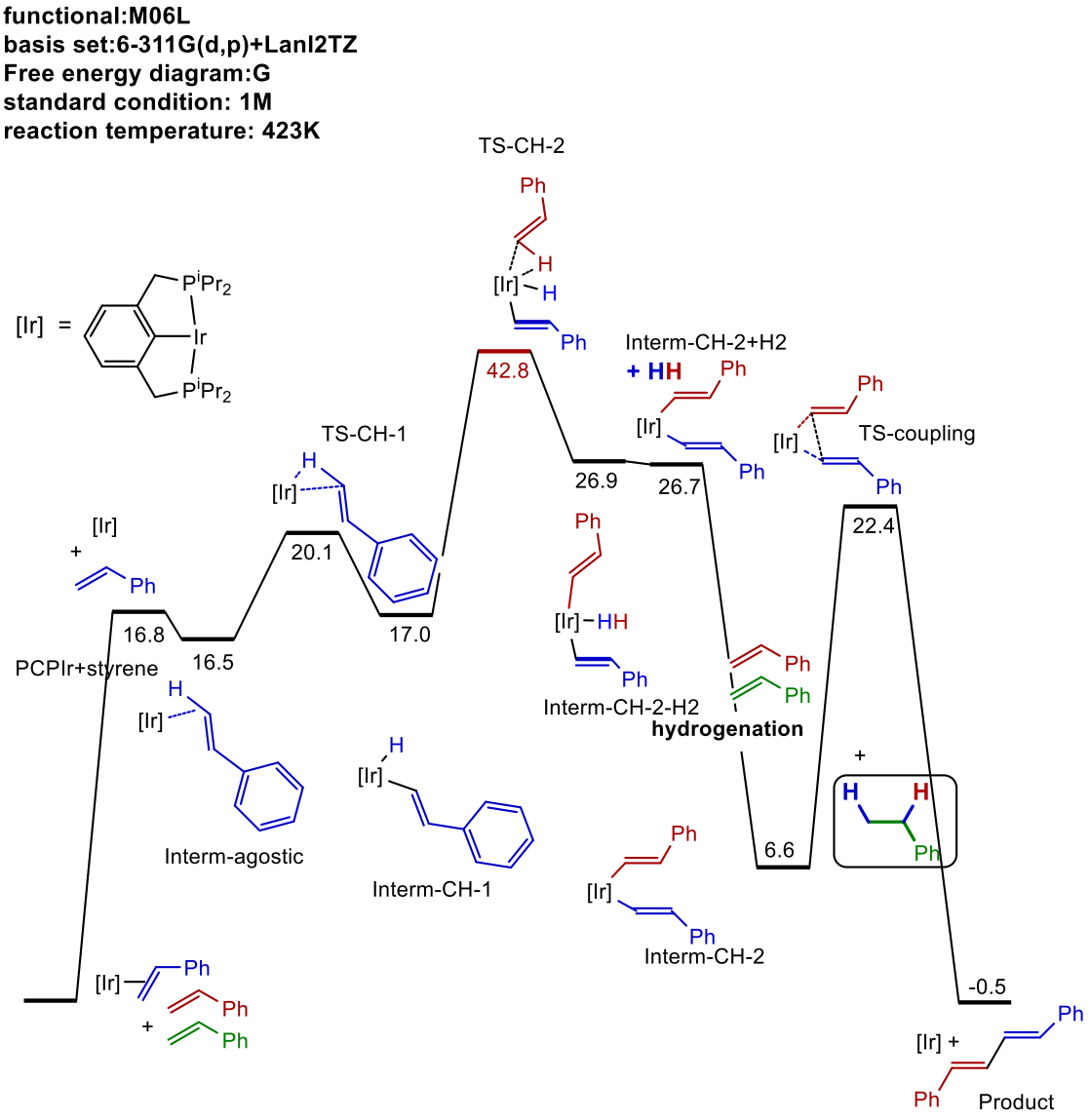

Table 3. 51. Ir(V) reaction mechanism and free energy values for styrene coupling catalyzed by (^{iPr}PCP)Ir.[a]

Species	E	H	G	S	G(corrected)[b]
Resting_state	0.0	0.0	0.0	0.0	0.0
PCPIr+styrene	40.0	38.8	24.6	47.5	16.8
Interm-agostic	19.9	19.4	18.7	2.3	16.5
TS-CH-1	26.9	24.0	22.6	4.7	20.1
Interm-CH-1	23.4	21.3	19.6	5.6	17.0
TS-CH-2	29.5	26.4	40.6	-47.8	42.8
Interm-CH-2-H2	13.3	11.6	25.0	-45.1	26.9
Interm-CH-2+H2	33.4	27.9	29.7	-6.1	26.7
Interm-CH-2	-3.9	-2.5	7.9	-34.9	6.6
TS-coupling	7.6	9.2	22.5	-44.7	22.4
Product	6.0	7.8	5.9	6.2	-0.5

[a]Units are kcal/mol for E, H, and G; units are cal/(deg·mol) for S. The standard state for concentrations is 1.0 M for each species participating in the reaction and T = 298.15 K. [b]G corrected to T = 423 K; units of kcal/mol.

Figure 3. 74. Vinylidene reaction mechanism and free energy values for styrene coupling catalyzed by (^{iPr}PCP)Ir.

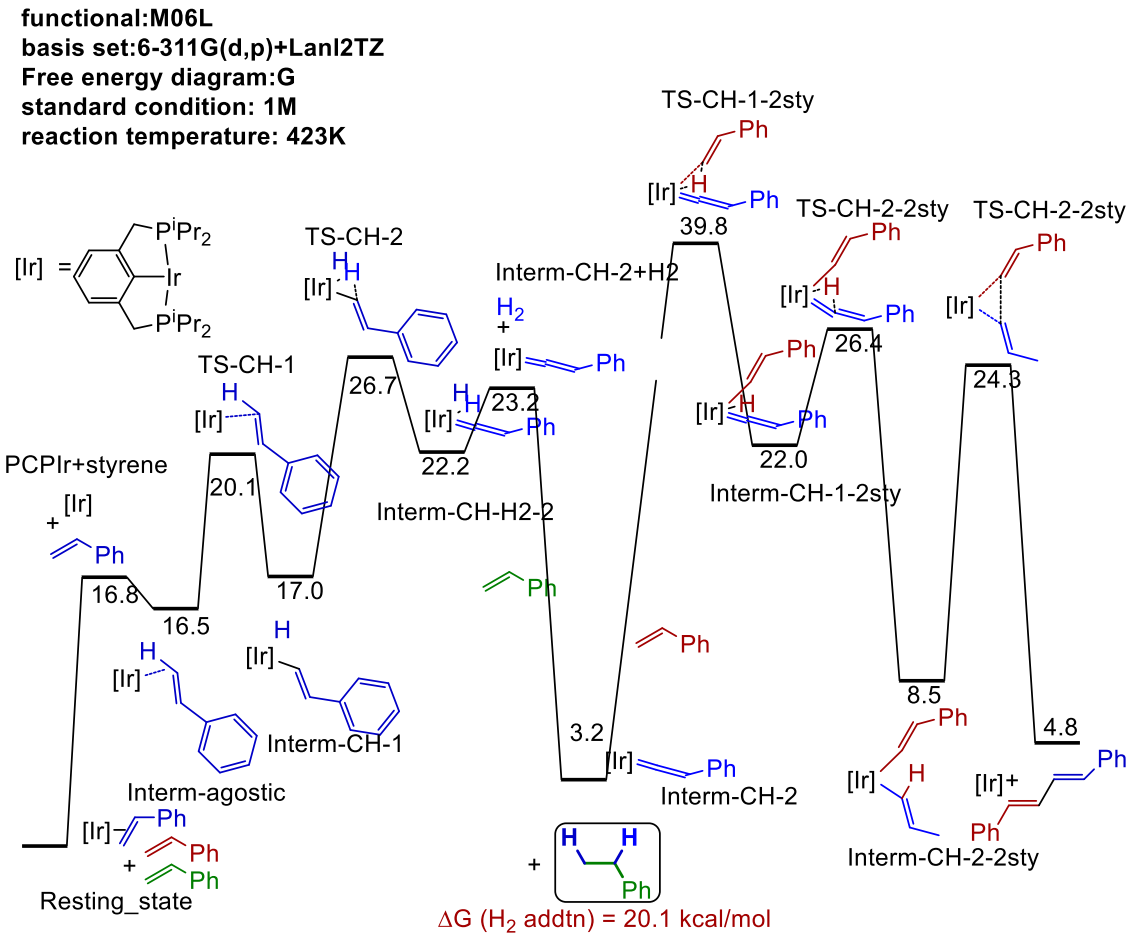

Table 3. 52. Vinylidene reaction mechanism and free energy values for styrene coupling catalyzed by (^{iPr}PCP)Ir.[a]

Species	E	H	G	S	G(corrected)[b]
Resting_state	0.0	0.0	0.0	0.0	0.0
PCPIr+styrene	40.0	38.8	24.6	47.5	16.8
Interm-agostic	19.9	19.4	18.7	2.3	16.5
TS-CH-1	26.9	24.0	22.6	4.7	20.1
Interm-CH-1	23.4	21.3	19.6	5.6	17.0
TS-CH-2	33.7	28.6	28.6	-0.2	26.7
Interm-CH-H2-2	29.0	24.8	24.3	1.6	22.2
Interm-CH-2+H2	44.8	38.3	29.0	31.1	23.2
Interm-CH-2	7.5	8.0	7.2	2.4	3.2
TS-C-C-coupling	7.6	9.2	22.5	-44.7	24.3
TS-CH-1-2sty	25.3	24.0	37.8	-46.2	39.8
TS-CH-2-2sty	11.7	10.6	24.4	-46.3	26.4
Interm-CH-1-2sty	8.1	8.0	20.6	-42.1	22.0
Interm-CH-2-2sty	-3.9	-2.5	7.9	-34.9	8.5

[a]Units are kcal/mol for E, H, and G; units are cal/(deg·mol) for S. The standard state for concentrations is 1.0 M for each species participating in the reaction and T = 298.15 K. [b]G corrected to T = 423 K; units of kcal/mol.

Figure 3. 75. Ir-C bond insertion reaction mechanism and free energy values for styrene coupling catalyzed by (^{iPr}PCP)Ir.

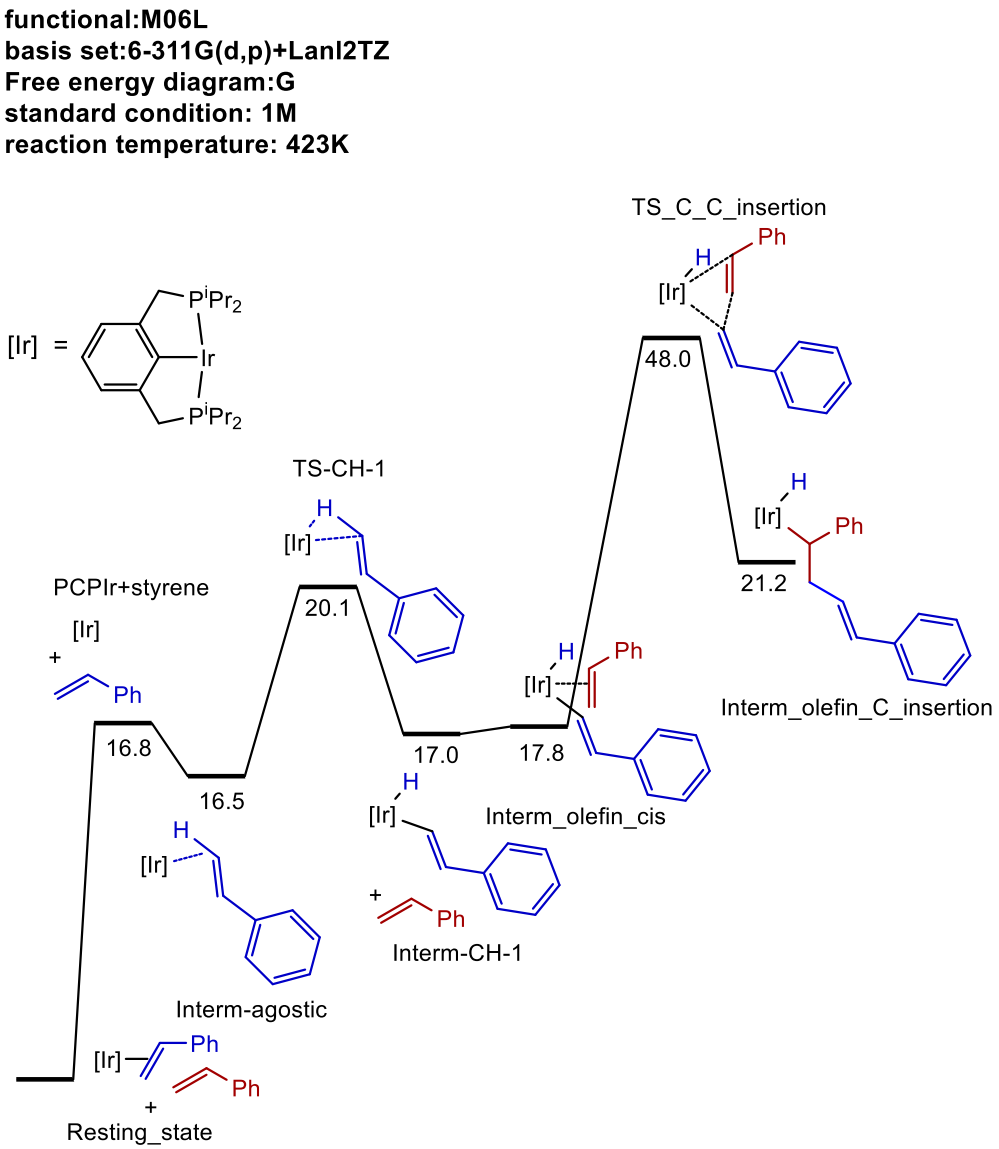

Table 3. 53. Ir-C bond insertion reaction mechanism and free energy values for styrene coupling catalyzed by (^{iPr}PCP)Ir.[a]

Species	E	H	G	S	G(corrected)[b]
Resting_state	0.0	0.0	0.0	0.0	0.0
PCPIr+styrene	40.0	38.8	24.6	47.5	16.8
Interm-agostic	19.9	19.4	18.7	2.3	16.5
TS-CH-1	26.9	24.0	22.6	4.7	20.1
Interm-CH-1	23.4	21.3	19.6	5.6	17.0
Interm_olefin_cis	-2.3	-2.1	14.6	-55.9	17.8
TS_C_C_insertion	30.1	29.4	45.2	-52.9	48.0
Interm_olefin_C_insertion	1.8	2.3	18.3	-53.6	21.2

[a]Units are kcal/mol for E, H, and G; units are cal/(deg·mol) for S. The standard state for concentrations is 1.0 M for each species participating in the reaction and T = 298.15 K. [b]G corrected to T = 423 K; units of kcal/mol.

Figure 3. 76. Ir-H bond insertion reaction mechanism and free energy values for styrene coupling catalyzed by (^{iPr}PCP)Ir.

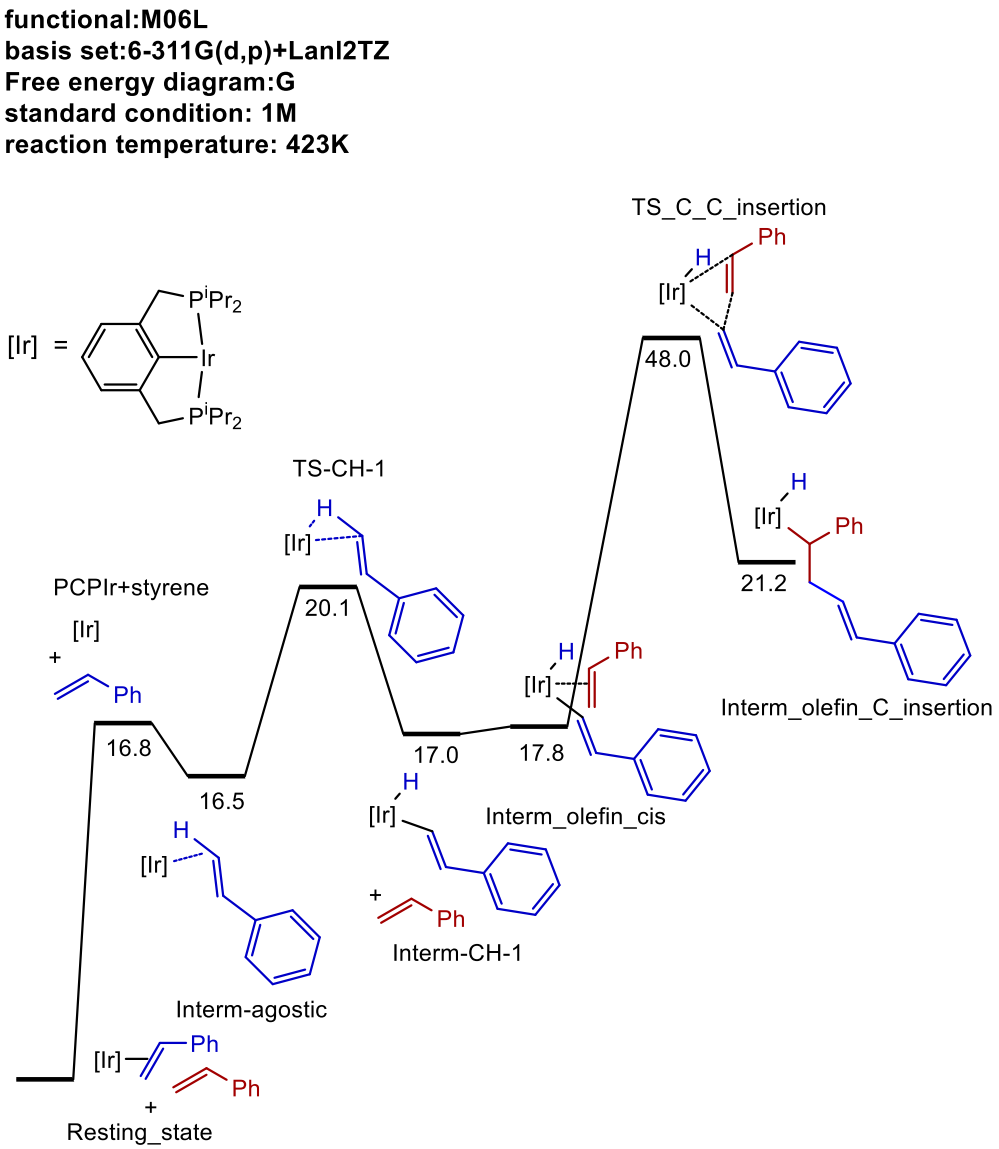

Table 3. 54. Ir-H bond insertion reaction mechanism and free energy values for styrene coupling catalyzed by (^{iPr}PCP)Ir.[a]

Species	E	H	G	S	G(corrected)[b]
Resting_state	0.0	0.0	0.0	0.0	0.0
PCPIr+styrene	40.0	38.8	24.6	47.5	16.8
Interm-agostic	19.9	19.4	18.7	2.3	16.5
TS-CH-1	26.9	24.0	22.6	4.7	20.1
Interm-CH-1	23.4	21.3	19.6	5.6	17.0
Interm_olefin_cis	-2.3	-2.1	14.6	-55.9	17.8
TS_C_H_insertion	13.4	12.3	28.5	-54.5	31.5
Interm_olefin_H_insertion	9.7	11.2	24.3	-43.9	26.0
TS_CC-coupling	31.4	33.1	47.9	-49.8	50.3
PCPIr+C_insertion_product	18.0	19.7	17.4	7.9	12.6

[a]Units are kcal/mol for E, H, and G; units are cal/(deg·mol) for S. The standard state for concentrations is 1.0 M for each species participating in the reaction and T = 298.15 K. [b]G corrected to T = 423 K; units of kcal/mol.

Figure 3. 77. Metalloindene reaction mechanism and free energy values for styrene coupling catalyzed by (^{iPr}PCP)Ir.

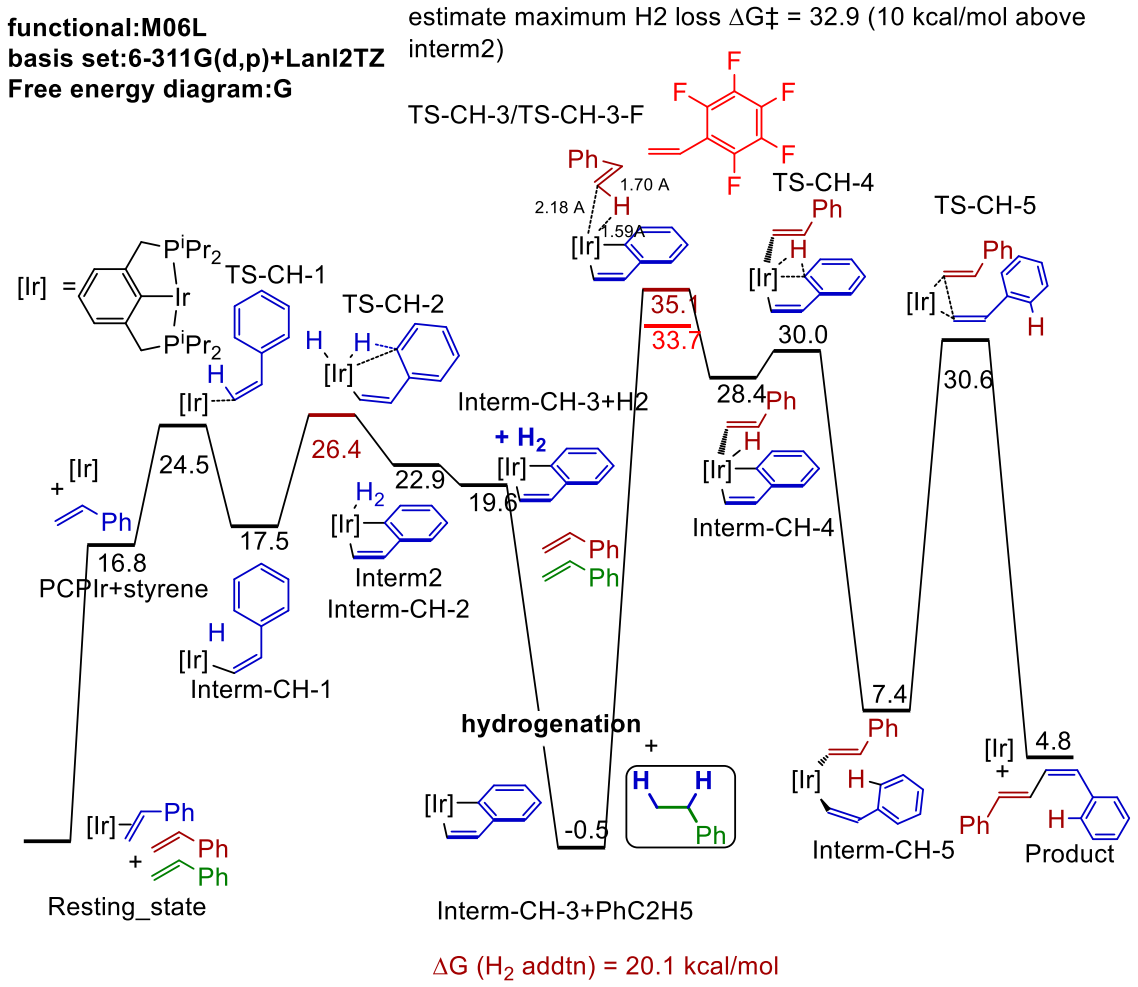

Table 3. 55. Metalloindene reaction mechanism and free energy values for styrene coupling catalyzed by (^{iPr}PCP)Ir.[a]

Species	E	H	G	S	G(corrected)[b]
Resting_state	0.0	0.0	0.0	0.0	0.0
PCPIr+styrene	40.0	38.8	24.6	47.5	16.8
Interm-agostic	19.9	19.4	18.7	2.3	16.5
TS-CH-1	27.9	24.9	26.0	-3.6	24.5
Interm-CH-1	18.7	16.4	18.6	-7.1	17.5
TS-CH-2	29.3	24.2	27.1	-9.6	26.4
Interm-CH-2	23.4	20.2	23.5	-11.0	22.9
Interm-CH-3+H2	38.7	31.7	24.5	24.2	19.6
Interm-CH-3+PhC2H5-styrene	1.5	1.4	2.7	-4.5	-0.5
TS-CH-3	15.6	15.2	31.9	-56.1	35.1
TS-CH-3-F	12.9	12.5	30.1	-59.0	33.7
Interm-CH-4	10.0	10.4	25.7	-51.3	28.4
TS-CH-4	12.0	11.2	27.1	-53.3	30.0
Interm-CH-5	-11.5	-10.0	5.0	-50.0	7.4
TS-CH-5	10.3	11.8	27.7	-53.6	30.6
Product	8.9	10.9	9.3	5.6	4.8

[a]Units are kcal/mol for E, H, and G; units are cal/(deg·mol) for S. The standard state for concentrations is 1.0 M for each species participating in the reaction and T = 298.15 K. [b]G corrected to T = 423 K; units of kcal/mol.

Figure 3. 78. Metalloindene reaction mechanism and corrected free energy values for 2,4,6-triMe-styrene coupling vs cyclization catalyzed by (^{iPr}PCP)Ir.

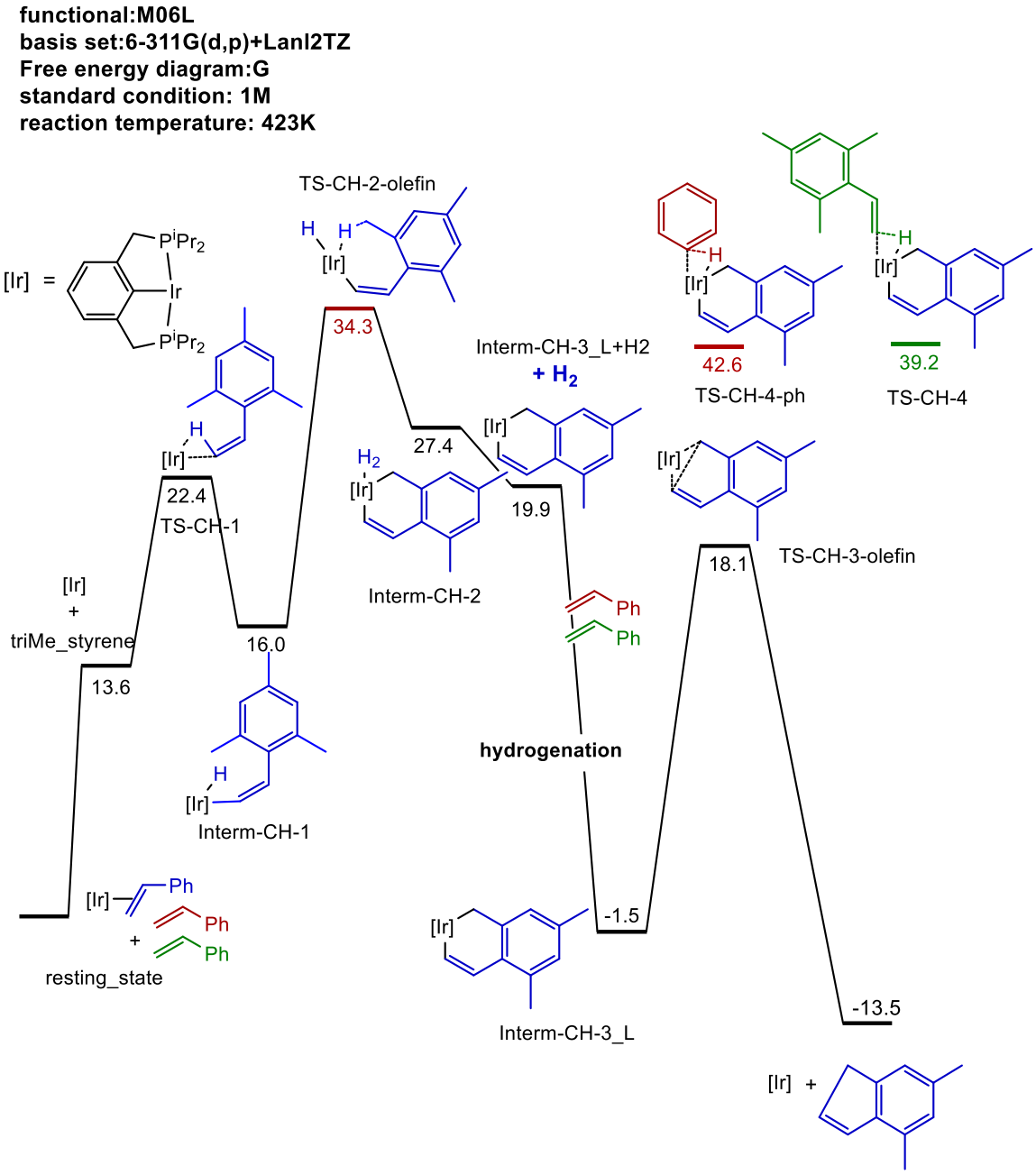

Table 3. 56. Metalloindene reaction mechanism and free energy values for 2,4,6-triMe-styrene coupling vs cyclization catalyzed by (^{iPr}PCP)Ir.[a]

Species	E	H	G	S	G(corrected)[b]
resting_state	0.0	0.0	0.0	0.0	0.0
Ir+styrene	41.3	39.8	22.7	57.5	13.6
TS-CH-1	28.0	24.5	24.4	0.5	22.4
Interm-CH-1	18.7	15.6	17.2	-5.5	16.0
TS-CH-2-olefin	37.3	32.4	35.1	-8.9	34.3
Interm-CH-2	29.3	25.9	28.2	-8.0	27.4
Interm-CH-3_L+H2	41.4	34.0	25.4	28.9	19.9
Interm-CH-3_L	1.7	1.3	2.0	-2.3	-1.5
TS-CH-3-olefin	20.4	19.3	21.1	-6.0	18.1
Interm-CH-3	-4.0	-2.1	13.7	-53.2	16.6
TS-CH-4	18.8	18.4	35.7	-58.1	39.2
Interm-CH-4	-7.0	-5.2	9.8	-50.3	12.3
TS-CH-5	9.7	10.9	27.8	-56.6	31.1
TS-CH-4-ph	25.0	24.0	39.8	-52.8	42.6
Interm-CH-3-ph	24.5	25.0	42.6	-58.8	46.1
TS-CH-5-ph	14.4	15.4	30.8	-52.0	33.6
Interm-CH-4-Ph	-1.5	0.6	16.5	-53.3	19.4

[a]Units are kcal/mol for E, H, and G; units are cal/(deg·mol) for S. The standard state for concentrations is 1.0 M for each species participating in the reaction and T = 298.15 K. [b]G corrected to T = 423 K; units of kcal/mol.

Table 3. 57. Energetic effects of solvation on the metalloindene reaction mechanism for styrene coupling by (^{iPr}PCP)Ir.

Species	E Gas	E Toluene	H Gas	H Toluene	G Gas	G Toluene	ΔG Gas - Toluene
(PCP)Ir-Styrene pi-complex + 2 Styrene (Resting State)	0.0	0.0	0.0	0.0	0.0	0.0	0.0
(PCP)Ir (+ 3 Styrene)	39.0	34.4	39.4	34.8	23.0	18.5	-4.5
Interm-agostic (+ 2 Styrene)	19.7	18.9	20.0	19.2	17.1	16.3	-0.8
TS-CH-1 (+ 2 Styrene)	25.4	25.5	25.5	25.6	24.3	24.4	0.1
Interm-CH-1 (+ 2 Styrene)	17.3	17.0	17.1	16.8	16.9	16.9	0.0
TS-CH-2 (+ 2 Styrene)	25.2	25.1	24.8	24.8	25.5	25.4	-0.1
Interm-CH-2 (+ 2 Styrene + H2)	21.2	20.6	20.8	20.3	21.8	21.3	-0.5
Interm-CH-3 (+ 2 Styrene + H2)	30.6	29.3	32.3	30.8	22.9	22.3	-0.6
(Interm-CH-3)-Styrene pi-complex (+PhC2H5)	-14.6	-13.6	-15.5	-14.4	1.5	2.2	0.7
TS-CH-3 (+PhC2H5)	16.4	17.1	15.8	16.4	30.2	31.1	0.9
Interm-CH-4 (+PhC2H5)	11.3		11.1		24.1		
TS-CH-4 (+PhC2H5)	12.2	13.2	11.9	12.8	25.5	27.1	1.6
Interm-CH-5 (+PhC2H5)	-9.4	-8.6	-9.4	-8.6	3.3	4.1	0.8
TS-CH-5 (+PhC2H5)	12.8	13.6	12.4	13.2	26.1	27.0	0.9
Product (+PhC2H5 + (PCP)Ir)	11.6	7.5	11.6	7.5	7.6	3.8	3.8

Units are kcal/mol for E, H, and G. The standard state for concentrations is P = 1 atm for each species participating in the reaction and T = 298.15 K.

The idealized gas-phase structures for the species involved in the metalloindene mechanism for styrene coupling proposed in Figure 3.6 were reoptimized (M06-L/LanL2TZ(+d)/6-311G(d,p)) incorporating the CPCM continuum dielectric model with toluene (the solvent used in the experiments described in the *MS*) as the model solvent. Energetic quantities (gas and liquid(toluene) phase) obtained with a standard state of T = 298.15 K and P = 1 atm for each species are compared in the Table below.

The dielectric constant of toluene is small (~ 2.4) and most species considered in the mechanism possess small dipole moments (μ < 2 D), so the energetic effects of bulk solvation are expected and found to be small, viz. the data presented in the ΔG(Gas-Toluene) = G(Toluene) – G(Gas) column. The largest effect is seen to occur in the two steps where the 3-coordinate unsaturated (^{iPr}PCP)Ir species is created (calculated μ(^{iPr}PCP)Ir) ~ 2.1 D). Toluene solvation is computed to increase the barrier for the C-H activation step producing the bis(vinyl) complex (^{iPr}PCP)Ir(*cis*-CH=CHPh)(*trans*-CH=CHPh) (**12**, Figure 3.6) by 1.6 kcal/mol; otherwise, the ΔG(Gas-Toluene) values are uniformly less than 1 kcal/mol.

3.8. References

1. Miyaura, N.; Suzuki, A., Palladium-Catalyzed Cross-Coupling Reactions of Organoboron Compounds. *Chem. Rev.* **1995,** *95* (7), 2457-2483.
2. Littke, A. F.; Fu, G. C., Palladium-catalyzed coupling reactions of aryl chlorides. *Angew. Chem., Intl. Ed.* **2002,** *41* (22), 4176-4211.
3. Kataoka, N.; Shelby, Q.; Stambuli, J. P.; Hartwig, J. F., Air stable, sterically hindered ferrocenyl dialkylphosphines for palladium-catalyzed C-C, C-N, and C-O bond-forming cross-couplings. *J. Org. Chem.* **2002,** *67* (16), 5553-5566.
4. Fagnou, K.; Lautens, M., Rhodium-Catalyzed Carbon-Carbon Bond Forming Reactions of Organometallic Compounds. *Chem. Rev.* **2003,** *103* (1), 169-196.
5. Nicolaou, K. C.; Bulger, P. G.; Sarlah, D., Palladium-catalyzed cross-coupling reactions in total synthesis. *Angew Chem Int Edit* **2005,** *44* (29), 4442-4489.
6. Suzuki, A., Carbon-carbon bonding made easy. *Chem. Commun.* **2005,** (38), 4759-4763.
7. Fu, G. C., The Development of Versatile Methods for Palladium-Catalyzed Coupling Reactions of Aryl Electrophiles through the Use of $P(t\text{-}Bu)_3$ and PCy_3 as Ligands. *Acc. Chem. Res.* **2008,** *41* (11), 1555-1564.
8. Martin, R.; Buchwald, S. L., Palladium-Catalyzed Suzuki-Miyaura Cross-Coupling Reactions Employing Dialkylbiaryl Phosphine Ligands. *Acc. Chem. Res.* **2008,** *41* (11), 1461-1473.
9. Seechurn, C. C. C. J.; Kitching, M. O.; Colacot, T. J.; Snieckus, V., Palladium-Catalyzed Cross-Coupling: A Historical Contextual Perspective to the 2010 Nobel Prize. *Angew. Chem., Intl. Ed.* **2012,** *51* (21), 5062-5085.
10. Kalyani, D.; Deprez, N. R.; Desai, L. V.; Sanford, M. S., Oxidative C-H Activation/C-C Bond Forming Reactions: Synthetic Scope and Mechanistic Insights. *J. Am. Chem. Soc.* **2005,** *127* (20), 7330-7331.
11. Chen, X.; Engle, K. M.; Wang, D. H.; Yu, J. Q., Palladium(II)-Catalyzed C-H Activation/C-C Cross-Coupling Reactions: Versatility and Practicality. *Angew Chem Int Edit* **2009,** *48* (28), 5094-5115.
12. Li, C. J., Cross-Dehydrogenative Coupling (CDC): Exploring C-C Bond Formations beyond Functional Group Transformations. *Acc. Chem. Res.* **2009,** *42* (2), 335-344.
13. Chiusoli, G. P.; Catellani, M.; Costa, M.; Motti, E.; Della Ca, N.; Maestri, G., Catalytic C-C coupling through C-H arylation of arenes or heteroarenes. *Coord. Chem. Rev.* **2010,** *254* (5-6), 456-469.
14. Neufeldt, S. R.; Sanford, M. S., Controlling Site Selectivity in Palladium-Catalyzed C-H Bond Functionalization. *Acc. Chem. Res.* **2012,** *45* (6), 936-946.
15. Le Bras, J.; Muzart, J., Intermolecular Dehydrogenative Heck Reactions. *Chemical Reviews* **2011,** *111* (3), 1170-1214.
16. Wu, Y.; Wang, J.; Mao, F.; Kwong, F. Y., Palladium-Catalyzed Cross-Dehydrogenative Functionalization of C(sp2)-H Bonds. *Chemistry – An Asian Journal* **2014,** *9* (1), 26-47.
17. Kitamura, T.; Fujiwara, Y., Dehydrogenative Heck-type Reactions: The Fujiwara-Moritani Reaction. In *From C-H to C-C Bonds: Cross-Dehydrogenative-Coupling*, Li, C.-J., Ed. The Royal Society of Chemistry: 2015; Vol. 26, pp 33-54.

18. Girard, S. A.; Knauber, T.; Li, C.-J., The Evolution of the Concept of Cross-Dehydrogenative-Coupling Reactions. In *From C-H to C-C Bonds: Cross-Dehydrogenative-Coupling*, Li, C.-J., Ed. Royal Society of Chemistry: 2015; Vol. 26, pp 1-32.
19. Shang, X.; Liu, Z.-Q., Transition metal-catalyzed Cvinyl-Cvinyl bond formation via double Cvinyl-H bond activation. *Chem. Soc. Rev.* **2013,** *42* (8), 3253-3260.
20. Yatsimirsky, A. K.; Ryabov, A. D.; Berezin, I. V., Olefin π-complex formation and kinetics of oxidative dimerisation in the palladium(II) acetate system. *J. Mol. Cat.* **1978,** *4* (2), 151-162.
21. Hwang, Y.-A.; Kim, D.-H.; Baek, D.-J., Activation of Aromatic Carbon-Hydrogen Bonds by Palladium Trifluoroacetate Complexes. *J. Korean Chem. Soc.* **2006,** *50* (5), 369-373.
22. Sun, Q.; Cai, L.; Ding, Y.; Xie, L.; Zhang, C.; Tan, Q.; Xu, W., Dehydrogenative Homocoupling of Terminal Alkenes on Copper Surfaces: A Route to Dienes. *Angew. Chem., Intl. Ed.* **2015,** *54* (15), 4549-4552.
23. Wen, Y.; Xie, J.; Deng, C.; Wu, Y., Synthesis of Buta-1,3-dienes through Palladium-Catalyzed Homocoupling of Aromatic Alkenes. *Synlett* **2015,** *26* (12), 1755-1758.
24. Arndtsen, B. A.; Bergman, R. G.; Mobley, T. A.; Peterson, T. H., Selective Intermolecular C-H Bond Activation by Synthetic Metal Complexes in Homogeneous Solution. *Acc. Chem. Res.* **1995,** *28*, 154-162.
25. Crabtree, R. H., The organometallic chemistry of alkanes. *Chem. Rev.* **1985,** *85* (4), 245-69.
26. Choi, J.; Goldman, A. S., Ir-Catalyzed Functionalization of C−H Bonds. *Top. Organomet. Chem.* **2011,** *34*, 139–168.
27. Choi, J.; MacArthur, A. H. R.; Brookhart, M.; Goldman, A. S., Dehydrogenation and Related Reactions Catalyzed by Iridium Pincer Complexes. *Chem. Rev.* **2011,** *111* (3), 1761-1779.
28. Findlater, M.; Choi, J.; Goldman, A. S.; Brookhart, M., Alkane dehydrogenation. In *Catal. Met. Complexes*, Springer: 2012; Vol. 38, pp 113-141.
29. Baratta, W.; Ballico, M.; Del Zotto, A.; Zangrando, E.; Rigo, P., C-H Activation and C-C Double Bond Formation Reactions in Iridium ortho-Methyl Arylphosphane Complexes. *Chem.-Eur. J.* **2007,** *13* (23), 6701-6709.
30. Polukeev, A. V.; Marcos, R.; Ahlquist, M. S. G.; Wendt, O. F., Formation of a C-C double bond from two aliphatic carbons. Multiple C-H activations in an iridium pincer complex. *Chem. Sci.* **2015,** *6* (3), 2060-2067.
31. Nie, S.-z.; Sun, X.; Wei, W.-t.; Zhang, X.-j.; Yan, M.; Xiao, J.-l., Unprecedented Construction of C═C Double Bonds via Ir-Catalyzed Dehydrogenative and Dehydrative Cross-Couplings. *Organic Letters* **2013,** *15* (10), 2394-2397.
32. Zhou, T.; Li, L.; Li, B.; Song, H.; Wang, B., Ir(III)-Catalyzed Oxidative Coupling of NH Isoquinolones with Benzoquinone. *Organic Letters* **2015,** *17* (17), 4204-4207.
33. Itoh, M.; Hirano, K.; Satoh, T.; Shibata, Y.; Tanaka, K.; Miura, M., Rhodium- and Iridium-Catalyzed Dehydrogenative Cyclization through Double C–H Bond Cleavages To Produce Fluorene Derivatives. *J. Org. Chem.* **2013,** *78* (4), 1365-1370.

34. Ghosh, R.; Emge, T. J.; Krogh-Jespersen, K.; Goldman, A. S., Combined experimental and computational studies on carbon-carbon reductive elimination from bis(hydrocarbyl) complexes of (PCP)Ir. *J. Am. Chem. Soc.* **2008,** *130* (34), 11317-11327.
35. Kanzelberger, M.; Singh, B.; Czerw, M.; Krogh-Jespersen, K.; Goldman, A. S., Addition of C-H bonds to the Catalytically Active Complex (PCP)Ir (PCP = η^3-2,6-$(R_2PCH_2)_2C_6H_3$). *J. Am. Chem. Soc.* **2000,** *122* (44), 11017-11018.
36. Wilklow-Marnell, M.; Brennessel, W. W.; Jones, W. D., Formation of 5-membered metallacycles at iPrPCPIr by C–H, O–H, and C–CO bond cleavage. *Polyhedron* **2016,** *116*, 38-46.
37. Laviska, D. A.; Zhou, T.; Kumar, A.; Emge, T. J.; Krogh-Jespersen, K.; Goldman, A. S., Single and Double C−H Activation of Biphenyl or Phenanthrene. An Example of C−H Addition to Ir(III) More Facile than Addition to Ir(I). *Organometallics* **2016,** *35*, 1613-1623.
38. Laviska, D. A.; Guan, C.; Emge, T. J.; Wilklow-Marnell, M.; Brennessel, W. W.; Jones, W. D.; Krogh-Jespersen, K.; Goldman, A. S., Addition of C-C and C-H Bonds by Pincer-Iridium Complexes: a Combined Experimental and Computational Study. *Dalton Trans.* **2014,** *43* (43), 16354-16365.
39. Göttker-Schnetmann, I.; White, P.; Brookhart, M., Iridium Bis(phosphinite) p-XPCP Pincer Complexes: Highly Active Catalysts for the Transfer Dehydrogenation of Alkanes. *J. Am. Chem. Soc.* **2004,** *126* (6), 1804 -1811.
40. Kumar, A.; Zhou, T.; Emge, T. J.; Mironov, O.; Saxton, R. J.; Krogh-Jespersen, K.; Goldman, A. S., Dehydrogenation of *n*-Alkanes by Solid-Phase Molecular Pincer-Iridium Catalysts. High Yields of α-Olefin Product. *J. Am. Chem. Soc.* **2015,** *137* (31), 9894-9911.
41. Laviska, D. A. Activation Of Aryl C-H And C-X Bonds By A Pincer-Ligated 'PCP' Iridium Complex. Ph.D. thesis, Rutgers University, 2013.
42. Zhang, X.; Kanzelberger, M.; Emge, T. J.; Goldman, A. S., Selective Addition to Iridium of Aryl C-H Bonds Ortho to Coordinating Groups. Not Chelation-Assisted. *J. Am. Chem. Soc.* **2004,** *126* (41), 13192-13193.
43. Choi, J.; Choliy, Y.; Zhang, X.; Emge, T. J.; Krogh-Jespersen, K.; Goldman, A. S., Cleavage of sp^3 C-O Bonds via Oxidative Addition of C-H Bonds. *J. Am. Chem. Soc.* **2009,** *131* (43), 15627-15629.
44. Sandoval, A.; Zechmeister, L., Some Spectroscopic Changes Connected with the Stereoisomerization of Diphenylbutadiene. *J. Am. Chem. Soc.* **1947,** *69* (3), 553-557.
45. Laviska, D. A.; Wang, D. Y.; Krogh-Jespersen, K.; Goldman, A. S. In *Effects of aryl substituents on the kinetics and thermodynamics of C-H bond activation by a pincer-ligated iridium complex*, Abstracts of Papers, 244th ACS National Meeting & Exposition, Philadelphia, PA, United States, August 19-23, 2012, American Chemical Society: 2012; pp INOR-1223.
46. Krogh-Jespersen, K.; Czerw, M.; Summa, N.; Renkema, K. B.; Achord, P. D.; Goldman, A. S., On the Mechanism of (PCP)Ir-catalyzed Acceptorless Dehydrogenation of Alkanes: a Combined Computational and Experimental Study. *J. Am. Chem. Soc.* **2002,** *124*, 11404-11416.
47. Ghosh, R.; Zhang, X.; Achord, P.; Emge, T. J.; Krogh-Jespersen, K.; Goldman, A. S., Dimerization of Alkynes Promoted by a Pincer Ligated Iridium Complex. C-C Reductive Elimination Inhibited by Steric Crowding. *J. Am. Chem. Soc.* **2007,** *129* (4), 853-866.

48. Heinekey, D. M.; Lledos, A.; Lluch, J. M., Elongated dihydrogen complexes: what remains of the H-H Bond? *Chem. Soc. Rev.* **2004,** *33* (3), 175-182.
49. Oxgaard, J.; Muller, R. P.; Goddard, W. A.; Periana, R. A., Mechanism of Homogeneous Ir(III) Catalyzed Regioselective Arylation of Olefins. *Journal of the American Chemical Society* **2004,** *126* (1), 352-363.
50. Oxgaard, J.; Periana, R. A.; Goddard, W. A., III, Mechanistic Analysis of Hydroarylation Catalysts. *J. Am. Chem. Soc.* **2004,** *126* (37), 11658-11665.
51. Krogh-Jespersen, K.; Czerw, M.; Zhu, K.; Singh, B.; Kanzelberger, M.; Darji, N.; Achord, P. D.; Renkema, K. B.; Goldman, A. S., Combined Computational and Experimental Study of Substituent Effects on the Thermodynamics of H_2, CO, Arene, and Alkane Addition to Iridium. *J. Am. Chem. Soc.* **2002,** *124*, 10797-10809.
52. Montag, M.; Schwartsburd, L.; Cohen, R.; Leitus, G.; Ben-David, Y.; Martin, J. M. L.; Milstein, D., The unexpected role of CO in C-H oxidative addition by a cationic rhodium(I) complex. *Angew. Chem., Int. Ed.* **2007,** *46* (11), 1901-1904.
53. Goldman, A. S.; Ghosh, R., C-H Transformation at Unfunctionalized Alkanes Handbook of C-H Transformations: Applications in Organic Synthesis. **2008,** *2*, 497-651.
54. Kumar, A.; Zhou, T.; Emge, T. J.; Mironov, O.; Saxton, R. J.; Krogh-Jespersen, K.; Goldman, A. S., Dehydrogenation of n-Alkanes by Solid-Phase Molecular Pincer-Iridium Catalysts. High Yields of α-Olefin Product. *Journal of the American Chemical Society* **2015,** *137* (31), 9894-9911.
55. Koch, W.; Holthausen, M. C., *A Chemist's Guide to Density Functional Theory*. Wiley: New York, 2001.
56. Zhao, Y.; Truhlar, D. G., A new local density functional for main-group thermochemistry, transition metal bonding, thermochemical kinetics, and noncovalent interactions. *J. Chem. Phys.* **2006,** *125* (19), 194101/1-194101/18.
57. Zhao, C. Y.; Truhlar, D. G., The M06 Suite of Density Functionals for Main Group Thermochemistry, Kinetics, Noncovalent Interactions, Excited States, and Transition Elements: Two New Functionals and Systematic Testing of Four M06 Functionals and Twelve Other Functionals. *Theo. Chem. Acc.* **2008,** *120*, 215-241.
58. Perdew, J. P.; Burke, K.; Ernzerhof, M., Generalized gradient approximation made simple. *Phys Rev. Lett.* **1996,** *77* (18), 3865-3868.
59. Hay, P. J.; Wadt, W. R., Ab initio effective core potentials for molecular calculations. Potentials for potassium to gold including the outermost core orbitals. *J. Chem. Phys.* **1985,** *82* (Copyright (C) 2012 American Chemical Society (ACS). All Rights Reserved.), 299-310.
60. Roy, L. E.; Hay, P. J.; Martin, R. L., Revised Basis Sets for the LANL Effective Core Potentials. *J. Chem. Theory Comput.* **2008,** *4* (7), 1029–1031.
61. outermost-d-LANL2TZ, Value obtained as one-half times the exponent of the outermost d-type function in the LANL2TZ basis set for Ir.
62. ValenceBasisSets2014, ValenceBasisSets2014 for JCSDT C-C Cleavage.
63. Hratchian-First40Years, Hratchian, H. P.; Schlegel, H. B. in Theory and Applications of Computational Chemistry: The First 40 Years, .
64. McQuarrie, D. A., *Statistical Thermodynamics*. Harper and Row: New York, 1973.
65. Wheeler, S. E.; Houk, K. N., Integration Grid Errors for Meta-GGA-Predicted Reaction Energies: Origin of Grid Errors for the M06 Suite of Functionals. *J. Chem. Theory Comput.* **2010,** *6* (2), 395-404.

66. Frisch, Æ.; Frisch, M. J.; Clemente, F. R.; G. W. Trucks, *Gaussian 09 User's Reference*, 147.
67. Frisch, M. J.; Trucks, G. W.; Schlegel, H. B.; Scuseria, G. E.; Robb, M. A.; Cheeseman, J. R.; Scalmani, G.; Barone, V.; Mennucci, B.; Petersson, G. A.; Nakatsuji, H.; Caricato, M.; Li, X.; Hratchian, H. P.; Izmaylov, A. F.; Bloino, J.; Zheng, G.; Sonnenberg, J. L.; Hada, M.; Ehara, M.; Toyota, K.; Fukuda, R.; Hasegawa, J.; Ishida, M.; Nakajima, T.; Honda, Y.; Kitao, O.; Nakai, H.; Vreven, T.; Montgomery, J. J. A.; Peralta, J. E. O., F.; Bearpark, M.; Heyd, J. J.; Brothers, E.; Kudin, K. N.; Staroverov, V. N.; Kobayashi, R.; Normand, J.; Raghavachari, K.; Rendell, A.; Burant, J. C.; Iyengar, S. S.; Tomasi, J.; Cossi, M.; Rega, N.; Millam, N. J.; Klene, M.; Knox, J. E.; Cross, J. B.; Bakken, V.; Adamo, C.; Jaramillo, J.; Gomperts, R.; Stratmann, R. E.; Yazyev, O.; Austin, A. J.; Cammi, R.; Pomelli, C.; Ochterski, J. W.; Martin, R. L.; Morokuma, K.; Zakrzewski, V. G.; Voth, G. A.; Salvador, P.; Dannenberg, J. J.; Dapprich, S.; Daniels, A. D.; Farkas, Ö.; Foresman, J. B.; Ortiz, J. V.; Cioslowski, J.; Fox, D. J., Gaussian 09, Revision D.01. Gaussian 09, Revision D.01, Gaussian, Inc., Wallingford, CT, 2009. See Supporting Information for the complete reference to Gaussian 09.
68. Hintermann, L.; Schmitz, M.; Chen, Y., A Direct Synthesis of Symmetrical (E,E)-1,4-Diaryl-1,3-butadienes by Wenkert Arylation of Thiophene. *Advanced Synthesis & Catalysis* **2010,** *352* (14-15), 2411-2415.
69. Babudri, F.; Farinola, G. M.; Naso, F.; Ragni, R.; Spina, G., A Novel Stereoselective Synthesis of Symmetrical (1E,3E)-1,4-Diarylbuta-1,3-dienes. *Synthesis* **2007,** *2007* (19), 3088-3092.
70. Liu, J.; Wendt, N. L.; Boarman, K. J., Trifluoromethyl Groups in Crystal Design of 1,4-Diphenyl-1,3-butadienes for Topochemical [2 + 2] Photodimerization. *Organic Letters* **2005,** *7* (6), 1007-1010.
71. Liu, J.; Boarman, K. J.; Wendt, N. L.; Cardenas, L. M., Regiospecific photoisomerization of fluorinated (E,E)-1,4-diphenyl-1,3-butadienes. *Tetrahedron Letters* **2005,** *46* (30), 4953-4956.
72. Yoshida, K.; Takahashi, H.; Imamoto, T., Synthesis of Substituted Benzenes and Phenols by Ring-Closing Olefin Metathesis. *Chemistry – A European Journal* **2008,** *14* (27), 8246-8261.
73. Call, A.; Franco, F.; Kandoth, N.; Fernandez, S.; Gonzalez-Bejar, M.; Perez-Prieto, J.; Luis, J. M.; Lloret-Fillol, J., Understanding light-driven H2 evolution through the electronic tuning of aminopyridine cobalt complexes. *Chemical Science* **2018**.
74. Laviska, D. A.; Guan, C. J.; Emge, T. J.; Wilklow-Marnell, M.; Brennessel, W. W.; Jones, W. D.; Krogh-Jespersen, K.; Goldman, A. S., Addition of C-C and C-H bonds by pincer-iridium complexes: a combined experimental and computational study. *Dalton T* **2014,** *43* (43), 16354-16365.
75. Laviska, D. A.; Zhou, T.; Kumar, A.; Emge, T. J.; Krogh-Jespersen, K.; Goldman, A. S., Single and Double C–H Activation of Biphenyl or Phenanthrene. An Example of C–H Addition to Ir(III) More Facile than Addition to Ir(I). *Organometallics* **2016**.

Chapter 4. Cross-dehydrogenative coupling vinyl arenes with aromatics and olefins

Abstract: The success of using a pincer-iridium complex as the catalyst to efficiently effect the dehydrogenative homo-coupling of vinyl arenes has driven us to apply this methodology to cross-dehydrogenative coupling of vinyl arenes with unfunctionalized aromatics and olefins based on the reported metalloindene mechanism. The cross-coupling reaction of styrene with benzene or tert-butyl ethylene (TBE) by pincer-iridium complex gave high selectivity and yield without oxidant or additives. Other vinyl arene with aromatics and alkenes could also effect the cross-coupling reaction with good selectivity and moderate yield. The reaction selectivity was greatly affected by the steric crowdedness of catalysts when benzene was used as substrate, while moderate effects were observed with TBE. The cross-coupling reaction of homo-coupling non-active substrates α-methyl styrene with benzene or TBE proceeded. Tandem dehydrogenation and coupling reaction could also be performed. All these cross-coupling reactions further supported the proposed metalloindene mechanism for homo-coupling vinyl arenes.

4.1. Introduction

As one of the most essential bonds in organic organisms, the carbon-carbon (C-C) bond has been the focus of lot researchers in the term of its formation and cleavage. Compared to the "ease" of cleavage of C-C bond at high temperature with heterogeneous catalysts, formation of C-C bond seems to be much more complicated, but also high demanded.[1] The quick development of transition metal complexes over the past several decades has demonstrated the ability to effect C-C bond formation via different methods. The most common methods for C-C bond formation catalyzed by transitional metals could be catalogued in three major groups, shown in scheme 4.1.[2] For the first route, which is also the most popular and widely used method, including Suzuki reaction, Stille reaction, and Negishi Reaction, requires pre-activated substrates C-X and C-Y together with an active organometallic species.[3-11] The second route takes the advantage of C-H activation by transitional metals,[12-14] coupling between C-H bond and C-X bond (heck reaction),[4, 7, 11, 15] which could possible reduce the cost of synthesizing C-Y from C-H. Significant progress of the dehydrogenative coupling (CDC, route 3), which forms C-C bond directly from two C-H bonds of non-functionalized alkanes, alkenes, and alkynes,[16-20] has been made since the initial work of Fujiwara and Moritani.[21-27] CDC showed the greatest potential among these three methodologies, considering reactant, atomic efficiency, economy, and environmental effects. However, this methodology suffered from a high catalyst (typically palladium complexes) loading, the requirement of stoichiometric amount of added oxidant and functional group, and poor selectivity and/or yields.[28-31] Developing simple dehydrogenative coupling reaction with less limitations has been the goal of most researchers in this field.

Scheme 4. 1. Different method for C-C bond formation by transitional metal

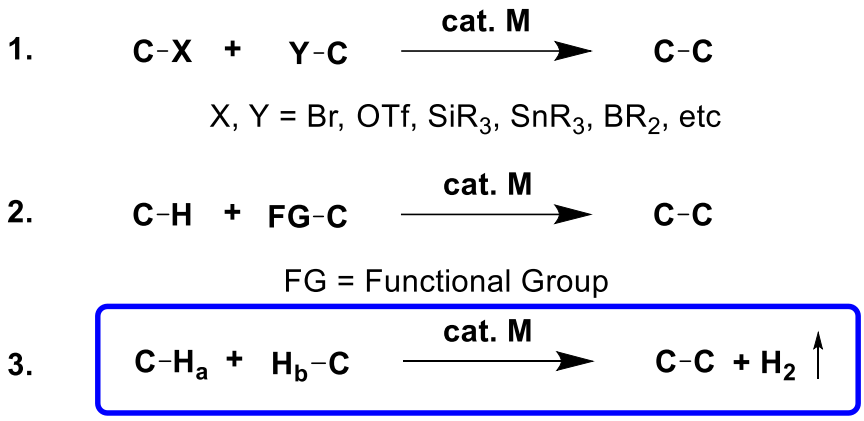

Figure 4. 1. Proposed mechanism for styrene homo-coupling reaction

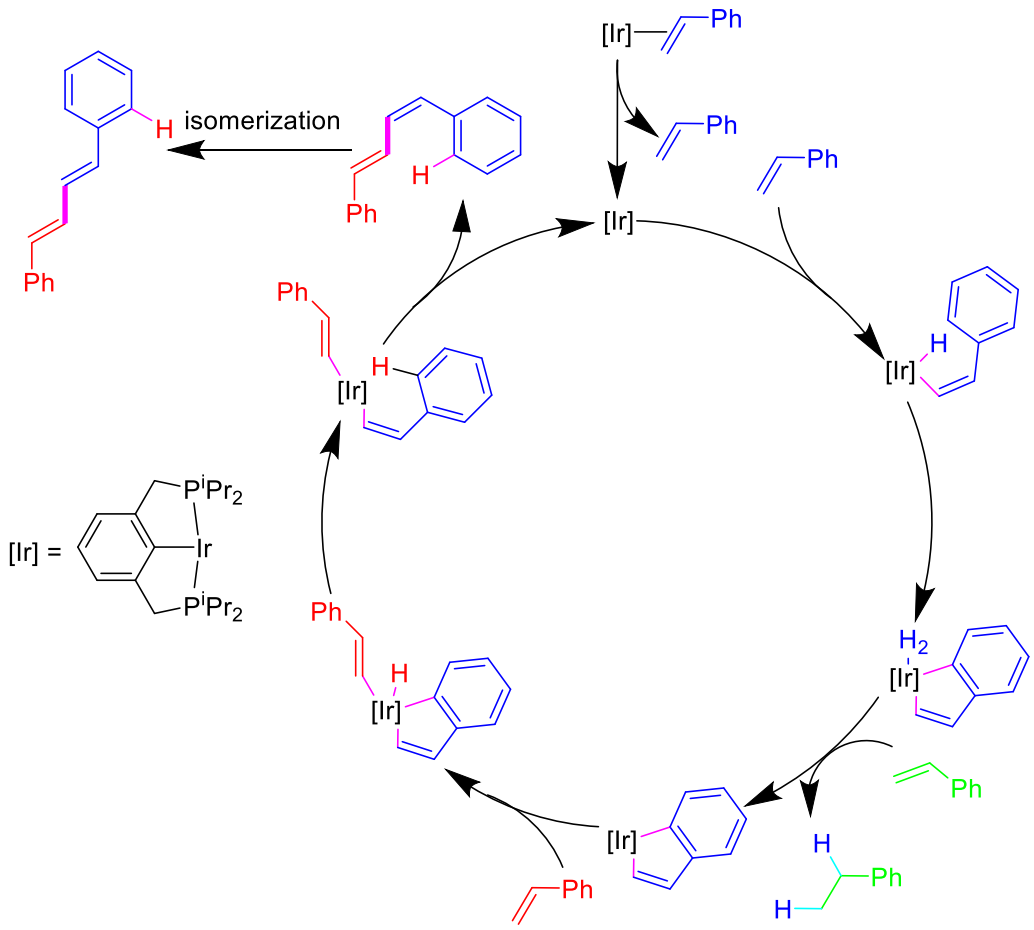

Using transition metal complexes for C-H activation and further functionalization has been widely studied in recently years.[32-38] The success of using pincer-iridium complex

as the catalyst to efficiently effect the dehydrogenative homo-coupling of vinyl arenes[39] has driven us to study the reaction in a wider scope. Based on the proposed metalloindene mechanism, showed in Figure 4.1, we figured out the oxidative addition of the third molecular styrene (in red color) to metalloindene complex does not involve any other moiety except for the β-vinylic C-H bond, which raises the possibility of replacing it with aromatics or olefins and, in effect, performing cross-dehydrogenative coupling. We proposed a cross-coupling reaction route based on the metalloindene complex for vinyl arene coupling with aromatics or alkenes, with reaction route shown in scheme 4.2 and the reaction equation displayed in scheme 4.3.

Scheme 4. 2. Proposed CDC reaction route

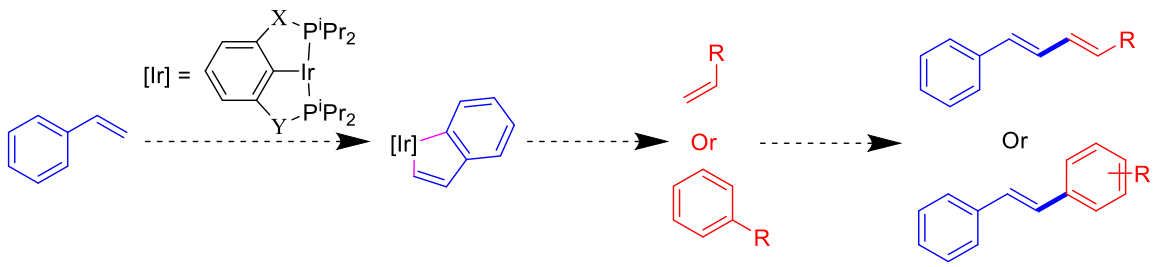

Scheme 4. 3. Proposed CDC reaction equation

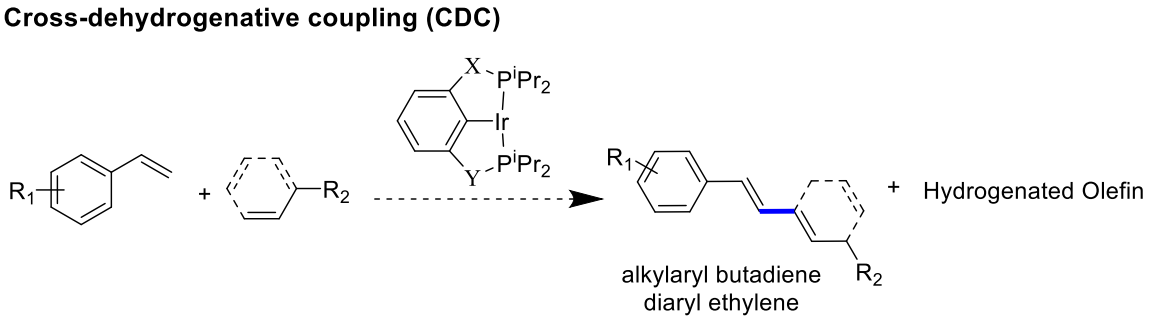

4.2. Results and discussion

4.2.1. Cross-coupling styrene with stoichiometric amount benzene or TBE using (^{iPr}PCP)Ir as catalyst

Initial cross-coupling reaction was run with 1:1 ratio styrene and benzene (simplest aromatic). With different pincer-iridium complexes as catalysts, showed in Figure 4.2, there was almost no to little amount stilbene (cross-coupling product) observed by either NMR or GC. Similar results were obtained for the cross-coupling with 1:1 ratio styrene and TBE (simplest non-gas and non-isomerizable olefin by pincer-iridium complex). Considering the β-vinylic C-H bond of styrene is highly activated through the conjugated π system, it is reasonable to predict better reactivity for it, which means the homo-coupling of styrene dominates the reaction. However, if excess amount of aromatics or alkenes is present, the kinetic effect would change the reaction selectivity. In this way, aromatics and alkenes, here benzene and TBE, would dominate the C-H oxidative addition to metalloindene complex, and then gave cross-coupling products as the major products, showed in scheme 4.4.

Figure 4. 2. Different pincer-iridium catalysts used for CDC reaction

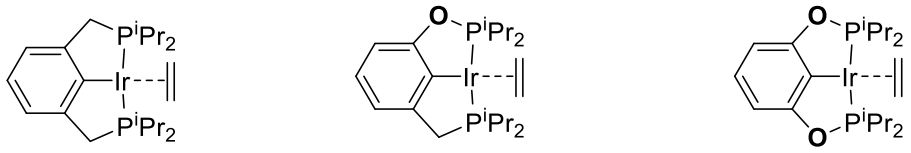

Cat-1 **Cat-2** **Cat-3**

Scheme 4. 4. Proposed CDC reaction route with excess amount of aromatics and alkene

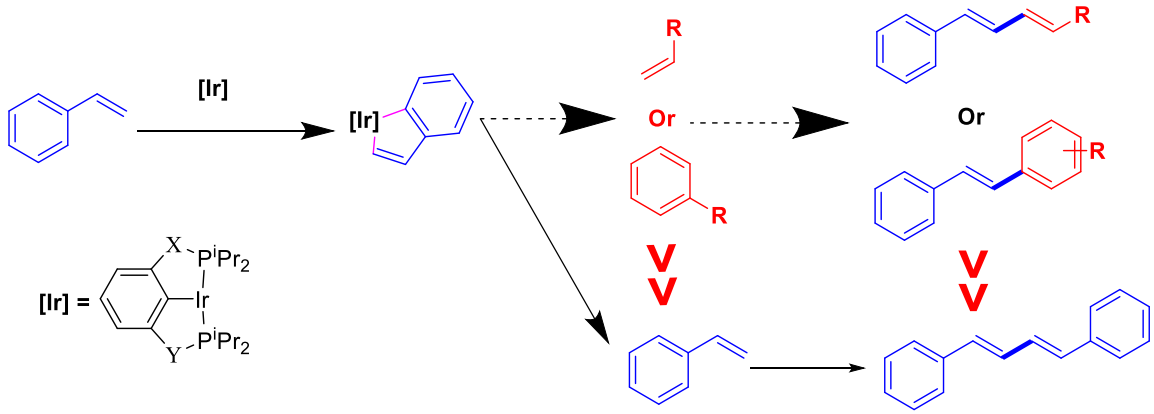

4.2.2. Cross-coupling styrene with excess amount benzene by pincer-iridium complex

The selectivity towards cross-coupling over homo-coupling was greatly enhanced with increasing amount of benzene added, which selectivities as high as 9.2:1 [cross coupling product vs homo-coupling products (C:H)], showed in table 4.1., entry 1-4. Increased product amounts and reaction conversion were also observed by increasing benzene concentration from 1.25 M to 5 M. However, increasing the concentration of benzene further to 10 M did not give better yield and conversion, which is probably due to the greater vaporization effect of mostly benzene (b.p. 80°C) under experiment condition (200°C), while styrene and catalyst remained in the solution. Compared to reported catalysis of cross-coupling benzene with styrene (using Pd catalyst and oxidant, with or without additives),[22, 40-45] we could achieve both high yield (73% vs highest reported 82% and most cases 20-40%) and high selectivity (86%) with only 20 eq benezene used (compared to 40-200 eq in reported examples). Also, this new catalysis by pincer-iridium complex did not require any oxidant, and additives with styrene served as both substrate and hydrogen acceptor. Similar to styrene homo-coupling reactions, there were up to 10%

Z isomer together with the major *E* isomer in cross-coupling reactions. In addition to that, there were also up to 10% hydrogenated coupling products showed in products due to the low amount of hydrogen acceptor presented.

Meanwhile, the catalyst played an even more important role in terms of selectivity. (^{iPr}PCP)Ir(ethylene) (**Cat-1**) showed the preference towards homo-coupling even with excess amount benzene, while (^{iPr}POCOP)Ir(ethylene) (**Cat-3**) totally reversed the selectivity and gave major cross-coupling product. (^{iPr}PCOP)Ir(ethylene) (**Cat-2**) presented a compromised selectivity of **Cat-1** and **Cat-3**. The selectivity difference among these three catalysts could be attribute to either steric or electronic effect, since the three catalyst has different steric crowdedness and electron density at the iridium center. To maximize both selectivity and yield, we set aromatics to vinyl arene ratio as 20:1 and used **Cat-3** as catalyst for the rest of the substrates.

Table 4. 1. Evaluation of reaction condition and catalysts

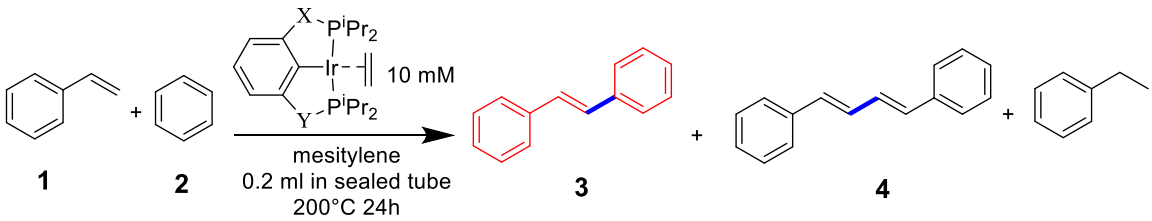

Reaction	Catalyst	1 (mM)	2 (M)	3 (mM)	4 (mM)	3:4 (C:H)	Conversion
1	**Cat-3**	250	1.25	22	17	1.3:1	87%
2	**Cat-3**	250	2.5	64	22	2.9:1	92%
3	**Cat-3**	250	5	91	15	6.1:1	95%
4	**Cat-3**	250	10	87	10	8.7:1	91%
5	**Cat-1**	250	5	25	47	0.5:1	99%
6	**Cat-2**	250	5	56	20	2.8:1	96%

Reaction conducted with 250 mM styrene, 1.25 - 10 M benzene, and 10 mM pincer-iridium complex in mesitylene (total 0.1 ml) sealed in glass tube and heated in GC oven under 200°C.

4.2.3. Cross-coupling vinyl arenes with aromatics by pincer-iridium complex

This cross-coupling reaction could also be applied for coupling other vinyl arenes with aromatics, showed in figure 4.3. However, the yield of cross-coupling products was significantly lowered (20-50%) compared to the cross-coupling reaction of styrene and benzene. The lower purity of the vinyl arene and aromatics could be the major obstacles. Better yield was achieved by purifying the substrates or increasing catalyst loading. The non-homo-coupling active substrate, α-methyl styrene, could also be used as substrate for this cross-coupling reaction. As was discussed in a previous chapter[39], although α-methyl styrene could form metalloindene complex with pincer-iridium, the steric crowdedness originating from the α-methyl group prevented the second molecular α-methyl styrene oxidative addition. Benzene, a planar molecule, showed the ability of accessing iridium center of metalloindene complex formed from α-methyl styrene and effecting the cross-coupling reaction. This cross-coupling only reaction by α-methyl styrene and benzene further supported the proposed metalloindene mechanism. Vinyl arenes with electron donating groups on the phenyl ring did not help the reaction yield, although they gave better yield in homo-coupling reaction.[39] On the contrary, electron donating groups (CH_3 and CH_3O) on vinyl arenes lowered the yield more than vinyl arenes with electron withdrawing group (CF_3) compared to styrene. However, benzene with electron donating group (CH_3) and withdrawing group (CF_3) substituents did not affect the selectivity and yield of the coupling reaction, which indicated the iridium center was not sensitive toward electronic effect for C-H addition to metalloindene complex.

Figure 4. 3. Cross-coupling vinyl arenes with aromatics

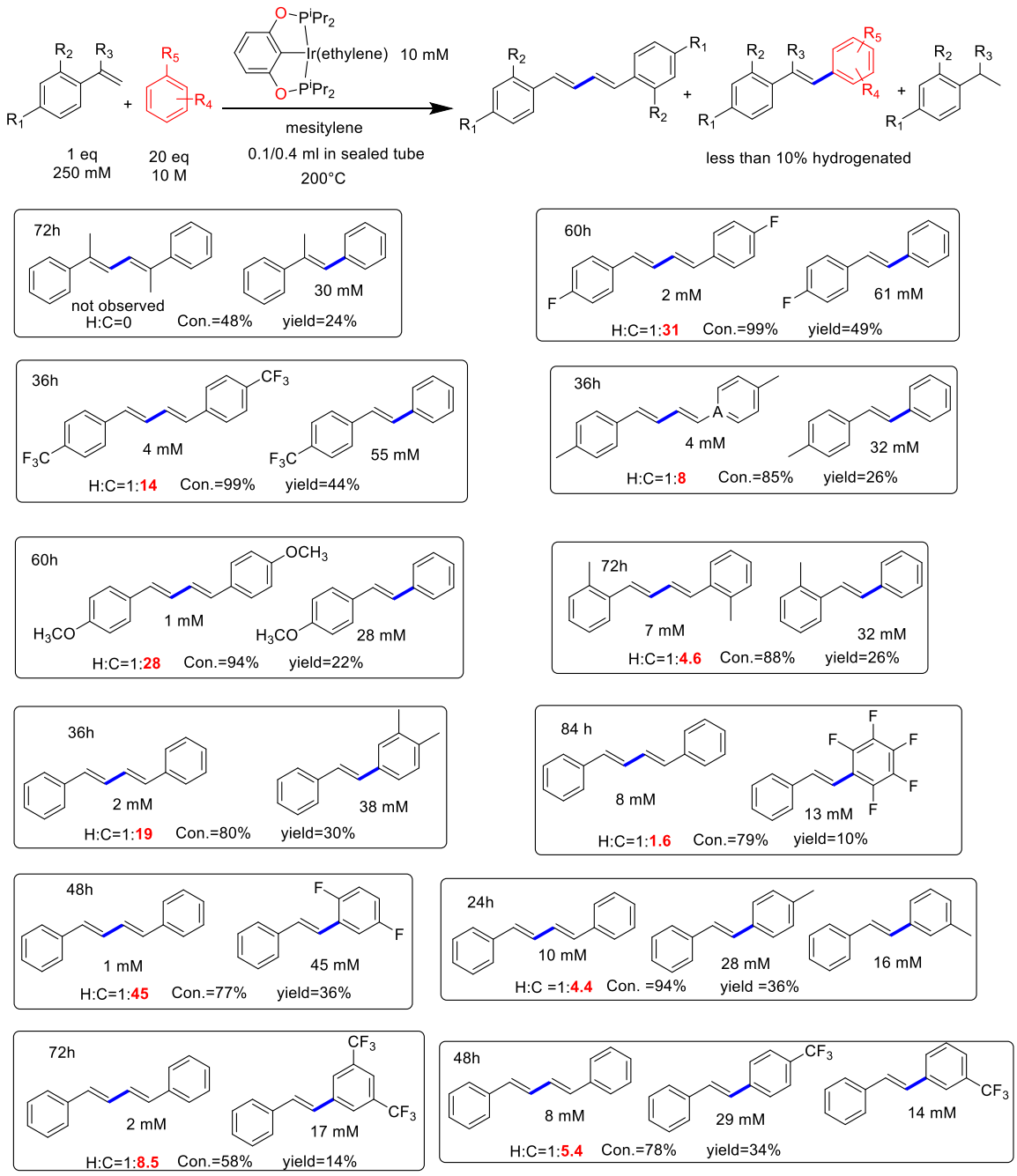

Reaction conducted with 250 mM vinyl arenes, 5 M aromatics, and 10 mM pincer-iridium complex in mesitylene (total 0.1 or 0.5 ml) sealed in glass tube and heat in GC oven under 200°C.

The insensitivity of this CDC reaction towards substrate electronic properties made us believe that iridium center crowdedness was the key reason of selectivity change among

these three catalysts. As discussed by Goldman, (^{tBu}POCOP)Ir is much less sterically hindered compared to (^{tBu}PCP)Ir, since the P-O-C angle is bigger than P-C-P.[46] Metalloindene formed from **Cat-1** disfavored the benzene oxidative addition due to the repulsion from alkyl group on phosphine, while the interaction of iso-propyl group from pincer-iridium with vinyl arene in homo-coupling reaction only happened at much less steric crowded vinyl group region. The intermolecular coupling between (^{tBu}PCP)Ir, with bigger alkyl group, and styrene described in chapter 2 further supported this hypothesis. Further evidence to support this is the absence of cross-coupling products from vinyl arene and phenyl on vinyl arene even at high vinyl arene concentration (up to 2 M). With two P-O-C motif, **Cat-3** presented the lowest repulsion from its alkyl group to substrates and gave best selectivity towards cross-coupling.

4.2.4. Cross-coupling vinyl arenes with heterocyclic compounds by pincer-iridium complex

Furan, with a reactive α-C-H bond, was one the best substrates for cross-coupling with vinyl arenes.[47-52] It was not surprising that furan also presented good selectivity in this CDC reaction catalyzed by a pincer-iridium complex. Reacted with 2 eq styrene (the other 1 eq styrene acted as hydrogen acceptor), furan gave over 99% selectivity towards cross-coupling products and over 80% yield. Substituents, such as methyl or phenyl, did not affect the reactivity. When its analog, thiophene, was used as substrates, poor selectivity and yield was achieved compared to furan. Compared to aromatics under same reaction condition, thiophene could showed better selectivity.

Figure 4. 4. Cross-coupling vinyl arenes with heterocyclic compound

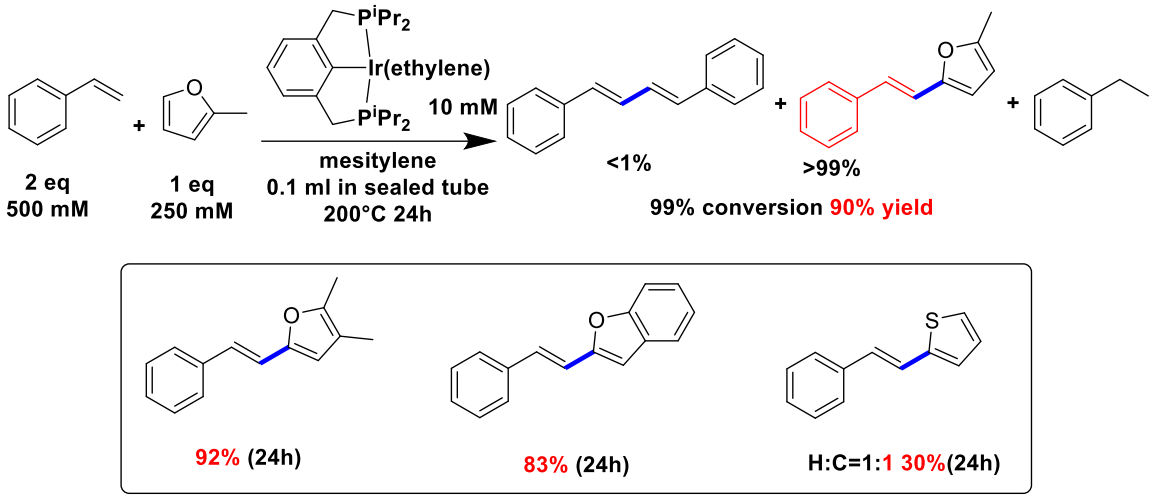

Reaction conducted with 500 mM styrene, 250 mM furan or thiophene, and 10 mM pincer-iridium complex in mesitylene (total 0.1 ml) sealed in glass tube and heat in GC oven under 200°C.

4.2.5. Cross-coupling vinyl arenes with non-functionalized alkenes by pincer-iridium complex

To the best of our knowledge, there have been no reports about the direct coupling reaction of vinyl arenes with non-functionalized alkenes (such as ethylene, propylene, and TBE). The challenge of cross-coupling vinyl arenes with non-functionalized alkenes is the much more active vinyl group from vinyl arene would dominate the reaction, while the regular vinyl group from non-functionalized alkenes remained unreacted. The strong ability of pincer-iridium complex in C-H activation made the reactivity difference between different vinyl group relatively smaller, which raised the possibility of effecting the cross-coupling reaction of vinyl arenes with non-functionalized alkenes. To prove this concept, we used TBE, the simplest non-gaseous and non-isomerizable olefin by pincer-iridium complex, as the model to study the cross-coupling reaction. With the same reaction condition as the cross-coupling of styrene with benzene, we successfully performed the

selective cross-coupling reaction of styrene with TBE by different pincer-iridium catalysts, showed in table 4.2. Together with the major (*E*, *E*) isomers, up to 10% (*E*, *Z*) isomers were also present in this reaction, while hydrogenated coupling products were not present due to excess amount hydrogen acceptor TBE in the reaction. Unlike the cross-coupling reaction of styrene with benzene, different catalysts showed limited influence on the selectivity of coupling styrene with TBE, which further supported our explanation of selectivity difference for styrene and benzene cross-coupling reaction using steric crowdedness of the catalysts. Although the less sterically-hindered pincer-iridium complex gave the best selectivity with slightly lower yield, the main reason behind was the poor ability of **Cat-3** for catalyzing the homo-coupling of styrene.

Table 4. 2. Evaluation of catalysts for cross-coupling styrene with TBE

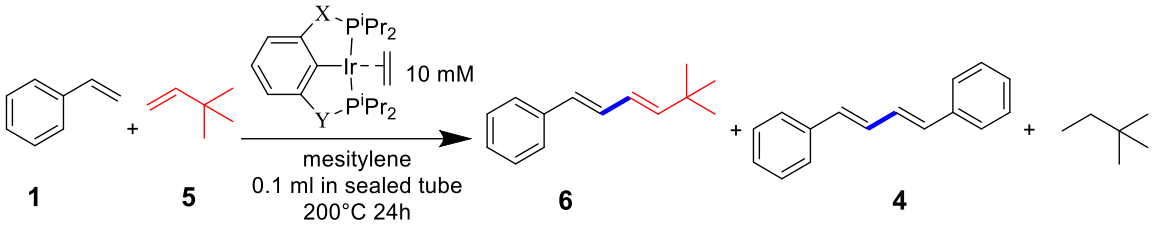

Reaction	Catalyst	1 (mM)	5 (M)	6 (mM)	4 (mM)	6:4 (C:H)	Conversion
1	**Cat-1**	250	33	145	33	4.4:1	99%
2	**Cat-2**	250	5	152	30	5.1:1	90%
3	**Cat-3**	250	10	120	10	12:1	95%

Reaction conducted with 250 mM styrene, 5 M TBE, and 10 mM pincer-iridium complex in mesitylene (total 0.1 ml) sealed in glass tube and heat in GC oven under 200°C.

One way to achieve better selectivity towards cross-coupling reaction was to generate the vinyl arene in situ, which could minimize the vinyl arene homo-coupling reaction. Dehydrogenation of alkyl benzene by pincer-iridium has been widely study by the Goldman group.[46, 53] Combining pincer-iridium complex's ability of dehydrogenation and coupling, we could effect cross-coupling reaction between ethylbenzene with TBE. In scheme 4.5, we showed **Cat-3** effected ethylbenzene with TBE coupling with similar yield

and better selectivity compared to styrene and TBE reaction. This was also one of the example to achieve a sp^2 C-C bond from one sp^3 and one sp^2 C-H bond through tandem dehydrogenation and coupling.

Scheme 4. 5. Tandem dehydrogenation and coupling

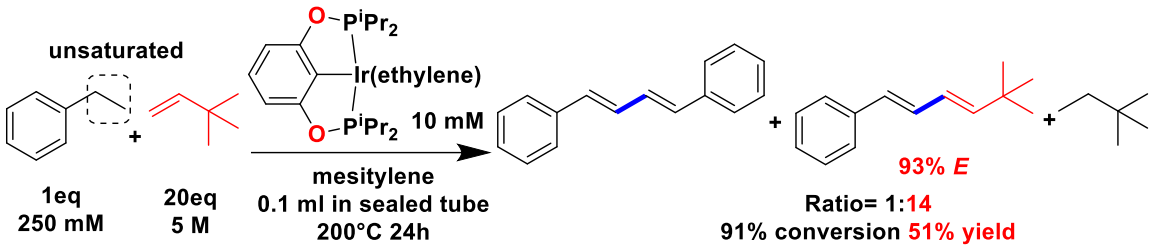

The quick isomerization reactions of alkenes by pincer-iridium complex greatly limited the reaction scope using alkene for cross-coupling reaction, since forming C-C bond at terminal position was preferred. As shown in figure 4.5, we achieved very good results with butadiene and isoprene, while propylene gave very poor selectivity due to the limited amount of propylene could be added in the reaction vessel. Different vinyl arenes gave different results, with electron donating groups on the phenyl ring giving better yield. However, compared to styrene, other vinyl arenes also gave low yields. The high reaction temperature required purer substrates for the reaction, otherwise, lower yield would be achieved. Cross-coupling α-methyl styrene with TBE also proceeded with moderate yield.

Figure 4. 5. Cross-coupling vinyl arenes with non-functionalized alkenes

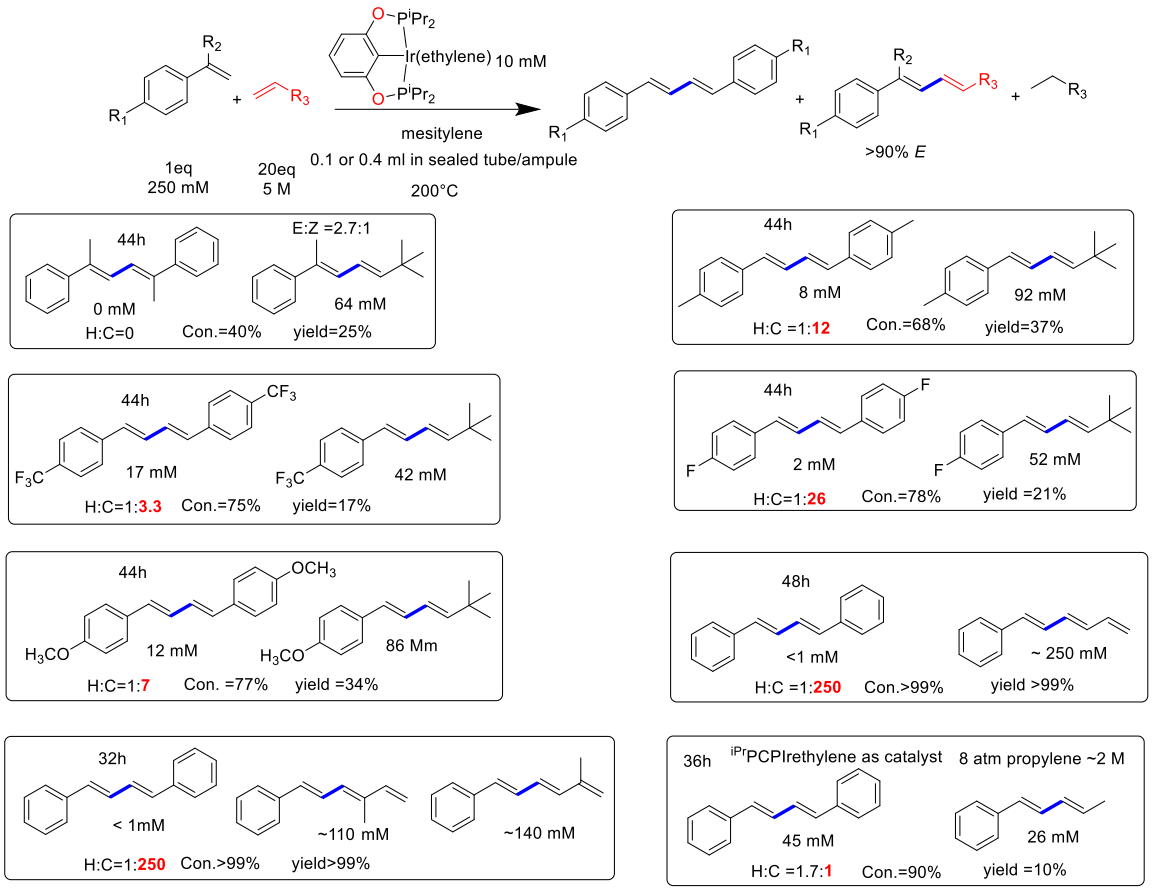

Reaction conducted with 250 mM vinyl arenes, 5 M alkene (if the alkene is gas then using 8 atm), and 10 mM pincer-iridium complex in mesitylene (total 0.1 or 0.5 ml) sealed in glass tube and heat in GC oven under 200°C.

4.3. Conclusion

Here, we reported a new methodology for cross-dehydrogenative coupling of vinyl arenes with non-functionalized aromatics and olefin based on the reported metalloindene mechanism of homo-coupling of vinyl arenes. This methodology gave high selectivity and yield when styrene and benzene (comparable to best example using CDC synthesis stilbene) or styrene and TBE were used as substrate, while good selectivity with moderate yield achieved for other substrates. The absence of oxidant and additives made the reaction easy and simple to execute. The steric crowdedness of catalysts great affected the selectivity

when aromatics were used as substrate, while moderate affects observed for alkene. The cross-coupling reaction of homo-coupling non-active substrates α-methyl styrene with benzene or TBE could also proceed. The tandem dehydrogenation and cross-coupling reaction could broaden the reactant scope and provide a new method to coupling alkanes to alkenes. All these results further supported the proposed metalloindene mechanism in a previous chapter for homo-coupling vinyl arenes.

4.4 Experimental information

4.4.1. General information

We conducted all our experiment either in an argon filled glovebox or using a schlenk line. NMR experiments were conducted on a 500 MHZ Varian VNMRS. ^{1}H and ^{13}C NMR spectra were referenced to residual deuterated solvent signal. All anhydrous solvents were purchased from Aldrich, flushed with argon, and stored in an argon atmosphere in a glovebox. All aromatic substrates were degassed, dried over activated alumina, and storage over 3-Å molecular sieves. Isoprene and TBE were degassed, dried over NaK alloy, removed NaK by vacuum transfer, and stored in glovebox freezer. All vinyl arenes were obtained from commercial sources or synthesized based on reported methods. Further treatment was carried out by drying them over calcium hydride, then distilling under reduced pressure. GC analysis was conducted using a Varian 430 GC with a 30 m capillary column, using helium carrier gas. GCMS analysis was conducted using a Varian 3900 GC with a 30 m capillary column coupled with a Saturn 2100T MS, using helium carrier gas. All pincer-iridium catalysts, (^{iPr}PCP)Ir(C_2H_4),[54] (^{iPr}PCOP)Ir(C_2H_4),[55] and (^{iPr}POCOP)Ir(C_2H_4)[56-57] were synthesized according reported methods.

General procedure for coupling of vinyl arenes with aromatics and alkenes: to a glass tube (4 or 6-inch-long borosilicate glass tube with ¼ inch inner diameter) were added 10 mM pincer-iridium complex, 250 mM vinyl arene, and 5 M aromatic or alkene in 0.1 or 0.4 mesitylene (0.1 ml sealed in 4-inch tube and 0.4 ml sealed in 6-inch tube). Then we used a piece of Tygon tubing connected the glass tube to a closed Kontes valve. For the reaction not involving gases, we removed the argon from the tube by freezing the contents in the tube with liquid nitrogen, then flame-sealed the tube under vacuum. For the reaction using gas, we first remove the argon in the tube and charged the tube with 8 atm of gases by condensating them. Then, the tubes were flame sealed under negative pressure. The sealed vessel was put in an aluminum block and then heated in a 200°C GC oven. The reaction was monitored by GC. Isolation of cross-coupling products was done by removing the volatiles and going through a flash chromatography with 1% EtOAc in hexane. Products could be further purified by distillation or recrystallization.

4.4.2. Product identification

All homo-coupling and cross-coupling products were identified either by comparison with reported ^{1}H and ^{13}C NMR spectra or authentic samples, or using GC-MS to identify. Cross-coupling products were isolated through flash chromatography.

[(1*E*,3*E*)-5,5-Dimethyl-1,3-hexadien-1-yl]benzene: ^{1}H NMR (500 MHz, Chloroform-*d*) δ 7.39 – 7.35 (m, 2H), 7.29 (ddt, *J* = 8.3, 6.7, 0.7 Hz, 2H), 7.18 (dddd, *J* = 8.7, 6.7, 2.3, 1.2 Hz, 1H), 6.74 (ddt, *J* = 15.6, 10.2, 0.9 Hz, 1H), 6.48 (d, *J* = 15.7 Hz, 1H), 6.16 (ddt, *J* = 15.4, 10.1, 0.8 Hz, 1H), 5.87 (dq, *J* = 15.5, 0.8 Hz, 1H), 1.09 (d, *J* = 0.9 Hz, 9H). ^{13}C NMR (126 MHz, Chloroform-*d*) δ 146.65, 137.81, 130.15, 129.88, 128.44, 126.92, 126.05, 125.42, 33.25, 29.53.

4.4.3. NMR Spectra of cross-coupling products

Figure 4. 6. ^{1}H NMR of [(1*E*,3*E*)-5,5-Dimethyl-1,3-hexadien-1-yl]benzene (500 MHz, $CDCl_3$)

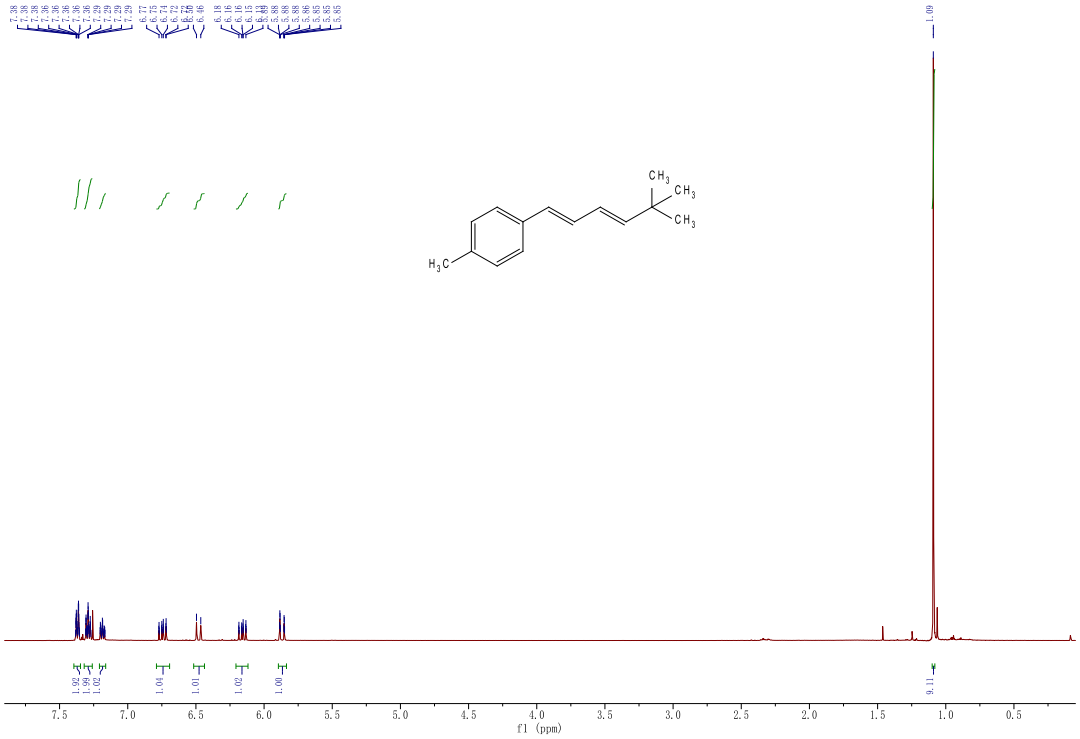

Figure 4. 7. ^{13}C NMR of [(1*E*,3*E*)-5,5-Dimethyl-1,3-hexadien-1-yl]benzene (500 MHz, $CDCl_3$)

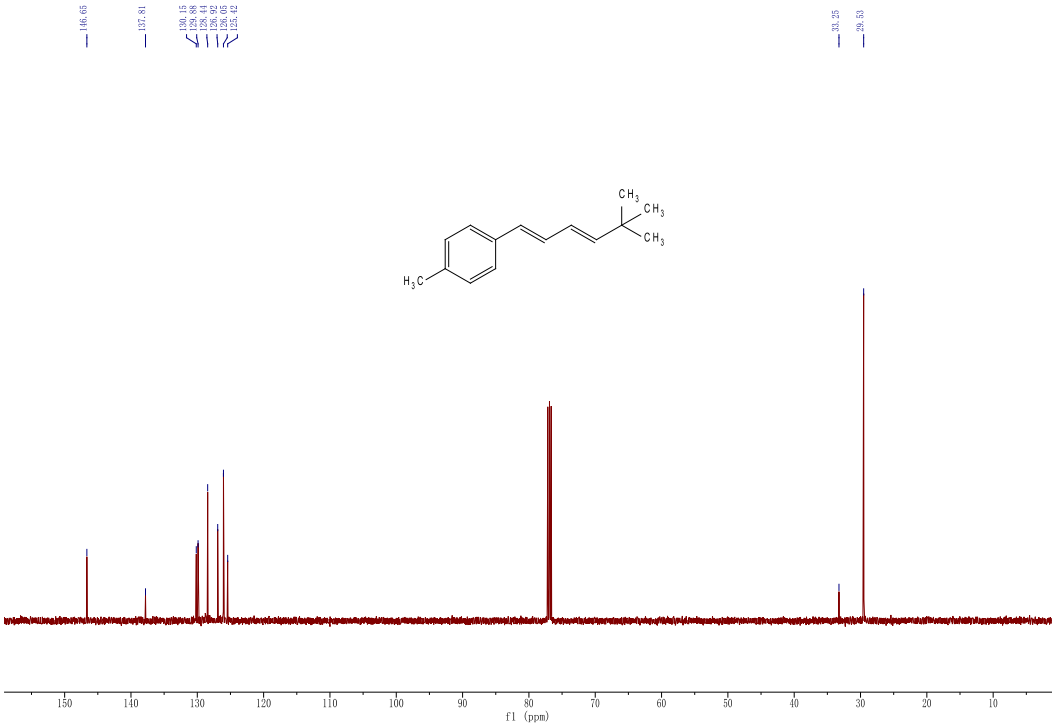

4.5. Reference

1. Yeung, C. S.; Dong, V. M., Catalytic Dehydrogenative Cross-Coupling: Forming Carbon−Carbon Bonds by Oxidizing Two Carbon−Hydrogen Bonds. *Chemical Reviews* **2011,** *111* (3), 1215-1292.
2. Li, Z.; Bohle, D. S.; Li, C.-J., Cu-catalyzed cross-dehydrogenative coupling: A versatile strategy for C–C bond formations via the oxidative activation of sp3 C–H bonds. *Proceedings of the National Academy of Sciences* **2006,** *103* (24), 8928-8933.
3. Miyaura, N.; Suzuki, A., Palladium-Catalyzed Cross-Coupling Reactions of Organoboron Compounds. *Chem. Rev.* **1995,** *95* (7), 2457-2483.
4. Littke, A. F.; Fu, G. C., Palladium-catalyzed coupling reactions of aryl chlorides. *Angewandte Chemie-International Edition* **2002,** *41* (22), 4176-4211.
5. Kataoka, N.; Shelby, Q.; Stambuli, J. P.; Hartwig, J. F., Air stable, sterically hindered ferrocenyl dialkylphosphines for palladium-catalyzed C-C, C-N, and C-O bond-forming cross-couplings. *J. Org. Chem.* **2002,** *67* (16), 5553-5566.
6. Fagnou, K.; Lautens, M., Rhodium-Catalyzed Carbon-Carbon Bond Forming Reactions of Organometallic Compounds. *Chem. Rev.* **2003,** *103* (1), 169-196.
7. Nicolaou, K. C.; Bulger, P. G.; Sarlah, D., Palladium-catalyzed cross-coupling reactions in total synthesis. *Angew Chem Int Edit* **2005,** *44* (29), 4442-4489.
8. Suzuki, A., Carbon-carbon bonding made easy. *Chem. Commun.* **2005,** (38), 4759-4763.
9. Fu, G. C., The Development of Versatile Methods for Palladium-Catalyzed Coupling Reactions of Aryl Electrophiles through the Use of $P(t\text{-}Bu)_3$ and PCy_3 as Ligands. *Acc. Chem. Res.* **2008,** *41* (11), 1555-1564.
10. Martin, R.; Buchwald, S. L., Palladium-Catalyzed Suzuki-Miyaura Cross-Coupling Reactions Employing Dialkylbiaryl Phosphine Ligands. *Acc. Chem. Res.* **2008,** *41* (11), 1461-1473.
11. Seechurn, C. C. C. J.; Kitching, M. O.; Colacot, T. J.; Snieckus, V., Palladium-Catalyzed Cross-Coupling: A Historical Contextual Perspective to the 2010 Nobel Prize. *Angew. Chem., Intl. Ed.* **2012,** *51* (21), 5062-5085.
12. Labinger, J. A.; Bercaw, J. E., Understanding and exploiting C–H bond activation. *Nature* **2002,** *417*, 507.
13. He, J.; Wasa, M.; Chan, K. S. L.; Shao, Q.; Yu, J.-Q., Palladium-Catalyzed Transformations of Alkyl C–H Bonds. *Chemical Reviews* **2017,** *117* (13), 8754-8786.
14. Crabtree, R. H., Organometallic alkane CH activation. *Journal of Organometallic Chemistry* **2004,** *689* (24), 4083-4091.
15. Daugulis, O.; Do, H.-Q.; Shabashov, D., Palladium- and Copper-Catalyzed Arylation of Carbon−Hydrogen Bonds. *Accounts of Chemical Research* **2009,** *42* (8), 1074-1086.
16. Kalyani, D.; Deprez, N. R.; Desai, L. V.; Sanford, M. S., Oxidative C-H Activation/C-C Bond Forming Reactions: Synthetic Scope and Mechanistic Insights. *J. Am. Chem. Soc.* **2005,** *127* (20), 7330-7331.
17. Chen, X.; Engle, K. M.; Wang, D. H.; Yu, J. Q., Palladium(II)-Catalyzed C-H Activation/C-C Cross-Coupling Reactions: Versatility and Practicality. *Angew Chem Int Edit* **2009,** *48* (28), 5094-5115.

18. Li, C. J., Cross-Dehydrogenative Coupling (CDC): Exploring C-C Bond Formations beyond Functional Group Transformations. *Acc. Chem. Res.* **2009,** *42* (2), 335-344.
19. Chiusoli, G. P.; Catellani, M.; Costa, M.; Motti, E.; Della Ca, N.; Maestri, G., Catalytic C-C coupling through C-H arylation of arenes or heteroarenes. *Coord. Chem. Rev.* **2010,** *254* (5-6), 456-469.
20. Neufeldt, S. R.; Sanford, M. S., Controlling Site Selectivity in Palladium-Catalyzed C-H Bond Functionalization. *Acc. Chem. Res.* **2012,** *45* (6), 936-946.
21. Fujiwara, Y.; Asano, R.; Moritani, I.; Teranishi, S., Aromatic substitution of olefins. XXV. Reactivity of benzene, naphthalene, ferrocene, and furan toward styrene, and the substituent effect on the reaction of monosubstituted benzenes with styrene. *The Journal of Organic Chemistry* **1976,** *41* (10), 1681-1683.
22. Fujiwara, Y.; Moritani, I.; Danno, S.; Asano, R.; Teranishi, S., Aromatic substitution of olefins. VI. Arylation of olefins with palladium(II) acetate. *Journal of the American Chemical Society* **1969,** *91* (25), 7166-7169.
23. Fujiwara, Y.; Moritani, I.; Asano, R.; Tanaka, H.; Teranishi, S., Aromatic substitution of olefin—VIII: Substituent effects on the reactions of styrene with monosubstituted benzenes in the presence of palladium(II) salts. *Tetrahedron* **1969,** *25* (19), 4815-4818.
24. fujiwara, Y.; Moritani, I.; Matsuda, M., Aromatic substitution of olefin—III: Reaction of styrene-palladium(II) chloride complex. *Tetrahedron* **1968,** *24* (13), 4819-4824.
25. Fujiwara, Y.; Moritani, I.; Matsuda, M.; Teranishi, S., Aromatic substitution of styrene-palladium chloride complex. II effect of metal acetate. *Tetrahedron Letters* **1968,** *9* (5), 633-636.
26. Fujiwara, Y.; Moritani, I.; Asano, R.; Teranishi, S., Aromatic substitution of olefin. V reaction of phenyl-substituted ethylenes with benzene. *Tetrahedron Letters* **1968,** *9* (57), 6015-6017.
27. Moritanl, I.; Fujiwara, Y., Aromatic substitution of styrene-palladium chloride complex. *Tetrahedron Letters* **1967,** *8* (12), 1119-1122.
28. Le Bras, J.; Muzart, J., Intermolecular Dehydrogenative Heck Reactions. *Chemical Reviews* **2011,** *111* (3), 1170-1214.
29. Wu, Y.; Wang, J.; Mao, F.; Kwong, F. Y., Palladium-Catalyzed Cross-Dehydrogenative Functionalization of C(sp2)-H Bonds. *Chemistry – An Asian Journal* **2014,** *9* (1), 26-47.
30. Kitamura, T.; Fujiwara, Y., Dehydrogenative Heck-type Reactions: The Fujiwara-Moritani Reaction. In *From C-H to C-C Bonds: Cross-Dehydrogenative-Coupling*, Li, C.-J., Ed. The Royal Society of Chemistry: 2015; Vol. 26, pp 33-54.
31. Girard, S. A.; Knauber, T.; Li, C.-J., The Evolution of the Concept of Cross-Dehydrogenative-Coupling Reactions. In *From C-H to C-C Bonds: Cross-Dehydrogenative-Coupling*, Li, C.-J., Ed. Royal Society of Chemistry: 2015; Vol. 26, pp 1-32.
32. Arndtsen, B. A.; Bergman, R. G.; Mobley, T. A.; Peterson, T. H., Selective Intermolecular C-H Bond Activation by Synthetic Metal Complexes in Homogeneous Solution. *Acc. Chem. Res.* **1995,** *28*, 154-162.

33. Crabtree, R. H., The organometallic chemistry of alkanes. *Chem. Rev.* **1985,** *85* (4), 245-69.
34. Choi, J.; Goldman, A. S., Ir-Catalyzed Functionalization of C−H Bonds. *Top. Organomet. Chem.* **2011,** *34*, 139–168.
35. Choi, J.; MacArthur, A. H. R.; Brookhart, M.; Goldman, A. S., Dehydrogenation and Related Reactions Catalyzed by Iridium Pincer Complexes. *Chem. Rev.* **2011,** *111* (3), 1761-1779.
36. Findlater, M.; Choi, J.; Goldman, A. S.; Brookhart, M., Alkane dehydrogenation. In *Catal. Met. Complexes*, Springer: 2012; Vol. 38, pp 113-141.
37. Liu, C.; Yuan, J.; Gao, M.; Tang, S.; Li, W.; Shi, R.; Lei, A., Oxidative Coupling between Two Hydrocarbons: An Update of Recent C–H Functionalizations. *Chemical Reviews* **2015**.
38. Chen, B.; Wu, L.-Z.; Tung, C.-H., Photocatalytic Activation of Less Reactive Bonds and Their Functionalization via Hydrogen-Evolution Cross-Couplings. *Accounts of Chemical Research* **2018,** *51* (10), 2512-2523.
39. Wilklow-Marnell, M.; Li, B.; Zhou, T.; Krogh-Jespersen, K.; Brennessel, W. W.; Emge, T. J.; Goldman, A. S.; Jones, W. D., Catalytic Dehydrogenative C–C Coupling by a Pincer-Ligated Iridium Complex. *Journal of the American Chemical Society* **2017**.
40. Weissman, H.; Song, X.; Milstein, D., Ru-Catalyzed Oxidative Coupling of Arenes with Olefins Using O2. *Journal of the American Chemical Society* **2001,** *123* (2), 337-338.
41. Yokota, T.; Tani, M.; Sakaguchi, S.; Ishii, Y., Direct Coupling of Benzene with Olefin Catalyzed by Pd(OAc)2 Combined with Heteropolyoxometalate under Dioxygen. *Journal of the American Chemical Society* **2003,** *125* (6), 1476-1477.
42. Tani, M.; Sakaguchi, S.; Ishii, Y., Pd(OAc)2-Catalyzed Oxidative Coupling Reaction of Benzenes with Olefins in the Presence of Molybdovanadophosphoric Acid under Atmospheric Dioxygen and Air. *The Journal of Organic Chemistry* **2004,** *69* (4), 1221-1226.
43. Kubota, A.; Emmert, M. H.; Sanford, M. S., Pyridine Ligands as Promoters in PdII/0-Catalyzed C–H Olefination Reactions. *Organic Letters* **2012,** *14* (7), 1760-1763.
44. Li, H.; He, K.-H.; Liu, J.; Wang, B.-Q.; Zhao, K.-Q.; Hu, P.; Shi, Z.-J., Straightforward synthesis of phenanthrenes from styrenes and arenes. *Chemical Communications* **2012,** *48* (56), 7028-7030.
45. Duan, H.; Li, M.; Zhang, G.; Gallagher, J. R.; Huang, Z.; Sun, Y.; Luo, Z.; Chen, H.; Miller, J. T.; Zou, R.; Lei, A.; Zhao, Y., Single-Site Palladium(II) Catalyst for Oxidative Heck Reaction: Catalytic Performance and Kinetic Investigations. *ACS Catalysis* **2015,** *5* (6), 3752-3759.
46. Choi, J.; MacArthur, A. H.; Brookhart, M.; Goldman, A. S., Dehydrogenation and related reactions catalyzed by iridium pincer complexes. *Chemical reviews* **2011,** *111* (3), 1761-79.
47. Sevov, C. S.; Hartwig, J. F., Iridium-Catalyzed Oxidative Olefination of Furans with Unactivated Alkenes. *Journal of the American Chemical Society* **2014,** *136* (30), 10625-10631.
48. Thiery, E.; Harakat, D.; Le Bras, J.; Muzart, J., Palladium-Catalyzed Oxidative Coupling of 2-Alkylfurans with Olefins through C−H Activation: Synthesis of Difurylalkanes. *Organometallics* **2008,** *27* (15), 3996-4004.

49. Aouf, C.; Thiery, E.; Le Bras, J.; Muzart, J., Palladium-Catalyzed Dehydrogenative Coupling of Furans with Styrenes. *Organic Letters* **2009,** *11* (18), 4096-4099.
50. Vasseur, A.; Muzart, J.; Le Bras, J., Dehydrogenative Heck Reaction of Furans and Thiophenes with Styrenes under Mild Conditions and Influence of the Oxidizing Agent on the Reaction Rate. *Chemistry – A European Journal* **2011,** *17* (45), 12556-12560.
51. Zhang, Y.; Li, Z.; Liu, Z.-Q., Pd-Catalyzed Olefination of Furans and Thiophenes with Allyl Esters. *Organic Letters* **2012,** *14* (1), 226-229.
52. Vasseur, A.; Harakat, D.; Muzart, J.; Le Bras, J., Aerobic Dehydrogenative Heck Reactions of Heterocycles with Styrenes: A Negative Effect of Metallic Co-Oxidants. *Advanced Synthesis & Catalysis* **2013,** *355* (1), 59-67.
53. Kumar, A.; Bhatti, T. M.; Goldman, A. S., Dehydrogenation of Alkanes and Aliphatic Groups by Pincer-Ligated Metal Complexes. *Chemical reviews* **2017,** *117* (19), 12357-12384.
54. Liu, F.; S. Goldman, A., Efficient thermochemical alkane dehydrogenation and isomerization catalyzed by an iridium pincer complex. *Chemical Communications* **1999,** (7), 655-656.
55. Ahuja, R.; Punji, B.; Findlater, M.; Supplee, C.; Schinski, W.; Brookhart, M.; Goldman, A. S., Catalytic dehydroaromatization of n-alkanes by pincer-ligated iridium complexes. *Nat Chem* **2011,** *3* (2), 167-171.
56. Morales-Morales, D.; Grause, C.; Kasaoka, K.; Redón, R. o.; Cramer, R. E.; Jensen, C. M., Highly efficient and regioselective production of trisubstituted alkenes through heck couplings catalyzed by a palladium phosphinito PCP pincer complex. *Inorganica Chimica Acta* **2000,** *300–302*, 958-963.
57. Mucha, N. T.; Waterman, R., Iridium Pincer Catalysts for Silane Dehydrocoupling: Ligand Effects on Selectivity and Activity. *Organometallics* **2015,** *34* (15), 3865-3872.

Chapter 5. Direct synthesis of indene and indole through intramolecular dehydrogenative coupling

Abstract: Indene and indole are important precursors used in chemical industry, agriculture, biology and pharmaceuticals. Discovering a simpler route for their synthesis is of great interest. The current synthetic route to indoles and indenes is via dehydrogenative coupling and is very limited. Here, we report a new method using pincer-iridium complexes as a catalyst to effect an intramolecular coupling reaction for synthesizing indole and indene from vinyl arenes and vinyl anilines respectively. This new methodology showed a simple new synthetic route with no substrate pre-functionalization, additives, or oxidants.

5.1. Introduction

Indole is prevalent in humans and other animals in the form of of L-tryptophan. It was not until 1869 that the chemical structure of indole was correctly assigned by Adolf von Baeyer,[1-2] as showed in figure 5.1. In addition to their biological applications, indoles and their derivatives have also been widely used in chemical industry, agriculture, and pharmaceuticals.[3-5] The great value of indoles has drawn extensive attention from researchers to develop different synthetic methodologies for them.[6-7] In general, Moody has divided the general synthetic methodologies of indoles into two categories: precursors with ortho substituted arenes and precursors without arene substitutions, as shown in scheme 5.1. Among all these methodologies, reactions are either limited by the availability of the staring materials, or complexity of their starting materials.

Figure 5. 1. Chemical structure of indole and indene

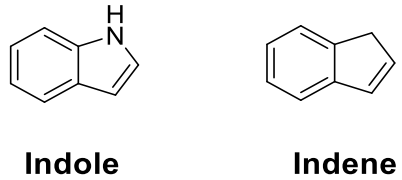

Similar to indole, indene (right in figure 5.1) is also an important motif in many natural products[8-9] and pharmaceuticals[10-13]. One of the important usages of indene in industrial applications is in making indene/coumarone thermoplastic resins. There are many methods developed to synthesize indenes, which include intramolecular electrophilic substitution reactions, nucleophilic cyclizations, metal-catalyzed cyclizations, cyclic precursor functionalization, ring expansion and contraction, and tandem reactions.[14-15] Different methods to synthesize indanes, which could be transferred to indenes through

dehydrogenation, were also available.[14, 16] Still, the development of new synthetic routes for indene with atomic efficiency and sustainable conditions is highly desired.

Scheme 5. 1. Two categories of indoles synthesis methods

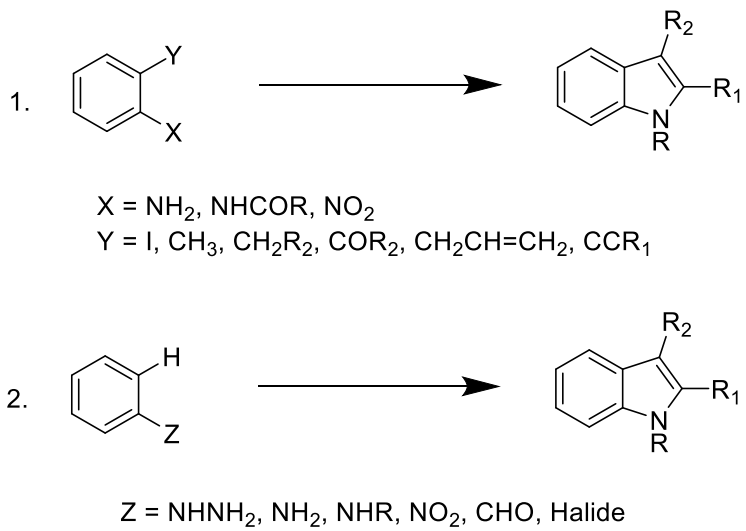

Use of cross-dehydrogenative coupling (CDC) to couple one C-H bond with one X-H bond to give C-X bond has become one of the most desired routes for bond formation.[17-23] However, using this method for indole and indene synthesis, is very limited. The synthesis of indoles using dehydrogenative coupling could be cataloged into C-C bond formation route[24-36] and C-N bond formation route,[29, 34, 37-49] as seen in scheme 5.2. These metal catalyzed coupling reactions mostly required the use of palladium and copper as catalysts together with stoichiometric amounts oxidant or base. In addition, functional groups to activate the C or N atom to facilitate the reaction were desired. Even with all of these restrictions, these reactions still suffered from low yield and generated large amounts of waste. There are rare examples of indene synthesis directly using CDC method[50-51] and those available focused on radical coupling reactions. Using a simple CDC reaction to synthesize indenes and indoles from simple substrates would be highly desired. Our success in using pincer-iridium complexes to effect homo- and cross-dehydrogenative

coupling, discussed in chapter 3 and 4, gave us new idea for intramolecular coupling for the synthesis of both indenes and indoles, as shown in scheme 5.3.

Scheme 5. 2. Synthesis indoles using dehydrogenative coupling

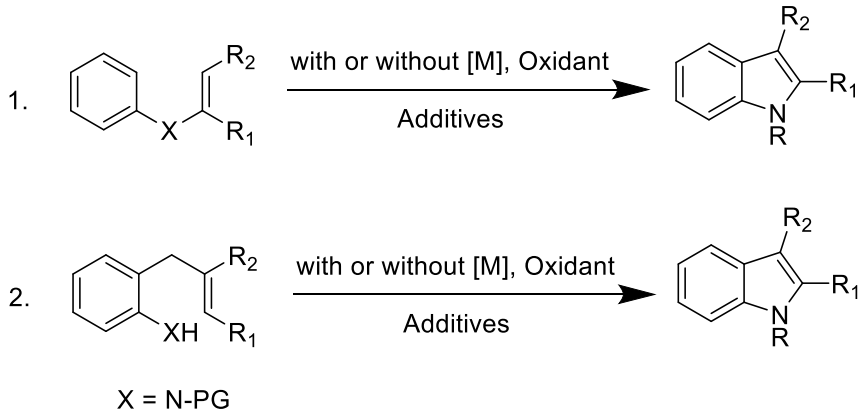

Scheme 5. 3. Intramolecular dehydrogenative coupling route for indenes and indoles synthesis

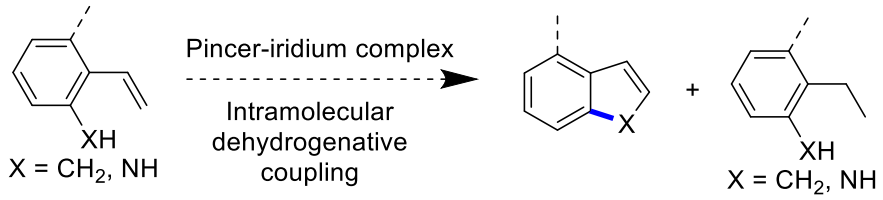

5.2. Results and discussion

5.2.1. Doubly ortho-methylated vinyl arenes undergo intramolecular dehydrogenative coupling

Scheme 5. 4. Intramolecular dehydrogenative coupling of 2,4,6-trimethylstyrene

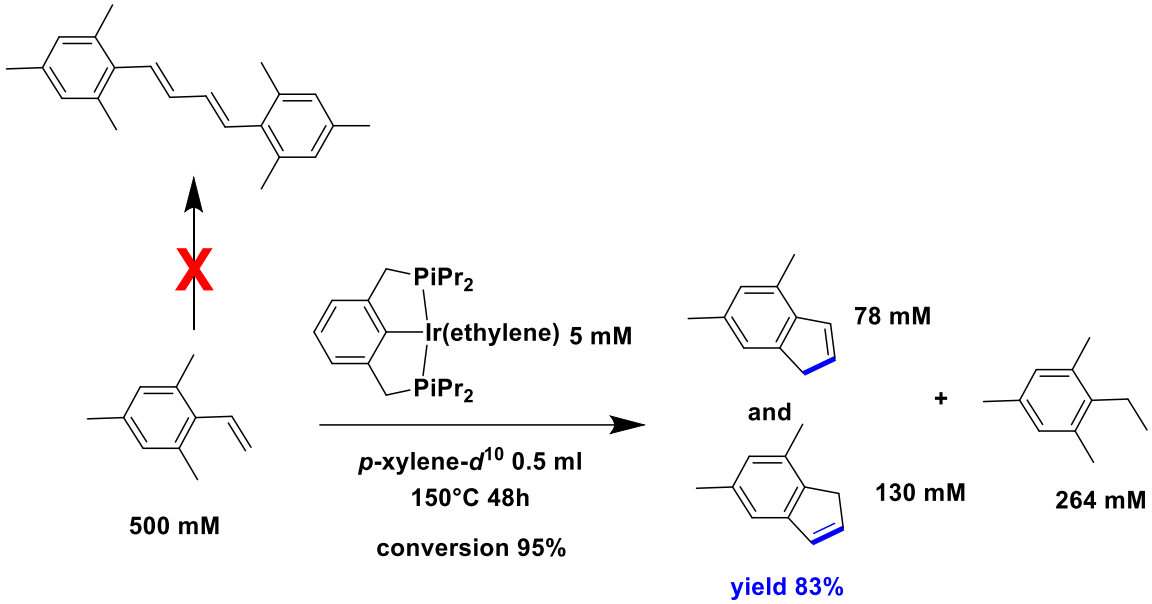

As reported in previous work,[52] the homo-coupling of vinyl arenes proceeds through a metalloindene intermediate via double C-H activation of both β-vinylic and ortho-aryl position. It has been well reported that sp^2 C-H is easier to break compared to sp^3 C-H bond. When the ortho hydrogen atom of the aryl ring was replaced with methyl group, the homo-coupling reaction of vinyl arene would not proceed. The reaction only formed other species, such as vinylidene species. When we run the reaction with 2,4,6-trimethylstyrene using similar condition of homo-coupling vinyl arene, we observed no homo-coupling products. Instead, two new species, identified as 4,6-dimethylindene and 5,7-dimethylindene, along with 1-ethyl-2,4,6-trimethylbenzene, shown in scheme 5.4. The products were the result of the coupling of the vinylic C-H bond with benzyl C-H bond to give new C-C bond and hydrogenated olefin. As far as we know, this is a rare example of generating indene directly from methyl group substituted styrene. Furthermore, the simple reaction condition with 2,4,6-trimethylstyrene as reactant, pincer-iridium as catalysts, p-xylene as solvent, and moderate heating condition (150°C) makes this methodology very

attractive. A mechanism including a six-member metallocycle complex as key intermediate was proposed based on experimental and computational results (detailed discussion in chapter 3). Similar to the metalloindene mechanism, this mechanism also went through double C-H activation, followed by hydrogenation of another molecule of styrene, and final reductive elimination to give the product, shown in figure 5.2. The isomerization of the double bond made the products appear as isomers.

Figure 5. 2. Mechanism for Intramolecular dehydrogenative coupling of 2,4,6-trimethylstyrene

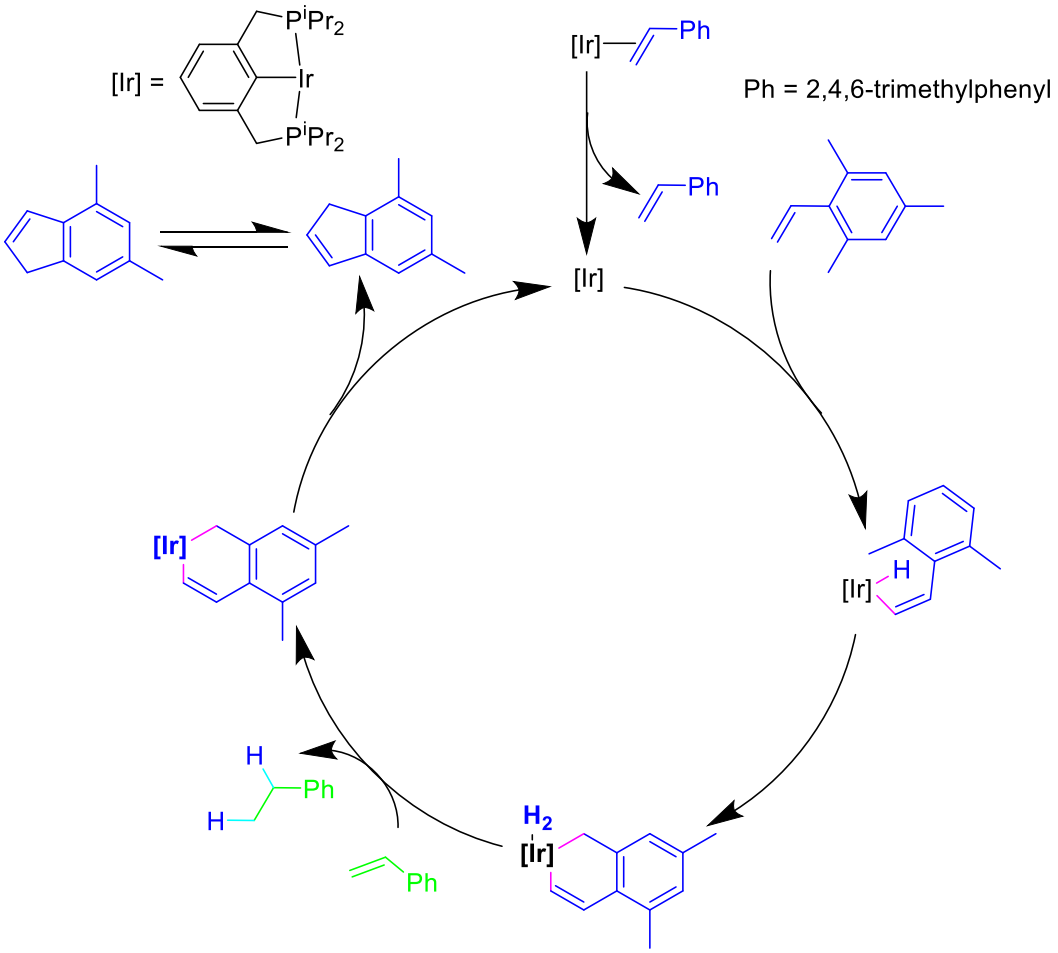

Although we could start with 1-ethyl-2,4,6-trimethylbenzene, or another substrate with similar structure, by tandem dehydrogenation and coupling, still, the availability of

both ortho-position methylated vinyl arene or ethylbenzene greatly limited our reaction scope. To broaden our reaction scope, we tried to effect the intramolecular dehydrogenative coupling of vinyl arenes with a methyl group at para-position and a methyl group at ortho position, assuming the para-methyl group will inhibit the activation of ortho C-H group. Unfortunately, the methyl group at para-position did not provide enough steric effect to prevent the C-H activation at ortho position. Homo-coupling detected just as other vinyl arenes, showed in scheme 5.5.

Scheme 5. 5. Coupling reaction of 2,5-dimethyl styrene

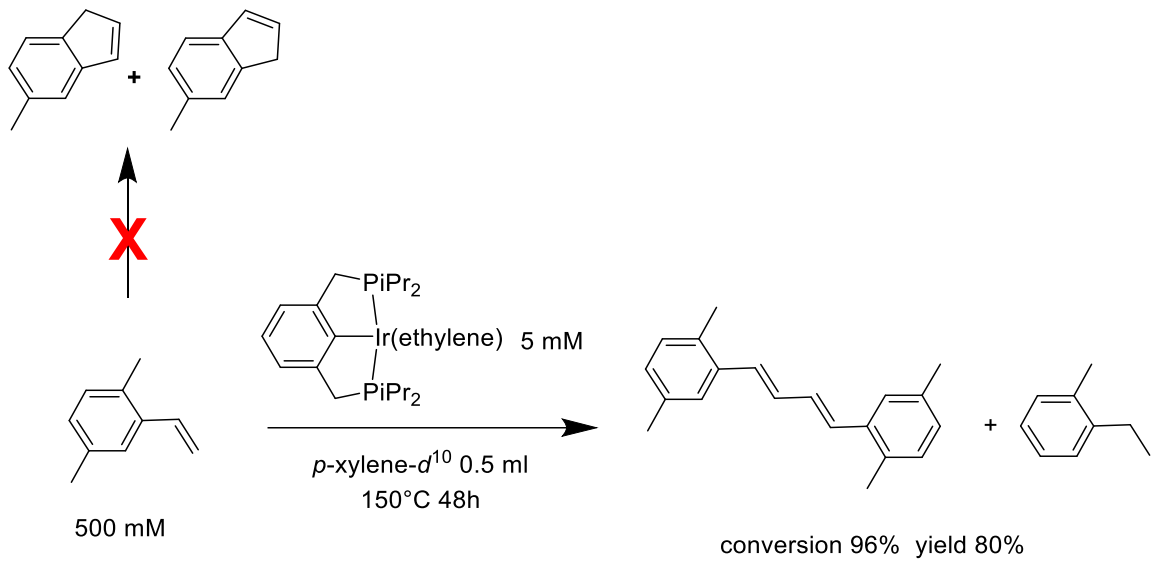

5.2.2. Intramolecular dehydrogenative coupling of vinyl aniline

The easy activation of N-H bond by pincer-iridium complexes[53] at room temperature makes vinyl aniline a good candidate for intramolecular coupling reactions. Unlike the double C-H activation of styrene, the activation of vinyl aniline starts with N-H activation. Stoichiometric experiments between pincer-iridium complex and 2-isopropenyl aniline gave N-H activated product (**Ir 1**) at room temperature, showed in scheme 5.6, while styrene only gave a π-adduct product (discussed in chapter 3). To confirm the structure of **Ir 1**, we used both NMR (including 1D and 2D, see experimental

information part) and X-Ray analysis, and the crystal structure was showed in figure 5.3. Further heating should result metalloindole formation by activating β-vinyl C-H bond, however, we could not manage to isolate and identify it.

Scheme 5. 6. N-H activation of 2-isopropenyl aniline by pincer-iridium complex

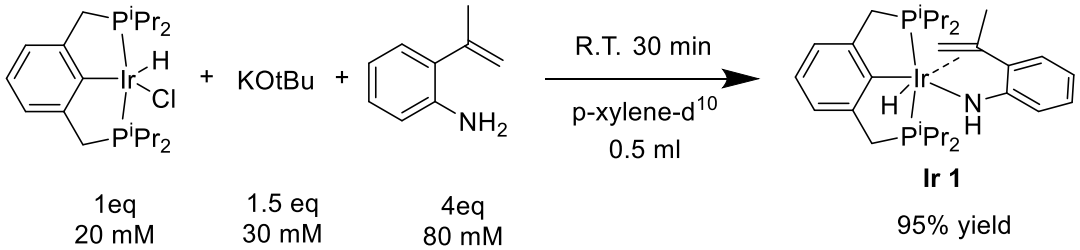

Figure 5. 3. ORTEP diagram of Ir 1

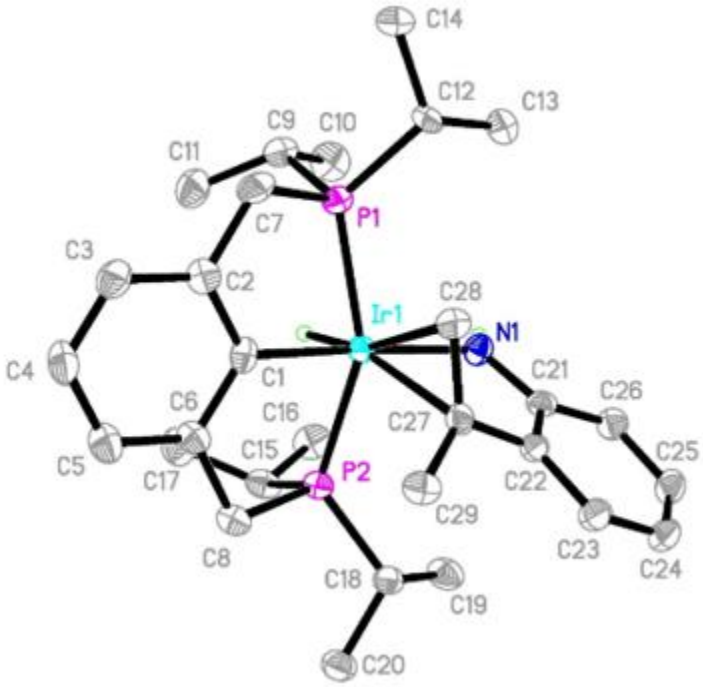

The catalytic reaction was run under similar condition as 2,4,6-trimethylstyrene coupling reaction, which could efficiently convert 2-isopropenyl aniline to 3-methyl indole, showed in scheme 5.7. Similar to the indene synthesis, this is also a rare direct synthetic methodology for indole from non-functionalized vinyl aniline.

Monitored by ^{1}H NMR, we could clearly see the two major products, 2-methyl indole and 2-isopropyl aniline, keeping 1:1 ratio during the reaction by referenced to the solvent residual peak (figure 5.4), which was a clear sign of dehydrogenative coupling. The ^{31}P NMR (figure 5.5) showed that one of the major peaks was **Ir 1** [δ 38.57 (dd, J = 248.1, 6.8 Hz), 20.23 (dd, J = 248.0, 9.0 Hz)], which was probably the resting state of the catalyst. We thought the singlet showed at δ 65.52 in the ^{31}P NMR could possibly be the metallocycle complex. Vinyl aniline was also tried with this type of reaction, however, the easy polymerization and formation of stable complexes with iridium prohibited the coupling by showing low yield.

Scheme 5. 7. Intramolecular dehydrogenative coupling of 2-isopropenylaniline

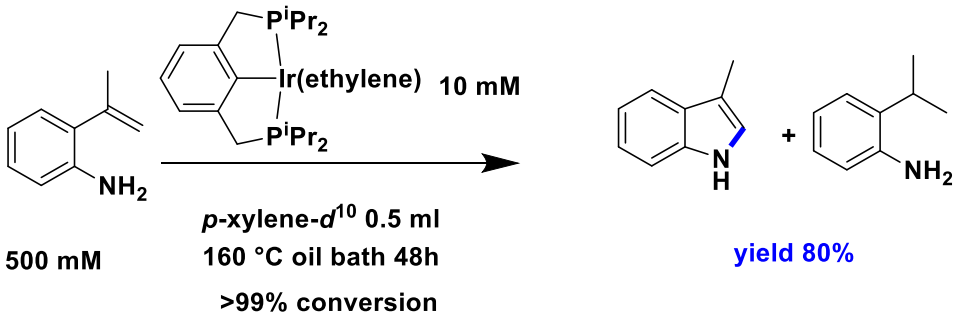

Figure 5. 4. ^{1}H NMR of intramolecular dehydrogenative coupling of 2-isopropenylaniline

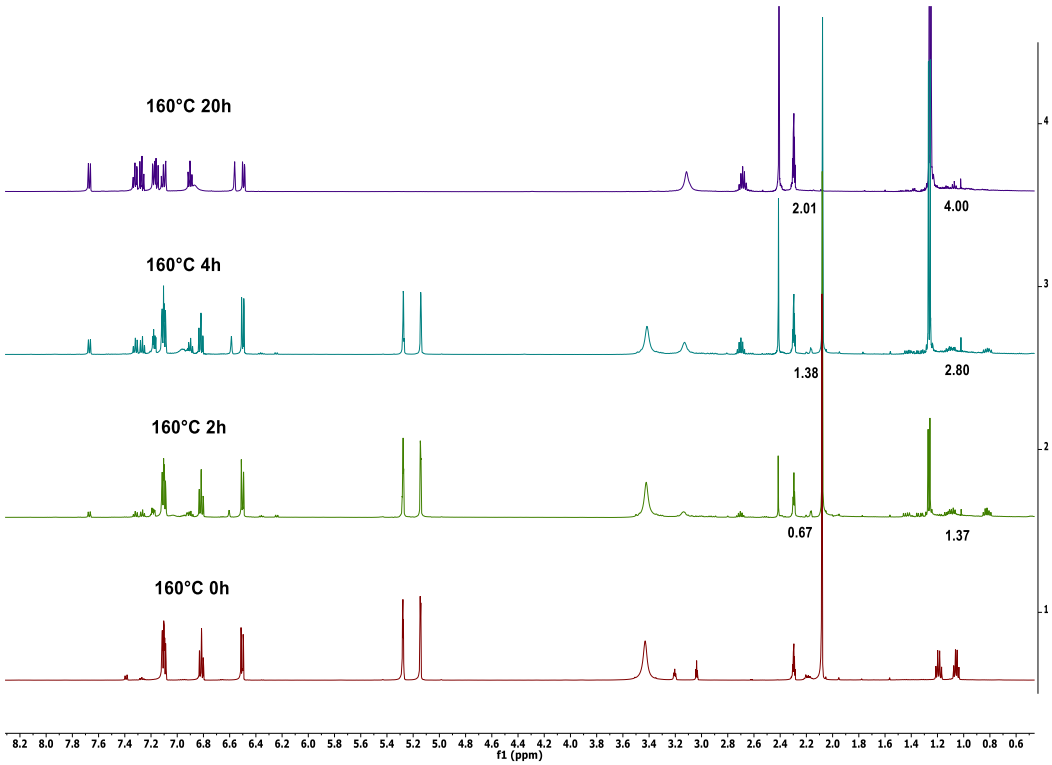

Figure 5. 5. ^{31}P NMR of intramolecular dehydrogenative coupling of 2-isopropenylaniline

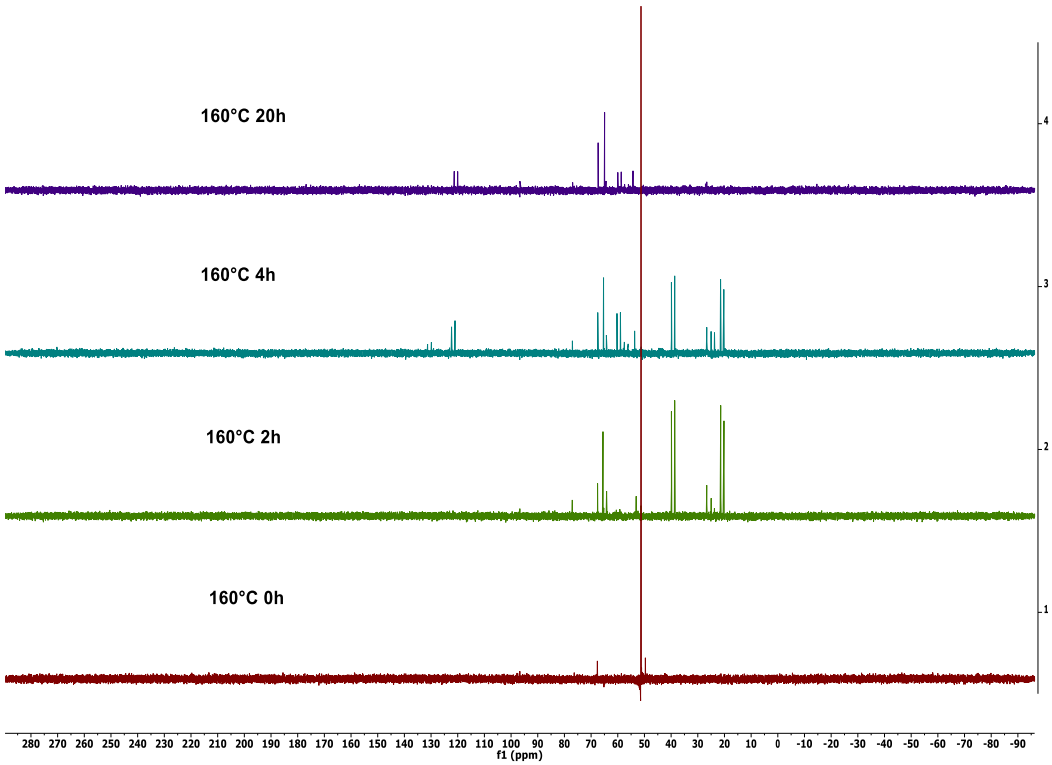

The reaction scope also got limited by the availability of vinyl aniline. However, different alkyl anilines, which could be easily synthesized through alkylation of aniline, were available. In Figure 5.6, we showed two examples of tandem dehydrogenation and coupling to synthesize indole from alkyl anilines. Although longer reaction time was required, due to the slow dehydrogenation process, we could still manage over 50% yield for both 2-methyl indole and 3-methyl indole. The other example shown in figure 5.6, 2-amino-biphenyl, coupling a N-H bond with a sp^2 C-H on phenyl ring, could strongly supported the dehydrogenative coupling mechanism, showed in figure 5.7. As if the reaction went through insertion mechanism, in scheme 5.8, then we had to break the π system of benzene ring, which has not been observed for pincer-iridium complexes. So

pincer-iridium complex effected coupling of 2-amino-biphenyl to give carbazole went through the dehydrogenative coupling route.

We proposed a similar reaction mechanism for this new indole synthesis methodology as intramolecular dehydrogenative coupling of vinyl arene, showed in figure 5.7. The reaction started with N-H activation, which could direct the β-vinylic C-H activation, followed by removing the dihydrogen by sacrificing a molecular vinyl aniline, and final reductive elimination gave the product.

Figure 5. 6. Substrates for indoles synthesis by intramolecular dehydrogenative coupling

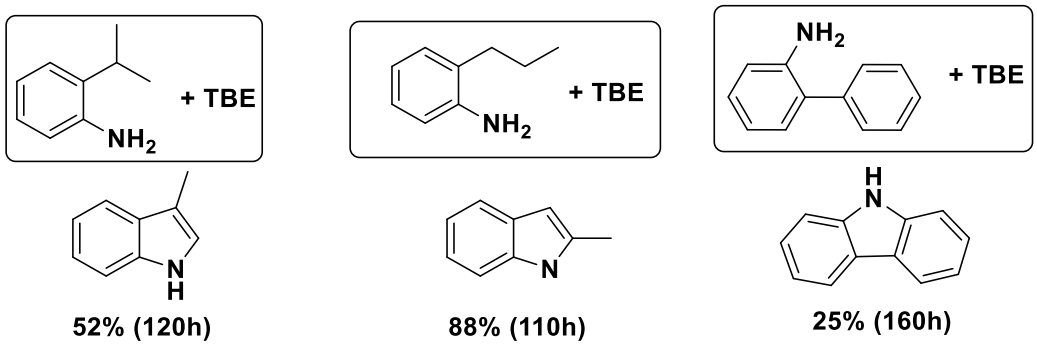

Experiments were run in a J. Young NMR tube with 200 mM aniline precursors and 500 mM TBE in 0.5 ml *p*-xylene-d^{10}. The reaction mixtures were refluxing in 160°C oil bath.

Figure 5. 7. Mechanism for intramolecular dehydrogenative coupling of 2-isopropenylaniline

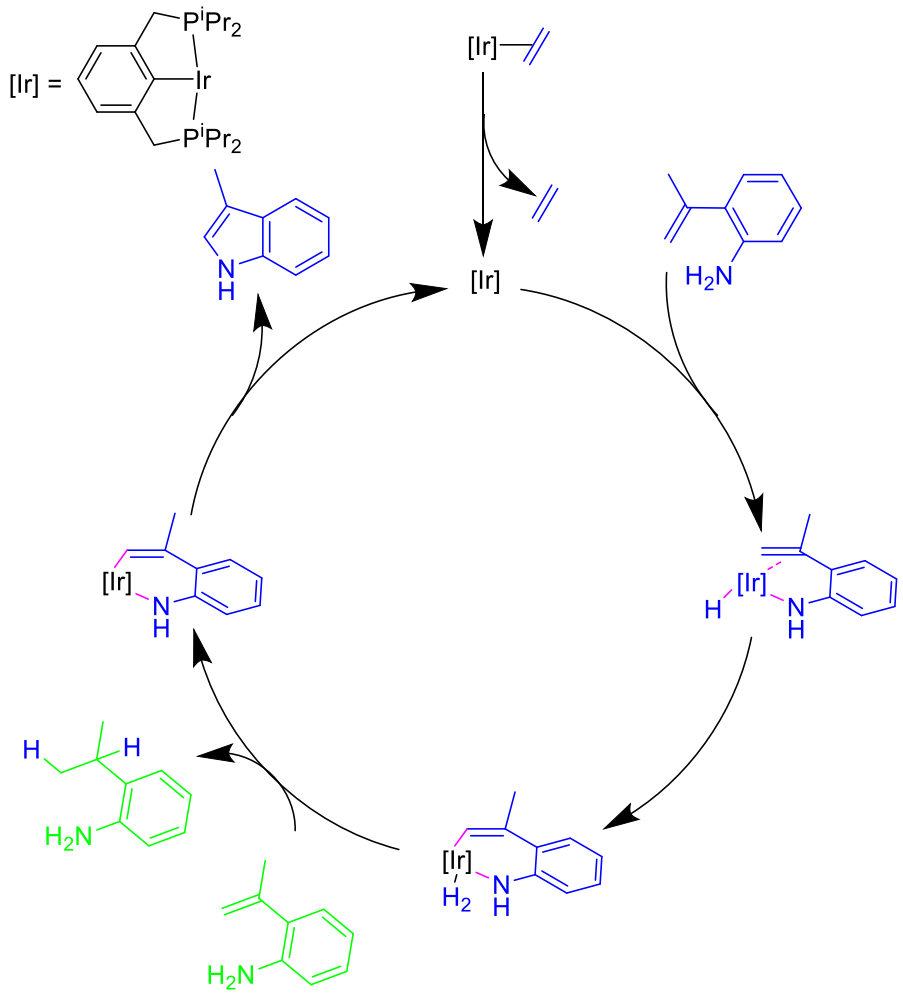

Figure 5. 8. Insertion mechanism

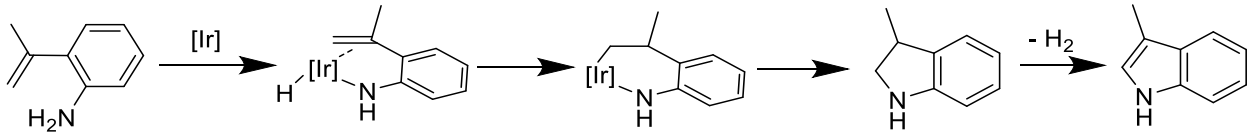

5.3. Conclusion

In summary, we reported a new synthetic methodology could be used for both indenes and indoles synthesis. The new method did not require any functionalization of the vinyl aniline, oxidant, and additives. It also showed the ability of pincer-iridium to do

different typed dehydrogenative coupling for C-C and C-N bond formation. Based on experiment results, we proposed a similar metallocycles mechanism for both of them.

5.4. Experiment information

5.4.1. General information

We conducted all our experiment either under argon filled glovebox or schlenk line. NMR experiment were conducted on 500-MHZ Varian VNMRS. ^{1}H and ^{13}C NMR spectra were referenced to residual deuterated solvent signal. ^{31}P NMR spectra was referenced with PMe_3 in capillary tube. All anhydrous solvents were purchased from Aldrich, flushed with argon, and stored in an argon atmosphere in a glovebox. All deuterium solvents were degassed, dried over activated alumina, and storage over 3-Å molecular sieves. TBE was degassed, dried over NaK alloy, removed NaK by vacuum transfer, and storage in glovebox freezer. All vinyl arenes, vinyl aniline and alkyl aniline were obtained from commercial sources or synthesized based on reported methods. Further treatment was carried out by distilling under reduced pressure. GC analysis was conducted using a Varian 430 GC with a 30-m capillary column, using helium carrier gas. GCMS analysis was conducted using a Varian 3900 GC with a 30-m capillary column coupled with a Saturn 2100T MS, using helium carrier gas. Pincer-iridium catalyst, (^{iPr}PCP)Ir(C_2H_4),[54] was synthesized according reported method.

General procedure for intramolecular dehydrogenative coupling: to J. Young Tube was added 10 mM pincer-iridium complex and 500 mM vinyl arene or vinyl aniline in 0.5 ml *p*-xylene-d^{10}. For tandem dehydrogenation and coupling reaction, 10 mM pincer-iridium complex, 200 mM alkyl aniline, and 500 mM TBE in 0.5 ml *p*-xylene-d^{10} were added to the J. Young Tubes. Then reaction was heated in oil bath at 150C°C or 160°C. The reaction

was monitored by both NMR and GC. Isolation of cross-coupling products was done by removing the volatiles and going through a flash chromatography with 1-20% EtOAc in hexane. Products could be further purified by distillation or recrystallization.

5.4.2. Product identification

All products were identified by either by compared with reported ^{1}H and ^{13}C NMR spectra or authentic samples. Mas was confirmed by GC-MS.

5.4.2.1. 3-methylindole

^{1}H NMR (500 MHz, Chloroform-*d*) δ 7.85 (s, 1H), 7.60 (dp, *J* = 7.9, 1.0 Hz, 1H), 7.35 (dq, *J* = 8.1, 1.0 Hz, 1H), 7.23 – 7.18 (m, 1H), 7.14 (ddt, *J* = 7.9, 7.0, 1.0 Hz, 1H), 6.97 (dq, *J* = 2.1, 1.1 Hz, 1H), 2.36 (t, *J* = 1.1 Hz, 3H). ^{13}C NMR (126 MHz, Chloroform-*d*) δ 136.24, 128.27, 121.84, 121.53, 119.09, 118.81, 111.72, 110.91, 9.66.

5.4.2.2. 2-methylindole

^{1}H NMR (500 MHz, Chloroform-*d*) δ 7.80 (s, 1H), 7.53 (ddq, *J* = 7.7, 1.7, 0.9 Hz, 1H), 7.28 (ddt, *J* = 8.0, 1.8, 0.9 Hz, 1H), 7.15 – 7.11 (m, 1H), 7.11 – 7.06 (m, 1H), 6.24 (tq, *J* = 1.8, 1.0 Hz, 1H), 2.45 (d, *J* = 1.1 Hz, 3H). ^{13}C NMR (126 MHz, Chloroform-*d*) δ 136.02, 135.01, 129.05, 120.91, 119.61, 110.18, 100.39, 13.71.

5.4.2.3. Ir 1

To a J. Young NMR tube, 5.6 mg (0.01 mmol) (^{iPr}PCP)IrHCl, 1.7 mg (0.015 mmol) KO*t*Bu, 4.1 μl (0.04 mmol) 2-isopropenylaniline, and 0.5 ml *p*-xylene-d^{10} were added, yielding a dark color solution. Two doublet of doublet were observed by ^{31}P NMR spectroscopy in ≥ 90% yield within 5-10 min. The volatiles were then removed by vacuum and the residues were washed by 0.2 ml pentane two times. Pure **Ir 1** was obtained by remove residue solvent under vacuum. Crystals suitable for X-ray diffraction were grown

from **Ir 1** solution in minimum amount hexane by slow evaporation at room temperature in glovebox. ^{1}H NMR (500 MHz, Benzene-d_6) δ 7.14 (d, J = 7.5 Hz, 1H), 6.91 (t, J = 7.6 Hz, 1H), 6.84 (d, J = 2.7 Hz, 3H), 6.34 (t, J = 7.2 Hz, 1H), 6.23 (d, J = 8.0 Hz, 1H), 3.41 (dt, J = 12.6, 2.3 Hz, 1H), 3.10 (dd, J = 16.9, 7.7 Hz, 1H), 2.96 (ddd, J = 16.7, 11.7, 2.1 Hz, 1H), 2.90 – 2.71 (m, 3H), 2.34 – 2.22 (m, 2H), 2.03 (d, J = 3.4 Hz, 3H), 1.97 – 1.79 (m, 3H), 1.23 (dd, J = 15.3, 7.4 Hz, 3H), 1.10 (dd, J = 15.8, 6.5 Hz, 3H), 1.01 (dd, J = 17.1, 7.3 Hz, 3H), 0.96 (dd, J = 14.7, 7.2 Hz, 3H), 0.82 (ddd, J = 11.6, 7.1, 4.7 Hz, 6H), 0.61 (dt, J = 14.1, 6.5 Hz, 6H), -11.43 (dd, J = 17.4, 13.9 Hz, 1H). ^{13}C NMR (126 MHz, Benzene-d_6) δ 146.98, 146.95, 146.90, 146.87, 145.72, 145.69, 145.64, 145.61, 120.48, 120.43, 120.36, 120.31, 28.06, 28.02, 27.86, 27.83, 24.88, 24.84, 24.78, 24.76, 24.72, 24.69, 20.64, 20.64, 20.62, 20.61, 17.82, 17.80, 17.79, 17.75, 17.73. ^{31}P NMR (202 MHz, Benzene-d_6) δ 38.57 (dd, J = 248.1, 6.8 Hz), 20.23 (dd, J = 248.0, 9.0 Hz).

5.4.3. NMR spectra

Figure 5. 9. ^{1}H NMR of 3-methylindole

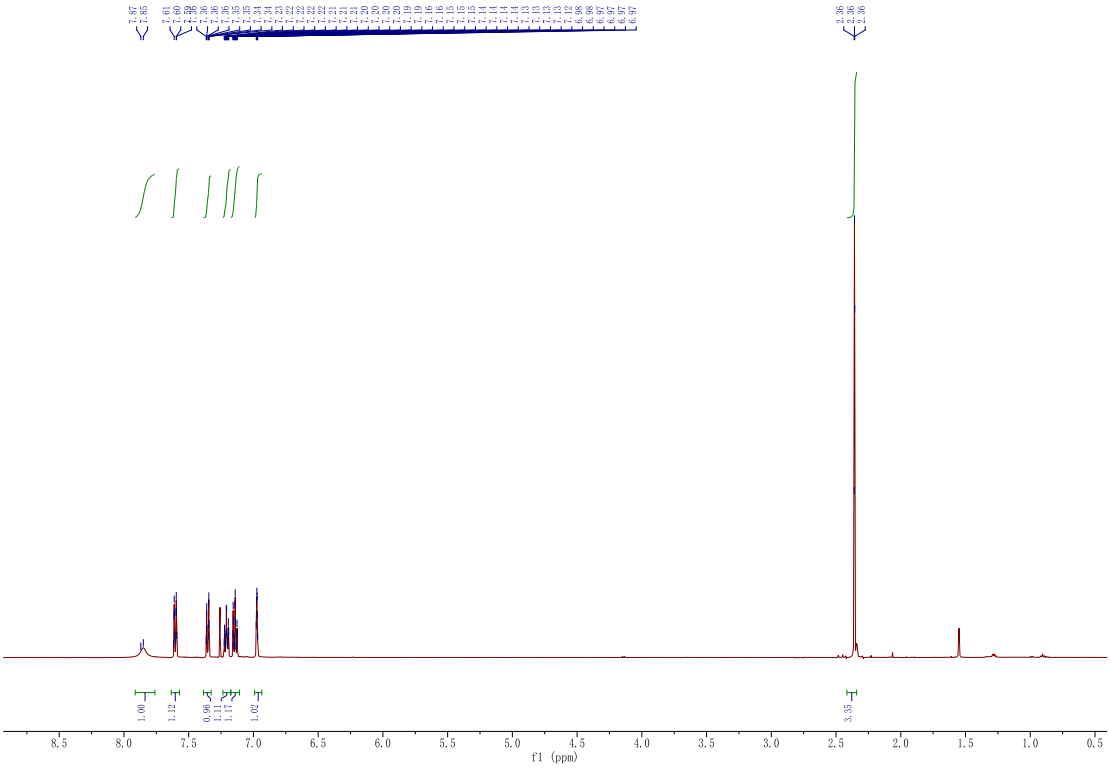

Figure 5. 10. ^{13}C NMR of 3-methylindole

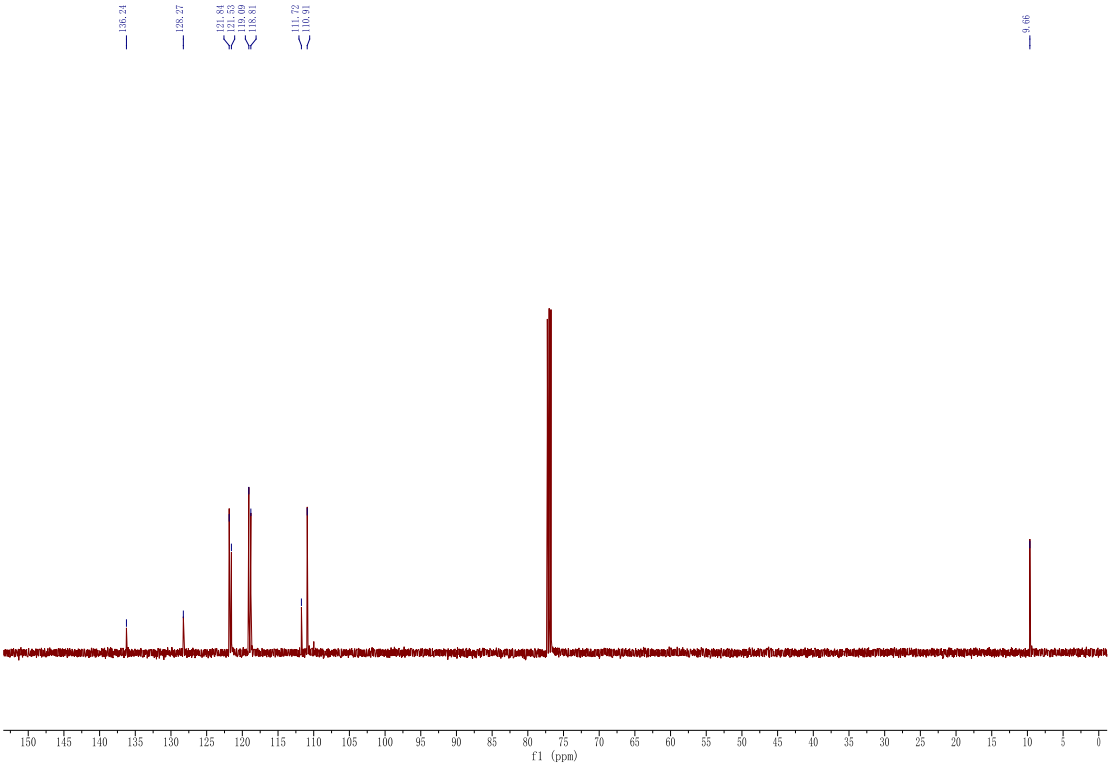

Figure 5. 11. ^{1}H NMR of 2-methylindole

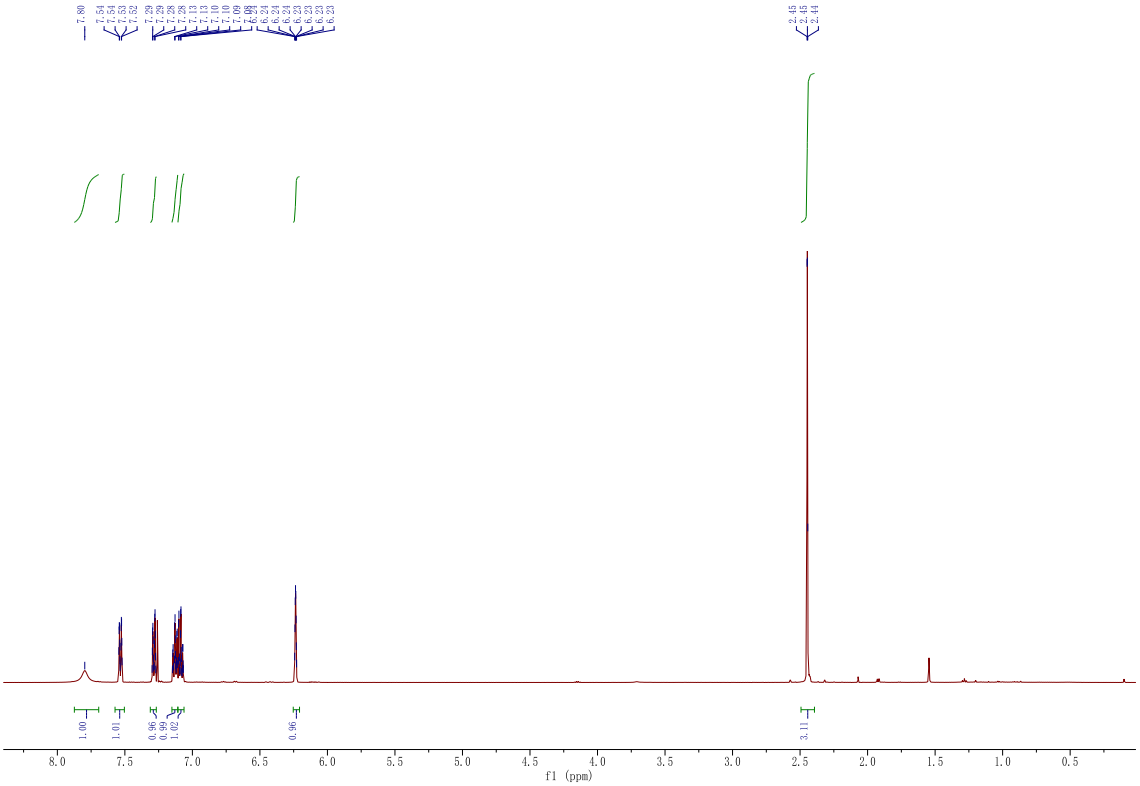

Figure 5. 12. ^{13}C NMR of 2-methylindole

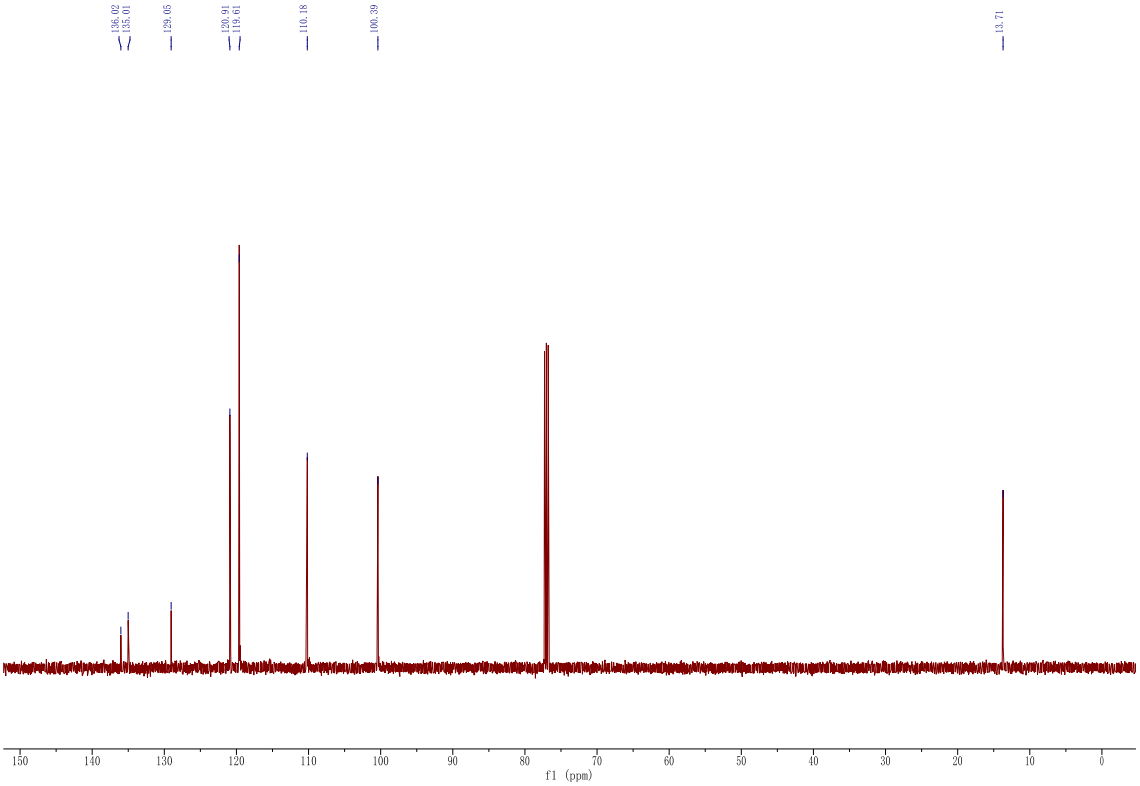

Figure 5. 13. ^{1}H NMR of Ir 1

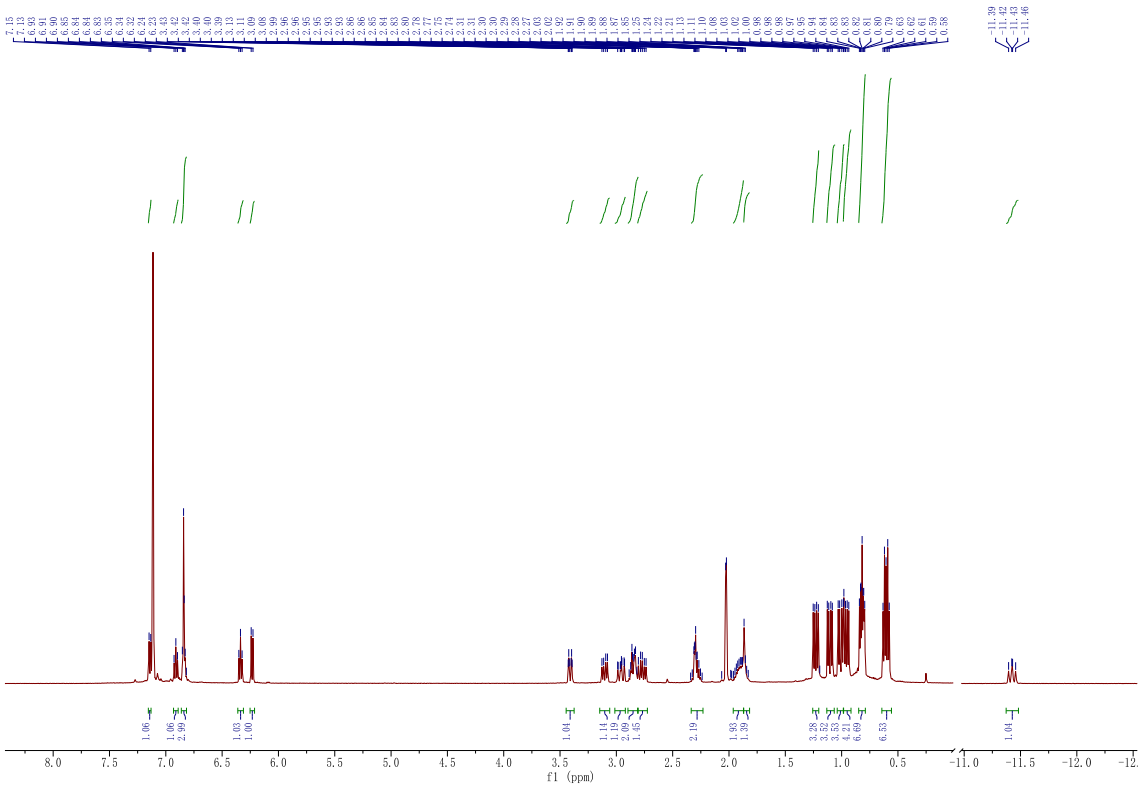

Figure 5. 14. ^{13}C NMR of Ir 1

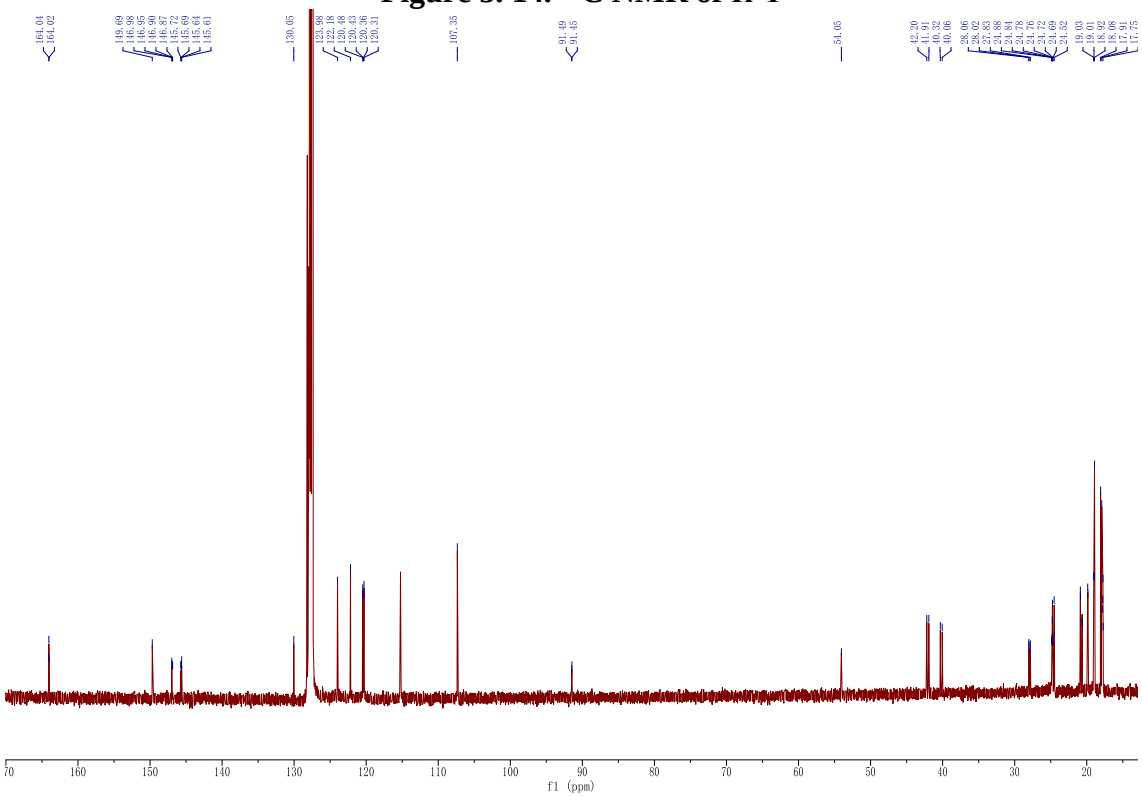

Figure 5. 15. ^{31}P NMR of Ir 1

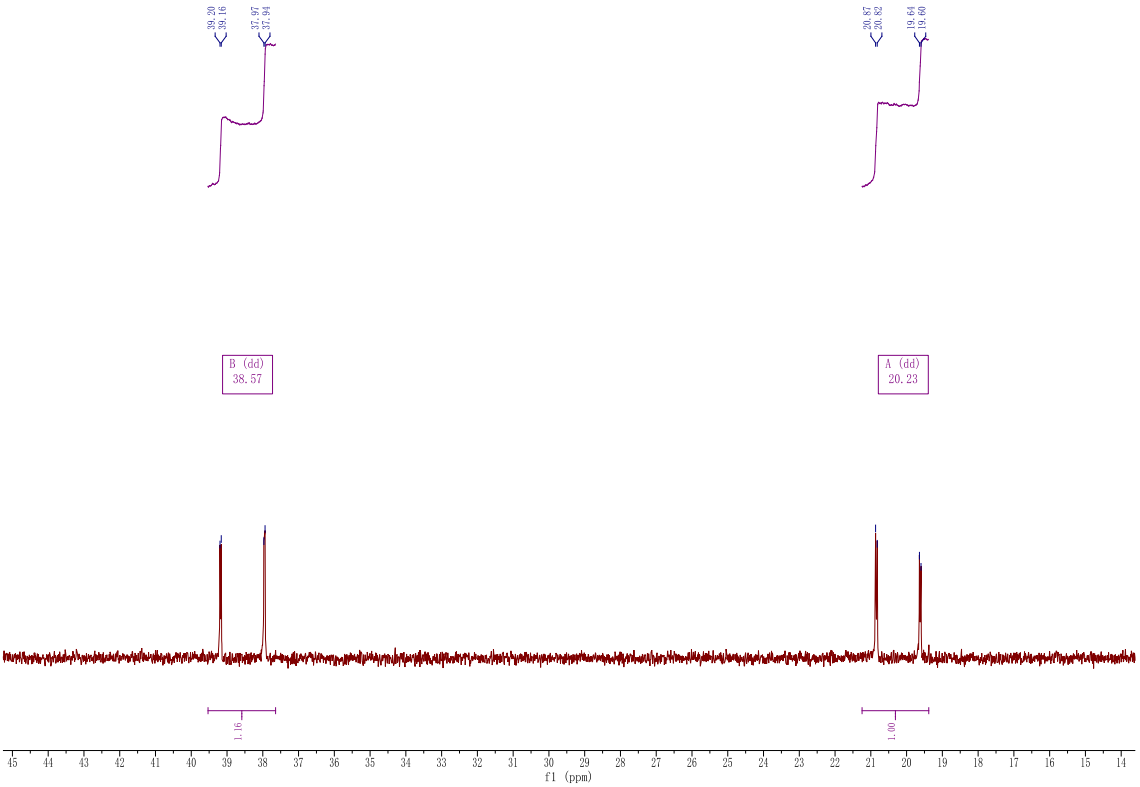

Figure 5. 16. COSY of Ir 1

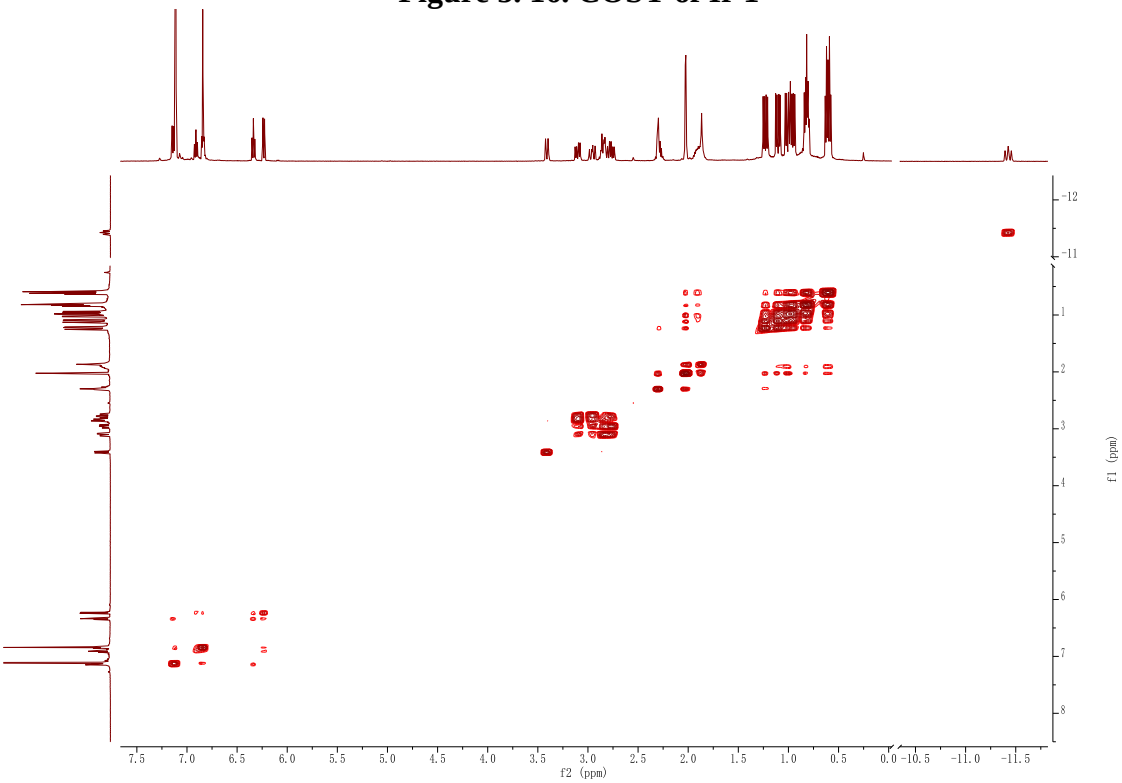

Figure 5. 17. HSQC of Ir 1

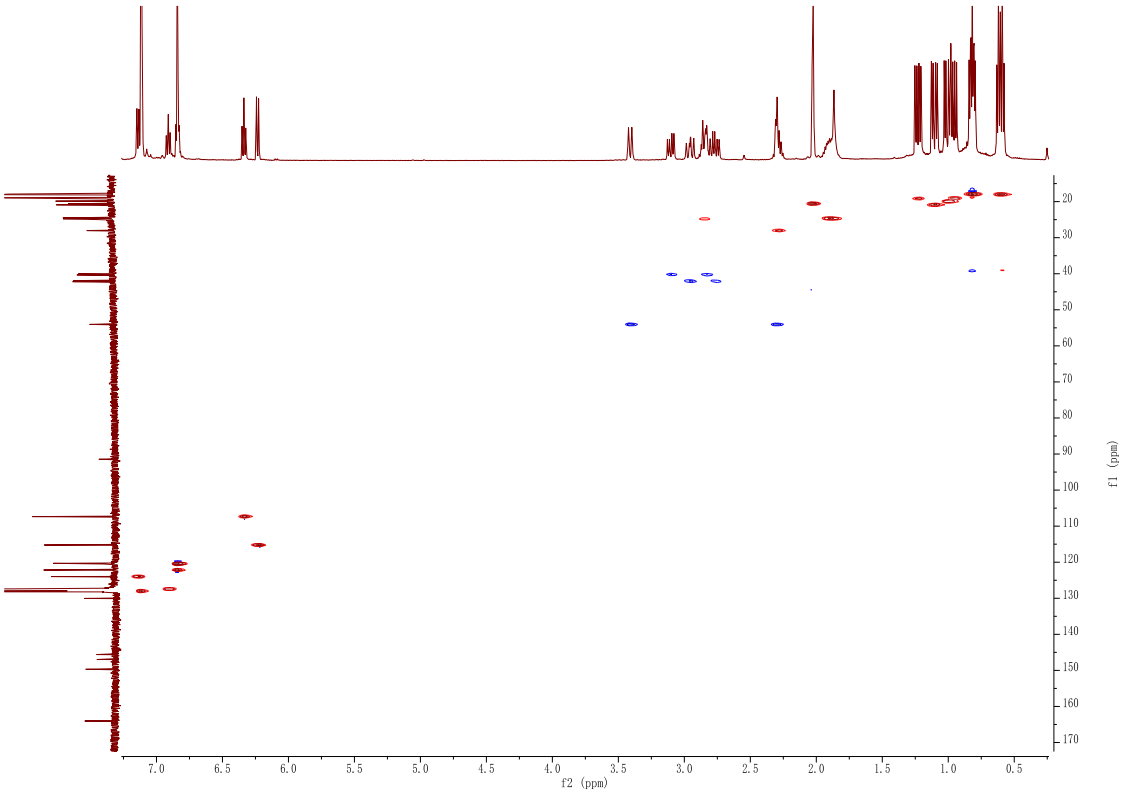

Figure 5. 18. HMBC of Ir 1

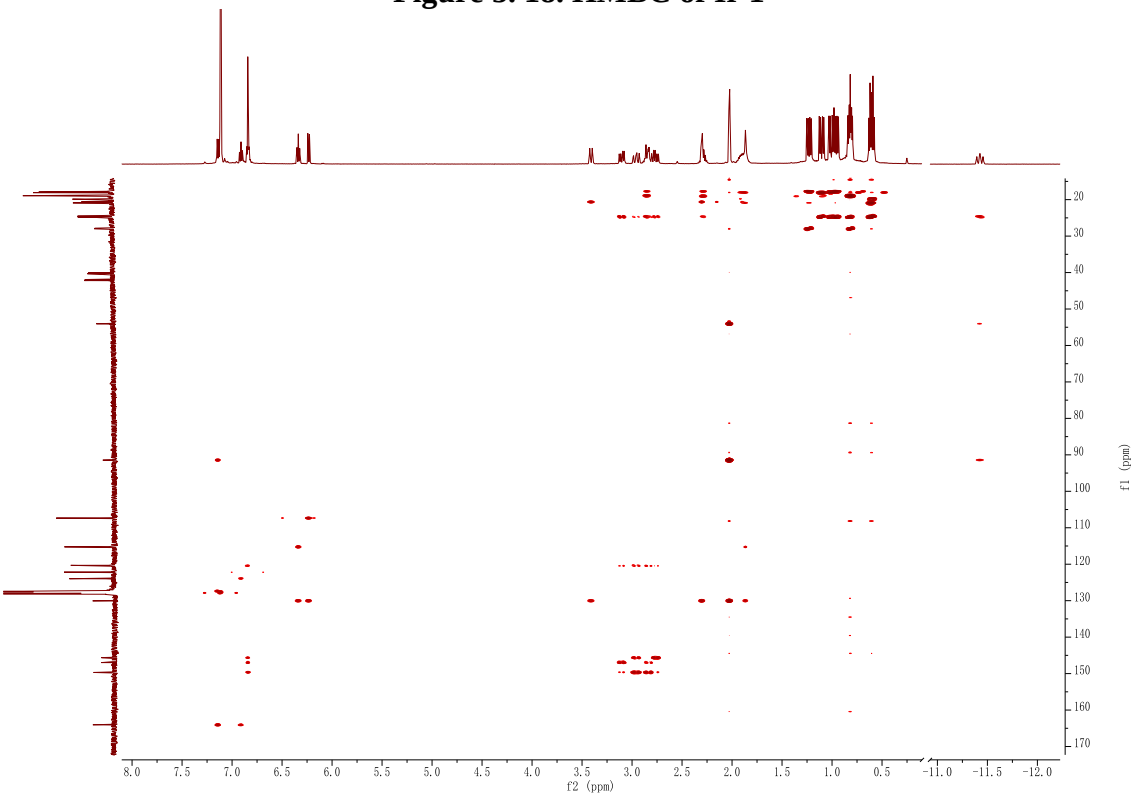

Figure 5. 19. NOSEY of Ir 1

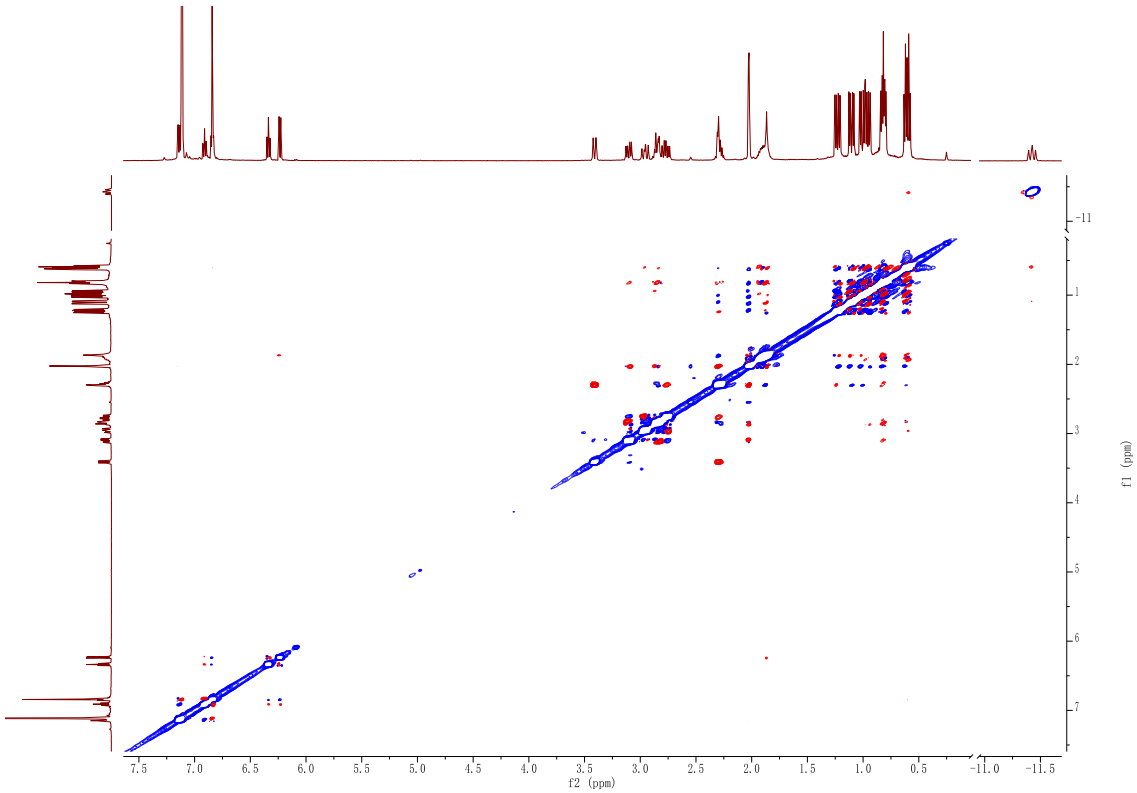

Figure 5. 20. ^{1}H NMR assignment of Ir 1

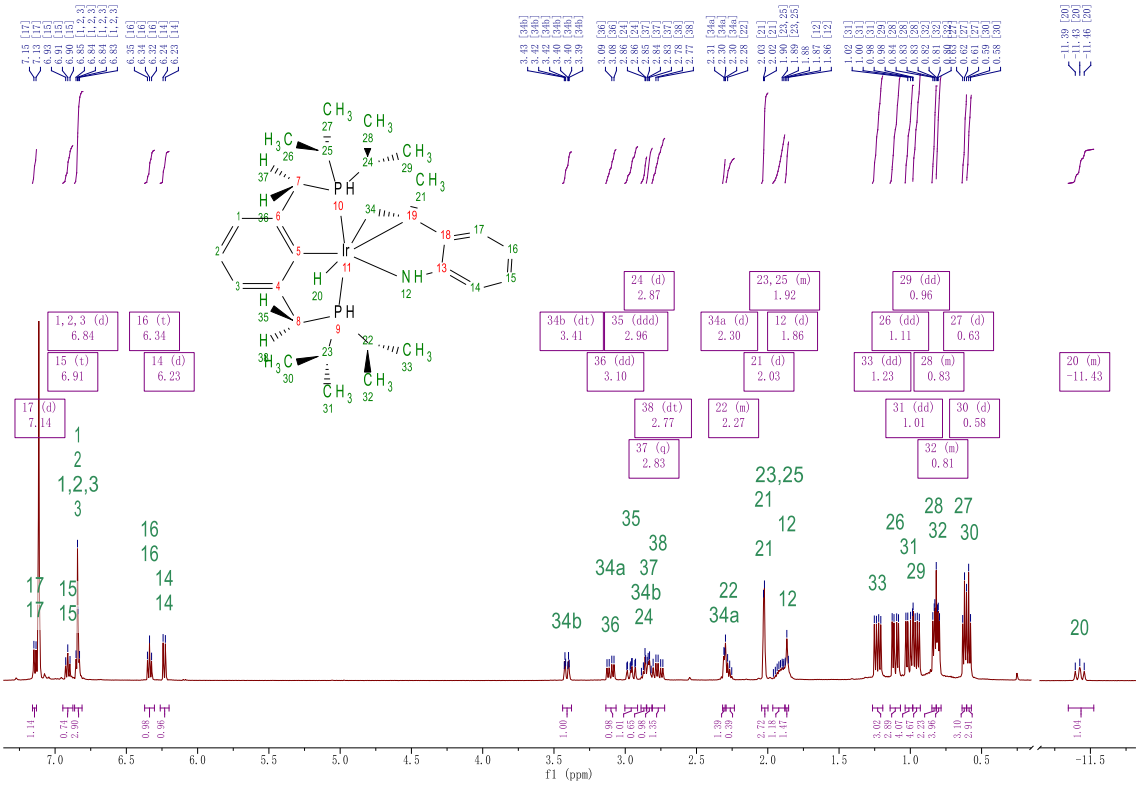

Figure 5. 21. ^{1}H NMR assignment of Ir 1

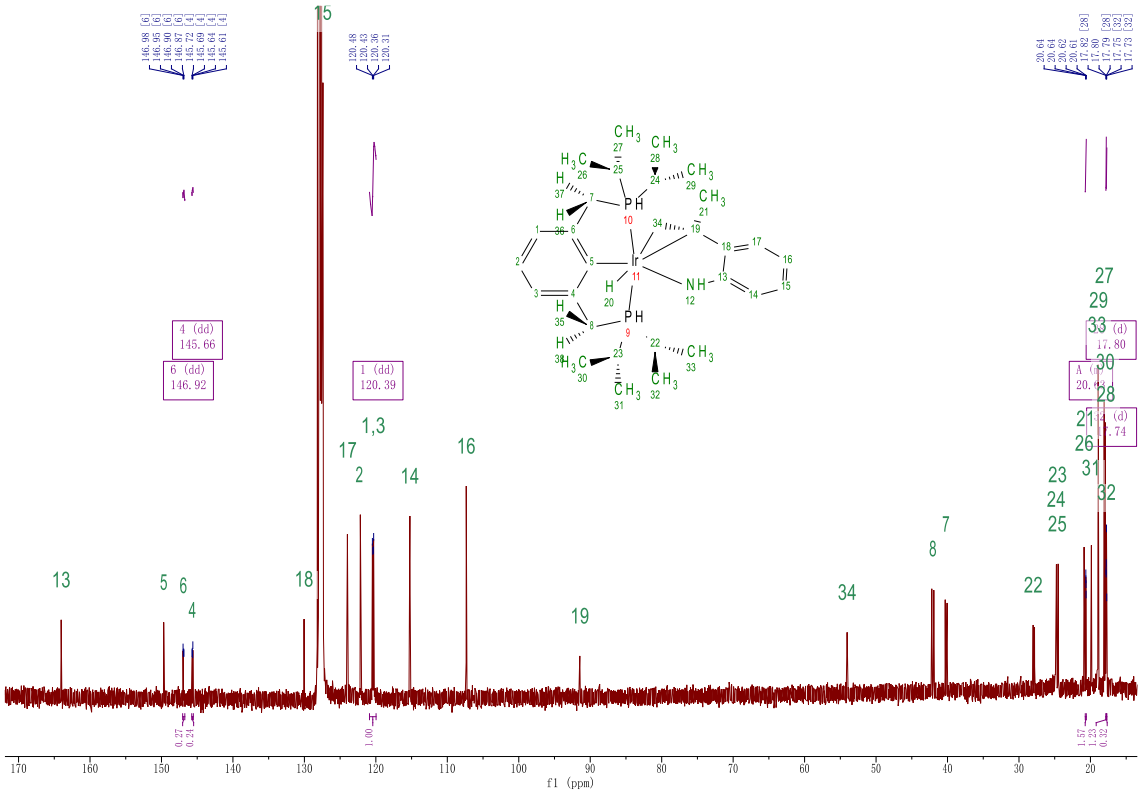

5.4.4. X-Ray structure data

5.4.3.1. ORTEP Diagram Ir 1

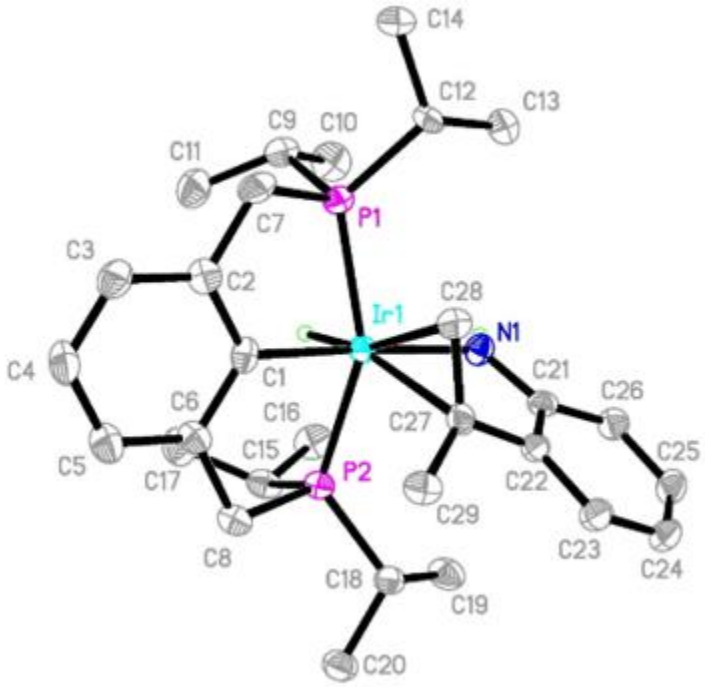

Table 5. 1. Crystal data and structure refinement for Ir 1.

Identification code	bo_li_0m	
Empirical formula	C29 H46 Ir N P2	
Formula weight	662.81	
Temperature	120(2) K	
Wavelength	0.71073 Å	
Crystal system	Monoclinic	
Space group	$P2_1/n$	
Unit cell dimensions	a = 15.820(3) Å	α= 90°.
	b = 12.643(3) Å	β= 118.954(3)°
	c = 15.992(3) Å	γ = 90°.
Volume	2798.9(10) $Å^3$	
Z	4	
Density (calculated)	1.573 Mg/m^3	
Absorption coefficient	4.902 mm^{-1}	
F(000)	1336	
Crystal size	0.350 x 0.160 x 0.080 mm^3	
Theta range for data collection	1.486 to 32.175°.	
Index ranges	-23<=h<=23, -18<=k<=18, -23<=l<=23	
Reflections collected	34343	
Independent reflections	9272 [R(int) = 0.0694]	
Completeness to theta = 25.242°	100.0 %	
Absorption correction	Numerical	
Max. and min. transmission	0.0424 and 0.0096	
Refinement method	Full-matrix least-squares on F^2	
Data / restraints / parameters	9272 / 4 / 319	
Goodness-of-fit on F^2	1.073	
Final R indices [I>2sigma(I)]	R1 = 0.0458, wR2 = 0.0906	
R indices (all data)	R1 = 0.0681, wR2 = 0.1005	
Extinction coefficient	n/a	
Largest diff. peak and hole	2.041 and -1.833 $e.Å^{-3}$	

Table 5. 2. Atomic coordinates (x 10^4) and equivalent isotropic displacement parameters (Å^{2}x 10^3) for Ir 1.

U(eq) is defined as one third of the trace of the orthogonalized U^{ij} tensor.

	x	y	z	U(eq)
Ir(1)	6231(1)	3807(1)	3662(1)	18(1)
P(1)	5697(1)	2093(1)	3596(1)	21(1)
P(2)	6042(1)	5506(1)	3057(1)	21(1)
N(1)	6579(3)	4245(3)	5074(3)	22(1)
C(1)	5991(3)	3415(4)	2309(3)	23(1)
C(2)	5806(4)	2364(4)	1964(3)	24(1)
C(3)	5576(4)	2133(4)	1028(4)	28(1)
C(4)	5563(4)	2904(4)	411(4)	31(1)
C(5)	5773(4)	3941(4)	733(4)	29(1)
C(6)	5975(4)	4202(4)	1663(3)	23(1)
C(7)	5847(4)	1504(4)	2625(4)	28(1)
C(8)	6201(4)	5329(4)	2001(3)	25(1)
C(9)	4398(4)	1911(4)	3202(4)	28(1)
C(10)	4108(4)	2416(5)	3885(4)	39(1)
C(11)	3768(4)	2315(5)	2189(4)	37(1)
C(12)	6343(4)	1143(4)	4597(3)	26(1)
C(13)	6414(4)	1528(4)	5535(4)	34(1)
C(14)	5948(5)	15(4)	4360(4)	39(1)
C(15)	4819(4)	6077(4)	2590(4)	26(1)
C(16)	4464(4)	6049(4)	3329(4)	34(1)
C(17)	4074(4)	5549(5)	1669(4)	36(1)
C(18)	6857(3)	6631(4)	3688(3)	22(1)
C(19)	6708(4)	7096(4)	4479(4)	31(1)
C(20)	6829(4)	7495(4)	3006(4)	30(1)
C(21)	7442(4)	4734(4)	5614(3)	22(1)
C(22)	8104(3)	4736(4)	5253(3)	22(1)
C(23)	8947(4)	5314(4)	5709(4)	26(1)
C(24)	9192(4)	5870(4)	6548(4)	31(1)

C(25)	8570(4)	5828(4)	6936(4)	29(1)
C(26)	7723(4)	5261(4)	6489(3)	26(1)
C(27)	7880(3)	4080(4)	4391(3)	22(1)
C(28)	7656(4)	3005(4)	4420(4)	23(1)
C(29)	8320(4)	4375(4)	3771(4)	25(1)

Table 5. 3. Bond lengths [Å] and angles [°] for Ir 1.

Ir(1)-C(1)	2.068(5)	C(10)-H(10A)	0.9800
Ir(1)-N(1)	2.122(4)	C(10)-H(10B)	0.9800
Ir(1)-C(28)	2.220(5)	C(10)-H(10C)	0.9800
Ir(1)-P(1)	2.3105(13)	C(11)-H(11A)	0.9800
Ir(1)-C(27)	2.311(5)	C(11)-H(11B)	0.9800
Ir(1)-P(2)	2.3152(13)	C(11)-H(11C)	0.9800
Ir(1)-H(1)	1.588(10)	C(12)-C(13)	1.529(7)
P(1)-C(7)	1.839(5)	C(12)-C(14)	1.529(7)
P(1)-C(9)	1.849(5)	C(12)-H(12)	1.0000
P(1)-C(12)	1.862(5)	C(13)-H(13A)	0.9800
P(2)-C(8)	1.837(5)	C(13)-H(13B)	0.9800
P(2)-C(15)	1.850(5)	C(13)-H(13C)	0.9800
P(2)-C(18)	1.856(5)	C(14)-H(14A)	0.9800
N(1)-C(21)	1.361(6)	C(14)-H(14B)	0.9800
N(1)-H(1N)	0.897(10)	C(14)-H(14C)	0.9800
C(1)-C(2)	1.414(7)	C(15)-C(17)	1.525(7)
C(1)-C(6)	1.427(7)	C(15)-C(16)	1.535(7)
C(2)-C(3)	1.389(7)	C(15)-H(15)	1.0000
C(2)-C(7)	1.496(7)	C(16)-H(16A)	0.9800
C(3)-C(4)	1.379(7)	C(16)-H(16B)	0.9800
C(3)-H(3)	0.9500	C(16)-H(16C)	0.9800
C(4)-C(5)	1.389(7)	C(17)-H(17A)	0.9800
C(4)-H(4)	0.9500	C(17)-H(17B)	0.9800
C(5)-C(6)	1.400(7)	C(17)-H(17C)	0.9800
C(5)-H(5)	0.9500	C(18)-C(19)	1.514(7)
C(6)-C(8)	1.503(7)	C(18)-C(20)	1.529(7)
C(7)-H(7A)	0.9900	C(18)-H(18)	1.0000
C(7)-H(7B)	0.9900	C(19)-H(19A)	0.9800
C(8)-H(8A)	0.9900	C(19)-H(19B)	0.9800
C(8)-H(8B)	0.9900	C(19)-H(19C)	0.9800
C(9)-C(10)	1.516(8)	C(20)-H(20A)	0.9800
C(9)-C(11)	1.521(7)	C(20)-H(20B)	0.9800
C(9)-H(9)	1.0000	C(20)-H(20C)	0.9800

C(21)-C(26)	1.413(7)	C(25)-H(25)	0.9500
C(21)-C(22)	1.422(7)	C(26)-H(26)	0.9500
C(22)-C(23)	1.379(6)	C(27)-C(28)	1.411(7)
C(22)-C(27)	1.496(7)	C(27)-C(29)	1.508(7)
C(23)-C(24)	1.394(7)	C(28)-H(28A)	0.957(10)
C(23)-H(23)	0.9500	C(28)-H(28B)	0.958(10)
C(24)-C(25)	1.396(8)	C(29)-H(29A)	0.9800
C(24)-H(24)	0.9500	C(29)-H(29B)	0.9800
C(25)-C(26)	1.376(7)	C(29)-H(29C)	0.9800

C(1)-Ir(1)-N(1)	175.92(17)	C(12)-P(1)-Ir(1)	121.98(16)
C(1)-Ir(1)-C(28)	94.93(19)	C(8)-P(2)-C(15)	105.0(2)
N(1)-Ir(1)-C(28)	82.32(17)	C(8)-P(2)-C(18)	103.1(2)
C(1)-Ir(1)-P(1)	81.33(15)	C(15)-P(2)-C(18)	103.6(2)
N(1)-Ir(1)-P(1)	101.17(12)	C(8)-P(2)-Ir(1)	102.93(16)
C(28)-Ir(1)-P(1)	81.29(13)	C(15)-P(2)-Ir(1)	115.35(17)
C(1)-Ir(1)-C(27)	98.90(18)	C(18)-P(2)-Ir(1)	124.66(16)
N(1)-Ir(1)-C(27)	77.10(16)	C(21)-N(1)-Ir(1)	117.3(3)
C(28)-Ir(1)-C(27)	36.21(17)	C(21)-N(1)-H(1N)	116(3)
P(1)-Ir(1)-C(27)	117.50(12)	Ir(1)-N(1)-H(1N)	122(3)
C(1)-Ir(1)-P(2)	82.18(15)	C(2)-C(1)-C(6)	116.4(4)
N(1)-Ir(1)-P(2)	96.75(12)	C(2)-C(1)-Ir(1)	122.2(4)
C(28)-Ir(1)-P(2)	122.92(13)	C(6)-C(1)-Ir(1)	121.4(4)
P(1)-Ir(1)-P(2)	151.77(5)	C(3)-C(2)-C(1)	121.0(5)
C(27)-Ir(1)-P(2)	87.61(12)	C(3)-C(2)-C(7)	120.5(5)
C(1)-Ir(1)-H(1)	87.5(19)	C(1)-C(2)-C(7)	118.5(4)
N(1)-Ir(1)-H(1)	96.1(19)	C(4)-C(3)-C(2)	121.9(5)
C(28)-Ir(1)-H(1)	161.2(18)	C(4)-C(3)-H(3)	119.1
P(1)-Ir(1)-H(1)	80.7(18)	C(2)-C(3)-H(3)	119.1
C(27)-Ir(1)-H(1)	161.4(18)	C(3)-C(4)-C(5)	118.9(5)
P(2)-Ir(1)-H(1)	75.9(18)	C(3)-C(4)-H(4)	120.5
C(7)-P(1)-C(9)	103.8(2)	C(5)-C(4)-H(4)	120.5
C(7)-P(1)-C(12)	102.9(2)	C(4)-C(5)-C(6)	120.4(5)
C(9)-P(1)-C(12)	105.7(2)	C(4)-C(5)-H(5)	119.8
C(7)-P(1)-Ir(1)	102.95(17)	C(6)-C(5)-H(5)	119.8
C(9)-P(1)-Ir(1)	117.00(17)	C(5)-C(6)-C(1)	121.3(5)

C(5)-C(6)-C(8)	119.8(4)	C(14)-C(12)-H(12)	106.1
C(1)-C(6)-C(8)	118.9(4)	P(1)-C(12)-H(12)	106.1
C(2)-C(7)-P(1)	108.9(3)	C(12)-C(13)-H(13A)	109.5
C(2)-C(7)-H(7A)	109.9	C(12)-C(13)-H(13B)	109.5
P(1)-C(7)-H(7A)	109.9	H(13A)-C(13)-H(13B)	109.5
C(2)-C(7)-H(7B)	109.9	C(12)-C(13)-H(13C)	109.5
P(1)-C(7)-H(7B)	109.9	H(13A)-C(13)-H(13C)	109.5
H(7A)-C(7)-H(7B)	108.3	H(13B)-C(13)-H(13C)	109.5
C(6)-C(8)-P(2)	109.4(3)	C(12)-C(14)-H(14A)	109.5
C(6)-C(8)-H(8A)	109.8	C(12)-C(14)-H(14B)	109.5
P(2)-C(8)-H(8A)	109.8	H(14A)-C(14)-H(14B)	109.5
C(6)-C(8)-H(8B)	109.8	C(12)-C(14)-H(14C)	109.5
P(2)-C(8)-H(8B)	109.8	H(14A)-C(14)-H(14C)	109.5
H(8A)-C(8)-H(8B)	108.2	H(14B)-C(14)-H(14C)	109.5
C(10)-C(9)-C(11)	110.8(5)	C(17)-C(15)-C(16)	109.5(4)
C(10)-C(9)-P(1)	112.1(4)	C(17)-C(15)-P(2)	112.8(4)
C(11)-C(9)-P(1)	111.6(4)	C(16)-C(15)-P(2)	112.5(4)
C(10)-C(9)-H(9)	107.4	C(17)-C(15)-H(15)	107.2
C(11)-C(9)-H(9)	107.4	C(16)-C(15)-H(15)	107.2
P(1)-C(9)-H(9)	107.4	P(2)-C(15)-H(15)	107.2
C(9)-C(10)-H(10A)	109.5	C(15)-C(16)-H(16A)	109.5
C(9)-C(10)-H(10B)	109.5	C(15)-C(16)-H(16B)	109.5
H(10A)-C(10)-H(10B)	109.5	H(16A)-C(16)-H(16B)	109.5
C(9)-C(10)-H(10C)	109.5	C(15)-C(16)-H(16C)	109.5
H(10A)-C(10)-H(10C)	109.5	H(16A)-C(16)-H(16C)	109.5
H(10B)-C(10)-H(10C)	109.5	H(16B)-C(16)-H(16C)	109.5
C(9)-C(11)-H(11A)	109.5	C(15)-C(17)-H(17A)	109.5
C(9)-C(11)-H(11B)	109.5	C(15)-C(17)-H(17B)	109.5
H(11A)-C(11)-H(11B)	109.5	H(17A)-C(17)-H(17B)	109.5
C(9)-C(11)-H(11C)	109.5	C(15)-C(17)-H(17C)	109.5
H(11A)-C(11)-H(11C)	109.5	H(17A)-C(17)-H(17C)	109.5
H(11B)-C(11)-H(11C)	109.5	H(17B)-C(17)-H(17C)	109.5
C(13)-C(12)-C(14)	111.6(4)	C(19)-C(18)-C(20)	110.9(4)
C(13)-C(12)-P(1)	112.8(4)	C(19)-C(18)-P(2)	113.8(3)
C(14)-C(12)-P(1)	113.6(4)	C(20)-C(18)-P(2)	112.8(3)
C(13)-C(12)-H(12)	106.1	C(19)-C(18)-H(18)	106.2

C(20)-C(18)-H(18)	106.2	C(25)-C(24)-H(24)	120.6
P(2)-C(18)-H(18)	106.2	C(26)-C(25)-C(24)	120.5(5)
C(18)-C(19)-H(19A)	109.5	C(26)-C(25)-H(25)	119.7
C(18)-C(19)-H(19B)	109.5	C(24)-C(25)-H(25)	119.7
H(19A)-C(19)-H(19B)	109.5	C(25)-C(26)-C(21)	121.4(5)
C(18)-C(19)-H(19C)	109.5	C(25)-C(26)-H(26)	119.3
H(19A)-C(19)-H(19C)	109.5	C(21)-C(26)-H(26)	119.3
H(19B)-C(19)-H(19C)	109.5	C(28)-C(27)-C(22)	117.0(4)
C(18)-C(20)-H(20A)	109.5	C(28)-C(27)-C(29)	117.6(4)
C(18)-C(20)-H(20B)	109.5	C(22)-C(27)-C(29)	119.3(4)
H(20A)-C(20)-H(20B)	109.5	C(28)-C(27)-Ir(1)	68.4(3)
C(18)-C(20)-H(20C)	109.5	C(22)-C(27)-Ir(1)	104.7(3)
H(20A)-C(20)-H(20C)	109.5	C(29)-C(27)-Ir(1)	118.2(3)
H(20B)-C(20)-H(20C)	109.5	C(27)-C(28)-Ir(1)	75.4(3)
N(1)-C(21)-C(26)	125.6(5)	C(27)-C(28)-H(28A)	119(3)
N(1)-C(21)-C(22)	116.9(4)	Ir(1)-C(28)-H(28A)	105(3)
C(26)-C(21)-C(22)	117.5(4)	C(27)-C(28)-H(28B)	116(3)
C(23)-C(22)-C(21)	120.0(5)	Ir(1)-C(28)-H(28B)	108(3)
C(23)-C(22)-C(27)	121.2(5)	H(28A)-C(28)-H(28B)	121(5)
C(21)-C(22)-C(27)	118.8(4)	C(27)-C(29)-H(29A)	109.5
C(22)-C(23)-C(24)	121.6(5)	C(27)-C(29)-H(29B)	109.5
C(22)-C(23)-H(23)	119.2	H(29A)-C(29)-H(29B)	109.5
C(24)-C(23)-H(23)	119.2	C(27)-C(29)-H(29C)	109.5
C(23)-C(24)-C(25)	118.8(5)	H(29A)-C(29)-H(29C)	109.5
C(23)-C(24)-H(24)	120.6	H(29B)-C(29)-H(29C)	109.5

Table 5. 4. Anisotropic displacement parameters ($Å^2$x 10^3) for Ir 1.

The anisotropic displacement factor exponent takes the form: $-2\pi p^2[h^2 a^{*2} U^{11} + ... + 2 h k a^* b^* U^{12}]$

	U^{11}	U^{22}	U^{33}	U^{23}	U^{13}	U^{12}
Ir(1)	20(1)	17(1)	18(1)	0(1)	9(1)	-1(1)
P(1)	24(1)	18(1)	22(1)	-1(1)	11(1)	-2(1)
P(2)	23(1)	19(1)	23(1)	1(1)	12(1)	1(1)
N(1)	21(2)	26(2)	21(2)	-3(2)	10(2)	-2(2)
C(1)	22(2)	27(2)	18(2)	-4(2)	8(2)	1(2)
C(2)	25(2)	25(2)	25(2)	-1(2)	13(2)	4(2)
C(3)	28(3)	26(3)	28(3)	-6(2)	13(2)	0(2)
C(4)	36(3)	35(3)	19(2)	0(2)	10(2)	6(2)
C(5)	33(3)	31(3)	24(2)	2(2)	14(2)	6(2)
C(6)	27(2)	20(2)	25(2)	2(2)	14(2)	6(2)
C(7)	33(3)	17(2)	34(3)	-6(2)	16(2)	-3(2)
C(8)	28(3)	23(2)	27(2)	3(2)	16(2)	1(2)
C(9)	27(3)	23(2)	33(3)	-1(2)	14(2)	-3(2)
C(10)	31(3)	45(4)	45(3)	2(3)	21(3)	2(3)
C(11)	27(3)	43(3)	33(3)	-3(2)	8(2)	-6(2)
C(12)	29(3)	23(2)	21(2)	7(2)	10(2)	-4(2)
C(13)	40(3)	32(3)	24(3)	3(2)	10(2)	-3(2)
C(14)	53(4)	20(3)	34(3)	3(2)	14(3)	-6(2)
C(15)	26(2)	21(2)	35(3)	7(2)	18(2)	7(2)
C(16)	31(3)	36(3)	43(3)	-5(2)	25(3)	0(2)
C(17)	26(3)	43(3)	31(3)	6(2)	9(2)	4(2)
C(18)	22(2)	21(2)	24(2)	2(2)	12(2)	0(2)
C(19)	42(3)	22(2)	33(3)	2(2)	20(3)	4(2)
C(20)	28(3)	27(3)	32(3)	7(2)	13(2)	0(2)
C(21)	26(2)	16(2)	24(2)	2(2)	12(2)	0(2)
C(22)	19(2)	18(2)	22(2)	2(2)	5(2)	0(2)
C(23)	24(2)	23(2)	28(3)	0(2)	10(2)	-2(2)
C(24)	30(3)	24(2)	29(3)	-3(2)	5(2)	-7(2)
C(25)	32(3)	25(2)	23(2)	-5(2)	9(2)	-1(2)
C(26)	27(3)	24(2)	25(2)	-2(2)	12(2)	1(2)

C(27)	18(2)	26(2)	20(2)	4(2)	6(2)	-1(2)
C(28)	22(2)	21(2)	28(3)	0(2)	13(2)	1(2)
C(29)	23(2)	24(2)	31(3)	2(2)	16(2)	2(2)

Table 5. 5. Hydrogen coordinates (x 10^4) and isotropic displacement parameters (Å^{2}x 10^3) for Ir 1.

	x	y	z	U(eq)
H(1)	5105(10)	4020(40)	3200(30)	28
H(1N)	6120(30)	4380(40)	5230(40)	27
H(3)	5424	1425	807	34
H(4)	5412	2728	-223	37
H(5)	5780	4477	320	35
H(7A)	6476	1133	2892	34
H(7B)	5328	983	2271	34
H(8A)	5764	5813	1485	30
H(8B)	6874	5499	2164	30
H(9)	4279	1133	3197	33
H(10A)	3412	2328	3637	58
H(10B)	4266	3172	3947	58
H(10C)	4459	2076	4512	58
H(11A)	3092	2138	1978	56
H(11B)	3971	1984	1761	56
H(11C)	3837	3085	2177	56
H(12)	7021	1107	4709	31
H(13A)	6918	1128	6069	51
H(13B)	5793	1420	5519	51
H(13C)	6577	2282	5619	51
H(14A)	6372	-462	4878	58
H(14B)	5922	-211	3762	58
H(14C)	5297	-5	4288	58
H(15)	4859	6837	2439	31
H(16A)	3856	6443	3083	51
H(16B)	4950	6373	3926	51
H(16C)	4358	5314	3449	51
H(17A)	3451	5908	1432	53
H(17B)	4005	4804	1794	53
H(17C)	4288	5595	1188	53

H(18)	7528	6340	4003	27
H(19A)	7253	7557	4880	47
H(19B)	6664	6524	4870	47
H(19C)	6108	7509	4200	47
H(20A)	7286	8057	3373	44
H(20B)	6176	7790	2659	44
H(20C)	7009	7193	2550	44
H(23)	9371	5333	5444	32
H(24)	9773	6270	6850	38
H(25)	8732	6194	7513	35
H(26)	7319	5223	6774	31
H(28A)	7690(40)	2730(40)	4990(20)	34
H(28B)	7720(40)	2550(40)	3980(30)	34
H(29A)	8259	5139	3655	38
H(29B)	7983	3999	3161	38
H(29C)	9005	4178	4096	38

Table 5. 6. Torsion angles [°] for Ir 1.

C(6)-C(1)-C(2)-C(3)	-3.1(7)	C(7)-P(1)-C(12)-C(14)	-58.1(5)
Ir(1)-C(1)-C(2)-C(3)	175.2(4)	C(9)-P(1)-C(12)-C(14)	50.5(5)
C(6)-C(1)-C(2)-C(7)	178.0(4)	Ir(1)-P(1)-C(12)-C(14)	-172.6(3)
Ir(1)-C(1)-C(2)-C(7)	-3.8(6)	C(8)-P(2)-C(15)-C(17)	42.5(4)
C(1)-C(2)-C(3)-C(4)	3.1(8)	C(18)-P(2)-C(15)-C(17)	150.3(4)
C(7)-C(2)-C(3)-C(4)	-177.9(5)	Ir(1)-P(2)-C(15)-C(17)	-70.0(4)
C(2)-C(3)-C(4)-C(5)	-0.8(8)	C(8)-P(2)-C(15)-C(16)	167.0(4)
C(3)-C(4)-C(5)-C(6)	-1.3(8)	C(18)-P(2)-C(15)-C(16)	-85.2(4)
C(4)-C(5)-C(6)-C(1)	1.3(8)	Ir(1)-P(2)-C(15)-C(16)	54.5(4)
C(4)-C(5)-C(6)-C(8)	-179.9(5)	C(8)-P(2)-C(18)-C(19)	167.6(4)
C(2)-C(1)-C(6)-C(5)	0.9(7)	C(15)-P(2)-C(18)-C(19)	58.4(4)
Ir(1)-C(1)-C(6)-C(5)	-177.3(4)	Ir(1)-P(2)-C(18)-C(19)	-76.3(4)
C(2)-C(1)-C(6)-C(8)	-177.9(4)	C(8)-P(2)-C(18)-C(20)	40.2(4)
Ir(1)-C(1)-C(6)-C(8)	3.9(6)	C(15)-P(2)-C(18)-C(20)	-69.1(4)
C(3)-C(2)-C(7)-P(1)	-158.3(4)	Ir(1)-P(2)-C(18)-C(20)	156.2(3)
C(1)-C(2)-C(7)-P(1)	20.7(6)	Ir(1)-N(1)-C(21)-C(26)	167.2(4)
C(9)-P(1)-C(7)-C(2)	97.0(4)	Ir(1)-N(1)-C(21)-C(22)	-11.1(6)
C(12)-P(1)-C(7)-C(2)	-153.1(4)	N(1)-C(21)-C(22)-C(23)	172.9(4)
Ir(1)-P(1)-C(7)-C(2)	-25.5(4)	C(26)-C(21)-C(22)-C(23)	-5.5(7)
C(5)-C(6)-C(8)-P(2)	161.7(4)	N(1)-C(21)-C(22)-C(27)	-8.7(6)
C(1)-C(6)-C(8)-P(2)	-19.5(6)	C(26)-C(21)-C(22)-C(27)	172.9(4)
C(15)-P(2)-C(8)-C(6)	-97.5(4)	C(21)-C(22)-C(23)-C(24)	2.7(7)
C(18)-P(2)-C(8)-C(6)	154.3(3)	C(27)-C(22)-C(23)-C(24)	-175.6(5)
Ir(1)-P(2)-C(8)-C(6)	23.6(4)	C(22)-C(23)-C(24)-C(25)	0.6(8)
C(7)-P(1)-C(9)-C(10)	-176.2(4)	C(23)-C(24)-C(25)-C(26)	-1.0(8)
C(12)-P(1)-C(9)-C(10)	75.9(4)	C(24)-C(25)-C(26)-C(21)	-2.0(8)
Ir(1)-P(1)-C(9)-C(10)	-63.6(4)	N(1)-C(21)-C(26)-C(25)	-173.1(5)
C(7)-P(1)-C(9)-C(11)	-51.3(4)	C(22)-C(21)-C(26)-C(25)	5.2(7)
C(12)-P(1)-C(9)-C(11)	-159.2(4)	C(23)-C(22)-C(27)-C(28)	126.4(5)
Ir(1)-P(1)-C(9)-C(11)	61.3(4)	C(21)-C(22)-C(27)-C(28)	-52.0(6)
C(7)-P(1)-C(12)-C(13)	173.7(4)	C(23)-C(22)-C(27)-C(29)	-25.6(7)
C(9)-P(1)-C(12)-C(13)	-77.7(4)	C(21)-C(22)-C(27)-C(29)	156.0(4)
Ir(1)-P(1)-C(12)-C(13)	59.2(4)	C(23)-C(22)-C(27)-Ir(1)	-160.7(4)

C(21)-C(22)-C(27)-Ir(1)	21.0(5)	C(29)-C(27)-C(28)-Ir(1)	-111.5(4)
C(22)-C(27)-C(28)-Ir(1)	96.0(4)		

Table 5. 7. Hydrogen bonds for Ir 1 [Å and °].

D-H...A	d(D-H)	d(H...A)	d(D...A)	<(DHA)
C(13)-H(13C)...N(1)	0.98	2.63	3.549(7)	156.2

5.5. Reference

1. Baeyer, A.; Emmerling, A., Synthese des Indols. *Berichte der deutschen chemischen Gesellschaft* **1869,** *2* (1), 679-682.
2. Wu, C.-J.; Meng, Q.-Y.; Lei, T.; Zhong, J.-J.; Liu, W.-Q.; Zhao, L.-M.; Li, Z.-J.; Chen, B.; Tung, C.-H.; Wu, L.-Z., An Oxidant-Free Strategy for Indole Synthesis via Intramolecular C–C Bond Construction under Visible Light Irradiation: Cross-Coupling Hydrogen Evolution Reaction. *ACS Catalysis* **2016,** *6* (7), 4635-4639.
3. Barden, T. C., Indoles: Industrial, Agricultural and Over-the-Counter Uses. In *Heterocyclic Scaffolds II: Reactions and Applications of Indoles*, Gribble, G. W., Ed. Springer Berlin Heidelberg: Berlin, Heidelberg, 2010; pp 31-46.
4. Bartoli, G.; Dalpozzo, R.; Nardi, M., Applications of Bartoli indole synthesis. *Chemical Society Reviews* **2014,** *43* (13), 4728-4750.
5. Baumann, M.; Baxendale, I. R.; Ley, S. V.; Nikbin, N., An overview of the key routes to the best selling 5-membered ring heterocyclic pharmaceuticals. *Beilstein Journal of Organic Chemistry* **2011,** *7*, 442-495.
6. Inman, M.; Moody, C. J., Indole synthesis – something old, something new. *Chemical Science* **2013,** *4* (1), 29-41.
7. Lancianesi, S.; Palmieri, A.; Petrini, M., Synthetic Approaches to 3-(2-Nitroalkyl) Indoles and Their Use to Access Tryptamines and Related Bioactive Compounds. *Chemical Reviews* **2014,** *114* (14), 7108-7149.
8. Majetich, G.; Shimkus, J. M., The Taiwaniaquinoids: A Review. *Journal of Natural Products* **2010,** *73* (2), 284-298.
9. Lee, B. H.; Choi, Y. L.; Shin, S.; Heo, J.-N., Stereoselective Palladium-Catalyzed α-Arylation of 3-Aryl-1-Indanones: An Asymmetric Synthesis of (+)-Pauciflorol F. *The Journal of Organic Chemistry* **2011,** *76* (16), 6611-6618.
10. Kahlon, A. K.; Negi, A. S.; Kumari, R.; Srivastava, K. K.; Kumar, S.; Darokar, M. P.; Sharma, A., Identification of 1-chloro-2-formyl indenes and tetralenes as novel antistaphylococcal agents exhibiting sortase A inhibition. *Applied Microbiology and Biotechnology* **2014,** *98* (5), 2041-2051.
11. Tye, H.; Mueller, S. G.; Prestle, J.; Scheuerer, S.; Schindler, M.; Nosse, B.; Prevost, N.; Brown, C. J.; Heifetz, A.; Moeller, C.; Pedret-Dunn, A.; Whittaker, M., Novel 6,7,8,9-tetrahydro-5H-1,4,7,10a-tetraaza-cyclohepta[f]indene analogues as potent and selective 5-HT2C agonists for the treatment of metabolic disorders. *Bioorganic & Medicinal Chemistry Letters* **2011,** *21* (1), 34-37.
12. Solomek, T.; Stacko, P.; Tazhe Veetil, A.; Pospisil, T.; Klan, P., Photoenolization-Induced Oxirane Ring Opening in 2,5-Dimethylbenzoyl Oxiranes To Form Pharmaceutically Promising Indanone Derivatives. *The Journal of Organic Chemistry* **2010,** *75* (21), 7300-7309.
13. Alcalde, E.; Mesquida, N.; López-Pérez, S.; Frigola, J.; Mercè, R., Indene-Based Scaffolds. 2. An Indole−Indene Switch: Discovery of Novel Indenylsulfonamides as 5-HT6 Serotonin Receptor Agonists. *Journal of Medicinal Chemistry* **2009,** *52* (3), 675-687.
14. Gabriele, B.; Mancuso, R.; Veltri, L., Recent Advances in the Synthesis of Indanes and Indenes. *Chemistry – A European Journal* **2016,** *22* (15), 5056-5094.
15. Qiu, G.; Wu, J., Generation of Indene Derivatives by Tandem Reactions. *Synlett* **2014,** *25* (19), 2703-2713.

16. Hong, B.-C.; Sarshar, S., RECENT ADVANCES IN THE SYNTHESIS OF INDAN SYSTEMS. A REVIEW. *Organic Preparations and Procedures International* **1999,** *31* (1), 1-86.
17. Yeung, C. S.; Dong, V. M., Catalytic Dehydrogenative Cross-Coupling: Forming Carbon−Carbon Bonds by Oxidizing Two Carbon−Hydrogen Bonds. *Chemical Reviews* **2011,** *111* (3), 1215-1292.
18. Cho, S. H.; Kim, J. Y.; Kwak, J.; Chang, S., Recent advances in the transition metal-catalyzed twofold oxidative C–H bond activation strategy for C–C and C–N bond formation. *Chemical Society Reviews* **2011,** *40* (10), 5068-5083.
19. Shi, Z.; Zhang, C.; Tang, C.; Jiao, N., Recent advances in transition-metal catalyzed reactions using molecular oxygen as the oxidant. *Chemical Society Reviews* **2012,** *41* (8), 3381-3430.
20. Samanta, R.; Matcha, K.; Antonchick, A. P., Metal-Free Oxidative Carbon-Heteroatom Bond Formation Through C–H Bond Functionalization. *European Journal of Organic Chemistry* **2013,** *2013* (26), 5769-5804.
21. Liu, C.; Yuan, J.; Gao, M.; Tang, S.; Li, W.; Shi, R.; Lei, A., Oxidative Coupling between Two Hydrocarbons: An Update of Recent C–H Functionalizations. *Chemical Reviews* **2015**.
22. Chen, B.; Wu, L.-Z.; Tung, C.-H., Photocatalytic Activation of Less Reactive Bonds and Their Functionalization via Hydrogen-Evolution Cross-Couplings. *Accounts of Chemical Research* **2018,** *51* (10), 2512-2523.
23. Baeten, M.; Maes, B. U. W., Chapter Five - Carbon–Nitrogen Bond Formation Through Cross-Dehydrogenative Coupling Reactions. In *Advances in Organometallic Chemistry*, Pérez, P. J., Ed. Academic Press: 2017; Vol. 67, pp 401-481.
24. Würtz, S.; Rakshit, S.; Neumann, J. J.; Dröge, T.; Glorius, F., Palladium-Catalyzed Oxidative Cyclization of N-Aryl Enamines: From Anilines to Indoles. *Angewandte Chemie International Edition* **2008,** *47* (38), 7230-7233.
25. Yu, W.; Du, Y.; Zhao, K., PIDA-Mediated Oxidative C−C Bond Formation: Novel Synthesis of Indoles from N-Aryl Enamines. *Organic Letters* **2009,** *11* (11), 2417-2420.
26. Guan, Z.-H.; Yan, Z.-Y.; Ren, Z.-H.; Liu, X.-Y.; Liang, Y.-M., Preparation of indolesvia iron catalyzed direct oxidative coupling. *Chemical Communications* **2010,** *46* (16), 2823-2825.
27. He, Z.; Liu, W.; Li, Z., I2-Catalyzed Indole Formation via Oxidative Cyclization of N-Aryl Enamines. *Chemistry – An Asian Journal* **2011,** *6* (6), 1340-1343.
28. Neumann, J. J.; Rakshit, S.; Dröge, T.; Würtz, S.; Glorius, F., Exploring the Oxidative Cyclization of Substituted N-Aryl Enamines: Pd-Catalyzed Formation of Indoles from Anilines. *Chemistry – A European Journal* **2011,** *17* (26), 7298-7303.
29. Maity, S.; Zheng, N., A Visible-Light-Mediated Oxidative C□N Bond Formation/Aromatization Cascade: Photocatalytic Preparation of N-Arylindoles. *Angewandte Chemie International Edition* **2012,** *51* (38), 9562-9566.
30. Xia, X.-D.; Xuan, J.; Wang, Q.; Lu, L.-Q.; Chen, J.-R.; Xiao, W.-J., Synthesis of 2-Substituted Indoles through Visible Light-Induced Photocatalytic Cyclizations of Styryl Azides. *Advanced Synthesis & Catalysis* **2014,** *356* (13), 2807-2812.
31. Zoller, J.; Fabry, D. C.; Ronge, M. A.; Rueping, M., Synthesis of Indoles Using Visible Light: Photoredox Catalysis for Palladium-Catalyzed C□H Activation. *Angewandte Chemie International Edition* **2014,** *53* (48), 13264-13268.
32. Cai, S.; Yang, K.; Wang, D. Z., Gold Catalysis Coupled with Visible Light Stimulation: Syntheses of Functionalized Indoles. *Organic Letters* **2014,** *16* (10), 2606-2609.

33. Sagadevan, A.; Ragupathi, A.; Hwang, K. C., Photoinduced Copper-Catalyzed Regioselective Synthesis of Indoles: Three-Component Coupling of Arylamines, Terminal Alkynes, and Quinones. *Angewandte Chemie International Edition* **2015,** *54* (47), 13896-13901.
34. Agasti, S.; Dey, A.; Maiti, D., Palladium-catalyzed benzofuran and indole synthesis by multiple C–H functionalizations. *Chemical Communications* **2017,** *53* (49), 6544-6556.
35. Festa, A. A., Synthesis of indoles under the action of visible light (microreview). *Chemistry of Heterocyclic Compounds* **2018,** *54* (1), 22-24.
36. Liu, W.-Q.; Lei, T.; Song, Z.-Q.; Yang, X.-L.; Wu, C.-J.; Jiang, X.; Chen, B.; Tung, C.-H.; Wu, L.-Z., Visible Light Promoted Synthesis of Indoles by Single Photosensitizer under Aerobic Conditions. *Organic Letters* **2017,** *19* (12), 3251-3254.
37. Prakash, S.; Kuppusamy, R.; Cheng, C.-H., Cobalt-Catalyzed Annulation Reactions via C−H Bond Activation. *ChemCatChem* **2018,** *10* (4), 683-705.
38. Peneau, A.; Guillou, C.; Chabaud, L., Recent Advances in [Cp*MIII] (M = Co, Rh, Ir)-Catalyzed Intramolecular Annulation Through C–H Activation. *European Journal of Organic Chemistry* **2018,** *2018* (42), 5777-5794.
39. Ghorai, J.; Reddy, A. C. S.; Anbarasan, P., Divergent Functionalization of N-Alkyl-2-alkenylanilines: Efficient Synthesis of Substituted Indoles and Quinolines. *Chemistry – An Asian Journal* **2018,** *13* (17), 2499-2504.
40. Li, Y.-L.; Li, J.; Ma, A.-L.; Huang, Y.-N.; Deng, J., Metal-Free Synthesis of Indole via NIS-Mediated Cascade C–N Bond Formation/Aromatization. *The Journal of Organic Chemistry* **2015,** *80* (8), 3841-3851.
41. Ortgies, S.; Breder, A., Selenium-Catalyzed Oxidative C(sp2)–H Amination of Alkenes Exemplified in the Expedient Synthesis of (Aza-)Indoles. *Organic Letters* **2015,** *17* (11), 2748-2751.
42. Jang, Y. H.; Youn, S. W., Metal-Free C–H Amination for Indole Synthesis. *Organic Letters* **2014,** *16* (14), 3720-3723.
43. Fra, L.; Millán, A.; Souto, J. A.; Muñiz, K., Indole Synthesis Based On A Modified Koser Reagent. *Angewandte Chemie International Edition* **2014,** *53* (28), 7349-7353.
44. Liwosz, T. W.; Chemler, S. R., Copper-Catalyzed Synthesis of N-Aryl and N-Sulfonyl Indoles from 2-Vinyl-anilines with O2 as Terminal Oxidant and TEMPO as Cocatalyst. *Synlett* **2015,** *26* (03), 335-339.
45. Harrington, P. J.; Hegedus, L. S., Palladium-catalyzed reactions in the synthesis of 3- and 4-substituted indoles. Approaches to ergot alkaloids. *The Journal of Organic Chemistry* **1984,** *49* (15), 2657-2662.
46. Liwosz, T. W.; Chemler, S. R., Copper-Catalyzed Oxidative Amination and Allylic Amination of Alkenes. *Chemistry – A European Journal* **2013,** *19* (38), 12771-12777.
47. Tsvelikhovsky, D.; Buchwald, S. L., Synthesis of Heterocycles via Pd-Ligand Controlled Cyclization of 2-Chloro-N-(2-vinyl)aniline: Preparation of Carbazoles, Indoles, Dibenzazepines, and Acridines. *Journal of the American Chemical Society* **2010,** *132* (40), 14048-14051.
48. Krolski, M. E.; Renaldo, A. F.; Rudisill, D. E.; Stille, J. K., Palladium-catalyzed coupling of 2-bromoanilines with vinylstannanes. A regiocontrolled synthesis of substituted indoles. *The Journal of Organic Chemistry* **1988,** *53* (6), 1170-1176.
49. Hegedus, L. S.; Toro, J. L.; Miles, W. H.; Harrington, P. J., Palladium-catalyzed reactions in the synthesis of 3- and 4-substituted indoles. 3. Total synthesis of (.+-.)-aurantioclavine. *The Journal of Organic Chemistry* **1987,** *52* (15), 3319-3322.

50. Wang, H.; Zhao, Y.-L.; Li, L.; Li, S.-S.; Liu, Q., ChemInform Abstract: Metal-Free 2,3-Dichloro-5,6-dicyano-1,4-benzoquinone (DDQ)-Mediated Cross-Dehydrogenative-Coupling (CDC) of Benzylic C(sp3)—H Bonds and Vinylic C(sp2)—H Bonds: Efficient One-Pot Synthesis of 1H-Indenes. *ChemInform* **2015,** *46* (11).
51. Wang, H.; Zhao, Y.-L.; Li, L.; Li, S.-S.; Liu, Q., Metal-Free 2,3-Dichloro-5,6-dicyano-1,4-benzoquinone (DDQ)-Mediated Cross-Dehydrogenative-Coupling (CDC) of Benzylic C(sp3)□H Bonds and Vinylic C(sp2)□H Bonds: Efficient One-Pot Synthesis of 1H-Indenes. *Advanced Synthesis & Catalysis* **2014,** *356* (14-15), 3157-3163.
52. Wilklow-Marnell, M.; Li, B.; Zhou, T.; Krogh-Jespersen, K.; Brennessel, W. W.; Emge, T. J.; Goldman, A. S.; Jones, W. D., Catalytic Dehydrogenative C–C Coupling by a Pincer-Ligated Iridium Complex. *Journal of the American Chemical Society* **2017**.
53. Zhao, J.; Goldman, A. S.; Hartwig, J. F., Oxidative addition of ammonia to form a stable monomeric amido hydride complex. *Science* **2005,** *307* (5712), 1080-2.
54. Liu, F.; S. Goldman, A., Efficient thermochemical alkane dehydrogenation and isomerization catalyzed by an iridium pincer complex. *Chemical Communications* **1999,** (7), 655-656.

Chapter 6. Partial deoxygenation of diols and triols by a pincer-ligated iridium complex

Abstract: Converting biomass to useful chemicals was an attractive alternative route for renewable energy. One of the key part of this conversion was removing the extra oxygen atom from the high oxygen content biomass. The successful discovery of dehydration reaction by pincer-iridium complex enabled us to design a special deoxygenation route to remove oxygen atom from diols and triols. With the help of hydrogen gas, we were able to partial deoxygenate of diols and triols to mono alcohol and diols respectively with high conversion and yield. Using the biodiesel fuel byproduct, glycerol, we could selectively generate valuable 1,2-propanediol (important polymer precursor) and its dehydrogenated product hydroxyacetone with up to 76% yield. Decarbonylation and hydrogenation by pincer-iridium could introduce ethylene glycol and methanol as side products (about 10-30%), which are also useful chemicals. A mechanism involved a key intermediate generated by a synergetic nucleophilic hydride attaching the electronic poor carbon and hydroxyl transferring to iridium center was proposed based on reaction scope, reaction selectivity and substrates effect.

6.1. Introduction

As global energy consumption increases, biomass may play a more prominent role in providing renewable fuels. However, the high oxygen content of biomass feedstock causes a few major problems that limit its value such as low energy density, low stability and corrosion.[1] Selective deoxygenation is the key to fulfill the potential of producing fuels from renewable biomass. Different catalytic systems for biomass conversion have been studied and their reactivity, selectivity and mechanisms have been described.[1-6] Finding new catalytic systems to convert biomass into desired products under mild condition with high selectivity and activity continues to be a research aim. In particular, the selective deoxygenation of mono alcohols, diols, and triols to alkanes would be of great value.

Glycerol, produced in abundance as a byproduct of biodiesel, is an attractive starting material for more value-added uses.[7-8] Different methods, including dehydration, oxidation, hydrogenolysis, esterification, and acetalization, have been developed to convert glycerol to more useful chemicals. Deoxygenation by hydrogenolysis is of great value in converting glycerol to either propanediol or propanol. Combining dehydration by acid catalysts and hydrogenation by homogeneous metal complexes[9] is one common strategy to produce 1,3-propanediol and 1-propanol[10-14] (Scheme 6.1). However, this only produces 1,3-propanediol due to the preference of the acid catalysts to react at the internal hydroxyl. This is unfortunate since 1,2-propanediols is of greater annual consumption and market value. Furthermore, the selectivity and yield of this route is poor due to acid-catalyzed side reactions.

Scheme 6. 1. Tandem acid and metal catalyst for partial deoxygenation of glycerol

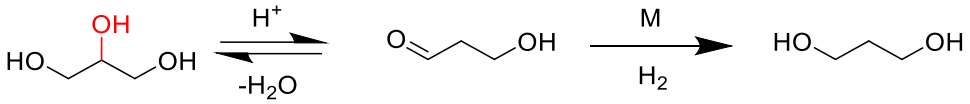

Although stoichiometric and catalytic C-O bond cleavage by pincer-iridium complexes has been reported by Goldman, Grubbs, and Agapie in recent years[15-19], dehydration, cleaving both C-H and C-O bond of an alcohol, has not been reported for these complexes. Hydrogenation reactions catalyzed by pincer-iridium complexes have been widely studied.[20-22] Alcohol deoxygenation via combined dehydration and hydrogenation has been reported for iridium, ruthenium and manganese complexes.[23-27] The discovery of alcohol dehydration by pincer iridium complexes (Scheme 6.2) enables partial deoxygenation of glycerol in a new way. We performed glycerol partial deoxygenation using only a pincer iridium complex as catalyst (Scheme 6.3). The different steric environments of the hydroxyl groups in glycerol is the source of the selectivity of deoxygenation by the pincer-iridium complex. Under hydrogen atmosphere to inhibit dehydrogenation, the less sterically hindered terminal hydroxyl is the preferred reaction site by the pincer iridium complex thereby affording commercially desirable 1,2-propanediol as the major product.

Scheme 6. 2. Dehydration by pincer-iridium complex

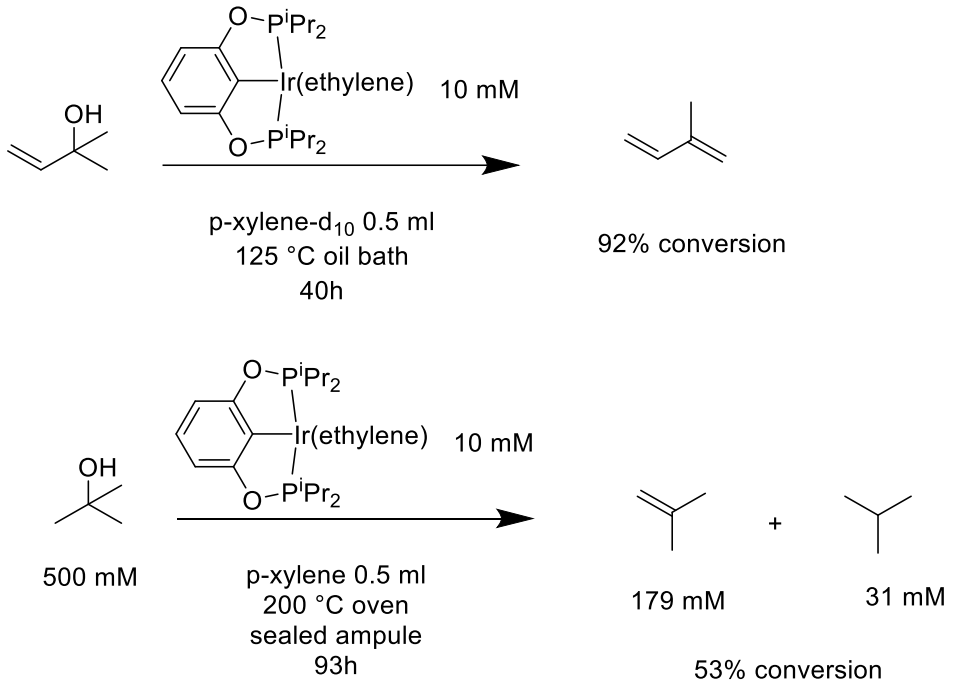

Scheme 6. 3. Pincer-iridium complex for partial deoxygenation of glycerol

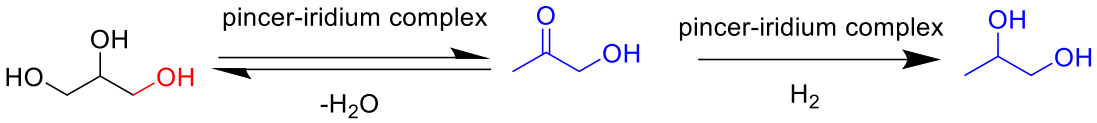

6.2. Results and discussion

6.2.1. Dehydration by pincer iridium complex

Pursuing a wider substrate scope for dehydrogenative coupling through metallocycle intermediates, we attempted the dehydrogenative coupling of 3-hydroxy-3-methyl-1-butene as using (^{iPr}POCOP)Ir(C_2H_4) as catalyst (Scheme 6.2). We predicted that facile O-H and *β*-vinylic C-H activation would lead to the formation of a new metallocycle (Figure 6.1) that could undergo further coupling. However, instead of observing C-C bond formation, we observed the formation of water and isoprene. This revealed that (^{iPr}POCOP)Ir(C_2H_4) is competent for alcohol dehdyration. However, dehydrogenation of alcohols to aldehydes or ketones[22] is a competitive side reaction that

limits the effectiveness of pincer-iridium complexes for primary and secondary alcohol dehydration. In contrast, the inability of tertiary alcohols to undergo dehydrogenation allows them to be ideal substrates for studying for pincer-iridium catalyzed dehydration. Tert-butanol easily underwent dehydration to isobutene, with certain amount isobutene product undergoing hydrogenation (Scheme 6.2). This inspired us to attempt transfer dehydrogenation of cyclooctane using isobutene generated *in-situ* by tert-butanol dehydration (Scheme 6.4). We were delighted to observe cyclooctene formation, showing that the dehydration is compatible with at least one other reaction also catalyzed by a pincer-iridium complex. This result also indicated the active catalyst in this tandem reaction should be the 14e$^-$ iridium complex given that it is active for transfer dehydrogenation. Also, based on the reported example of C-O bond cleavage[15-19], C-H activation likely precedes C-O bond cleavage.

Figure 6. 1. Proposed new metallocycle

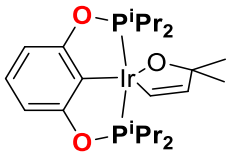

Scheme 6. 4. Tandem dehydration and transfer dehydrogenation

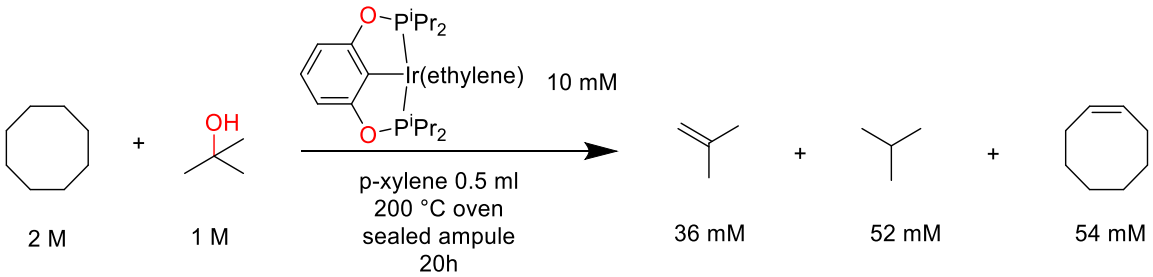

6.2.2. Partial deoxygenation of diols

The ability of (^{iPr}POCOP)Ir(C_2H_4) to perform both dehydration and hydrogenation enabled a novel deoxygenation reaction. To further explore this reaction, we successfully converted 1,3-propanediol to 1-propanol with high conversion and yield (96% and 56%, respectively) in 1:1

pyridine/*p*-xylene-d^{10} (pyridine was used to dissolve the alcohol, and *p*-xylene-d^{10} was used as NMR solvent) under 4 atm H_2 pressure, showed in scheme 6.5. Together with the major products, small amount ethanol and methanol formed. Monitoring the reaction by both ^1H and ^{31}P NMR revealed that the catalyst species present in the reaction after heating were Ir-CO and two $Ir(CO)(H)_2$ species (cis and trans) (Figure 6.2). Generation of Ir-CO and $Ir(CO)(H)_2$ species from $14e^-$ iridium complex in the presence of alcohol has previously been reported.[28-29] Using (^{iPr}POCOP)Ir(CO) instead of (^{iPr}POCOP)Ir(C_2H_4) gave the same results. Although catalytic hydrogenation using pincer iridium carbonyl complexes of (^{tBu}POCOP)Ir(CO) and (Me_2N-^{tBu}POCOP)Ir(CO) has been studied by Goldberg group,[11-12, 30] using (^{iPr}POCOP)Ir(CO) for dehydration was unclear, since there are a big difference for $14e^-$ iridium complex and $16e^-$ iridium complex. In a previous report of C-O bond cleavage by a pincer-iridium complex,[15-19] direct C-O oxidative addition was unfavorable. Instead, C-H bond activation was reported to mediate the C-O bond cleavage. In these C-H bond activation mediated C-O bond cleavage reactions, $14e^-$ iridium complex was determined to be the active catalytic species. It is also noteworthy that sp C-H oxidative addition of phenyl acetylene, which is facile for the 14e- Ir(I) complex (^{tBu}PCP)Ir, is very slow for (^{tBu}PCP)Ir(CO) in the absence of an acid catalyst.[31] Whether or not (^{iPr}POCOP)Ir(CO) is an active catalyst for dehydration or it dissociates CO under experimental conditions is not yet determined."

Scheme 6. 5. Partial deoxygenation of 1,3-propanediol

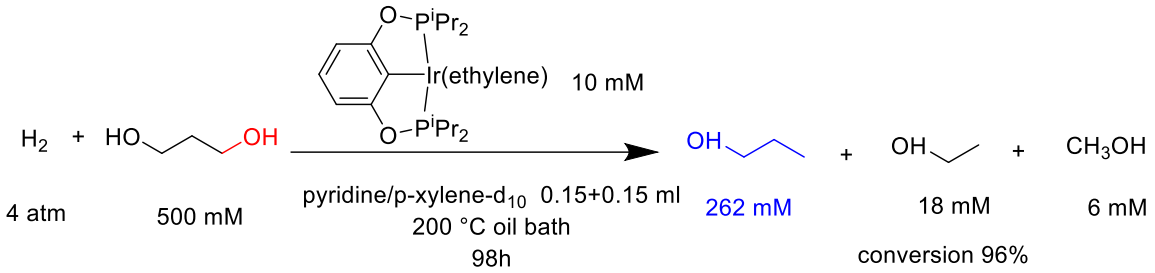

Figure 6. 2. Catalyst species in the reaction

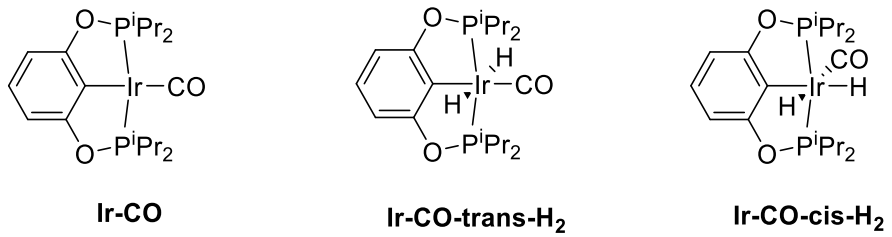

Although the dehydration reactions are performed under hydrogen atmosphere, the high reaction temperature could enable the iridium catalyst to generate small amounts of aldehyde through dehydrogenation. This has been observed by NMR, but is not listed as a major product. The decarbonylation reaction of alcohol and aldehyde by pincer-iridium complexes has been reported.[28-29] This occurs in catalytic manner in the present reaction based on the formation of small amounts ethanol and methanol. Based on former group member Jason D. Hackenberg's dissertation,[32] we know that aldehydes undergo decarbonylation via sequence of C-H oxidative addition to form Ir(CO)(alkyl)(H) complexes (cis and trans isomers) followed by sp^3 C-H reductive elimination to give an equivalent of alkane (or, in the present case, ethanol) and Ir-CO (Scheme 6.6). The resulting Ir(CO) species can undergo either hydrogenation to afford methanol or disassociation to give CO and the $14e^-$ iridium(I) complex. Considering ethanol could also go through decarbonylation to give methanol, the amount of methanol formed should be greater than ethanol, while we observed greater amount of ethanol than methanol. The amount difference in

formed ethanol and methanol could only explained by loss as CO, since Ir-CO went through disassociation route could give CO.

Scheme 6. 6. Decarbonylation route of 1,3-propanediol by pincer-iridium complex

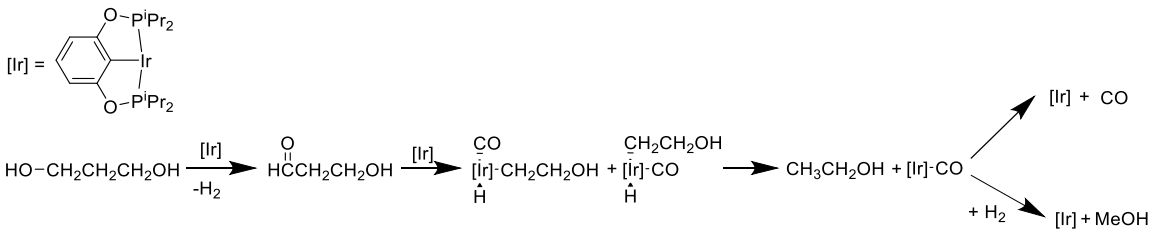

The hypothesis that CO disassociates from (^{iPr}POCOP)Ir(CO) complex under experimental conditions to form the catalytically active 14e- complex (^{iPr}POCOP)Ir was tested by performing catalytic dehydration under mixed CO/H_2 atmosphere (Table 6.1). 50% CO in H_2 slowed down the reaction by a factor of 2.5 in comparison to the reaction performed under 50% Argon in H_2. The greater amount of CO present in the solution would inhibit CO dissociation from iridium and thereby reduce the equilibrium concentration of 14e$^-$ iridium complex. Increasing total gas pressure increases both product yield and reaction rate. This change in reaction rate and yield may be attributed to the change of reaction temperature, since we run the reaction in a reflux condition. Higher reaction temperatures would favor the dehydration process and make more deoxygenated product.

Table 6. 1. Partial deoxygenation of 1,3-propanediol with different gases component

Reaction	H_2(atm)	CO (atm)	Ar (atm)	Reaction time (h)	1-propanol (mM)	ethanol (mM)	methanol (mM)	Conversion
1	4	0	0	6	77	26	20	55%
				24	156	33	20	82%
				72	191	36	24	98%
2	4	0	1[a]	6	99	28	22	43%
				24	189	41	29	68%
				72	253	46	31	94%
				98	278	54	36	96%
3	4	0	4	6	65	11	2	22%
				24	281	14	4	84%
				48	318	14	4	99%
4	4	4	0	6	29	9	6	9%
				24	115	24	12	32%
				72	174	24	12	59%
				120	256	29	10	91%

Reaction conducted with 500 mM 1,3-propanediol, and 10 mM (^{iPr}PCOP)Ir(ethylene) in 0.3 ml mixture solvent with 1:1 ration pyridine and *p*-xylene-d^{10} in high pressure NMR tube, the NMR tube was degas under vacuum and charged gases or gas mixtures with different pressure, a) without remove the initial 1 atm argon from glovebox. Then heated in 200°C oil bath and monitored by NMR. Yield calculated through product peaks in ^{1}H spectra by comparing residual solvent peak.

The isomer 1,2-propanediol gave totally different results (scheme 6.7). No partial deoxygenation was observed; instead, only products from dehydrogenation and decarbonylation were present. Increasing the hydrogen pressure only resulted in a lower amount dehydrogenation product. The same catalyst speciation was observed for this reaction. Higher hydrogen pressure decreased the amount of Ir-CO and increased the amount of *trans*-Ir(CO)$(H)_2$, similar to the reported results of H_2 addition to Ir-CO by Goldberg.[33]

Scheme 6. 7. Partial deoxygenation of 1,2-propanediol

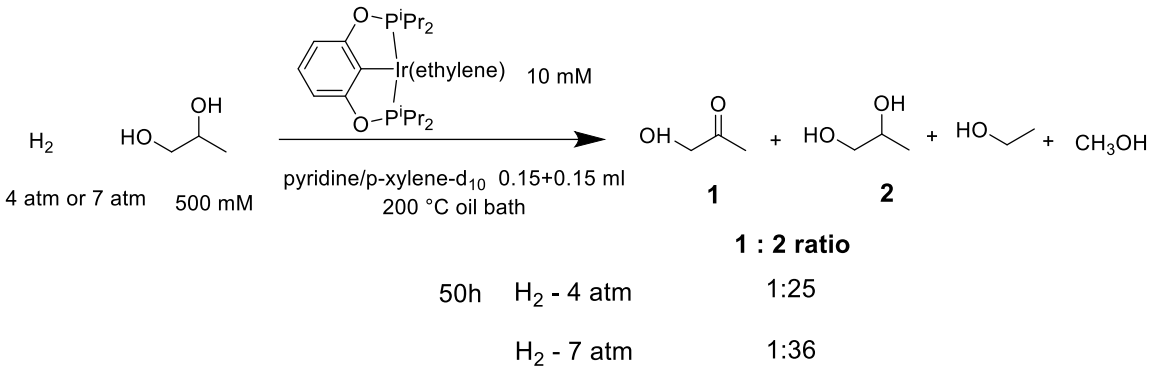

Interesting, only diols with 1,3- hydroxyl groups underwent dehydration (figure 6.3). Similar to 1,3-propanediol, 2-methyl-1,3-propanediol underwent deoxygenation to give isobutanol but with a slower rate. Interestingly, deoxygenation of 1,3-butanediol gave both 1-butanol and 2-butanol as products with slightly preference to 1-butanol. This indicates that there is no dominant selectivity difference for pincer-iridium complex catalyzed deoxygenation of primary versus secondary alcohols, which is different from our initial assumption.

Figure 6. 3. Diols with 1,3-hydroxyl group went through deoxygenation

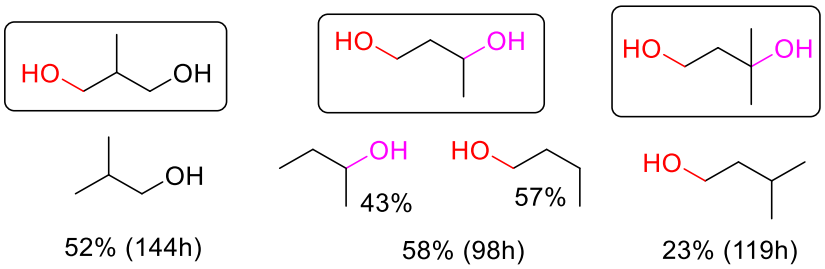

Reaction conducted with 500 mM substrates, and 10 mM (^{iPr}PCOP)Ir(ethylene) in 0.3 ml mixture solvent in high pressure NMR tube, the NMR tube was degas under vacuum and charged gases with 4 atm H_2 gas, then heated in 200°C oil bath and monitored by NMR. Yield calculated through product peaks in ^{1}H spectra by comparing residual solvent peak.

Not every substrate with 1,3-diols underwent deoxygenation. For example, 2,2-Dimethyl-1,3-propanediol and 2,2-Dimethyl-1,3-butanediol (figure 6.4), showed no activity for deoxygenation. We can rationalize this by considering the steric effect brought by these two 2 methyl groups at 2-position, which may prevent the hydroxyl group from being approached by the

iridium center. Also 2,5-pentanediol, with a relative similar internal hydroxyl group, only underwent retro-aldol reaction to break a C-C bond and give ethanol and isopropanol as the hydrogenated products.

Figure 6. 4. Diols with 1,3-hydroxygroup did not go through deoxygenation

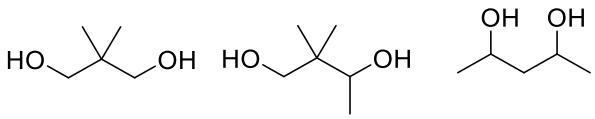

Substrates without 1,3-hydroxyl groups do not undergo deoxygenation (Figure 6.5). When 1-propanol, the product of partial deoxygenation of 1,3-propanediol, was used as substrate, the reactions observed were decarbonylation, dehydrogenation, dehydrogenative coupling with ethane and methanol. Propionaladehyde and propyl propionate were observed products. In addition to those reactions observed for 1-propanol, intramolecular dehydrogenative coupling was the dominant reaction when 1,4-butanediol was used as substrate. For 1,2-butanediol and 2,3-butanediol only decarbonylation and dehydrogenation were observed.

Figure 6. 5. Diols could not undergo deoxygenation

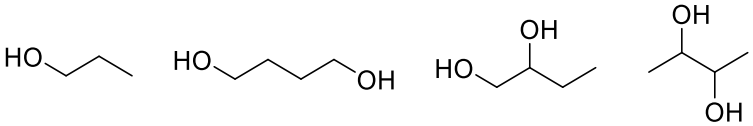

6.2.3. Partial deoxygenation of triols

The success of using 1,3-propanediol as substrate for deoxygenation motivated us to pursue glycerol partial deoxygenation. As discussed in the previous section, we observed a unique 1,3-hydroxyl groups selectivity, which enabled us selectively convert glycerol to 1,2-propanediol. The partial deoxygenation of glycerol selectively gave 1,2-propanediol and its dehydrogenated product hydroxyacetone as well as small amounts of ethylene glycol and methanol as side products (87% conversion and 56% yield for heating 200°C 144 h) (Figure 6.6). The reaction was fast with almost

zero-order for the first 36h and then slowed down, which may be due to the accumulation of CO and consequent reaction inhibition. Hydroxyacetone formed by alcohol dehydrogenation. The amount of methanol was also less than the amount of ethylene glycol formed, which is also attributed to the difference of decarbonylation versus CO hydrogenation: in other words, the amount of CO released. The amount of CO produced was not quantified and neither was the amount of starting materials polymerized under the experimental conditions. These are the sources of the mass imbalance, which corresponds to the significant difference between conversion and yield.

Figure 6. 6. Partial deoxygenation of glycerol

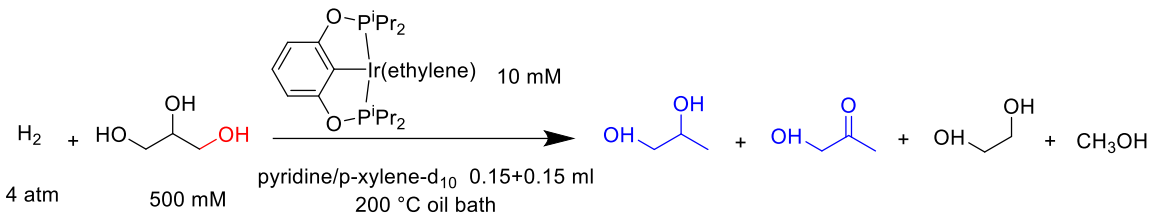

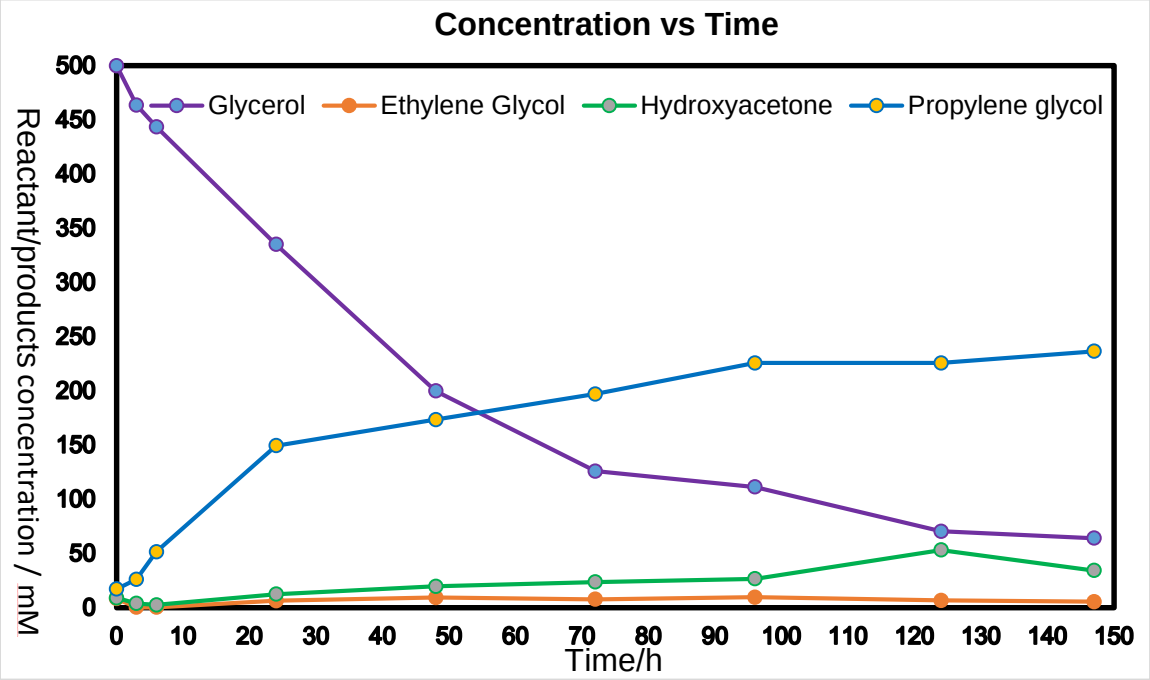

Reaction conducted with 500 mM substrates, and 10 mM (^{iPr}POCOP)Ir(ethylene) in 0.3 ml mixture solvent in high pressure NMR tube, the NMR tube was degas under vacuum and charged gases

with 4 atm H_2 gas, then heated in 200°C oil bath and monitored by NMR. Yield calculated through product peaks in ^1H spectra by comparing residual solvent peak.

The hydrogen gas pressure added to the reactor could also be a factor affecting the reaction. Unlike previously reported systems using pincer-iridium complexes for partial deoxygenation of glycerol which required high hydrogen pressure (40-80 bar)[12], increasing the hydrogen pressure from 4 atm to 7 atm *suppressed* the reaction rate (Table 6.2). Reducing the hydrogen gas pressure led to higher conversions conversion in shorter time, but the yield of desired products dropped greatly due to side reactions. The major side reaction was the production of aldehyde and ketone from the dehydrogenation of glycerol. This competitive reaction is inhibited by increasing the hydrogen pressure. Therefore 4 atm hydrogen gas was chosen as the optimal reaction parameter to balance the yield and reaction rate.

A difference in the ratio of catalyst species was observed by monitoring the reaction at room temperature using ^1H and ^{31}P NMR (Table 6.2, last column). A higher proportion of *trans*-$Ir(CO)(H)_2$ is observed at 7 atm than at 4 atm. As mentioned earlier, *trans*-$Ir(CO)(H)_2$ is slower to convert to 16e- Ir(CO) complex (and then the active $14e^-$ iridium complex) than the isomeric *cis*-$Ir(CO)(H)_2$. Thus, a greater proportion of the *trans* isomer versus the *cis* isomer in the catalyst resting state may explain the decrease in reaction rate at higher hydrogen pressure.

Table 6. 2. (^{iPr}POCOP)Ir catalyzed partial deoxygenation of glycerol with different hydrogen pressure

Reaction	H_2(atm)	Reaction time (h)	1,2-propanediol (mM)	hydroxyacetone (mM)	Ethylene glycol (mM)	methanol (mM)	Conversion	Ir-CO-trans-H_2 and Ir-CO-trans-H_2 ratio
1	4	3	34	6	6	3	22%	1:2.2
		6	51	6	7	3	30%	1:3.7
		24	153	14	13	8	48%	1:3.7
		93	225	35	15	8	89%	1:8.2
2	7	3	25	3	6	2	6%	1:1.5
		6	33	3	6	4	15%	1:1.5
		24	104	5	11	7	37%	1:1.5
		93	203	9	9	9	72%	1:2.5

Reaction conducted with 500 mM substrates, and 10 mM (^{iPr}POCOP)Ir(ethylene) in 0.3 ml mixture solvent in high pressure NMR tube, the NMR tube was degas under vacuum and charged gases with 4 atm H_2 gas, then heated in 200°C oil bath and monitored by NMR. Yield calculated through product peaks in ^{1}H spectra by comparing residual solvent peak.

The use of mixed solvents containing pyridine greatly enhances the solubility of the hydrophilic diols and triols. However, the basicity of pyridine raised a question of whether it was somehow involved in the catalytic process. To answer this question, we tested this reaction with non-basic mixed solvents (Table 6.3). The poor solubility of THF and 1,4-dioxane for glycerol required a large ratio of them in the mixed solvent system in comparison to pyridine. As changing the ratio of pyridine to *p*-xylene-d^{10} from 1:1 to 5:1 had only a slight effect on the reaction rate and yield, the ratio difference for THF and 1,4-dioxane should not be the source of any observed reactivity differences. With THF as solvent, comparable amounts of products formed but with different selectivity after 24 hours. Reaction in 1,4-dioxane produced less products in 24 hours. However, a greater yield is observed at 167 hours in 1,4-dioxane. These results suggest that pyridine is simply acting as a solvent.

Table 6. 3. Partial deoxygenation of glycerol in mixed solvents

Reaction	H_2(atm)	Solvent	Reaction time (h)	1,2-propanediol (mM)	hydroxyacetone (mM)	Ethylene glycol (mM)	methanol (mM)	Conversion
1	4	pyridine/*p*-xylene-d^{10} 0.15 ml + 0.15 ml	24	153	14	13	8	48%
			93	225	35	15	8	89%
2	4	1,4-dioxane-d^8 /*p*-xylene-d^{10} 0.2 ml + 0.1 ml	24	50	5	10	n/a	n/a
			167	285	42	63	n/a	n/a
3	4	THF-d^8/*p*-xylene-d^{10} 0.2 ml + 0.1 ml	24	84	29	31	n/a	n/a

Reaction conducted with 500 mM glycerol, and 10 mM (^{iPr}POCOP)Ir(ethylene) in 0.3 ml mixture solvent in high pressure NMR tube, the NMR tube was degas under vacuum and charged gases with 4 atm H_2 gas, then heated in 200°C oil bath and monitored the reaction by NMR. Methanol concentration and product conversion not given here due to the peak overlapping in NMR spectra. The stability of THF under reaction condition prohibited it running for long time experiment. Yield calculated through product peaks in ^{1}H spectra by comparing residual solvent peak.

The steric and electronic differences of different pincer iridium catalysts may affect their reactivity and selectivity. We compared three different pincer-iridium complexes, shown in figure 6.7, for partial deoxygenation of glycerol (Table 6.4). **Cat-1** showed the highest activity. The activity of **Cat-3** decreased significantly after 24h. Plotting the total products concentration reveals that **Cat-2** has the best selectivity and yield (Figure 6.8). However, there were no certain trends to show how the electronic and steric factors from the catalysts affected the reaction. Notably, **Cat-2** achieved 86% conversion and 80% yield under only 4 atm H_2 ranks it as one of the best catalysts for this reaction.

Figure 6. 7. Different catalysts used for partial deoxygenation of glycerol

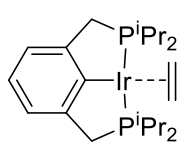

Cat-1

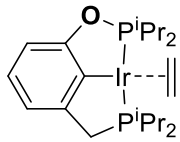

Cat-2

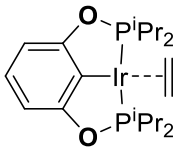

Cat-3

Table 6. 4. Partial deoxygenation of glycerol with different catalysts

Reaction	H_2(atm)	Catalyst	Reaction time (h)	1,2-propanediol (mM)	hydroxyacetone (mM)	Ethylene glycol (mM)	methanol (mM)	Conversion
1	4	**Cat-1**	3	52	4	7	6	13%
			6	98	7	16	10	25%
			24	192	21	33	22	63%
			72	322	31	42	29	93%
2	4	**Cat-2**	3	8	3	4	3	6%
			6	31	7	8	6	10%
			24	154	16	21	7	42%
			72	312	37	31	13	78%
			96	340	39	30	16	86%
3	4	**Cat-3**	3	26	4	6	3	22%
			6	52	6	7	3	30%
			24	149	12	13	8	48%
			72	197	24	13	8	75%
			96	226	27	15	8	86%

Figure 6. 8. Partial deoxygenation of glycerol with different catalysts

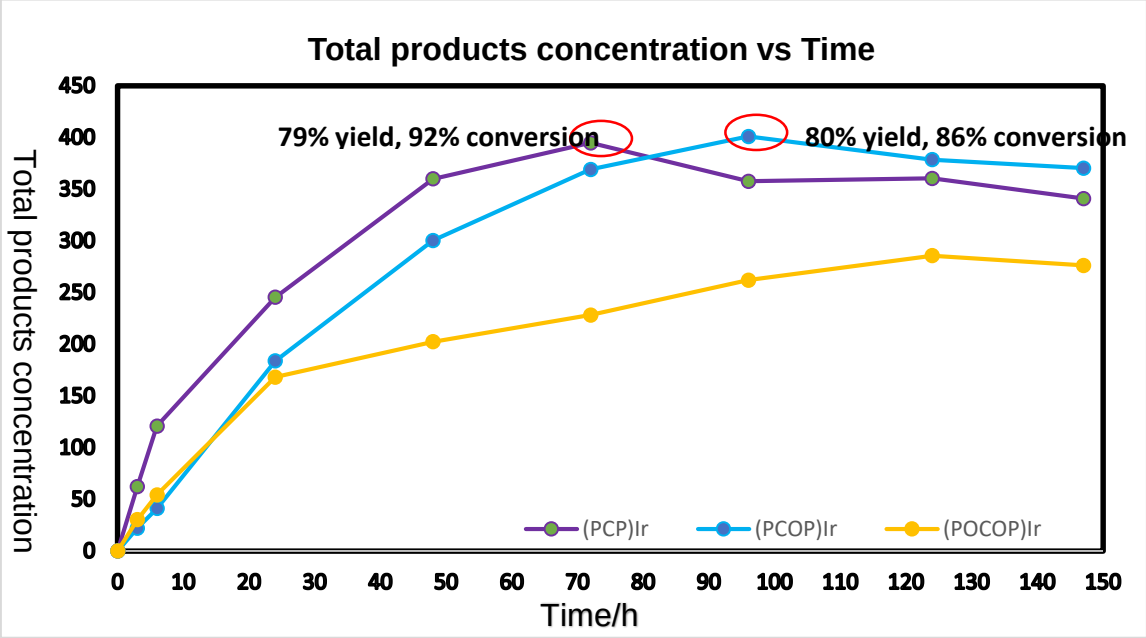

Reaction conducted with 500 mM glycerol, and 10 mM pincer-iridium complex in 0.3 ml mixture solvent with 1:1 ration pyridine and *p*-xylene-d^{10} in high pressure NMR tube, the NMR tube was degas under vacuum and charged gases with different pressure, then heated in 200°C oil bath and monitored the reaction by NMR. Yield calculated through product peaks in ^{1}H spectra by comparing residual solvent peak.

CO had a similar effect on glycerol partial deoxygenation as seen in earlier examples (Figure 6.9). Small amounts of CO could be easily generated by the reaction; so under an atmosphere of 1% CO in H_2, the reaction showed no rate change for the first 24 hours. However, large amount CO (4 atm) significantly depressed the reaction rate by inhibiting CO disassociation to generate active catalyst. As we discussed earlier, an extra 4 atm CO would help to suppress side reactions and increase the reaction temperature, thus affording a better yield.

Figure 6. 9. Partial deoxygenation of glycerol under varied CO partial pressure

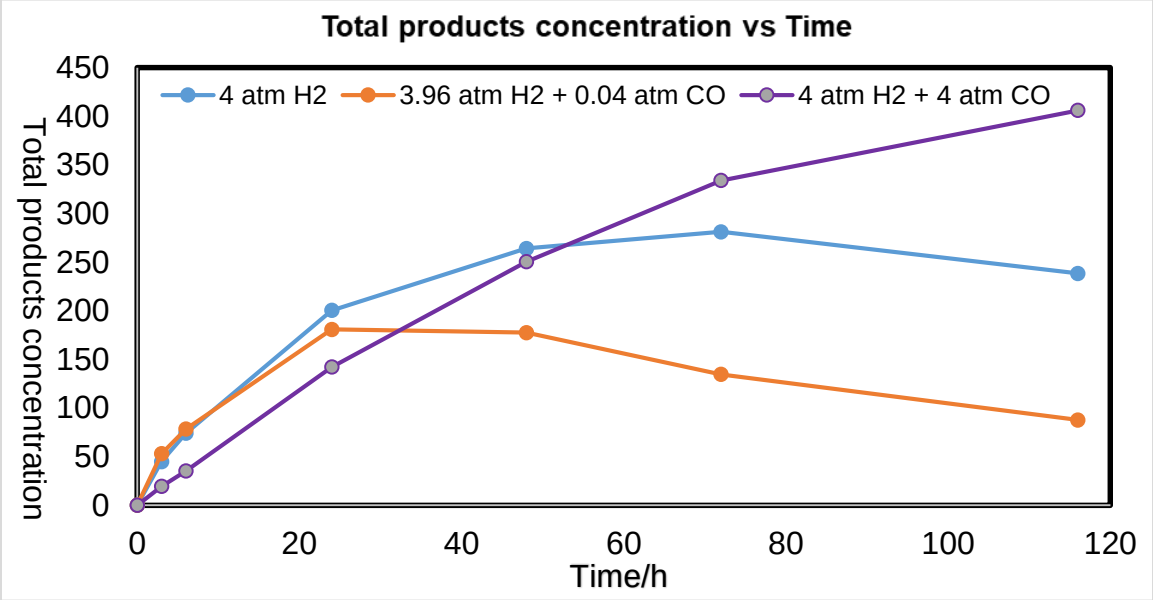

Reaction conducted with 500 mM glycerol, and 10 mM (^{iPr}PCOP)Ir(ethylene) in 0.3 ml mixture solvent with 1:1 ration pyridine and *p*-xylene-d^{10} in high pressure NMR tube, the NMR tube was degas under vacuum and charged different gas mixtures with different pressures. Then heated in 200°C oil bath and monitored the reaction by NMR. Yield calculated through product peaks in ^{1}H spectra by comparing residual solvent peak.

Other triols with 1,3-hydroxyl groups were also tested for partial deoxygenation, (figure 6.10). 1,2,4-butanetriol gave only 1,2-butanediol and 1,4-butanediol, consistent with 1,3-hydroxyl groups selectivity. 1,2,3-butanetriol showed the same selectivity pattern, deoxygenating at either the 1 or 3-hydroxyl group. Compared to butanediol as substrates, when butanetriol was used, the selectivity towards hydroxyl group on primary carbon over secondary carbon was present, which should originate from the interaction of the extra hydroxyl group with iridium complex.

Figure 6. 10. Triols could effect partial deoxygenation

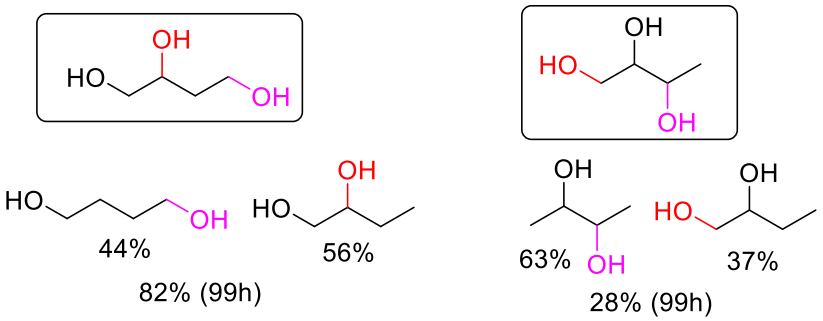

Reaction conducted with 500 mM substrates, and 10 mM (^{iPr}PCOP)Ir(ethylene) in 0.3 ml mixture solvent in high pressure NMR tube, the NMR tube was degas under vacuum and charged gases with 4 atm H_2 gas, then heated in 200°C oil bath and monitored the reaction by NMR. Yield calculated through product peaks in ^{1}H spectra by comparing residual solvent peak.

6.2.4. Demethoxylation of 3-methoxy-1-propanol

Under the reaction conditions described thus far, (^{iPr}NCOP)Ir(C_2H_4) is capable of reducing methoxy groups to saturated aliphatic groups. When 3-methoxy-1-propanol was used as substrate, we observed the replacement of methoxy group by hydrogen atom (Scheme 6.8). Deoxygenation of the hydroxyl group was not observed. Notably, propyl methyl ether did not undergo demethoxylation, highlighting the importance of a hydroxyl group being present in the substrate. We believe the 3-hydroxyl group acts as mediate for this type reaction.

Scheme 6. 8. Catalytic hydrogenation of ether

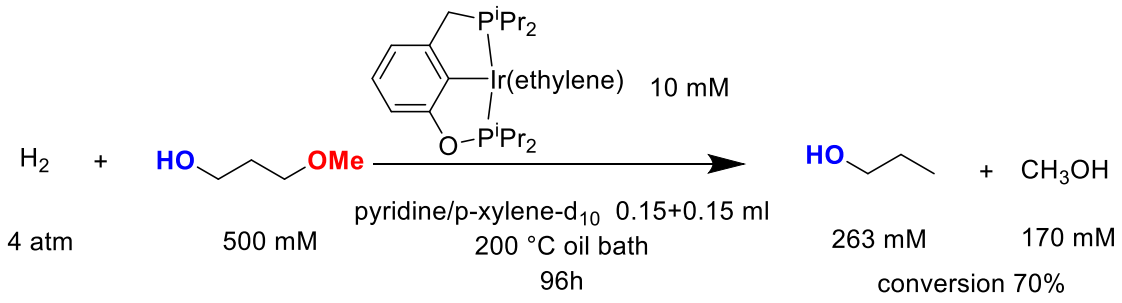

6.2.5. Mechanism studies

To gain insight into the reaction mechanism, we compared the effects of substrate electronics and structure on reaction outcome. Compared to 1,3-propanediol, 2-methyl-1,3-propanediol and glycerol introduces an electronic donating group and an electronic withdrawing group respectively, which could make the carbon skeletal electron rich or poor. In scheme 6.9, we could see a trend for the reaction favored electronic poor with fastest rate for glycerol. To clearly study the trend, two reactions of mixed substrates was conducted in figure 6.11 and 6.12. The clearly faster rate for glycerol and slower rate of 2-methyl-1,3-propanediol compared to 1,3-propanediol further supported the idea of this reaction favored electronic poor carbon skeletal. The more electronic poor carbon skeletal, the C-O bond being more polarized, which would be favored for cleaving.

Scheme 6. 9. Electronic effects of substrates

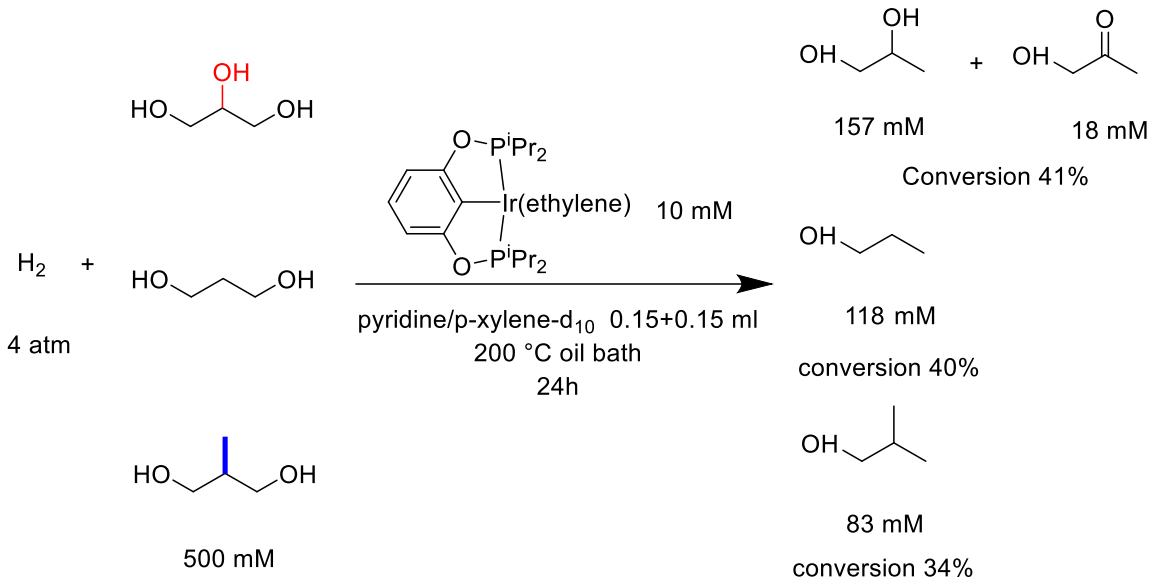

Figure 6. 11. Comparing glycerol and 1,3-propanediol as substrate

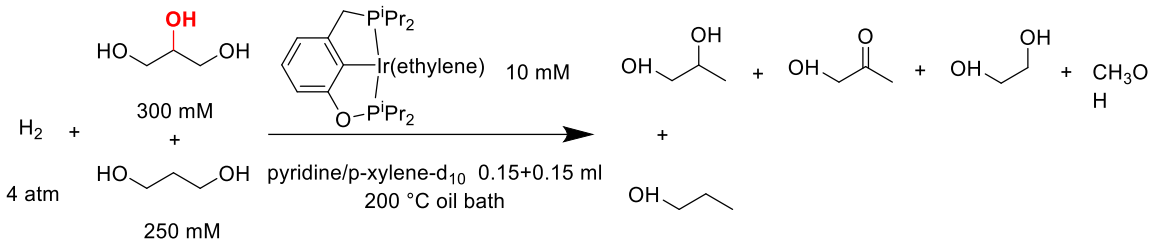

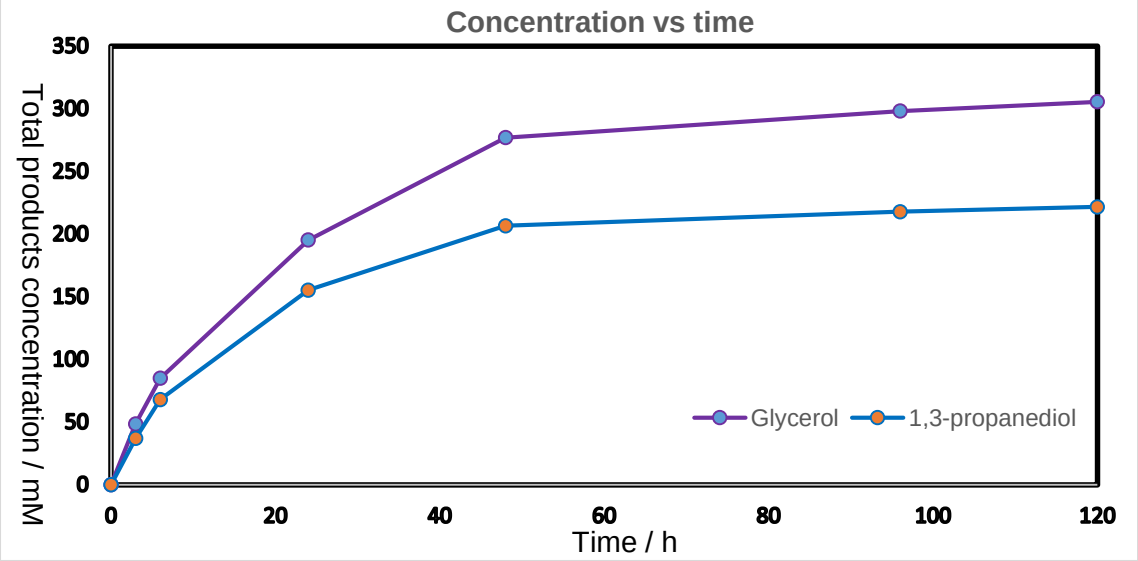

Figure 6. 12. Comparing 2-methyl-1,3-propanediol and 1,3-propanediol as substrate

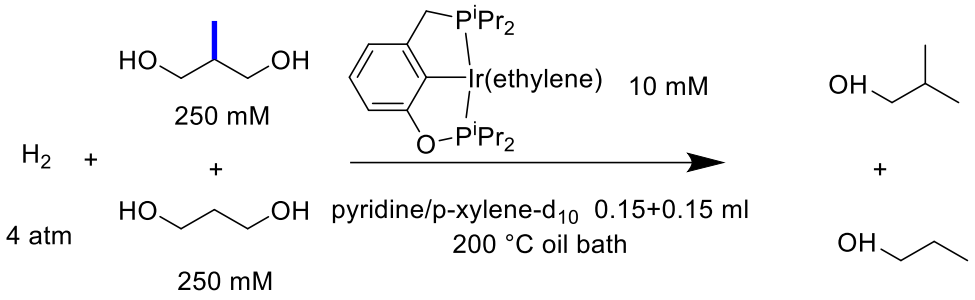

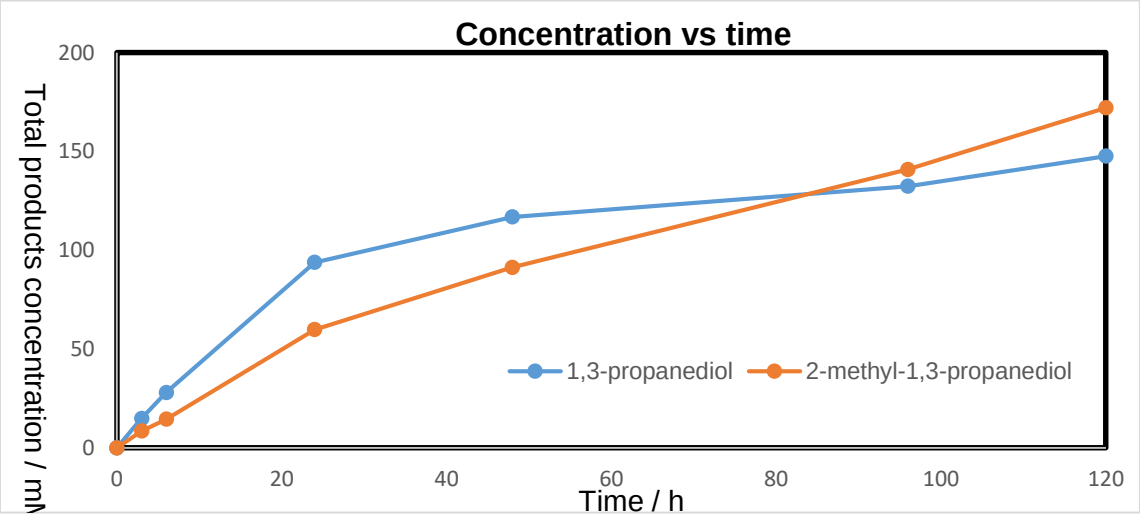

Considering the requirement of 1,3-hydroxyl groups for reactants, reactivity differences for different substrates, and product selectivity, we could provide two mechanisms involving an active 14 e^- iridium (I) complex (using 1,3-propanediol as substrate, side reaction has already discussed in previous section), showed in Figure 6.11. Mechanisms involving Ir-CO were ruled out by the reaction depression from CO. Both mechanisms begin with O-H activation. In route 1, a synergetic key step involving the nucleophilic hydride attacking the electronic poor carbon and hydroxyl transferring to iridium center is proposed, which is believed to be rate determining. The route was perfect agree with the electronic effect from the substrates, since electron withdrawing group making the carbon easier go through nucleophilic attacking. The formed complex from this step should easily go through hydrogenation to give 1-propanol, and further reductive elimination

gave both 14e$^-$ iridium specie and water. In route 2, the first O-H bond addition would mediate the C-O bond cleavage to give a Ir(V) intermediate. Although we have proposed a pseudo Ir(V)intermediate for the dehydrogenative coupling, which was based on the quick hydride transfer would get iridium quickly reduced back to Ir(III), the oxidative addition of C-O bond to Ir(III) intermediate to give Ir(V) was very unfavorable since the following reductive elimination did not seems to provide a strong driving force. In all, we preferred route 1 as the reaction mechanism for this special selective deoxygenation reaction.

Figure 6. 13. Proposed reaction mechanism for deoxygenation

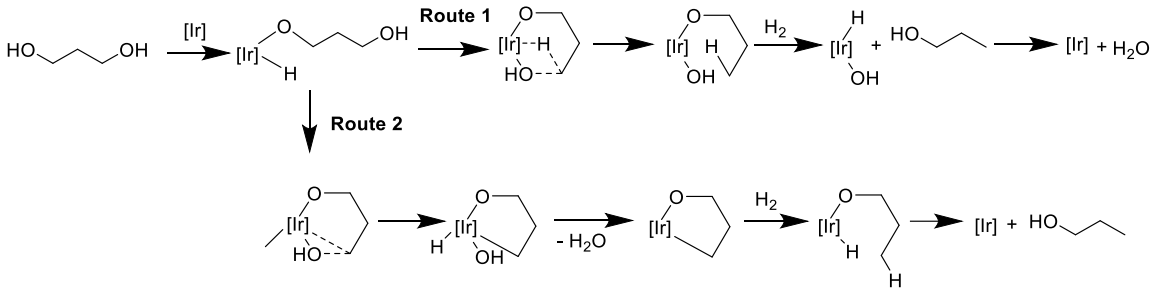

6.3. Conclusion

The discovery of dehydration by pincer-iridium complex led us to discover partial deoxygenation reaction of diols and triols, which may be a useful strategy for transforming biomass to value-added chemicals. Using pincer-iridium complexes as catalysts under modest pressures of hydrogen gas, we could transform diols and triols with 1,3-hydroxyl groups to the respective mono alcohols and diols with high conversion and yield. Notably, glycerol, the biodiesel fuel byproduct could be selectively transformed to valuable 1,2-propanediol (important polymer precursor) and its dehydrogenated product hydroxyacetone with up to 76% yield. Side products (about 10-30%)—ethylene glycol and methanol—created by decarbonylation and hydrogenation, are also useful chemicals. Based on the requirement of 1,3-hydroxyl groups for reactant, reactivity difference of different substrates, and product selectivity, we proposed a key intermediate

generated by a synergetic key step involving nucleophilic hydride attacking the alpha carbon and hydroxyl transferring to the iridium center.

6.4. Experimental information

6.4.1. General experimental information

We conducted all our experiment either under argon filled glovebox or schlenk line. NMR experiment were conducted on 400-MHZ Varian VNMRS. ^{1}H and ^{13}C NMR spectra were referenced to residual deuterated solvent signal. residual deuterated solvent signal. ^{31}P NMR spectra was referenced with PMe_3 in capillary tube. All anhydrous solvents were purchased from Aldrich, flushed with argon, and stored in an argon atmosphere in a glovebox. All deuterium solvents were degassed, dried over activated alumina, and storage over 3-Å molecular sieves. All alcohols were brought into glovebox after degassed under vacuum. All reactant gases were bought from Airgas with ultra-high purity. GC analysis was conducted using a Varian 430 GC with a 30-m capillary column, using helium carrier gas. GCMS analysis was conducted using a Varian 3900 GC with a 30-m capillary column coupled with a Saturn 2100T MS, using helium carrier gas. All pincer-iridium catalysts, (^{iPr}PCP)Ir(C_2H_4),[34] (^{iPr}PCOP)Ir(C_2H_4),[35] and (^{iPr}POCOP)Ir(C_2H_4)[36-37] were synthesized according reported methods.

General Procedure for partial deoxygenation of diols and triols: to a high pressure NMR tube (5 mm Medium Wall Precision Quick Pressure Valve NMR Sample Tube 7" L from Wilmad-Labglass) 500 mM glycerol, and 10 mM pincer-iridium complex in 0.3 ml mixture solvent with 1:1 ration pyridine and p-xylene-d10 were added. The NMR tube was degas under vacuum and charged with 4 atm H_2 gas. Then merge the most the glass part of the NMR tube in oil bath and heated at 200°C. The reaction was monitored by NMR, and final mixtures were also monitored by GC. Products were identified by compared to authentic sample in NMR spectra and GC run track.

Further identification was using GCMS. All yield calculated through reactant peaks and products peaks in ^{1}H spectra by comparing residual solvent peak (or internal standard 1,4-dimethoxybenzene and 4-Dimethylaminotoluene).

6.5. Reference

1. Tran, N.; Uemura, Y.; Chowdhury, S.; Ramli, A., *A Review of Bio-Oil Upgrading by Catalytic Hydrodeoxygenation*. 2014; Vol. 625, p 255-258.
2. Kay Lup, A. N.; Abnisa, F.; Wan Daud, W. M. A.; Aroua, M. K., A review on reactivity and stability of heterogeneous metal catalysts for deoxygenation of bio-oil model compounds. *Journal of Industrial and Engineering Chemistry* **2017,** *56*, 1-34.
3. Rogers, K. A.; Zheng, Y., Selective Deoxygenation of Biomass-Derived Bio-oils within Hydrogen-Modest Environments: A Review and New Insights. *ChemSusChem* **2016,** *9* (14), 1750-1772.
4. Kay Lup, A. N.; Abnisa, F.; Daud, W. M. A. W.; Aroua, M. K., A review on reaction mechanisms of metal-catalyzed deoxygenation process in bio-oil model compounds. *Applied Catalysis A: General* **2017,** *541*, 87-106.
5. Hermida, L.; Abdullah, A. Z.; Mohamed, A. R., Deoxygenation of fatty acid to produce diesel-like hydrocarbons: A review of process conditions, reaction kinetics and mechanism. *Renewable and Sustainable Energy Reviews* **2015,** *42*, 1223-1233.
6. Krishna, S. H.; Huang, K.; Barnett, K. J.; He, J.; Maravelias, C. T.; Dumesic, J. A.; Huber, G. W.; De bruyn, M.; Weckhuysen, B. M., Oxygenated commodity chemicals from chemo-catalytic conversion of biomass derived heterocycles. *AIChE Journal* **2018,** *64* (6), 1910-1922.
7. Pagliaro, M.; Ciriminna, R.; Kimura, H.; Rossi, M.; Della Pina, C., From Glycerol to Value-Added Products. *Angewandte Chemie International Edition* **2007,** *46* (24), 4434-4440.
8. Yang, F.; Hanna, M. A.; Sun, R., Value-added uses for crude glycerol--a byproduct of biodiesel production. *Biotechnology for Biofuels* **2012,** *5* (1), 13.
9. Foley, N. A.; Lee, J. P.; Ke, Z.; Gunnoe, T. B.; Cundari, T. R., Ru(II) Catalysts Supported by Hydridotris(pyrazolyl)borate for the Hydroarylation of Olefins: Reaction Scope, Mechanistic Studies, and Guides for the Development of Improved Catalysts. *Accounts of Chemical Research* **2009,** *42* (5), 585-597.
10. Schlaf, M.; Ghosh, P.; Fagan, P. J.; Hauptman, E.; Bullock, R. M., Catalytic Deoxygenation of 1,2-Propanediol to Give n-Propanol. *Advanced Synthesis & Catalysis* **2009,** *351* (5), 789-800.
11. Ahmed Foskey, T. J.; Heinekey, D. M.; Goldberg, K. I., Partial Deoxygenation of 1,2-Propanediol Catalyzed by Iridium Pincer Complexes. *ACS Catalysis* **2012,** *2* (6), 1285-1289.
12. Lao, D. B.; Owens, A. C. E.; Heinekey, D. M.; Goldberg, K. I., Partial Deoxygenation of Glycerol Catalyzed by Iridium Pincer Complexes. *ACS Catalysis* **2013,** *3* (10), 2391-2396.
13. Braca, G.; Raspolli Galletti, A. M.; Sbrana, G., Anionic ruthenium iodorcarbonyl complexes as selective dehydroxylation catalysts in aqueous solution. *Journal of Organometallic Chemistry* **1991,** *417* (1), 41-49.
14. Thibault, M. E.; DiMondo, D. V.; Jennings, M.; Abdelnur, P. V.; Eberlin, M. N.; Schlaf, M., Cyclopentadienyl and pentamethylcyclopentadienyl ruthenium complexes as catalysts for the total deoxygenation of 1,2-hexanediol and glycerol. *Green Chemistry* **2011,** *13* (2), 357-366.
15. Choi, J.; Choliy, Y.; Zhang, X. W.; Emge, T. J.; Krogh-Jespersen, K.; Goldman, A. S., Cleavage of sp(3) C-O Bonds via Oxidative Addition of C-H Bonds. *Journal of the American Chemical Society* **2009,** *131* (43), 15627-+.
16. Kundu, S.; Choi, J.; Wang, D. Y.; Choliy, Y.; Emge, T. J.; Krogh-Jespersen, K.; Goldman, A. S., Cleavage of Ether, Ester, and Tosylate C(sp(3))-O Bonds by an Iridium Complex, Initiated

by Oxidative Addition of C-H Bonds. Experimental and Computational Studies. *Journal of the American Chemical Society* **2013,** *135* (13), 5127-5143.
17. Haibach, M. C.; Lease, N.; Goldman, A. S., Catalytic Cleavage of Ether C-O Bonds by Pincer Iridium Complexes. *Angew Chem Int Edit* **2014,** *53* (38), 10160-10163.
18. Edouard, G. A.; Kelley, P.; Herbert, D. E.; Agapie, T., Aryl Ether Cleavage by Group 9 and 10 Transition Metals: Stoichiometric Studies of Selectivity and Mechanism. *Organometallics* **2015,** *34* (21), 5254-5277.
19. Romero, P. E.; Whited, M. T.; Grubbs, R. H., Multiple C−H Activations of Methyl tert-Butyl Ether at Pincer Iridium Complexes: Synthesis and Thermolysis of Ir(I) Fischer Carbenes1. *Organometallics* **2008,** *27* (14), 3422-3429.
20. Wang, W.-H.; Himeda, Y.; Muckerman, J. T.; Manbeck, G. F.; Fujita, E., CO2 Hydrogenation to Formate and Methanol as an Alternative to Photo- and Electrochemical CO2 Reduction. *Chemical Reviews* **2015,** *115* (23), 12936-12973.
21. Sordakis, K.; Tang, C.; Vogt, L. K.; Junge, H.; Dyson, P. J.; Beller, M.; Laurenczy, G., Homogeneous Catalysis for Sustainable Hydrogen Storage in Formic Acid and Alcohols. *Chemical Reviews* **2018,** *118* (2), 372-433.
22. Choi, J.; MacArthur, A. H.; Brookhart, M.; Goldman, A. S., Dehydrogenation and related reactions catalyzed by iridium pincer complexes. *Chemical reviews* **2011,** *111* (3), 1761-79.
23. Isomura, M.; Petrone, D. A.; Carreira, E. M., Coordination-Induced Stereocontrol over Carbocations: Asymmetric Reductive Deoxygenation of Racemic Tertiary Alcohols. *Journal of the American Chemical Society* **2019,** *141* (11), 4738-4748.
24. Yang, S.; Tang, W.; Yang, Z.; Xu, J., Iridium-Catalyzed Highly Efficient and Site-Selective Deoxygenation of Alcohols. *ACS Catalysis* **2018,** *8* (10), 9320-9326.
25. Bauer, J. O.; Chakraborty, S.; Milstein, D., Manganese-Catalyzed Direct Deoxygenation of Primary Alcohols. *ACS Catalysis* **2017,** *7* (7), 4462-4466.
26. Huang, J.-L.; Dai, X.-J.; Li, C.-J., Iridium-Catalyzed Direct Dehydroxylation of Alcohols. *European Journal of Organic Chemistry* **2013,** *2013* (29), 6496-6500.
27. Dai, X.-J.; Li, C.-J., En Route to a Practical Primary Alcohol Deoxygenation. *Journal of the American Chemical Society* **2016,** *138* (16), 5433-5440.
28. Kloek, S. M.; Heinekey, D. M.; Goldberg, K. I., Stereoselective Decarbonylation of Methanol to Form a Stable Iridium(III) trans-Dihydride Complex. *Organometallics* **2006,** *25* (12), 3007-3011.
29. Melnick, J. G.; Radosevich, A. T.; Villagrán, D.; Nocera, D. G., Decarbonylation of ethanol to methane, carbon monoxide and hydrogen by a [PNP]Ir complex. *Chemical Communications* **2010,** *46* (1), 79-81.
30. Goldberg, J. M.; Goldberg, K. I.; Heinekey, D. M.; Burgess, S. A.; Lao, D. B.; Linehan, J. C., Detection of an Iridium–Dihydrogen Complex: A Proposed Intermediate in Ionic Hydrogenation. *Journal of the American Chemical Society* **2017,** *139* (36), 12638-12646.
31. Hackenberg, J. D.; Kundu, S.; Emge, T. J.; Krogh-Jespersen, K.; Goldman, A. S., Acid-Catalyzed Oxidative Addition of a C-H Bond to a Square Planar d(8) Iridium Complex. *Journal of the American Chemical Society* **2014,** *136* (25), 8891-8894.
32. C-H activation involving three- and four-coordinate iridium(I) pincer complexes. **2014**.
33. Goldberg, J. M.; Cherry, S. D. T.; Guard, L. M.; Kaminsky, W.; Goldberg, K. I.; Heinekey, D. M., Hydrogen Addition to (pincer)IrI(CO) Complexes: The Importance of Steric and Electronic Factors. *Organometallics* **2016,** *35* (20), 3546-3556.

34. Liu, F.; S. Goldman, A., Efficient thermochemical alkane dehydrogenation and isomerization catalyzed by an iridium pincer complex. *Chemical Communications* **1999,** (7), 655-656.
35. Ahuja, R.; Punji, B.; Findlater, M.; Supplee, C.; Schinski, W.; Brookhart, M.; Goldman, A. S., Catalytic dehydroaromatization of n-alkanes by pincer-ligated iridium complexes. *Nat Chem* **2011,** *3* (2), 167-171.
36. Morales-Morales, D.; Grause, C.; Kasaoka, K.; Redón, R. o.; Cramer, R. E.; Jensen, C. M., Highly efficient and regioselective production of trisubstituted alkenes through heck couplings catalyzed by a palladium phosphinito PCP pincer complex. *Inorganica Chimica Acta* **2000,** *300–302*, 958-963.
37. Mucha, N. T.; Waterman, R., Iridium Pincer Catalysts for Silane Dehydrocoupling: Ligand Effects on Selectivity and Activity. *Organometallics* **2015,** *34* (15), 3865-3872.

Chapter 7. Synthesis and reactivity of a new pincer-ligated iridium complex for C-C bond formation and C-O bond cleavage

Abstract: To obtain better reactivity toward C-C bond formation and C-O cleavage catalysis, we designed a sterically open catalyst with a possibly hemi-labile amine arm, (^{iPr}NCOP)Ir. This complex catalyzed styrene homo-coupling at lower temperatures; however, catalyst decomposition under experimental conditions limited TON. An efficient non-dehydrogenative coupling of methyl acrylate to form dimethyl (*E*)-hex-2-enedioate through hydroalkenylation was observed with this catalyst. Interestingly, (^{iPr}NCOP)Ir catalyzes C-O cleavage of vinyl acetate under H_2 atmosphere to give acetic acid and ethylene, which was a direct hydrogenation of unsaturated ester to olefin and acid. Other vinylic ester substrates also worked for this reaction. A carbonyl group mediated vinylic carbon insertion mechanism was proposed for this reaction.

7.1. Introduction

Although pincer-iridium complexes were first created in 1976 by Moulton and Shaw[1], it was not until 1996, when Jensen and Kaska used it for homogenous transfer dehydrogenation[2], that people realized the great potential of this complex for organic compound transformation. Further study by Goldman and other group showed that pincer-iridium complexes could be used for multiple purposes.[3-4] In addition to transfer dehydrogenation, the more economic efficient and desired acceptorless dehydrogenation was discovered.[5] Amine-Boranes,[6] alcohols,[7-8] amines,[9] ethers,[10] amongst others, were also introduced as substrates for dehydrogenation reaction catalyzed by pincer-iridium complexes. Reactions based on pincer-iridium complexes catalyzed dehydrogenation, dehydroaromatization, and could convert linear alkanes to alkylbenzenes.[11] Tandem reactions where dehydrogenation by pincer-iridium complexes was followed by another type of reaction were also explored. For example, tandem olefin metathesis reactions could convert low carbon number hydrocarbons to higher number hydrocarbons.[12-14] Tandem zeolite catalyzed alkylation could covert alkylbenzene to valuable methyl naphthalene (discussed in chapter 2).[15] Beyond the original application of dehydrogenation, this new growing family shows a strong ability to activate different type of bonds, such as X-H (X = C, N, O) bonds[16-18] and C-Y (Y = C, N, O, F) bonds[19-23]. The Goldman group has recently reported iridium-catalyzed olefin hydroaryloxylation[24] cleavage of simple aryl alkyl ethers[25] and dehydrogenative coupling of vinyl arenes [26] and ethylene[27] emphasized the potential of using pincer-iridium as catalysts in C-O bond formation and cleavage reaction.

Recently, pincer-ligated iridium complexes have grown rapidly to include a family of derivatives, as shown in figure 7.1. As we can see in figure 7.1, variables were introduced at aryl backbone,[28-35] linker Y_1 and Y_2,[36-43] ligating atoms (E_1 and E_2),[44-50] and alkyl group on ligating

atoms.[51-53] The introduction of the Anthraphos backbone and adamantyl groups on ligating atoms improved the thermal stability of pincer-iridium complexes. The replacement of CH_2 arm to O or S atom and bulkier alkyl groups on ligating atoms to small alkyl group could reduce the steric crowdedness the of iridium center. Using sp^2 N as ligating atom could possibly make the pincer-iridium complex air and moisture stable. Compared to its mother (PCP)Ir and (POCOP)Ir, "hybrid" phosphine−phosphinite pincer ligands (PCOP) showed unique properties in terms of reactivity and selectivity.

Figure 7. 1. Various pincer-ligated iridium complexes

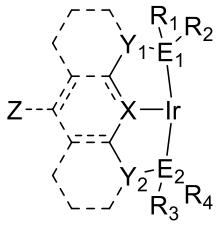

Most common elements
E_1, E_2: P, N, S, O, As
X: C, N, B
Y_1, Y_2: CH_2, O, NH
R_1, R_2, R_3, R_4: *i*-Pr, *t*-Bu, Me, CF_3, Ad
Z: CH_3O, $(CH_3)_2N$, CO_2Me, C_6F_5

Driven by discovering better catalysis for C-C bond formation and C-O bond cleavage, we tried to design a new catalyst based on our knowledge of structure and property relation of pincer-iridium complexes. The success of introducing "hybrid" ligand inspired us to develop the new catalyst with two different ligating atom. Although there were success examples of using P and N as the ligating atom, only sp^2 N atom was used for pincer-iridium complexes. In the meantime, pincer-palladium complex with "hybrid" ligand containing sp^3 N and P ligating atoms had been reported by the Punji group[54]. In a conference report by former group member Dr. Jaime A. Flores, (^{iPr}NCOP^{tBu})Ir was synthesized with a possibly hemi-labile amine arm.[55] As discussed in previous chapters, the less sterically hindered catalysts usually lead to better catalysis. So we attempted to synthesize (^{iPr}NCOP)Ir, the less steric hindered analog. The weaker coordination ability of sp^3 N allowed for a possibly hemi-labile amine arm, which could disassociate and associate with the

iridium center. The extra vacant site created by the amine arm could be of great interest in terms of reactivity or new typed reaction.

Figure 7. 2. Design of new catalyst with a possible hemi-labile amine arm

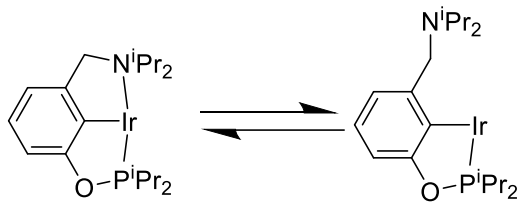

7.2. Results and discussion

7.2.1. Catalyst synthesis

Figure 7. 3. Synthetic route for ^{iPr}NCOPH ligand

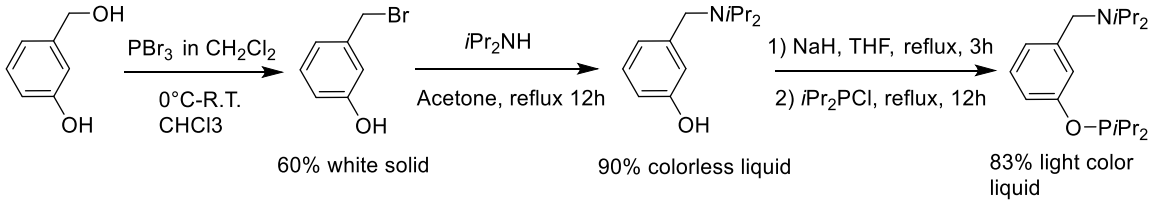

The ligand synthesis followed the same procedure reported by the Punji group, showed in figure 7.3. The first metalation reaction was carried out in a similar fashion to the synthesis of (^{iPr}POCOP)Ir(HCl) complex. Refluxing 1 eq ligand and 0.45 eq $[Ir(COE)_2Cl]_2$ in toluene resulted in a lot of different products, which could not be identified and isolated. The second trial, we used metalation condition similar to (^{iPr}PCOP)Ir(HCl) by heating 1 eq ligand and 0.45 eq $[Ir(COD)Cl]_2$ in toluene at 110°C. After 2 h heating, we could observe a doublet at δ143.18 (J = 20.7 Hz) together with three other doublets and starting materials (major species) on ^{31}P NMR, showed in Figure 7.5. Introducing hydrogen gas greatly promoted the reaction, after heating with H_2 for another 2 h, the doublet at δ 147.59 (over 80%) with three small singlets were the only remaining peaks in ^{31}P NMR. Further heating did not make any change for reaction result. Later experiments showed that even better metalation could be performed with mixing ligand and iridium precursor in toluene

heating at 80°C for 2 h under H_2 atmosphere. (^{iPr}PNOP)Ir(HCl) was obtained by removing solvent under vacuum and extracting the residue with pentane. Although it showed to be very pure in ^{31}P spectra, the ^{1}H was not ideal. However, treat this complex with base (KO*t*Bu) under ethylene atmosphere would give a single pure complex [(^{iPr}NCOP)Ir(ethylene)], which confirmed by both ^{1}H and ^{31}P NMR spectra (figure 7.13 and figure 7.14). This new complex was further confirmed by single crystal structure, showed in (figure 7.4). The weaker coordination of N was clearly presented by comparing the bond lengths of Ir-N (2.275 Å) and Ir-P (2.150 Å).

Scheme 7. 1. Metalation of ^{iPr}NCOPH ligand

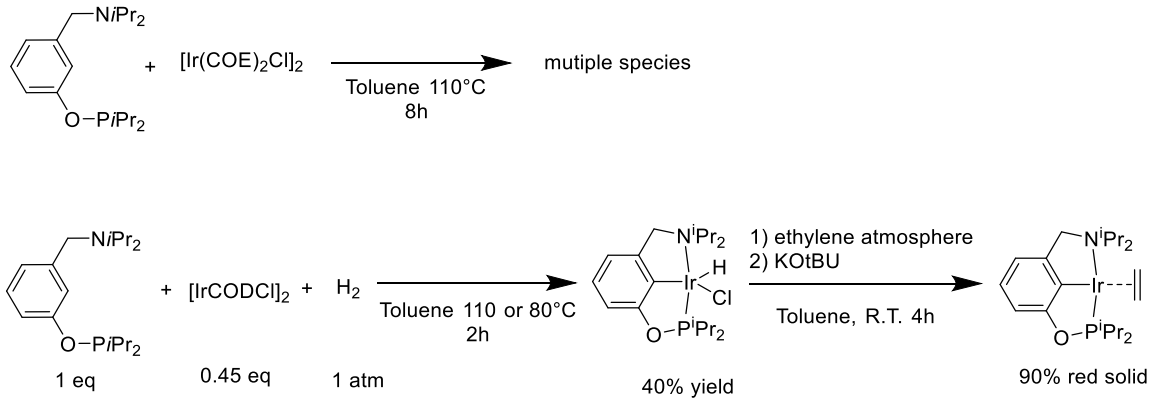

Figure 7. 4. ORTEP diagram of (^{iPr}NCOP)Ir(ethylene)

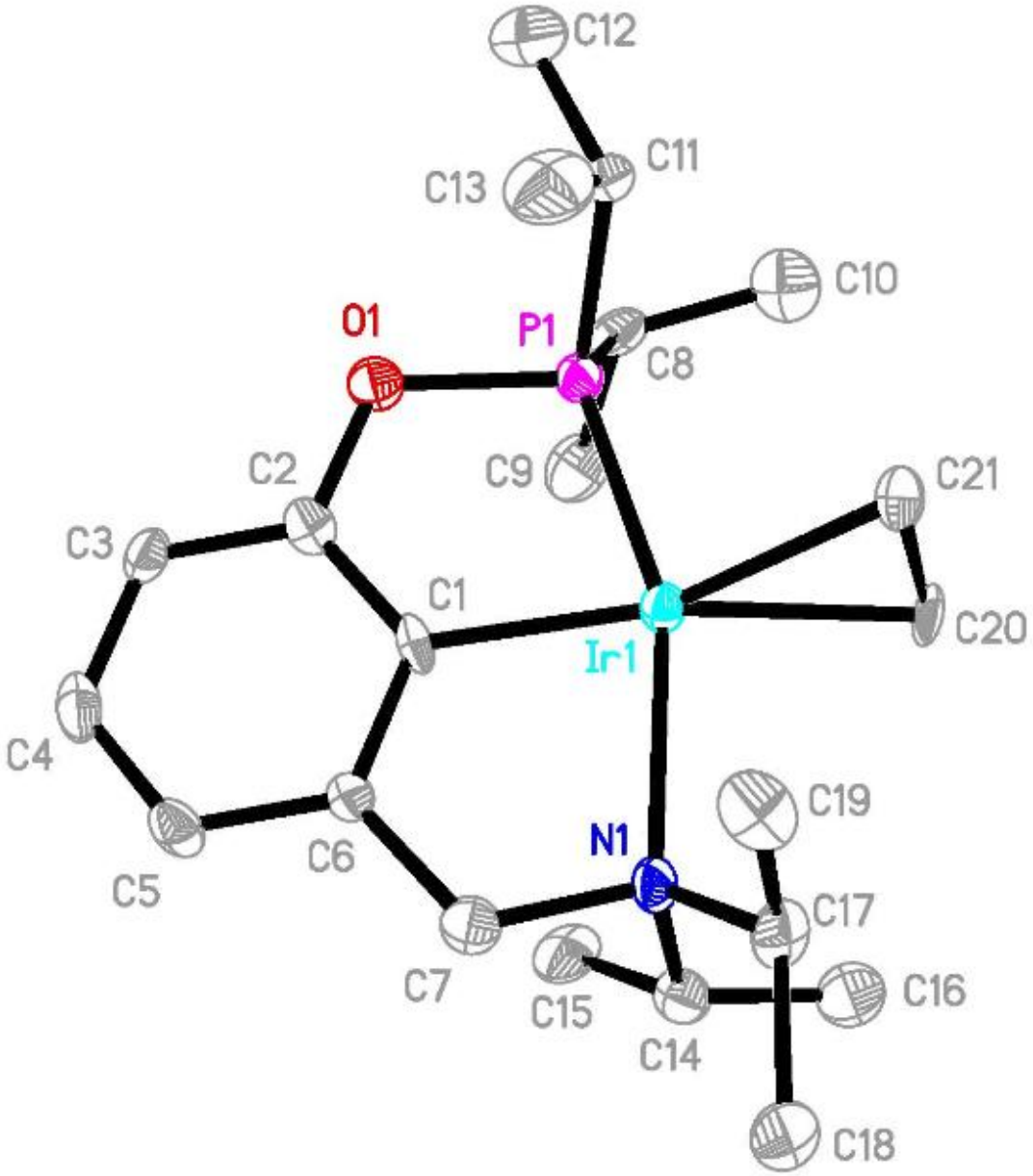

Figure 7. 5. ^{31}P NMR of ^{iPr}NCOPH ligand metalation

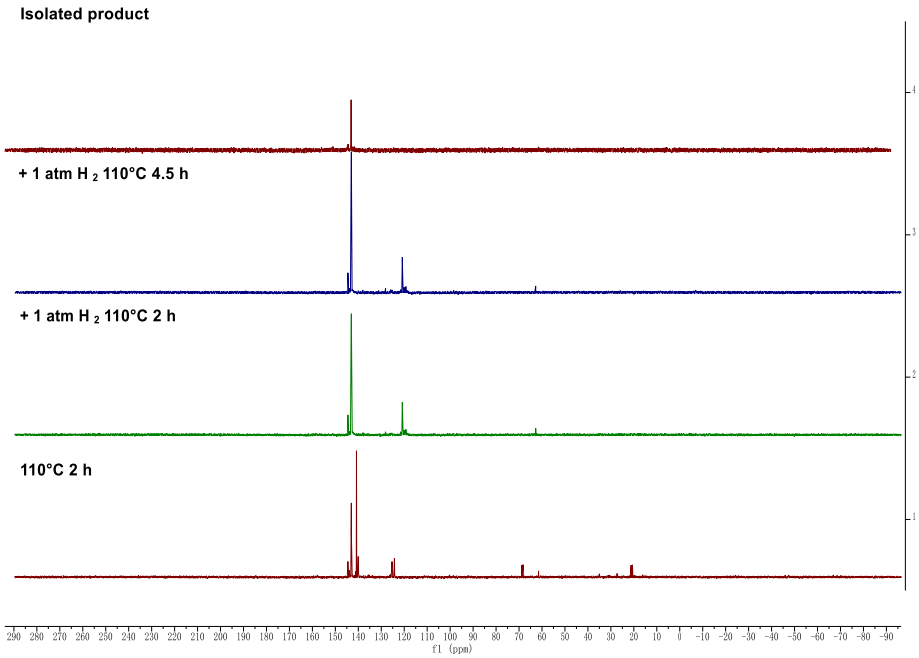

7.2.2. Using (^{iPr}NCOP)Ir(ethylene) for C-C bond formation

When (^{iPr}NCOP)Ir(ethylene) was used as catalyst for styrene homo-coupling reaction, product diphenylbutadiene was observed at 100°C, which was much lower compared to 150°C for (^{iPr}PCP)Ir. However, increasing temperature or heating for longer time did not quite increase the yield, while the ^{31}P signal of the catalyst quickly decreased, which indicated the catalyst decomposition happened. Despite the poor thermal stability of this new complex in styrene homo-coupling reaction, the lowered reaction barrier by this complex indicated better reactivity at the iridium center.

Scheme 7. 2. Homo-coupling of styrene by (^{iPr}NCOP)Ir(ethylene)

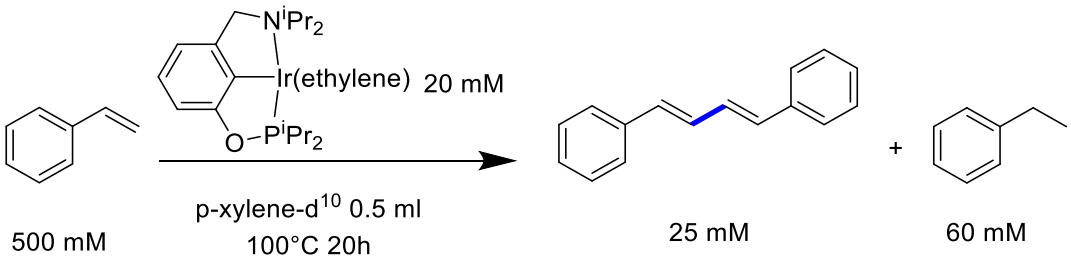

The possible hemi-labile amine arm of this complex could create an extra vacant site on iridium center by disassociating from metal center. The catalytic tail to tail dimerization reaction of methyl acrylate reaction reported by Brookhart group[56] inspired us to use the special property of this new complex. We designed a catalytic cycle, showed in figure 7.6, based on the mechanism proposed by Brookhart in his work. Unlike the dehydrogenative route, this route does not involve any dehydrogenation step, instead, it would go through hydroalkenylation route. Under similar experiment condition as the homo-coupling styrene by pincer-iridium complex, we could successfully couple two methyl acrylate molecules, showed in scheme 7.3. The low stability of methyl acrylate under 150°C and H_2 from the glovebox resulted the low yield of this reaction. Although the result was very poor compared to Brookhart's report with thousands TON under low temperature (25°C and 60°C), this was still one the rare example using pincer-iridium complex for hydroalkenylation reaction. Together with the dehydrogenative coupling system we developed, we managed developed two total different methodologies for C-C bond formation.

Figure 7. 6. Designed catalytic cycle for methyl acrylate dimerization

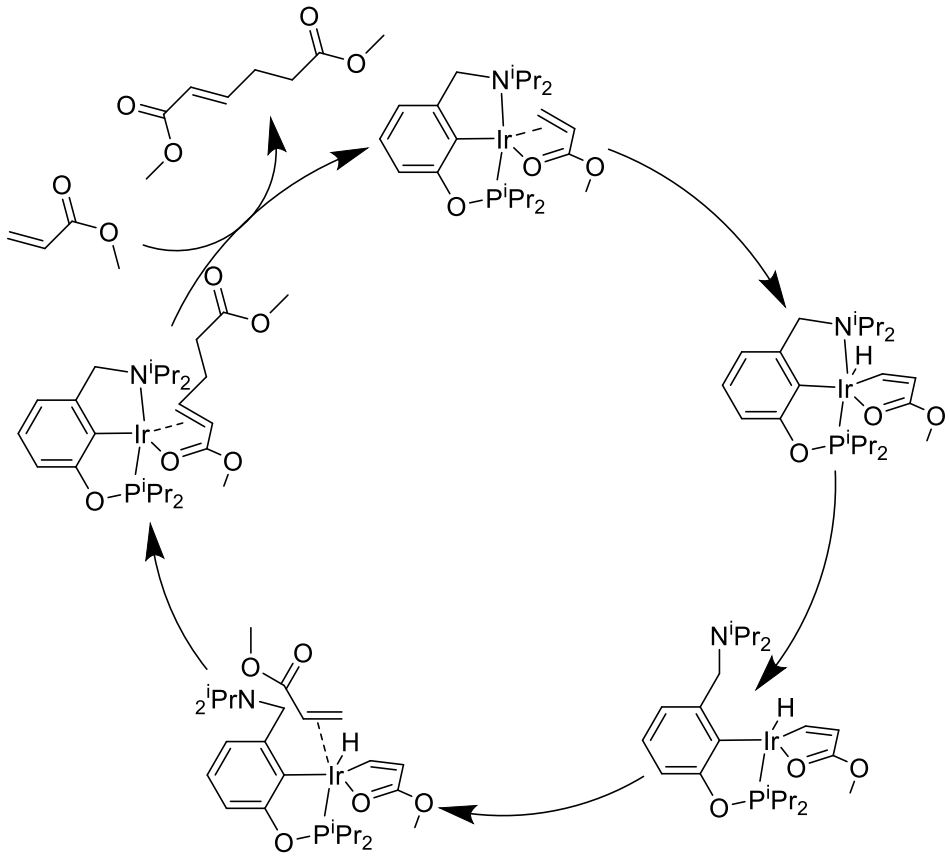

Scheme 7. 3. Methyl acrylate dimerization

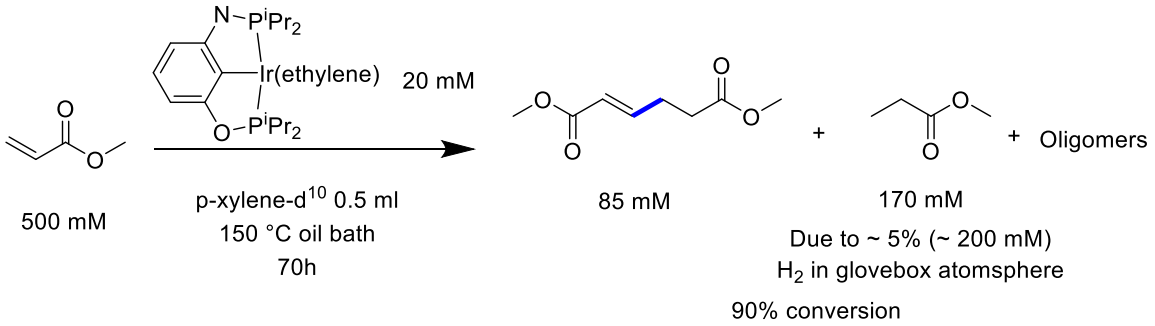

7.2.3. Discovering C-O bond cleavage reaction by new catalyst (^{iPr}NCOP)Ir(ethylene)

Vinyl acetate shares the same functional group in a different structure and could also possibly go through hydroalkenylation reaction. As showed in route 1 of Figure 7.7, we designed vinyl acetate reaction coupling route to make the dimer. When we attempted to use vinyl acetate

as a substrate to do the coupling action, we did not observe any of the desired products, instead, characteristic peaks represent ethylene and acetate acid showed up in ^{1}H NMR. It would be surprised to see ethylene and vinyl acetate could be direct generated from vinyl acetate, since the balanced equation need a molecule H_2 gas. As mentioned above, we observed large amount of methyl acrylate hydrogenation during the reaction. Also when we run this reaction under vacuum by degassing the reactor before heating resulted in almost no reaction observed by NMR. So the assumption was that H_2 gas was present in our reaction. Later we figured out that the regeneration gases (5% H_2 in argon) for glovebox was brought into our reactor. So in fact, the real reaction was vinyl acetate hydrogenation by H_2 gas. It was surprising to see pincer-iridium complex prefers the hydrogenation of ester C-O bond over C=C bond.

Figure 7. 7. Reaction involved vinyl acetate and (^{iPr}NCOP)Ir(ethylene)

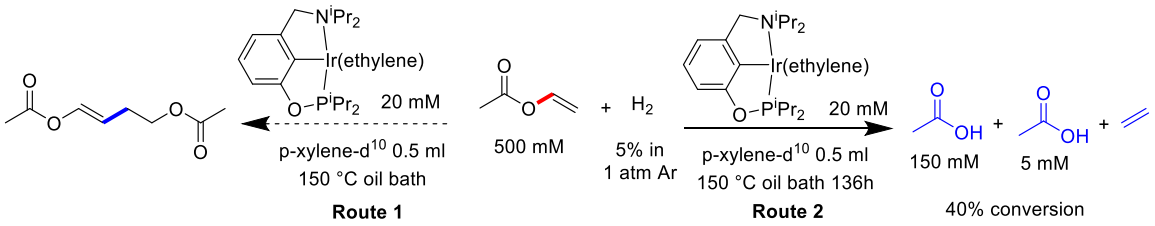

To further explore this reaction, we increased the hydrogen amount in the reaction. In scheme 7.4, we could see better conversion and yield were achieved when more H_2 gas (1 atm) was used. Beside acetic acid, small amounts of acetaldehyde was also formed. Unlike the acetic acid formed through cleavage vinylic C-O bond, two molecules acetaldehyde formed by cleavage of the carboxylic C-O bond of one molecule vinyl acetate, which seemed to be unfavorable. Compared to reported ester C-O bond cleavage reactions by pincer-metal complexes that required high temperature and high pressure of H_2 gas[57], this reaction was unique in terms of reaction conditions. Using NMR to monitor the reaction, we could see no hydride peak in ^{1}H spectra and two major peaks at δ134.91 and 134.00 ppm in ^{31}P spectra.

Scheme 7. 4. C-O bond cleavage by (^{iPr}NCOP)Ir(ethylene)

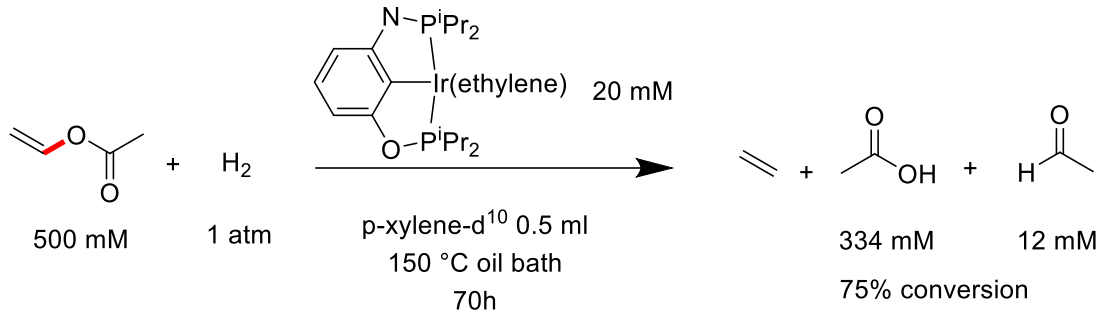

In the meantime, this new pincer-iridium complex could possibly decarbonylate aldehyde to give Ir-CO complex. When we started to perform the reaction with (^{iPr}NCOP)Ir(CO), as showed in scheme 7.5, a similar result was observed. Monitoring the reaction by ^{1}H and ^{31}P NMR, we could see no hydride peaks and one major ^{31}P peaks at δ 169.35 (one minor ^{31}P peaks at δ 168.92 ppm), which were different with the major ^{31}P peaks in experiment starting with (^{iPr}NCOP)Ir(ethylene). Despite different iridium species being present in those two systems, C-O cleavage happened in both of them with similar results.

Scheme 7. 5. C-O bond cleavage by (^{iPr}NCOP)Ir(CO)

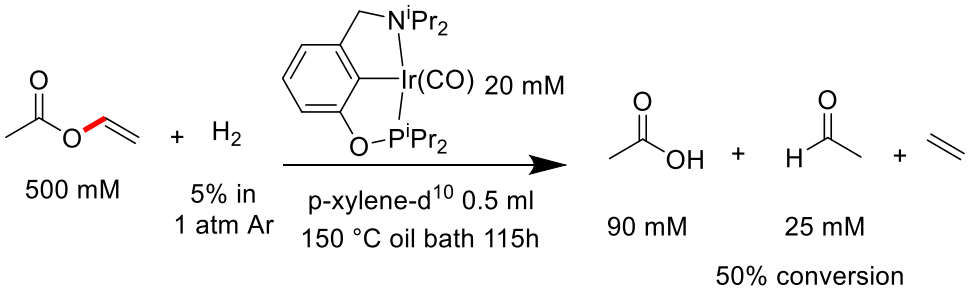

Starting with ethyl acetate as substrate gave no reaction, even when heated to 175°C. This results emphasized the importance of the double bond in the substrates for C-O bond cleavage. Using other well-known pincer-iridium complexes, for example, (^{iPr}POCOP)Ir(ethylene), gave poor results with Ir-CO complex as the major iridium species after heating, showed in figure 7.8. When there were no other iridium species besides Ir-CO, the reaction stopped. Increasing the

hydrogen content and using (^{iPr}PCP)Ir(ethylene) as catalyst could increase both the amount of hydrogenation product and C-O bond cleavage products. It was interesting to see the reaction proceeded fast in the beginning and slowed down after 2 h, while ^{31}P NMR showed that one of the catalytic species was Ir-CO complex, which slowly dominated all the other iridium species. As previously, the catalytic C-O bond cleavage stopped when Ir-CO was the only species. Considering hydrogenation of vinyl acetate using (^{iPr}PCP)Ir(CO) was not observed, the real catalytic species for the hydrogenation and C-O cleavage reaction should be the Ir(I)14 e^- species.

The significant difference between this new (^{iPr}NCOP)Ir complex with well-known pincer-iridium complexes, (^{iPr}PCP)Ir and (^{iPr}POCOP)Ir, in terms of C-O bond cleavage could attribute to the hemi-labile amine arm of this new complex. When CO replaced the ligating N atom of (^{iPr}NCOP)Ir, Ir(I) 14 e^- specie, as a new ligand, the product complex could still be Ir(I)14 e^- species. In case of (^{iPr}PCP)Ir and (^{iPr}POCOP)Ir, there was no hemi-labile amine arm to help keep the complex remain at 14 e^-, which possibly indicated the catalytic cycle involved 18 e^- intermediate since the Ir 16 e^- showed no reactivity.

Figure 7. 8. Other substrate and catalyst for C-O bond cleavage

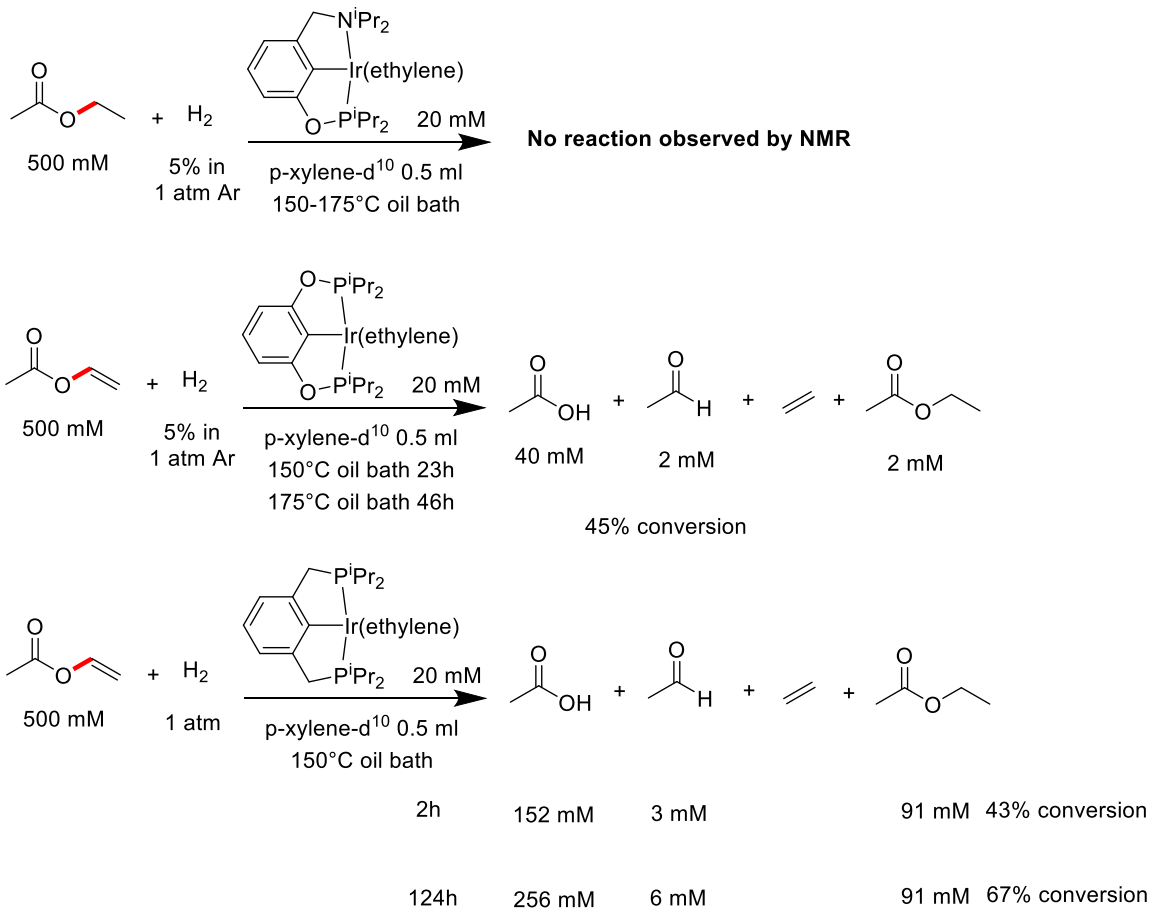

7.2.4. C-O bond cleavage reaction scope and proposed mechanism

This new catalytic cleavage reaction by (^{iPr}NCOP)Ir complex could be successfully applied for other substrates with vinylic ester bond, showed in Figure 7.9. As we can see, different substrates with vinylic ester bond, no matter bearing electron donating or electron withdrawing functional groups, could all effect the reaction with high yield.

Figure 7. 9. Substrates could undergo C-O bond cleavage

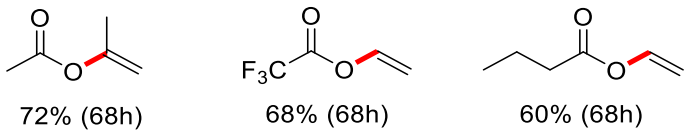

Reaction was run in a J. Young tube under 1 atm H_2 atmosphere with 500 mM substrates and 20 mM catalyst in p-xylene-d^{10}.

As far as we know, there was no reported catalytic system for this typed reaction, only a few examples of stoichiometric reactions were reported[58-62]. Although catalytic cleaving C-O bond of vinyl ester or allyl ester reactions were used in coupling reaction[63], the strong driving force from coupling reaction drove the reaction moving, otherwise, only stoichiometric reaction were observed. Using H_2 as driving force to perform the C-O cleavage was unique, but it should share similar mechanism as the mechanism of previous reported C-O bond cleavage. The chelating of carbonyl group facilitated the bond activation of metal complex in all the reported works. In Figure 7.10, we proposed a mechanism were the carbonyl group mediates vinylic carbon insertion into the iridium center as the key step. The iridium complex formed could easily go through a hydrogenation process and gave final product. In this mechanism, we could see multiple intermediates, such as 1, 4, and 5, were all feasible 18 e^- species. CO displacement of the hemi-lable amine arm in a similar mechanism could still be proposed.

Figure 7. 10. Proposed mechanism

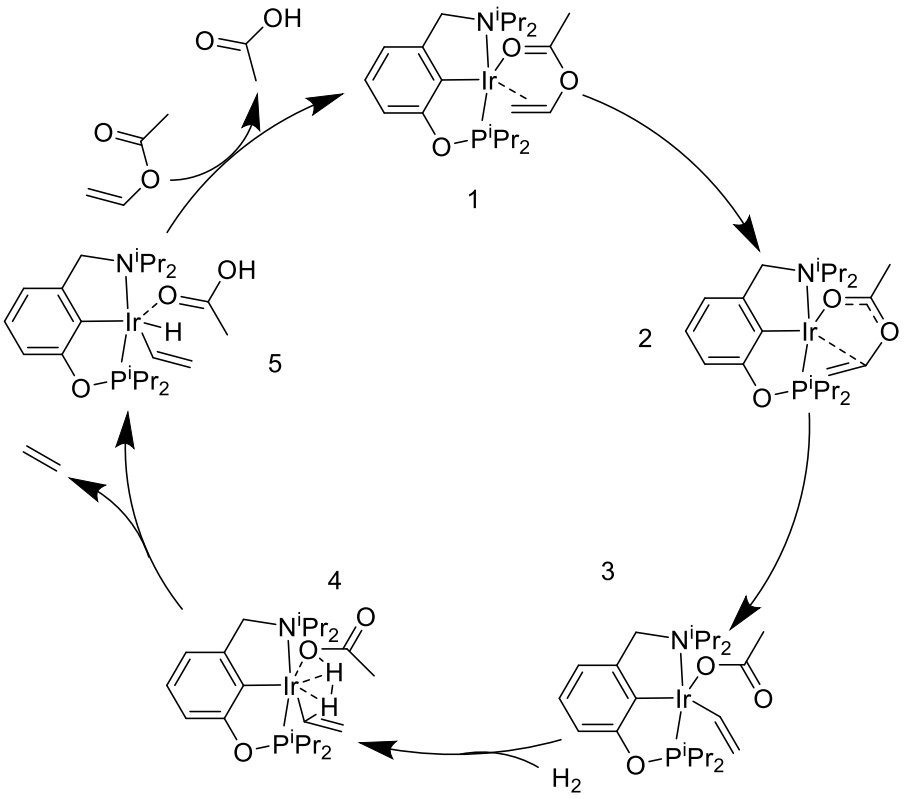

7. 3. Conclusion

We synthesized a new pincer-iridium complex with a possibly hemi-lable amine arm. Although this new complex could perform dehydrogenative coupling at low temperature, the thermal stability of it limited the desired activity. However, this new complex could be used for hydroalkenylation, which could affect tail to tail dimerization of vinyl acrylate. Moreover, this new complex could catalyze C-O bond cleavage for vinyl ester under H_2 atmosphere. The hemi-lable amine could possible enable this complex to catalyze the same reaction with different ligating components. A mechanism based on previous reports was proposed with key step involved carbonyl group mediated vinylic carbon insertion to iridium center.

7. 4. Experimental information

7.4.1. General information

We conducted all our experiment either under argon filled glovebox or schlenk line. NMR experiment were conducted on 500-MHZ Varian VNMRS. ^{1}H and ^{13}C NMR spectra were referenced to residual deuterated solvent signal. ^{31}P NMR spectra was referenced with PMe_3 in capillary tube. All anhydrous solvents were purchased from Aldrich, flushed with argon, and stored in an argon atmosphere in a glovebox. All deuterium solvents were degassed, dried over activated alumina, and storage over 3-Å molecular sieves. Vinyl esters were degassed and storage in glovebox freezer. GC analysis was conducted using a Varian 430 GC with a 30-m capillary column, using helium carrier gas. GCMS analysis was conducted using a Varian 3900 GC with a 30-m capillary column coupled with a Saturn 2100T MS, using helium carrier gas.

General procedure for C-O bond cleavage: to a J. Young Tube were added 20 mM pincer-iridium complex and 500 mM vinyl ester in 0.5 ml *p*-xylene-d^{10}. Then either directly run the reaction or removed the argon from glovebox and charged with 1 atm H_2 gas. Then reaction was heated in oil bath at 150C°C or 175°C. The reaction was monitored by both NMR and GC.

7.4.2. Catalyst synthesis and product identification

All products were identified by either compared to reported ^{1}H and ^{13}C NMR spectra or NMR spectra of authentic samples. Further confirmation was made by GC-MS.

7.4.2.1. (^{iPr}NCOP)Ir(HCl) synthesis and NMR data

In glovebox, to a 100ml schlenk flask were added 355mg (1.1 mmol) ligand ^{iPr}NCOPH, 346 mg (0.5 mmol) $[Ir(COD)Cl]_2$, and 20ml toluene. Then the flask brought outside glovebox and connected to a dry condenser under strong argon flow. The flask atmosphere was changed to hydrogen by bubble H_2 gas through a needle and heating in 80°C for 2 h. The solution changed color from yellow to red after heating. The solvent removed under vacuum and residues were

extracted by pentane (50 ml x 3). The final product (red solid) was gained by removing the pentane (0.3g, 54%). ^{1}H NMR (500 MHz, Benzene-d_6) δ 6.83 – 6.75 (m, 2H), 6.58 (dq, *J* = 7.2, 1.0 Hz, 1H), 4.53 (pd, *J* = 6.6, 1.3 Hz, 1H), 3.99 (d, *J* = 16.7 Hz, 1H), 3.73 (d, *J* = 16.9 Hz, 1H), 3.15 (pd, *J* = 6.4, 4.9 Hz, 1H), 2.26 (dq, *J* = 14.4, 7.2 Hz, 1H), 2.08 – 1.99 (m, 1H), 1.46 (d, *J* = 6.4 Hz, 3H), 1.20 (dd, *J* = 17.3, 7.2 Hz, 3H), 1.13 (dd, *J* = 18.2, 7.1 Hz, 3H), 1.01 (dd, *J* = 14.7, 7.1 Hz, 3H), 0.94 (dd, *J* = 15.8, 7.0 Hz, 3H), 0.89 (dd, *J* = 6.5, 2.8 Hz, 3H), 0.63 (d, *J* = 6.5 Hz, 6H), 0.51 (d, *J* = 6.5 Hz, 3H). ^{31}P NMR (202 MHz, Benzene-d_6) δ 143.19 (d, *J* = 21.6 Hz).

7.4.2.2. (^{iPr}NCOP)Ir(ethylene) synthesis and NMR data

In glovebox, to a 100ml schlenk flask were added 300mg (0.5 mmol) ligand (^{iPr}NCOP)Ir(HCl) and 20ml toluene. Then the flask was bubbled with ethylene gas with solution color changed from red to brown. Then 67 mg (0.6 mmol) KOtBu in 5 ml THF was added dropwise. The color immediately changed to dark after KOtBu added. After 4 h, the solvent removed under vacuum and residues extracted with pentane (50 ml x 2). Removed the pentane under vacuum to give the final product in dark red (0.24 g, 90% yield) ^{1}H NMR (500 MHz, Benzene-d_6) δ 7.08 – 7.02 (m, 2H), 6.75 (dd, *J* = 6.0, 2.4 Hz, 1H), 3.84 (s, 2H), 3.11 (hd, *J* = 6.5, 2.8 Hz, 2H), 2.82 (d, *J* = 1.5 Hz, 4H), 2.12 (pd, *J* = 7.1, 5.3 Hz, 2H), 1.22 (d, *J* = 6.4 Hz, 6H), 1.11 (dd, *J* = 13.6, 6.9 Hz, 6H), 0.97 (dd, *J* = 16.6, 7.2 Hz, 6H), 0.87 (d, *J* = 6.3 Hz, 6H). ^{31}P NMR (202 MHz, Benzene-d_6) δ 152.37.

7.4.2.3. (^{iPr}NCOP)Ir(CO) synthesis and NMR data

This complex was synthesized in situ of a J. Young tube. In glovebox, to a J. Young tube were added 5.4g (0.01mmol) (^{iPr}NCOP)Ir(ethylene) and 0.5 ml benzene. Then the J. Young tube was degassed under vacuum and charged with 1 atm CO, the red solution immediately turned into yellow. Then the solvent was removed and the remaining solid was the desired

(^{iPr}NCOP)Ir(CO). The J. Young tube was refreshed with benzene-d_6 for NMR study. ^{1}H NMR (500 MHz, Benzene-d_6) δ 7.03 (t, J = 7.6 Hz, 1H), 6.96 (d, J = 7.8 Hz, 1H), 6.79 (d, J = 7.4 Hz, 1H), 4.16 (s, 2H), 3.45 (dtd, J = 12.2, 8.2, 7.1, 4.0 Hz, 2H), 2.25 (dq, J = 14.0, 7.4, 7.0 Hz, 2H), 1.70 (d, J = 6.4 Hz, 6H), 1.35 – 1.33 (m, 6H), 1.32 – 1.29 (m, 6H), 1.09 (dd, J = 10.5, 6.6 Hz, 6H). ^{31}P NMR (202 MHz, Benzene-d_6) δ 168.26.

7.4.3. NMR spectra

Figure 7. 11. ^{1}H NMR of (^{iPr}NCOP)Ir(HCl)

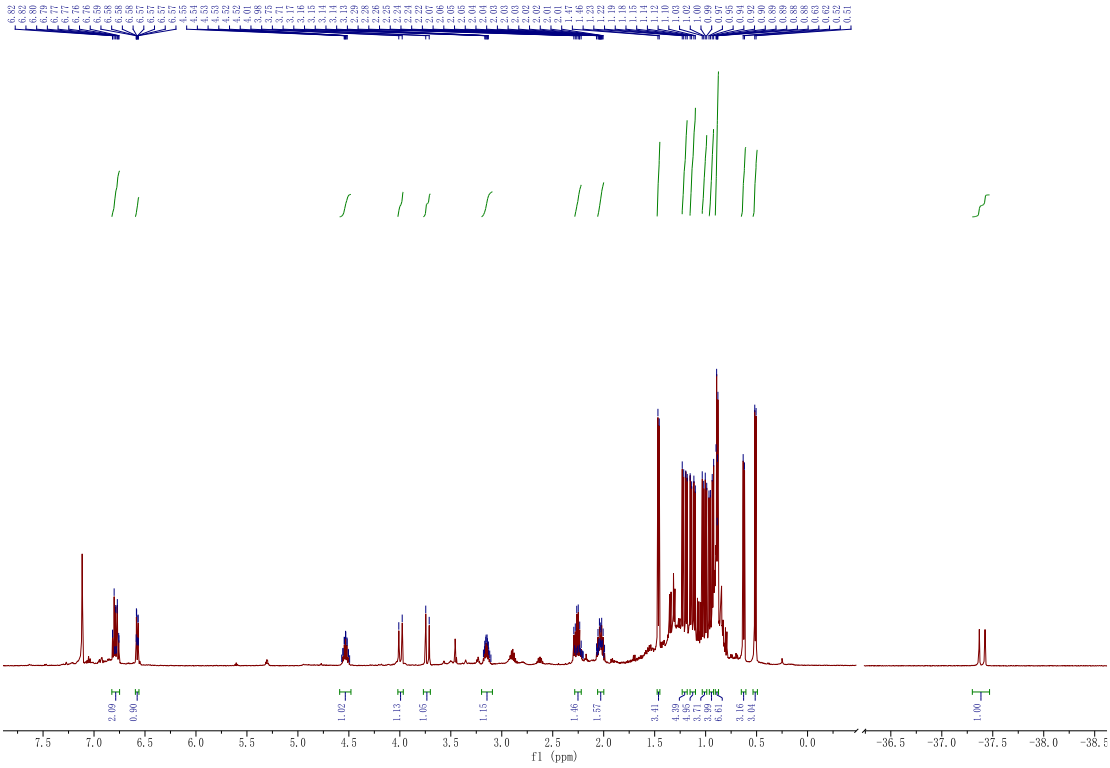

Figure 7. 12. ^{31}P NMR of (^{iPr}NCOP)Ir(HCl)

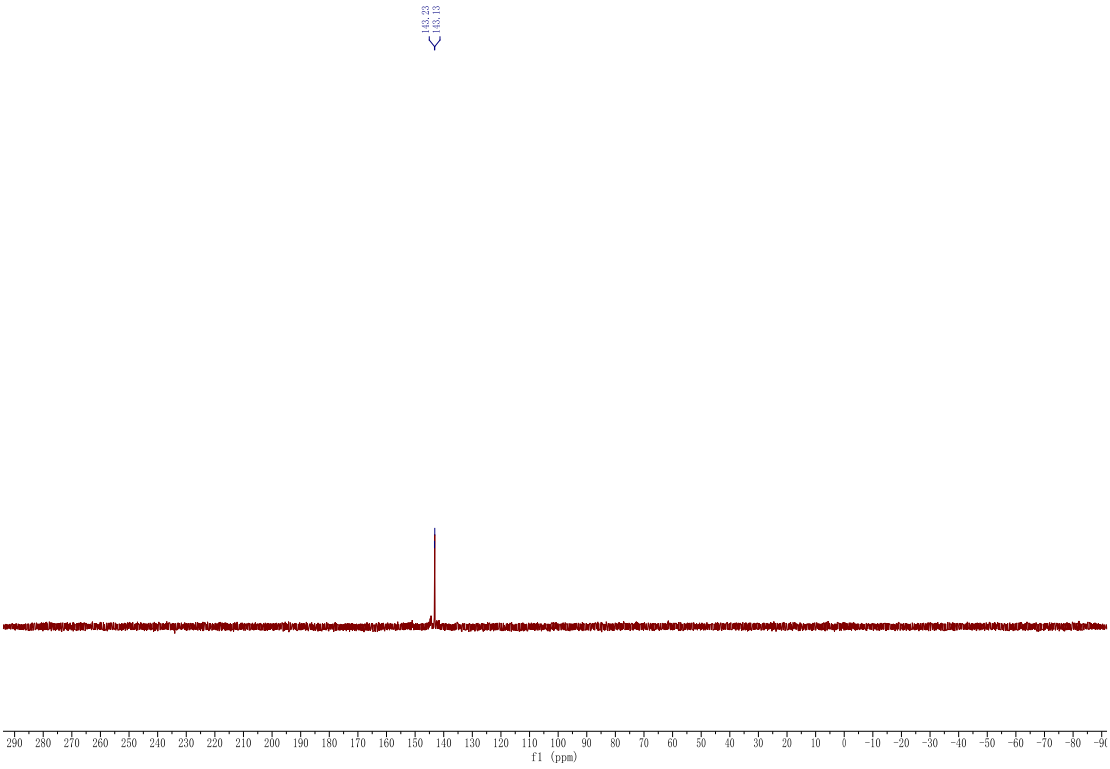

Figure 7. 13. ^{1}H NMR of (^{iPr}NCOP)Ir(ethylene)

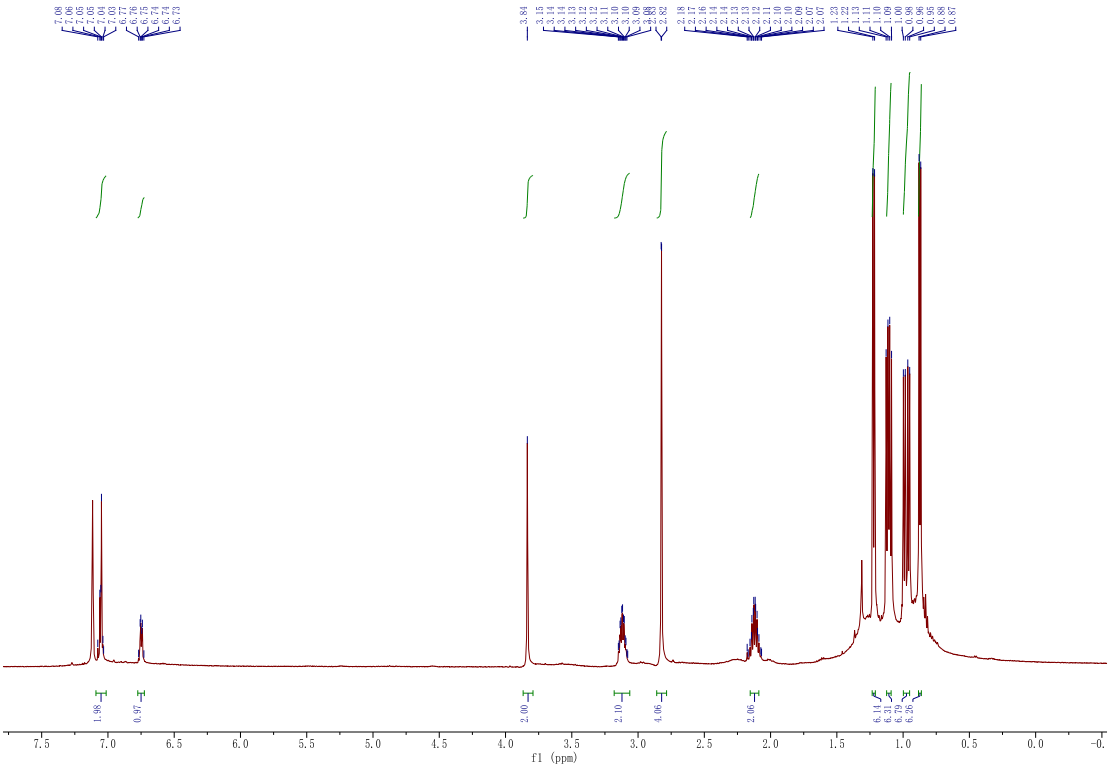

Figure 7. 14. ^{31}P NMR of (^{iPr}NCOP)Ir(ethylene)

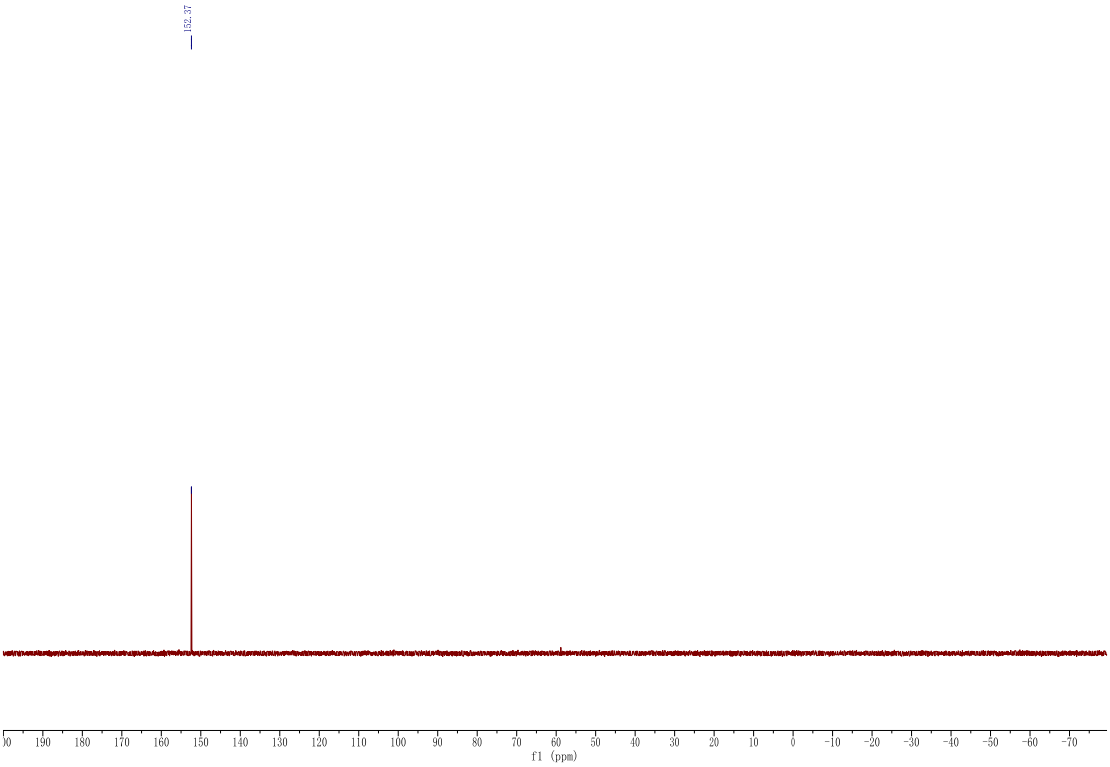

Figure 7. 15. ^{1}H NMR of (^{iPr}NCOP)Ir(CO)

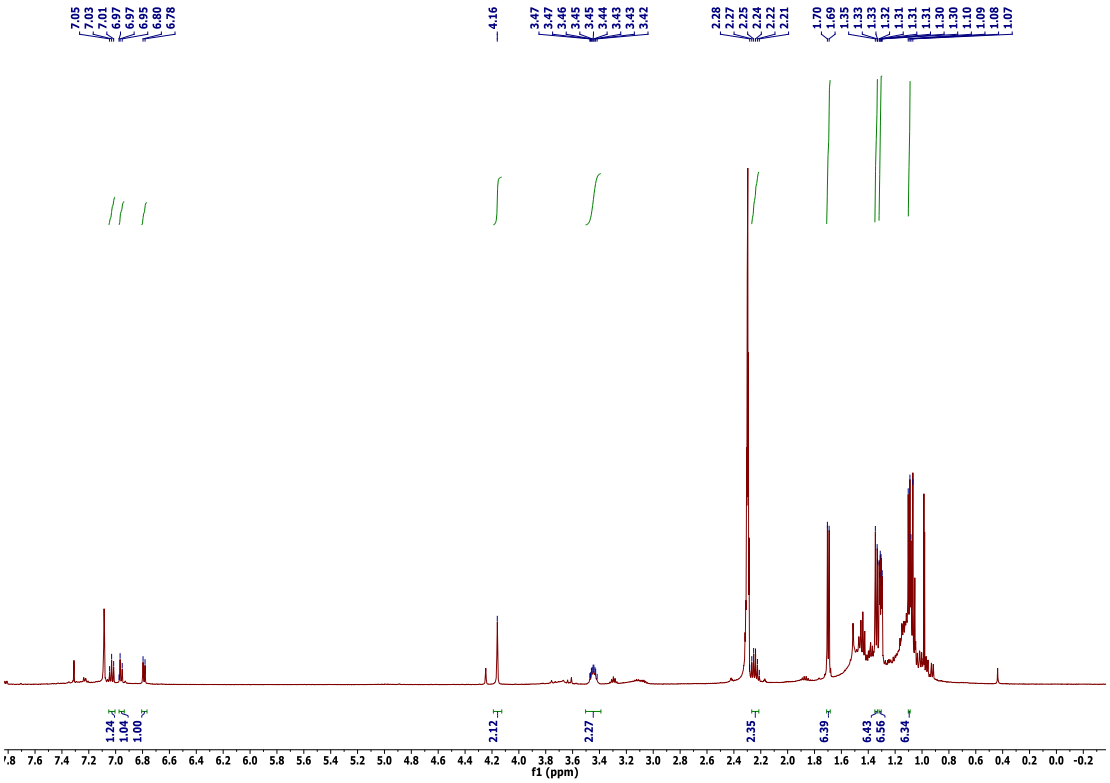

Figure 7. 16. ^{31}P NMR of (^{iPr}NCOP)Ir(CO)

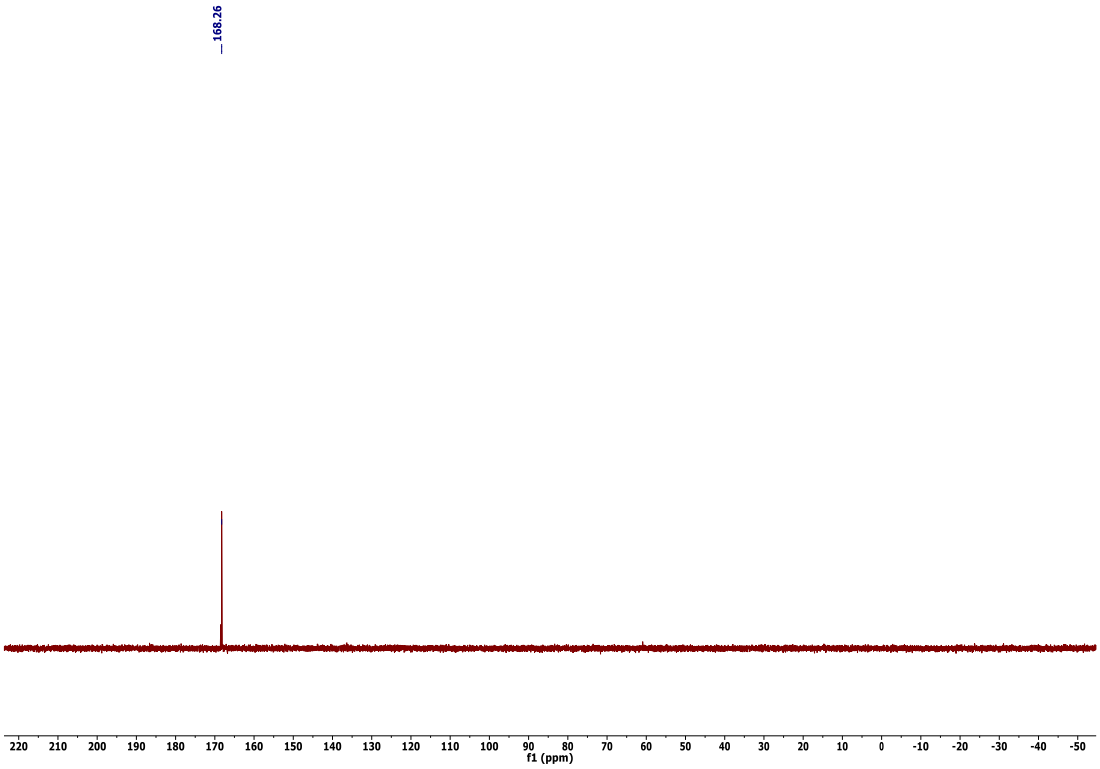

7.4.4. X-Ray structure data

Figure 7. 17. ORTEP diagram of (^{iPr}NCOP)Ir(ethylene)

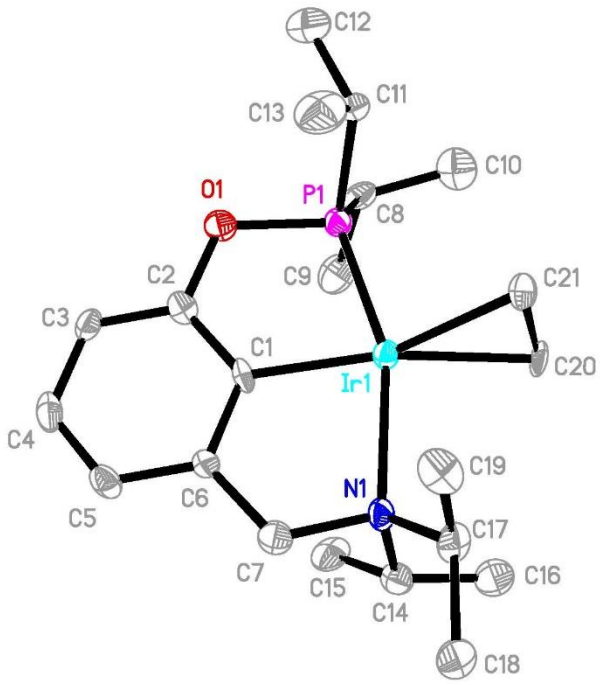

Table 7. 1. Crystal data and structure refinement for (^{iPr}NCOP)Ir(ethylene)

Identification code	irNCOPethane_Pbca_a	
Empirical formula	C21 H37 Ir N O P	
Formula weight	542.68	
Temperature	120(2) K	
Wavelength	0.71073 Å	
Crystal system	Orthorhombic	
Space group	Pbca	
Unit cell dimensions	a = 15.558(6) Å	α= 90°.
	b = 13.733(5) Å	β= 90°.
	c = 20.110(8) Å	γ = 90°.
Volume	4297(3) $Å^3$	
Z	8	
Density (calculated)	1.678 Mg/m^3	
Absorption coefficient	6.298 mm^{-1}	
F(000)	2160	
Crystal size	.33 x .07 x .03 mm^3	
Theta range for data collection	2.025 to 29.574°.	
Index ranges	-3<=h<=21, -17<=k<=17, -27<=l<=27	
Reflections collected	15009	
Independent reflections	5753 [R(int) = 0.0969]	
Completeness to theta = 25.242°	98.8 %	
Absorption correction	Semi-empirical from equivalents	
Max. and min. transmission	0.7461 and 0.5168	
Refinement method	Full-matrix least-squares on F^2	
Data / restraints / parameters	5753 / 363 / 235	
Goodness-of-fit on F^2	1.000	
Final R indices [I>2sigma(I)]	R1 = 0.0529, wR2 = 0.1123	
R indices (all data)	R1 = 0.0953, wR2 = 0.1313	
Extinction coefficient	0.00025(5)	
Largest diff. peak and hole	2.239 and -1.850 $e.Å^{-3}$	

Table 7. 2. Atomic coordinates (x 10^4) and equivalent isotropic displacement parameters (Å^{2}x 10^3) for (^{iPr}NCOP)Ir(ethylene)

U(eq) is defined as one third of the trace of the orthogonalized U^{ij} tensor.

	x	y	z	U(eq)
Ir(1)	5497(1)	6855(1)	6583(1)	15(1)
P(1)	6050(1)	7376(2)	5670(1)	16(1)
O(1)	5496(4)	8377(4)	5439(3)	22(1)
N(1)	4536(4)	6694(5)	7428(3)	19(1)
C(1)	4753(5)	8034(6)	6425(4)	18(2)
C(2)	4837(5)	8593(7)	5851(4)	20(2)
C(3)	4278(5)	9336(6)	5704(4)	21(2)
C(4)	3613(5)	9545(7)	6145(4)	25(2)
C(5)	3532(5)	9023(7)	6725(4)	22(2)
C(6)	4103(5)	8253(6)	6868(4)	17(2)
C(7)	4074(5)	7679(6)	7500(4)	22(2)
C(8)	5966(5)	6669(6)	4903(4)	21(2)
C(9)	5040(6)	6336(7)	4806(5)	34(2)
C(10)	6586(6)	5795(7)	4909(5)	35(2)
C(11)	7143(5)	7873(6)	5650(5)	23(2)
C(12)	7412(6)	8296(8)	4983(5)	40(3)
C(13)	7247(6)	8593(8)	6199(5)	41(3)
C(14)	3823(5)	5960(6)	7296(4)	22(2)
C(15)	3352(5)	6176(7)	6648(5)	31(2)
C(16)	4108(6)	4913(7)	7294(5)	32(2)
C(17)	4975(5)	6476(7)	8082(4)	22(2)
C(18)	4380(6)	6369(8)	8689(4)	32(2)
C(19)	5694(6)	7203(8)	8220(5)	31(2)
C(20)	6053(6)	5421(6)	6767(5)	25(2)
C(21)	6668(5)	6128(7)	6850(5)	28(2)

Table 7. 3. Bond lengths [Å] and angles [°] for (^{iPr}NCOP)Ir(ethylene).

Ir(1)-C(1)	2.016(8)	C(11)-C(13)	1.491(13)
Ir(1)-P(1)	2.150(2)	C(11)-C(12)	1.520(13)
Ir(1)-C(21)	2.144(8)	C(11)-H(11)	1.0000
Ir(1)-C(20)	2.183(8)	C(12)-H(12A)	0.9800
Ir(1)-N(1)	2.275(7)	C(12)-H(12B)	0.9800
P(1)-O(1)	1.688(6)	C(12)-H(12C)	0.9800
P(1)-C(8)	1.828(8)	C(13)-H(13A)	0.9800
P(1)-C(11)	1.832(8)	C(13)-H(13B)	0.9800
O(1)-C(2)	1.351(9)	C(13)-H(13C)	0.9800
N(1)-C(17)	1.512(10)	C(14)-C(16)	1.505(12)
N(1)-C(14)	1.521(10)	C(14)-C(15)	1.524(12)
N(1)-C(7)	1.538(10)	C(14)-H(14)	1.0000
C(1)-C(6)	1.380(11)	C(15)-H(15A)	0.9800
C(1)-C(2)	1.392(11)	C(15)-H(15B)	0.9800
C(2)-C(3)	1.373(11)	C(15)-H(15C)	0.9800
C(3)-C(4)	1.394(11)	C(16)-H(16A)	0.9800
C(3)-H(3)	0.9500	C(16)-H(16B)	0.9800
C(4)-C(5)	1.374(11)	C(16)-H(16C)	0.9800
C(4)-H(4)	0.9500	C(17)-C(19)	1.525(13)
C(5)-C(6)	1.412(11)	C(17)-C(18)	1.540(12)
C(5)-H(5)	0.9500	C(17)-H(17)	1.0000
C(6)-C(7)	1.497(11)	C(18)-H(18A)	0.9800
C(7)-H(7A)	0.9900	C(18)-H(18B)	0.9800
C(7)-H(7B)	0.9900	C(18)-H(18C)	0.9800
C(8)-C(9)	1.524(12)	C(19)-H(19A)	0.9800
C(8)-C(10)	1.540(13)	C(19)-H(19B)	0.9800
C(8)-H(8)	1.0000	C(19)-H(19C)	0.9800
C(9)-H(9A)	0.9800	C(20)-C(21)	1.373(13)
C(9)-H(9B)	0.9800	C(20)-H(20A)	0.9900
C(9)-H(9C)	0.9800	C(20)-H(20B)	0.9900
C(10)-H(10A)	0.9800	C(21)-H(21A)	0.9900
C(10)-H(10B)	0.9800	C(21)-H(21B)	0.9900
C(10)-H(10C)	0.9800		

C(1)-Ir(1)-P(1)	80.1(2)	C(4)-C(5)-C(6)	120.3(7)
C(1)-Ir(1)-C(21)	154.3(4)	C(4)-C(5)-H(5)	119.8
P(1)-Ir(1)-C(21)	91.6(3)	C(6)-C(5)-H(5)	119.8
C(1)-Ir(1)-C(20)	168.3(3)	C(1)-C(6)-C(5)	119.6(8)
P(1)-Ir(1)-C(20)	106.6(2)	C(1)-C(6)-C(7)	117.1(7)
C(21)-Ir(1)-C(20)	37.0(3)	C(5)-C(6)-C(7)	123.2(7)
C(1)-Ir(1)-N(1)	79.5(3)	C(6)-C(7)-N(1)	111.6(6)
P(1)-Ir(1)-N(1)	158.96(17)	C(6)-C(7)-H(7A)	109.3
C(21)-Ir(1)-N(1)	109.1(3)	N(1)-C(7)-H(7A)	109.3
C(20)-Ir(1)-N(1)	92.7(3)	C(6)-C(7)-H(7B)	109.3
O(1)-P(1)-C(8)	99.4(4)	N(1)-C(7)-H(7B)	109.3
O(1)-P(1)-C(11)	99.5(4)	H(7A)-C(7)-H(7B)	108.0
C(8)-P(1)-C(11)	104.2(4)	C(9)-C(8)-C(10)	111.1(8)
O(1)-P(1)-Ir(1)	107.6(2)	C(9)-C(8)-P(1)	109.6(6)
C(8)-P(1)-Ir(1)	121.0(3)	C(10)-C(8)-P(1)	111.2(6)
C(11)-P(1)-Ir(1)	121.0(3)	C(9)-C(8)-H(8)	108.3
C(2)-O(1)-P(1)	113.4(5)	C(10)-C(8)-H(8)	108.3
C(17)-N(1)-C(14)	110.5(7)	P(1)-C(8)-H(8)	108.3
C(17)-N(1)-C(7)	107.7(6)	C(8)-C(9)-H(9A)	109.5
C(14)-N(1)-C(7)	105.0(6)	C(8)-C(9)-H(9B)	109.5
C(17)-N(1)-Ir(1)	111.8(5)	H(9A)-C(9)-H(9B)	109.5
C(14)-N(1)-Ir(1)	114.4(5)	C(8)-C(9)-H(9C)	109.5
C(7)-N(1)-Ir(1)	107.0(5)	H(9A)-C(9)-H(9C)	109.5
C(6)-C(1)-C(2)	119.0(7)	H(9B)-C(9)-H(9C)	109.5
C(6)-C(1)-Ir(1)	119.6(6)	C(8)-C(10)-H(10A)	109.5
C(2)-C(1)-Ir(1)	121.3(6)	C(8)-C(10)-H(10B)	109.5
O(1)-C(2)-C(3)	120.7(8)	H(10A)-C(10)-H(10B)	109.5
O(1)-C(2)-C(1)	117.3(7)	C(8)-C(10)-H(10C)	109.5
C(3)-C(2)-C(1)	121.9(8)	H(10A)-C(10)-H(10C)	109.5
C(2)-C(3)-C(4)	119.1(8)	H(10B)-C(10)-H(10C)	109.5
C(2)-C(3)-H(3)	120.5	C(13)-C(11)-C(12)	111.7(8)
C(4)-C(3)-H(3)	120.5	C(13)-C(11)-P(1)	109.3(6)
C(5)-C(4)-C(3)	120.1(8)	C(12)-C(11)-P(1)	114.7(6)
C(5)-C(4)-H(4)	119.9	C(13)-C(11)-H(11)	106.9
C(3)-C(4)-H(4)	119.9	C(12)-C(11)-H(11)	106.9

P(1)-C(11)-H(11)	106.9	N(1)-C(17)-C(19)	111.1(7)
C(11)-C(12)-H(12A)	109.5	N(1)-C(17)-C(18)	115.9(7)
C(11)-C(12)-H(12B)	109.5	C(19)-C(17)-C(18)	111.0(8)
H(12A)-C(12)-H(12B)	109.5	N(1)-C(17)-H(17)	106.0
C(11)-C(12)-H(12C)	109.5	C(19)-C(17)-H(17)	106.0
H(12A)-C(12)-H(12C)	109.5	C(18)-C(17)-H(17)	106.0
H(12B)-C(12)-H(12C)	109.5	C(17)-C(18)-H(18A)	109.5
C(11)-C(13)-H(13A)	109.5	C(17)-C(18)-H(18B)	109.5
C(11)-C(13)-H(13B)	109.5	H(18A)-C(18)-H(18B)	109.5
H(13A)-C(13)-H(13B)	109.5	C(17)-C(18)-H(18C)	109.5
C(11)-C(13)-H(13C)	109.5	H(18A)-C(18)-H(18C)	109.5
H(13A)-C(13)-H(13C)	109.5	H(18B)-C(18)-H(18C)	109.5
H(13B)-C(13)-H(13C)	109.5	C(17)-C(19)-H(19A)	109.5
C(16)-C(14)-C(15)	109.0(8)	C(17)-C(19)-H(19B)	109.5
C(16)-C(14)-N(1)	114.8(7)	H(19A)-C(19)-H(19B)	109.5
C(15)-C(14)-N(1)	111.8(7)	C(17)-C(19)-H(19C)	109.5
C(16)-C(14)-H(14)	107.0	H(19A)-C(19)-H(19C)	109.5
C(15)-C(14)-H(14)	107.0	H(19B)-C(19)-H(19C)	109.5
N(1)-C(14)-H(14)	107.0	C(21)-C(20)-Ir(1)	70.0(5)
C(14)-C(15)-H(15A)	109.5	C(21)-C(20)-H(20A)	116.6
C(14)-C(15)-H(15B)	109.5	Ir(1)-C(20)-H(20A)	116.6
H(15A)-C(15)-H(15B)	109.5	C(21)-C(20)-H(20B)	116.6
C(14)-C(15)-H(15C)	109.5	Ir(1)-C(20)-H(20B)	116.6
H(15A)-C(15)-H(15C)	109.5	H(20A)-C(20)-H(20B)	113.6
H(15B)-C(15)-H(15C)	109.5	C(20)-C(21)-Ir(1)	73.0(5)
C(14)-C(16)-H(16A)	109.5	C(20)-C(21)-H(21A)	116.2
C(14)-C(16)-H(16B)	109.5	Ir(1)-C(21)-H(21A)	116.2
H(16A)-C(16)-H(16B)	109.5	C(20)-C(21)-H(21B)	116.2
C(14)-C(16)-H(16C)	109.5	Ir(1)-C(21)-H(21B)	116.2
H(16A)-C(16)-H(16C)	109.5	H(21A)-C(21)-H(21B)	113.2
H(16B)-C(16)-H(16C)	109.5		

Table 7. 4. Anisotropic displacement parameters ($Å^2$x 10^3) for (^{iPr}NCOP)Ir(ethylene)

The anisotropic displacement factor exponent takes the form: $-2\pi^2[h^2 a^{*2} U^{11} + ... + 2 h k a^* b^* U^{12}]$

	U^{11}	U^{22}	U^{33}	U^{23}	U^{13}	U^{12}
Ir(1)	17(1)	14(1)	13(1)	0(1)	0(1)	2(1)
P(1)	18(1)	17(1)	15(1)	2(1)	1(1)	2(1)
O(1)	25(3)	26(3)	15(3)	2(2)	4(2)	4(2)
N(1)	21(3)	21(4)	15(3)	3(3)	-1(3)	7(3)
C(1)	15(3)	16(4)	22(4)	-1(3)	-4(3)	7(3)
C(2)	20(3)	22(4)	19(4)	-2(3)	-1(3)	3(3)
C(3)	22(4)	17(4)	23(4)	8(4)	-1(3)	1(3)
C(4)	24(4)	17(4)	35(5)	1(4)	-4(3)	6(3)
C(5)	23(4)	27(5)	15(4)	-3(3)	2(3)	9(3)
C(6)	15(3)	18(4)	18(3)	2(3)	1(3)	2(3)
C(7)	26(4)	23(4)	17(4)	-2(4)	2(3)	2(3)
C(8)	29(4)	24(5)	11(3)	2(3)	4(3)	-3(3)
C(9)	42(5)	29(6)	32(5)	0(5)	-3(4)	-4(4)
C(10)	42(5)	35(6)	28(5)	-9(5)	0(4)	3(4)
C(11)	17(3)	21(4)	31(4)	8(4)	2(3)	-1(3)
C(12)	31(5)	41(7)	47(6)	10(5)	6(4)	-6(4)
C(13)	34(5)	41(6)	47(6)	0(5)	-6(5)	-16(5)
C(14)	21(4)	20(4)	25(4)	-2(4)	2(3)	-1(3)
C(15)	19(4)	33(5)	42(5)	11(5)	-4(4)	-12(4)
C(16)	29(5)	28(5)	40(6)	2(5)	1(4)	-6(4)
C(17)	31(4)	26(5)	11(4)	0(3)	-5(3)	5(4)
C(18)	43(5)	44(6)	11(4)	6(4)	4(4)	14(5)
C(19)	30(4)	38(6)	25(5)	-8(4)	-4(3)	4(4)
C(20)	34(4)	12(4)	30(4)	10(3)	8(3)	13(3)
C(21)	23(4)	32(5)	28(4)	13(4)	-3(3)	7(3)

Table 7. 5. Hydrogen coordinates (x 10^4) and isotropic displacement parameters (Å^{2}x 10^3) for (^{iPr}NCOP)Ir(ethylene).

	x	y	z	U(eq)
H(3)	4345	9703	5306	25
H(4)	3214	10048	6045	30
H(5)	3089	9183	7032	26
H(7A)	3467	7565	7626	26
H(7B)	4349	8059	7860	26
H(8)	6125	7101	4522	26
H(9A)	4988	5996	4380	51
H(9B)	4659	6904	4809	51
H(9C)	4878	5895	5168	51
H(10A)	6479	5386	4519	53
H(10B)	6495	5413	5315	53
H(10C)	7181	6032	4899	53
H(11)	7543	7321	5747	28
H(12A)	7998	8551	5016	60
H(12B)	7019	8824	4860	60
H(12C)	7391	7785	4643	60
H(13A)	7860	8726	6267	61
H(13B)	7000	8328	6609	61
H(13C)	6951	9199	6082	61
H(14)	3395	6032	7663	26
H(15A)	2944	5649	6555	47
H(15B)	3768	6223	6284	47
H(15C)	3040	6793	6690	47
H(16A)	3602	4487	7298	48
H(16B)	4459	4785	7689	48
H(16C)	4448	4784	6893	48
H(17)	5261	5830	8024	27
H(18A)	4726	6224	9085	49
H(18B)	3972	5838	8612	49

H(18C)	4064	6978	8759	49
H(19A)	6120	6905	8517	46
H(19B)	5454	7785	8432	46
H(19C)	5971	7386	7801	46
H(20A)	5860	5078	7173	30
H(20B)	6120	4988	6376	30
H(21A)	7134	6143	6515	33
H(21B)	6874	6233	7310	33

Table 7. 6. Torsion angles [°] for (^{iPr}NCOP)Ir(ethylene).

C(8)-P(1)-O(1)-C(2)	124.6(6)	O(1)-P(1)-C(8)-C(9)	-69.3(6)
C(11)-P(1)-O(1)-C(2)	-129.1(6)	C(11)-P(1)-C(8)-C(9)	-171.7(6)
Ir(1)-P(1)-O(1)-C(2)	-2.2(6)	Ir(1)-P(1)-C(8)-C(9)	47.9(7)
P(1)-O(1)-C(2)-C(3)	-174.5(7)	O(1)-P(1)-C(8)-C(10)	167.4(6)
P(1)-O(1)-C(2)-C(1)	5.6(10)	C(11)-P(1)-C(8)-C(10)	65.1(7)
C(6)-C(1)-C(2)-O(1)	178.0(8)	Ir(1)-P(1)-C(8)-C(10)	-75.4(7)
Ir(1)-C(1)-C(2)-O(1)	-6.9(11)	O(1)-P(1)-C(11)-C(13)	68.9(7)
C(6)-C(1)-C(2)-C(3)	-1.8(13)	C(8)-P(1)-C(11)-C(13)	171.2(7)
Ir(1)-C(1)-C(2)-C(3)	173.2(7)	Ir(1)-P(1)-C(11)-C(13)	-48.3(7)
O(1)-C(2)-C(3)-C(4)	-179.2(8)	O(1)-P(1)-C(11)-C(12)	-57.4(7)
C(1)-C(2)-C(3)-C(4)	0.7(13)	C(8)-P(1)-C(11)-C(12)	44.9(8)
C(2)-C(3)-C(4)-C(5)	1.3(13)	Ir(1)-P(1)-C(11)-C(12)	-174.6(6)
C(3)-C(4)-C(5)-C(6)	-2.2(13)	C(17)-N(1)-C(14)-C(16)	-56.7(9)
C(2)-C(1)-C(6)-C(5)	1.0(13)	C(7)-N(1)-C(14)-C(16)	-172.5(7)
Ir(1)-C(1)-C(6)-C(5)	-174.2(6)	Ir(1)-N(1)-C(14)-C(16)	70.5(8)
C(2)-C(1)-C(6)-C(7)	-175.9(7)	C(17)-N(1)-C(14)-C(15)	178.5(7)
Ir(1)-C(1)-C(6)-C(7)	9.0(11)	C(7)-N(1)-C(14)-C(15)	62.7(8)
C(4)-C(5)-C(6)-C(1)	1.0(13)	Ir(1)-N(1)-C(14)-C(15)	-54.3(8)
C(4)-C(5)-C(6)-C(7)	177.6(8)	C(14)-N(1)-C(17)-C(19)	179.7(7)
C(1)-C(6)-C(7)-N(1)	-22.9(11)	C(7)-N(1)-C(17)-C(19)	-66.1(9)
C(5)-C(6)-C(7)-N(1)	160.4(8)	Ir(1)-N(1)-C(17)-C(19)	51.1(8)
C(17)-N(1)-C(7)-C(6)	144.1(7)	C(14)-N(1)-C(17)-C(18)	-52.3(10)
C(14)-N(1)-C(7)-C(6)	-98.1(8)	C(7)-N(1)-C(17)-C(18)	61.8(10)
Ir(1)-N(1)-C(7)-C(6)	23.8(8)	Ir(1)-N(1)-C(17)-C(18)	179.1(6)

7.5. Reference

1. Moulton, C. J.; Shaw, B. L., Transition metal–carbon bonds. Part XLII. Complexes of nickel, palladium, platinum, rhodium and iridium with the tridentate ligand 2,6-bis[(di-t-butylphosphino)methyl]phenyl. *Journal of the Chemical Society, Dalton Transactions* **1976,** (11), 1020-1024.
2. Gupta, M.; Hagen, C.; Flesher, R. J.; Kaska, W. C.; Jensen, C. M., A highly active alkane dehydrogenation catalyst: stabilization of dihydrido rhodium and iridium complexes by a P-C-P pincer ligand. *Chemical Communications* **1996,** (17), 2083-2084.
3. Choi, J.; MacArthur, A. H.; Brookhart, M.; Goldman, A. S., Dehydrogenation and related reactions catalyzed by iridium pincer complexes. *Chemical reviews* **2011,** *111* (3), 1761-79.
4. Kumar, A.; Bhatti, T. M.; Goldman, A. S., Dehydrogenation of Alkanes and Aliphatic Groups by Pincer-Ligated Metal Complexes. *Chemical reviews* **2017,** *117* (19), 12357-12384.
5. Xu, W.-w.; P. Rosini, G.; Krogh-Jespersen, K.; S. Goldman, A.; Gupta, M.; M. Jensen, C.; C. Kaska, W., Thermochemical alkane dehydrogenation catalyzed in solution without the use of a hydrogen acceptor. *Chemical Communications* **1997,** (23), 2273-2274.
6. Denney, M. C.; Pons, V.; Hebden, T. J.; Heinekey, D. M.; Goldberg, K. I., Efficient Catalysis of Ammonia Borane Dehydrogenation. *Journal of the American Chemical Society* **2006,** *128* (37), 12048-12049.
7. Morales-Morales, D.; Redón, R.; Wang, Z.; Lee, D. W.; Yung, C.; Magnuson, K.; Jensen, C. M., Selective dehydrogenation of alcohols and diols catalyzed by a dihydrido iridium PCP pincer complex. *Canadian Journal of Chemistry* **2001,** *79* (5-6), 823-829.
8. Levy, R.; Azerraf, C.; Gelman, D.; Rueck-Braun, K.; Kapoor, P. N., Cyclometalated phosphine-based Ir(III) pincer complex as a catalyst for Oppenauer-type oxidation of alcohols. *Catalysis Communications* **2009,** *11* (4), 298-301.
9. Gu, X.-Q.; Chen, W.; Morales-Morales, D.; Jensen, C. M., Dehydrogenation of secondary amines to imines catalyzed by an iridium PCP pincer complex: initial aliphatic or direct amino dehydrogenation? *Journal of Molecular Catalysis A: Chemical* **2002,** *189* (1), 119-124.
10. Gupta, M.; C. Kaska, W.; M. Jensen, C., Catalytic dehydrogenation of ethylbenzene and tetrahydrofuran by a dihydrido iridium P–C–P pincer complex. *Chemical Communications* **1997,** (5), 461-462.
11. Ahuja, R.; Punji, B.; Findlater, M.; Supplee, C.; Schinski, W.; Brookhart, M.; Goldman, A. S., Catalytic dehydroaromatization of n-alkanes by pincer-ligated iridium complexes. *Nat Chem* **2011,** *3* (2), 167-171.
12. Haibach, M. C.; Kundu, S.; Brookhart, M.; Goldman, A. S., Alkane Metathesis by Tandem Alkane-Dehydrogenation-Olefin-Metathesis Catalysis and Related Chemistry. *Accounts of Chemical Research* **2012,** *45* (6), 947-958.
13. Goldman, A. S.; Roy, A. H.; Huang, Z.; Ahuja, R.; Schinski, W.; Brookhart, M., Catalytic alkane metathesis by tandem alkane dehydrogenation olefin metathesis. *Science* **2006,** *312* (5771), 257-261.
14. Dobereiner, G. E.; Yuan, J.; Schrock, R. R.; Goldman, A. S.; Hackenberg, J. D., Catalytic Synthesis of n-Alkyl Arenes through Alkyl Group Cross-Metathesis. *Journal of the American Chemical Society* **2013,** *135* (34), 12572-12575.

15. Dinh, L. V.; Li, B.; Kumar, A.; Schinski, W.; Field, K. D.; Kuperman, A.; Celik, F. E.; Goldman, A. S., Alkyl–Aryl Coupling Catalyzed by Tandem Systems of Pincer-Ligated Iridium Complexes and Zeolites. *ACS Catalysis* **2016**, 2836-2841.
16. Kanzelberger, M.; Zhang, X. W.; Emge, T. J.; Goldman, A. S.; Zhao, J.; Incarvito, C.; Hartwig, J. F., Distinct thermodynamics for the formation and cleavage of N-H bonds in aniline and ammonia. Directly-observed reductive elimination of ammonia from an isolated amido hydride complex. *Journal of the American Chemical Society* **2003,** *125* (45), 13644-13645.
17. Lee, D. W.; Jensen, C. M.; Morales-Morales, D., Reactivity of Iridium PCP Pincer Complexes toward CO and CO2. Crystal Structures of IrH(κ2-O2COH){C6H3-2,6-(CH2PBut2)2} and IrH(C(O)OH){C6H3-2,6-(CH2PBut2)2}·H2O. *Organometallics* **2003,** *22* (23), 4744-4749.
18. Zhao, J.; Goldman, A. S.; Hartwig, J. F., Oxidative addition of ammonia to form a stable monomeric amido hydride complex. *Science* **2005,** *307* (5712), 1080-2.
19. Zhang, X.; Emge, T. J.; Ghosh, R.; Goldman, A. S., Selective Cleavage of the C−C Bonds of Aminoethyl Groups, via a Multistep Pathway, by a Pincer Iridium Complex. *Journal of the American Chemical Society* **2005,** *127* (23), 8250-8251.
20. Laviska, D. A.; Guan, C.; Emge, T. J.; Wilklow-Marnell, M.; Brennessel, W. W.; Jones, W. D.; Krogh-Jespersen, K.; Goldman, A. S., Addition of C–C and C–H bonds by pincer-iridium complexes: a combined experimental and computational study. *Dalton T* **2014,** *43* (43), 16354-16365.
21. Choi, J.; Choliy, Y.; Zhang, X.; Emge, T. J.; Krogh-Jespersen, K.; Goldman, A. S., Cleavage of sp3 C−O Bonds via Oxidative Addition of C−H Bonds. *Journal of the American Chemical Society* **2009,** *131* (43), 15627-15629.
22. Kundu, S.; Choi, J.; Wang, D. Y.; Choliy, Y.; Emge, T. J.; Krogh-Jespersen, K.; Goldman, A. S., Cleavage of Ether, Ester, and Tosylate C(sp3)–O Bonds by an Iridium Complex, Initiated by Oxidative Addition of C–H Bonds. Experimental and Computational Studies. *Journal of the American Chemical Society* **2013,** *135* (13), 5127-5143.
23. Choi, J.; Wang, D. Y.; Kundu, S.; Choliy, Y.; Emge, T. J.; Krogh-Jespersen, K.; Goldman, A. S., Net Oxidative Addition of C(sp³)-F Bonds to Iridium via Initial C-H Bond Activation. *Science* **2011,** *332* (6037), 1545-1548.
24. Haibach, M. C.; Guan, C. J.; Wang, D. Y.; Li, B.; Lease, N.; Steffens, A. M.; Krogh-Jespersen, K.; Goldman, A. S., Olefin Hydroaryloxylation Catalyzed by Pincer-Iridium Complexes. *Journal of the American Chemical Society* **2013,** *135* (40), 15062-15070.
25. Haibach, M. C.; Lease, N.; Goldman, A. S., Catalytic Cleavage of Ether C□O Bonds by Pincer Iridium Complexes. *Angewandte Chemie International Edition* **2014,** *53* (38), 10160-10163.
26. Wilklow-Marnell, M.; Li, B.; Zhou, T.; Krogh-Jespersen, K.; Brennessel, W. W.; Emge, T. J.; Goldman, A. S.; Jones, W. D., Catalytic Dehydrogenative C–C Coupling by a Pincer-Ligated Iridium Complex. *Journal of the American Chemical Society* **2017**.
27. Gao, Y.; Emge, T. J.; Krogh-Jespersen, K.; Goldman, A. S., Selective Dehydrogenative Coupling of Ethylene to Butadiene via an Iridacyclopentane Complex. *Journal of the American Chemical Society* **2018,** *140* (6), 2260-2264.
28. Kovalenko, O. O.; Wendt, O. F., An electron poor iridium pincer complex for catalytic alkane dehydrogenation. *Dalton T* **2016,** *45* (40), 15963-15969.

29. Bézier, D.; Brookhart, M., Applications of PC(sp3)P Iridium Complexes in Transfer Dehydrogenation of Alkanes. *ACS Catalysis* **2014,** *4* (10), 3411-3420.
30. Huang, Z.; Brookhart, M.; Goldman, A. S.; Kundu, S.; Ray, A.; Scott, S. L.; Vicente, B. C., Highly Active and Recyclable Heterogeneous Iridium Pincer Catalysts for Transfer Dehydrogenation of Alkanes. *Advanced Synthesis & Catalysis* **2009,** *351* (1-2), 188-206.
31. Kuklin, S. A.; Sheloumov, A. M.; Dolgushin, F. M.; Ezernitskaya, M. G.; Peregudov, A. S.; Petrovskii, P. V.; Koridze, A. A., Highly Active Iridium Catalysts for Alkane Dehydrogenation. Synthesis and Properties of Iridium Bis(phosphine) Pincer Complexes Based on Ferrocene and Ruthenocene. *Organometallics* **2006,** *25* (22), 5466-5476.
32. Zhu, K.; Achord, P. D.; Zhang, X.; Krogh-Jespersen, K.; Goldman, A. S., Highly Effective Pincer-Ligated Iridium Catalysts for Alkane Dehydrogenation. DFT Calculations of Relevant Thermodynamic, Kinetic, and Spectroscopic Properties. *Journal of the American Chemical Society* **2004,** *126* (40), 13044-13053.
33. Haenel, M. W.; Oevers, S.; Angermund, K.; Kaska, W. C.; Fan, H.-J.; Hall, M. B., Thermally Stable Homogeneous Catalysts for Alkane Dehydrogenation. *Angewandte Chemie International Edition* **2001,** *40* (19), 3596-3600.
34. Tanoue, K.; Yamashita, M., Synthesis of Pincer Iridium Complexes Bearing a Boron Atom and iPr-Substituted Phosphorus Atoms: Application to Catalytic Transfer Dehydrogenation of Alkanes. *Organometallics* **2015,** *34* (16), 4011-4017.
35. Shih, W.-C.; Ozerov, O. V., Synthesis and Characterization of PBP Pincer Iridium Complexes and Their Application in Alkane Transfer Dehydrogenation. *Organometallics* **2017,** *36* (1), 228-233.
36. Yao, W.; Jia, X.; Leng, X.; Goldman, A. S.; Brookhart, M.; Huang, Z., Catalytic alkane transfer-dehydrogenation by PSCOP iridium pincer complexes. *Polyhedron* **2016,** *116*, 12-19.
37. Yao, W.; Zhang, Y.; Jia, X.; Huang, Z., Selective Catalytic Transfer Dehydrogenation of Alkanes and Heterocycles by an Iridium Pincer Complex. *Angewandte Chemie International Edition* **2014,** *53* (5), 1390-1394.
38. Nawara-Hultzsch, A. J.; Hackenberg, J. D.; Punji, B.; Supplee, C.; Emge, T. J.; Bailey, B. C.; Schrock, R. R.; Brookhart, M.; Goldman, A. S., Rational Design of Highly Active “Hybrid” Phosphine–Phosphinite Pincer Iridium Catalysts for Alkane Metathesis. *ACS Catalysis* **2013,** *3* (11), 2505-2514.
39. Ahuja, R.; Punji, B.; Findlater, M.; Supplee, C.; Schinski, W.; Brookhart, M.; Goldman, A. S., Catalytic dehydroaromatization of n-alkanes by pincer-ligated iridium complexes. *Nat Chem* **2010,** *3*, 167.
40. Morales-Morales, D.; Redón, R. o.; Yung, C.; Jensen, C. M., Dehydrogenation of alkanes catalyzed by an iridium phosphinito PCP pincer complex. *Inorganica Chimica Acta* **2004,** *357* (10), 2953-2956.
41. Göttker-Schnetmann, I.; White, P. S.; Brookhart, M., Synthesis and Properties of Iridium Bis(phosphinite) Pincer Complexes (p-XPCP)IrH2, (p-XPCP)Ir(CO), (p-XPCP)Ir(H)(aryl), and {(p-XPCP)Ir}2{μ-N2} and Their Relevance in Alkane Transfer Dehydrogenation. *Organometallics* **2004,** *23* (8), 1766-1776.
42. Göttker-Schnetmann, I.; White, P.; Brookhart, M., Iridium Bis(phosphinite) p-XPCP Pincer Complexes: Highly Active Catalysts for the Transfer Dehydrogenation of Alkanes. *Journal of the American Chemical Society* **2004,** *126* (6), 1804-1811.

43. Göttker-Schnetmann, I.; Brookhart, M., Mechanistic Studies of the Transfer Dehydrogenation of Cyclooctane Catalyzed by Iridium Bis(phosphinite) p-XPCP Pincer Complexes. *Journal of the American Chemical Society* **2004,** *126* (30), 9330-9338.
44. Jia, X.; Zhang, L.; Qin, C.; Leng, X.; Huang, Z., Iridium complexes of new NCP pincer ligands: catalytic alkane dehydrogenation and alkene isomerization. *Chemical Communications* **2014,** *50* (75), 11056-11059.
45. Brayton, D. F.; Beaumont, P. R.; Fukushima, E. Y.; Sartain, H. T.; Morales-Morales, D.; Jensen, C. M., Synthesis, Characterization, and Dehydrogenation Activity of an Iridium Arsenic Based Pincer Catalyst. *Organometallics* **2014,** *33* (19), 5198-5202.
46. Chianese, A. R.; Shaner, S. E.; Tendler, J. A.; Pudalov, D. M.; Shopov, D. Y.; Kim, D.; Rogers, S. L.; Mo, A., Iridium Complexes of Bulky CCC-Pincer N-Heterocyclic Carbene Ligands: Steric Control of Coordination Number and Catalytic Alkene Isomerization. *Organometallics* **2012,** *31* (21), 7359-7367.
47. Knapp, S. M. M.; Shaner, S. E.; Kim, D.; Shopov, D. Y.; Tendler, J. A.; Pudalov, D. M.; Chianese, A. R., Mechanistic Studies of Alkene Isomerization Catalyzed by CCC-Pincer Complexes of Iridium. *Organometallics* **2014,** *33* (2), 473-484.
48. Chianese, A. R.; Drance, M. J.; Jensen, K. H.; McCollom, S. P.; Yusufova, N.; Shaner, S. E.; Shopov, D. Y.; Tendler, J. A., Acceptorless Alkane Dehydrogenation Catalyzed by Iridium CCC-Pincer Complexes. *Organometallics* **2014,** *33* (2), 457-464.
49. Chianese, A. R.; Mo, A.; Lampland, N. L.; Swartz, R. L.; Bremer, P. T., Iridium Complexes of CCC-Pincer N-Heterocyclic Carbene Ligands: Synthesis and Catalytic C−H Functionalization. *Organometallics* **2010,** *29* (13), 3019-3026.
50. Oakley, S. H.; Coogan, M. P.; Arthur, R. J., Synthesis of Bis(imino)aryl Iridium Pincer Complexes and Demonstration of Catalytic Hydrogen-Transfer Activity. *Organometallics* **2007,** *26* (9), 2285-2290.
51. Kundu, S.; Choliy, Y.; Zhuo, G.; Ahuja, R.; Emge, T. J.; Warmuth, R.; Brookhart, M.; Krogh-Jespersen, K.; Goldman, A. S., Rational Design and Synthesis of Highly Active Pincer-Iridium Catalysts for Alkane Dehydrogenation. *Organometallics* **2009,** *28* (18), 5432-5444.
52. Adams, J. J.; Arulsamy, N.; Roddick, D. M., Acceptor PCP Pincer Iridium(I) Chemistry: Stabilization of Nonmeridional PCP Coordination Geometries. *Organometallics* **2011,** *30* (4), 697-711.
53. Adams, J. J.; Lau, A.; Arulsamy, N.; Roddick, D. M., Acceptor PCP Pincer Iridium Chemistry: (CF3PCP)IrIII Coordination Properties. *Organometallics* **2011,** *30* (4), 689-696.
54. Khake, S. M.; Soni, V.; Gonnade, R. G.; Punji, B., Design and development of POCN-pincer palladium catalysts for C–H bond arylation of azoles with aryl iodides. *Dalton T* **2014,** *43* (42), 16084-16096.
55. Flores, J.; Haibach, M.; Emge, T.; Goldman, A., *New NCOP Pincer Ligands Supporting Iridium Catalysts for the Catalytic Activation of Alkanes*. 2012.
56. Brookhart, M.; Sabo-Etienne, S., Catalytic tail-to-tail dimerization of methyl acrylate using rhodium(III) catalysts. *Journal of the American Chemical Society* **1991,** *113* (7), 2777-2779.
57. Valdés, H.; García-Eleno, M. A.; Canseco-Gonzalez, D.; Morales-Morales, D., Recent Advances in Catalysis with Transition-Metal Pincer Compounds. *ChemCatChem* **2018,** *10* (15), 3136-3172.

58. Sanshiro, K.; Jun-ichi, S.; Kunio, M.; Nobutami, K., Oxidative Addition of Vinyl Acetate to Ruthenium(0) Involving Carbon Oxygen Bond Cleavage Forming a Novel Vinyl(acetato)tris(triethylphosphine)ruthenium(II). *Chemistry Letters* **1987,** *16* (7), 1287-1290.

59. Komiya, S.; Kabasawa, T.; Yamashita, K.; Hirano, M.; Fukuoka, A., C□O bond cleavage and oxidative addition of allyl carboxylate to ruthenium(0) complex. Isolation of (π-allyl)(trifluoroacetato)tris(triethylphosphine)ruthenium(II). *Journal of Organometallic Chemistry* **1994,** *471* (1), C6-C7.

60. Ferrando, G.; Coalter, I. I. I. J. N.; Gérard, H.; Huang, D.; Eisenstein, O.; Caulton, K. G., Facile C(sp2)/O2CR bond cleavage by Ru or Os. *New Journal of Chemistry* **2003,** *27* (10), 1451-1462.

61. Planas, J. G.; Marumo, T.; Ichikawa, Y.; Hirano, M.; Komiya, S., Carbon–oxygen and carbon–sulfur bond activation of vinyl esters, ethers and sulfides by low valent ruthenium complexes. *Journal of the Chemical Society, Dalton Transactions* **2000,** (15), 2613-2625.

62. Komiya, S.; Hirano, M., Bond activation by low valent ruthenium complexes. *Dalton T* **2003,** (8), 1439-1453.

63. Kuwano, R., Usage of the Carboxylate Leaving Group in Transition-metal-catalyzed Cross-coupling and Related Reactions. *有機合成化学協会誌* **2011,** *69* (11), 1263-1270.

64. Liu, F.; S. Goldman, A., Efficient thermochemical alkane dehydrogenation and isomerization catalyzed by an iridium pincer complex. *Chemical Communications* **1999,** (7), 655-656.